NATIONAL ADVISORY COMMITTEE FOR AERONAUTICS

NACA - UNIVERSITY CONFERENCE ON AERODYNAMICS

A COMPILATION OF THE PAPERS PRESENTED

Langley Aeronautical Laboratory
Langley Field, Va.

June 21-23, 1948

NACA – UNIVERSITY CONFERENCE

ON AERODYNAMICS

A Compilation of the Papers Presented

Langley Aeronautical Laboratory
Langley Field, Virginia

June 21–23, 1948

TABLE OF CONTENTS

INTRODUCTION

This document contains reproductions of the technical papers presented at the NACA – University Conference on Aerodynamics held at the Langley Aeronautical Laboratory on June 21, 22, and 23, 1948. The conference was held in recognition of the difficulties, imposed by security restrictions, in keeping abreast of the rapid advances in aerodynamics. The papers were prepared to review the status of a number of fields of interest, to summarize the more important wartime advances that are no longer classified, and to orient reference material for further study.

The papers in this document are in the same form in which they were presented at the conference so that distribution of them might be prompt. The original presentation and this record are considered as complementary to, rather than as substitutes for, the Committee's system of complete and formal reports.

A list of the conferees is included.

LIST OF CONFEREES

The following were registered at the NACA – University Conference on Aerodynamics, Langley Aeronautical Laboratory, Langley Field, Virginia, June 21–23, 1948:

Abbott, Ira H.	NACA
Abel, William	Sparton College of Aeronautical Engineering
Akerman, John D.	University of Minnesota
Alden, Henry L.	Massachusetts Institute of Technology
Ames, Milton B.	NACA
Ashley, Holt	Massachusetts Institute of Technology
Barzelay, M. E.	Syracuse University
Becker, John V.	NACA
Beeson, Lt. Col. Thomas H.	U. S. Military Academy
Bergman, Stefan	Harvard University
Bicknell, Joseph	Massachusetts Institute of Technology
Binder, R. C.	Purdue University
Black, S. D.	Case Institute of Technology
Blaisdell, Allen H.	Carnegie Institute of Technology
Bock, Arthur E.	U. S. Naval Academy
Brown, Clinton E.	NACA
Bruhn, E. F.	Purdue University
Brush, Edward E.	Agricultural and Mechanical College of Texas
Buchman, Walter H.	University of Cincinnati
Burroughs, K. L.	Aeronautical University, Inc.
Campbell, John P.	NACA
Chang, C. C.	Johns Hopkins University
Chieri, Pericle A.	Newark College of Engineering
Churchill, L. S.	University of Louisville
Corson, Blake W., Jr.	NACA
Crook, Louis	Catholic University
Daley, Capt. Daniel H.	Air Force Institute of Technology
de Graffenried, A. L.	Rensselaer Polytechnic Institute
Deters, O. J.	NACA
Diamond, Anisley H.	Agricultural and Mechanical College of Oklahoma
Diederich, Franklin W.	NACA
Dobyns, Capt. S. W.	Virginia Military Institute
Donaldson, Coleman duP.	NACA
Donlan, C. J.	NACA
Doty, L. T.	University of Cincinnati
Dryden, H. L.	NACA
Duke, Charles E.	Pennsylvania State College
Erdoss, B. K.	Lehigh University

Fairbanks, A. J.	Rensselaer Polytechnic Institute
Fedziuk, Henry A.	NACA
Ferri, Antonio	NACA
Ganzer, Victor M.	University of Washington
Garrick, I. E.	NACA
Gatewood, B. E.	Air Force Institute of Technology
Gessow, Alfred	NACA
Goddard, Frank E., Jr.	Massachusetts Institute of Technology
Guerrieri, S. A.	University of Delaware
Hanson, K. P.	North Carolina State College of Agriculture and Engineering
Harrington, R. P.	Polytechnic Institute of Brooklyn
Hawkins, Harold V.	Illinois Institute of Technology
Hemke, Paul E.	Rensselaer Institute of Technology
Houser, Jacque	University of Illinois
Hugli, W. C., Jr.	Stevens Institute of Technology
Hunter, W. H.	NACA
Johnson, Harold A.	University of California, Berkeley
Jones, Bradley	University of Cincinnati
Jones, Robert T.	NACA
Kaplan, Carl	NACA
Katzoff, S.	NACA
Korvin-Kroukovsky, B. V.	Stevens Institute of Technology
Korycinski, Peter F.	NACA
Kotcher, Ezra	Air Force Institute of Technology
Kuethe, Arnold M.	University of Michigan
Laitone, Edmund V.	University of California, Berkeley
Langhaar, H. L.	University of Illinois
Larsen, Lt. Harold C.	Air Force Institute of Technology
LaVier, H. W. S.	Georgia Institute of Technology
Libby, Paul A.	Polytechnic Institute of Brooklyn
Loftin, Laurence K., Jr.	NACA
Lomax, Harvard	NACA
Ludloff, J. F.	New York University
Lundquist, Elmer C.	State University of Iowa
Maggin, B.	NACA
Malmberg, Ben O.	Rutgers University
Martin, George P.	Lawrence Institute of Technology
Maser, Ernest E.	Louisiana State University
McBride, J. W.	Purdue University
McCoy, Kenneth L.	Louisiana State University
Merriam, Kenneth G.	Worcester Polytechnic Institute
Miles, John W.	University of California, Los Angeles

Miller, Jay W.	Rensselaer Polytechnic Institute
Morkovin, M.	University of Michigan
Morse, Fred T.	University of Virginia
Mueller, Robert K.	Massachusetts Institute of Technology
Neumann, Ernest P.	Massachusetts Institute of Technology
Newkirk, Burt L.	Rensselaer Polytechnic Institute
Nikolsky, A. A.	Princeton University
Pai, S. I.	Cornell University
Parkinson, L. R.	Syracuse University
Pearce, Clinton E.	Kansas State College of Agriculture and Applied Sciences
Pierce, C. J.	Ohio State University
Pell, William H.	Brown University
Perkins, Courtland D.	Princeton University
Perna, Angelo J.	Newark College of Engineering
Phillips, William H.	NACA
Pope, Alan	Georgia Institute of Technology
Power, R. B.	Pennsylvania State College
Prior, John A.	University of Pennsylvania
Razak, Kenneth	University of Wichita
Reid, Elliott G.	Stanford University
Reissner, Eric	Massachusetts Institute of Technology
Rhodes, J. E., Jr.	Georgia Institute of Technology
Rightmire, B. G.	Massachusetts Institute of Technology
Rinkoski, Donald W.	University of Akron
Ritter, W. K.	NACA
Robinson, R. G.	NACA
Ross, R. S.	University of Akron
Rowland, A. E.	Virginia Polytechnic Institute
Rutkowski, Joseph	University of Michigan
Scanlan, R. H.	Rensselaer Polytechnic Institute
Seamens, Robert C.	Massachusetts Institute of Technology
Sheldon, H. H.	University of Miami
Sherwood, A. W.	University of Maryland
Sims, Leland W.	Aeronautical University, Inc.
Sivells, James C.	NACA
Smith, Josiah E.	California Institute of Technology
Smith, J. F. D.	Iowa State College of Agriculture and Mechanic Arts
Smith, Kenneth E.	University of Detroit
Smith, Norman F.	NACA
Smull, T. L. K.	NACA
Soulé, H. A.	NACA
Stack, John	NACA
Sternfield, Leonard	NACA
Stillwell, H. S.	University of Illinois
Stott, A. F.	Aeronautical University, Inc.

Taylor, Edward S.	Massachusetts Institute of Technology
Teplitz, J.	NACA
Tetervin, Neal	NACA
Theodorides, P.	Harvard University
Thompson, F. L.	NACA
Toll, Thomas A.	NACA
Truitt, R. W.	North Carolina State College of Agriculture and Engineering
Vincenti, Walter G.	NACA
Von Doenhoff, Albert E.	NACA
Von Eschen, G. L.	Ohio State University
Von Mises, Richard	Harvard University
Wang, C. T.	New York University
Webber, D. H.	St. Louis University, Parks College of Aeronautical Technology
Weber, Paul	Georgia Institute of Technology
Wild, John M.	Cornell University
Wilsey, Edward F.	Ohio University
Witunski, Michael	Massachusetts Institute of Technology
Wood, K. D.	University of Colorado
Yates, C. C.	University of Pittsburgh
Zener, Clarence	University of Chicago

BOUNDARY LAYER

STABILITY OF THE LAMINAR BOUNDARY LAYER

By Neal Tetervin

Langley Aeronautical Laboratory

This paper treats the stability theory for the laminar boundary layer and its applications. First, a short history of the theory similar to that in a paper by Pillow (reference 1), which contains a comprehensive list of references, is given; then, an outline of the theory for incompressible flow (reference 2) is presented. This is followed by a summary of the recent applications of the theory for incompressible flow. Finally, the results of investigations concerning the effect of compressibility and the effect of curvature on the stability of the laminar boundary layer is summarized.

In Prandtl's paper of 1904 (reference 3), which founded boundary-layer theory, the region of flow around a body was divided into two parts. One region includes almost the entire flow field and has the property that the viscosity of the fluid in this region has no effect on its motion. The other region is a narrow one next to the body where the fluid velocity rises rapidly from zero at the surface to a value which then changes slowly or not at all with further increase in distance from the surface. The narrow region in which the velocity changes so rapidly that the viscous forces are not negligible even in fluids of small viscosity is called the boundary layer. To this boundary layer can be traced the origin of the differences between the behavior of bodies in real and in nonviscous fluids.

Boundary layers are generally classified as either laminar or turbulent. Laminar flow is defined as one in which almost all of the interchange of momentum between adjacent layers of flowing fluid takes place by molecular diffusion (reference 4). At the stagnation point of a body and usually for some distance downstream, the flow in the boundary layer is laminar. Far enough from the stagnation point, however, the flow in the boundary layer changes from the smooth laminar flow to a violently fluctuating one – the turbulent flow. As shown in figure 1, the turbulent flow is associated with a different manner of increase of the average velocity with distance from the surface and with a higher skin friction. The skin friction for turbulent flow is usually several times the skin friction for laminar flow.

In normal flight attitudes the profile drag of wings and fuselages is almost directly proportional to their skin friction. It is thus possible to reduce greatly the drag of aircraft by so constructing them that extensive regions of laminar flow can exist. One method is to design shapes that are favorable for long lengths of laminar flow; another is to act directly upon the laminar boundary layer. The first method has led to the NACA 6-series airfoils (reference 5); the second which includes various types of suction and blowing is still in the relatively early stages of development (reference 6). The close connection between aircraft drag and the type of flow in the boundary layer thus makes it important to understand how the change from laminar to

turbulent flow occurs. Such an understanding may eventually lead to aircraft with considerably lower drag (reference 7).

The change from laminar to turbulent flow is known as transition. Several causes of transition are (1) disturbances that originate in the outer stream such as those that occur when the free stream is turbulent, (2) disturbances introduced into the laminar boundary layer itself, for example, by surface roughness, and (3) a rising static pressure in the direction of flow that causes a complete reversal of the flow and eddies near the surface. Historically the subject first attracted attention because an apparently smooth flow would suddenly become turbulent.

It is interesting to note that the problem of the stability of laminar flow drew the attention of investigators years before modern aeronautics and boundary-layer theory began. The first recorded suggestion that the Navier-Stokes equation of motion might have unstable solutions was made by Stokes in 1843 (reference 8). Twenty-five years later Helmholtz (see reference 11 of reference 1) showed that, in a nonviscous fluid, surfaces across which there was a discontinuity in the velocity were inherently unstable. Rayleigh (reference 9) was the first to really attack the problem. He published his first paper on the subject of stability in 1879 and his last on the same subject thirty-five years later (references 10 and 11). Rayleigh investigated the stability of various hypothetical velocity distributions with the effect of viscosity on the disturbed motion neglected.

In 1883, Reynolds (see reference 48 of reference 1) published the results of his classic experiments on the transition from laminar to turbulent flow in pipes. Later, in 1895 (reference 12), he investigated the transition problem theoretically by seeking to determine the smallest Reynolds number above which an arbitrary disturbance would increase initially. The work was criticized by Sharpe in 1905 (see reference 46 of reference 1) and by Lorentz (see reference 29 of reference 1) in 1907 on the ground that the critical Reynolds number depended strongly on the form of the disturbance. Between 1907 and 1909, Orr (reference 13) improved Reynolds' method by using the calculus of variations to find the largest Reynolds number below which all disturbances decrease. Orr's work, however, has in turn been criticized because it allows all disturbances and, therefore, gives critical Reynolds numbers that are much smaller than those observed for quiet flows.

In 1908, a short time after Orr's work was published, Sommerfeld (see reference 26 of reference 1) independently set up the problem for the two-dimensional flow in which the velocity is parallel to the wall and is dependent only on the distance from the wall. Sommerfeld's and Orr's investigations formed the basis of the work leading up to the present theory of boundary-layer instability. During the following years, Von Mises (see references 27 and 28 of reference 1) and Hopf (reference 14), by making use of the work of Orr and Sommerfeld, found

plane Couette flow, the flow which exists when two parallel planes separated by fluid slide past one another, to be stable for all the Reynolds numbers that were investigated. For the plane Couette flow the velocity varies directly with the distance from the wall.

Taylor, in 1923, (reference 15) investigated the Couette motion between rotating cylinders theoretically and checked the results experimentally. In contrast to most of the work on plane flows where the disturbances were assumed to be two dimensional, Taylor's theory was based on three-dimensional disturbances. For a number of years Taylor's work was a high-water mark in the understanding of the breakdown of laminar flow.

In 1924, Heisenberg (reference 16) successfully studied the stability of a variable continuous vorticity distribution by making use of the work of Orr and Sommerfeld. As an example he showed that plane Poiseuille flow, the flow under a uniform pressure gradient between fixed parallel planes, is unstable for sufficiently large Reynolds numbers. This flow has a parabolic velocity distribution. Heisenberg's theory was not generally accepted, perhaps, because his computations were incomplete and rough.

The first to investigate the stability of the boundary layer was Tietjens (reference 17) in 1925. He replaced the velocity profile by line segments and applied Rayleigh's theory, taking account of viscosity near the wall. Tietjens did not obtain a critical Reynolds number for the flat plate. The use of line segments to replace a velocity profile had already been shown to be invalid by Heisenberg. The next to investigate the stability of the boundary layer were Tollmien in 1929 (reference 18) and Schlichting in 1932 (reference 19). Both used what was essentially Heisenberg's theory and during the 1930's developed it sufficiently for use as a research tool (references 20 and 21). In 1945, Lin published his comprehensive work on the stability of two-dimensional parallel flows. (See reference 2.) This work made the theory more rigorous mathematically, provided a rapid approximate means of determining the minimum critical Reynolds number of a flow, and improved the physical picture of the instability. In addition it provided stability limits for the flow over a flat plate that agree better with experimental results than do the calculations of Tollmien and Schlichting.

The following is an outline of Lin's stability theory (reference 2). The purpose of the theory is to determine whether a particular flow is unstable for sufficiently large Reynolds numbers, to determine the minimum critical Reynolds number at which instability begins, and to understand the physical mechanism of the growth or decay of disturbances. The basic assumptions of the theory are that (1) the disturbances are small, (2) two-dimensional disturbances alone are considered, (3) the flow is essentially parallel to one direction (thus, the boundary-layer approximation that the derivative parallel to the surface of any quantity connected with the main flow is negligible compared with the

derivative normal to the surface of the same quantity is applicable), (4) the velocity distribution normal to the surface is everywhere the same, and (5) the boundary conditions are everywhere the same.

The development of the theory is begun by writing the Navier–Stokes equation of motion for two-dimensional incompressible flow in a form that uses the vorticity ζ and thereby eliminates the pressure. The equation of motion then appears as:

$$\Delta\psi_t + \psi_y\Delta\psi_x - \psi_x\Delta\psi_y = \nu\Delta\Delta\psi \qquad (1)$$

where x is the coordinate along the surface, y is the coordinate normal to the surface,

$$U = \psi_y = \frac{\partial\psi}{\partial y}$$

is the velocity parallel to the surface,

$$V = -\psi_x = -\frac{\partial\psi}{\partial x}$$

is the velocity normal to the surface,

$$\zeta = \frac{\partial V}{\partial x} - \frac{\partial U}{\partial y} = -\Delta\psi$$

$$\Delta = \frac{\partial^2}{\partial x^2} + \frac{\partial^2}{\partial y^2}$$

and ν is the kinematic viscosity.

The stream function ψ is assumed to be the sum of the stream function of the steady flow Ψ and of the stream function of the disturbance ψ'. The introduction of the stream functions makes both the mean and the disturbance velocities satisfy the equation of continuity. Thus, let

$$\psi = \Psi(x,y) + \psi'(x,y,t)$$

and substitute into equation (1). Then, because the disturbance is small, terms quadratic in ψ' and its derivatives can be neglected. Equation (1) then becomes

$$\Delta\psi'_t + \Psi_y\Delta\psi'_x - \Psi_x\Delta\psi'_y + \psi'_y\Delta\Psi_x - \psi'_x\Delta\Psi_y = \nu\Delta\Delta\psi' \qquad (2)$$

The flow is now assumed to be essentially parallel to the x-axis, thus making the boundary-layer approximations applicable. Therefore, it is permissible to neglect the x-derivative of any quantity connected with the main flow compared with the y-derivative of the same quantity. For the disturbance, however, the quantities ψ'_y and ψ'_x, which are the disturbance velocities u' and $-v'$ along the x- and y-axes, respectively, are of the same order of magnitude. After making the boundary-layer approximation, equation (2) becomes

$$\Delta\psi'_t + \bar{\Psi}_y \Delta\psi'_x - \psi'_x \frac{\partial^3 \bar{\Psi}}{\partial y^3} = \nu\Delta\Delta\psi' \tag{3}$$

The approximation that the velocity distribution normal to the wall is independent of x now makes it permissible to use the local values at a given value of x for $\bar{u} = \frac{\partial \bar{\Psi}}{\partial y} = \bar{\Psi}_y$ and for $\frac{\partial^2 \bar{u}}{\partial y^2} = \frac{\partial^3 \bar{\Psi}}{\partial y^3}$. Equation (3) then becomes

$$\Delta\psi'_t + \bar{u}(y)\Delta\psi'_x - \frac{\partial^2 \bar{u}(y)}{\partial y^2} \psi'_x = \nu\Delta\Delta\psi' \tag{4}$$

A main flow with an arbitrary distribution of velocity $\bar{u}(y)$ is now assumed to exist between two parallel planes $y = y_1$ and $y = y_2$. Then the disturbance stream function $\psi'(x,y,t)$ must be made to satisfy both equation (4) and the conditions $u' = v' = 0$ at $y = y_1$ and $y = y_2$ where u' and v' are the disturbance velocities. The disturbance stream function is now assumed to be given by

$$\psi' = \phi(y)e^{i\alpha(x-ct)}$$

where ϕ disturbance amplitude function

$$\alpha = \frac{2\pi}{\text{Wave length of disturbance}}$$

x coordinate along the plate

t time

and c is complex; the real part of c, that is, c_r, is the velocity with which the disturbance moves downstream; and the imaginary part of c, that is, c_i, determines whether the disturbance dies out $(c_i < 0)$, does not change with time $(c_i = 0)$, or increases in amplitude with time $(c_i > 0)$

After all the velocities have been referred to a reference velocity U and all lengths, to a reference length l, a Reynolds number $R = \frac{Ul}{\nu}$ has been defined, and the equation for ψ' has been used, equation (4) becomes the linearized differential equation for $\phi(y)$ which is known as the Orr-Sommerfeld equation.

$$(\bar{u} - c)\left(\frac{\partial^2\phi}{\partial y^2} - \alpha^2\phi\right) - \frac{\partial^2\bar{u}}{\partial y^2}\phi = -\frac{i}{\alpha R}\left(\frac{\partial^4\phi}{\partial y^4} - 2\alpha^2\frac{\partial^2\phi}{\partial y^2} + \alpha^4\phi\right) \tag{5}$$

Equation (5) is a homogoneous, linear, ordinary differential equation of the fourth order. Its solution is

$$\phi = C_1\phi_1 + C_2\phi_2 + C_3\phi_3 + C_4\phi_4 \tag{6}$$

where the ϕ's are particular solutions and the C's are constants of integration.

The four boundary conditions which are independent of x and which must be satisfied are

$$\left.\begin{aligned} &\phi(y_1) = 0 \\ &\phi(y_2) = 0 \end{aligned}\right\}$$

that is, $v' = 0$ at $y = y_1$ and $y = y_2$, and

$$\left.\begin{aligned} &\left(\frac{d\phi}{dy}\right)_{y_1} = 0 \\ &\left(\frac{d\phi}{dy}\right)_{y_2} = 0 \end{aligned}\right\} \tag{7}$$

that is, $u' = 0$ at $y = y_1$ and $y = y_2$.

When these boundary conditions are used with equation (6), the result is the determinant

$$\begin{vmatrix} \phi_1(y_1) & \phi_2(y_1) & \phi_3(y_1) & \phi_4(y_1) \\ \phi_1(y_2) & \phi_2(y_2) & \phi_3(y_2) & \phi_4(y_2) \\ \left(\frac{d\phi_1}{dy}\right)_{y_1} & \left(\frac{d\phi_2}{dy}\right)_{y_1} & \left(\frac{d\phi_3}{dy}\right)_{y_1} & \left(\frac{d\phi_4}{dy}\right)_{y_1} \\ \left(\frac{d\phi_1}{dy}\right)_{y_2} & \left(\frac{d\phi_2}{dy}\right)_{y_2} & \left(\frac{d\phi_3}{dy}\right)_{y_2} & \left(\frac{d\phi_4}{dy}\right)_{y_2} \end{vmatrix} = 0 \qquad (8)$$

which involves the solution of equation (5). After the functions ϕ_1, ϕ_2, ϕ_3, and ϕ_4 which contain the parameters α, R, and c have been determined with sufficient precision, which is a very involved process, the determinant (8) is written out and the real and imaginary parts equated to zero. The result is two real equations involving the parameters α, R, c_r, and c_i. If c_i is made zero and c_r is eliminated between the two real equations, the result is a relation between α and R. This relation between α, a quantity inversely proportional to the wave length of the disturbance, and R, the Reynolds number, defines the neutral curve along which the disturbances are neither damped nor amplified. The curve divides the α,R-plane into a stable region and an unstable region. The smallest value of the Reynolds number for which amplification can occur is called the minimum critical Reynolds number. Above the minimum critical Reynolds number, disturbances in the correct frequency range are amplified and, if they grow large enough, cause transition to turbulent flow. Lin has found that all velocity distributions of the symmetrical type and of the boundary-layer type are unstable for sufficiently large, but finite, Reynolds numbers. In his paper, Lin has given a useful approximate rule

for the determination of the minimum critical Reynolds number; the rule is

$$R_\delta = \frac{25\left(\frac{d\bar{u}}{dy}\right)_1}{c^4}$$

where

$$R_\delta = \frac{U_\delta \delta}{\nu}$$

and where c is equal to the value of $\bar{u}$ for which

$$-\pi\left(\frac{d\bar{u}}{dy}\right)_1 \left[3 - \frac{2\left(\frac{d\bar{u}}{dy}\right)_1 y}{\bar{u}}\right]\left[\frac{\bar{u}\left(\frac{d^2\bar{u}}{dy^2}\right)}{\left(\frac{d\bar{u}}{dy}\right)^3}\right] = 0.58$$

U_δ is the velocity at the edge of the boundary layer, δ is the thickness of the boundary layer, and subscript 1 denotes "at surface." The velocities are referred to the velocity at the boundary-layer edge and the lengths, to the distance from the wall to where $\bar{u} = 1$.

The physical interpretation of the instability process (references 2 and 22) is that the viscosity shifts the phase between the x- and y-components of the disturbance in such a way that energy is drawn from the main flow and builds up the amplitude of the disturbance.

The validity of the assumption that for a parallel flow it is necessary to investigate only two-dimensional disturbances was confirmed by Squire (reference 23). In 1933 he showed that a two-dimensional disturbance produces instability at a smaller Reynolds number than a corresponding three-dimensional disturbance.

In 1941, Pretsch (reference 24) showed that the relations between the parameters α, R, and c are the same whether both the mean and the disturbance velocities in the boundary layer are functions of x and y or of y alone as assumed in the development of the theory. This important result means that the stability of the boundary layer at any value of x is dependent only on the local velocity distribution. The present theory can therefore be used when both the velocity distribution in the boundary layer and its thickness change along the surface.

It should be kept in mind that the theory is a small-disturbance theory. Therefore, conclusions drawn from it should not be applied to cases where finite disturbances are introduced into the boundary layer. Such disturbances are often introduced by roughness particles, which although small, may easily produce disturbances much greater than the vanishingly small disturbances allowed by the theory. It should also be noted that the theory merely predicts when infinitesimal disturbances will begin to grow. The disturbance cannot be traced by the theory to the stage where the disturbance has grown large enough to produce turbulent flow. The growth of the infinitesimal disturbance takes time; and, therefore, when transition develops from the growth of infinitesimal disturbances, the transition point lies some distance downstream of the instability point. The magnitude of the distance depends on the rate of amplification of the disturbance and therefore on the flow conditions.

Because of the many assumptions and because of the complexity of the mathematical development, the theory and its predictions were not taken seriously by many until fairly recently. In 1943 the results of the outstanding experimental work of Schubauer and Skramstad appeared (reference 25). The results showed that the laminar boundary-layer oscillations predicted by the stability theory of Tollmien and Schlichting not only were present but that the theory correctly predicted their characteristics. Figure 2 shows the neutral curve calculated by Lin, probably the most accurate calculation to date, and the experimental points obtained by Schubauer and Skramstad for flow over a flat plate. The circle symbols should lie on branch I; the cross symbols, on branch II.

In Germany during the war, the theory was used to calculate stability limits for flows in which there were small velocities through the surface. For these suction or blowing flows, the same stability theory was used as for impervious walls. This use is permissible because both the equations describing the motion and the boundary conditions that have to be satisfied by the disturbances are unchanged by small flows through the wall. The stability limits were computed for four exact solutions of the Prandtl boundary-layer equations. A boundary-layer velocity distribution must be known precisely before its stability limits can be determined accurately. The following results were taken from a paper by Ulrich (reference 26). The first case is the "Asymptotic Case." It applies to flow over a flat plate with a constant flow velocity into the plate and concerns only the region that is so far from the leading edge that no boundary-layer characteristic changes with a further increase in distance from the leading edge. For this case, the surface friction coefficient is independent of the viscosity and, for equal boundary-layer Reynolds numbers, is 1.75 times greater than the surface friction on the plate without suction. The minimum critical Reynolds number $\frac{U_0\delta^*}{\nu}$, where δ^* is the displacement thickness, is given by Pretsch as 55,200 (reference 27) in contrast to 575 obtained by Schlichting for the flat

plate without suction. Other German investigators have obtained the value 70,000 for R_{δ}^* (reference 28) instead of 55,200 so that there seems to be some differences caused by different calculating procedures. In order to keep the boundary-layer Reynolds number always less than the minimum critical Reynolds number, and thus to keep the boundary layer stable, making the suction ratio $-\frac{v_o}{U_o} > 1.8 \times 10^{-5}$ is sufficient when 55,200 is used for the value of $R_{\delta}^*{}_{cr}$; v_o is the suction velocity and is negative when its direction is into the plate and U_o is the free-stream velocity.

The second case is the "Constant Suction" flow. Here also, there is a constant suction velocity through the surface of the plate, but the entire plate is treated and the velocity profiles are not similar to one another. Near the leading edge of the plate, the profile is the Blasius flat-plate profile (reference 29); but as the distance from the leading edge increases, the profile becomes more convex and finally approaches the asymptotic profile at large distances from the leading edge. When the suction ratio $\frac{-v_o}{U_o} > 1.2 \times 10^{-4}$, the flow is stable over the entire plate. This suction ratio, 1.2×10^{-4} is about seven times the ratio necessary for stability with the asymptotic profile. The greater suction is necessary because the velocity profiles near the leading edge of the plate are not as stable as the more convex asymptotic profile. Note, however, that the required suction ratio is still very small. The flow velocity through the plate is about 0.001 of the free-stream velocity.

Another case for which the stability computations based on exact solutions of the boundary-layer equations were made is the one in which the suction velocity varies inversely as $\sqrt{x}$ from the leading edge of a flat plate. The results are shown in figure 3. For this flow all the velocity profiles are similar to one another and change their form only when the suction coefficient C_Q is changed. The suction coefficient is defined by

$$C_Q = -\frac{Q}{lbU_o}$$

where

l length of plate

b width of plate

U_o free-stream velocity

Q total suction quantity

The value 575 for R_{δ}^* corresponds to the value 1.1×10^5 for R_x; the value 10^4 for R_{δ}^* corresponds to the value 8.3×10^7 for R_x, an increase in R_x of about 750 times. Figure 3 clearly shows that sucking, positive C_Q, increases the stability of the flow over that on an impervious flat plate and that blowing, negative C_Q, decreases the stability. In general, suction increases the stability of a boundary layer both because the boundary layer is kept thin and because the velocity profile is made more convex.

The fourth case for which stability computations based on exact solutions of the boundary-layer equation exist is that for the flow near the stagnation point of a two-dimensional body which has a constant suction or blowing velocity through its surface. The region considered is that region where the velocity at the edge of the boundary layer varies directly as the distance from the stagnation point. The results are shown in figure 4. In this region $U = u_1 x$, where U is the velocity at the edge of the boundary layer, u_1 is a constant, and x is the distance from the stagnation point measured along the surface. Here again, all the velocity profiles are similar to one another and change in shape only when C_o, the suction coefficient, is changed. The boundary-layer thickness is independent of x. It should be noticed that the flow near the stagnation point has a falling pressure in the direction of the flow; the previously mentioned flows were all for zero pressure gradient. The increased stability caused by the falling pressure is shown in figure 4. An amount of blowing corresponding to $C_o < -3$, where $C_o = \frac{-v_o}{\sqrt{u_1 \nu}}$, is necessary before stability is reduced from that for no flow through the surface to that for the impervious flat plate. When there is no flow through the surface, the boundary layer near a stagnation point has a critical Reynolds number of 12,300 in contrast to the value of 575 for the flat plate; the increase of about 20 times is caused by the falling pressure along the surface.

In figure 5 is shown the theoretically predicted drag reduction for two types of flow over flat plates with just enough suction to maintain stability; one is the "Constant Suction" case and the other is the case for which the suction velocity is inversely proportional to $\sqrt{x}$. The drag reduction is a large percentage of the drag of a plate with a completely turbulent boundary layer and, for R_x less than 10^8, a constant suction velocity is better than a suction velocity inversely proportional to $\sqrt{x}$.

The skin-friction values upon which the comparison in figure 5 is based are obtained from the velocity derivative at the surface. The sucked-in fluid remains at rest in the plate and the power required to suck the fluid into the plate is not considered. If, however, it is

assumed that the sucked-in fluid is ejected with free-stream total head and that, in order to do this, total head is added to the fluid with an efficiency of unity, then the drag reduction shown is the true drag reduction if the total-head loss through the surface is equal to the free-stream dynamic pressure. If the total-head loss through the surface is greater than the free-stream dynamic pressure, then the drag reduction will be less than shown and vice versa. Because only small quantities of suction air are required to maintain laminar flow, the percentage drag reduction changes fairly slowly with a change of total-head loss through the plate.

These results are the sum total of the known stability computations based on exact solutions of the laminar boundary-layer equations. The only case directly applicable to flow about an airfoil is the stagnation-point flow.

Before the stability boundaries for an airfoil can be computed, the velocity distributions through the boundary layer must be known. During the war, Schlichting developed an approximate method for the computation of the laminar boundary layer over an arbitrary two-dimensional body with an arbitrary distribution of suction along the surface (reference 30). The method is related to the Pohlhausen method which treats flows without suction. Schlichting's method uses the boundary-layer momentum equation for the case where there is flow through the surface and assumes a one-parameter family of curves for the boundary-layer velocity distributions. The parameter for the velocity distribution depends on the pressure distribution over the body and on the suction flow through the surface.

The critical Reynolds number of a velocity profile is sensitive to its shape. Therefore, the accuracy of an approximate method, such as Schlichting's, when the results are to be used for stability computations, can be tested only by comparing the critical Reynolds numbers with those from an accurate computation of the boundary layer.

The foregoing discussion was restricted to incompressible flow. The problem of the stability of the laminar boundary layer in a compressible gas has, however, not been neglected. The increase in flight speeds has given the problem practical, as well as purely scientific, importance.

The stability theory for compressible flow has been developed by Lees and Lin (references 31 and 32) to about the same state as the theory for incompressible flow. The development of the theory for compressible flow is similar to that for incompressible flow. In the theory for compressible flow, however, in contrast to the theory for incompressible flow, the heat energy is important and the physical properties of the gas are not fixed. Nevertheless, the main physical mechanism is not changed. The stability of a velocity distribution depends on the distribution of the product of density and vorticity and on the effect of the viscous

forces but not directly on the heat conductivity. The expression $\frac{\partial}{\partial y}\left(\rho\frac{\partial u}{\partial y}\right)$ for compressible flow takes the place of the expression $\frac{\partial}{\partial y}\left(\frac{\partial u}{\partial y}\right)$ for incompressible flow as an important factor in determining the stability. It is noted, however, that as yet for compressible flow there is no rigorous proof that the two-dimensional disturbances upon which the theory is based are more unstable than three-dimensional disturbances.

The main results of Lees' and Lins' work can be summed up in the following statements:

(1) When the free-stream velocity is subsonic, every laminar boundary-layer flow is unstable at sufficiently large Reynolds numbers.

(2) At all free-stream Mach numbers the flow is unstable at sufficiently large Reynolds numbers if the y derivative of $\rho\frac{\partial u}{\partial y}$ is zero for a value of $u > 1 - \frac{1}{M_o}$.

(3) An approximate expression for the minimum critical Reynolds number is obtained, similar to the expression obtained by Lin for incompressible flow.

(4) As shown in figure 6 the stability of the laminar boundary layer on an insulated surface decreases with increase in Mach number. At $M_o = 1$, $R_{x_{cr_{min}}}$ is less than half its value at $M_o = 0$.

(5) As shown in figure 7, the ratio of the surface temperature to the free-stream temperature has a large effect on the boundary-layer stability. Thus, at a Mach number of 0.7 the value of the boundary-layer Reynolds number R_θ, based on the momentum thickness as the length, at which the boundary layer first becomes unstable increases about 40 times when the surface temperature is changed from 110 percent of the free-stream temperature, the stagnation-temperature ratio for a Mach number of 0.7, to 70 percent of the free-stream temperature. On the other hand, an increase of surface temperature from 110 percent of the free-stream temperature to 125 percent of the free-stream temperature halves the Reynolds number at which the flow becomes unstable.

(6) At supersonic free-stream velocities, the boundary layer can be made stable at all Reynolds numbers by maintaining the surface temperature at a small enough fraction of the free-stream temperature. For $M_o > 3$ at 50,000 feet altitude and for $M_o > 2$ at 100,000 feet altitude, the radiation of heat from a surface can make the ratio of the surface temperature to the free-stream temperature small enough to ensure a stable boundary layer at all Reynolds numbers, in the absence of an adverse pressure gradient.

The stability theories for both the incompressible and the compressible laminar boundary layer, which have just been discussed, were developed for flows in which the effects of surface curvature were negligible. Because most aircraft components are curved, it was not clear whether the stability theory for flat surfaces was directly applicable. The effect of curvature on the stability of the incompressible boundary layer was investigated theoretically by Görtler about 1940 (references 33 to 35) and experimentally by Liepmann (references 36 and 37) in the following years.

Görtler found that the two-dimensional wavelike disturbances were hardly affected by wall curvature. When, however, the stability of the boundary layer on curved walls was considered by investigating the behavior of vortices with their axis parallel to the main flow, analogous to the Taylor vortices in flow between concentric rotating cylinders, an instability caused by these vortices was found to be possible only on concave walls. The effect was so large that the effect of the usual two-dimensional disturbances was completely overshadowed. Görtler's theory is, like the two-dimensional disturbance theory, a small-disturbance theory that assumes the main boundary-layer flow to be the same over the entire surface. Also, the boundary-layer thickness is assumed to be small compared with the radius r of the wall. It was found, as shown in figure 8, that the wall curvature and the Reynolds number occur in the combination $R_\theta\sqrt{\frac{\theta}{r}}$ and that instability occurs above a value of $R_\theta\sqrt{\frac{\theta}{r}}$ that depends on $\alpha\theta$, where α is inversely proportional to the wave length and θ is the boundary-layer momentum thickness. The neutral curve shown is for the Blasius velocity distribution. Görtler found that the instability region was only slightly affected by the shape of the velocity distribution through the boundary layer when the momentum thickness θ was used as the measure of the boundary-layer thickness.

In agreement with Görtler's theoretical work, Liepmann found experimentally that $R_\theta\sqrt{\frac{\theta}{r}}$ was the parameter defining the stability of the boundary layer on concave surfaces. Liepmann concluded that transition can be expected when the value of $R_\theta\sqrt{\frac{\theta}{r}}$ reaches about 9.0. It may be observed that Görtler found the minimum critical value of $R_\theta\sqrt{\frac{\theta}{r}}$ to be 0.58. It should be noted, however, that Liepmann's criterion concerns transition, whereas Görtler's concerns the stability of the boundary layer. Liepmann also found, in agreement with Görtler's work, that in contrast to flow over convex or plane surfaces, a pressure gradient along the wall had a negligible effect on the stability of the flow over concave walls. Thus, on convex and plane surfaces instability of the boundary layer is caused by the Tollmien-Schlichting waves; whereas the instability on concave walls is caused by three-dimensional disturbances. In figure 9 is shown the dependence of Reynolds number for transition $R_{\theta_{tr}}$ on the effective curvature θ/r. The value of $R_{\theta_{tr}}$ is practically

independent of curvature for convex walls and is about equal to the value for the flat plate. The value of $R_{\theta_{tr}}$ for concave walls, however, decreases rapidly as the effective curvature increases. The data in figure 10 show that the experimentally determined stability limits for the boundary layer on a convex wall and the calculated stability limits for the boundary layer on a flat plate are about the same except at the lowest Reynolds numbers. The upright triangles should lie on the upper branch of the neutral curve; the inverted triangles, on the lower branch. The neutral curve for the experimental points for $r = 20$ feet and also the curve for the points for $r = 2\frac{1}{2}$ feet, not shown in the figure, have a slightly higher minimum critical Reynolds number than the neutral curve for the flat plate. The reason for the difference is not definitely known.

This paper has attempted to present a short history of the theory of the stability of laminar flow, an outline of the theory for incompressible plane flow, a summary of the applications of the theory in combination with suction flows, a resumé of the results of the theory for compressible plane flow, and a summary of the theoretical and experimental results for curved flows. The stability theory based on infinitesimal disturbances may be regarded as experimentally verified for incompressible flow over plane surfaces and, probably, also for curved surfaces. Experimental work remains to be done in verifying the stability theory for compressible flows. An extension of the stability theory to the realm of finite disturbances for the purpose of calculating transition points is desirable.

REFERENCES

1. Pillow, A. F.: A Review of Hydrodynamic Stability and Its Bearing on Transition to Turbulent Flow in the Boundary Layer. Council for Sci. and Ind. Res., Div. Aero., Commonwealth of Australia, Rep. A.35, 1945.

2. Lin, C. C.: On the Stability of Two-Dimensional Parallel Flows. Part I. Quarterly Appl. Math., vol. III, no. 2, July 1945, pp. 117-142; Part II, vol. III, no. 3, Oct. 1945, pp. 218-234; and Part III, vol. III, no. 4, Jan. 1946, pp. 277-301.

3. Prandtl, L.: Motion of Fluids with Very Little Viscosity. NACA TM No. 452, 1928.

4. Fluid Motion Panel of the Aeronautical Research Committee and Others: Modern Developments in Fluid Dynamics. Vols. I and II, S. Goldstein, ed., The Clarendon Press (Oxford), 1938.

5. Abbott, Ira H., von Doenhoff, Albert E., and Stivers, Louis S., Jr.: Summary of Airfoil Data. NACA Rep. No. 824, 1945.

6. Goldstein, Sydney: Low-Drag and Suction Airfoils. Jour. Aero. Sci., vol. 15, no. 4, April 1948, pp. 189-214.

7. Squire, H. B., and Young, A. D.: The Calculation of the Profile Drag of Aerofoils. R. & M. No. 1838, British A.R.C., 1938.

8. Stokes, George Gabriel: On Some Cases of Fluid Motion. Mathematical and Physical Papers, vol. I, Univ. Press (Cambridge), 1880, pp. 17-68.

9. Rayleigh, Lord: On the Instability of Jets. Scientific Papers, vol. I, no. 58, Univ. Press (Cambridge), 1879, pp. 361-371.

10. Rayleigh, Lord: On the Stability or Instability of Certain Fluid Motions. Scientific Papers: Part I, vol. I, no. 66, 1880, pp. 474-487. Part II, vol. III, no. 144, 1887, pp. 17-23. Part III, vol. IV, no. 216, 1895, pp. 203-210.

11. Rayleigh, Lord: Stability of the Laminar Motion of an Inviscid Fluid. Phil. Mag., no. 26, Dec. 1913, pp. 1001-1010.

12. Reynolds, Osborne: On the Dynamical Theory of Incompressible Viscous Fluids and the Determination of the Criterion. Phil. Trans. Roy. Soc. (London), ser. A, vol. 186, 1895, pp. 123-164.

13. Orr, William M'Fadden: The Stability or Instability of the Steady Motions of a Liquid. Proc. Roy. Irish Acad., vol. XXVII, ser. A, no. 3, 1907, pp. 9–138.

14. Hopf, L.: Decrement of Small Vibrations in the Flow of a Viscous Fluid. Ann. d. Physik, vol. 44, no. 4, April 28, 1914, pp. 1–60.

15. Taylor, G. I.: Stability of Viscous Liquid Contained between Two Rotating Cylinders. Phil. Trans. Roy. Soc. (London), vol. 223, Feb. 8, 1923, pp. 289–343.

16. Heisenberg, Werner: Über Stabilität und Turbulenz von Flüssigkeitsströmen. Ann. d. Phys., Vierte Folge, Bd. 74, no. 15, 1924, pp. 577–627.

17. Tietjens, O.: Beiträge zur Entstehung der Turbulenz. Z.f.a.M.M., Bd. 5, Heft 3, June 1925, pp. 200–217.

18. Tollmien, W.: The Production of Turbulence. NACA TM No. 609, 1931.

19. Schlichting, H.: Zur Entstehung der Turbulenz bei der Plattenströmung. Nachr. d. Ges. d. Wiss. zu Göttingen, Math.-Phys. Kl., 1933, pp. 181–208.

20. Tollmien, W.: General Instability Criterion of Laminar Velocity Distributions. NACA TM No. 792, 1936.

21. Schlichting, H.: Amplitudenverteilung und Energiebilanz der kleinen Störungen bei der Plattenströmung. Nachr. d. Ges. d. Wiss. zu Göttingen, Math.-Phys. Kl., Neue Folge, Bd. 1, Nr. 4, 1935, pp. 47–78.

22. Prandtl, L.: The Mechanics of Viscous Fluids. Vol. III of Aerodynamic Theory, div. G, W. F. Durand, ed., Julius Springer (Berlin), 1935, pp. 34–208.

23. Squire, H. B.: Stability for Three-Dimensional Disturbances of Viscous Fluid Flow between Parallel Walls. Proc. Roy. Soc. (London), ser. A, vol. 142, no. , Nov. 1, 1933, pp. 621–628.

24. Pretsch, J.: Die Stabilität einer ebenen Laminarströmung bei Druckgefälle und Druckanstieg. Jahrb. 1941 der deutschen Luftfahrtforschung, R. Oldenbourg (Munich), pp. I 158 – I 175.

25. Schubauer, G. B., and Skramstad, H. K.: Laminar-Boundary-Layer Oscillations and Transition on a Flat Plate. NACA ACR, April 1943.

26. Ulrich, A.: Theoretical Investigation of Drag Reduction in Maintaining the Laminar Boundary Layer by Suction. NACA TM No. 1121, 1947.

27. Pretsch, J.: Umschlagbeginn und Absaugung. Jahrb. 1942 der deutschen Luftfahrtforschung, R. Oldenbourg (Munich), pp. I 1 – I 7.

28. Bussmann, K., and Münz, H: Die Stabilität der laminaren Reibungsschicht mit Absaugung. Jahrb. 1942 der deutscher Luftfahrtforschung, R. Oldenbourg (Munich), pp. I 36 – I 39.

29. Iglisch, Rudolf: Exakte Berechnung der laminaren Grenzschicht an der längsangeströmten ebenen Platte mit honogener Absaugung. Schriften der Deutsche Akademie der Luftfahrtforschung, Bd. 8B, Heft 1, 1944.

30. Schlichting, H.: Ein Näherungsverfahren zur Berechnung der laminaren Grenzschicht mit Absaugung bei beliebiger Körperform. Bericht 43/14, Aerodynamisches Institut der T. H. Braunschweig, June 12, 1943.

31. Lees, Lester, and Lin, Chia Chiao: Investigation of the Stability of the Laminar Boundary Layer in a Compressible Fluid. NACA TN No. 1115, 1946.

32. Lees, Lester: The Stability of the Laminar Boundary Layer in a Compressible Fluid. NACA TN No. 1360, 1947.

33. Görtler, H.: Über den Einfluss der Wandkrümmung auf die Entstehung der Turbulenz. Z.f.a.M.M., Bd. 20, Heft 3, June 1940, pp. 138–147.

34. Görtler, H.: Über eine dreidimensionale Instabilität laminarer Grenzschichten an konkaven Wanden. Göttinger Nachrichten Neue Folge, 2 Nr. 1.

35. Görtler, H.: Instability of Laminar Boundary Layers on Concave Walls against Certain Three-Dimensional Disturbances. R.T.P. Translation No. 1588, British Ministry of Aircraft Production. (From Z.f.a.M.M., Bd. 21, Heft 4, Aug. 1941, pp. 250–252.)

36. Liepmann, Hans W.: Investigations on Laminar Boundary-Layer Stability and Transition on Curved Boundaries. NACA ACR No. 3H30, 1943.

37. Liepmann, H. W.: Investigation of Boundary-Layer Transition on Concave Walls. NACA ACR No. 4J28, 1945.

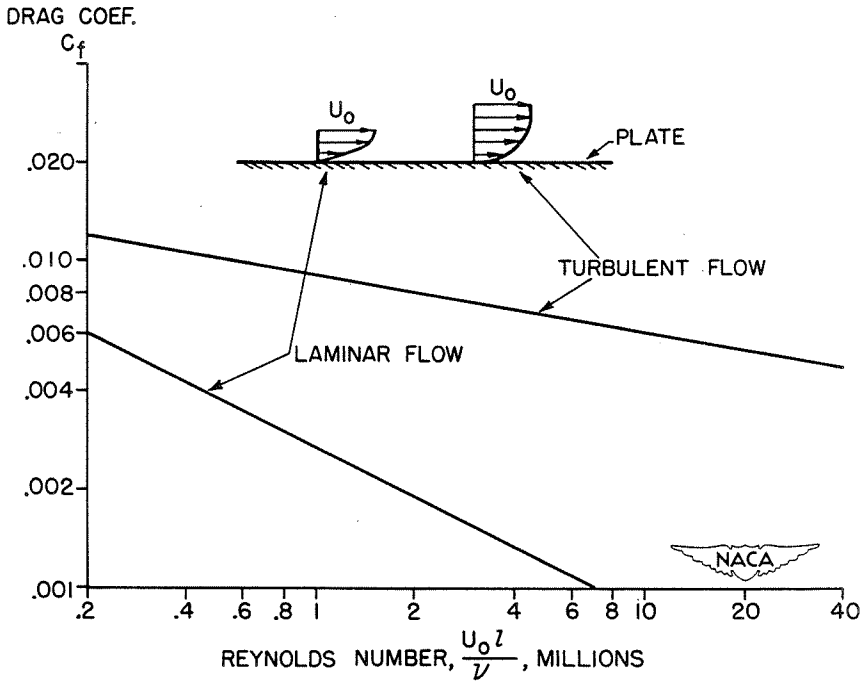

Figure 1.- Flat-plate drag coefficients for turbulent and laminar flow.

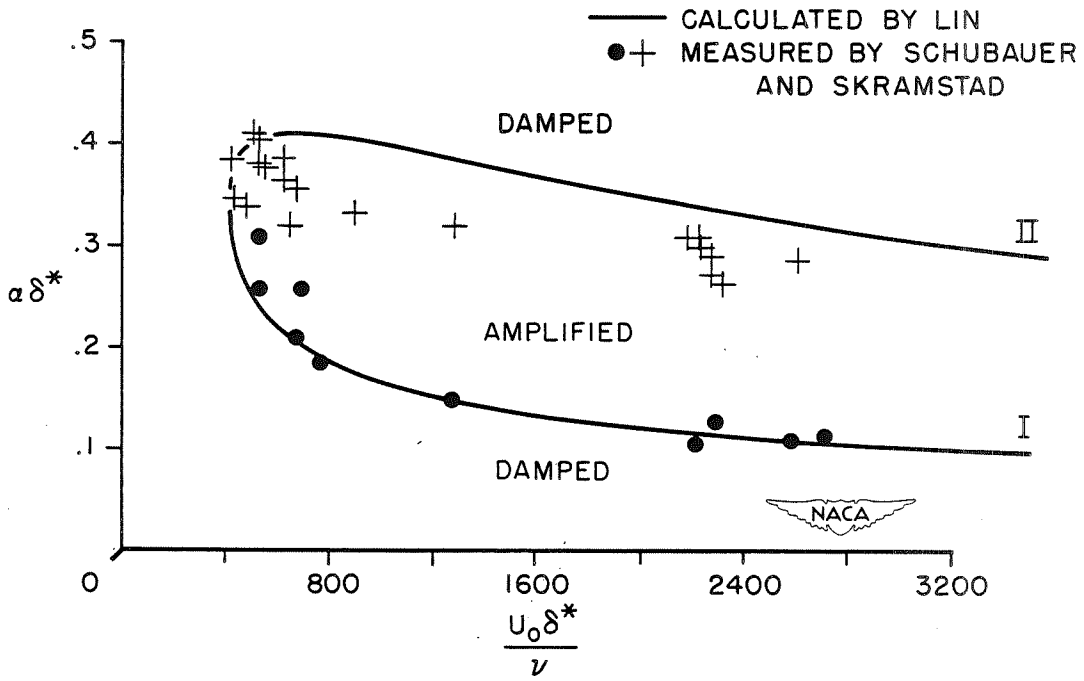

Figure 2.- Curve of neutral stability for Blasius profile.

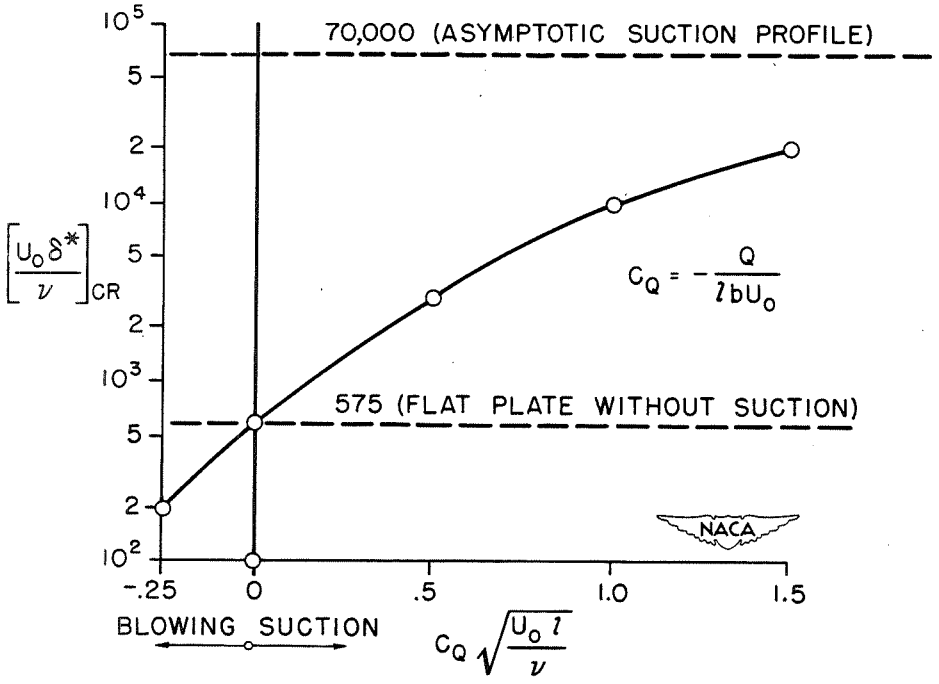

Figure 3.- Flow over a flat plate $\left(V_o \propto \frac{1}{\sqrt{x}}\right)$.

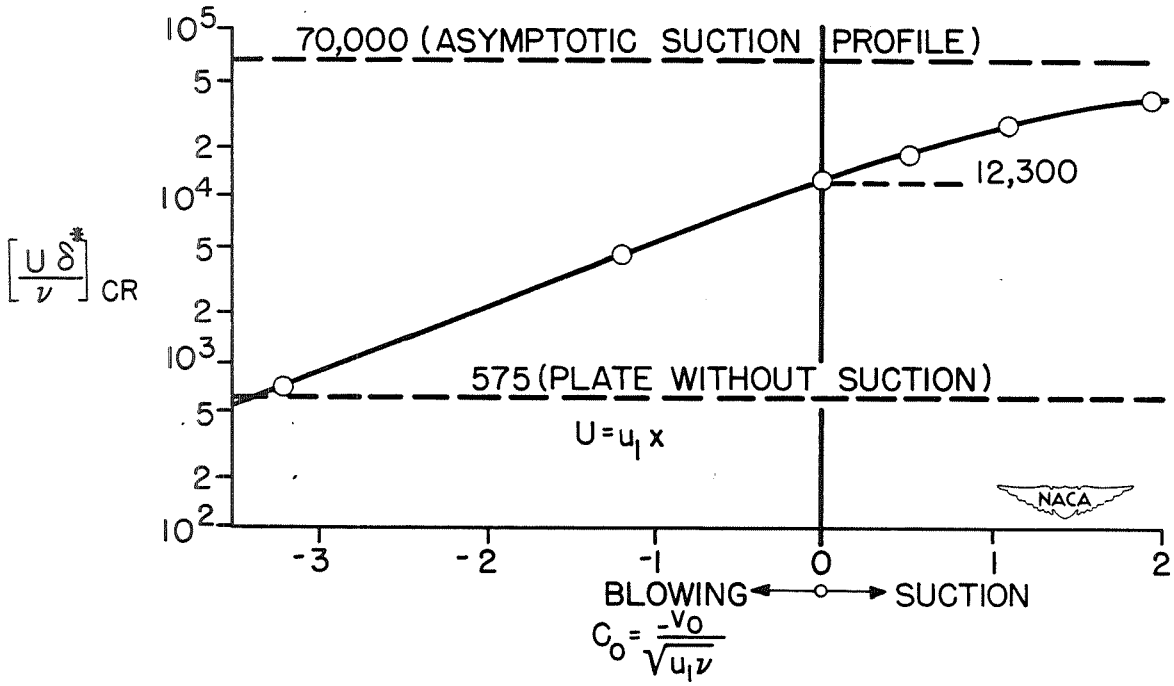

Figure 4.- Flow near a stagnation point.

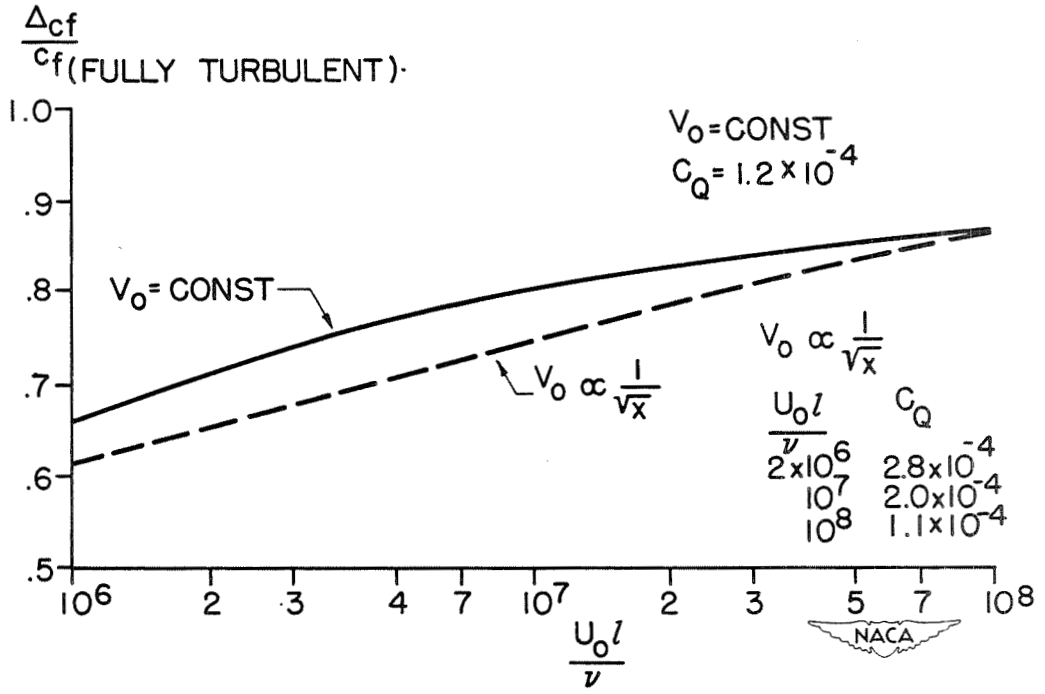

Figure 5.- Relative drag reduction for V_o = Constant and $V_o \propto \frac{1}{\sqrt{x}}$.

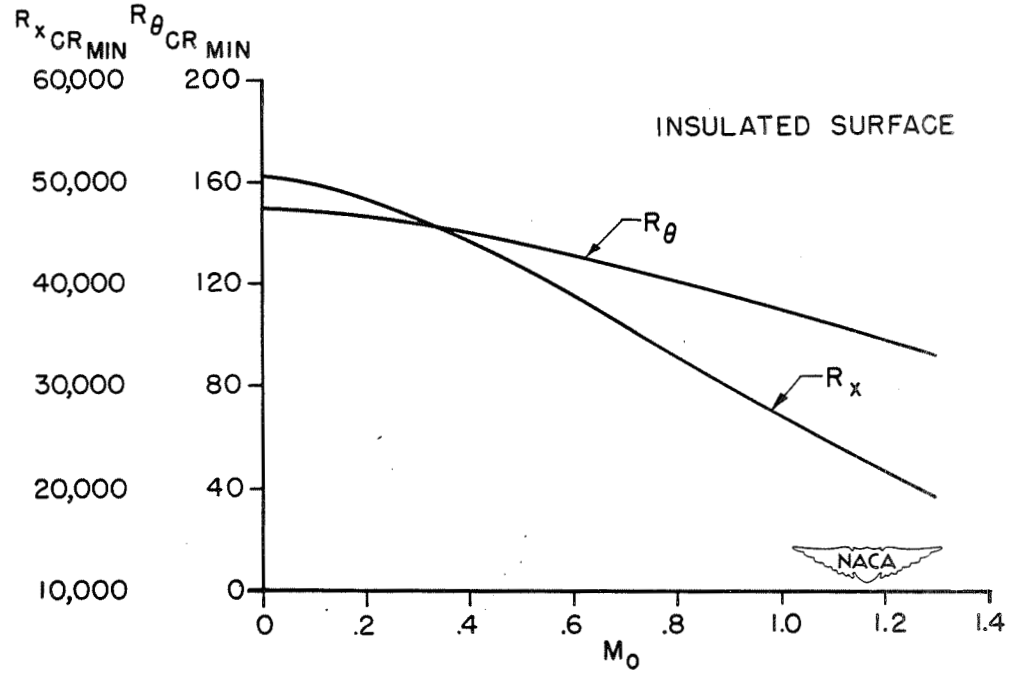

Figure 6.- Critical Reynolds number against Mach number.

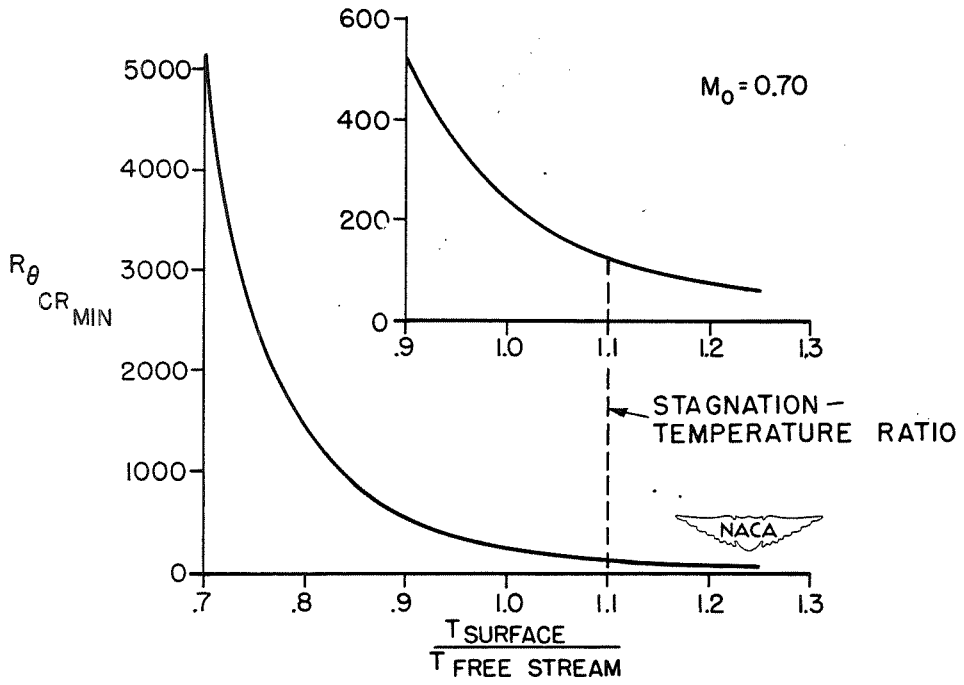

Figure 7.- Critical Reynolds number against surface temperature ratio.

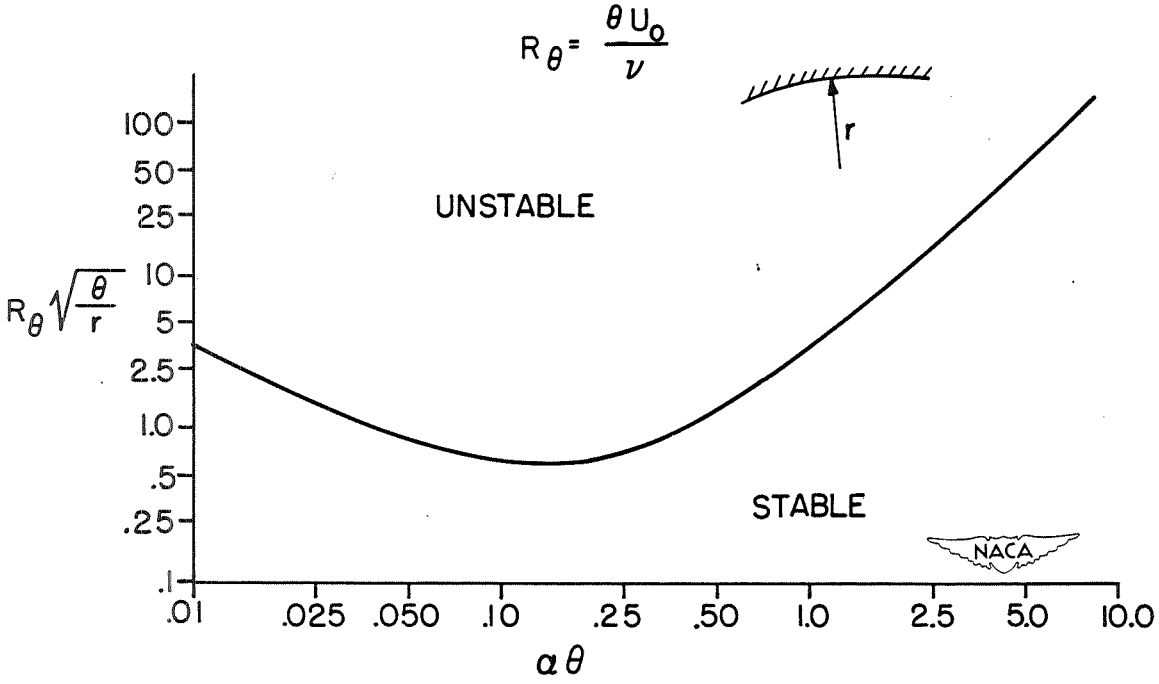

Figure 8.- Neutral curve for boundary layer on concave wall.

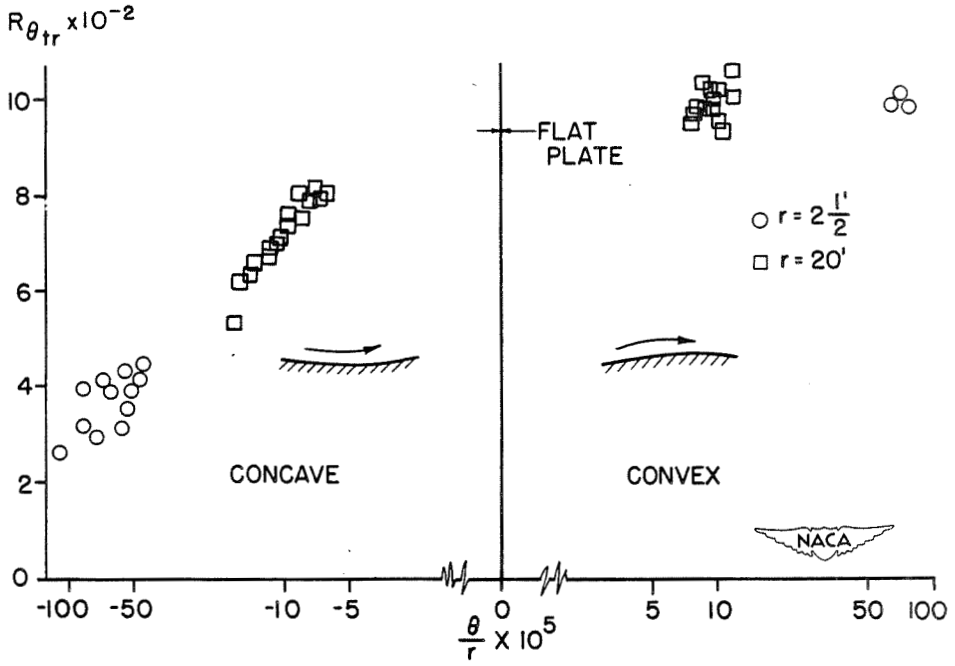

Figure 9.- Curvature effect on transition Reynolds number.

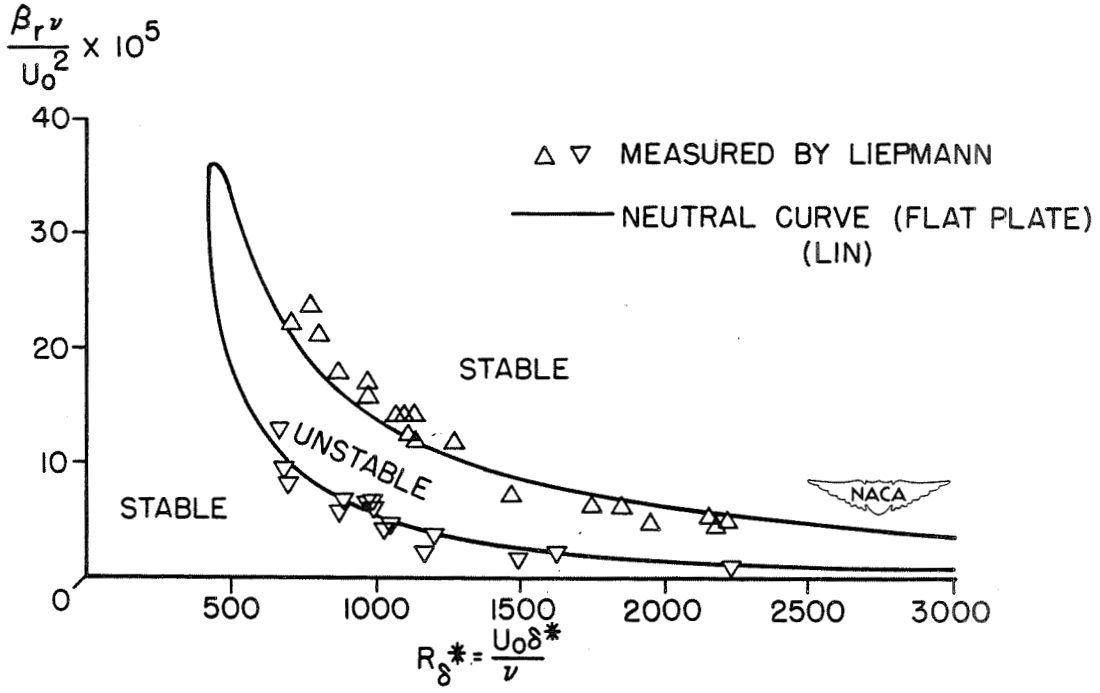

Figure 10.- Stability data for convex plate (r = 20 ft). β_r is the frequency of the oscillation.

SUBSONIC COMPRESSIBLE FLOW

A REVIEW OF APPROXIMATE METHODS IN SUBSONIC COMPRESSIBLE FLOW

By Carl Kaplan

Langley Aeronautical Laboratory

INTRODUCTION

The purpose of this paper is to review several methods developed in recent years for the calculation of the flow of a compressible fluid past a prescribed body. These methods have evolved largely because of the inherent difficulty of handling the nonlinear partial differential equations which govern the flow of a compressible fluid. In the discussion of these methods several points of mathematical interest will be noted for possible future investigations.

The study of fluid-flow phenomena at high speeds requires the consideration of compressibility and therefore of the thermodynamics of the fluid. For a real fluid, this would be a practically impossible problem. In this review, therefore, the fluid is considered to be a perfect one with vanishingly small viscosity and heat conductivity. The discussion is confined, moreover, mainly to irrotational flow in two dimensions with a subsonic undisturbed flow.

It is assumed that the fluid is a perfect gas so that the equation of state is

$$p = RT\rho \tag{1}$$

The equations of motion for the fluid are

$$\left.\begin{aligned} u\frac{\partial u}{\partial x} + v\frac{\partial u}{\partial y} &= -\frac{1}{\rho}\frac{\partial p}{\partial x} \\ u\frac{\partial v}{\partial x} + v\frac{\partial v}{\partial y} &= -\frac{1}{\rho}\frac{\partial p}{\partial y} \end{aligned}\right\} \tag{2}$$

and the equation of continuity is

$$\frac{\partial \rho u}{\partial x} + \frac{\partial \rho v}{\partial y} = 0 \tag{3}$$

where

x, y rectangular coordinates in plane of flow

u, v components of velocity vector

p pressure in fluid

ρ density of fluid

T temperature of fluid

R gas constant

With the assumption of vanishingly small viscosity and heat conductivity, the behavior of the fluid in motion is closely isentropic so that p and ρ are related by the equation

$$p = k\rho^{\gamma} \tag{4}$$

where γ is the ratio of specific heats at constant pressure and constant volume and k is an arbitrary constant. The Bernoulli integral of the equations of motion (2) then becomes

$$c^2 = c_\infty^2\left[1 - \frac{\gamma - 1}{2} M_\infty^2\left(\frac{q^2}{U^2} - 1\right)\right] \tag{5}$$

where

c local velocity of sound $\left(c = \sqrt{\frac{dp}{d\rho}}\left(= \sqrt{\gamma\frac{p}{\rho}}\right)\right)$

c_∞ velocity of sound in undisturbed stream

q magnitude of fluid velocity

U velocity of undisturbed stream

M_∞ Mach number in undisturbed stream $\left(\frac{U}{c_\infty}\right)$

With the assumption of irrotationality, a velocity potential ϕ can be introduced, where

$$\left.\begin{aligned} u &= \frac{\partial\phi}{\partial x} \\ v &= \frac{\partial\phi}{\partial y} \end{aligned}\right\} \tag{6}$$

Then the elimination of ρ from equations (2) and (3) yields the fundamental differential equation governing the flow; namely,

$$\left(c^2 - u^2\right) \frac{\partial^2 \phi}{\partial x^2} - 2uv \frac{\partial^2 \phi}{\partial x \partial y} + \left(c^2 - v^2\right) \frac{\partial^2 \phi}{\partial y^2} = 0 \tag{7}$$

a nonlinear, second-order partial differential equation.

METHODS OF APPROXIMATE SOLUTION

The rigorous treatment of the fundamental differential equation (7) for nonlinearized flow past closed shapes with general boundary conditions has up to the present time proved to be impossible. In place of rigorous analytical solutions it is necessary to be satisfied in general with approximation methods essentially based on the linearization of equation (7). The mathematical difficulties are considerably greater for subsonic flow (elliptic potential equation) than for supersonic flow (hyperbolic potential equation), for which the theory of characteristics leads to very simple approximation methods. Three of the methods which have been utilized for subsonic flow will be described in the remainder of this paper.

Method of Expansion in Powers of the Mach Number

In the Rayleigh-Janzen method the velocity potential ϕ is expanded in a series of powers of M_∞^2,

$$\phi = \phi_0 + M_\infty^2 \phi_1 + M_\infty^4 \phi_2 + \cdots \tag{8}$$

where ϕ_0 is the velocity potential of the incompressible fluid flow and thus satisfies the boundary conditions. The appropriate form of the differential equation for ϕ is obtained by rewriting equation (7) with the aid of equation (5). Thus

$$\left[1 - \frac{\gamma - 1}{2} M_\infty^2 \left(\frac{q^2}{U^2} - 1\right)\right] \Delta\phi = \frac{1}{2} M_\infty^2 \left[\frac{\partial \phi}{\partial x} \frac{\partial}{\partial x}\left(\frac{q^2}{U^2}\right) + \frac{\partial \phi}{\partial y} \frac{\partial}{\partial y}\left(\frac{q^2}{U^2}\right)\right] \tag{9}$$

where the symbol Δ denotes the Laplacian operator

$$\frac{\partial^2}{\partial x^2} + \frac{\partial^2}{\partial y^2}$$

The expression for ϕ from equation (8) is then inserted in equation (9) and coefficients of corresponding powers of M_∞ on either side are equated, yielding successively the equations for ϕ_0, ϕ_1, ... Thus

$$\left.\begin{aligned} \Delta\phi_0 &= 0 \\ \Delta\phi_1 &= \frac{1}{2}\left[\frac{\partial\phi_0}{\partial x}\frac{\partial}{\partial x}\left(\frac{q_0^2}{U^2}\right) + \frac{\partial\phi_0}{\partial y}\frac{\partial}{\partial y}\left(\frac{q_0^2}{U^2}\right)\right] \\ &\cdots\cdots \end{aligned}\right\} \qquad (10)$$

where q_0 is the magnitude of the incompressible flow velocity.

Rayleigh (reference 1) and Janzen (reference 2) were the first to consider the second of equations (10) and gave a series solution for ϕ_1 in the case of the flow past a circular cylinder. Later, Poggi (reference 3) introduced a method that consists essentially in considering the compressible fluid to be an incompressible fluid with a continuous distribution of sinks and sources in the entire region external to the solid boundary. According to Poggi, the right-hand sides of equations (10) represent successive terms in an infinite series giving this sink-source distribution. Poggi and later Kaplan (references 4 and 5) and Imai (reference 6) obtained the solution from this point of view for the flow past such shapes as a circular cylinder, an elliptic cylinder, and a Joukowski profile with angle of attack and circulation. The calculations proved to be extremely laborious, involving a large number of double integrals. In order to ease the labor involved in the original Poggi method, Imai and Aihara (reference 7) and Kaplan (reference 8) developed elegant and useful methods which utilized the theory of functions of a complex variable. The one to be described in this review is that due to Kaplan, which makes use of the calculus of residues. Thus, if new independent variables $z = x + iy$ and $\bar{z} = x - iy$ are introduced, the expression for the strength of the sink-source distribution obtained from the right-hand side of the second of equations (10) may be written as follows:

$$-\frac{1}{4\pi U^2}\left(w_0^2\frac{d\bar{w}_0}{d\bar{z}} + \bar{w}_0^2\frac{dw_0}{dz}\right)dx\,dy \qquad (11)$$

where w_o and $\overline{w}_o$ are, respectively, the complex and conjugate complex velocities of the incompressible fluid past the prescribed shape; that is, $w_o = -u + iv$ and $\overline{w}_o = -u - iv$ and these are, respectively, functions of z and $\overline{z}$ only, since they are obtained from solutions of Laplace's equation. Now, the expression, equation (11), involves non-analytic functions of z and $\overline{z}$. In order, however, to utilize the methods of the calculus of residues, functions of only a single complex variable must appear. For this purpose the plane z of the obstacle is represented conformally on the plane Z of the corresponding circle. Since the strengths of the sink-source distribution of corresponding elements of the two planes are equal, the expression for the strength of the sink-source distribution of an element of the plane Z is

$$-\frac{1}{4\pi U^2}\left[W_o^2 \frac{dZ}{dz}\frac{d}{d\overline{Z}}\left(\overline{W}_o \frac{d\overline{Z}}{dz}\right) + \overline{W}_o^2 \frac{d\overline{Z}}{d\overline{z}}\frac{d}{dZ}\left(W_o \frac{dZ}{dz}\right)\right] dX\, dY \qquad (12)$$

where W_o and $\overline{W}_o$ are, respectively, the complex and conjugate complex velocities of the incompressible fluid past the circular profile in the plane Z.

It is a simple matter to obtain an expression for the complex velocity W_1 induced at any point Z_p external to the circular boundary by a sink-source distribution originating in the physical plane z and at the same time to preserve the boundary conditions of zero normal velocity at the circular boundary and zero induced velocity at infinity. The essential fact to remember is that corresponding to a unit external source there is a unit source at the inverse point with respect to the circle and a unit sink at the center of the circle. The actual velocity w_1 of the fluid in the physical plane z is related to the velocity W_1 at the corresponding point in the plane Z of the circle by the equation

$$w_1 = W_1 \frac{dZ}{dz} \qquad (13)$$

The expression for W_1 consists of double integrals whose integrands are non-analytic functions of Z and $\overline{Z}$. The double integrations over the entire region external to the circular boundary can be replaced by line integrals involving functions of Z and $\overline{Z}$ only by the use of Stokes' theorem for the plane. Thus, it can be shown that if $F(Z,\overline{Z})$

is a function of Z and $\bar{Z}$, continuous and differentiable in the area S enclosed by the contour C, then

$$\left.\begin{aligned} \int_C F(Z,\bar{Z})d\bar{Z} &= -2i\int_S \frac{\partial F}{\partial Z}\,dS \\ \int_C F(Z,\bar{Z})dZ &= 2i\int_S \frac{\partial F}{\partial \bar{Z}}\,dS \end{aligned}\right\} \qquad (14)$$

The line integrals, in the present case, are taken around the circular boundary corresponding to the actual profile in the z-plane, around an infinitely small circle surrounding the point at which W_1 is to be evaluated, and around an infinitely large circle concentric with the internal circular boundary. The important point to note is that, since all the contours involved in the line integrations are circular, the integrands can be made analytic in Z or $\bar{Z}$, since on a circular boundary $Z\bar{Z}$ = Constant. It then follows that the line integrals can be evaluated by means of Cauchy's theorem on residues. This theorem states that, if a function is analytic on a contour C and throughout its interior except at a number of poles inside the contour, then

$$\left.\begin{aligned} \int_C G(Z)dZ &= 2\pi iM \\ \int_C H(\bar{Z})d\bar{Z} &= -2\pi iN \end{aligned}\right\} \qquad (15)$$

where M and N are, respectively, the sum of the residues at those poles which lie within the contour C.

The device of introducing z and $\bar{z}$ as independent variables, then utilizing the conformal mapping of the plane of the obstacle into the plane of a circle, and finally replacing the double integrals by line integrals thus enables one to evaluate by the method of residues the first effect of compressibility on the velocity of the fluid past an arbitrary shape. The point of interest to an applied mathematician is that here is a method whereby a Poisson equation involving rather complicated boundary conditions can be solved with the aid of analytic functions of a single complex variable. The subject is certainly worthy of further investigation.

Method of Small Perturbations

Whereas the preceding treatment started with the incompressible flow, the Prandtl-Busemann or Ackeret method starts with the undisturbed flow. It is applicable to the flow past thin shapes placed in a uniform stream, in which the changes in the velocity of the fluid as it passes over the body are small compared with the main stream velocity. The velocity potential is developed in a power series of a perturbation parameter ϵ (which may be the thickness coefficient, the camber coefficient, or the angle of attack) in which the first term is the velocity potential of the undisturbed stream $\phi_0 = Ux$. Thus, it is assumed that

$$\phi = Ux + \epsilon\phi_1 + \epsilon^2\phi_2 + \epsilon^3\phi_3 + \cdots \tag{16}$$

where the ϕ_n are functions of x, y and of M_∞ and show successively the effects of compressibility on the flow.

The assumed series, equation (16), is inserted into the combined nonlinear equations (7) and (5) and the successive linear equations for $\phi_1, \phi_2, \ldots$ can then be obtained by equating the coefficients of successive powers of the perturbation parameter ϵ. The first two equations obtained by this procedure are

$$\left.\begin{aligned} \left(1 - M_\infty^2\right)\frac{\partial^2\phi_1}{\partial x^2} + \frac{\partial^2\phi_1}{\partial y^2} &= 0 \\ \left(1 - M_\infty^2\right)\frac{\partial^2\phi_2}{\partial x^2} + \frac{\partial^2\phi_2}{\partial y^2} &= M_\infty^2\left[(\gamma + 1)\frac{\partial\phi_1}{\partial x}\frac{\partial^2\phi_1}{\partial x^2}\right. \\ &\quad \left. + (\gamma - 1)\frac{\partial\phi_1}{\partial x}\frac{\partial^2\phi_1}{\partial y^2} + 2\frac{\partial\phi_1}{\partial y}\frac{\partial^2\phi_1}{\partial x\partial y}\right] \end{aligned}\right\} \tag{17}$$

These differential equations may be put into more familiar forms by

introducing a new set of independent variables X and Y by means of the following affine transformation:

$$\left.\begin{aligned} X &= x \\ Y &= \sqrt{1 - M_\infty^2}\, y \end{aligned}\right\} \tag{18}$$

Thus, for $M < 1$, the first of equations (17) is transformed into a Laplace equation and the succeeding equations for ϕ_2, ϕ_3, ... into Poisson equations in which the right-hand sides are known functions of X and Y determined from the preceding approximations. The solution of the first of equations (17) yields the well-known Prandtl-Glauert rule, whereas the solutions of the succeeding Poisson equations provide higher approximations to the flow of the compressible fluid and thus will apply for larger departures from the undisturbed uniform flow.

The general procedure followed in solving equations (17) is simple in principle. The first step is to obtain an expression for the velocity potential of the incompressible flow past the prescribed boundary in the form of a power series in the perturbation parameter ϵ. Then the solution for the first approximation ϕ_1 to the compressible flow is easily obtained by analogy from the coefficient of the first power of ϵ. The higher approximations ϕ_2, ϕ_3, ... are obtained by solving the corresponding Poisson equations, at the same time satisfying the boundary conditions to the same power of the perturbation parameter ϵ as is involved in the expression for the velocity potential ϕ.

Thus, consider the first approximation ϕ_1; if

$$\phi = UX + \epsilon\phi_1 (X,Y) \tag{19}$$

represents the incompressible flow past a body, then to the same order of approximation,

$$\left.\begin{aligned} \phi &= Ux + \frac{\epsilon}{\beta}\,\phi_1 (x,\beta y) \\ \beta &= \sqrt{1 - M_\infty^2} \end{aligned}\right\} \tag{20}$$

represents the compressible flow past the same body.

Now, if q_c and q_i denote the magnitudes of the velocity at the surface of the prescribed shape for the compressible and incompressible flows, respectively, then to the first power of ϵ the perturbation term (evaluated at the boundary) is the same for the two cases. The result is a relation between q_c and q_i, independent of the particular shape prescribed; namely,

$$\frac{q_c}{q_i} = \frac{1}{\beta} - \left(\frac{1}{\beta} - 1\right)\frac{U}{q_i} \tag{21}$$

Equation (21) represents the so-called velocity correction formula for the Prandtl-Glauert approximation.

This method of iteration by powers of a perturbation parameter ϵ has been applied to a family of symmetrical shapes (bumps, reference 9) and to a family of circular arcs (reference 10), specifically chosen because they possess no stagnation points and hence satisfy the primary assumption of the method; namely, small disturbances to the oncoming uniform stream. The iterations included the third power of the thickness coefficient in the case of the family of symmetrical shapes and the third power of the camber coefficient in the case of the family of circular arcs. It is important to remark that, although extensive use was made of the affine transformation, equation (18), the boundary conditions were always satisfied in the plane of the actual profiles.

In general, the affine transformation, equation (18), introduces a distortion of the solid boundary which depends on the stream Mach number. This distortion, therefore, in general precludes the use of analytic function methods. In the case of a family of elliptic profiles, however, the affine transformation produces another family of elliptic profiles. Since one ellipse differs from another only with respect to the thickness coefficient, it is possible to treat the problem in the plane of the circle corresponding to the plane of the affine ellipse. For this purpose it is simpler, from the point of view of satisfying the boundary conditions, to treat the equations for the stream function corresponding to equations (17). The results obtained in the plane of the circle, making extensive and elegant use of functions of a single complex variable, are easily transferred into the physical plane of the actual elliptic profile. Such calculations have been performed for the case of an elliptic cylinder with both angle of attack and circulation (references 11, 12, and 13). Typical of the results obtained is the following formula relating the lift on an elliptic cylinder in a compressible and an incompressible flow:

$$\frac{L_c}{L_i} = \frac{1}{\beta} + \frac{1}{2}\left(1 - e^{-2\lambda}\right)\left[\frac{1-\beta}{\rho^2} + \frac{1}{4}(\gamma+1)\left(\frac{1-\beta^2}{\rho^2}\right)^2\right] \tag{22}$$

where

$\beta = \sqrt{1 - M_\infty^2}$

γ ratio of specific heats at constant pressure and at constant volume

e^λ proportional to radius of circle conformal to actual ellipse in physical plane

Equation (22) is an extension of the well-known Prandtl-Glauert rule to thicker profiles and is applicable not only to an ellipse but to an arbitrary symmetrical shape.

The method just described, utilizing the powerful tool of complex-function theory, could be extended to arbitrary profiles if the answer to the purely mathematical question of the effect of an affine transformation on the coefficients of the conformal mapping function to a circle were known. Another interesting and important problem is the convergence of the precedure herein described. Calculations indicate that the power-series development of the velocity potential or of the stream function in powers of a perturbation parameter may converge somewhat beyond the critical stream Mach number, but a rigorous discussion of this question has yet to be given.

In order to show the entent to which the methods of Rayleigh and Janzen and of Prandtl and Busemann apply to practical airfoils, figure 1 has been prepared. The stream Mach number M_∞ is the abscissa and the thickness coefficient t is the ordinate. The critical stream Mach number curve bounds the subsonic flows. The method of Rayleigh and Janzen proceeds in the direction of increasing stream Mach number and yields at each stage exact information with regard to the geometry of the profile. The vertical lines separate the regions of the second and third approximations, the line $M_\infty = 0$ being the incompressible solution. It is clear that many approximations would be necessary to penetrate into the region of interest to aeronautics, that is, between $t = 5$ percent and $t = 15$ percent.

The method based on the Prandtl-Glauert linearized result proceeds in the direction of increasing thickness and yields at each stage exact information with regard to the stream Mach number. The horizontal lines separate the regions in which the Prandtl-Glauert correction holds and the first additional step. This figure shows clearly that, already by a first-step improvement of the Prandtl-Glauert result, significant results are obtained in the region of interest to aeronautics whereas similar success by means of the Rayleigh-Janzen method would entail a prohibitive amount of labor.

Method of the Hodograph

It is clear from the discussion in the foregoing sections that both the Rayleigh–Janzen and the Prandtl–Busemann procedures become rather laborious after one or two steps; moreover, such calculations must be repeated from the beginning for each prescribed solid boundary. Consequently, many attempts have been made to set up a correspondence between incompressible flows and compressible flows of the nature of correction factors. Among the better known results of such attempts are the Prandtl–Glauert (reference 14), von Kármán–Tsien (reference 15), Temple–Yarwood (reference 16), and Garrick–Kaplan (references 17 and 18) velocity correction formulas – all of which depend only on the incompressible fluid velocity and the stream Mach number.

Before proceeding with the discussion of velocity correction formulas, a rather instructive comparison is given of the compressibility effect on the maximum velocity of a series of bumps and circular arcs. The thickness coefficients of the bumps and the camber coefficients of the corresponding circular arcs were so chosen that the incompressible speeds were the same. Table I shows the results calculated by the Prandtl–Busemann iteration method – the calculations included the third power of the thickness and camber coefficients. For moderate values of thickness and camber the differences are seen to be negligible over most of the subsonic range. These calculations indicate that, to a very good approximation, the effect of compressibility in the subsonic range depends essentially only on the incompressible fluid velocity and on the undisturbed stream Mach number and is largely independent of the particular solid boundary treated. This result substantiates the feasibility of velocity correction formulas in the subsonic range of speeds.

From the nature of velocity correction formulas it would seem that the hodograph plane variables are the appropriate ones to consider. The hodograph variables are q, the magnitude of the fluid velocity, and θ, the angle included by the velocity vector and the positive direction of the x-axis. Corresponding to q^k in the incompressible case, there appear functions $P_k(q)$ and $Q_k(q)$ in the compressible case, where

$$\left.\begin{aligned} \frac{1}{k}\log Q_k &= \log q + f_k(\tau) \\ \frac{1}{k}\log P_k &= \log q + g_k(\tau) \end{aligned}\right\} \qquad (23)$$

The functions $P_k(q)$ and $Q_k(q)$ are associated, respectively, with the velocity potential and the stream function in the compressible case; the functions $f_k(\tau)$ and $g_k(\tau)$ are related to the particular solutions of Chaplygin's basic differential equation of the hypergeometric type

for compressible flow. The variable τ is a dimensionless speed variable defined as follows:

$$\tau = \frac{q^2}{q_{max}^2} = \frac{M^2}{\frac{2}{\gamma - 1} + M^2}$$

where q_{max} is the maximum fluid velocity corresponding to expansion into a vacuum. Figure 2 shows the graphs of several of the (hypergeometric) functions f_k and g_k for positive values of k with the Mach number as abscissa. The value of γ chosen was 1.4 for air. Note that, as the subscript k is increased, both sets of functions approach the single function $f_\infty = g_\infty = h(\tau)$ defined between the limits $M = 0$ and $M = 1$. According to equations (23) then, as $k \to \infty$,

$$P_k \approx Q_k \approx \left[q e^{h(\tau)} \right]^k \tag{24}$$

The nature of the correspondence between incompressible and compressible flow is assumed to be such that

$$\left.\begin{aligned} \phi_i(q_i, \theta) &= \phi_c \left[q_c e^{f_k(\tau)}, \theta \right] \\ \psi_i(q_i, \theta) &= \psi_c \left[q_c e^{g_k(\tau)}, \theta \right] \end{aligned}\right\} \tag{25}$$

where ψ denotes the stream function and the subscripts i and c refer, respectively, to incompressible and compressible flow. In order to obtain a correspondence of velocities, it is necessary that also for the compressible case the speed variable be the same for both the velocity potential and the stream function. The function $h(\tau)$ separating, as it does, the two sets of functions $f_k(\tau)$ and $g_k(\tau)$ is peculiarly suited for this purpose. Thus, the correspondence of velocities in the incompressible and the compressible case is given by

$$q_i = q_c e^{h(\tau)} \tag{26}$$

Equation (26) constitutes the geometric-mean type of velocity correction formula introduced in reference 16 and is limited to the subsonic range $0 \leq M \leq 1$. As already noted, for positive values of k, $h(\tau)$ lies

between $f_k(\tau)$ and $g_k(\tau)$ in magnitude. Moreover, the deviation of $e^{h(\tau)}$ from $e^{f_k(\tau)}$ and $e^{g_k(\tau)}$ is quite small in the entire subsonic range.

The geometric-mean type of velocity correction formula contains the results of Chaplygin, von Kármán and Tsien, Temple and Yarwood, and, in the limiting case of small disturbances to the main flow, the exact Prandtl-Glauert rule. For example, the von Kármán-Tsien velocity correction formula is obtained from the geometric-mean type of approximation by taking $\gamma = -1$. The geometric-mean type of velocity correction formula just described seems to be the most logical one from a mathematical point of view. It is interesting to note, however, that the choice of $\gamma = -1$, yielding the Kármán-Tsien formula, appears to cancel the effect of boundary distortion inherent in the correspondence equations (25). This fortuitous circumstance, together with the simplicity of the calculations involved, makes it very useful for most purposes. Figure 3 illustrates in general the usefulness of velocity correction formulas and in particular the one given by von Kármán and Tsien. The solid curves show the variation of the maximum pressure coefficient with the stream Mach number for several members of a family of symmetrical profiles (bumps) calculated by means of the Prandtl-Busemann iteration in powers of the thickness coefficient (reference 9). The small circles show the results obtained by means of the von Kármán-Tsien velocity correction formula. The agreement between the two methods over such a wide range in thickness coefficients and stream Mach numbers is remarkable. Indeed, the development of velocity correction formulas and their use in the prediction of compressibility effects should be considered as an outstanding achievement of theoretical aerodynamics. For, consider that the problem of compressible flow involves a nonlinear differential equation for which very little mathematical treatment is available; nevertheless, with the aid of a few simple ideas and very little labor the essential results can be obtained by means of velocity correction formulas. One must be cautioned, however, that their use is limited to the subsonic range and must not be extended into the transonic or mixed subsonic and supersonic range of speeds.

REFERENCES

Method of Expansion in Powers of the Mach Number

1. Rayleigh, (Lord): On the Flow of Compressible Fluid past an Obstacle. Phil. Mag., ser. 6, vol. 32, no. 187, July 1916, pp. 1–6.

2. Janzen, O.: Beitrag zu einer Theorie der stationären Strömung kompressibler Flüssigkeiten. Phys. Zeitschr. Jahrg. 14, Nr. 14, July 15, 1913, pp. 639–643.

3. Poggi, Lorenzo: Campo di velocità in una corrente piana di fluido compressible. L'Aerotecnica, vol. XII, fasc. 12, Dec. 1932, pp. 1579–1593, and vol. XIV, fasc. 5, May 1934, pp. 532–549.

4. Kaplan, Carl: Two-Dimensional Subsonic Compressible Flow past Elliptic Cylinders. NACA Rep. No. 624, 1938.

5. Kaplan, Carl: Compressible Flow about Symmetrical Joukowski Profiles. NACA Rep. No. 621, 1938.

6. Imai, Isao: On the Flow of a Compressible Fluid past a Circular Cylinder. Proc. Phys.-Math. Soc. of Japan, ser. 3, vol. 20, no. 8, Aug. 1938, pp. 636–645.

7. Imai, Isao, and Aihara, Takasi: On the Subsonic Flow of a Compressible Fluid past an Elliptic Cylinder. Rep. No. 194, vol. XV, no. 8, Aero. Res. Inst., Tokyo Imperial Univ., Aug. 1940.

8. Kaplan, Carl: On the Use of Residue Theory for Treating the Subsonic Flow of a Compressible Fluid. NACA Rep. No. 728, 1942.

Method of Small Perturbations

9. Kaplan, Carl: The Flow of a Compressible Fluid past a Curved Surface. NACA Rep. No. 768, 1943.

10. Kaplan, Carl: The Flow of a Compressible Fluid past a Circular Arc Profile. NACA Rep. No. 794, 1944.

11. Kaplan, Carl: Effect of Compressibility at High Subsonic Velocities on the Lifting Force Acting on an Elliptic Cylinder. NACA TN No. 1118, 1946.

12. Kaplan, Carl: Effect of Compressibility at High Subsonic Velocities on the Moment Acting on an Elliptic Cylinder. NACA TN No. 1218, 1947.

13. Hantzsche, W., and Wendt, H.: Der Kompressibilitätseinfluss für dünne wenig gekrümmte Profile bei Unterschallgeschwindigkeit. Z.f.a.M.M., Bd. 22, Nr. 2, April 1942, pp. 72–86. (Available as R.T.P. Translation No. 2198, British Ministry of Aircraft Production.)

Method of the Hodograph

14. Glauert, H.: The Effect of Compressibility on the Lift of an Aerofoil. R. & M. No. 1135, British A.R.C., 1927.

15. Von Kármán, Th.: Compressibility Effects in Aerodynamics. Jour. Aero. Sci., vol. 8, no. 9, July 1941, pp. 337–356.

16. Temple, G., and Yarwood, J.: The Approximate Solution of the Hodograph Equations for Compressible Flow. Rep. No. S.M.E. 3201, British R.A.E., June 1942.

17. Garrick, I. E., and Kaplan, Carl: On the Flow of a Compressible Fluid by the Hodograph Method. I – Unification and Extension of Present–Day Results. NACA Rep No. 789, 1944.

18. Garrick, I. E., and Kaplan, Carl: On the Flow of a Compressible Fluid by the Hodograph Method. II – Fundamental Set of Particular Flow Solutions of the Chaplygin Differential Equation. NACA Rep. No. 790, 1944.

TABLE I.- VALUES OF MAXIMUM VELOCITY FOR CORRESPONDING BUMP AND CIRCULAR ARC PROFILE

M	q_{max}									
	Camber coefficient, h					Thickness coefficient, t				
	0.02	0.04	0.06	0.08	0.10	0.052	0.100	0.145	0.186	0.226
0	1.0815	1.1659	1.2527	1.3415	1.4320	1.0816	1.1660	1.2527	1.3414	1.4320
.2	1.0834	1.1701	1.2597	1.3520	1.4466	1.0834	1.1701	1.2595	1.3513	1.4454
.3	1.0859	1.1759	1.2695	1.3668	1.4673	1.0859	1.1757	1.2689	1.3651	1.4641
.4	1.0899	1.1851	1.2855	1.3913	1.5024	1.0900	1.1847	1.2840	1.3876	1.4950
.5	1.0960	1.1997	1.3116	1.4324	1.5627	1.0959	1.1988	1.3084	1.4245	1.5467
.6	1.1056	1.2239	1.3572	1.5078	1.6780	1.1052	1.2217	1.3492	1.4879	1.6373
.7	1.1223	1.2705	1.4530	1.6780	------	1.1213	1.2640	1.4298	1.6197	------
.8	1.1594	1.3979	------	------	------	1.1557	1.3701	------	------	------
.9	1.2055	------	------	------	------	1.1960	------	------	------	------

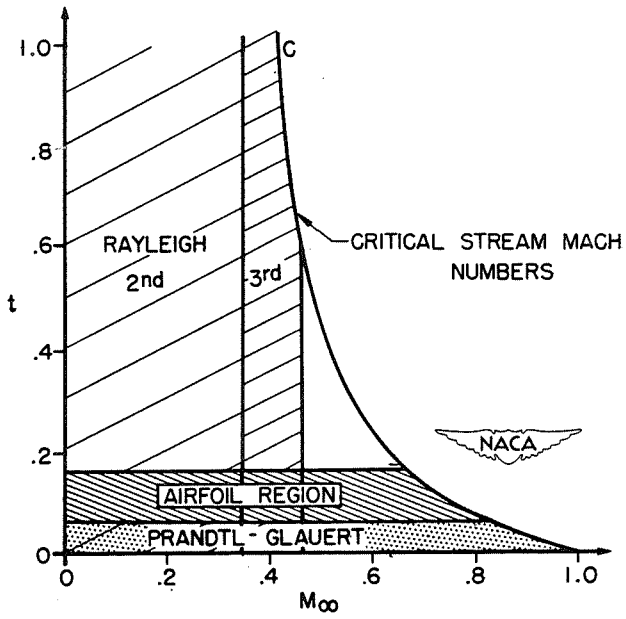

Figure 1.- Regions of application of the approximation methods.

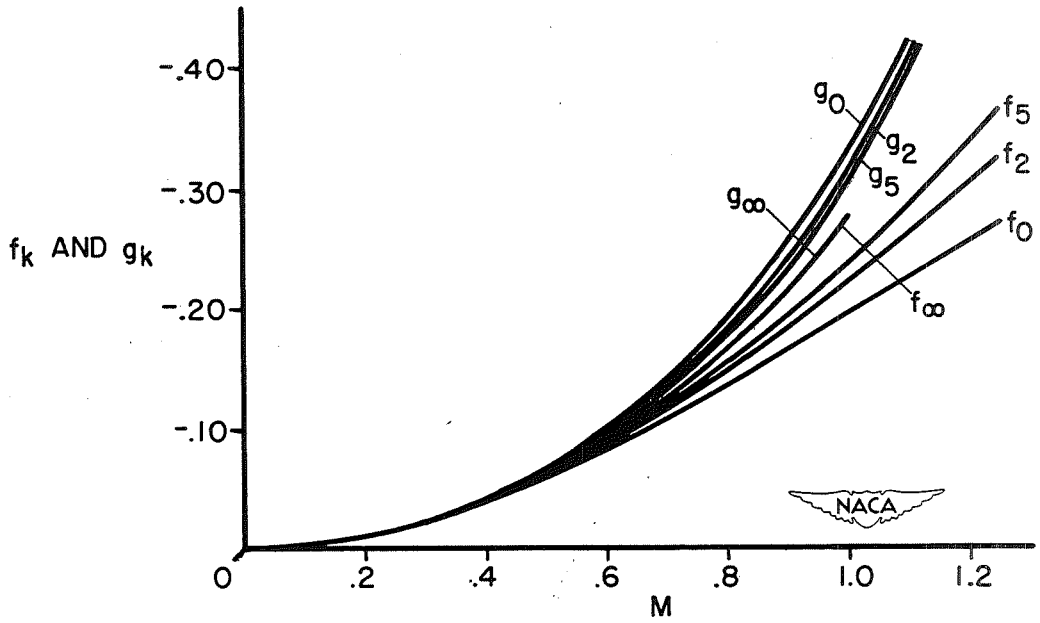

Figure 2.- The f_k and g_k functions against M.

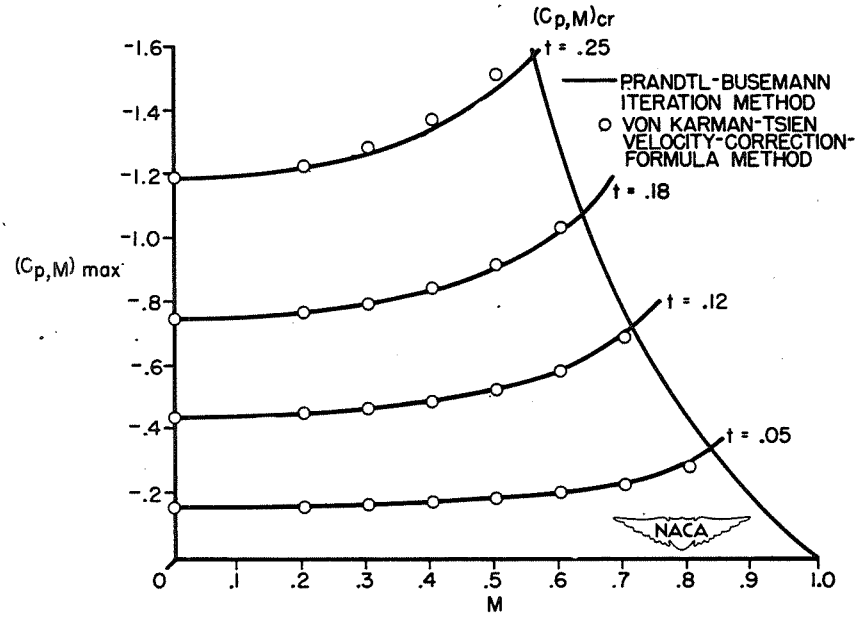

Figure 3.- Maximum pressure coefficient as function of Mach number.

WIND-TUNNEL-WALL CORRECTIONS

WIND-TUNNEL-WALL CORRECTIONS

By S. Katzoff

Langley Aeronautical Laboratory

BOUNDARY CONDITIONS

When the wind tunnel was first developed as a practical approach to experimental aerodynamics, it was recognized that the flow about a body in a wind tunnel was not the same as the flow about the same body in flight. Since that time, mainly during the past 30 years, there has appeared a steady stream of research papers, some offering improvements in recognized corrections in keeping with the improvements in wind-tunnels, equipment, techniques, and general understanding of aerodynamics and others deriving necessary corrections for new types of aerodynamic configurations or new types of measuring techniques.

The problem arises from the fact that, although the differential equations of the flow are the same in the tunnel as in flight, the outer boundary conditions are different. In flight, the condition is simply that the flow at infinity is uniform; in the tunnel, certain other conditions, depending on the type of tunnel, must be satisfied at the tunnel boundaries. For the closed tunnel, the condition is obviously that the velocity component normal to the wall be zero. For the open tunnel, where the jet traverses a region of comparatively quiescent air, the condition is that the pressure at the boundary be uniform. By Bernoulli's law, it follows that the tunnel velocity must be uniform on the boundary. If this velocity is considered as the sum of the undisturbed tunnel velocity U and a small perturbation velocity (u, v, w) resulting from the presence of the body in the jet, the condition is then that $(U + u)^2 + v^2 + w^2 \approx U^2 + 2Uu$ be constant, from which it follows that u is constant over the entire surface. Furthermore, since u is obviously zero far in front of the body, it must be zero over the entire surface, whence it can be easily shown that the perturbation potential itself is constant over the entire surface. The somewhat obvious condition that the perturbation velocity (u, v, w) is zero far in front of the body may need special emphasis; neglect of this condition has in the past sometimes led to erroneous results (reference 1).

Some attention has been directed recently to a third case; namely, that of an open tunnel in which the body is so far forward in the jet that the presence of the closed entrance bell cannot be neglected. This case involves a mixed-boundary-value problem in which the normal velocity is zero on the closed portion of the boundary and the longitudinal perturbation velocity u is zero (or constant) over the open portion of the boundary. An interesting further boundary condition arises here, namely, that the flow velocities be continuous at the edge of the entrance bell. This condition is similar to the Kutta condition at the trailing edge of an airfoil. It arises because of the finite viscosity of air, and it provides uniqueness where otherwise an infinity of solutions would exist.

BASIC VIEWPOINT

The approach to the problem usually follows a fairly well defined pattern, although variations are sometimes necessary. In general, no effort is made to predict the complete flow and the corresponding aerodynamic characteristics for the model in the tunnel. These are normally measured by the wind-tunnel survey apparatus, the wind-tunnel balances, or other measuring equipment. The usual problem is rather to determine, primarily, by how much the presence of the tunnel boundaries modifies the "free-stream" flow at the model location and, secondly, by how much the model characteristics are altered by this flow modification.

The mathematical approach, for example, is first to assume within the model a set of singularities - sources, sinks, doublets, vortices - that, on the basis of model geometry, air-flow measurements, force measurements, and any other sources of information, are believed to effectively represent the contribution of the model to the flow field. These singularities induce a field that, in general, violates the desired condition at the tunnel boundary. An additional potential flow is now sought, having singularities only on or outside the tunnel boundary, such that when it is added to the field of the model, the desired boundary conditions will be satisfied. This additional flow is called the tunnel interference flow. Its determination and, in particular, its evaluation in the neighborhood of the model constitutes the previously mentioned primary problem. Vertical components of this additional flow are normally interpreted (after division by the main tunnel velocity) as a correction to the local flow angle; horizontal components are normally interpreted as a correction to the tunnel velocity.

In figure 1 is indicated an airplane model in a closed wind tunnel, together with several of the more important components of the interference flow. Associated with the lift of the model is a strong downflow of the air behind it; and the corresponding tunnel interference flow is essentially an upflow which neutralizes the downflow at the walls and, in the neighborhood of the model, introduces the upflow velocities indicated in the figure. The upflow velocity has a certain value near the wing, rapidly approaches twice this value behind the wing, and rapidly approaches zero in front of the wing. Since the lift of an airfoil section in a curved flow is determined roughly by the angle of attack as measured at the three-quarter-chord point, the upflow at the three-quarter-chord line is used to correct the angle of attack of the airplane. Since the lift itself (or the bound vorticity) is centered about the quarter-chord line, however, the drag correction is determined from the product of the lift and the upflow velocity at the quarter-chord line. This flow curvature is effectively an induced camber of the wing and results in a corresponding change in the wing moment and in its maximum lift coefficient. Since the upflow at the tail is greater than that

at the wing three-quarter-chord line, the difference must be applied as a correction to the stabilizer setting or to the downwash angle. A correction would also be applied for the additional moment of the fuselage caused by its presence in a curved flow field.

Because the tunnel walls prevent the normal outward displacement of the streamlines about the model, there is a corresponding effective increase of the airspeed in the neighborhood of the body (constriction effect), indicated by the horizontal vector at the left of figure 1. If the drag of the model becomes fairly high, as in tests with extended flaps or at supercritical speeds, a large wake of slowly moving air exists downstream of the model, and the surrounding air of the main stream experiences a corresponding velocity increase that persists far behind the model (indicated by the horizontal vector at the right of the figure). Somewhat over half of this increase is considered to apply in the neighborhood of the model itself, in addition to the normal constriction effect due to the volume of the body; the sum is indicated by the horizontal vector near the center of the figure. Associated with the longitudinal increase of velocity along the model resulting from the wake, there is a decrease of stream static pressure toward the rear of the model. Corresponding to this effect is a longitudinal buoyancy force, roughly equal to the product of the model volume and the pressure gradient, which should be applied as a correction to the drag. Normally, however, this last correction is fairly small, and it may be noted, in any case, that if this longitudinal pressure gradient is large enough to cause a fairly large correction, it may also appreciably affect the flow phenomena, such as separation, associated with the high drag.

METHODS OF SOLUTION

Almost any interference problem for two-dimensional closed tunnels can be solved by complex-variable methods. The interference is merely the field of the system of mirror images of the model extending to infinity above and below the model. If the model can be considered as adequately represented by several simple singularities - for example, a doublet and a vortex - the interference field is simple to compute since the flow fields for infinite rows of such singularities are given by relatively simple expressions (references 2 and 3). For the exact solution of an airfoil in a closed tunnel, modern cascade theory provides applicable methods (reference 4). Corresponding solutions for an open two-dimensional tunnel (that is, a tunnel with vertical walls, but open at the top and bottom) can be similarly derived. Solutions for singularities in the open tunnel with closed entrance and exit regions are also readily possible (references 5 and 6). In all such solutions for an open tunnel, however, it is assumed that the tunnel boundary is not appreciably deformed by the singularities within the jet. Various experimental results indicate that this assumption introduces no significant error in the interference flow

near the airfoil but may lead to some error in the region behind the airfoil (references 7 and 8). Exact solutions, taking into account the boundary deformation, have been obtained for special cases (reference 9); in general, however, the deformation is not considered.

For three-dimensional tunnels the problem is much more difficult. For a small-chord, unswept, and unyawed wing, however, the interference at the wing can be readily shown to reduce to a two-dimensional flow problem - that of a vortex within a contour having the shape of the tunnel cross section and on which the normal or the tangential velocity is zero for the closed or the open tunnel, respectively. Many interesting two-dimensional problems of this nature have been solved by complex-variable methods (for example, references 10 to 12). For the interference at swept or yawed wings, or for the problem of corrections to the downwash angle at the tail, no similar simplification is possible.

For rectangular tunnels with closed, open, or partly open cross sections, solutions can be obtained by the method of images in which the interference field is that due to the doubly infinite array of mirror images of the model reflected in the tunnel walls (reference 13). The infinite summation can generally be readily approximated with adequate accuracy.

For singularities within circular tunnels, solutions can be found by expansions in Bessel functions (references 14 to 16); either the open or the closed tunnel, or the open tunnel with closed entrance and exit regions, can be treated in this way (reference 17). Solutions for elliptical tunnels are found in terms of Mathieu functions (reference 14).

For tunnels of other cross-section shapes, as the NACA full-scale tunnels or the octagonal tunnels, results for the nearest rectangle or the nearest ellipse or, perhaps, an average of the results for the nearest rectangle and the nearest ellipse may be used. An indication of the accuracy of such an approximation (and also some indication of the direction in which further modification might be made) can be found by comparing the estimated interference flow at an unswept lifting line with that for the true shape (which, as previously mentioned, can be rigorously solved as a two-dimensional problem).

It may also be mentioned that solutions of the boundary-value problems that arise in the study of tunnel interference can be found by electrical-analogy methods (references 18 and 19) or by empirical comparisons between the characteristics of the model in the tunnel and those of the same model in a tunnel that is so large relative to the model that interference is negligible (reference 7).

It is not possible in the present paper to describe in further detail any of the solution procedures that have just been mentioned or the analytical studies that have been made of the reaction of the model to the interference flows (for example, reference 20). Instead, in the remainder of

the paper are discussed several problems that may be of interest to those currently associated with wind-tunnel laboratories, namely, tunnel interference for swept wings, compressibility corrections, and choking.

TUNNEL INTERFERENCE FOR SWEPT WINGS

It might be supposed that, in order to be prepared with tunnel-interference calculations for any swept wing that might be proposed for test in a given tunnel, calculations would be needed for a series of wings having a range of sweep angles and a range of spans - that is, a two-parameter set of calculations. Actually, however, such extensive calculations are quite unnecessary, at least for rectangular tunnels. Consider the sweptback wing (yawed for greater generality) shown at the top center of figure 2. Associated with some point concentration of lift on the wing is a horseshoe vortex of zero span (that is, a doublet line) extending downstream to infinity from the point. The lower part of figure 2 shows the rear view of the wing in the tunnel, together with the doublet line and the image system of tunnels and doublet lines. The doublets are marked plus or minus according as they are the same as or opposite to the wing doublet. Examination of the doublet system shows that it is composed of two superimposed lattices, one of which is indicated by circles and the other, by squares. The vertical spacing in each lattice is equal to the tunnel height; the lateral spacing in each is equal to twice the tunnel width. The two lattices are thus identical and, furthermore, are determined only by the tunnel dimensions and not by the location of the lifting element in the tunnel. Accordingly, once the field of such a lattice has been calculated for the horizontal center plane of the tunnel, it can be used for determining the complete flow field regardless of the location of the lifting element. The interference flow field for the given lifting element is found by subtracting from the field of the two complete lattices the field of the single doublet that trails from the lifting element itself. Finally, by repeating the indicated procedures for a series of lifting elements on the wing, distributed according to the estimated wing lift distribution, the net tunnel interference is obtained.

Contour charts of the vertical component of the flow in the field of the lattice have been prepared for several NACA tunnels, including the 7- by 10-foot tunnels.

This procedure would not apply to nonrectangular tunnels. For circular tunnels, the NACA has published fairly complete interference fields for lifting lines of various spans and various sweep angles (reference 15). The sweep angles do not exceed 45°; however, it should be pointed out that, when necessary, interference calculations for any sweep angle can be used for any other sweep angle. This fact follows from the observation that a reasonably rough approximation to the wing loading is generally adequate for predicting tunnel interference; and the procedure is illustrated in figure 3. In the left half of the figure is shown how the loading on a

60° swept wing may be approximated by a single horseshoe vortex and two pairs of unswept horseshoe vortices, where the inner vortex of each pair has the same strength as the superimposed outer vortex but has opposite rotation. In the right half of the figure is shown similarly how a pair of horseshoe vortices and a single horseshoe vortex, all swept 45°, might be used for the same purpose.

FIRST-ORDER COMPRESSIBILITY CORRECTIONS

Consider a streamline object (fig. 4, upper left) in the (x, y, z) space, to be flown or tested at Mach number M and velocity U. It is desired to predict the perturbation velocities (u, v, w) at various points on the object or in the field about the object. According to the Glauert-Prandtl method, which takes into account only the first-order compressibility effects, the procedure for predicting the perturbation velocities involves the three following steps. (A short derivation of this procedure is given in the appendix. See also references 21 to 23.)

1. An object is constructed in the x', y', z' space that is related to the physical object according to the relations

$$x' = \frac{x}{\sqrt{1 - M^2}}$$

$$y' = y$$

$$z' = z$$

Essentially, this corresponds merely to a longitudinal stretching of the object by the factor $\frac{1}{\sqrt{1 - M^2}}$. For the model indicated in the figure, the fineness ratio of the fuselage, the wing chord, and the sweepback angle are increased by this stretching; the aspect ratio, the wing thickness ratio, and the angle of attack are reduced. If the model is in a tunnel, the cross section of the tunnel remains unchanged.

2. The incompressible flow about this elongated body is found. Specifically, the perturbation velocities u', v', w' on, or near, the object are found for an incompressible flow of stream velocity U. The problem of determining this flow may, of course, be quite difficult; however, since it is an incompressible-flow problem, it can presumably be solved by known methods.

3. The desired perturbation velocities u, v, w in the desired compressible flow are related to the perturbation velocities u', v', w' in the incompressible flow about the elongated object at corresponding points by the following equations:

$$u = \frac{u'}{1 - M^2}$$

$$v = \frac{v'}{\sqrt{1 - M^2}}$$

$$w = \frac{w'}{\sqrt{1 - M^2}}$$

To within the accuracy of the first-order approximation, this procedure applies for determining velocities on the object in flight or in the tunnel, or for determining tunnel interference velocities. In particular, constriction corrections are found by first determining the constriction effect in the x', y', z' space and then multiplying by $\frac{1}{1 - M^2}$. Angle-of-attack or downwash-angle corrections are found by first determining the correction in the x', y', z' space and then multiplying by $\frac{1}{\sqrt{1 - M^2}}$. The measured lift multiplied by $\sqrt{1 - M^2}$ gives the value of the lift that should be assumed for the incompressible flow in the x', y', z' space. Because the aerodynamic characteristics of the elongated object, in general, may bear no simple relation to those of the actual object in low-speed flight, combining the preceding three steps into a simple formula for the "compressibility effect" on tunnel interference is not possible for most cases. The constriction effect on short objects, however, does permit such a simple correction formula.

Consider an airfoil in a two-dimensional closed tunnel. It is roughly represented by a source-sink body on the left side of figure 5, where are also shown the nearest images. The constriction effect is merely the velocity contributed by these images in the region of the body. For incompressible flow, the constriction of the first upper image is indicated by the velocity vectors shown. The lower vector is due to the source at the nose of the image; the upper vector is due to the sink at the rear of the image; and the short horizontal vector is the resultant.

A similar construction applies to all the other images. Now, if the constriction effect at some Mach number M is desired, it is first necessary to construct an elongated body and determine its interference in incompressible flow. Examination of the right side of figure 5 shows that, if the body is elongated by $\frac{1}{\sqrt{1 - M^2}}$, the constriction velocity due to the first image is roughly $\frac{1}{\sqrt{1 - M^2}}$ as much as before, and similarly for the constriction velocity due to all the other images. If now, according to step 3 of the indicated procedure, this increase is multiplied by $\frac{1}{1 - M^2}$, it follows that the constriction effect for a reasonably short body in the tunnel varies as $\frac{1}{(1 - M^2)^{3/2}}$. Furthermore, although the preceding derivation was for an airfoil in a two-dimensional tunnel, it can be readily seen that the identical derivation method and final formula would apply for the open two-dimensional tunnel or for a body in a three-dimensional tunnel, either open or closed (reference 24).

From considerations of the field of the airfoil and its images in the two-dimensional closed-tunnel case, a simple rule can be derived for the body-constriction effect in the absence of an appreciable wake, namely, that the constriction effect at the airfoil is one-third the total velocity increase at the wall opposite the airfoil. This rule, which applies for both compressible and incompressible flow, provides a means of estimating the constriction effect from simple pressure measurements at the wall. For bodies in three-dimensional tunnels the factor is about one-half.

CHOKING

The choking speed of a closed tunnel containing a model is that speed for which the passage around the model serves roughly as a sonic throat and prevents further increase of the flow. Although all the flow in this minimum section may not be precisely at sonic speed, the choking speed is usually fairly accurately predicted, on the basis of the one-dimensional flow equations, from the ratio of the tunnel cross-sectional area to the minimum cross-sectional area of the passage around the model. After this condition has been reached, any further reduction of the back pressure results merely in an increase in the extent of the supersonic flow region just after the minimum without increasing the flow quantity or the upstream Mach number. Any measurements made under such conditions will obviously bear no relation to the characteristics of the model in flight. The question still remains, however, as to whether results obtained just

at choking are meaningful, or, if not, what is the highest Mach number for which meaningful results can be obtained. Certain investigators have concluded that tunnel Mach numbers should not be closer than 0.02 to 0.03 to the choking Mach numbers; others, by comparing results for models of different size in the same tunnel, have concluded that the safe margin is 0.04 to 0.05, depending on the model size (reference 25); still others have concentrated on the study of constriction effects almost up to choking itself, presumably with the hope of using the measurements made under such conditions. A review of these studies seems to indicate some variations among the types of results obtained in the different tunnels. Possibly the differences are related to the differences in relative boundary-layer thicknesses on the tunnel walls; in any case, it seems desirable, for the present, that further studies be made in the different wind tunnels where the problem arises.

Figure 6 illustrates the nature of the phenomena observed. Several 5-inch-chord airfoils were mounted across the Langley 24-inch high-speed tunnel and pressures were measured on the wall opposite the models (reference 26). On the left side of the figures, these pressures, interpreted in terms of local wall Mach number, have been plotted against distance along the wall for several tunnel indicated Mach numbers. It can be seen that the constriction effect is quite small at $M_{indicated} = 0.602$ but begins to become appreciable at 0.705. At higher Mach numbers it becomes quite large and, in addition, the wake constriction effect becomes very large (indicated by the fact that the wall Mach number downstream of the model never returns to the wall Mach number upstream of the model). Finally, just before choking, the peak Mach number rises very rapidly toward 1.0. On the right side of figure 6, the peak Mach number at the wall has been plotted against tunnel indicated Mach number in order to show more clearly how rapidly the peak Mach number rises just before the tunnel chokes.

In the case of the lifting airfoil (fig. 7, left side), a variation of the choking problem arises. The stagnation streamline effectively splits the flow into two parts which pass, respectively, above and below the airfoil. The distribution of cross-sectional areas, generally, is such that choking of the upper passage, in the region just above the airfoil leading edge, occurs before choking of the lower passage. In this case, the tunnel flow quantity can continue to increase until the lower passage is also choked, although, obviously, any data obtained in this flow regime bears no relation to the true airfoil characteristics. It is therefore desirable to determine, by some means other than observation of the tunnel indicated Mach number, the existence of a choked condition in the upper passage. Pressure orifices on the wall opposite the model should be useful to detect the approach of choking, as shown in figure 6. It may also be possible to compute the streamline pattern by the method previously discussed (indicated on the right of fig. 7) - the airfoil is considered to be elongated in the stream direction by the factor $\frac{1}{\sqrt{1 - M^2}}$ and the incompressible flow

pattern about this airfoil is determined. The area ratios above the stagnation streamline in this flow should apply to the compressible flow. Determination of the location of this streamline involves the solution of the flow in the infinite double cascade of airfoils consisting of the airfoil and all its mirror images. (The cascade is referred to as "double" because it consists of two superimposed cascades, one containing airfoils at a positive angle of attack and one containing airfoils at a negative angle of attack.) Although modern cascade theory can provide exact solutions to this flow, an approximate solution, such as that calculated in reference 27, should be satisfactory for this purpose.

Unsymmetrical choking of a type similar to that just discussed is a basic characteristic of any test setup in which the model supports extend below the model to the floor of the tunnel. The normal slight asymmetry introduced by such supports at low speeds becomes progressively more pronounced as the Mach number increases, and, finally, choking occurs in the region between the supports or perhaps in most of the region below the wing. Such a support system therefore becomes quite unacceptable at high speeds, and other arrangements have accordingly been developed. In one of these, a half-span model is mounted from the tunnel wall or, to avoid the thick wall boundary layer, from a plate in the center of the tunnel. In another arrangement, the complete model is supported from a sting at the rear.

The use of an open instead of a closed tunnel is also of interest with regard to choking (reference 28). At the lower speeds, the tunnel constriction effect is, in any case, about half as much as for a closed tunnel (and of opposite sign); and at very high speeds it offers the advantages that the wake constriction effect is inappreciable and that choking in the sense previously described cannot occur. The disadvantages of the open tunnel are, of course, the greater flow irregularity and the lower energy ratio, as compared with the closed tunnel.

APPENDIX

THE PRANDTL-GLAUERT METHOD FOR THREE-DIMENSIONAL FLOW

A brief derivation of a form of the Prandtl-Glauert method, correct for three dimensions, may be given as follows: A first-order approximation to the subsonic compressible flow about a thin body B, the surface of which has the equation

$$S(x, y, z) = 0$$

may be obtained by finding a solution of the linearized differential equation for the potential φ of the incremental velocities,

$$\beta^2\varphi_{xx} + \varphi_{yy} + \varphi_{zz} = 0 \tag{A1}$$

where the x-axis is in the stream direction and the incremental velocities φ_x, φ_y, and φ_z are small compared with the stream velocity U. At all points on the surface of B, the potential φ must satisfy the boundary condition

$$\left(U + \varphi_x\right)S_x + \varphi_y S_y + \varphi_z S_z = 0 \tag{A2}$$

which states that the flow is tangential to B. Since B is assumed thin, S_x is small compared with S_y and S_z; consequently, the second-order term $\varphi_x S_x$ may be neglected, and the boundary condition becomes

$$US_x + \varphi_y S_y + \varphi_z S_z = 0$$

In order to solve the boundary-value problem given by equations (A1) and (A2) in terms of incompressible flow, the following transformation of variables is used

$$\left.\begin{aligned} x' &= \frac{x}{\beta} \\ \varphi' &= \beta\varphi \end{aligned}\right\} \qquad (A3)$$

Under this transformation, equations (A1) and (A2) become, respectively,

$$\varphi'_{x'x'} + \varphi'_{yy} + \varphi'_{zz} = 0 \qquad (A4)$$

$$US_{x'} + \varphi'_y S_y + \varphi'_z S_z = 0 \qquad (A5)$$

Equations (A4) and (A5) are, respectively, the differential equation and boundary condition for the potential φ' of the incremental velocities of an incompressible flow with free-stream velocity U, in the x', y, z space, about a thin body B', the surface of which has the equation

$$S(\beta x', y, z) = 0$$

The incremental velocities in the compressible flow are thus given by

$$u = \varphi_x = \frac{1}{\beta^2}\varphi'_{x'} = \frac{1}{\beta^2}u'$$

$$v = \varphi_y = \frac{1}{\beta}\varphi'_y = \frac{1}{\beta}v'$$

$$w = \varphi_z = \frac{1}{\beta}\varphi'_z = \frac{1}{\beta}w'$$

where u, v, and w and u', v', and w' are the incremental velocities

at corresponding points in the compressible flow about B and the incompressible flow about B', respectively.

The foregoing analysis establishes the Prandtl-Glauert method for three-dimensional flow in the following form: The incremental velocities at a point P on the surface of a thin body B in compressible flow may be obtained in three steps:

(1) The x-coordinates of all points of B are increased by the factor $1/\beta$, where

$$\beta = \sqrt{1 - M^2}$$

and where the x-axis is in the stream direction. This transformation changes B into a stretched body B'.

(2) The incremental velocities u', v', w', in the direction of the x-, y-, and z-axes, respectively, at the point P' on B' corresponding to the point P on B are calculated as though B' were in an incompressible flow having the same free-stream velocity as the original compressible flow.

(3) The values u, v, and w of the incremental velocities at the point P on the original unstretched body B in compressible flow are then found by the equations

$$u = \frac{1}{\beta^2} u'$$

$$v = \frac{1}{\beta} v'$$

$$w = \frac{1}{\beta} w'$$

REFERENCES

1. Van Schliestett, George: Experimental Verification of Theodorsen's Theoretical Jet-Boundary Correction Factors. NACA TN No. 506, 1934.

2. Abbott, Ira H., Von Doenhoff, Albert E., and Stivers, Louis S., Jr.: Summary of Airfoil Data. NACA Rep. No. 824, 1945, appendix.

3. Vincenti, Walter G., and Graham, Donald J.: The Effect of Wall Interference upon the Aerodynamic Characteristics of an Airfoil Spanning a Closed-Throat Circular Wind Tunnel. NACA ACR No. 5D21, 1945.

4. Katzoff, S., Finn, Robert S., and Laurence, James C.: Interference Method for Obtaining the Potential Flow past an Arbitrary Cascade of Airfoils. NACA TN No. 1252, 1947.

5. Poggi, L.: Sulla variazione da apportarsi ai resultati delle esperienze eseguite al tunnel aerodinamico su di un modello alare. L'Aerotecnica, vol. XI, fasc. 4, April 1931, pp. 424-445.

6. Vandrey, F.: Der Düseneinfluss auf die Windkanalkorrekturen bei ebener Strömung. Jahrb. 1942 der deutschen Luftfahrtforschung, R. Oldenbourg (Munich), pp. I 786 - I 793.

7. Silverstein, Abe, and Katzoff, S.: Experimental Investigation of Wind-Tunnel Interference on the Downwash behind an Airfoil. NACA Rep. No. 609, 1937.

8. Theodorsen, Theodore, and Silverstein, Abe: Experimental Verification of the Theory of Wind-Tunnel Boundary Interference. NACA Rep. No. 478, 1934.

9. Imai, Isao: On the Deformation of Free Boundary Due to Line Vortices. Rep. No. 183 (vol. 14, 12), Aero. Res. Inst., Tokyo Imperial Univ., Aug. 1939, pp. 395-438.

10. Davison, B., and Rosenhead, L.: Wind Tunnel Correction for a Circular Open Jet Tunnel with a Reflection Plate. Proc. Roy. Soc. (London), ser. A, vol. 177, no. 970, Feb. 24, 1941, pp. 366-382.

11. Sivells, James C., and Deters, Owen J.: Jet-Boundary and Plan-Form Corrections for Partial-Span Models with Reflection Plane, End Plate, or No End Plate in a Closed Circular Wind Tunnel. NACA TN No. 1077, 1946.

12. Kondo, Kazuo: Boundary Interference of Partially Closed Wind Tunnels. Rep. No. 137 (vol. XI, 5), Aero. Res. Inst., Tokyo Imperial Univ., Mar. 1936, pp. 165-190.

13. Silverstein, Abe, and White, James A.: Wind-Tunnel Interference with Particular Reference to Off-Center Positions of the Wing and to the Downwash at the Tail. NACA Rep. No. 547, 1935.

14. Lotz, Irmgard: Correction of Downwash in Wind Tunnels of Circular and Elliptic Sections. NACA TM No. 801, 1936.

15. Eisenstadt, Bertram J.: Boundary-Induced Upwash for Yawed and Swept-Back Wings in Closed Circular Wind Tunnels. NACA TN No. 1265, 1947.

16. Allen, H. Julian, and Vincenti, Walter G.: The Wall Interference in a Two-Dimensional-Flow Wind Tunnel with Consideration of the Effect of Compressibility. NACA Rep. No. 782, 1944.

17. Küchemann, Dietrich, and Vandrey, Friedrich: On the Influence of the Entrance (or Exit Cone) on Measurements of Resistance in a Free Jet. Z.f.a.M.M., Bd. 21, Feb. 1941, pp. 17-31.

18. Malavard, Lucien: Etude de quelques problèmes techniques relevant de la théorie des ailes. Application à leur solution de la méthode rhéoélectrique. Pub. No. 153, Pub. Sci. et Tech. du Ministère de l'Air (Paris), 1939.

19. Katzoff, S., and Finn, Robert S.: Determination of Jet-Boundary Corrections to Cowling-Flap-Outlet Pressures by an Electrical Analogy Method. NACA ARR No. 4B23, 1944.

20. Swanson, Robert S.: Jet-Boundary Corrections to a Yawed Model in a Closed Rectangular Wind Tunnel. NACA ARR, Feb. 1943.

21. Hess, Robert V., and Gardner, Clifford, S.: Study by the Prandtl-Glauert Method of Compressibility Effects and Critical Mach Number for Ellipsoids of Various Aspect Ratios and Thickness Ratios. NACA RM No. L7B03a, 1947.

22. Göthert, B.: Ebene und räumliche Strömung bei hohen Unterschallgeschwindigkeiten (Erweiterung der Prandtlschen Regel). Bericht 127 der Lilienthal-Gesellschaft für Luftfahrtforschung, 1940, pp. 97-101.

23. Göthert, B.: Windkanalkorrekturen bei hohen Unterschallgeschwindigkeiten unter besonderer Berücksichtigung des geschlossenen Kreiskanals. Forschungsbericht Nr. 1216, Deutsche Luftfahrtforschung (Berlin-Adlershof), 1940.

24. Young, A. D., and Squire, H. B.: Blockage Corrections in a Closed Rectangular Tunnel. (Part I.- Simple, Approximate Formulae for General Application by Young and Squire; Part II.- Note on the Blockage Correction for Streamline Bodies of Revolution by Young.) R. & M. No. 1984, British A.R.C., June 1945.

25. Petersohn, E.: On Maximum Model Size for Wind Tunnel Investigations at High Subsonic Mach Numbers. Rep. No. 23, Aero. Res. Inst. of Sweden (Stockholm), 1948.

26. Byrne, Robert W.: Experimental Constriction Effects in High-Speed Wind Tunnels. NACA ACR No. L4L07a, 1944.

27. Goethert, Bernhard A.: Choking Mach Number in High Speed Wind Tunnel with Consideration of the Model Lift. AF TR No. 5666, Air Materiel Command, U. S. Air Force, Feb. 9, 1948.

28. Wright, Ray H., and Donaldson, Coleman duP.: Comparison of Two-Dimensional Air Flows about an NACA 0012 Airfoil of 1-Inch Chord at Zero Lift in Open and Closed 3-Inch Jets and Corrections for Jet-Boundary Interference. NACA TN No. 1055, 1946.

BIBLIOGRAPHY

Glauert, H.: Wind Tunnel Interference on Wings, Bodies, and Airscrews. R. & M. No. 1566, British A.R.C., 1933.

Toussaint, A.: Experimental Methods - Wind Tunnels. Influence of the Dimensions of the Air Stream. Vol. III of Aerodynamic Theory, div. I, part 1, ch. III, W. F. Durand, ed., Julius Springer (Berlin), 1935, pp. 280-319.

Von Kármán, Th., and Burgers, J. M.: General Aerodynamic Theory - Perfect Fluids. Influence of Boundaries in the Field of Motion around Airfoil Systems. Vol. II of Aerodynamic Theory, div. E., ch. IV, pt. C, W. F. Durand, ed., Julius Springer (Berlin), 1935, pp. 236-280.

Pope, Alan: Wind-Tunnel Testing. John Wiley & Sons, Inc., 1947.

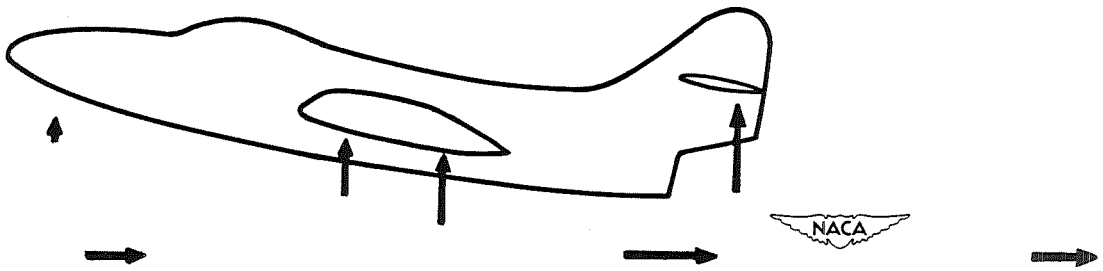

Figure 1.- Airplane model in closed wind tunnel. Several of more important components of interference flow shown.

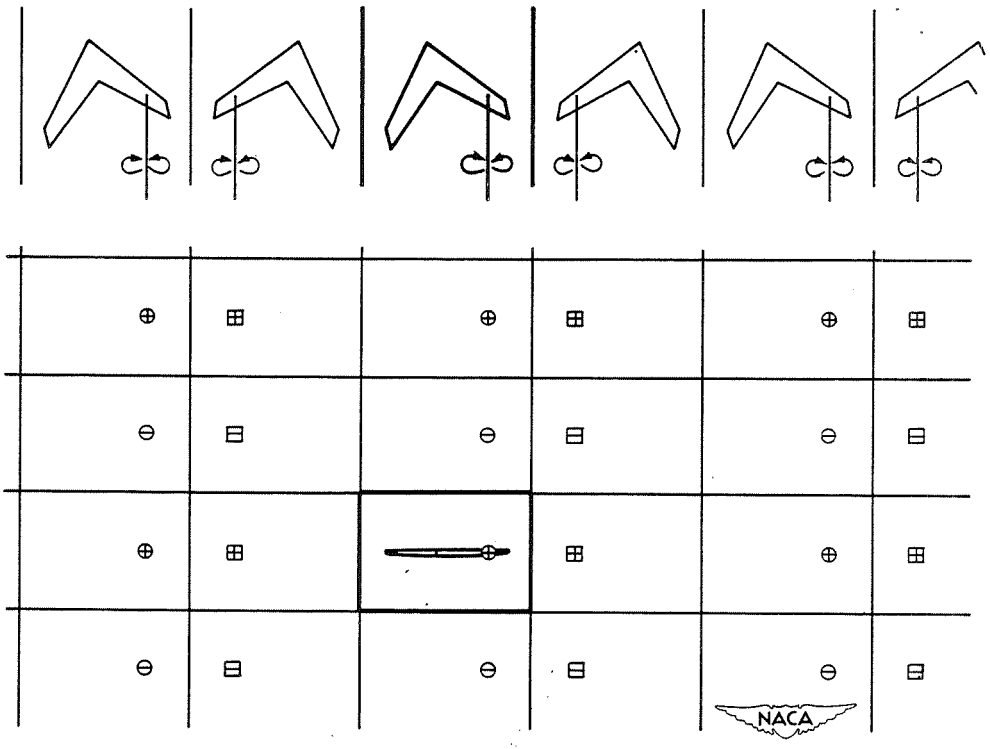

Figure 2.- Image system of doublets for a lifting element in a closed rectangular wind tunnel.

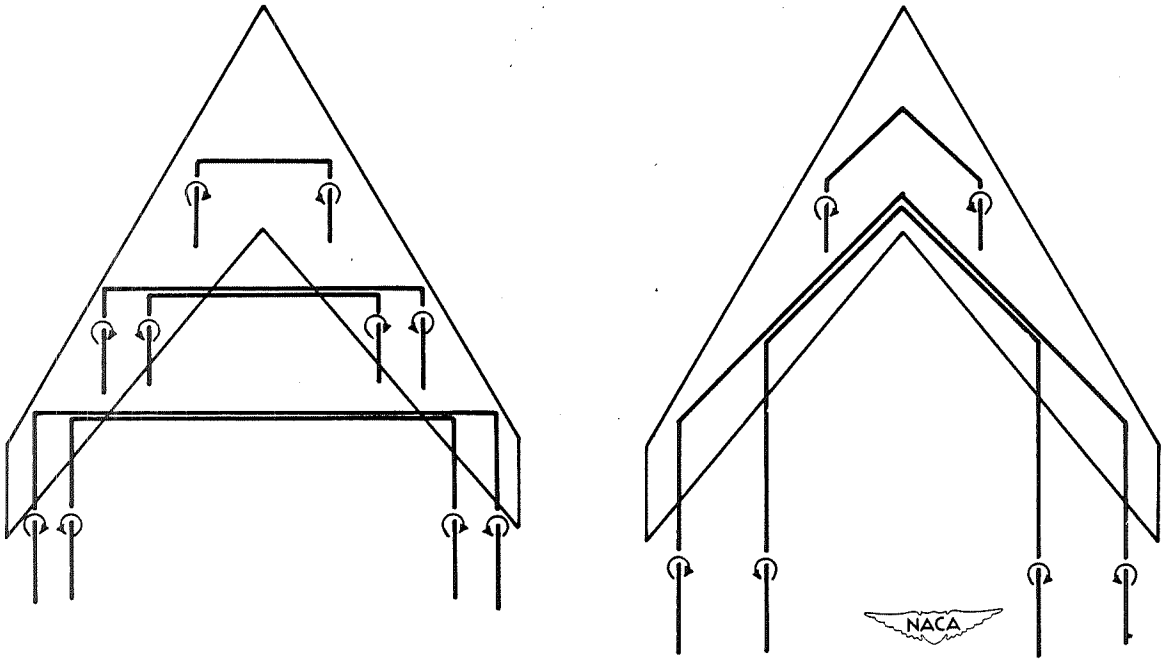

Figure 3.- Representations of the loading on a 60° swept wing by means of horseshoe vortices of other sweep angles.

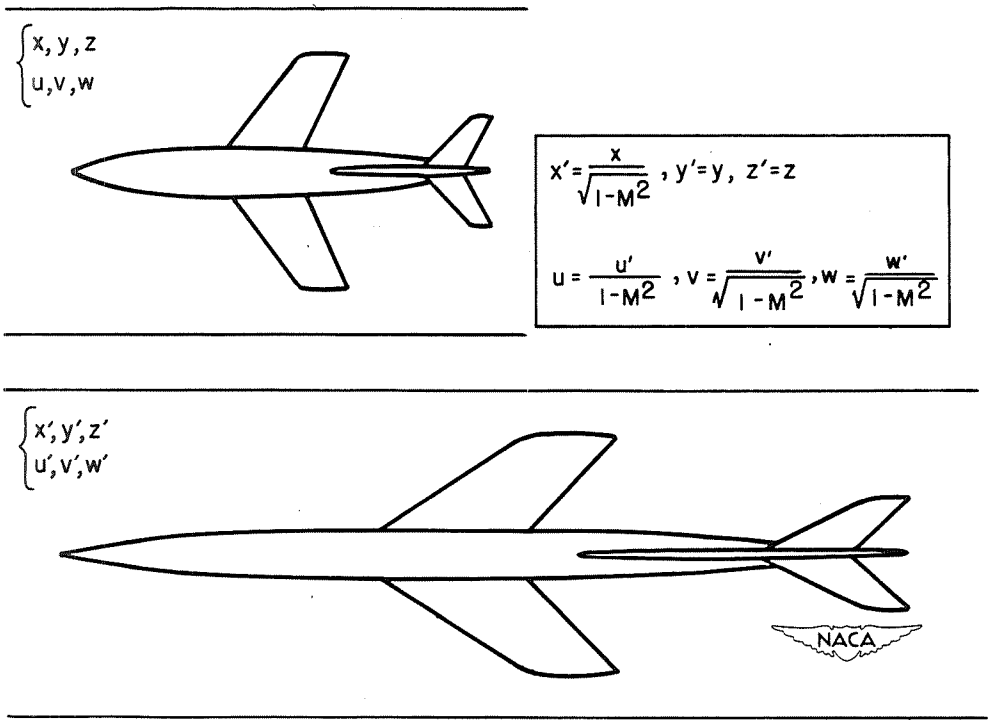

Figure 4.- Scheme for calculation of first-order compressibility effects.

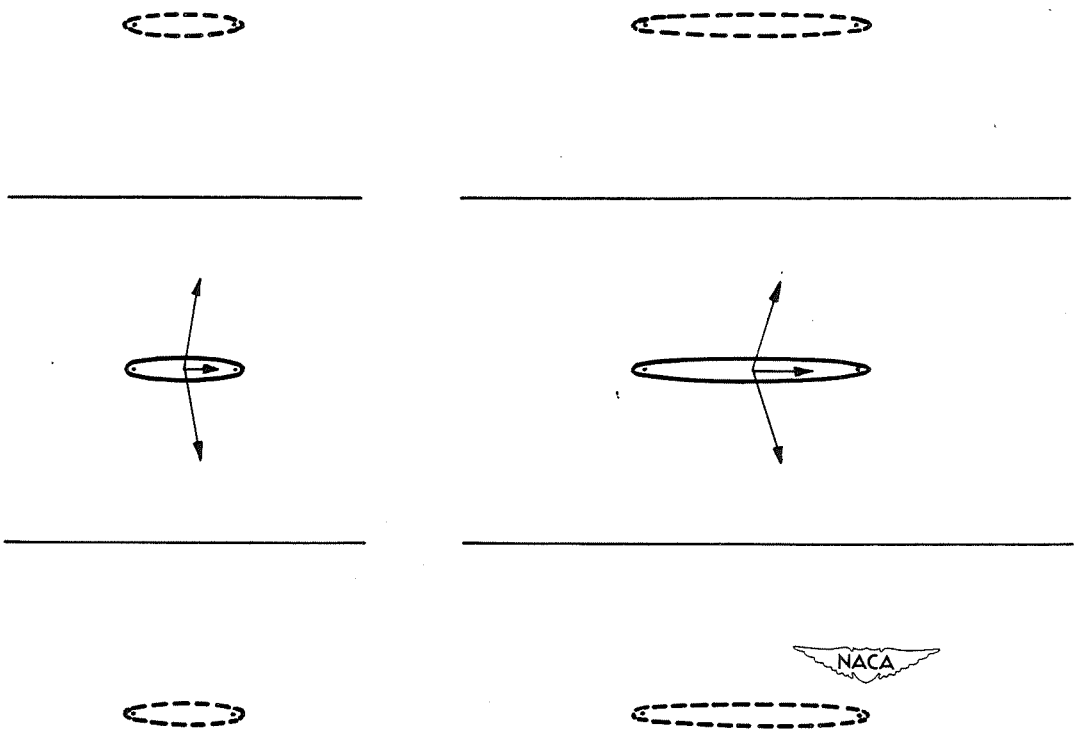

Figure 5.- Source-sink body in a two-dimensional tunnel, and its nearest images.

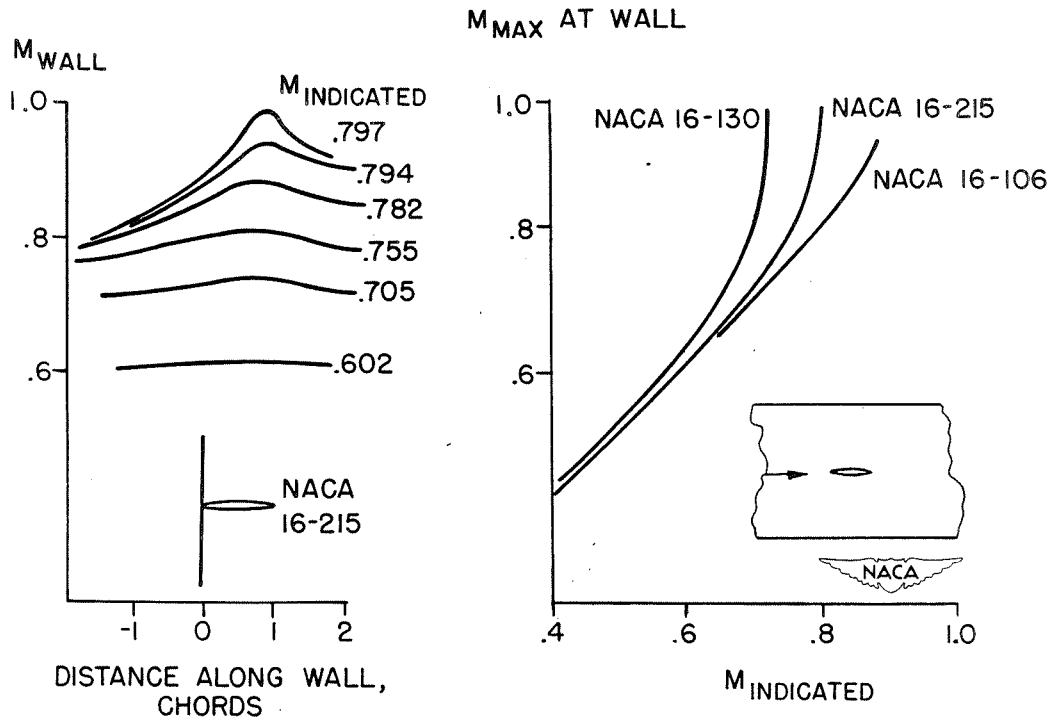

Figure 6.- Variation of wall Mach number with tunnel indicated Mach number. Five-inch chord airfoils in the Langley 24-inch high-speed tunnel.

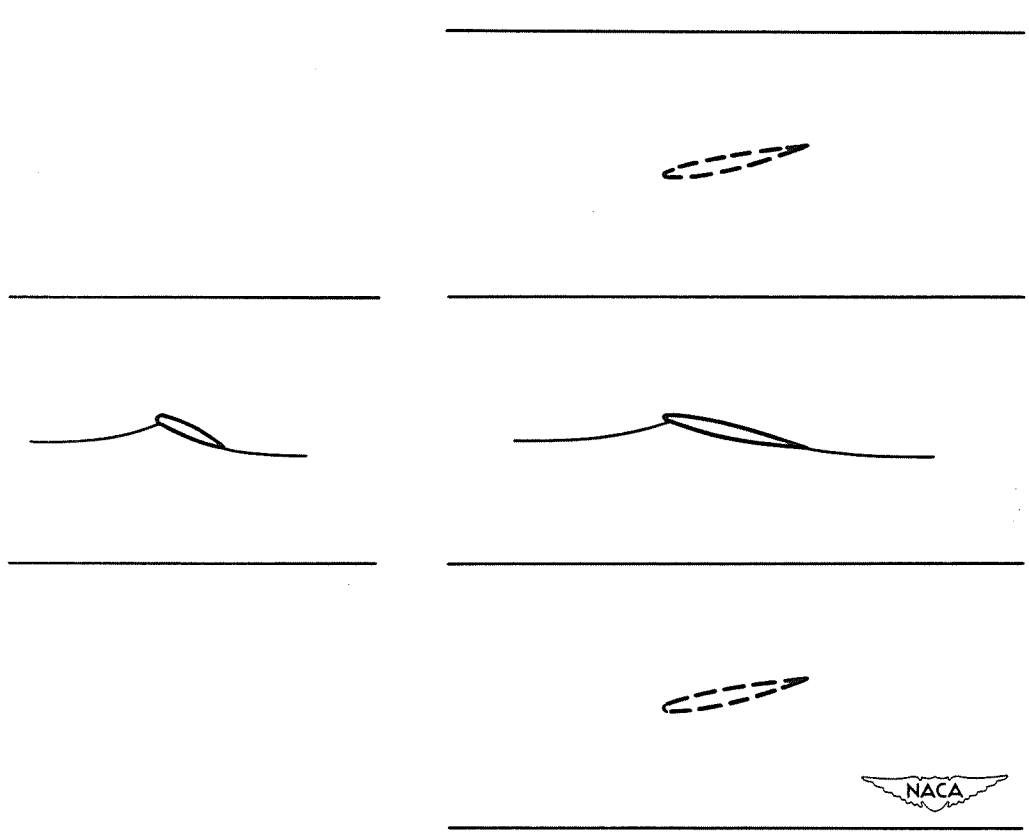

Figure 7.- Figure illustrating calculation of choking for a lifting airfoil in a closed two-dimensional tunnel.

PROPELLER THEORY

A REVIEW OF PROPELLER THEORY

By Blake W. Corson, Jr.

Langley Aeronautical Laboratory

INTRODUCTION

Although the use of screw propellers for boats was introduced at least as early as 1836, the scientific study of propellers may be regarded as having begun in 1865 with the introduction of the slipstream-momentum theory by Rankine which was followed in 1878 by an alternative concept, the simple blade-element theory of W. Froude. In view of the extreme simplicity of the assumptions upon which the early theory is based, the agreement of the analytical results with experience is remarkably good. The fact that no further major advances in propeller theory were made until about 1915 is due in part to the relatively satisfactory results obtained with the early simple theory and indicates that progress in propeller theory awaited the development of aircraft and airfoil theory.

In the history of propeller theory there appear to be five outstanding contributions which serve as a background for a great number of associated significant contributions. The major contributions are the axial-momentum theory introduced by Rankine (reference 1) in 1865, the simple blade-element theory of W. Froude (reference 2), 1878, the concept of the vortex propeller theory by Lanchester (reference 3), 1907, the screw propeller with minimum induced energy loss by Betz (reference 4), 1919, and Goldstein's solution for the radial distribution of circulation for highest efficiency for a lightly loaded propeller having a finite number of blades (reference 5), 1929. Since 1929 a number of notable contributions have been made to aerodynamic propeller theory, most of which stem from an attempt to extend the work of Betz and Goldstein to consideration of a heavily loaded propeller and the development of dual-rotation propeller theory.

A review of only the significant contributions to propeller theory affords material for a voluminous textbook. The purpose of this paper is to mention briefly the significant features of the major contributions and to discuss some of the more important developments made since the introduction of Goldstein's work, especially those made during the recent war years which have not received widespread publicity.

A list of the symbols used in this paper is included in the appendix.

EARLY THEORY

Simple Momentum Theory

In the development of the slipstream-axial-momentum theory Rankine regarded the propeller as an actuator disk immersed in a fluid having a uniform relative motion normal to the plane of the disk as shown in figure 1. The thrust exerted by the propeller results in a discontinuous increase in total pressure of the slipstream as it passes through the disk which is manifest as a continuous increase in slipstream axial velocity and an abrupt rise in static pressure. In the derivation, use is made of the laws of motion, Bernoulli's equation, continuity equation, and conservation of energy. The analysis indicates that the axial-velocity increase in the fully developed slipstream, where the static pressure is the same as that of the surrounding medium, is twice the increase at the propeller. The fundamental and very useful relation for jet propulsive efficiency is

$$\eta = \frac{1}{1 + a} \tag{1}$$

By assuming conservation of energy, an alternate expression involving power coefficient, advance ratio, and efficiency is derived:

$$C_p = \frac{\pi}{2} J^3 \frac{\eta - 1}{\eta^3} \tag{2}$$

Equation (2) represents the absolute ultimate in efficiency obtainable with a loaded propeller operating in an undisturbed stream; the only loss considered is the axial kinetic energy in the slipstream which is inseparable from the production of thrust. The variation of ideal efficiency with advance ratio as indicated by the simple momentum theory is shown in figure 2 and is compared with the efficiency indicated by modern theory.

The simple momentum theory was inadequate in that it gave no indication of the rate of slipstream contraction, failed to deal with the friction losses of a real propeller, and failed to fix propeller geometry except to demand the largest possible diameter.

Simple Blade-Element Theory

The simple blade-element theory introduced by W. Froude in 1878 and extended by Drzewiecki (reference 1 on p. 179 of reference 6) in 1892 ignored the concept of slipstream momentum and considered only the

force and velocity vectors acting on the propeller blade sections. The blade section at each radial distance from the axis of rotation was treated as an airfoil of indefinitely short span operating in a fluid whose relative velocity was determined only by the propeller's rotational speed and its forward motion. Application of the theory required the use of experimentally determined airfoil characteristics (lift and drag coefficients) and arbitrary assumptions of effective aspect ratio.

This theory, though far from being satisfactory, did enable designers to fix propeller size and shape for given operating conditions and permitted the calculation of propeller thrust, power, and profile efficiency. The efficiency computation accounts for no losses except the blade-section profile-drag or friction losses. The efficiency of a blade element η' is expressed as

$$\eta' = \frac{\tan \phi_o}{\tan \left(\phi_o + \gamma \right)} \tag{3}$$

where ϕ_o is the nominal helix angle and γ is the angle whose tangent is the drag-lift ratio. The foregoing relation is simply the efficiency of any screw involving friction and working without slip. The theory is useless for conditions of low rates of advance but gives reasonably good results at high advance ratios and does indicate that highest efficiency can be obtained when the most effective parts of the propeller blade have helix angles slightly less than 45°. Inasmuch as the energy relations between the propeller and the surrounding medium are ignored, the theory is incomplete and gives no information for selection of optimum number of blades or optimum blade shape. The optimum diameter indicated would be merely that which resulted in lowest profile losses which is entirely dependent upon the arbitrary selection of airfoil characteristics.

MODERN THEORY

The Vortex Theory

In the quarter century preceding World War I, considerable effort was spent in trying to develop the older basic theories to have a more realistic application to actual propellers. Most investigators realized that the axial-velocity increment demanded by the simple momentum theory must also exist to some extent for the blade-element theory, and early attempts to improve the latter theory followed this approach. That is, the effective axial velocity in which the propeller operated was assumed to be the sum of the flight velocity and the velocity increment (at the disk) calculated from the simple momentum theory or an empirically determined portion thereof (reference 1 on p. 180 of reference 6 and references 7 and 8). Also, during this period the slipstream-momentum

theory was extended to include the slipstream rotation resulting from propeller torque and was designated as the general momentum theory.

With the advent of modern airfoil theory characterized by the association of lift with circulation and the related concept of a vortex system for a finite airfoil consisting of bound and trailing vortices, a new approach to the propeller problem was opened.

The concept proposed by Lanchester in 1907 (reference 3), upon which the vortex theory of the propeller is based, is that the effective velocity at which the blade sections of a propeller operate includes, in addition to the translational and rotational velocities, the velocity induced by the propeller itself which is the strength at the propeller blades of the velocity field of the trailing vortex system. This concept is based on Prandtl's airfoil theory. The simplest possible representation of such a system, analogous to the use of a horseshoe vortex to represent a finite lifting airfoil, is shown in figure 3. The diagram illustrates the propeller blades, each with a bound vortex and its associated pair of trailing vortices, all of equal strength. From each propeller blade one vortex trails directly downstream with circulation about the axis of rotation in the same sense as the propeller rotation, the other vortex springing from the propeller tip trails along a helical path with circulation opposite in sense to that of the axial trailing vortex. It was realized, of course, that the real vortex system would be determined by the radial distribution of load on the blade and would be composed of a helicoidal sheet of vortex filaments springing from all points along the blade. Employing such a concept, Joukowski developed a vortex theory of screw propellers in 1912 (reference 8 on p. 180 of reference 6) which he presented in final form in 1918, being forced by the involved nature of the problem to the simplifying assumption of an infinite number of blades. Original contributions in the development of the vortex theory of propellers with an infinite number of blades have been made by other investigators (references A5 and A7 of reference 9 and references 10 to 13) of whom the most widely known in English speaking countries is H. Glauert.

The essential feature of the vortex theory is that the induced velocity at the propeller blade can be calculated from a knowledge of the vortex system of the wake and that in the resultant flow the blade elements can be assumed to operate with the characteristics of an airfoil having infinite aspect ratio. A further assumption made in the application of blade-element theory is that the operation of a blade element is not influenced by the operation of adjacent elements of the same blade. Though not theoretically tenable, experiment has shown that the assumption of independence of blade elements results in no appreciable error (reference 14).

A typical vector diagram of the velocities assumed to act on a propeller blade element for the vortex theory is presented in figure 4. The axial and rotational components, v and $2\pi rn$, respectively, are

specified by the operating conditions. The critical problem in any screw-propeller theory is the determination of the induced velocity w_1 which is the real velocity at the propeller blade element of the air adjacent to the vortex sheet in a direction normal to the sheet. In the application of the vortex theory it has been customary to resolve the induced velocity into axial and rotational components and to compute these "interference" velocities by means of the general momentum equations. Satisfactory routing procedures for application of the vortex theory have been set up by Glauert and by Weick (references 15 and 16, respectively).

Again referring to the vector diagram (fig. 4) the efficiency of a blade element by the vortex theory is shown to be

$$\eta' = \frac{\tan \phi}{\tan (\phi + \gamma)} \frac{1 - a'}{1 + a} \tag{4}$$

Equation (4) conveniently indicates the magnitudes of the three sources of loss considered, that is, profile-drag loss and the axial and rotational induced losses.

When the vortex theory is simplified by the assumption of a propeller having an infinite number of frictionless blades, the induced velocity at the propeller w_1 of the trailing-vortex system is the same as that obtained by the general momentum equations and is given by

$$w_1 = \frac{B\Gamma}{4\pi r \sin \phi} \tag{5}$$

where the product $B\Gamma$ is the total circulation about all blade elements at the radius r.

In spite of the necessary simplifying assumptions, the vortex theory has given results which agree reasonably well with experience and forms the basis of modern propeller theory. It did fail, however, in the important detail of showing the effect of the number of blades and, as originally developed, did not indicate the optimum radial distribution of blade loading.

Screw Propeller with Minimum Induced Energy Loss

Adopting the concept of a propeller operating in accordance with the vortex theory and producing a slipstream composed of a system of trailing vortices, Betz proposed to determine the radial distribution of circulation along the propeller blade (or distribution of vorticity in

the slipstream) which for a given thrust would result in the smallest energy loss (reference 4). Prandtl had shown that the condition of minimum induced energy loss for a lifting airfoil is obtained when the induced velocity in the wake, opposed to the direction of the lift, is uniform along the span, which results in an elliptical spanwise loading. Betz's solution represents an extension of Prandtl's airfoil theory to the case of a propeller. Just as in the case of a finite wing, the system of vortex filaments trailing the spanwise wing elements is regarded as forming a rigid sheet; so, for a propeller the vortex filaments trailing along helical paths downstream from the propeller blade elements are regarded as forming, behind each blade, a rigid helicoidal vortex sheet (without any assumption at this point as to whether the individual filaments continue to maintain their positions relative to one another as they pass downstream).

In the wake of a thrusting propeller the helicoidal sheets have both axial and rotational velocity components which, if the sheets are rigid, can be resolved into a pure apparent axial motion or pure apparent rotation. In any case the fluid between adjacent sheets adopts the same general motion and, in addition, a radial velocity produced by its tendency to flow around the edges of the sheets which produces the so-called "tip loss" associated with a finite number of blades. In his early treatment Betz assumed a lightly loaded propeller with negligible slipstream contraction. He dealt with conditions in the wake far behind the propeller and made use of Munk's displacement theorem by which a small change in circulation can be assumed to be added at a point in the wake rather than at the propeller blade.

Betz assumed that the radial distribution of circulation could be varied at will by adding or subtracting increments of circulation at various radii. He showed that to maintain a constant value of over-all thrust an increment of circulation removed at one radius had to be replaced at another by an increment having a strength inversely proportional to the respective radii. He then investigated the possibility of reducing the circulation at those radii where the induced loss was high and increasing the circulation at radii where the induced loss was small and thereby established the condition of minimum induced energy loss to be that for which the helicoidal vortex sheets formed apparently rigid screw surfaces of uniform pitch, under which conditions the blade elements at all radii operated with equal efficiency (drag losses not being considered).

Betz used rigorous proofs to establish the condition for minimum induced energy loss for a screw propeller, to justify the use of Munk's displacement theorem, and to show that the induced velocities in the fully developed slipstream were twice as great as for corresponding points at the propeller blades.

The condition for minimum induced energy loss is illustrated by the vector diagrams of figure 5 for velocities in the wake far downstream from the propeller. Betz's conclusion was that the induced velocity w_1

normal to the local surface of the vortex sheet should vary radially so that

$$\frac{w_1}{\cos \phi} = w = \text{Constant}$$

where w is the apparent axial motion of the rigid vortex sheets. The real velocity w_1 of the air at the surface of the helicoidal sheet has both axial and rotational components which vary continuously along the blade. However, to an observer far to one side of the slipstream viewing the wake system in a direction normal to its axis, the vortex sheets would appear to form rigid screw surfaces of uniform pitch and would appear to move as a whole without rotation with the pure axial velocity w.

The foregoing concept of a rigid-wake system is adopted for convenience in the mathematical treatment of the potential flow in the propeller wake. Because the induced velocities in the far wake are twice as great as at the propeller, the helicoidal vortex sheets undergo an initial distortion in the region where the slipstream contracts and are assumed then to form rigid screw surfaces of infinite length. Actually, the surfaces roll up into concentrated spiral vortices, one for each blade, and a single vortex along the axis equal to the combined strength of the spiral vortices.

In the development of propeller theory various authors deal sometimes with conditions at the propeller blades and at other times with those in the fully developed slipstream. In nearly all modern treatments of the vortex theory conditions in the final wake (especially, the apparent axial motion of the trailing helicoidal sheets) are the design criterions. It is the responsibility of the individual to make certain of an author's nomenclature before applying his results. The symbol w is found in the literature to represent axial velocity of the helices both in the final wake and at the propeller blades.

Effect of Number of Blades

In the development of the vortex theory the treatment of the propeller was simplified by the assumption of an infinite number of blades. In this way the spacing between adjacent helicoidal vortex sheets is made indefinitely small, the radial velocity components of the flow around the edges of the vortex sheets are eliminated from the considerations, and the circulation in a bound vortex does not become zero at the blade tip. For physical propellers the foregoing simplification must be abandoned; the spacing between the helicoidal sheets increases as a function of advance ratio and inversely as the number of blades; and further, the circulation in a bound vortex must become zero at the blade tip as well as at the axis. However, the Betz condition for

minimum induced energy loss that the helicoidal vortex sheets form screw surfaces of uniform pitch remains valid.

Prandtl's solution.- In an addendum to Betz's paper (reference 4), Prandtl gave an approximate solution for the radial distribution of circulation for a propeller having few blades. Prandtl ignored the helical nature of the flow behind a propeller and assumed the helicoidal vortex sheets to be replaced by a succession of semi-infinite, rigid-plane laminae normal to the propeller axis. The distance between laminae was taken equal to the normal distance at the slipstream boundary between the corresponding helicoidal surfaces, and the edges of the laminae were taken to lie in a plane tangent to the slipstream boundary. Prandtl investigated the two-dimensional field of flow around the edges of the laminae when the ambient fluid moved normal to their planes with a relative velocity w. Regarding the circulation as equal to the change in the velocity potential across the laminae, Prandtl obtained a distribution of circulation which was zero at the edge and increased with distance from the edge. The results applied to a propeller give a radial distribution of circulation which is a function of number of blades and advance ratio and is zero at the blade tip. When equations presented in reference 17 are combined, the approximate solution for optimum distribution of circulation along the blade obtained by Prandtl is given by equation (6) in terms of the circulation function

$$K(x) = \frac{B\Gamma_n}{Vw} = \frac{x^2}{1 + x^2}\frac{2}{\pi}\arccos e^{-\left[\frac{B}{2}(1-x)\sqrt{\left(\frac{\pi}{J}\right)^2+1}\right]} \qquad (6)$$

When Goldstein's exact solution (discussed subsequently) is used as a criterion, Prandtl's approximate solution gives good results for propellers having a large number of blades or having a small advance ratio, that is, when the spacing between adjacent helicoidal sheets is relatively small. For operation at large values of advance ratio, or with few blades, the approximate solution is not accurate. In all cases the approximate solution gives values of circulation larger than those obtained by Goldstein's exact solution.

Goldstein's solution.- An exact solution for the radial distribution of circulation in the helical wake of a propeller having few blades was obtained by Goldstein and presented in 1929 (reference 5). Lock (reference 18) states that the problem of pure hydrodynamics considered by Goldstein is that of the potential flow of fluid past a rigid body of a certain form moving with a uniform velocity. The form of the body is a helicoidal surface of infinite length but finite radius, moving parallel to its axis with uniform velocity w, or more generally any finite number of such surfaces equally spaced on the same axis and of the same radius, corresponding in number to the number of blades of the airscrew.

Goldstein deals with a propeller having few blades operating in an inviscid fluid so that the consideration of blade drag loss is eliminated. He accepts as valid the Betz condition for minimum energy loss as being realized when, at a great distance from the propeller, the vortex sheets trailing the propeller blades form screw surfaces of uniform pitch. Goldstein notes that acceptance of the foregoing condition is equivalent to neglecting the slipstream contraction and is therefore valid only for lightly loaded propellers. In obtaining his solution Goldstein deals only with conditions in the final wake and states, as does Betz, that the induced velocity at a propeller blade is one-half as great as that at a corresponding point in the wake.

In a few brief steps Goldstein establishes the differential equation for the potential flow which satisfies the boundary conditions. However, the mathematical procedures used to obtain a solution are intricate. The solution is obtained in terms of a circulation function $K(x)$

$$K(x) \equiv \frac{B\Gamma n}{Vw} = f(B, \phi, x)$$

The determination of the value of $K(x)$ for a specific operating condition involves the use of Bessel functions and the evaluation of infinite series.

A diagram of a propeller with its trailing vortex system is presented in figure 6 to illustrate the definition of the circulation function $K(x)$. This figure was taken in part from one presented in reference 19. A four-blade propeller operating at a flight speed V and rotational tip speed πnD is represented. On the lower blade in the figure the bound vorticity is represented by equipotential lines which, when shed, continue downstream as trailing-vortex filaments, the aggregate of which build the helicoidal vortex sheets. Goldstein assumed a lightly loaded propeller with negligible slipstream contraction so that at the surface of a vortex sheet in the far wake the circulation at a given radius could be equated to the circulation about the propeller blade at the same radius. The circulation Γ at a point on a vortex sheet is equivalent to the difference in the velocity potential between the upstream and downstream faces of the sheet taken along a path around the edge of the sheet.

By hypothesis the wake vortex system conforms to the Betz condition for minimum energy loss and moves axially with velocity w with respect to the surrounding medium. The axial spacing between adjacent helicoidal sheets is

$$\frac{V + w}{Bn}$$

The quantity

$$\left(\frac{V + w}{Bn}\right)w$$

represents the equivalent velocity potential resulting from the action of the velocity w through the axial distance between adjacent sheets. The circulation function $K(x)$ is defined as the ratio of the circulation Γ to this velocity potential:

$$K(x) = \frac{\Gamma}{\left(\frac{V + w}{Bn}\right)w}$$

$$= \frac{B\Gamma n}{(V + w)w}$$

The helix angle in the far wake is determined by the relation

$$\tan \phi = \frac{V + w}{2\pi rn}$$

In defining the circulation function for lightly loaded propellers, Goldstein regarded the wake velocity w as small compared to the flight speed so that

$$K(x) = \frac{B\Gamma n}{Vw}$$

For propellers with a moderately heavy loading he notes that it is more exact to define

$$K(x) = \frac{B\Gamma n}{(V + w)w}$$

One concept of the circulation function $K(x)$ is that it represents the fraction of the axial spacing between surfaces which, if acted through by the constant velocity w, produces the same potential as does the average of the real axial-velocity component acting through the full distance of the axial spacing. In other words, $K(x)w$ is the average value of the axial component of the induced velocity at a given radius.

In the simple case of a propeller with an infinite number of blades this is easily visualized. The helicoidal surfaces are indefinitely closely spaced; there is no radial flow; and the average axial induced velocity is the same as at the helicoidal surface and is $w \cos^2 \phi$:

$$K(x)w = w \cos^2 \phi$$

$$= \frac{B\Gamma}{\frac{V + w}{n}}$$

The total circulation $B\Gamma$ at a given radius is equivalent to the velocity potential produced by the average axial induced velocity acting through the axial distance traversed in one turn.

In figure 6 a qualitative representation of the streamlines referred to axes fixed in the surrounding fluid is shown on a plane approximately normal to the helicoidal sheets at their edges. The component of air velocity normal to a helicoidal sheet at any radius is the same on both faces of the sheet. The radial component of the velocity, however, is different, being directed inward at the upstream face and outward at the downstream face as a result of the tendency of the air to flow around the edge of the sheet. This discontinuity of the radial velocity at opposite faces of the helicoidal surface is a measure of the vortex strength or circulation. The energy of the radial flow accounts for the so-called "tip loss."

Goldstein presents values of the circulation function for a two-blade propeller plotted as a function of the cotangent of the helix angle with π/J as a parameter. He compares the values obtained by his exact solution with those obtained from Prandtl's approximate solution. Goldstein's results are shown in figure 7.

A comparison of the radial distribution of load for the simple momentum theory, the vortex theory ($B = \infty$), and Goldstein theory is presented in figure 8. In each case the propeller operates at an advance ratio of 2.0 and a power coefficient of 0.2. The comparison is of the thrust-grading curves. For the simple momentum theory this curve is a straight line through the origin corresponding to a uniform pressure rise across the disk. For the vortex theory for an infinite number of blades there is no tip loss, and thrust is assumed to be maintained at the blade tips. The curve for the Goldstein theory illustrates that the circulation must drop to zero at the tip. The table in the figure indicates the values of apparent axial velocity of the vortex system resulting in each case, as well as the respective values of efficiency.

Lock.- Prior to Goldstein's work on propeller theory, the vortex theory for an infinite number of blades had come into widespread use, and propeller investigators were familiar with the somewhat standardized form of equations by which the vortex theory was applied. Lock and Yeatman, in reference 20, show that the insertion of a factor κ into the standard equations for the vortex theory made these equations applicable to propellers having a finite number of blades where

$$\kappa = \frac{K(x)}{\cos^2\phi}$$

The circulation function $K(x)$ is defined by Goldstein for moderately loaded propellers as

$$K(x) = \frac{B\Gamma h}{(V + w)w}$$

For the vortex theory for infinite number of blades the circulation function so defined is found to be

$$K(x) = \frac{B\Gamma h}{(V + w)w}$$

$$= \cos^2\phi$$

Hence, for an infinite number of blades the function κ defined by Lock is unity:

$$\kappa = \frac{K(x)}{\cos^2\phi} = 1.0$$

The critical velocity component in propeller-blade-element theory is the induced velocity w_1 at the propeller blade normal to the resultant velocity. For the vortex theory for infinite number of blades this induced velocity, where $B\Gamma$ is the total circulation around the disk at radius r, is

$$w_1 = \frac{B\Gamma}{4\pi r \sin\phi}$$

Lock shows that the equivalent expression for the vortex theory with Goldstein's correction for a finite number of blades is

$$w_1 = \frac{B\Gamma}{4\pi r \kappa \sin \phi}$$

Values of κ lie, in general, between zero and unity. When the number of blades approaches infinity, Goldstein's $K(x)$ approaches $\cos^2\phi$ and κ approaches unity. Lock and Yeatman have extended the computation of Goldstein's $K(x)$ to cases for propellers having two, three, and four blades and have presented the results in charts showing κ as a function of $\sin \phi$ with the radius as a parameter (reference 20). A sample chart is shown in figure 9.

Crigler and Talkin (reference 21) present charts of $K(x)/\cos^2\phi$ for propellers having two, three, four, six, and eight blades. For such propellers they also give very useful charts of ideal efficiency (blade-section drag neglected) as a function of power coefficient, with blade loading σc_l at $x = 0.7$ and advance ratio as parameters, and show how these charts may be used to estimate quickly the over-all efficiency, thrust coefficient, and power coefficient, including the effects of drag.

Effect of Blade Profile Drag

In the development of propeller theory the potential-flow problem is usually set up for idealized conditions. The flow field of the propeller is regarded as being established by the flight speed, propeller rotational speed, and the velocities induced by the vortex system. The propeller blades are replaced by bound vortices of the desired strength, and the physical shape of a blade is ignored. The effects of the blade section drag on potential flow are regarded as of second order and are neglected. This is a logical procedure for establishing optimum ideal blade loading and the associated induced flow field.

In the application of theory to design the blade section drag must be considered because a large portion of the energy loss for a propeller is that due to profile drag. Lock (reference 22) makes a direct computation of the profile-drag power loss as being, for each blade element, the product of section drag and resultant velocity, which, when integrated, gives the loss for the entire propeller. Weick (reference 16) bases propeller drag loss on the section drag-lift ratio,

$$\eta_o' = \frac{\tan \phi}{\tan (\phi + \gamma)}$$

where

$$\tan \gamma = \frac{c_d}{c_l}$$

He shows that highest elemental efficiency is obtained when

$$\phi = 45^\circ - \frac{\gamma}{2}$$

and, consequently, that from consideration of only drag, a propeller of highest efficiency should be designed for an advance ratio slightly less than 2.20 which corresponds to a helix angle of 45° at $x = 0.7$.

In a study of the induced flow field of propellers of highest efficiency having a finite number of blades, Ferri (reference 23) considers the effect of blade section drag upon the ideal radial distribution of circulation. He shows that as the drag-lift ratio is increased an inboard shift of the blade loading is required to maintain highest over-all efficiency.

Hartman and Feldman (reference 24), basing their work on that of Goldstein and Lock, offer a systematic procedure for the design of propellers of highest efficiency including the effect of blade-section profile drag. They investigate the relation between the induced loss and drag loss for a propeller and show that when a specific propeller operates at its highest efficiency the drag loss is equal to the induced loss. Their treatment of the propeller is analogous to that which, for a finite wing, shows the maximum lift-drag ratio to be obtained when the induced drag equals the profile drag. Although their analysis is not rigorous, the conclusion is apparently substantiated by experiment. In figure 10 the envelope efficiency and corresponding values of power coefficient plotted against advance ratio are shown as solid-line curves. These data, from reference 25, were obtained in the Langley propeller-research tunnel for a 10-foot-diameter three-blade propeller, designated as 5868-9, with spinner. For identical values of power coefficient and advance ratio, the ideal efficiency of a three-blade propeller is shown as a dash line. At the advance ratio for maximum efficiency the induced loss is found to be very nearly equal to the drag loss. Similar computations for a number of different propellers have yielded like results. This type of analysis provides one means of judging the excellence of a propeller design. Also, in selection of diameter, when the propeller geometrical shape and operating conditions are fixed, the optimum diameter is that which results in equal induced and profile-drag losses.

The systematic design procedure offered by Hartman and Feldman is most readily applied when the NACA 16-series airfoil sections

(reference 26) are used. These sections which were developed especially for application to propellers have very high critical speeds and, at present, are the blade sections most widely used in the design of high-speed propellers.

Dual-Rotation Propellers

The history of dual-rotation propellers in the inventional stage begins almost as early as that for single-rotation propellers, but the development of fundamental theory for dual propellers has not progressed to a comparable stage. No rigorous proof for the optimum wake configuration comparable to Betz's treatment for single-rotation propellers has been established, nor has a mathematical solution for the distribution of the circulation along the blade been obtained. A large amount of literature exists which deals with the practical phases of dual rotation. An approximate design procedure, proposed by Lock, based essentially on single-rotation-propeller theory is presented in reference 27. A consideration of the periodic effects in dual-rotation propellers is treated in reference 28. A treatment of dual-rotation-propeller theory and design believed to be basically sound, but dependent upon an experimental approach, has been presented by Theodorsen (references 29 to 33). A simplified design procedure for dual propellers based upon Theodorsen's work has been presented by Crigler (reference 34).

The principal contributions to propeller theory made by Theodorsen are (1) the demonstration that the circulation function for any propeller could be determined by an electrical analogy with relatively simple apparatus and (2) the experimental determination of the circulation function for dual-rotation propellers, a problem which presents formidable difficulties to the mathematical approach.

Circulation function.- In dealing with single-rotation propellers having a finite number of blades, both Prandtl and Goldstein solved for the radial distribution of circulation along the propeller blade which they expressed as a nondimensional ratio equal to a function of number of blades, helix angle, and radius. For lightly loaded propellers,

$$K(x) = \frac{B\Gamma n}{Vw} = f(B, \phi, x)$$

or alternatively for moderately loaded propellers,

$$K(x) = \frac{B\Gamma n}{(V + w)w} = f(B, \phi, x)$$

Theodorsen uses the latter definition.

Mass coefficient.- A factor which Theodorsen uses extensively in his treatment of propeller theory is the mass coefficient k which is the average value over the propeller disk of the circulation function $K(x)$. The mass coefficient is the ratio of the equivalent mass of air accelerated to the uniform velocity w in unit time to the mass of air which passes through the propeller disk during the same time. For a propeller with a finite number of blades, the equivalent mass of air in a cylindrical element of thickness dr to which is imparted the axial velocity w in one turn is

$$dm = \rho(2\pi r\, dr)K(x)\frac{V + w}{n}$$

By an integration over the disk, the equivalent total mass accelerated to velocity w is

$$m = \rho 2\pi R^2 \frac{V + w}{n} \int_0^{1.0} K(x)x\, dx$$

By definition,

$$\frac{m}{\rho\pi R^2 \frac{V + w}{n}} = k = 2\int_0^{1.0} K(x)x\, dx$$

Theodorsen has used an electrical-analogy method to determine values of both the circulation function and the mass coefficient for a wide variety of propellers.

Electrical analogy.- For dual-rotation propellers with symmetrically loaded front and rear units, there is no net rotation in the slipstream; the wake is composed of two sets of helicoidal surfaces spiraling in opposite directions. The configuration of the wake helices is the same whether the oppositely spiraling surfaces of vorticity are regarded as intersecting each other, or as being reflected from one another. For conditions far downstream in the wake of a single-rotation propeller, the value of $K(x)$ at a specified radius on the helicoidal surface is obviously independent of axial position. This independence of axial position does not hold for the circulation function for dual-rotation propellers. The oppositely spiraled vortex sheets intersect (or reflect) to form a symmetrical pattern moving downstream with the velocity w. The circulation function $K(x, \theta)$ for dual-rotation propellers is a periodic function of axial position, one cycle

being the axial distance between successive intersections. The problems involved in determining mathematically the circulation function for dual-rotation propellers were regarded as insurmountably difficult, and Theodorsen turned to the more expedient method of devising a calculating machine to obtain this function. Theodorsen considered investigation of the flow field about and forces on a rigid helicoid when immersed in a liquid and oscillated axially but discarded this scheme as too dependent upon mechanical perfection. However, the mathematical identity of the flow of an ideal fluid with the flow of an electric current in a field of uniform resistance, when boundary conditions are the same, made possible the experimental solution of this problem by electrical analogy.

In the electrical method the counterpart of the rigid helicoidal surfaces trailing the propeller blades is a geometrically similar model of the wake surfaces made of nonconducting material (celluloid). A photograph of several of the wake models is presented as figure 11. The wake model is immersed in a weak electrolytic solution (tap water) in which an electric current flows in a uniform field parallel to the model axis. In this setup electric current and electrical potential are analogous to the velocity and velocity potential of fluid motion, respectively.

Apparatus.- The two types of measurements made with the electrical method were determination point by point of the radial distribution of the circulation function $K(x)$ and determination of the mass coefficient k.

A diagram of the apparatus used for measuring the value of the circulation function $K(x)$ at points along the radius of the helical surface is shown in figure 12. The arrangement is simply a Wheatstone bridge with the usual galvanometer replaced by earphones, and the power supply is alternating current having a frequency of 1000 cycles per second. The null point is established by adjusting the variable resistance until the signal becomes inaudible. The measurement is very precise. The drop in electrical potential δE across a helicoidal surface can be measured accurately at any radius and compared with the potential drop E in a length of the uniform flow field equivalent to the axial spacing between adjacent sheets. The electrical analogy shows the circulation function to be

$$K(x) = \frac{\delta E}{E}$$

Somewhat similar apparatus (fig. 13) is used for measuring the mass coefficient k which, being an integrated quantity, requires only a single measurement for each model. Two arms of the Wheatstone bridge are known resistances and the other two are the identical tanks of electrolyte. The tank walls are nonconducting, but the top and bottom

are copper plates in contact with the electrolyte. Between the copper plates of one tank is inserted a model of the helicoidal wake coaxially with the tank. The increase in electrical resistance caused by the presence of the wake model is equivalent to the addition of a potential opposing that of the uniform flow and results in a decreased current. Theodorsen gives rigorous proof that the mass coefficient is

$$k = \frac{\Delta I}{\left(\frac{F}{S}\right) I_o}$$

where F and S are the cross-sectional areas of the wake model and tank, respectively, I_o is the current flowing in the unobstructed tank, and ΔI is the change in current due to the presence of the wake model.

The reliability of the electrical-analogy method was verified by a comparison of the experimental results with those obtained by the exact theory (Goldstein) for the known case of a single-rotation propeller having two blades. The comparison is given in figure 14 which presents the mass coefficient plotted against the advance ratio of the wake. The agreement is excellent.

The difference in radial distribution of the circulation function for single-rotation and dual-rotation propellers is illustrated in figure 15 for four-blade propellers operating at an advance ratio of 6.0. The dual-rotation propeller is composed of two units of two blades each, rotating in opposite directions. The value of $K(x)$ is of necessity zero at the blade tip for both propellers and zero at the axis also for the single-rotation propeller, but for the dual-rotation propeller $K(x)$ increases continuously with distance from the tip and reaches a maximum value at the axis of rotation. In order to draw an analogy between the propeller and a wing, the single-rotation-propeller blade behaves in effect as a wing having a span equal to the propeller radius, whereas the dual-rotation-propeller blade acts as the semispan of a wing the full span of which is the propeller diameter. Consider two oppositely rotating blades of an ideal dual-rotation propeller when 180° apart. The bound circulations on the two blades are symmetrical, equal, and are in the same sense; hence there is no concentration of vorticity shed along the axis of rotation as in the case of the single-rotation propeller. If a comparison were made of the radial distribution of thrust for the two propeller types, the thrust-grading curves for both would be zero at the axis and at the tip, but the elemental values of thrust for the dual-rotation propeller would, at all radii, be greater than those for the single-rotation propeller if the same value of wake velocity w is assumed for both cases.

As mentioned in the discussion of the mass coefficient this factor represents the portion of the slipstream flow effectively worked on by

the propeller. A comparison of the mass coefficients for four-blade single-rotation and dual-rotation propellers is shown in figure 16. At values of advance ratio currently in use for cruising operation, $J = 1.5$ to 3.0, the mass coefficient for the dual-rotation propeller is about twice that for the single, and about three times as great at values of advance ratio from 4.0 to 5.0. This comparison shows that for the case selected, for operation at equal values of induced loss the power capacity of a dual-rotation propeller is much greater than that of a single-rotation propeller of equal diameter and solidity.

DISCUSSION

In his book on propeller theory (reference 33) Theodorsen comments that the theory for dual-rotation propellers may be overidealized. The ideal distribution of circulation cannot be obtained in practice by any means known at present, because the theory demands a cyclic change in the circulation function which in turn requires a cyclic change in blade angle. The required cyclic pitch change is different for each radial station and, therefore, cannot be obtained by a simple oscillation of a blade in the hub.

The validity of the electrical analogy, though apparently well verified by comparison with theory for single-rotation propellers, is not completely established for dual-rotation propellers. The radial lines of intersection of the sets of oppositely spiraling vortex sheets represent regions of discontinuity. There is no guarantee that the application of the electrical analogy with celluloid models of dual-propeller wakes faithfully represents the operation of actual dual-rotation air propellers, especially in the practical case in which the dual units operate in tandem rather than in the same plane.

All propeller theory has been developed for operation in an incompressible fluid. The theories apply well in a compressible fluid at subsonic speeds up to those at which the blade sections reach their critical values of Mach number. At higher subsonic speeds some portion of the blade always operates in a region of transonic flow, the blade section lift and drag characteristics undergo rapid changes, and the load distribution calculated for ideal conditions is meaningless. With adequate knowledge of airfoil characteristics at transonic speeds, however, a propeller can be designed to operate with the ideal load distribution for one particular operating condition in the transonic region. The design of an efficient propeller with least induced energy loss for operation at transonic and low supersonic speeds depends only on the availability of airfoil characteristics for the corresponding values of blade-section Mach number. Inasmuch as the propeller wake velocity is only a few percent of the velocity of flight, the induced velocities are entirely subsonic even for transonic and supersonic propellers. The theoretically desirable distribution of circulation along the blade for incompressible flow should hold for transonic and low supersonic flight speeds as well as it does in the low subsonic range.

APPENDIX

SYMBOLS

a	inflow velocity factor ($B = \infty$)
a'	rotational interference velocity factor ($B = \infty$)
B	number of blades
b	blade width (chord)
c_d	section drag coefficient
c_l	section lift coefficient
C_P	power coefficient $\left(P/\rho n^3 D^5\right)$
C_T	thrust coefficient $\left(T/\rho n^2 D^4\right)$
D	propeller diameter
E	electrical potential, volts
F	cross-sectional area of model helicoidal wake projected on a plane normal to axis
H	total pressure
I	electric current, amperes
I_o	electric current in uniform field, amperes
J	advance ratio (V/nD)
$K(x)$	the circulation function $\left(\frac{B\Gamma n}{(V + w)w}\right)$
k	mass coefficient $\left(2\int_0^{1.0} K(x)x\,dx\right)$
L	lift
m	mass flow, slugs per second

n rotational speed, revolutions per second

P power

p static pressure

p_o free-stream static pressure

R propeller tip radius; electrical resistance, ohms

r radius to blade element

S electrolytic-tank cross-sectional area

T thrust

V velocity of advance

W resultant velocity at blade section

w apparent axial velocity of wake helicoidal vortex sheets

w_1 induced velocity normal to helicoidal surface ($w \cos \phi$)

x fraction of propeller-tip radius (r/R)

Γ circulation

$\gamma = \tan^{-1} \frac{c_d}{c_l}$

η efficiency

η_i ideal efficiency, when no drag loss is assumed

η' blade-element efficiency

η_o' blade-element efficiency, when no induced energy loss is assumed

θ angle measured in any plane normal to the axis of rotation, with axis as center

κ Lock's factor $\left(\frac{K(x)}{\cos^2 \phi} \right)$

ρ mass density of air, slugs per cubic foot

σ propeller solidity ($Bb/\pi xD$)

ϕ aerodynamic helix angle

ϕ_o geometric helix angle $\left(\tan^{-1} \frac{J}{\pi x}\right)$

Ω angular velocity, radians per second

REFERENCES

1. Rankine, W. J. M.: On the Mechanical Principles of the Action of Propellers. Trans. Inst. Naval Architects, vol. 6, 1865, pp. 13-39.

2. Froude, W.: On the Elementary Relation between Pitch, Slip, and Propulsive Efficiency. Trans. Inst. Naval Architects, vol. 19, 1878, pp. 47-65.

3. Lanchester, F. W.: Aerodynamics. Constable & Co., Ltd. (London), 1907.

4. Betz, Albert: Schraubenpropeller mit geringstem Energieverlust. Nachrichten d. Kgl. Ges. d. Wissensch. zu Göttingen. Math.-phys. Kl., 1919, pp. 193-217.

5. Goldstein, Sydney: On the Vortex Theory of Screw Propellers. Proc. Roy. Soc. (London), ser. A, vol. 123, no. 792, April 6, 1929, pp. 440-465.

6. Glauert, H.: Airplane Propellers. Airscrew Theory. Vol. IV of Aerodynamic Theory, div. L, ch. I, sec. 4, W. F. Durand, ed., Julius Springer (Berlin), 1935, pp. 179-180.

7. Fage, A., and Collins, H. E.: An Investigation of the Magnitude of the Inflow Velocity of the Air in the Immediate Vicinity of an Airscrew, with a View to an Improvement in the Accuracy of Prediction from Aerofoil Data of the Performance of an Airscrew. R. & M. No. 328, British A.C.A., 1917.

8. Bairstow, Leonard: Applied Aerodynamics. Longmans, Green and Co., 1920.

9. Pistolesi, E.: L'Aerodinamica dell'elica aerea. Estratto dal volume: Sistemi di propulsione per la navigazione aerea e marittima. R. Accad. Sci. Torino, 1942.

10. Glauert, H.: An Aerodynamic Theory of the Airscrew. R. & M. No. 786, British A. R. C., 1922.

11. Helmbold, H. B.: Zur Aerodynamik der Treibschraube. Z.F.M., Jahrg. 15, Heft 13 and 14, 1924, pp. 150-153, and Heft 15 and 16, pp. 170-173.

12. Bienen, Th., and v. Kármán, Th.: Zur Theorie der Luftschrauben. Zeitschr. V.D.I., Bd. 68, Nr. 48, 1924, pp. 1237-1242 and 1315-1318.

13. Kawada, Sandi: Theory of Airscrews. Rep. No. 14 (vol. I, 14) Aero. Res. Inst., Tokyo Imperial Univ., March 1926.

14. Lock, C. N. H., Bateman, H., and Townend, H. C. H.: Experiments to Verify the Independence of the Elements of an Airscrew Blade. R. & M. No. 953, British A.R.C., 1925.

15. Glauert, H.: The Elements of Aerofoil and Airscrew Theory. Cambridge Univ. Press, 1926.

16. Weick, Fred E.: Aircraft Propeller Design. McGraw-Hill Book Co., Inc., 1930.

17. Glauert, H.: Airplane Propellers. Propellers of Highest Efficiency. Vol. IV of Aerodynamic Theory, div. L, ch. VII, sec. 4, W. F. Durand, ed., Julius Springer (Berlin), 1935, p. 263.

18. Lock, C. N. H.: The Application of Goldstein's Theory to the Practical Design of Airscrews. R. & M. No. 1377, British A.R.C., 1932.

19. Lock, C. N. H.: Airscrew Theory. R. & M. No. 1746, British A.R.C., 1936.

20. Lock, C. N. H., and Yeatman, D.: Tables for Use in an Improved Method of Airscrew Strip Theory Calculation. R. & M. No. 1674, British A.R.C., 1935.

21. Crigler, John L., and Talkin, Herbert W.: Charts for Determining Propeller Efficiency. NACA ACR No. L4I29, 1944.

22. Lock, C. N. H.: A Graphical Method of Calculating the Performance of an Airscrew. R. & M. No. 1849, British A.R.C., 1938.

23. Ferri, Antonio: La Determinazione delle velocità indotte da un vortice elicoidale e alcune sue applicazioni allo studio delle eliche. Atti di Guidonia, no. 57-58, 1941.

24. Hartman, Edwin P., and Feldman, Lewis: Aerodynamic Problems in the Design of Efficient Propellers. NACA ACR, Aug. 1942.

25. Biermann, David, and Hartman, Edwin P.: Tests of Two Full-Scale Propellers with Different Pitch Distributions, at Blade Angles up to 60°. NACA Rep. No. 658, 1939.

26. Stack, John: Tests of Airfoils Designed to Delay the Compressibility Burble. NACA Rep. No. 763, 1943.

27. Naiman, Irven: Method of Calculating Performance of Dual-Rotating Propellers from Airfoil Characteristics. NACA ARR No. 3E24, 1943.

28. Collar, A. R.: On the Periodic Effects Experienced by the Blades of a Contra-Rotating Airscrew Pair. R. & M. No. 1995, British A.R.C., 1941.

29. Theodorsen, Theodore: The Theory of Propellers. I - Determination of the Circulation Function and the Mass Coefficient for Dual-Rotating Propellers. NACA Rep. No. 775, 1944.

30. Theodorsen, Theodore: The Theory of Propellers. II - Method for Calculating the Axial Interference Velocity. NACA Rep. No. 776, 1944.

31. Theodorsen, Theodore: The Theory of Propellers. III - The Slip-stream Contraction with Numerical Values for Two-Blade and Four-Blade Propellers. NACA Rep. No. 777, 1944.

32. Theodorsen, Theodore: The Theory of Propellers. IV - Thrust, Energy, and Efficiency Formulas for Single- and Dual-Rotating Propellers with Ideal Circulation Distribution. NACA Rep. No. 778, 1944.

33. Theodorsen, Theodore: Theory of Propellers. McGraw-Hill Book Co., Inc., 1948.

34. Crigler, John L.: Application of Theodorsen's Theory to Propeller Design. NACA RM No. L8F30, 1948.

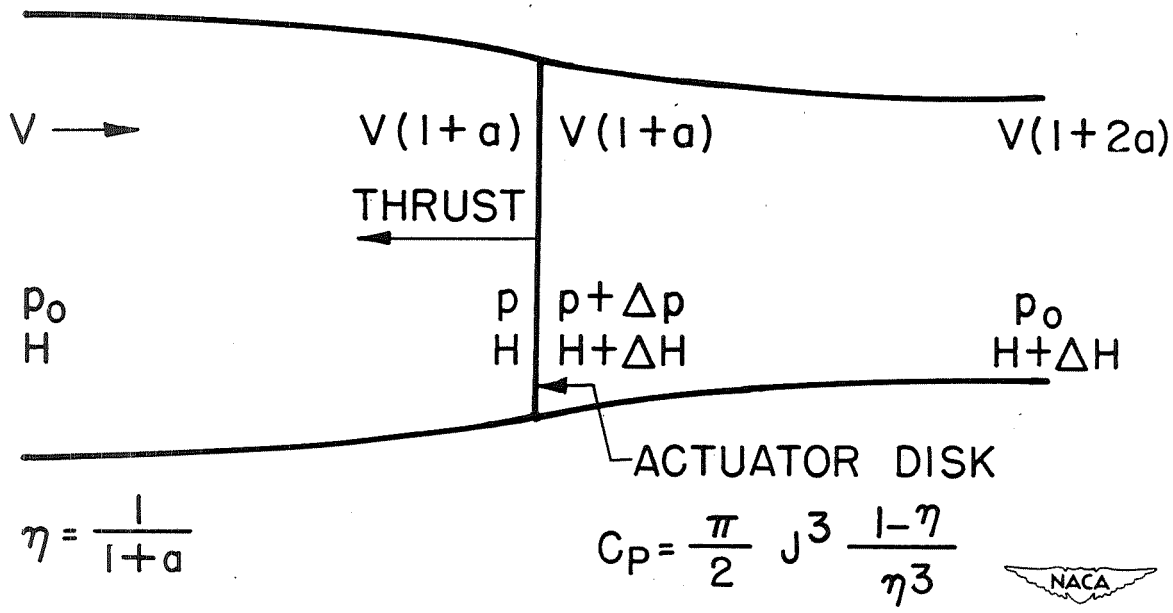

Figure 1.- Simple momentum theory.

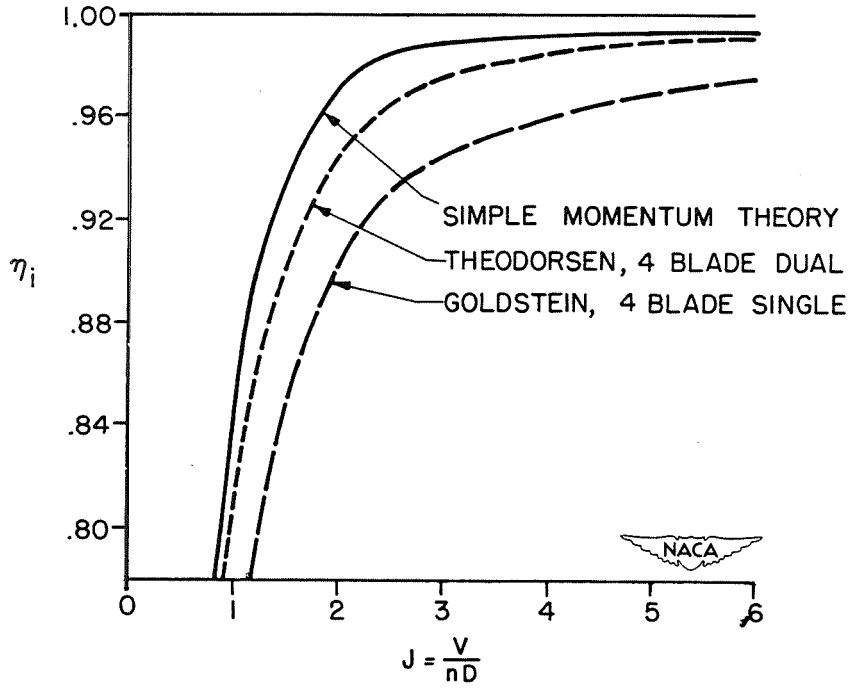

Figure 2.- Ideal efficiency (frictionless propeller); $C_p = 0.4$.

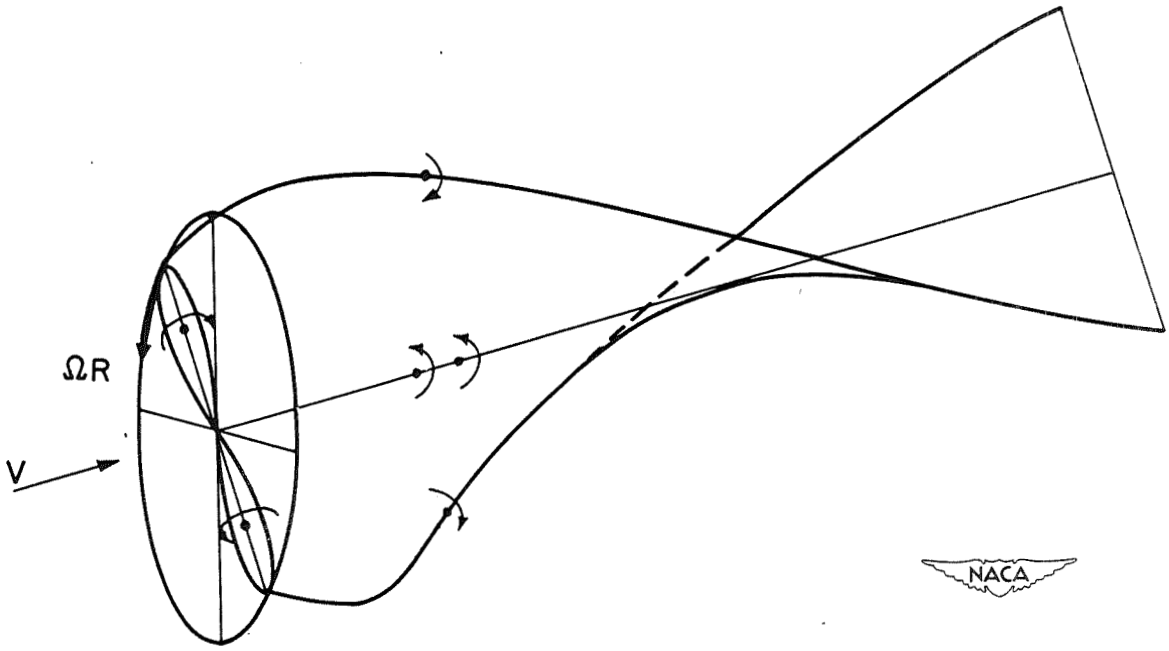

Figure 3.- Basic vortex system for a propeller.

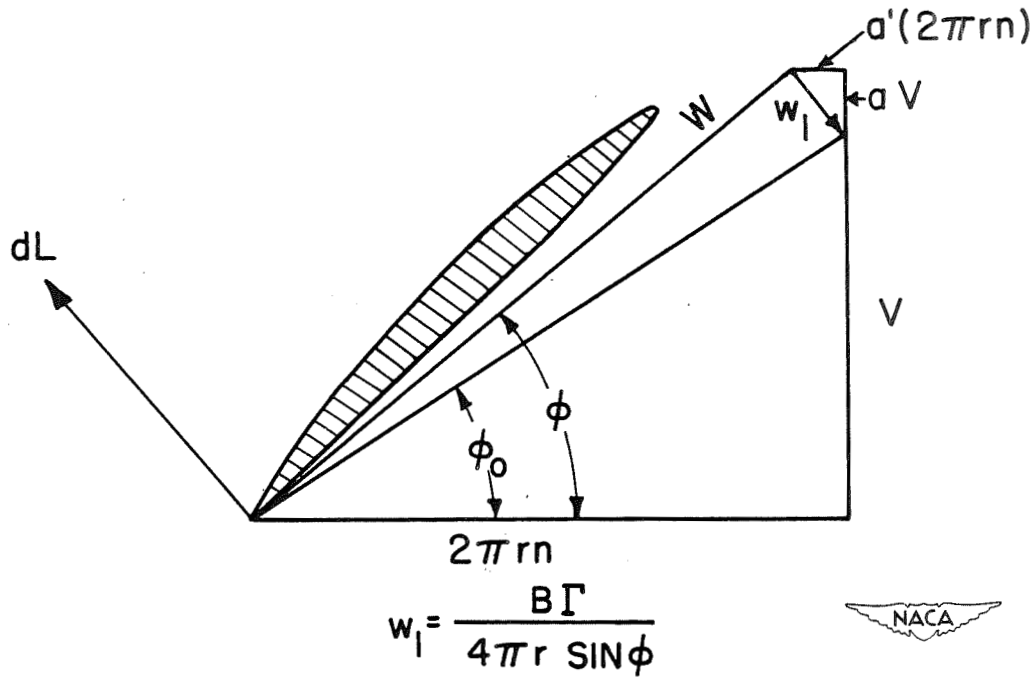

Figure 4.- Vector diagram of vortex blade-element theory; infinite number of blades.

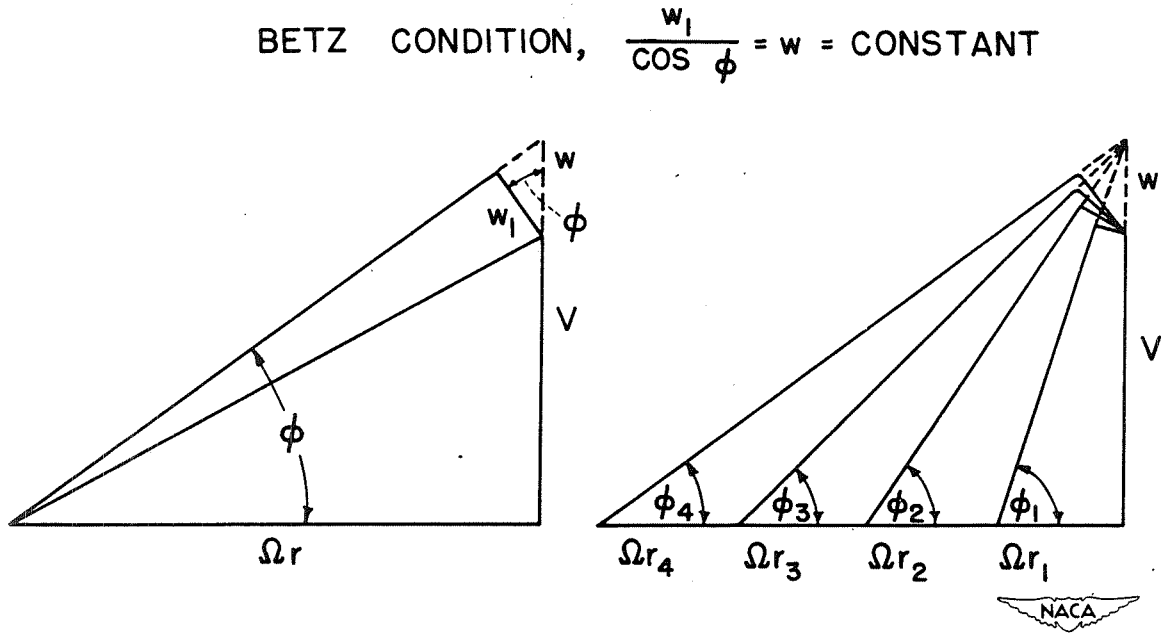

Figure 5.- Radial distribution of induced velocity in rigid helicoidal wake.

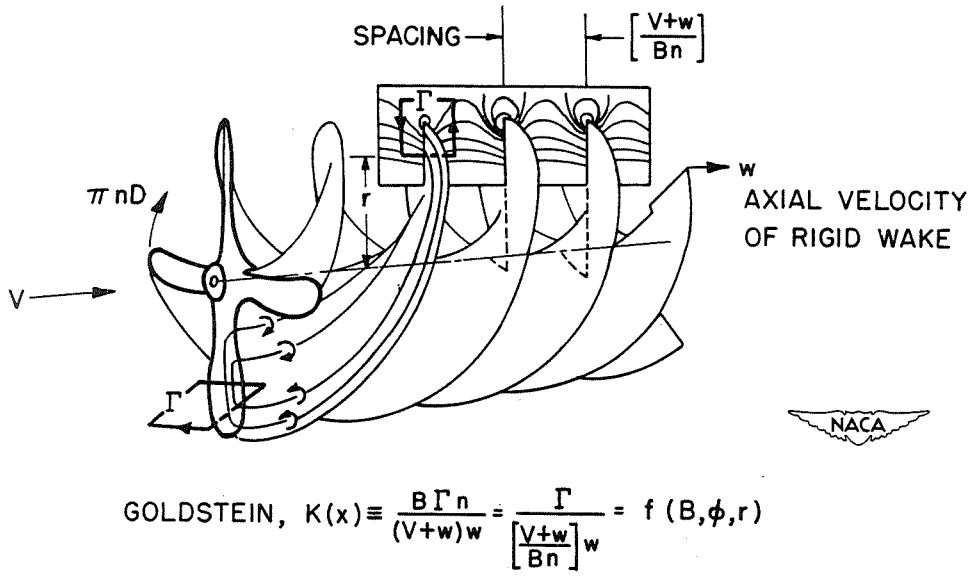

Figure 6.- Circulation function, K(x); finite number of blades.

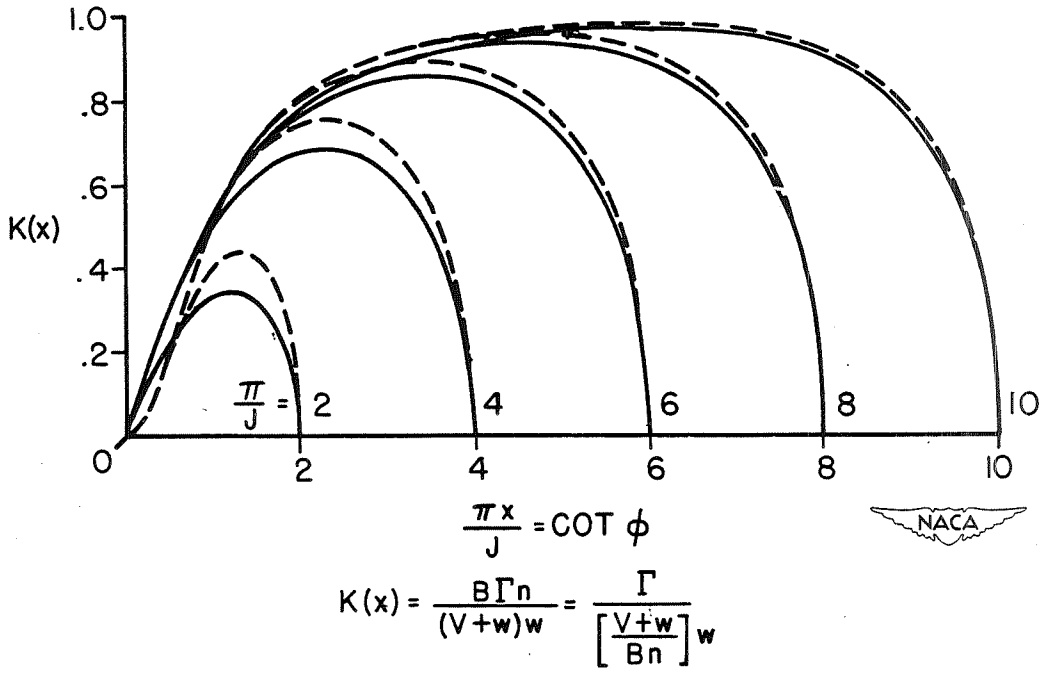

Figure 7.- Goldstein's circulation function; two-blade propeller.

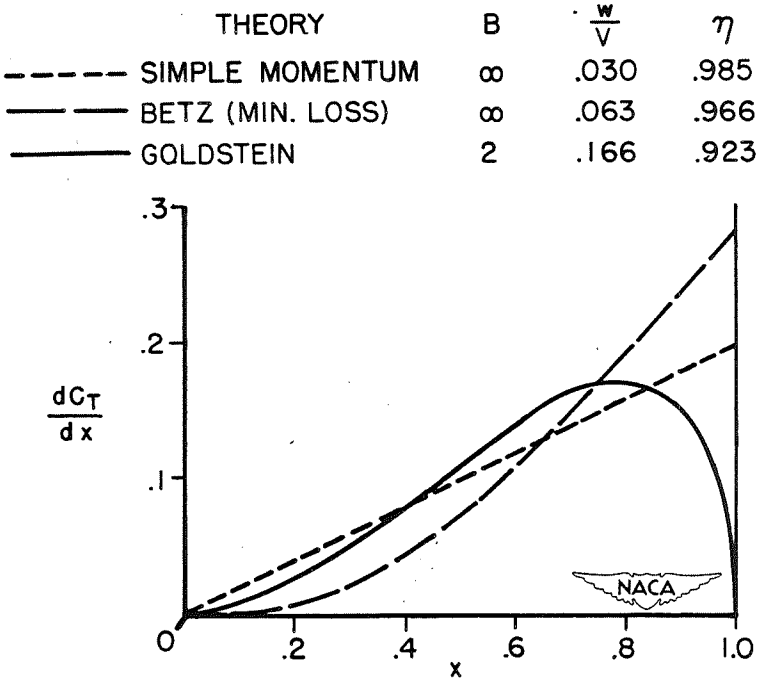

Figure 8.- Comparison of thrust grading curves; $C_p = 0.2$; $J = 2.0$.

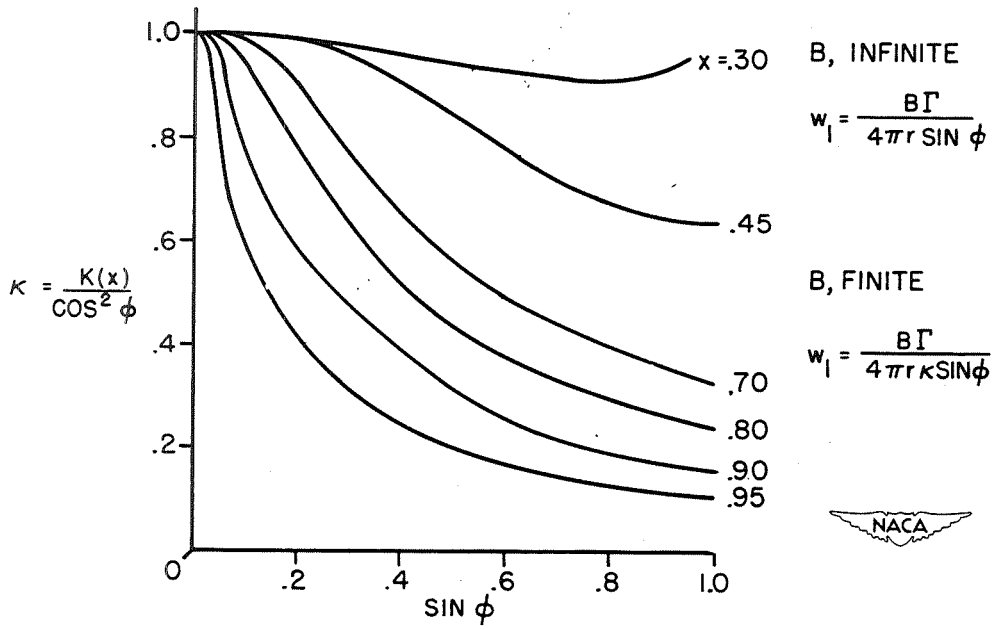

Figure 9.- Lock's presentation of Goldstein circulation function; two-blade propeller.

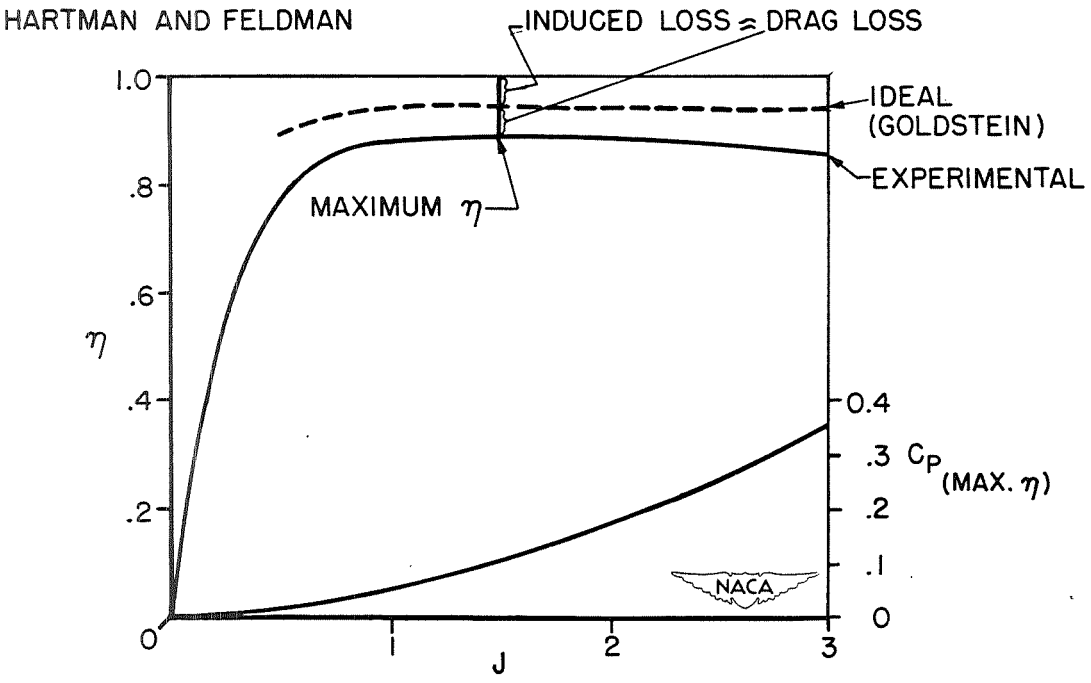

Figure 10.- Envelope efficiency compared with ideal efficiency.

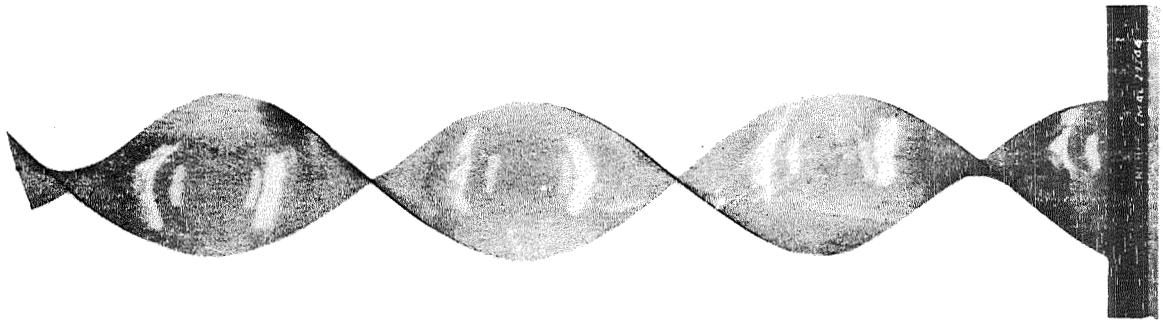

(a) Two-blade single rotation.

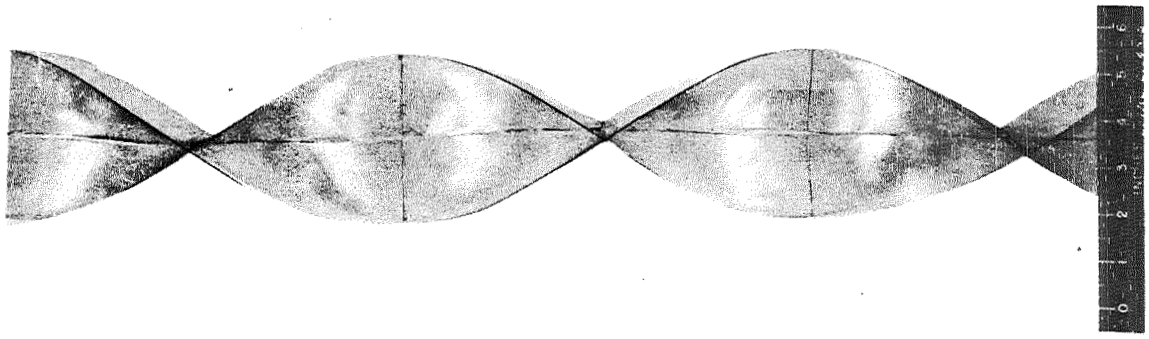

(b) Four-blade dual rotation.

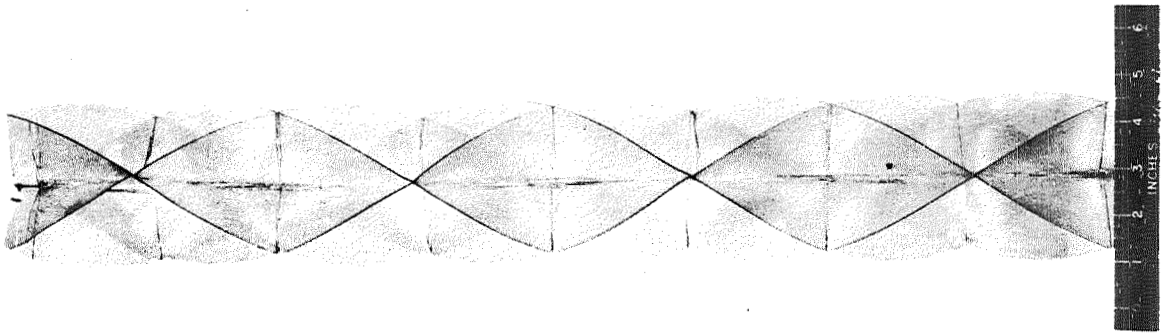

(c) Six-blade dual rotation.

Figure 11.- Typical celluloid wake models used in the electrical-analogy experiments.

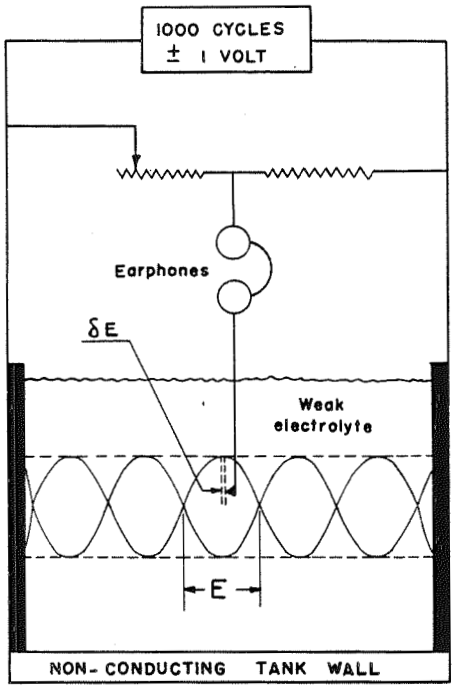

ANALOGY

AERODYNAMIC $\approx$ ELECTRICAL

$$\omega \approx I$$

$$\left[\frac{V+\omega}{Bn}\right] \approx R$$

$$\omega\left[\frac{V+\omega}{Bn}\right] \approx E = IR$$

$$\Gamma \approx \delta E$$

$$K(x) = \frac{\Gamma}{\omega\left[\frac{V+\omega}{Bn}\right]} = \frac{\delta E}{E}$$

NACA

Figure 12.- Schematic diagram of apparatus for measuring the circulation function.

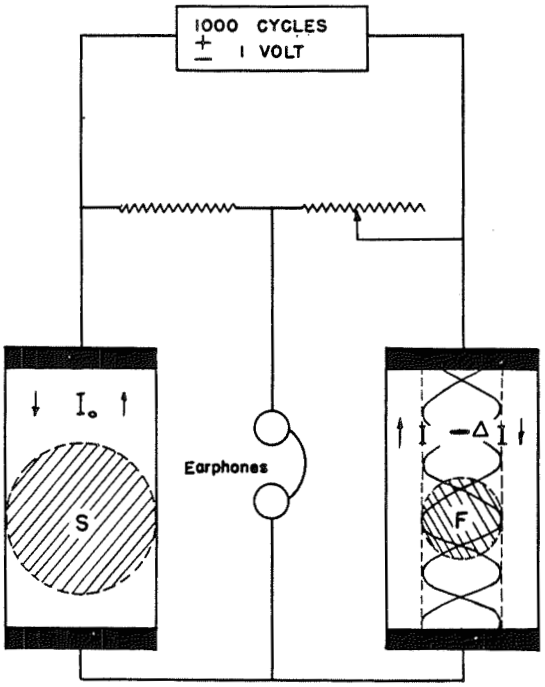

AERODYNAMIC

$$k = 2\int K(x)\, x\, dx$$

$$= \frac{2\int \Gamma x\, dx}{\left[\frac{V+\omega}{Bn}\right]}$$

ELECTRICAL

$$k = \frac{\Delta I}{\left(\frac{F}{S}\right) I_o}$$

NACA

Figure 13.- Schematic diagram of apparatus for measuring the mass coefficient.

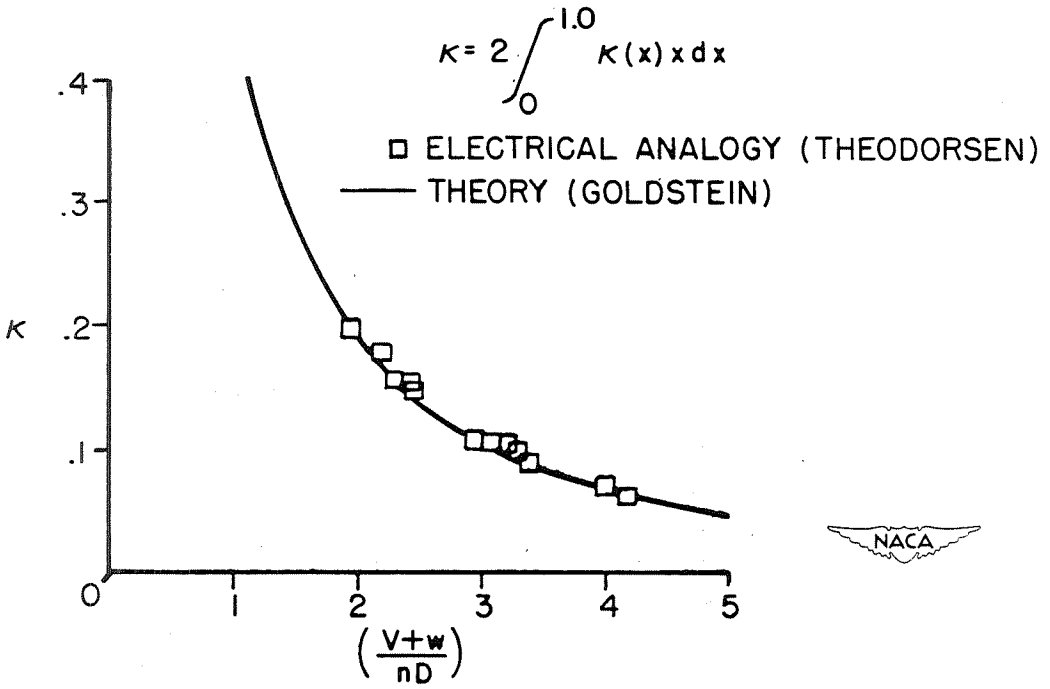

Figure 14.- Electrical-analogy results compared with theory; B = 2.

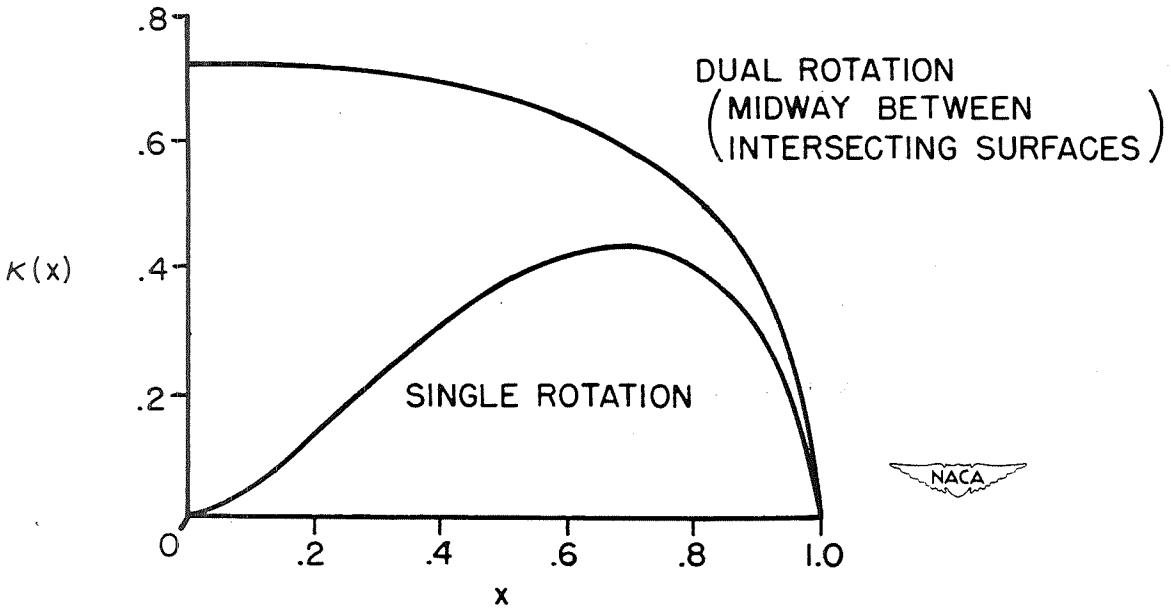

Figure 15.- Radial distribution of load; four-blade propellers; $\frac{V + w}{\pi nD} = 1.89$.

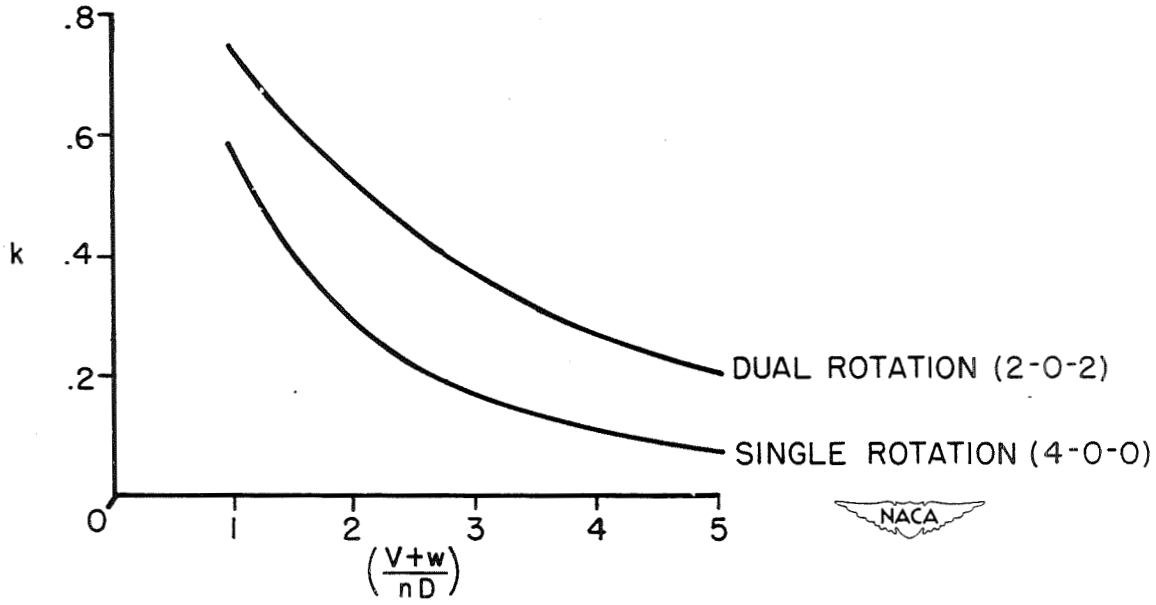

Figure 16.- Mass coefficient for comparable four-blade single- and dual-rotation propellers.

WINGS

D5

Preceding page blank

CHARACTERISTICS OF WING SECTIONS AT SUBCRITICAL SPEEDS

By Albert E. von Doenhoff and Laurence K. Loftin, Jr.

Langley Aeronautical Laboratory

The characteristics of wing sections at subcritical speeds have been the subject of intensive research since the airplane was first invented. The problem has been attacked both experimentally and theoretically. As a result of these investigations, we have today a qualitative understanding of nearly all the flow phenomena associated with the various characteristics and we are able to calculate many of the characteristics theoretically. The present paper represents an attempt to summarize briefly some of the more important aspects of our theoretical and experimental knowledge of the flow about airfoil sections and to indicate the way in which this knowledge was used in the design of NACA 6-series or low-drag airfoils. Acknowledgement is gratefully expressed for the expert guidance and many original contributions of Mr. Eastman N. Jacobs, who supervised much of the experimental work to be discussed and the application of the theoretical methods to the design of improved airfoil sections.

One of the concepts most useful in understanding the behavior of airfoil sections is that of the thin airfoil. For the purpose of determining the chordwise load distribution at various angles of attack, and hence the angle of zero lift, the slope of the lift curve, and the pitching-moment coefficient, the airfoil is considered to be replaced by a curved line that is midway between the upper and lower surfaces of the airfoil; that is, the airfoil is considered to be replaced by its mean line. The usual form of mean-line theory as developed by Munk, Birnbaum, Glauert, Theodorsen (references 1 to 5) and others assumes that the angle of attack is small and that the slopes and ordinates are sufficiently small that all effects of these quantities are proportional to their magnitude. In other words, the mean-line theory is a linearized theory. For the purposes of the theory, the air is assumed to be nonviscous and incompressible.

The basic relations of thin-airfoil theory are given in figure 1. Abscissas and ordinates are represented by x and y, respectively. The vertical component of induced velocity is v, the free-stream velocity is V, and the angle of attack is α. Circulation of strength γ per unit length is assumed to be distributed along the mean line. This circulation per unit length is equal to the difference in tangential components of velocity between the upper and lower surfaces. Equation (1) in figure 1 states that the flow must be tangential to the surface, that is, there can be no flow through the mean line. Equation (2) is a formula for calculating the vertical component of induced velocity at any station x_0 in terms of the distribution of circulation along the chord. A problem can be solved by simultaneous solution of equations (1) and (2) either by finding the distribution of γ associated with a given mean line at a given angle of attack, or by finding the mean line for a given distribution of γ.

Most practical airfoil sections are sufficiently thin that the approximations of mean-line theory hold with good accuracy. Numerous comparisons between theoretical and experimental results are available in the literature for many types of airfoil sections. (See references 6 and 7.) In general, good agreement can be expected except in cases where the flow has separated from the surface of the airfoil, as at high angles of attack, large flap deflections, and so forth.

In spite of the many useful results obtained from thin-airfoil or mean-line theory, the nature of the information required for a particular problem may frequently be beyond the scope of this simplified approach. No information, of course, is given concerning the actual distribution of pressure over the surfaces of an airfoil, and as will be pointed out later, such information is necessary for the design of improved airfoil sections. In order to be able to compute the actual pressure distribution about an airfoil, as opposed to the calculation of the chordwise loading, the more elaborate methods of thick-airfoil theory must be used. This theory as developed by Theodorsen and Garrick (references 8 and 9) is a rigorous treatment of the problem of finding the perfect-fluid pressure distribution about an airfoil of arbitrary shape. The method consists essentially of finding suitable conformal transformations to relate the known flow about a circle to the unknown flow about the airfoil. An analysis made by Joukowski which permits the direct transformation of the flow about a circle into the flow about a particular type of airfoil, called a Joukowski airfoil, has been known for a long time. In the Theodorsen method, as shown in figure 2, the Joukowski transformation $\zeta = Z' + \frac{a^2}{Z'}$ is applied, in reverse, to the arbitrary airfoil. Since all airfoils can be roughly approximated by a Joukowski airfoil of about the same thickness, the application of the Joukowski transformation to the arbitrary airfoil (ζ-plane) results in a nearly circular curve in the Z'-plane, the equation of which is given by the relation $Z' = ae^{(\psi+i\theta)}$. According to the Reimann theorem, any simple closed curve can be transformed into a circle. Theodorsen found a particularly convenient process for accomplishing this result. By a process of successive approximations, the first one or two steps of which are generally sufficient in practice, the distorted circle is transformed into a true circle whose equation is $Z = ae^{(\psi_0+i\phi)}$ where ψ_0 is a constant. The transformation is given by $\frac{Z'}{Z} = e^{\left[(\psi-\psi_0)+i(\theta-\phi)\right]}$, where the quantities $(\psi - \psi_0)$ and $(\theta - \phi)$ represent the radial and angular distortions between corresponding points in the near- and true-circle planes. The flow about the arbitrary airfoil is found by applying these transformations in reverse order to the known field of flow about the true circle.

A comparison between the pressure distribution found experimentally and that computed by the Theodorsen method at a low angle of attack is given in figure 3. (See also reference 7.) The solid line is the result of the theoretical calculation and the test points represent the experimental results.

At higher angles of attack and lift coefficients, the agreement between theory and experiment is generally not so close. This is due to the formation of a relatively thick boundary layer primarily along the rear portion of the upper surface. Under such conditions, the angle of attack at which a given lift coefficient is obtained experimentally is not the same as the theoretical angle of attack. Pinkerton (reference 10) found that it was possible to obtain nearly perfect agreement between measured and calculated pressure distributions by reducing the theoretical circulation at a given angle of attack to the value corresponding to the measured lift coefficient and then modifying the trailing-edge shape in such a manner that the Kutta-Joukowski condition is satisfied. The modification of the airfoil shape corresponded closely to the estimated change in the effective shape of the airfoil caused by the thickening of the boundary layer.

It is often desirable to determine the effects of airfoil thickness, thickness form, and type and amount of camber on the pressure distribution for large numbers of airfoils. Such calculations could, of course, be carried out by using the Theodorsen method for each individual case. The amount of computational labor involved in such a procedure, however, would probably be excessive. Great simplification of methods for calculating airfoil pressure distributions approximately was made possible by the work of Allen which showed that the effects of thickness form and load distribution could be considered separately. (See reference 11.)

The method is based essentially on the assumption that the velocity distribution about an airfoil may be approximated by the following three independent components (see fig. 4):

(1) The velocity over the symmetrical airfoil at zero angle of attack (thickness). This velocity distribution can be obtained by the Theodorsen method as previously discussed.

(2) The incremental velocity distribution corresponding to the load distribution of the mean line at the design lift coefficient (camber). The design lift coefficient is the lift coefficient at which the flow enters the leading edge of the mean line smoothly. This type of incremental velocity distribution is a function only of the mean-line geometry and can be obtained by the methods of thin-airfoil theory.

(3) The additional type of incremental velocity distribution associated with departure of the angle of attack or lift coefficient from the design conditions (angle). This type of velocity distribution is, according to thin-airfoil theory, independent of airfoil geometry and depends only on this departure of the angle of attack. The additional type of velocity distribution obtained from thin-airfoil theory is of limited practical application, however, because this simple theory leads to infinite values of the velocity at the leading edge. This difficulty, together with the slight dependence of the additional velocity distribution on airfoil

shape, is taken into account by calculating the velocity increments for each symmetrical airfoil by the methods of thick-airfoil theory.

The final pressure distribution at an arbitrary angle of attack is found by summing the three components of velocity: $S = \left(\frac{v}{V} \pm \frac{\Delta v}{V} \pm \frac{\Delta v_a}{V}\right)^2$. The plus sign is used for the upper surface and the minus sign for the lower surface. The final diagram in figure 4 shows the results of summing the various components of the pressure distribution. The short-dash line represents the pressure distribution about the symmetrical airfoil at zero lift. The long-dash line gives the pressure distribution about the cambered airfoil at the design lift coefficient. The solid line gives the pressure distribution about the cambered section at a lift coefficient higher than the design value.

The convenience of this method of calculating the pressure distribution is primarily due to the availability of tabulated values of the necessary component velocity distributions for large numbers of symmetrical airfoils and mean lines. (See reference 7.)

Although the theories just discussed permit the calculation of a number of airfoil characteristics with good accuracy, since they are essentially based on the concept of a perfect fluid, they give no direct information about one of the most important airfoil characteristics, namely, the drag. As will be shown later, however, these theories have proved invaluable in the design of low-drag airfoil sections. Another important characteristic about which no direct theoretical information has been obtained is the maximum lift coefficient. Some discussion of the maximum lift coefficient will be given in a paper by Sivells entitled "Maximum-Lift and Stalling Characteristics of Wings." The present discussion is concerned primarily with the drag.

From 1929 to 1937, extensive experimental investigations were made of families of related airfoil sections in the NACA variable-density wind tunnel. (See references 6 and 12 to 15.) A large amount of information on the drag was accumulated in these investigations. In figure 5 are shown typical drag data at a low lift coefficient for one of the airfoils tested. (See reference 14.) The drag coefficient c_d is plotted as a function of Reynolds number R. The upper line is the drag coefficient for a flat plate with completely turbulent boundary-layer flow. The lower line is the drag coefficient for a flat plate with completely laminar flow. The comparison between the airfoil drag data and the flat-plate skin friction indicates that nearly all the profile drag is attributable to skin friction. Comparisons, such as this, made it apparent that any pronounced reduction of the profile drag must be obtained by a reduction of the skin friction through increasing the relative extent of the laminar boundary layer. Theoretical and experimental work on this problem was begun late in 1937.

The basic requirement for obtaining extensive regions of laminar flow is that the pressure continuously decreases in the direction of flow throughout the region in which laminar flow is expected. This requirement necessitated the development of methods which would permit the design of airfoil sections having specified types of pressure distribution. The method developed consists of a process of successive approximations in which the ordinates and corresponding pressure distribution are calculated with a high degree of accuracy. The pressure-distribution characteristics thus obtained are compared with the characteristics desired. The nature of the Theodorsen relations (shown in fig. 2) for thick airfoils is such that it is not feasible to express the airfoil velocity distribution directly as a function of the airfoil coordinates. There are, however, relatively simple relations between the distortion parameters $(\psi - \psi_0)$ and $(\theta - \phi)$ relating the near and true circles and the airfoil coordinates on one hand, and between these distortion parameters and the airfoil velocity distribution on the other hand. (See reference 5.) The airfoil coordinates and corresponding velocity distribution were, therefore, calculated from assumed values of the distortion parameters. The choice is subject to certain simple conditions that insure closed symmetrical shapes for the basic thickness forms. (See reference 7.) Approximate relations were found by means of which it is possible to modify successively the original choice of parameters so as to yield airfoils having the desired type of velocity distribution. (See references 7 and 16.) Another method of solving this problem has been developed by Goldstein and was described in his recent Wright Brothers lecture. (See reference 17.)

A typical pressure distribution for one of the low-drag airfoils derived is shown in figure 6. It was noted previously that the type of loading resulting from changes in angle of attack tends to make the pressures along one of the airfoil surfaces increase in the direction of flow. Because of the desirability of obtaining low drag over a range of lift coefficient, the magnitude of the favorable pressure gradient over the forward part of the basic thickness form at zero lift should, therefore, be greater than that of the unfavorable gradient corresponding to the additional type of loading throughout a reasonable range of lift coefficient The requirements of a wide low-drag range, good characteristics at high subsonic speeds, and good maximum-lift characteristics are somewhat conflicting. These conflicting requirements place an upper limit on the magnitude of the low-drag range of lift coefficient for which the airfoil should be designed. The optimum form for the pressure distribution is such that at the extremities of the low-drag range of lift coefficient, the pressure gradient on the suction side of the airfoil becomes substantially flat from a point near the leading edge to the original position of minimum pressure. For the airfoil shown in figure 6, this condition exists at a lift coefficient of 0.22. A more complete discussion of the problem of finding the proper type of pressure distribution is given in reference 7.

The desirability of obtaining low drag corresponding to extensive laminar flow at lift coefficients higher than those possible with the basic

thickness form alone indicated the necessity for mean camber lines which would shift the low-drag range to higher values of the lift coefficient, but which would not at the same time decrease the range of lift coefficient for low drag. These requirements define a type of mean line that has, at design conditions, a uniform chordwise distribution of load at least as far back as the position of minimum pressure on the basic thickness form. The method of deriving mean lines to have such prescribed load distributions employs the previously discussed thin-airfoil theory, and is relatively simple compared with the more usual problem of finding the load distribution corresponding to a given mean line.

By the use of the theoretical methods discussed, a large number of related airfoil sections designed for extensive laminar flow were derived. Some method of designating members of this group of airfoils is necessary. The NACA method can be explained by the designation shown in figure 6:

NACA 64_2-015

The first digit is merely a series designation. The second digit gives the position of minimum pressure on the basic thickness form at zero lift in tenths of the chord measured from the leading edge. The subscript gives the range of lift coefficient on either side of the design lift coefficient through which the pressure gradients on both surfaces are favorable for laminar flow. The first digit following the dash gives the design lift coefficient in tenths. (In this case, since the airfoil is symmetrical, the value is 0.) The last two digits give the thickness ratio in percent of the chord.

Approximately 100 of these related airfoils were investigated experimentally. (See reference 7.) In order actually to achieve extensive laminar flow at high Reynolds numbers, it is necessary that the turbulence level of the wind-tunnel air stream be extremely small so as to simulate flight conditions correctly. A description of the development of low-turbulence wind tunnels is given in recent papers by Dryden and Schubauer (reference 18) and Von Doenhoff and Abbott (reference 19).

Some of the results obtained from the experimental investigation of NACA 6-series airfoils are presented in the next few figures. The value of the drag coefficient in the low-drag range for smooth airfoils is mainly a function of the Reynolds number and the relative extent of the laminar layer and is moderately affected by the airfoil thickness ratio and camber. The effect on minimum drag of the position of minimum pressure, which determines the possible extent of laminar flow, is shown in figure 7 for some NACA 6-series airfoils. (See reference 7.) The data show a regular decrease in drag coefficient with rearward movement of minimum pressure. Also shown in this figure is the minimum drag coefficient of the older NACA 2415 airfoil section. Comparison shows that savings in minimum drag of from 20 percent to 50 percent, depending upon the position of minimum pressure, are possible by the use of the newer NACA 6-series airfoils.

The effect of Reynolds number upon the minimum drag of the NACA 65_4-421 airfoil section is illustrated in figure 8. The data show that the drag first decreases with increasing Reynolds number, after which it levels off, then increases, and finally levels off again as the Reynolds number is further increased. The behavior of the minimum drag with increasing Reynolds number can be attributed to the variation in relative strength of two interacting boundary-layer changes. The initial decrease in minimum drag coefficient can be explained by the usual decrease in skin-friction coefficient which accompanies an increase in Reynolds number. After a certain Reynolds number is reached, however, the transition position begins to move forward along the airfoil. The forward movement of transition, of course, decreases the relative extent of low-drag laminar flow on the airfoil, and hence, the drag increases. The Reynolds number range in which the data in the figure show the drag to be relatively constant is a region in which the general decrease in skin friction and forward movement of transition are balanced with respect to their opposite effects upon the drag. The subsequent increase of drag with Reynolds number indicates that forward movement of transition is predominating in this region. The drag ceases to increase when the transition position comes fairly close to the leading edge. The data in the chart for the highest Reynolds number correspond to this condition. Further increases in Reynolds number should cause the drag coefficient to decrease. The scale-effect curve shown in the figure is characteristic of those obtained for NACA 6-series airfoils. The Reynolds number at which the transition position moves forward, however, depends upon the degree to which the pressure gradients on the airfoil are favorable. The Reynolds number at which the different effects occur depends, therefore, upon the detail design of the particular airfoil.

The development of mean lines designed to shift the low-drag range to different values of the lift coefficient has already been discussed. The effect of the addition of camber on the experimental drag polar is shown in figure 9. (See also reference 7.) The solid curve represents the polar for a symmetrical 6-series airfoil section. The "bucket" in the curve is the low-drag range; that is, the range of lift coefficient through which extensive laminar flow is obtained on both surfaces. As shown by the dash-line curve, the primary effect of the addition of camber is to shift the low-drag range. The center of this range corresponds to the design lift coefficient. The width of the low-drag range increases with increasing airfoil thickness ratio.

The results discussed have been obtained from airfoil tests in which the model surfaces were smooth and fair. Unfortunately, the surfaces of airplane wings are oftentimes both rough and unfair. Since laminar flow cannot be maintained at practical values of the Reynolds number unless the airfoil surfaces are aerodynamically smooth, it seemed desirable to investigate the characteristics of NACA 6-series airfoils with surfaces roughened sufficiently near the leading edge that fully developed turbulent layers would exist. Results corresponding to such a surface condition would give the most pessimistic view of what might be expected from

an airplane wing under any conditions short of physical damage or heavy accretions of ice or mud, whereas the results for the smooth condition would correspond to an optimum for which to strive. The effect of roughness on the lift and drag characteristics of a typical NACA 6-series airfoil section is shown in figure 10. (See also reference 7.) It is apparent that the roughness causes large decreases in the maximum lift and large increases in the drag. Similar data from tests of various types of airfoil sections show that the lift and drag characteristics of airfoils of a given thickness ratio are relatively insensitive to the shape of the basic thickness distributions when the leading edges are rough.

The entire discussion so far has been limited to Mach numbers sufficiently low so that the flow could be considered incompressible. As the Mach number is increased, the first-order effects of compressibility are given by the Prandtl-Glauert relation (reference 20) which states essentially that, in two-dimensional flow, the values of all pressure coefficients formed from differences between local static pressure and free-stream static pressure are increased by the relation $\frac{1}{\sqrt{1 - M_0^2}}$, where M_0 is the free-stream Mach number. This means, of course, that the lift-curve slope is theoretically increased by the same factor, thus,

$$\left(\frac{dc_l}{d\alpha}\right)_c = \frac{\left(\frac{dc_l}{d\alpha}\right)_i}{\sqrt{1 - M_0^2}}$$

where the subscript c indicates compressible flow and the subscript i indicates incompressible flow. A comparison of the theoretical and experimental values of the lift-curve slope for an NACA 6-series airfoil section of 10-percent thickness is shown in figure 11. (See also reference 21.) The expression for the first-order effects of compressibility appears to be valid for thin airfoils up to surprisingly high values of the Mach number. A second-order correction developed by Kaplan (reference 22) gives results in better agreement with experiment at high subcritical values of the Mach number. In general, the increase of lift coefficient with Mach number becomes less as the airfoil thickness ratio is increased, and the agreement between theory and experiment for the thicker sections is less satisfactory.

The effect of compressibility on the drag at speeds below the critical is rather difficult to evaluate. This difficulty arises from the fact that most high-speed test equipment is incapable of separating the effect of increasing Reynolds number which accompanies an increase in Mach number. Some indication of the relative importance of the effect of Mach

number on the drag at subcritical speeds, however, may be gained from figure 12. (See also references 23 and 24.) The drag of the NACA 0012-34 airfoil section at zero lift is plotted against Mach number for a range of Reynolds number from 0.34×10^6 to 0.42×10^6 and for a range of Reynolds number from 2.3×10^6 to 4.6×10^6. The large increment in drag between the high- and low-scale data in the subcritical region is of about the magnitude that would be expected for such a change in the Reynolds number. The data for the higher Reynolds number range are in agreement with recent low-speed tests ($M < 0.2$) of a similar airfoil which show a negligible scale effect on the minimum drag between Reynolds numbers of 3.0×10^6 and 6.0×10^6. From this discussion, it would seem that the effect of Reynolds number is far more important at subcritical speeds than the effect of Mach number. Since in any case the pressure drag is a small part of the total drag, it would not be expected that changes in local-pressure coefficients in accordance with the Prandtl-Glauert relation would have any direct effect upon the drag.

The rather brief summary of the status of the airfoil problem just presented indicates that we have a fairly complete understanding of the behavior of airfoil sections at subcritical speeds. The attainment of laminar flow on airplane wings remains a problem because the surfaces of such wings are usually not sufficiently fair and smooth. Methods of reducing the sensitivity of the laminar layer to surface imperfections are now being investigated. The flow phenomena about an airfoil at maximum lift also remain a problem. We have a qualitative understanding of this problem, but research is needed before our ideas can be extended to quantitative calculation.

REFERENCES

1. Munk, Max M.: The Determination of the Angles of Attack of Zero Lift and of Zero Moment, Based on Munk's Integrals. NACA TN No. 122, 1923.

2. Munk, Max M.: Elements of the Wing Section Theory and of the Wing Theory. NACA Rep. No. 191, 1924.

3. Birnbaum, Walter: Die Tragende Wirbelpläche als Hilfsmittel fur Behandlung des ebenen Problems der Tragflügeltheorie. Z.a.M.M., vol. 3, no. 4, Aug. 1923, pp. 290-297.

4. Glauert, H.: The Elements of Aerofoil and Airscrew Theory. Cambridge Univ. Press, 1926.

5. Theodorsen, Theodore: On the Theory of Wing Sections with Particular Reference to the Lift Distribution. NACA Rep. No. 383, 1931.

6. Jacobs, Eastman N., Ward, Kenneth E., and Pinkerton, Robert M.: The Characteristics of 78 Related Airfoil Sections from Tests in the Variable-Density Wind Tunnel. NACA Rep. No. 460, 1933.

7. Abbott, Ira H., Von Doenhoff, Albert E., and Stivers, Louis S., Jr.: Summary of Airfoil Data. NACA Rep. No. 824, 1945.

8. Theodorsen, Theodore: Theory of Wing Sections of Arbitrary Shape. NACA Rep. No. 411, 1931.

9. Theodorsen, T., and Garrick, I. E.: General Potential Theory of Arbitrary Wing Sections. NACA Rep. No. 452, 1933.

10. Pinkerton, Robert M.: Calculated and Measured Pressure Distribution over the Midspan Section of the N.A.C.A. 4412 Airfoil. NACA Rep. No. 563, 1936.

11. Allen, H. Julian: A Simplified Method for the Calculation of Airfoil Pressure Distribution. NACA TN No. 708, 1939.

12. Jacobs, Eastman N., and Pinkerton, Robert M.: Tests in the Variable-Density Wind Tunnel of Related Airfoils Having the Maximum Camber Unusually Far Forward. NACA Rep. No. 537, 1935.

13. Jacobs, Eastman N., Pinkerton, Robert M., and Greenberg, Harry: Tests of Related Forward-Camber Airfoils in the Variable-Density Wind Tunnel. NACA Rep. No. 610, 1937.

14. Jacobs, Eastman N., and Sherman, Albert: Airfoil Section Characteristics as Affected by Variations in the Reynolds Number. NACA Rep. No. 586, 1937.

15. Jacobs, Eastman N., and Abbott, Ira H.: Airfoil Section Data Obtained in the N.A.C.A. Variable-Density Tunnel as Affected by Support Interference and Other Corrections. NACA Rep. No. 669, 1939.

16. Theodorsen, Theodore: Airfoil-Contour Modifications Based on ϵ-Curve Method of Calculating Pressure Distribution. NACA ARR No. L4G05, 1944.

17. Goldstein, Sydney: Low-Drag and Suction Airfoils. Jour. Aero. Sci., vol. 15, no. 4, April 1948, pp. 189-214.

18. Dryden, Hugh L., and Schubauer, G. B.: The Use of Damping Screens for the Reduction of Wind-Tunnel Turbulence. Jour. Aero. Sci., vol. 14, no. 4, April 1947, pp. 221-228.

19. Von Doenhoff, Albert E., and Abbott, Frank T., Jr.: The Langley Two-Dimensional Low-Turbulence Pressure Tunnel. NACA TN No. 1283, 1947.

20. Glauert, H.: The Effect of Compressibility on the Lift of an Aerofoil. R. & M. No. 1135, British A.R.C., 1927.

21. Graham, Donald J.: High-Speed Tests of an Airfoil Section Cambered to Have Critical Mach Numbers Higher Than Those Attainable with a Uniform-Load Mean Line. NACA TN No. 1396, 1947.

22. Kaplan, Carl: The Effect of Compressibility at High Subsonic Velocities on the Lifting Force Acting on an Elliptic Cylinder. NACA TN No. 1118, 1946.

23. Ferri, Antonio: Completed Tabulation in the United States of Tests of 24 Airfoils at High Mach Numbers (Derived from Interrupted Work at Guidonia, Italy, in the 1.31- by 1.74-Foot High-Speed Tunnel). NACA ACR No. L5E21, 1945.

24. Göthert, B.: Hochgeschwindigkeits-Untersuchungen an symmetrischen Profilen mit verschiedenen Dickenverhältnissen im DVL-Hochgeschwindigkeits-Windkanal (2,7 m Durchm.) und Vergleich mit Messungen in anderen Windkanälen. Forschungsbericht Nr. 1506, Deutsche Luftfahrtforschung, 1941.

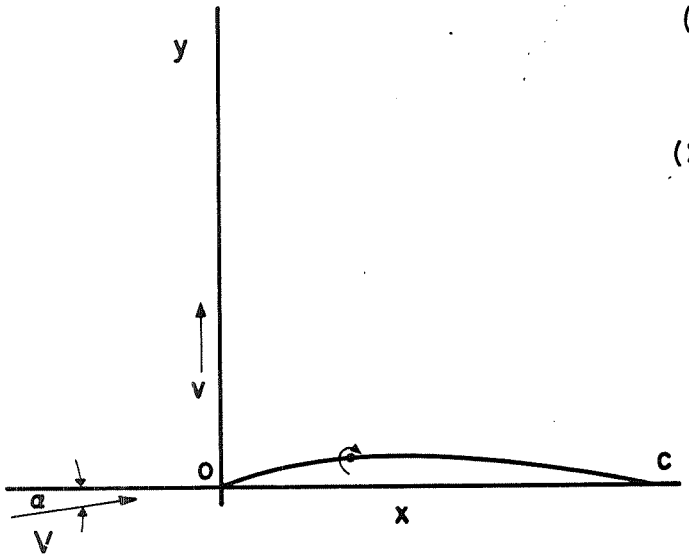

$$(1)\quad \frac{dy}{dx} = \frac{v}{V} - \alpha$$

$$(2)\quad v(x_0) = \int_0^c \frac{\gamma\, dx}{2\pi(x - x_0)}$$

γ = CIRCULATION PER UNIT LENGTH

NACA

Figure 1.- Basic relations of thin-airfoil theory.

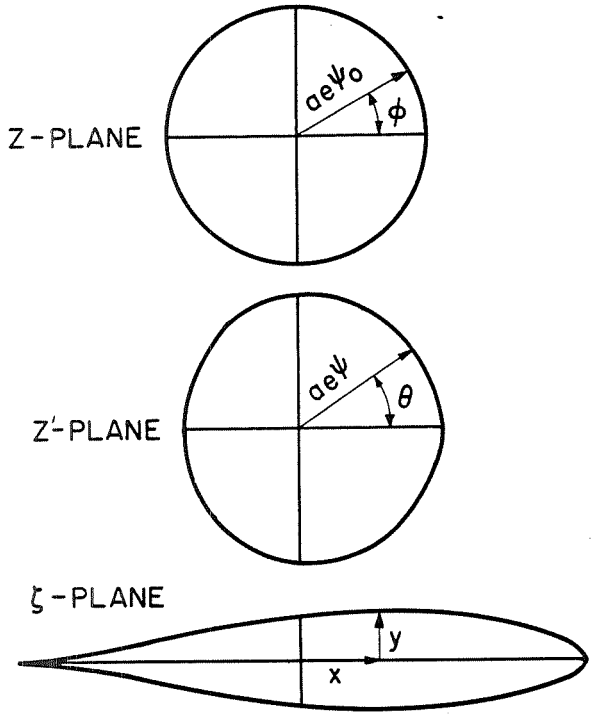

$$Z = ae(\psi_0 + i\phi)$$

$$\frac{Z'}{Z} e[(\psi - \psi_0) + i(\theta - \phi)]$$

$$Z' = ae(\psi + i\theta)$$

$$\zeta = Z' + \frac{a^2}{Z'}$$

NACA

$$\zeta = x + iy$$

Figure 2.- Transformations used to calculate pressure distributions.

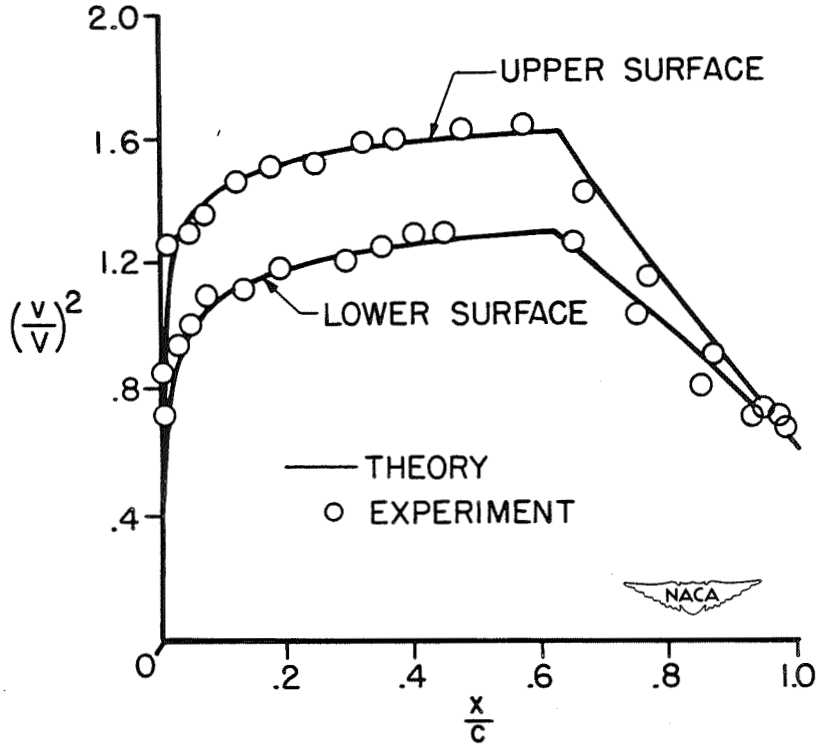

Figure 3.- Comparison of theoretical and experimental pressure distributions.

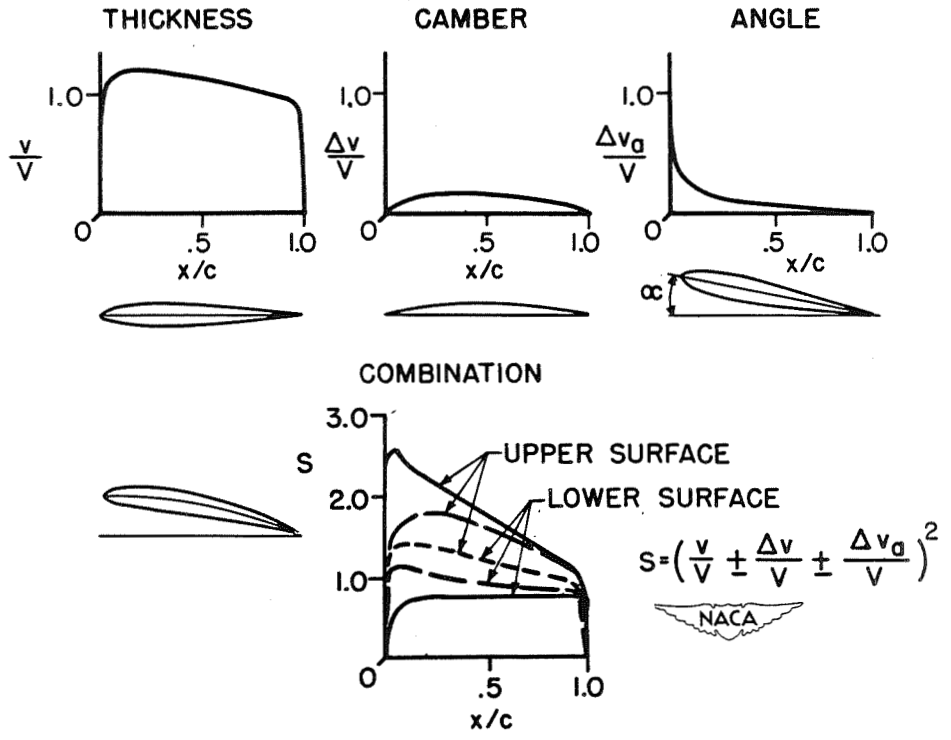

Figure 4.- Synthesis of pressure distribution.

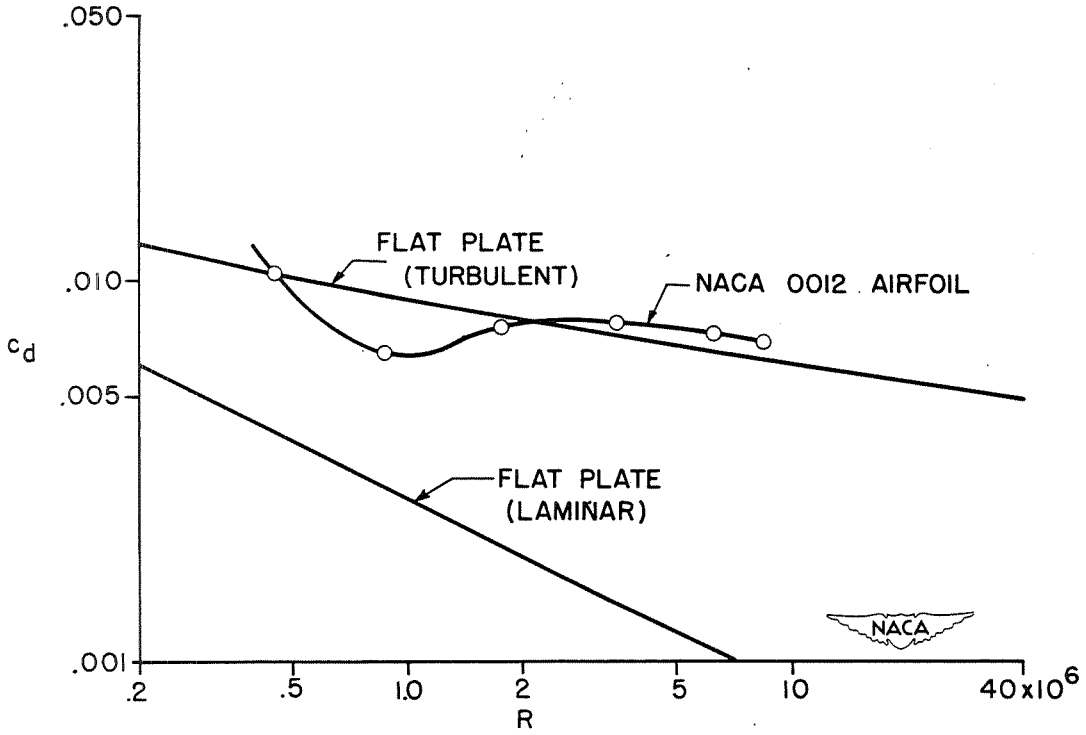

Figure 5.- Section drag coefficient c_d of airfoil and flat plate plotted as function of Reynolds number R.

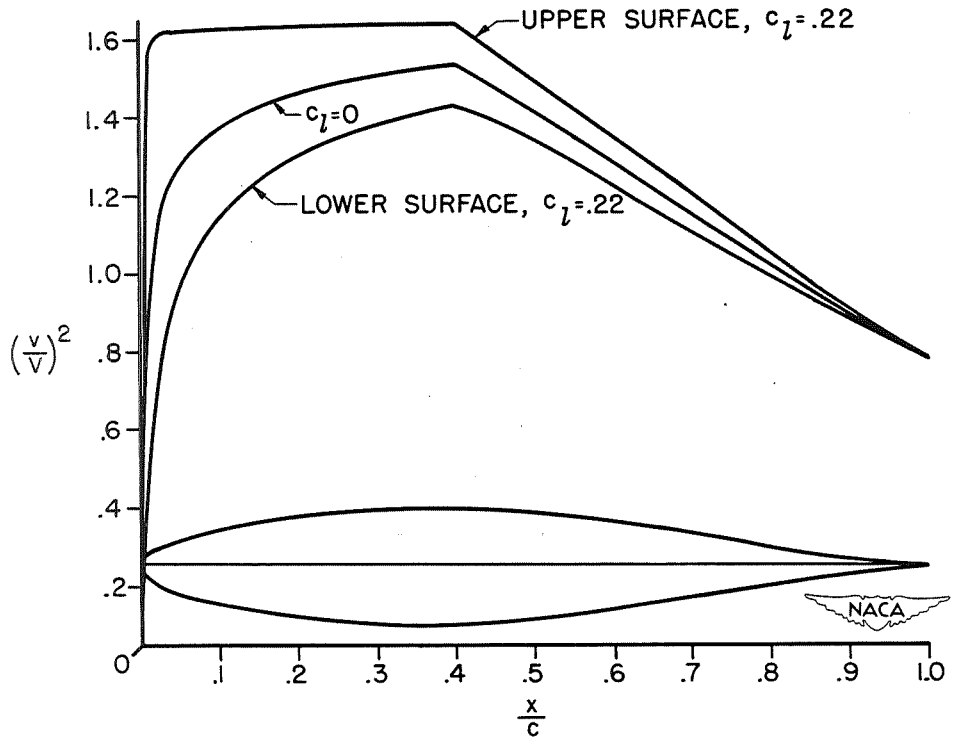

Figure 6.- Pressure distribution for NACA 64_2-015 airfoil section.

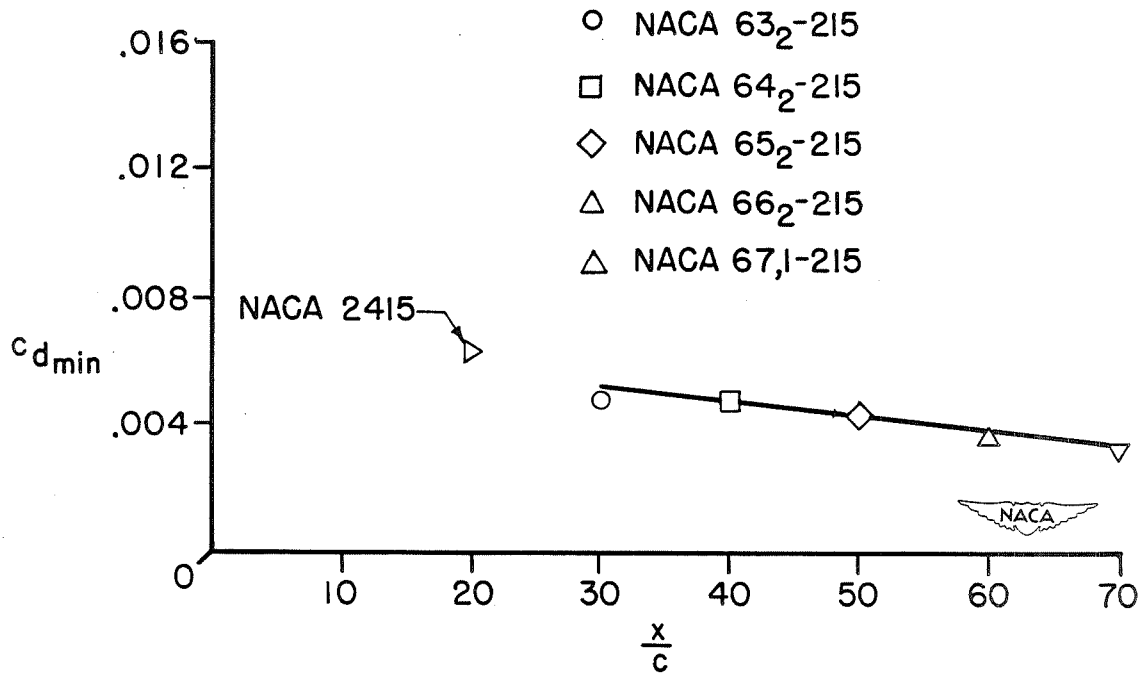

Figure 7.- Variation of minimum drag coefficient $c_{d_{min}}$ with position of minimum pressure x/c.

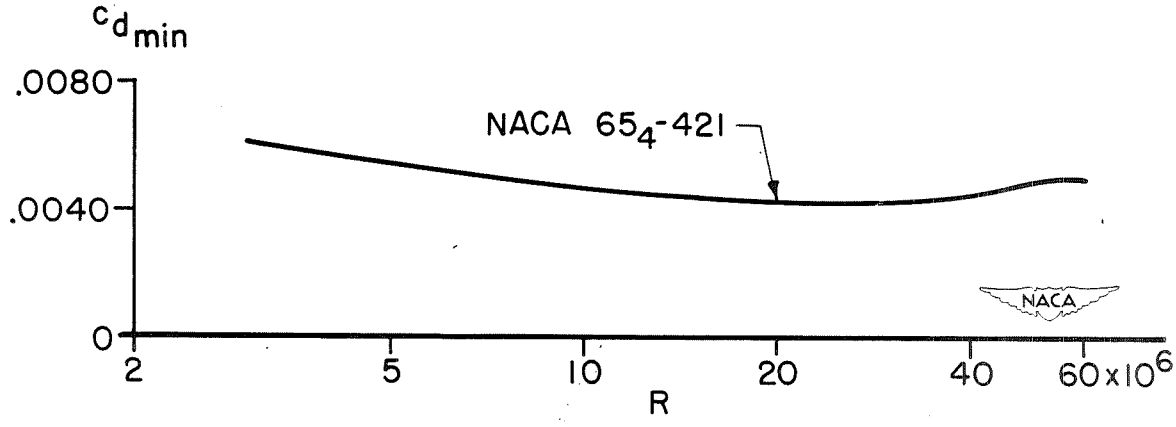

Figure 8.- Effect of Reynolds number on the minimum drag of the NACA 65_4-421 airfoil section.

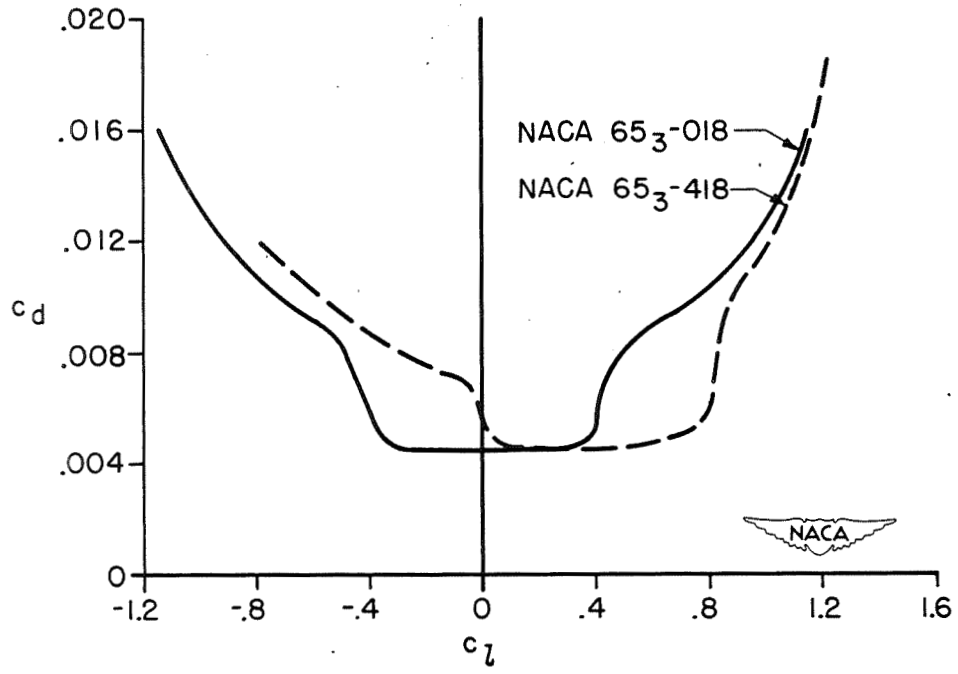

Figure 9.- Effect of camber on the experimental drag polar.

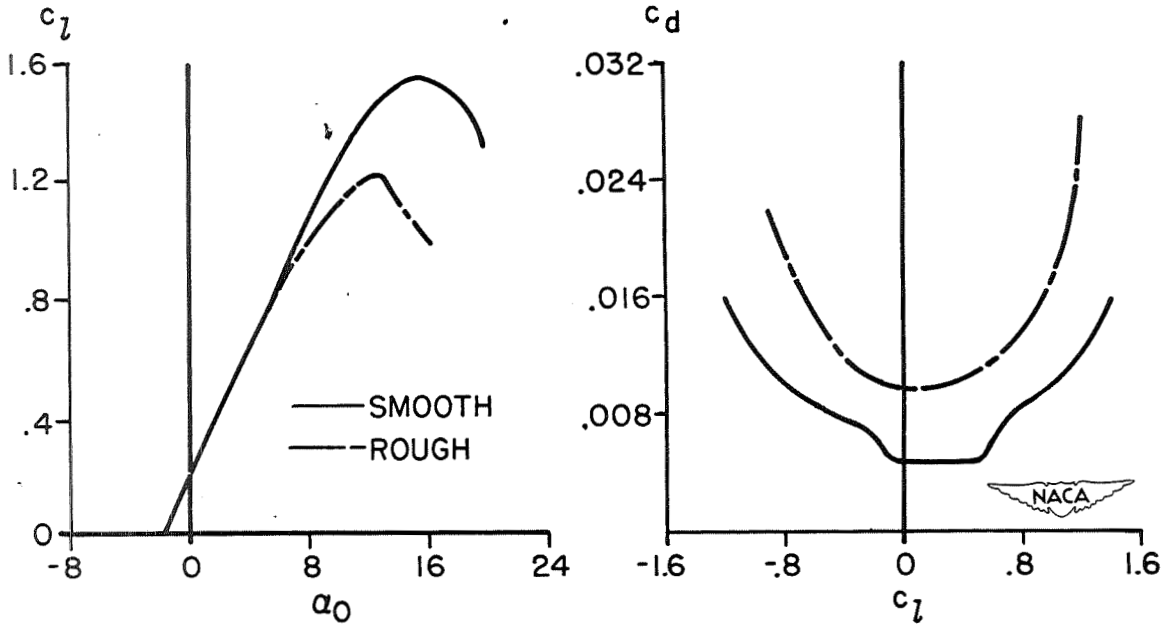

Figure 10.- Effect of roughness on the lift and drag characteristics of a typical NACA 6-series airfoil section.

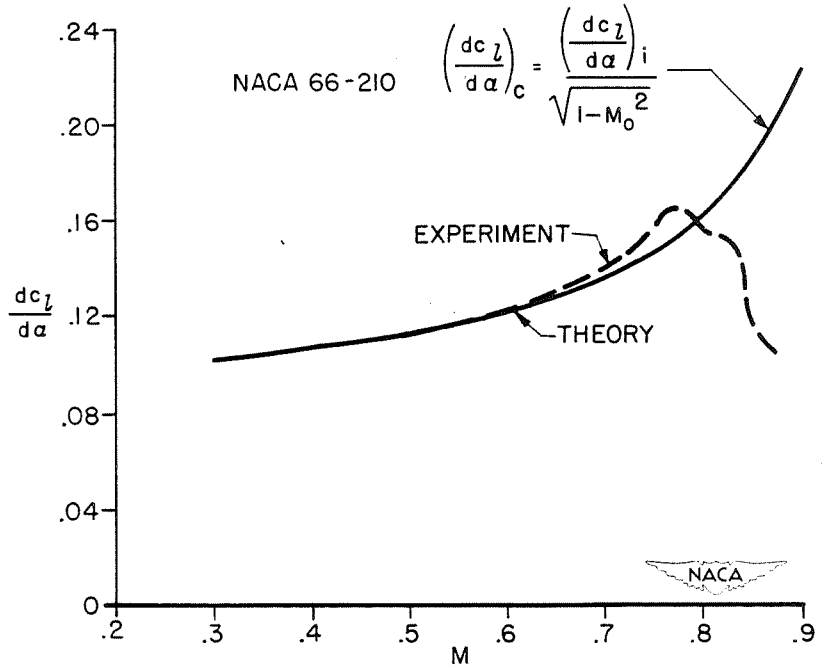

Figure 11.- Comparison of the theoretical and experimental values of the lift-curve slope for an NACA 6-series airfoil section of 10-percent thickness.

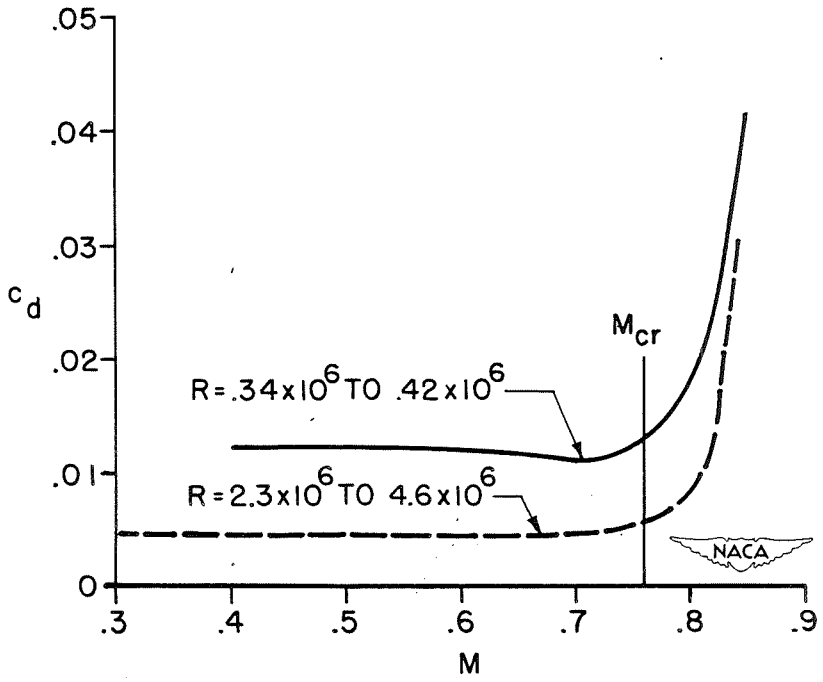

Figure 12.- Effect of Mach number on drag of NACA 0012-34 airfoil section at zero lift.

CHARACTERISTICS OF WING SECTIONS AT TRANSONIC SPEEDS

By John V. Becker

Langley Aeronautical Laboratory

INTRODUCTION

The transonic regime is presumed to begin with the first appearance of a local region of supersonic flow near the airfoil surface and to end when the flow field has become entirely supersonic. The development of theory for transonic flows has been impeded by the coexistence of subsonic and supersonic flow regions and the presence of shock. Shock boundary-layer interaction effects which exert a controlling influence in the transonic region cannot be treated by rigorous theory. The major part of existing knowledge of wing-section behavior at transonic speeds is therefore derived from experimental research, and any review of the current status such as the present one must depend largely on experimental results.

FLOW CHANGES IN THE TRANSONIC REGIME

The progressive changes in flow pattern which occur in the transonic regime are illustrated schematically in figure 1. The diagram at the upper left ($M = 0.70$) represents a condition slightly beyond the critical Mach number (M_{cr} at which sonic velocity is attained locally). A small region of supersonic flow exists, usually terminated by shock. The possibility that local supersonic flows of this type can exist without shock is a matter of considerable speculation. Theoretical studies have indicated that shock-free flows in an ideal fluid are possible in certain special cases. (See references 1 to 4, for example.) From the practical standpoint, however, the important fact is that the presence of shock does not have any seriously adverse effects on airfoil performance unless it precipitates boundary-layer separation.

As the Mach number is increased, the shock moves rearward and the local supersonic region expands rapidly. The rearward movement is analogous to shock behavior in channels, which has been treated theoretically in reference 5. Shock-stall occurs (diagram for $M = 0.90$ in fig. 1) when the adverse pressure gradient through the shock becomes large enough to precipitate separation. Considerable compression of the flow takes place ahead of the main shock (references 6 and 7) as a consequence of thickening of the boundary layer. It is important to note that shock-stall is basically a shock boundary-layer interaction phenomenon and that there is no adequate method for predicting the shock-stall Mach number. "Limiting" or "upper critical" Mach numbers predicted by theories which do not consider shock boundary-layer interaction (references 4 and 8) are at variance with experimental shock-stall Mach numbers.

Rearward movement of the shock continues at speeds beyond shock-stall. When the shock nears the trailing edge, reattachment of the flow takes place, accompanied by an increase in lift coefficient and pressure drag. The flow over the airfoil surface is now predominantly supersonic except for a region near the nose. (See diagram for $M = 0.95$ in fig. 1.)

The diagram for $M = 1.05$ in figure 1 indicates that the nature of the flow at the airfoil surface is similar to that for $M = 0.95$. A bow wave of weak intensity has appeared, marking the forward boundary of the field of influence of the airfoil but having no first-order effect on the airfoil characteristics. The transition from high subsonic to low supersonic speeds has been the subject of recent theoretical studies by Busemann and Guderley (references 9 to 12); no theoretical reasons have been found to prohibit the existence of stable flows at and near sonic velocity, and no abrupt or discontinuous changes in airfoil characteristics are anticipated in traversing sonic velocity.

As the supersonic Mach number advances, the bow wave moves closer to the airfoil nose with an attendant shrinking of the subsonic region near the nose (see diagram for $M = 1.30$ in fig. 1). For sharp-edge sections the region of subsonic flow will disappear entirely at a speed dependent on the angle through which the flow must be deviated (references 13 and 14, for example). Guderley's theoretical work (reference 10) leads to the conclusion that the process of bow-wave attachment is entirely continuous.

Force data for wings throughout the transonic range of speeds have been obtained by the "wing-flow" method both in flight (reference 15) and in the wind tunnel (reference 16). Typical data (reference 16) for a wing of aspect ratio 6.4 and NACA $65_{(112)}$-213 section are presented in figure 2. The results are considered illustrative of transonic wing-section characteristics. It is striking that all the major changes in lift, drag, and moment coefficient take place between $M = 0.75$ and 0.95; the aerodynamic center shifts from 0.25 chord at low speeds to about 0.40 chord at speeds beyond $M = 0.95$; the angle of zero lift changes from a negative low-speed value to a slightly positive value. Reattachment appears to start at $M = 0.90$, becoming complete at $M = 0.95$. These changes are in qualitative accord with theoretical requirements for transition from subsonic-type to supersonic-type flow. The wing performance at $M = 0.95$ is obviously more nearly supersonic than subsonic in character. In fact, the coefficients are in crude agreement with calculated values appropriate to $M = 1.30$, for a sharp-edge cambered wing in pure supersonic flow. It may therefore be reasoned that no first-order changes in performance will appear at speeds beyond $M \approx 0.95$.

Typical changes in pressure distribution in the transonic region are shown in figure 3 for the NACA 23012 section (references 17 and 18). Lift and drag data corresponding to the pressure distributions are given in the upper left diagram. The effect of increasing Mach number on the pressure coefficients at subcritical speeds (compare curves for $M = 0.29$

and $M = 0.59$ in fig. 3) is predictable by approximate theoretical methods. (See reference 3, for example.) The presence of supersonic flow terminated by a strong shock (but no obvious flow separation) is clearly evident in the diagram for $M = 0.74$ in figure 3. In the last diagram in figure 3, for $M = 0.88$, the shocks lie just ahead of the trailing edge. The supersonic character of the flow is illustrated by comparison of the measured pressures with those predicted by supersonic (Prandtl-Meyer) theory applied to the part of the section aft of the sonic point. The shapes of the measured and computed curves are similar although the measured suction pressures are, of course, considerably lower because the depth of the supersonic region is actually finite rather than infinite as assumed by the theory. The development of pressure drag is apparent from the progressive increase of pressure at the nose beyond M_{cr} together with the large decrease of pressure over the rear portion beyond shock-stall.

SYSTEMATIC INVESTIGATION OF SHAPE PARAMETERS AT HIGH SUBSONIC SPEEDS

Wind-tunnel investigations of a large number of related wing sections have been made at speeds up to $M = 0.94$. The succeeding discussion consists of a brief review of the effects of the more important shape parameters as determined from this research.

Thickness ratio.- The transonic characteristics of two symmetrical airfoils differing only in thickness ratio (reference 19) are shown in figure 4. The thinner airfoil has not only a higher shock-stall speed but also smaller undesirable changes in force characteristics after shock-stall. It will be noted that the critical Mach number does not coincide with the speed of shock-stall. In fact, the 6-percent-thick airfoil which has the higher force-break speed and superior supercritical characteristics has the lower critical speed. This result leads to the conclusion that the critical Mach number is useful only to denote the beginning of the transonic region; it does not coincide with the speed of force-break and is no criterion of airfoil behavior beyond the point of force-break.

The values of the drag coefficients at sonic velocity were estimated from wing-flow data (references 15 and 16), the transonic similarity rule (reference 20) being used to correct the available data to the desired thickness ratio. The drags of the two sections at $M = 1.0$ (fig. 4) are about three times and eight times the low-speed values, respectively, for the 6- and 12-percent-thick sections at these Reynolds numbers.

Figure 5 is a plot of minimum drag coefficient against thickness ratio. At subcritical speeds (curve for $M = 0.65$) the drag is not

greatly affected by thickness ratio but, beginning at a speed somewhat below shock–stall, the drag rises steeply with increasing thickness. According to the transonic similarity rule (references 20 and 21) the drag coefficient of a family of thin airfoils differing only in thickness is related to the thickness and Mach number as follows:

$$\frac{M^2 c_d}{(t/c)^{5/3}} = f\left[\frac{M-1}{(t/c)^{2/3}}\right]$$

At $M = 1$ this relation yields

$$c_{d_{M=1.0}} \propto (t/c)^{5/3}$$

Systematic drag data (fig. 5) at the highest speed for which data were obtained in reference 19 ($M = 0.94$) appear to agree with this five–thirds power rule. (The theoretical (dashed) curves of figure 5 were fitted to the test data at $\frac{t}{c} = 0.09$). For cambered sections the agreement is somewhat less satisfactory than for symmetrical sections. In purely supersonic flow the pressure drag varies approximately as the second power of the thickness ratio. Thus, the effect of thickness ratio will probably not change appreciably in the region between sonic speed and the speed at which bow–wave attachment occurs.

Camber.– Figure 6 compares the performance of two sections differing only in camber (reference 22). These sections are modified versions of the NACA four–digit series and are designed to have higher critical speeds than the four–digit series. The significance of the designation numbers can be seen from the following specifications for the cambered section 2,35,12–.55,40:

Maximum camber, percent chord	2
Position of maximum camber, percent chord	35
Maximum thickness, percent chord	12
Leading–edge radius	$0.55c\left(\frac{t}{c}\right)^2$
Position of maximum thickness, percent chord	40

The symmetrical section operating at $c_l = 0.20$ has not only higher force–break Mach numbers but also much smaller undesirable changes in angle of attack and changes in moment after force–break; the change in angle of attack, for example, is only 1.7° for the symmetrical section as compared with 4.5° for the cambered airfoil. A contributing factor to the large trim change of the cambered section is the shift in angle of zero lift inherent in the transition from subsonic–type to supersonic–type flows. (See fig. 2.)

The 0,00,12–.55,40 airfoil of figure 6 is identical with the NACA 0012–34 airfoil of figure 4 except for leading-edge radius. The results shown for the two sections were obtained at Reynolds numbers differing by a factor of about 10. Comparison of the data from the two tests indicates differences which are believed to be attributable primarily to scale effects, although the model-support methods used also differed and some uncertainty exists as to the possibility of tunnel-wall constriction effects, particularly for the 0,00,12–.55,40 data at the highest test speeds. It is important to note, however, that analysis of the data from either of these investigations (reference 19 or 22) leads to the same conclusions regarding optimum shapes.

Further insight into the effects of camber on shock-stall characteristics can be obtained by a study of typical pressure distributions such as those shown in figure 7. When operating at an appreciable lift coefficient, the thin symmetrical section has a high suction peak near the leading edge, while the cambered section chosen for comparison has a flat pressure-distribution diagram. The symmetrical section obviously has the lower critical Mach number of the two, but it is important to note that sonic velocity and shock will first occur near the nose. The cambered section, on the other hand, will develop shock on the rear of the airfoil where the boundary layer is more susceptible to separation. The high-speed lift characteristics of these two sections, which are also shown in figure 7, indicate that shock-stall occurs shortly after the formation of shock on the rear portion of the cambered airfoil. Shock develops at a lower free-stream speed on the symmetrical section but has no deleterious effects on performance until M_{cr} is exceeded by about 0.17. The critical Mach numbers in this figure were obtained from high-speed pressure-distribution data; thus, there is no question involved as to the adequacy of methods of estimating M_{cr} from low-speed data. In spite of its lower critical speed, the symmetrical section has a higher lift-break Mach number than the cambered section for either of the two angles of attack shown in figure 7.

Substantiation of this line of reasoning is obtained from schlieren flow photographs for these two airfoils obtained in the Langley rectangular high-speed tunnel. Figure 8 for the symmetrical section indicates that the main shock is still near the leading edge, even though the critical Mach number has been exceeded by 0.10. There is no evidence of flow separation; measurement of the wake width at the trailing edge indicates the same value as was found for $M = 0.30$. The schlieren photograph for the cambered section (fig. 9) indicates the occurrence of shock just ahead of the trailing edge and the presence of flow separation at a Mach number only 0.05 above the critical. The flow separation was actually observed to start at a Mach number about 0.02 above the critical value. An analysis of the schlieren diagrams of figures 8 and 9 is made in figure 10. A maximum local Mach number of 1.20 was measured for the symmetrical section as compared with 1.11 for the cambered section. It would, therefore, be expected that the shock at the nose of the symmetrical section is considerably more intense than the shock for the cambered section. This difference in shock strength is probably accentuated by the

fact that the boundary layer thickens extensively ahead of the main shock on the cambered airfoil, thereby reducing the local Mach number to a value close to unity just ahead of the shock (reference 23). Flow separation is thus precipitated by a very weak shock when the shock occurs near the rear of the airfoil. This explains the behavior of high-critical-speed and low-drag types of airfoils when operating at lift coefficients near their design values (references 24 to 26). Figure 11 shows the force-break characteristics of the NACA 66-210 airfoil (reference 26) as an example. In the vicinity of design lift the force-breaks occur shortly after the first appearance of shock at M_{cr}. At lift coefficients appreciably higher or lower than the design value, high suction pressure peaks develop at the airfoil nose but the existence of shock in this position does not cause force-break, and the critical Mach number is exceeded by a wide margin before the occurrence of force-break.

A photograph of the flow taken near the Mach number of force-break of the symmetrical NACA 0009-64 section is shown in figure 12. The main shock has moved from the vicinity of the nose to the 0.45-chord position, where it causes an appreciable disturbance of the boundary layer but no extensive flow separation. An analysis of this photograph and comparison with the cambered section is made in figure 13 in which both sections are operating at the same speed, the same geometric angle of attack, and approximately the same lift coefficient prior to force-break. The cambered section again has a weak shock preceded by a maximum Mach number close to unity. As in the previous illustration, appreciable flow separation and force-break have occurred, although the critical Mach number has been exceeded only by 0.05. The symmetrical section, on the other hand, carries a relatively strong shock of about equal depth normal to the airfoil without any evidence of shock stall. The shock losses for the symmetrical section will obviously be high, but no appreciable separation losses are present. The cambered section on the other hand encounters no appreciable shock loss but has a high separation loss. It is therefore difficult to determine from this analysis the relative lift-drag values of the two sections and this question must be answered by force data. An analysis of typical force-test results for related airfoils of varying camber (reference 22) is shown in figure 14. The camber in percent of chord which resulted in the maximum lift-drag ratio is plotted against Mach number for various operating lift coefficients. At low speed appreciable camber is desirable, but the optimum camber is seen to decrease as the Mach number increases. When the critical Mach number is exceeded, the optimum amount of camber drops rapidly to zero. For the 12-percent-thick sections used in the illustration, the symmetrical section has the best lift-drag ratios at all Mach numbers beyond 0.76 for all the lift coefficients tested. An NACA investigation of 16-series sections of various camber (reference 24) revealed a similar trend of decreasing optimum camber with increasing Mach number. Previous discussion of figure 6 revealed that symmetrical sections are desirable for transonic applications from consideration of trim and moment changes as well as from consideration of best lift-drag ratio.

Trailing-edge angle.- Virtually no information is available showing the effect of trailing-edge angle as an isolated variable. If the angle is large, the flow is subject to separation at transonic speeds which results in high drag, low lift-curve slope, and poor control-surface effectiveness (references 27 to 29). The maximum recommended values for trailing-edge angle lie in the range of 10° to 15°; smaller values are preferable.

Positions of maximum thickness.- Test data bearing on the optimum position of maximum thickness for symmetrical sections are given in references 19 and 30. The best location appears to lie between 0.4 chord and 0.5 chord.

Leading-edge radius.- At lift coefficients near zero (say, less than 0.1) the value of the leading-edge radius is not critical for symmetrical sections at high subsonic speeds (reference 31). At higher lifts the best lift-drag ratio is obtained with a leading-edge radius of about one-half the value used in the NACA four-digit series. The radii used on the NACA 16-series and 6-series airfoils are near the optimum value. The leading edge should be sharp in supersonic flow if the speed is high enough to permit bow-wave attachment (reference 32), in order to avoid the relatively high shock losses occurring near the apex of a detached bow wave. If, however, the supersonic Mach number is so low that an attached shock is not possible even if the leading edge is sharp (reference 14), then there is no reason to believe that sections having a small leading-edge radius will have inferior characteristics to comparable sharp-edge sections.

The behavior of sharp-edge supersonic-type sections has been the subject of a recent investigation at high subsonic speeds (reference 33). An unexpected phenomenon was discovered which is illustrated in figures 15 and 16. At all speeds up to $M = 0.75$ the anticipated extensive region of separated flow starting at the sharp leading edge was present as depicted in figure 15. Local supersonic velocities terminated by shock are present over the forward part of the section outside of the region of flow separation. The separated flow vanished abruptly when the Mach number was increased by 0.02 to $M = 0.77$ (fig. 16). The ability of the flow to negotiate the sharp edge is explained by the fact that the local velocity field in the vicinity of the leading edge is supersonic (reference 34). A small bubble of separation is present immediately behind the corner. In expanding about this bubble the flow is directed towards the surface, giving rise to the oblique compression shock. The origin of the foremost oblique disturbance apparent in figure 16 is uncertain. It is believed, however, that since the disturbance disappears at some distance above the airfoil it does not have any major effect on the reattachment phenomenon.

This reattachment of the flow is accompanied by an increase in lift and, in a majority of cases, little change in drag. The increased pressure drag after attachment tends to offset the reduction of separation

losses. It is important to note that, although the lift–drag ratio is increased by this phenomenon, the lift–drag ratios reached are not as high as are obtainable with round–edge sections at the same speeds (reference 33).

OPTIMUM SHAPES FOR LOW SUPERSONIC SPEED RANGE

The high–subsonic test data utilized in the foregoing discussion point towards an optimum section shape for the high–subsonic speed range which has no camber, a maximum–thickness position near the midchord point, as small values as possible of the thickness and trailing–edge angle, and a small but finite leading–edge radius. With the exception of the leading–edge radius, these specifications closely approach the theoretical requirements for an optimum section in purely supersonic flow at low supersonic speeds. There is little reason to suspect that a sharp leading edge would prove more desirable than a small rounded edge in the transonic speed range where a detached bow wave would occur with either shape. It may be conjectured, therefore, that the airfoil shape which is optimum for high–subsonic speeds will also have the best characteristics in the supersonic part of the transonic regime. It is obvious, however, that further research is needed to establish the details of airfoil performance at low supersonic speeds.

PROFILES SUITABLE FOR TRANSONIC APPLICATIONS

The following symmetrical profiles meet the approximate specifications for optimum shape discussed in the preceding sections of this paper:

NACA 0009–44	(see reference 35)
NACA 65–009	(see reference 36)
NACA 65A–009	(see reference 37)

The latter two sections could be made thicker than 9 percent without exceeding the arbitrary limit imposed on the trailing–edge angle (15°). The use of thicker sections, however, is usually prohibitive for transonic applications from consideration of power requirements as well as adverse trim and moment changes. Obviously, thinner sections having the same thickness distribution as the above profiles will also meet the approximate optimum shape requirements.

REFERENCES

1. Taylor, G. I.: The Flow of Air at High Speeds past Curved Surfaces. R. & M. No. 1381, British A.R.C., 1930.

2. Ringleb, Friedrich: Exakte Lösungen der Differentialgleichungen einer adiabatischen Gasströmung. Z.f.a.M.M., Bd. 20, Heft. 4, Aug. 1940, pp. 185–198.

3. Von Kármán, Th.: Compressibility Effects in Aerodynamics. Jour. Aero. Sci., vol. 8, no. 9, July 1941, pp. 337–356.

4. Kaplan, Carl: The Flow of a Compressible Fluid past a Curved Surface. NACA Rep. No. 768, 1943.

5. Stodola, A.: Steam and Gas Turbines. Vol. I. McGraw-Hill Book Co., Inc., 1927.

6. Ackeret, J., Feldmann, F., and Rott, N.: Investigations of Compression Shocks and Boundary Layers in Gases Moving at High Speed. NACA TM No. 1113, 1947.

7. Liepmann, Hans Wolfgang: The Interaction between Boundary Layer and Shock Waves in Transonic Flow. Jour. Aero. Sci., vol. 13, no. 12, Dec. 1946, pp. 623–638.

8. Greene, Leonard Michael: The Attenuation Method for Compressible Flow Systems. Jour. Aero. Sci., vol. 12, no. 3, July 1945, pp. 329–338.

9. Busemann, A., and Guderley, G.: The Problem of Drag at High Subsonic Speeds. Reps. and Translations No. 184, British M.O.S.(A) Völkenrode, March 1947. (Wright Field translation F-TS-3492-RE in preparation.)

10. Guderley, G.: Considerations of the Structure of Mixed Subsonic–Supersonic Flow Patterns. Tech. Rep. No. F-TR-2168-ND, Air Materiel Command (Wright Field), Oct. 1947.

11. Guderley, G.: On the Transition from a Transonic Potential Flow to a Flow with Shocks. Tech. Rep. No. F-TR-2160-ND, Air Materiel Command (Wright Field), Aug. 1947.

12. Guderley, G.: Singularities at the Sonic Velocity. Tech. Rep. No. F-TR-1171-ND, Air Materiel Command (Wright Field), Nov. 1947. (Preprint.)

13. Crocco, Luigi: Singolarità della corrente gassosa imperacustica nell'intorno di una prora a diedro. L'Aerotecnica, vol. XVII, fasc. 6, June 1937, pp. 519–534.

14. Burcher, Marie A.: Compressible Flow Tables for Air. NACA TN No. 1592, 1948.

15. Gilruth, R. R., and Wetmore, J. W.: Preliminary Tests of Several Airfoil Models in the Transonic Speed Range. NACA ACR No. L5E08, 1945.

16. Weaver, John H.: A Method of Wind–Tunnel Testing through the Transonic Range. Jour. Aero. Sci., vol. 15, no. 1, Jan. 1948, pp. 28–34.

17. Göthert, B.: Druckverteilungsschaubilder für das Profil NACA 230–12 bei hohen Unterschallgeschwindigkeiten. UM Nr. 1260/2, Deutsche Luftfahrtforschung (Berlin–Adlershof), 1944.

18. Göthert, B.: Hochgeschwindigkeitsmessungen an Profilen der Reihe NACA 230 mit verschiedenen Dickenverhältnissen. UM Nr. 1259/2, Deutsche Luftfahrtforschung (Berlin–Adlershof), 1944.

19. Ferri, Antonio: Completed Tabulation in the United States of Tests of 24 Airfoils at High Mach Numbers (Derived from Interrupted Work at Guidonia, Italy, in the 1.31– by 1.74–Foot High–Speed Tunnel). NACA ACR No. L5E21, 1945.

20. Von Kármán, Theodore: The Similarity Law of Transonic Flow. Jour. Math. and Phys., vol. XXVI, no. 3, Oct. 1947, pp. 182–190.

21. Kaplan, Carl: On Similarity Rules for Transonic Flow. NACA TN No. 1527, 1948.

22. Göthert, B.: Hochgeschwindigkeitsmessungen an Profilen gleicher Dickenverteilung mit verschiedener Krümmung im DVL–Hochgeschwindigkeitswindkanal (2.7m Durchm.) FB Nr. 1910, Deutsche Luftfahrtforschung (Berlin–Adlershof), 1944.

23. Stack, John: Compressible Flows in Aeronautics. Jour. Aero. Sci., vol. 12, no. 2, April 1945, pp. 127–143.

24. Lindsey, W. F., Stevenson, D. B., and Daley, Bernard N.: Aerodynamic Characteristics of 24 NACA 16–Series Airfoils at Mach Numbers between 0.3 and 0.8. NACA TN No. 1546, 1948.

25. Anderson, Joseph L.: Tests of NACA 65(216)–420 and 66(218)–420 Airfoils at High Speeds. NACA MR, April 1944.

26. Graham, Donald J.: High-Speed Tests of an Airfoil Section Cambered to Have Critical Mach Numbers Higher Than Those Attainable with a Uniform-Load Mean Line. NACA TN No. 1396, 1947.

27. Stevenson, David B., and Bryne, Robert W.: High-Speed Wind-Tunnel Tests of an NACA 16-009 Airfoil Having a 32.9-Percent-Chord Flap with an Overhang of 20.7 Percent of the Flap Chord. NACA TN No. 1406, 1947.

28. Stevenson, David B., and Adler, Alfred A.: High-Speed Wind-Tunnel Tests of an NACA 0009-64 Airfoil Having a 33.4-Percent-Chord Flap with an Overhang 20.1 Percent of the Flap Chord. NACA TN No. 1417, 1947.

29. Lindsey, W. F.: Effect of Compressibility on the Pressures and Forces Acting on a Modified NACA 65,3-019 Airfoil Having a 0.20-Chord Flap. NACA ACR No. L5G31a, 1946.

30. Göthert, B.: Hochgeschwindigkeits-Untersuchungen an symmetrischen Profilen mit verschiedenen Dickenverhältnissen im DVL-Hochgeschwindigkeitswindkanal (2.7m Durchm.) und Vergleich mit Messungen in anderen Windkanälen. FB Nr. 1506, Deutsche Luftfahrtforschung (Berlin-Adlershof), 1941.

31. Göthert, B.: Widerstandsanstieg bei Profilen im Bereich hoher Unterschallgeschwindigkeiten. Tech. Berichte, Bd. II, Teil 7, 1944.

32. Busemann, A., and Walchner, O.: Profileigenschaften bei Überschallgeschwindigkeit. Forsch. auf dem Geb. des Ingenieurw. Ausg. A; Bd. 4, Heft 2, March/April 1933, pp. 87-92.

33. Lindsey, W. F., Daley, Bernard N., and Humphreys, Milton D.: The Flow and Force Characteristics of Supersonic Airfoils at High Subsonic Speeds. NACA TN No. 1211, 1947.

34. Stack, John: Shock Stalled Flows for Supersonic Type Airfoils at Transonic Speeds. Paper presented at 6th Int. Cong. Appl. Mech. (Paris), Sept. 22-29, 1946.

35. Stack, John, and Von Doenhoff, Albert E.: Tests of 16 Related Airfoils at High Speeds. NACA Rep. No. 492, 1934.

36. Abbott, Ira H., Von Doenhoff, Albert E., and Stivers, Louis S., Jr.: Summary of Airfoil Data. NACA Rep. No. 824, 1945.

37. Loftin, Laurence K., Jr.: Theoretical and Experimental Data for NACA 6A-Series Airfoil Sections. NACA TN No. 1368, 1947.

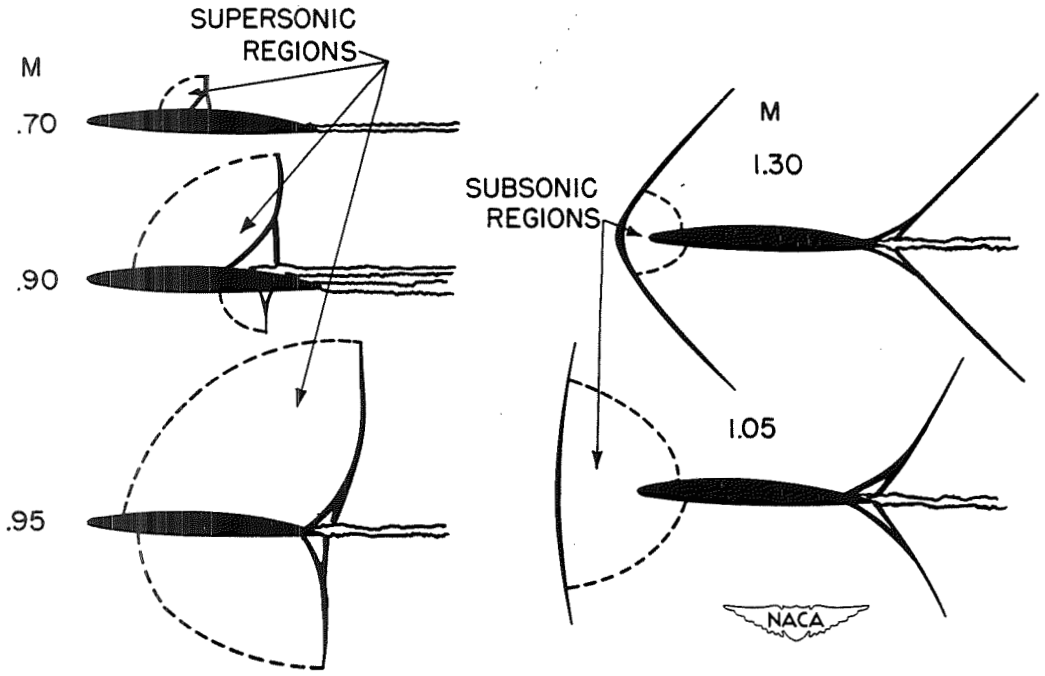

Figure 1.- Transonic flow patterns.

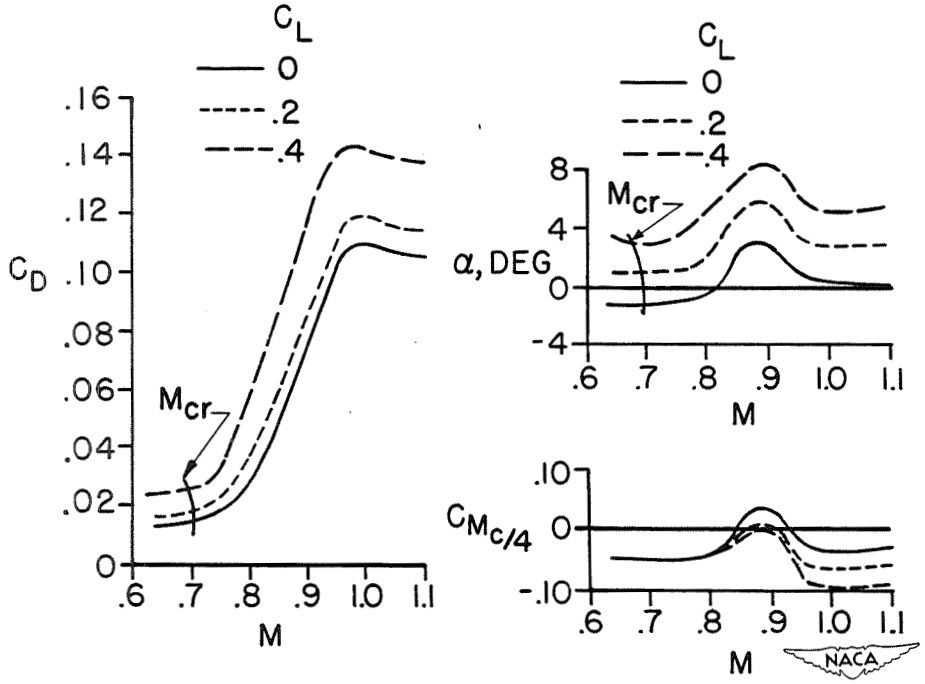

Figure 2.- Transonic force data for a typical wing. NACA $65_{(112)}$-213, a = 0.5 airfoil; aspect ratio, 6.4.

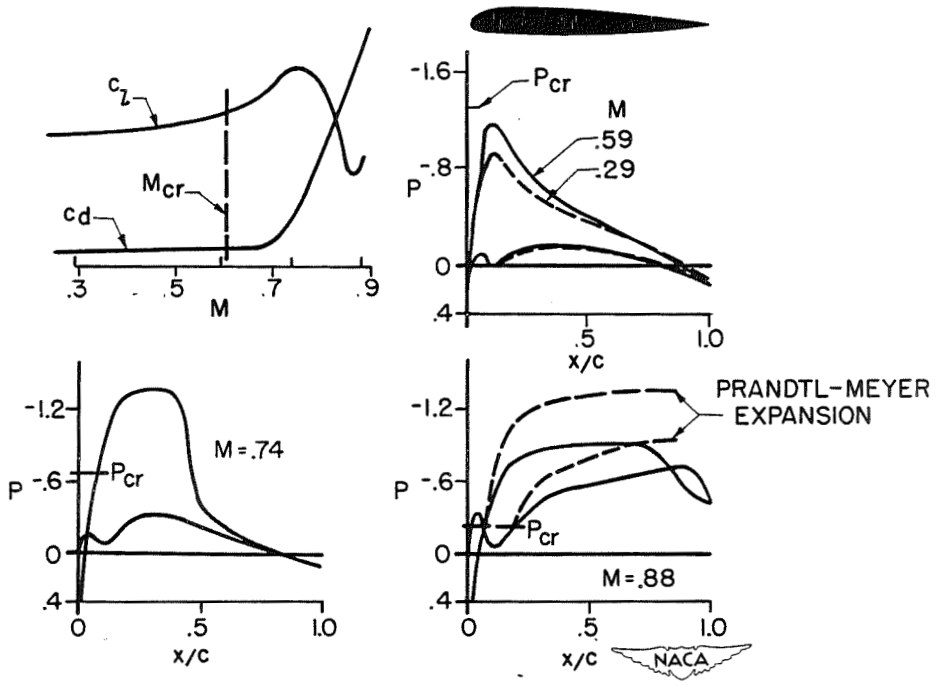

Figure 3.- Typical pressure-distribution data. NACA 23012 airfoil; $\alpha = 1.6^{\circ}$.

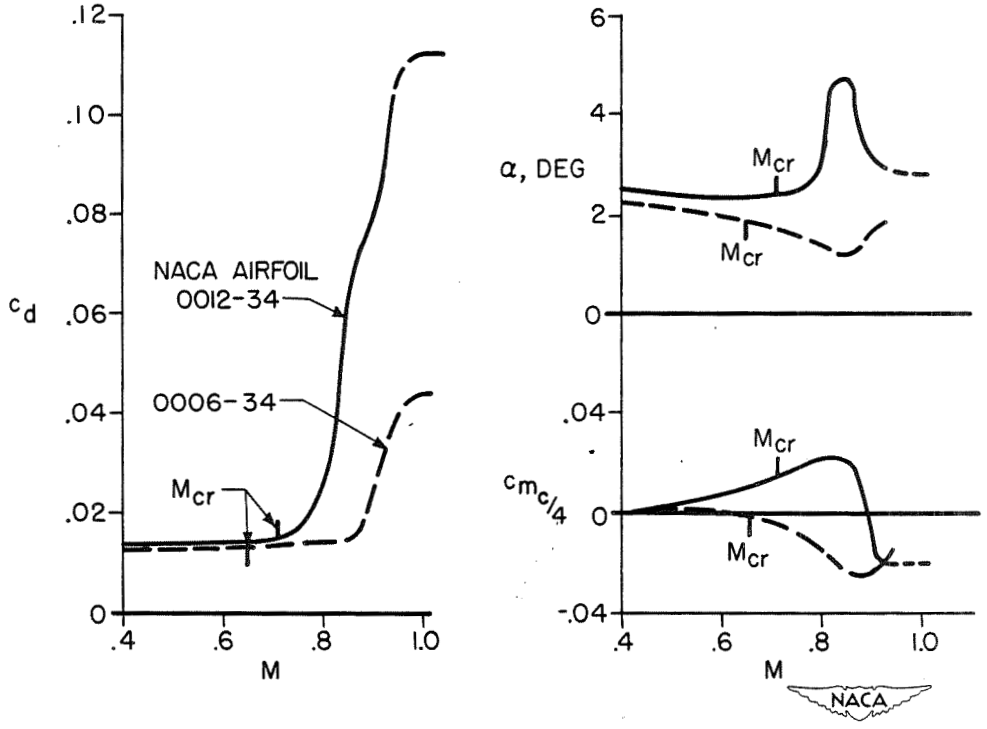

Figure 4.- Effects of thickness ratio. $c_l = 0.20$; $R \approx 0.4 \times 10^6$.

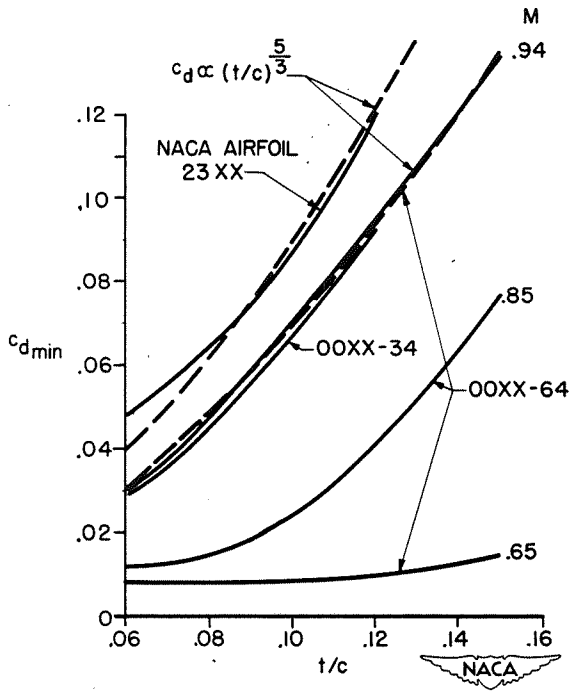

Figure 5.- Effect of thickness ratio on minimum drag.

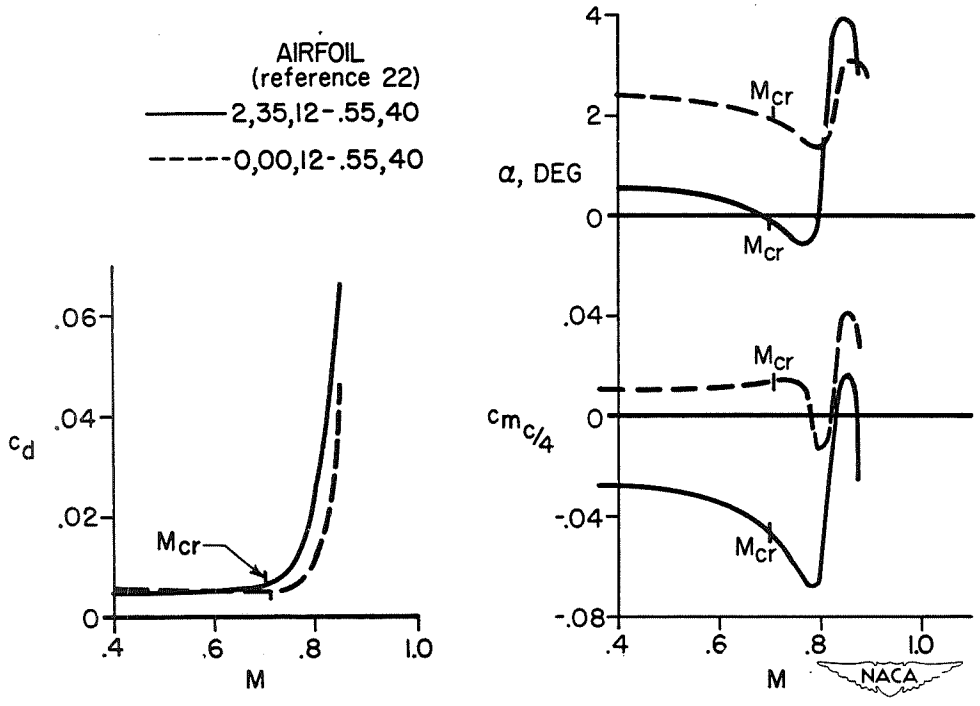

Figure 6.- Effects of camber. $c_l = 0.20$; $R \approx 4 \times 10^6$.

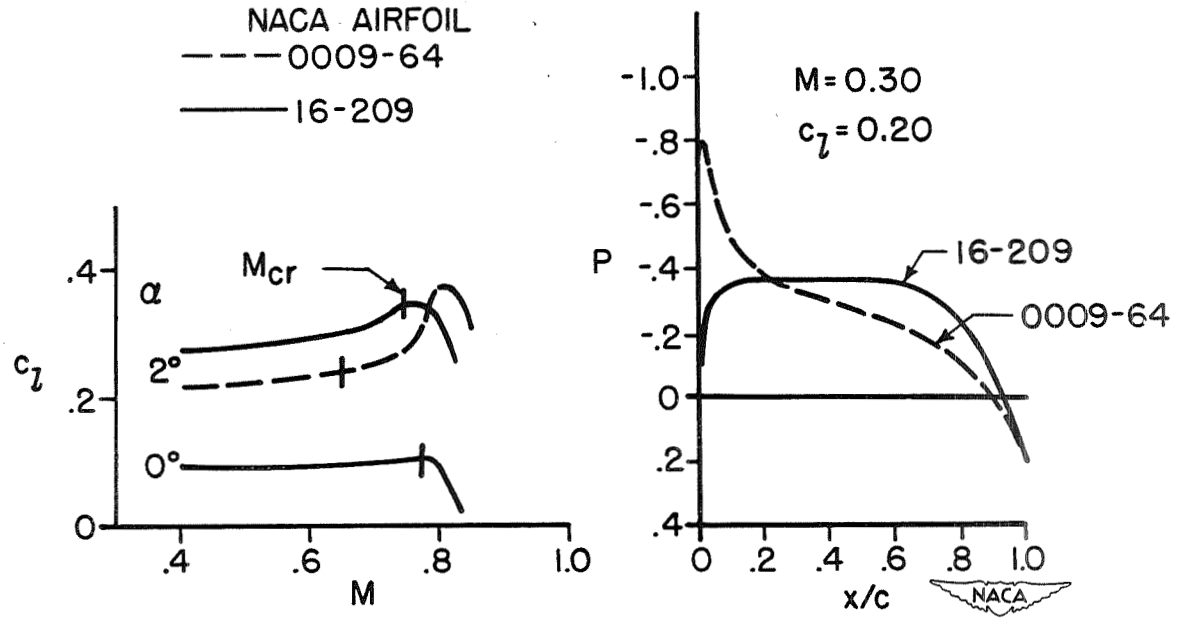

Figure 7.- Effects of camber on lift and upper-surface pressure-distribution characteristics of thin sections.

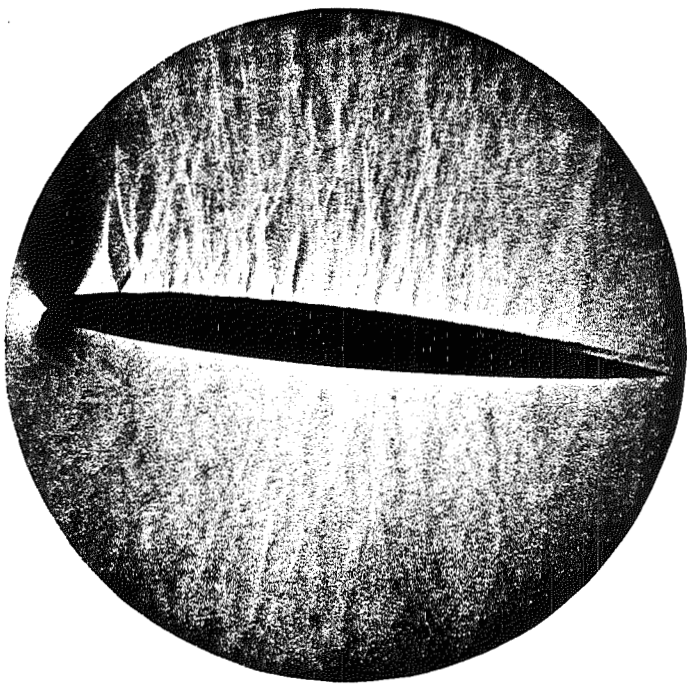

Figure 8.- Schlieren flow photograph of NACA 0009-64 airfoil. $\alpha = 2^{\circ}$; $M = 0.75 = M_{cr} + 0.10$.

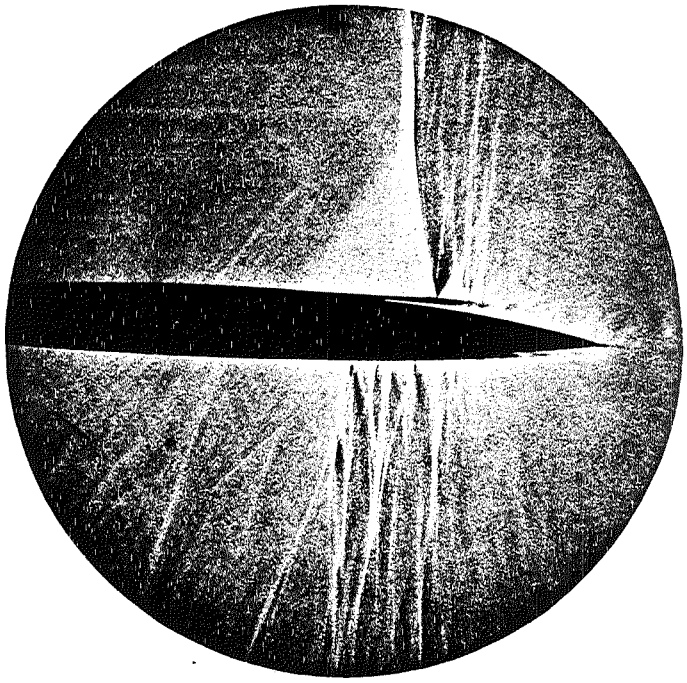

NACA

Figure 9.- Schlieren flow photograph of NACA 16-209 airfoil. $\alpha = 0^{\circ}$; $M = 0.83 = M_{cr} + 0.05$.

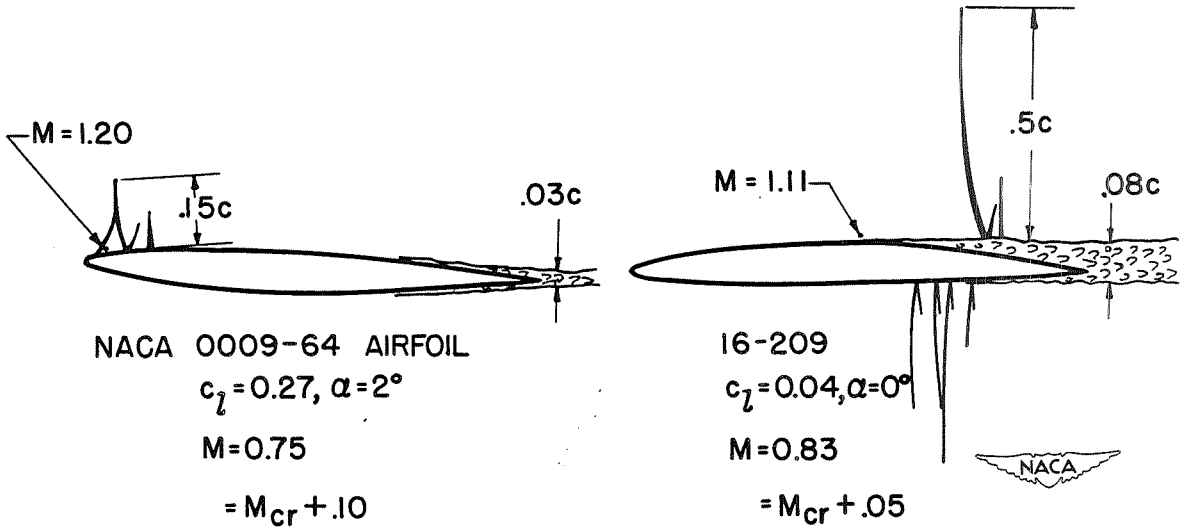

Figure 10.- Analysis of flow photographs (figs. 8 and 9).

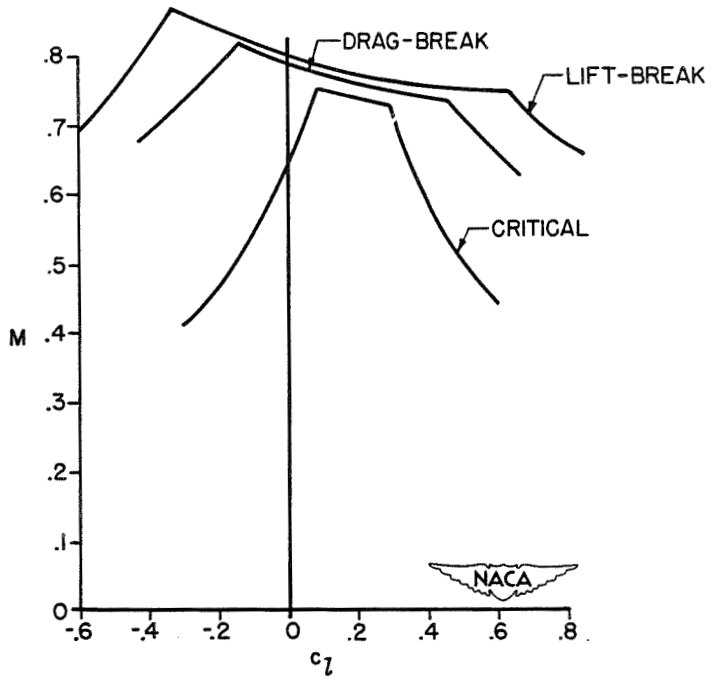

Figure 11.- Critical and force-break Mach numbers for an NACA 66-210 airfoil.

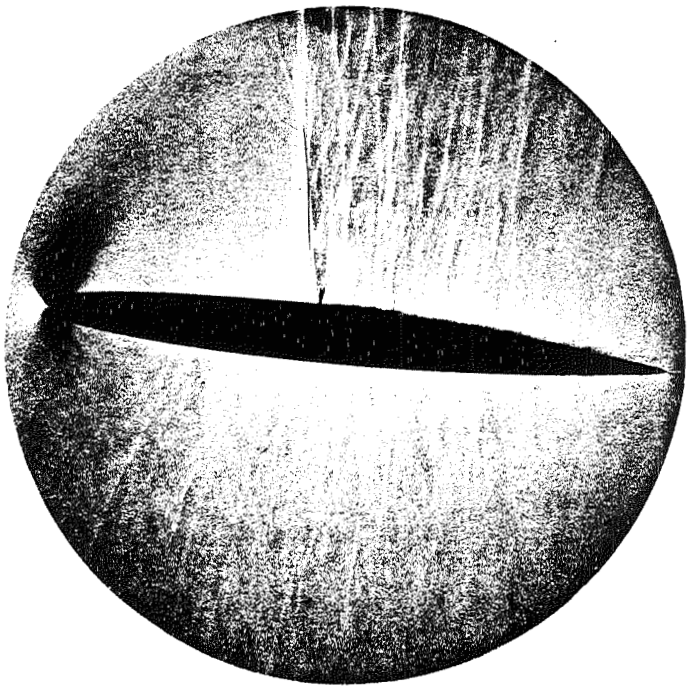

Figure 12.- Schlieren flow photograph of NACA 0009-64 airfoil. $\alpha = 2^{\circ}$; $M = 0.80 = M_{cr} + 0.15$.

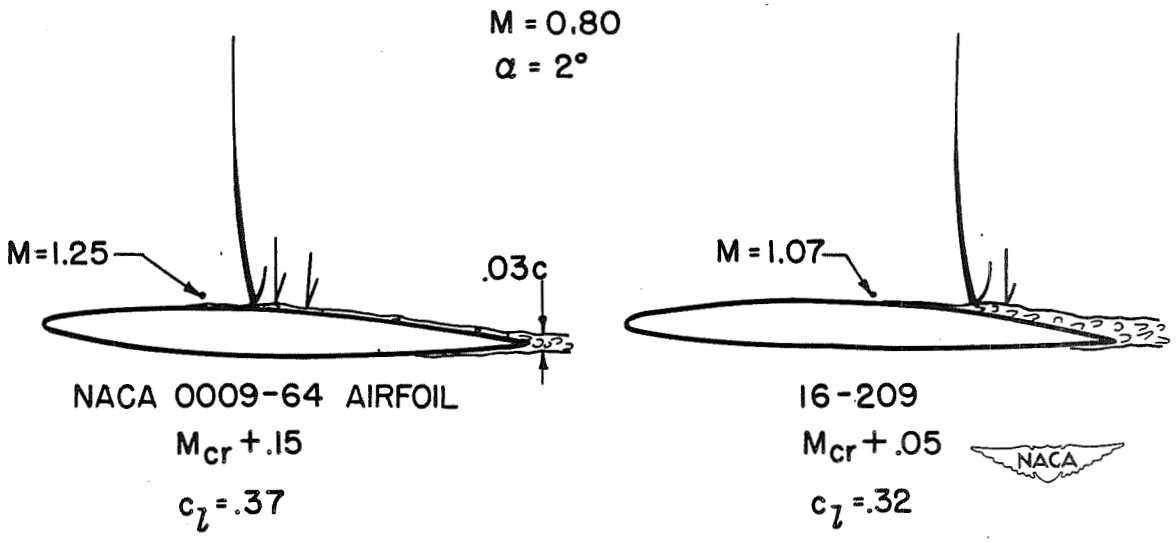

Figure 13.- Analysis of flow photograph for NACA 0009-64 airfoil (fig. 12) and comparison with NACA 16-209 airfoil.

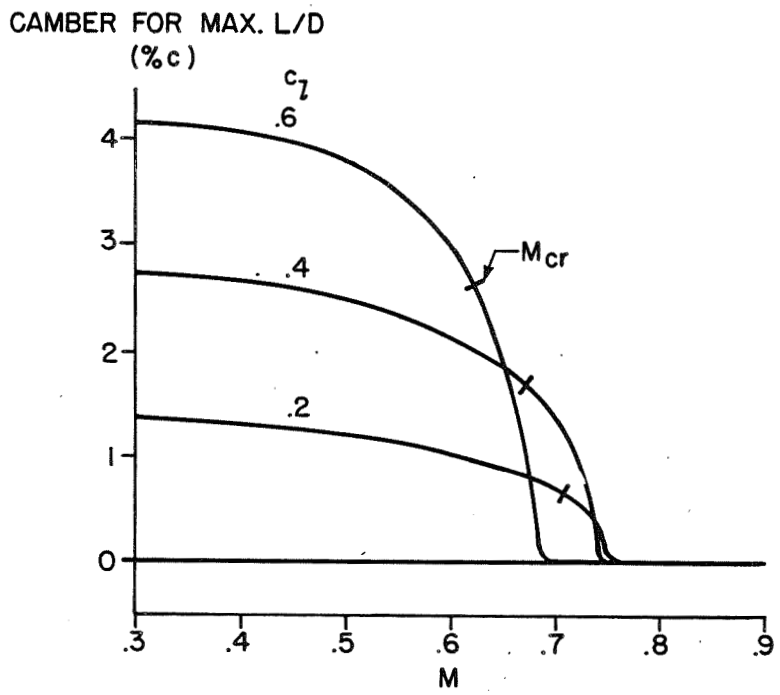

Figure 14.- Effect of Mach number on optimum camber. X,35,12-.55,40 airfoils (reference 22).

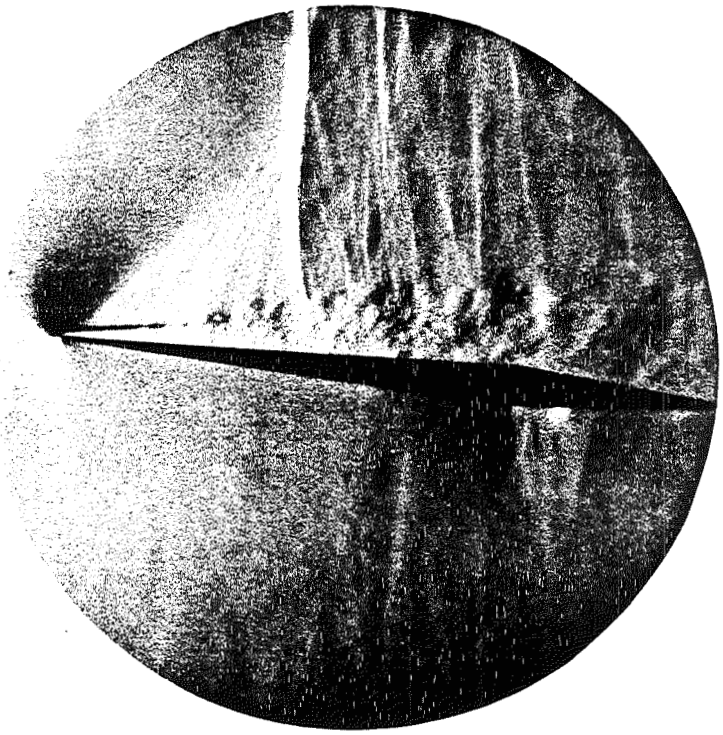

Figure 15.- Schlieren flow photograph of NACA 1S-(70)(03)(70)(03) airfoil. $\alpha = 5.5^{\circ}$; M = 0.75.

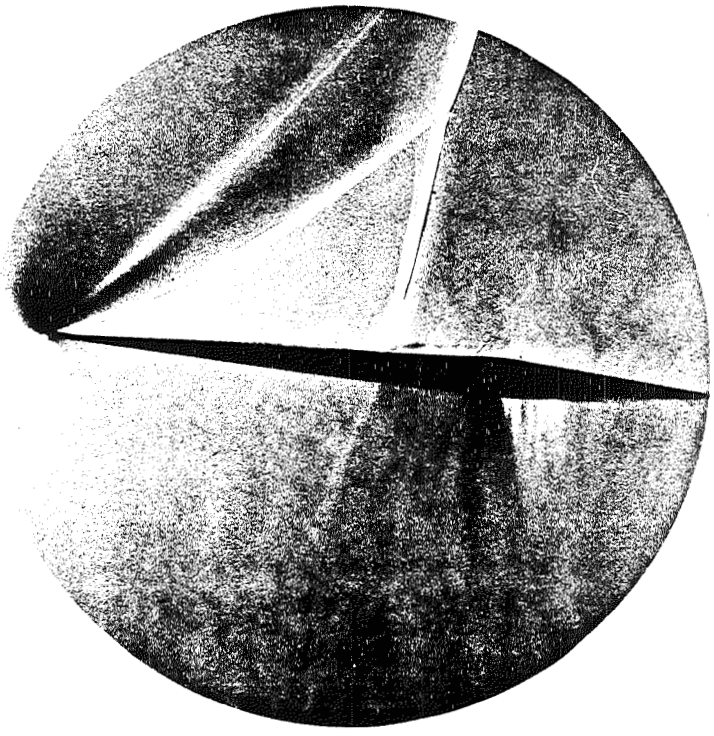

Figure 16.- Schlieren flow photograph of NACA 1S-(70)(03)(70)(03) airfoil. $\alpha = 5.5^{\circ}$; M = 0.77.

D7

Preceding page blank

PREDICTION OF WING CHARACTERISTICS

By Thomas A. Toll and Franklin W. Diederich

Langley Aeronautical Laboratory

INTRODUCTION

The problem of the prediction of wing characteristics is not necessarily restricted to the characteristics of the main lifting wing of an airplane. The characteristics of tail surfaces and of movable controls usually are also included since the factors that influence such characteristics are very similar to the factors that influence the characteristics of the main lifting wing. The general problem, therefore, is very broad and the number of aerodynamic quantities that need to be evaluated is considerable. Some of the important quantities are the lift, drag, and aerodynamic center, corresponding to various attitudes of the wing, the distribution of lift over the wing surface, the various forces and moments that affect the stability of the wing under dynamic flight conditions, the effectiveness of tail surfaces or of controls, and the aerodynamic forces that must be overcome in order to operate the controls. The present discussion is concerned with the various theoretical and empirical processes that have been found suitable for use in evaluating such quantities at flight speeds below the critical Mach number.

DISCUSSION

In order to evaluate the desired quantities, the theory of wing sections must be either supplemented or replaced by a theory of finite-span wings. In many instances, the desired quantities bear only a secondary relationship to the characteristics of wing sections. An example is the spanwise distribution of wing loading, which is influenced largely by the flow about the wing tips rather than by section characteristics. The chordwise distribution of loading also is affected by finite span; but in many instances, this effect is relatively unimportant. The assumption of a two-dimensional chordwise load distribution, therefore, is one reasonable simplification of the finite-wing theory.

A number of wing theories, based on various simplifying assumptions, have been developed. (See references 1 to 8.) The theories differ in accuracy and in the extent of their applicability. Before discussing specific details of the various theories, consideration will be given to some of the important factors that determine the usefulness of a wing theory. One important factor concerns the variety of wing plan forms to which the theory can be applied. Of equal importance, is the number of aerodynamic characteristics that may be treated by a given wing theory. A third factor concerns the suitability of a wing theory for consideration of appropriate wing section characteristics. This is important, since experiments have indicated that, through the action of the boundary layer,

there may be large effects of the profile shape or of the surface condition. A fourth factor concerns the suitability of the theory for engineering applications or, more specifically, the time required for routine computations. With these items in mind, some of the physical concepts upon which the present-day theories are based might now be considered.

The practical wing theories make use of vortex lines for determining the load carried by the wing. (See fig. 1.) The theories differ in the manner in which the vorticity is assumed to be distributed over the wing surface and in the method employed for fixing the strength of the vorticity and, thereby, the magnitude of the lift. According to a very simple concept, which was proposed by Prandtl about 30 years ago and which is commonly called lifting-line theory (reference 1), the vorticity is assumed to be divided into bound and trailing elements, with the bound elements concentrated in a single line which should run approximately through the centers of pressure of the wing sections. The trailing vorticity leaves the wing in the form of a sheet and extends downstream to infinity. Downwash angles usually are calculated at a finite number of control points along the lifting line. The effective angle of attack of the wing is assumed to be the difference between the geometric angle of attack and the downwash angle. The strength of the vorticity, and hence the wing lift, is determined from section characteristics corresponding to the effective angle of attack. The lifting-line method, therefore, provides no indication of any possible distortion of the chordwise load distribution. Also, because the lifting line is necessarily straight, the method must be restricted to small angles of sweep.

Because of the recent emphasis on highly swept wings, consideration is being given to a more general (or lifting-surface) concept such as has been used by Falkner (reference 5) and Cohen (reference 6). According to this concept, the vorticity is assumed to be distributed both chordwise and spanwise over the wing surface. The strength of the vorticity is fixed by the condition that, at any point on the surface, the flow must be tangent to the surface. This method gives both the chordwise and the spanwise load distributions under potential-flow conditions. Wing section characteristics do not enter into the solution and, therefore, the effects of viscosity can be accounted for only in an indirect manner. For practical applications, the surface lift must be represented by a finite number of vortex lines and the boundary conditions must be satisfied at a finite number of control points. The simplest arrangement, which uses only one lifting vortex, is designated in figure 1 as the "simplified lifting-surface concept." This particular concept was suggested by Wieghardt (reference 3) and has been developed by Weissinger (reference 7) and Mutterperl (reference 8). The single lifting vortex is located along the wing quarter chord, and the boundary condition is satisfied along the wing three-quarter-chord line. Because the boundary condition is not satisfied at the lifting vortex, as in the case of lifting-line theory, the lifting vortex does not have to be a straight line; and the method, therefore, is applicable to swept wings. As in the case of lifting-line theory, however, this method does not account for any distortion of the two-dimensional chord loading.

All of the subsonic wing theories are based on the assumption of incompressible potential flow. The so-called first-order effects of compressibility can be accounted for, however, by resorting to a generalization of the Prandtl-Glauert rule (references 9 to 11), as indicated in figure 2. This rule implies that characteristics of a wing in compressible flow can be obtained by analyzing an equivalent wing in incompressible flow. The equivalent wing is obtained by increasing all longitudinal dimensions of the actual wing by the factor $1/\sqrt{1 - M^2}$. This results in a decrease in the aspect ratio A and an increase in the sweep angle Λ, as indicated by the equations given in figure 2. The compressible-flow pressures P_{comp} are obtained by multiplying the incompressible-flow pressures $P_{e_{inc}}$ for the equivalent wing by the factor $1/\sqrt{1 - M^2}$. This procedure, of course, does not account for changes in boundary-layer effects which may accompany changes in Mach number.

The general utility of the three wing-theory concepts is summarized in table I. The comparison is made on the basis of the Multhopp, Falkner, and Weissinger adaptations, which are considered to be the most suitable for practical use. With regard to applicability to wing geometry, the lifting-line method is subject to the most severe restrictions inasmuch as it is limited to high aspect ratio and low sweep angle. The lifting-surface theory has general applicability, and the simplified lifting-surface theory of Weissinger is applicable to all wings having straight leading and trailing edges. The lifting-line theory is readily applicable to a wide variety of wing characteristics (references 12 to 21); whereas, the lifting-surface and simplified lifting-surface theories, being considerably more cumbersome, have so far been applied to only a limited number of characteristics. Wing section characteristics can be easily accounted for only by the lifting-line concept. The lifting-line theory is most desirable from the standpoint of the time required for solutions. For example, in calculating a spanwise load distribution, the lifting-surface method takes about 60 times as long as the lifting-line method which uses four control points, and the simplified lifting-surface method takes about eight times as long as the lifting-line method for the same number of control points. Doubling the number of control points approximately quadruples the time required for solutions.

The importance of one of the factors considered in table I, that is, the suitability of a theory for consideration of wing section characteristics, is illustrated in figure 3. Chordwise load distributions resulting from angle of attack and from flap deflection, $(\Delta P)_\alpha$ and $(\Delta P)_\delta$, are shown. The particular distributions shown were obtained from two-dimensional thin-airfoil theory (references 16 and 22) and from tests of a two-dimensional NACA 0009 airfoil with a thickened trailing-edge portion (reference 23). As has been mentioned previously, some distortion of the two-dimensional chordwise load distributions would be expected to result from finite-span effects. The comparison of the experimental and theoretical load curves for the two-dimensional airfoil nevertheless provides a qualitative indication of differences that exist for finite-span wings.

The areas of the chordwise load curves represent the lift due to angle of attack and the lift due to flap deflection. The rates of change of these quantities with angle of attack and with flap deflection are commonly represented by the symbols C_{l_α} and C_{l_δ}, respectively. Integration for moment, about the flap hinge point, of the parts of the loads carried by the flap yields the hinge moment due to angle of attack and the hinge moment due to flap deflection. The rates of change of these latter quantities with angle of attack and with flap deflection are conventionally represented by the symbols C_{h_α} and C_{h_δ}, respectively. The greatest differences between the experimental and theoretical distributions are in the trailing-edge region where the boundary layer is relatively thick. Because of the convex contour in the vicinity of the trailing edge of the selected airfoil, the differences between theory and experiment are greater than would normally be obtained. The indicated differences do, however, provide a qualitative representation of usual conditions. Comparison of the total areas of the load curves indicates that the theoretical value of the lift due to angle of attack C_{l_α} would be subject to only a small error and that the lift due to flap deflection C_{l_δ} would be subject to a somewhat larger error. The theoretical values of the hinge moment due to angle of attack C_{h_α} and of the hinge moment due to flap deflection C_{h_δ} would be considerably different from the experimental values because of the large differences in the loads near the trailing edge. If a theory is to be applied to determination of the effectiveness and hinge moments of finite-span controls, it is important, therefore, that some means be provided for accounting for the effects of viscosity on the wing section characteristics.

The effects of viscosity also influence the variation of characteristics with Mach number, as is illustrated in figure 4. Comparisons are shown for the actual and theoretical variations with Mach number of the lift-curve slope C_{l_α} and of the rate of change of aileron hinge-moment coefficient with deflection C_{h_δ} for the wing of a fighter-type airplane (reference 24). The calculated curves are based on applications of the generalized Prandtl-Glauert rule which assumes no viscosity (reference 9). The calculated results for the lift-curve slope C_{l_α} are in good agreement with experiment almost up to the Mach number for which the force break occurs. Good agreement was not obtained, however, for the hinge-moment parameter C_{h_δ} even at moderate Mach numbers. The poor agreement probably is caused by variations, with Mach number, of the characteristics of the boundary layer, which were shown in figure 3 to have an important effect on hinge moments. As yet, there is no satisfactory method of accounting for such boundary-layer effects.

The fact that the lifting-line theory is inadequate at small aspect ratios, such as may be employed for tail surfaces or for high-speed wings, is illustrated in figure 5. This figure shows theoretical variations with aspect ratio of the lift-curve slope C_{L_α} and of the hinge-moment parameters C_{h_α} and C_{h_δ}. Results given by lifting-line-theory equations are compared with results indicated by a lifting-surface-theory method. (See references 25 to 28.) In the latter method, lifting-surface theory was used only to obtain corrections that could be applied to the usual lifting-line-theory equations. By this procedure, equations in terms of arbitrary section parameters could be retained. The curves shown were calculated from the measured section characteristics of an NACA 0009 airfoil equipped with a 30-percent-chord plain sealed flap. The results indicate that the difference between the two theories increases as the aspect ratio decreases; and, in the case of the hinge-moment parameters, the differences may be very large. The two test points in figure 5 represent results obtained from tests of two specific configurations. The results tend to be in better agreement with the lifting-surface theory than with the lifting-line theory; and, in general, tests of other models have given similar results. The errors of the lifting-line theory are of such a magnitude as to be intolerable for most design purposes.

As had been mentioned previously, the lifting-line theory cannot be applied to wings with large sweep angles. The simplified lifting-surface theory of Weissinger (reference 7) has been found to be very useful for the calculation of certain swept-wing characteristics, as, for example, the spanwise load distribution. Calculations of the load distributions have been carried out for a wide variety of wing plan forms (reference 29); and, in general, good agreement has been obtained with experiment, at least for low lift coefficients. (See reference 30.) Comparisons of measured and theoretical load distributions for an unswept wing, a sweptback wing, and a sweptforward wing are shown in figure 6. The agreement is fairly typical of what has been obtained for all but the most extreme plan forms. Comparison of the load curves for the unswept and sweptback plan forms shows the usual reduction in load near the wing root and increase in load near the wing tip as the wing is swept back. An increase in load near the root and a decrease in load near the wing tip is obtained as the wing is swept forward. These effects of sweep on the load distribution cause a tendency for the tip sections of sweptback wings to stall before the root sections; whereas, for sweptforward wings, the root sections generally stall before the tip sections.

The peculiar stalling characteristics of swept wings limit the lift-coefficient range over which any theory, if based on potential-flow concepts, can be expected to give reliable results. This fact is illustrated in figure 7. Comparisons of theoretical and experimental values of the aerodynamic-center location are given for an unswept wing and a wing with 45° sweepback (reference 31). Both wings had an aspect ratio

of 4.1. For the unswept wing the aerodynamic center showed little movement to a lift coefficient at least as high as 1.0, and the experimental results were in good agreement with the value given by the Weissinger theory. For the wing with 45° sweepback, however, the aerodynamic center showed a large rearward movement, starting at a lift coefficient of about 0.6. Although the theoretical value was in good agreement with experiment at low lift coefficients, the agreement was very poor in the high lift-coefficient range where the wing probably was partially stalled. This limitation of the theory is illustrated only for the case of the aerodynamic center, but similar limitations have been observed for almost all of the aerodynamic characteristics. At the present time, it is possible only to make qualitative estimates of the characteristics at high lift. Wind-tunnel tests must be relied upon in order to obtain quantitative answers.

Rigorous theories have not yet been applied to all of the characteristics which are of interest. For certain purposes, however, reasonably reliable indications of the effects of a given geometric variable can be obtained from very simple considerations. The effects of sweep on finite-span wings, for example, are sometimes assumed to be the same as the effects of sweep on infinite-span wings. (See reference 32.) This approach neglects any consideration of the induced angle of attack or of the effects of sweep on the span loading. An example of the reliability of such an approach for one particular characteristic is shown in figure 8. This figure gives a comparison of experimental and calculated values of the aileron rolling-monent effectiveness C_{l_δ}. Infinite-span considerations indicate that the aileron rolling-moment effectiveness should decrease as the square of the cosine of the sweep angle. By applying this correction factor to the effectiveness parameter measured for the unswept wing, the dashed curve is obtained. Test results (reference 33) obtained with two sweptback wings were in reasonably good agreement with the calculated curve. Since unswept wings have been investigated rather thoroughly, both by theory and experiment, rough estimates of the aileron rolling-moment effectiveness for almost any swept-wing plan form can be obtained by this simple procedure. Several other wing characteristics have been handled in a similar manner. A somewhat different approach, in which consideration is given to the induced angle of attack, as well as to the infinite-span effect but with the effects on the load distribution still neglected, has been applied to the estimation of the stability derivatives of swept wings (reference 34).

There are certain problems that can be handled most satisfactorily by purely empirical procedures. An example is the determination of the control-surface balance configuration required in order to obtain specified values of the hinge-moment parameters. Theoretical procedures have so far been indequate for analyzing the characteristics of the various balancing devices; consequently, the effects of the many details of control-surface balances have been studied experimentally (references 35 to 38). Some of the important results of this work are summarized in figure 9.

The form of figure 9 has been found convenient for a number of different analyses of hinge-moment characteristics. It is a plot of the parameter C_{h_α} against the parameter C_{h_δ}; and the dashed line represents combinations of these parameters that would result in zero control force for a typical aileron. Lines of constant values of the control force for a given flight speed and a given altitude could be represented by lines drawn parallel to the zero-force line. Increasing heaviness, or underbalance, is obtained in moving to the left of the zero-force line, and increasing overbalance results from moving to the right of the zero-force line. A point, determined by the characteristics of a plain aileron (without balance), is represented on the chart by the small circle. The manner in which the hinge-moment parameters are altered through the addition of various aerodynamic balances is indicated by the lines radiating from the point for the plain aileron. The distance moved along a given line depends, of course, on the size or geometry of the balancing device. Empirical procedures are available for estimating the extent to which the geometry of the various balances must be altered in order to produce prescribed changes in the hinge-moment parameters (reference 37). The chart shows that the different devices vary considerably in the manner in which they affect the hinge-moment parameters. The balancing tab, for example, may have a large effect on C_{h_δ}, but a negligible effect on C_{h_α}. The addition of a beveled-trailing-edge balance, on the other hand, affects C_{h_α} and C_{h_δ} almost equally. Intermediate variations are obtained with a sealed internal balance and with balances of the plain overhang type. By proper choice of the balance or by combinations of various balances, it is possible to obtain almost any desired values of the hinge-moment parameters.

CONCLUDING REMARKS

In the foregoing discussion, a brief description has been given of the physical principles of the wing theories that are presently available to the aerodynamicist, and an indication has been given of some of the procedures that are being used to obtain solutions to specific problems. The procedures in use do not always utilize sound fundamental principles. The reason for this is not lack of a sound theory, but rather that the present theories are, in many instances, too cumbersome for practical applications. None of the present theories is satisfactory with regard to all of the points mentioned at the beginning of this paper. A theory that would combine applicability to arbitrary geometry with the many advantages of the present lifting-line theory would be extremely useful. The effects of compressibility, particularly for thick finite-span wings, and the effects of the boundary layer cannot yet be adequately accounted for. There is no reliable method of anticipating the conditions under which the flow first begins to break down on swept wings or of estimating

the characteristics after the breakdown occurs. Many of the problems are complicated by the fact that wing flexibility enters as an important additional factor for some of the wing plan forms that are of current interest. The extent to which wing flexibility may have to be considered has not yet been well-established.

REFERENCES

1. Prandtl, L.: Theory of Lifting Surfaces. Part I. NACA TN No. 9, 1920.

2. Multhopp, H.: Die Berechnung der Auftriebsverteilung von Tragflügeln. Luftfahrtforschung, Bd. 15, Lfg. 4, April 6, 1938, pp. 153-169.

3. Wieghardt, Karl: Chordwise Load Distribution of a Simple Rectangular Wing. NACA TM No. 963, 1940.

4. Krienes, Klaus: The Elliptic Wing Based on the Potential Theory. NACA TM No. 971, 1941.

5. Falkner, V. M.: The Calculation of Aerodynamic Loading on Surfaces of Any Shape. R. & M. No. 1910, British A.R.C., 1943.

6. Cohen, Doris: A Method for Determining the Camber and Twist of a Surface to Support a Given Distribution of Lift. NACA Rep. No. 826, 1945.

7. Weissinger, J.: The Lift Distribution of Swept-Back Wings. NACA TM No. 1120, 1947.

8. Mutterperl, William: The Calculation of Span Load Distributions on Swept-Back Wings. NACA TN No. 834, 1941.

9. Goldstein, S., and Young, A. D.: The Linear Perturbation Theory of Compressible Flow with Applications to Wind-Tunnel Interference. R. & M. No. 1909, British A.R.C., 1943.

10. Göthert, B.: Plane and Three-Dimensional Flow at High Subsonic Speeds. NACA TM No. 1105, 1946.

11. Hess, Robert V., and Gardner, Clifford S.: Study by the Prandtl-Glauert Method of Compressibility Effects and Critical Mach Number for Ellipsoids of Various Aspect Ratios and Thickness Ratios. NACA RM No. L7B03a, 1947.

12. Lotz, Irmgard: Berechnung der Auftriebsverteilung beliebig geformter Flügel. Z.F.M., Jahrg. 22, Heft 7, April 14, 1931, pp. 189-195.

13. Anderson, Raymond F.: Determination of the Characteristics of Tapered Wings. NACA Rep. No. 572, 1936.

14. Pearson, H. A.: Span Load Distribution for Tapered Wings with Partial-Span Flaps. NACA Rep. No. 585, 1937.

15. Pearson, Henry A., and Jones, Robert T.: Theoretical Stability and Control Characteristics of Wings with Various Amounts of Taper and Twist. NACA Rep. No. 635, 1938.

16. Glauert, H.: Theoretical Relationships for an Aerofoil with Hinged Flap. R. & M. No. 1095, British A.R.C., 1927.

17. Perring, W. G. A.: The Theoretical Relationships for an Aerofoil with a Multiply Hinged Flap System. R. & M. No. 1171, British A.R.C., 1928.

18. Ames, Milton B., Jr., and Sears, Richard I.: Determination of Control-Surface Characteristics from NACA Plain-Flap and Tab Data. NACA Rep. No. 721, 1941.

19. Jones, Robert T.: Theoretical Correction for the Lift of Elliptic Wings. Jour. Aero. Sci., vol. 9, no. 1, Nov. 1941, pp. 8-10.

20. Sivells, James C., and Neeley, Robert H.: Method for Calculating Wing Characteristics by Lifting-Line Theory Using Nonlinear Section Lift Data. NACA TN No. 1269, 1947.

21. Boshar, John: The Determination of Span Load Distribution at High Speeds by Use of High-Speed Wind-Tunnel Section Data. NACA ACR No. 4B22, 1944.

22. Glauert, H.: A Theory of Thin Aerofoils. R. & M. No. 910, British A.R.C., 1924.

23. Hoggard, H. Page, Jr., and Bulloch, Marjorie E.: Wind-Tunnel Investigation of Control-Surface Characteristics. XVI - Pressure Distribution over an NACA 0009 Airfoil with 0.30-Airfoil-Chord Beveled-Trailing-Edge Flaps. NACA ARR No. L4D03, 1944.

24. Laitone, Edmund V.: An Investigation of 0.15-Chord Ailerons on a Low-Drag Tapered Wing at High Speeds. NACA ARC No. 4I25, 1944.

25. Swanson, Robert S., and Gillis, Clarence L.: Limitations of Lifting-Line Theory for Estimation of Aileron Hinge-Moment Characteristics. NACA CB No. 3L02, 1943.

26. Swanson, Robert S., and Crandall, Stewart M.: An Electromagnetic-Analogy Method of Solving Lifting-Surface-Theory Problems. NACA ARR No. L5D23, 1945.

27. Swanson, Robert S., and Priddy, E. LaVerne: Lifting-Surface-Theory Values of the Damping in Roll and of the Parameter Used in Estimating Aileron Stick Forces. NACA ARR No. L5F23, 1945.

28. Swanson, Robert S., and Crandall, Stewart M.: Lifting-Surface-Theory Aspect-Ratio Corrections to the Lift and Hinge-Moment Parameters for Full-Span Elevators on Horizontal Tail Surfaces. NACA TN No. 1175, 1947.

29. DeYoung, John: Theoretical Additional Span Loading Characteristics of Wings with Arbitrary Sweep, Aspect Ratio, and Taper Ratio. NACA TN No. 1491, 1947.

30. Van Dorn, Nicholas H., and DeYoung, John: A Comparison of Three Theoretical Methods of Calculating Span Load Distribution on Swept Wings. NACA TN No. 1476, 1947.

31. Letko, William, and Goodman, Alex: Preliminary Wind-Tunnel Investigation at Low Speed of Stability and Control Characteristics of Swept-Back Wings. NACA TN No. 1046, 1946.

32. Betz, A.: Applied Airfoil Theory. Unsymmetrical and Non-Steady Types of Motion. Vol. IV of Aerodynamic Theory, div. J, ch. IV, sec. 4, W. F. Durand, ed., Julius Springer (Berlin), 1935, pp. 102-107.

33. Bennett, Charles V., and Johnson, Joseph L.: Experimental Determination of the Damping in Roll and Aileron Rolling Effectiveness of Three Wings Having 2°, 42°, and 62° Sweepback. NACA TN No. 1278, 1947.

34. Toll, Thomas A., and Queijo, M. J.: Approximate Relations and Charts for Low-Speed Stability Derivatives of Swept Wings. NACA TN No. 1581, 1948.

35. Rogallo, F. M.: Collection of Balanced-Aileron Test Data. NACA ACR No. 4A11, 1944.

36. Sears, Richard I.: Wind-Tunnel Data on Aerodynamic Characteristics of Airplane Control Surfaces. NACA ACR No. 3L08, 1943.

37. Langley Research Department (Compiled by Thomas A. Toll): Summary of Lateral-Control Research. NACA TN No. 1245, 1947.

38. Morgan, M. B., and Thomas, H. H. B. M.: Control Surface Design in Theory and Practice. Jour. R.A.S., vol. XLIX, no. 416, Aug. 1945, pp. 431-514.

TABLE I.- COMPARISON OF WING THEORIES

CONCEPT	LIFTING LINE	LIFTING SURFACE	SIMPLIFIED LIFTING SURFACE
METHOD	MULTHOPP	FALKNER	WEISSINGER
APPLICABILITY TO WING GEOMETRY	HIGH ASPECT RATIO, LOW SWEEP	GENERAL	STRAIGHT L.E. AND T.E.
APPLICABILITY TO WING CHARACTERISTICS	WIDE	LIMITED	LIMITED
WING-SECTION CHARACTERISTICS	EASILY HANDLED	NOT EASILY HANDLED	NOT EASILY HANDLED
*RELATIVE TIME REQUIRED	4 POINTS: 1 8 POINTS: 4	60	4 POINTS: 8 8 POINTS: 30

*FOR SPAN LOAD CALCULATIONS

NACA

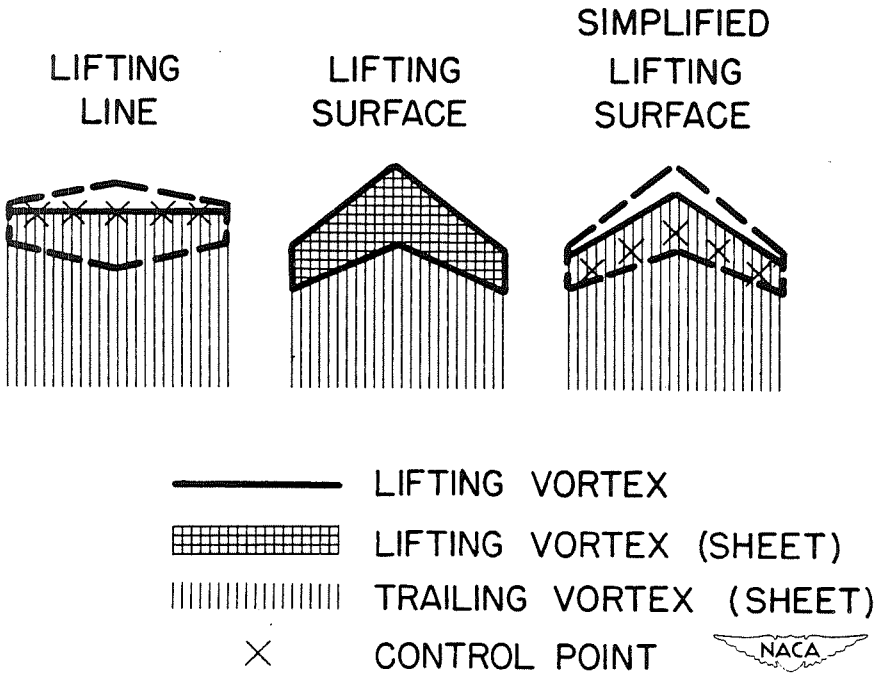

Figure 1.- Basic wing-theory concepts.

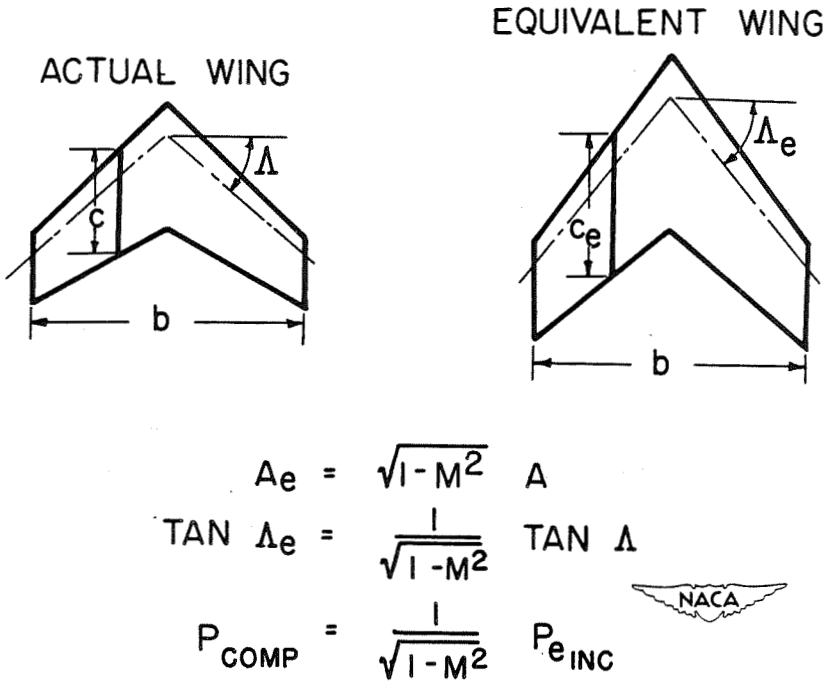

Figure 2.- Actual and equivalent wings in compressible flow.

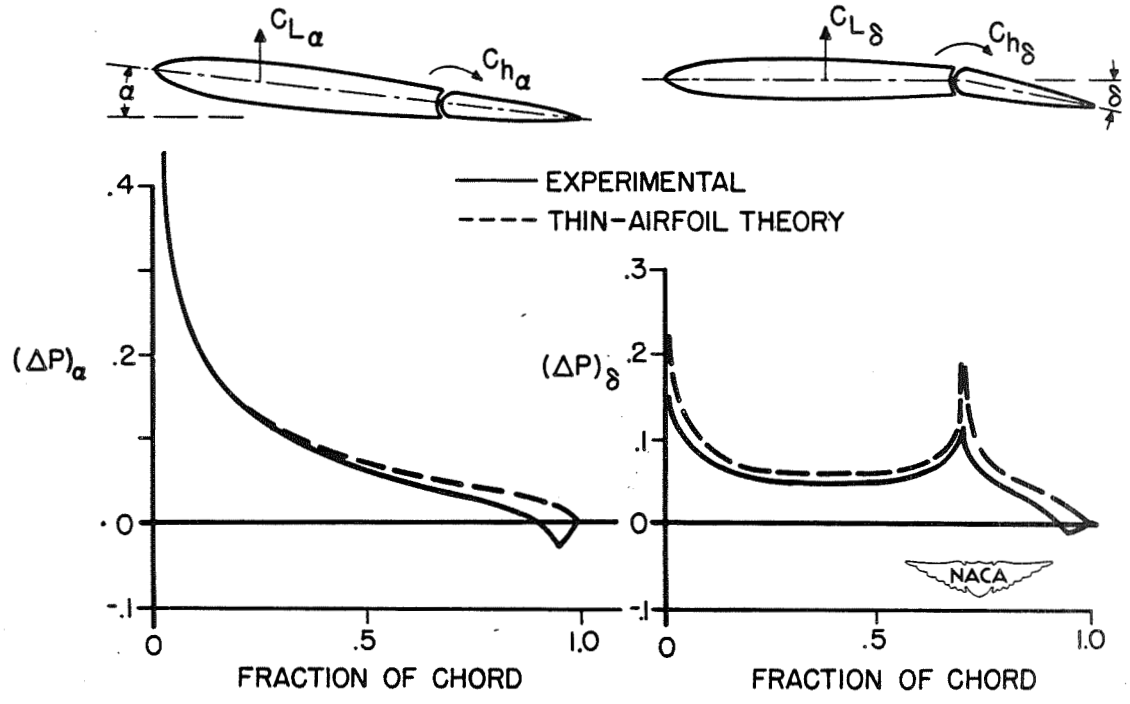

Figure 3.- Chordwise pressures for two-dimensional airfoil

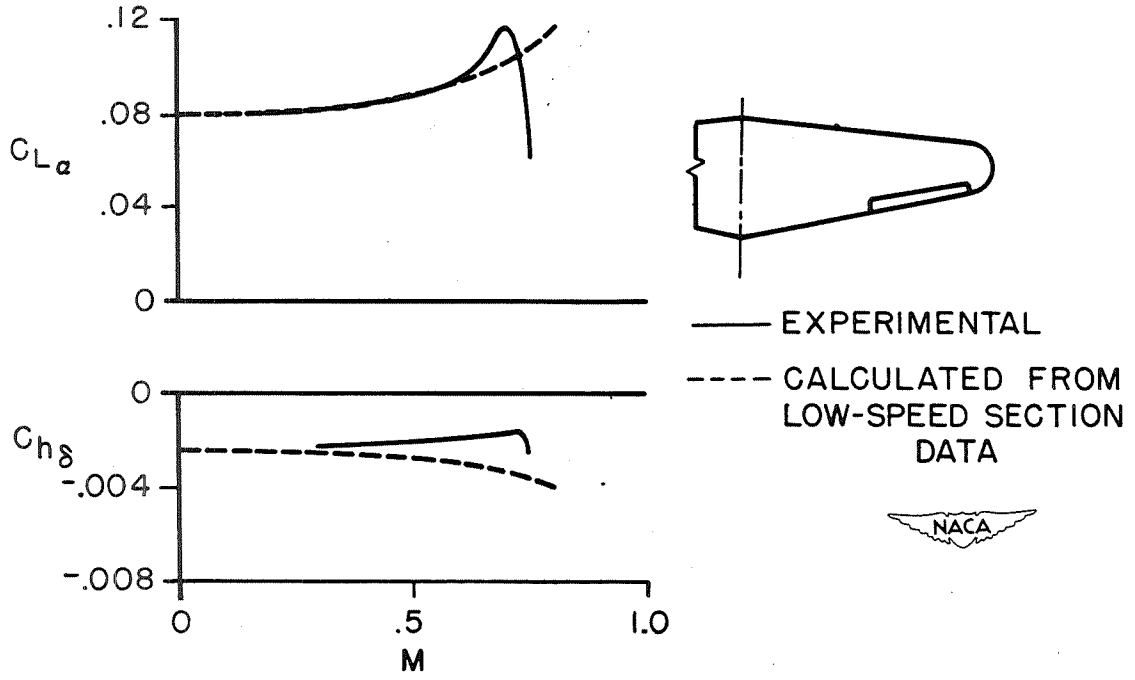

Figure 4.- Effect of Mach number on lift and hinge moments.

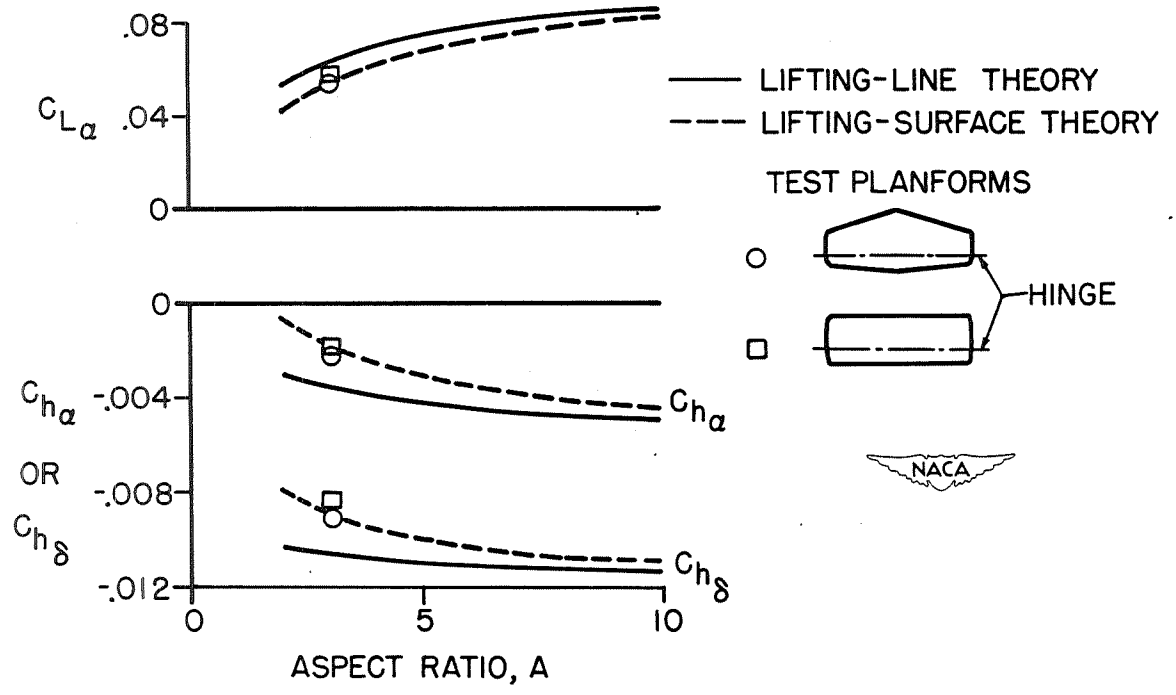

Figure 5.- Lift and hinge-moment parameters for 0.3 chord flaps. NACA 0009 section.

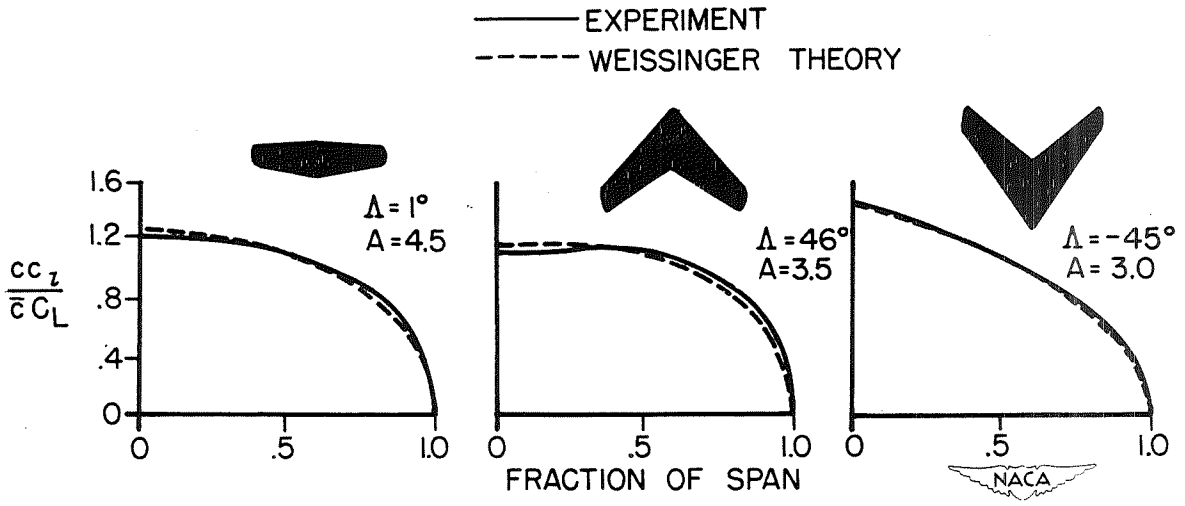

Figure 6.- Experimental and theoretical spanwise load distributions.

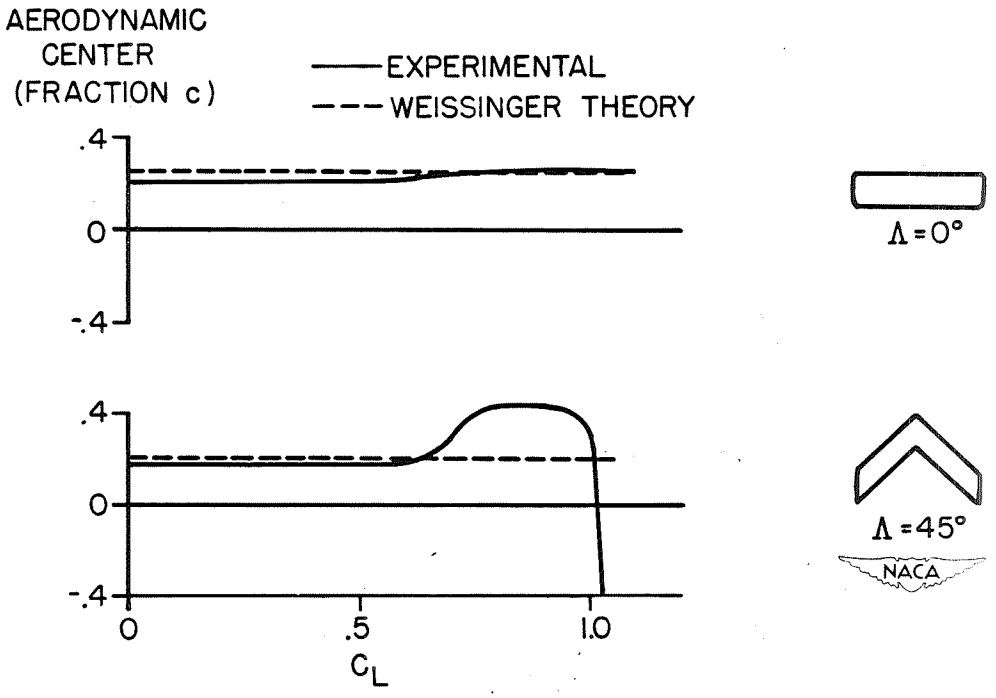

Figure 7.- Effect of sweep on aerodynamic center.

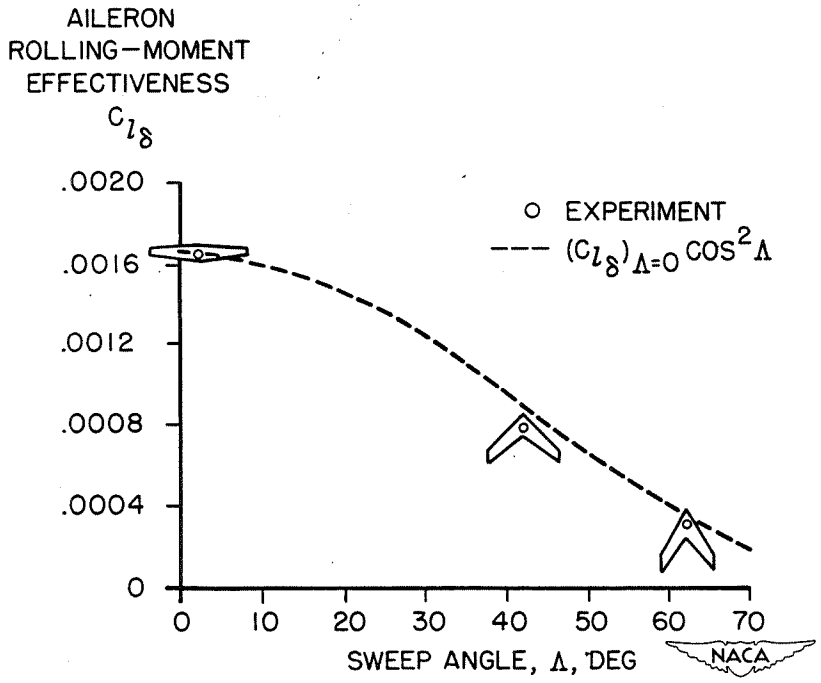

Figure 8.- Effect of sweep on aileron effectiveness.

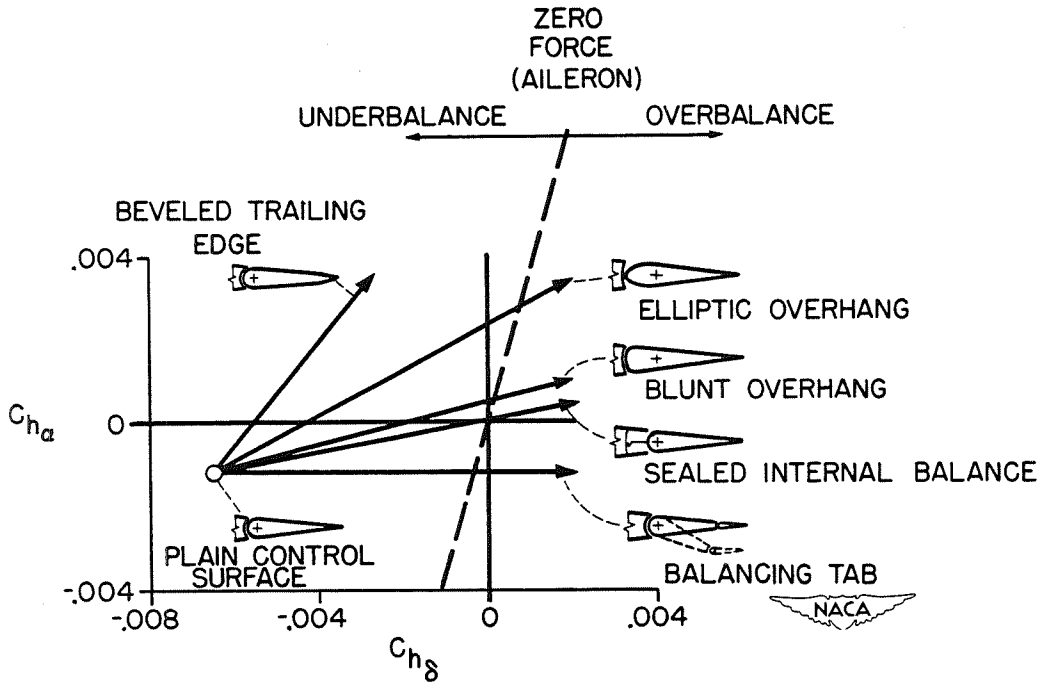

Figure 9.- Effects of control-surface balance on hinge moments.

MAXIMUM-LIFT AND STALLING CHARACTERISTICS OF WINGS

By James C. Sivells

Langley Aeronautical Laboratory

The maximum-lift and stalling characteristics of wings constitute a subject that is common to all types of airplanes, small or large, low speed or high speed. The problems associated with each type may, however, be widely different. The old biplanes and early monoplanes had stalling characteristics which were usually fairly good. The wing loadings were low so that the landing speeds were relatively low. The relatively thick, rectangular wings tended to stall near the center and gave the pilots adequate stall warning. As the airplane designs became more efficient, the structural designers demanded that the wings be tapered to decrease the stresses at the wing roots. Tapering the wings, however, tended to move outboard the spanwise position of the incipient stall, so that a compromise has to be made between the structural and aerodynamic desiderations. Recently the use of thinner and smoother wing sections, higher wing loadings, and unconventional plan forms has resulted in further compromises, both structural and aerodynamic, since the factors which are necessary for high-speed performance are usually not conducive to low-speed performance. All present-day airplanes represent the results of such compromises which have been made in their designs.

Since it is desirable to be able to predict the maximum-lift and stalling characteristics of an airplane at a very early stage in its design, a large amount of research has been done with this end in mind. This research has been undertaken along three lines - theoretical work, wind-tunnel experiments, and flight tests - which must be closely correlated to provide the maximum amount of useful information. The theoretical work can indicate trends due to variations in the wing geometry but cannot adequately include the interference effects of the fuselage or nacelles. The wind-tunnel experiments can determine the maximum lift values for a smooth model or one with standard leading-edge roughness but oftentimes at values of Reynolds number or Mach number different than those at which the airplane will fly. Moreover, the stalling characteristics determined in most wind tunnels are obtained for models which are restrained at a given attitude so that the motions of a stalled airplane cannot be simulated. The final analysis of the maximum-lift and stalling characteristics of an airplane comes in the flight tests where all the factors which influence the characteristics are integrated. At this stage of the design, however, it may be too late or very expensive to make alterations necessary to improve the characteristics. In spite of all the research which has been done along these lines, much more remains to be done before accurate predictions can be made of the characteristics of every type of airplane.

One of the major factors which influence the maximum-lift and stalling characteristics of a wing is its airfoil section. Comparisons

of various airfoil sections can best be made from the results of two-dimensional wind-tunnel tests. The NACA 6-series airfoil sections have been described in the paper by von Doenhoff and Loftin. In figure 1, the values of the maximum lift coefficient of the NACA 64-series sections are shown for a Reynolds number of 6×10^6. (See reference 1.) In order to provide an indication of the maximum-lift capabilities of an airfoil with various types of high-lift flaps, nearly all sections are tested with and without 20-percent-chord split flaps deflected 60°. Varying the airfoil thickness ratio has approximately the same effect on the maximum lift of the NACA 6-series airfoils as it does on the older 4- and 5-digit airfoil sections. (See reference 2.) Without flaps, the highest values are for thickness ratios of about 12 to 15 percent. With flaps, the highest values are for thickness ratios of about 18 to 21 percent. The airfoil thickness also has an appreciable effect on the sharpness of the lift-curve peak (reference 3) which, in turn, may influence the stalling characteristics of a wing. The very thin sections, up to about 6 percent thick, have flat-top lift curves, characteristic of flat plates. The sections from about 9 to 12 percent thick have relatively sharp-peak lift curves characterized by abrupt separation of the flow from the entire upper surface initiated by laminar separation near the leading edge. The actual flow mechanism is quite complex but is described more fully in reference 3. The thicker sections have more rounded lift-curve peaks characterized by separation of the turbulent boundary layer starting at the trailing edge. Not only the thickness but also the airfoil contour, particularly the forward part, has an effect on the section stalling characteristics so that different families of airfoils do not necessarily exhibit the same characteristics. For example, for equal thicknesses, the NACA 6-series sections do not have as sharp lift-curve peaks as the NACA 230-series sections.

The addition of camber of the uniform-load type generally increases the values of maximum lift coefficient as shown in figure 1 for values of design lift coefficient c_{l_i} of 0.2 and 0.4. Still greater amounts of camber do not further increase the maximum lift coefficient. These curves are typical of all the NACA 6-series sections. The values for NACA 63-series sections are generally a little higher than those shown while those for the NACA 65- and 66-series are a little lower. The effects of Reynolds number on the values of maximum lift coefficient are about the same as for the older types of airfoils. These data were all obtained with the airfoils in a smooth condition. With so-called standard leading-edge roughness applied to the forward 8 percent of the airfoil surface, the effects of thickness and Reynolds number are materially reduced. For example, at the Reynolds number of 6×10^6, the values of maximum lift coefficient for the 6-percent-thick sections are little affected by roughness, for the 12-percent-thick sections losses of 0.3 to 0.5 are caused by roughness, and for the thicker sections the losses due to roughness are of the order of 0.2 to 0.3. These losses in $c_{l_{max}}$ are accompanied by a rounding-off of the lift-curve peaks.

The thicker sections with split flaps give fairly high values of maximum lift coefficient, of the order of 2.8. For high-speed performance, however, much thinner sections must be used, usually less than 12 percent thick. It then becomes imperative to use some more powerful type of high-lift device in order to obtain high values of maximum lift coefficient. In figure 2 are shown typical values which can be obtained for various types and combinations of high-lift devices. The difference between the two sections shown is mainly that of camber. The double slotted flap is one of the most powerful types of trailing-edge flap and on the NACA 64_1A212 section produces a value of $c_{l_{max}}$ of about 2.85 for a Reynolds number of 6×10^6 as compared with a value of 2.41 obtained with a split flap. (See references 4 and 5.) The addition of a leading-edge slat increases the value of $c_{l_{max}}$ to about 3.38. A still further increase can be obtained by removing part of the boundary layer by suction through one or more slots. For a single slot located at 40 percent of the chord and a flow coefficient of 0.025, a maximum lift coefficient of 3.72 has been obtained in conjunction with a double slotted flap and a leading-edge slat.

Another type of leading-edge device is the extensible leading-edge flap. (See reference 6.) Two types of flap are shown with the NACA 64_1-012 section; one is intended to be hinged at the lower surface near the nose of the airfoil and the other is intended to be retracted into the upper surface. The lower-surface flap is probably simpler from a construction standpoint but produces a discontinuity at the nose and is, therefore, not as effective as the upper-surface flap. Used in conjunction with a split flap, however, the lower-surface leading-edge flap produces a fairly high value of $c_{l_{max}}$ One advantage of the leading-edge flap as a high-lift device is that it produces approximately the same values of $c_{l_{max}}$ on still thinner airfoil sections (reference 7) even though the values obtained for the plain airfoil decrease rapidly with decreasing thickness.

Although the two-dimensional data give a fairly good indication of the relative merits of various airfoil sections, the other factors which influence the maximum-lift and stalling characteristics of wings must be investigated in three-dimensional flow on wings of finite span. Complete wings may be divided into two catagories: those having little or no sweep and those which are sweptback or sweptforward enough that the sweep has an influence on the wing characteristics. Since much more is known about the characteristics of unswept wings, these are discussed first.

Except for wings of very low aspect ratio, the various sections of an unswept wing behave very much as they do in two-dimensional flow but at an effective angle of attack as predicted by lifting-line theory. Even the nonlinearity of the section lift curves in the vicinity of

maximum lift can be taken into account by a method developed for calculating the wing characteristics using actual two-dimensional data. (See reference 8.) Figure 3 shows the results of such calculations for one of a series of wings. (See references 9 to 11.) The calculated curve is here superimposed on the points obtained experimentally. This particular wing has the fairly high aspect ratio of 10 and a taper ratio of 0.4. The sections varied in thickness from 20 percent at the root to 12 percent at the tip and account was taken of the variation in Reynolds number from root to tip due to the taper. The agreement between the calculated and experimental results was very good for this wing and at least reasonably good for all the wings of the series investigated. In all cases the agreement was better than if no account were taken of the nonlinearity of the section lift curves.

In addition to the value of the maximum lift coefficient, the stalling characteristics of a wing can be predicted by this method as shown in figure 4. This is for the same wing as the previous figure. The upper, or dotted, curve shows the spanwise variation of the maximum lift coefficient for the various sections as determined from two-dimensional tests. The variations of thickness and Reynolds number along the span are taken into account. The lower, or solid, curve is the spanwise variation of the local section lift coefficient at the maximum value of wing lift coefficient as calculated by the method mentioned. Where the curves are tangent, the sections have reached their maximum values of lift coefficient and the stall has begun. The divergence between the curves is an indication of the progression of the stall. In this particular case, the difference between the curves at the root is probably insufficient to prevent separation, so that the wing would be predicted to be stalled over about 90 percent of the semispan. From wind-tunnel tests with tufts attached to the wing, the area indicated was stalled at maximum lift. The agreement between the wind-tunnel tests and the predicted stall is reasonable. Whether this wing would have satisfactory stalling characteristics in flight cannot be predicted from these data inasmuch as the motions of the stalled airplane are not known. It can be conjectured that some loss in aileron effectiveness would be experienced near maximum lift but, because of the thick root sections which experience separated flow at values of lift coefficient somewhat below the maximum, the pilot may have warning of the incipient stall in the nature of tail buffeting.

Although the maximum-lift and stalling characteristics of unswept wings are believed to be predicted better by the method using nonlinear section lift data than by older methods in which the section lift curves are assumed to be linear, much useful information has been obtained by the latter methods as to the effects of various geometric parameters. One such theoretical investigation (references 12 and 13) provides the information shown in figure 5. It has been generally accepted that a rectangular wing (taper ratio of 1) will possess good stalling characteristics inasmuch as the stall tends to start at the root and progress slowly outboard as indicated by the lower left-hand curves. There may be certain combinations of variables, however, for which such a

generalization is not true. Furthermore, too early a root stall may seriously reduce the maximum lift or cause too much tail buffeting. It may, therefore, be desirable from an aerodynamic as well as a structural standpoint to taper the wing. A taper ratio of 1/2, which many designers consider to be moderate, moves the incipient-stall position dangerously far outboard for a wing with this particular combination of airfoil sections. If other design criterions allow the root thickness to be increased to 21 percent, the stall can again be moved inboard because the thicker sections have lower values of $c_{l_{max}}$. It is thus readily seen that it is extremely important to consider not only the taper ratio but also the airfoil section and other variables in the design of a wing with good stalling characteristics. The lower right-hand curves show that more taper again shifts the stall outboard even though the root section is quite thick.

A few general remarks should be made at this time. The use of nonlinear section lift data has oftentimes indicated that the stall would be more severe than that indicated by the use of linear data. These four examples shown are for an aspect ratio of 6, constant camber from root to tip, and no washout. The effect of increasing aspect ratio is to level off the local-lift-coefficient distributions thereby making the stalling characteristics better or worse depending upon the shape of the maximum-section-lift-coefficient distribution. An increase in camber from root to tip will usually improve the stalling characteristics if the maximum section lift coefficients are increased near the tip. Washout will also improve the stalling characteristics by increasing the local lift coefficients near the root and decreasing them near the tip. The use of either camber increase or washout may be limited, however, by the high-speed requirements for the airplane. The high-speed requirements may also dictate the shape and thickness of the airfoil section which may greatly influence the stalling characteristics in a manner not shown in the above type of analysis or even in wind-tunnel tests. The use of an airfoil section with a sharp-peak lift curve may result in a rapid roll-off or pitching motion when the airplane stalls in flight. Another factor which may affect the stalling characteristics of an airplane is the slipstream from a tractor propeller. (See reference 14.) The increased velocity in the slipstream increases the local Reynolds number of the wing sections behind the propeller. The downwash behind an inclined propeller tends to reduce the effective angle of attack of the wing sections. Both of these effects tend to delay stalling in the affected regions and may allow the outboard sections of the wing to stall first. Another effect is that of slipstream rotation which causes the sections behind the upgoing propeller blades to stall before the sections behind the downgoing propeller blades.

Where the high-speed requirements influence the design so that a poor-stalling wing results, the designer may resort to the use of stall control devices such as the sharp leading edge and leading-edge slat.

Figure 6 shows the use of a sharp leading edge on a wing with a taper ratio of 1/3. (See reference 15.) The outboard stall of the plain wing is corrected by decreasing the maximum section lift coefficients near the root; the stall is thereby caused to move inboard. The use of this type of stall control device results in a lower maximum lift coefficient of the wing and would probably not be used except where absolutely necessary. Figure 7 shows the use of a leading-edge slat over the outboard part of the wing. (See reference 12.) In this case the tip stall is prevented by increasing the maximum-lift capabilities of the outboard sections and a higher wing lift is obtained. Although this analysis indicates that the stall would be localized near the inboard end of the flap, it is extremely difficult to predict the flight characteristics.

Associated with the maximum-lift and stalling characteristics of airplanes is the sinking speed in the landing approach. This may be a deciding factor as to what type of high-lift device to use. Figure 8 shows the lift-drag polars of a wing-fuselage combination with three types of 60-percent-span flaps. (See reference 16.) To place the flaps on a more comparable basis, a tail length was assumed and the negative lift on the tail, necessary to trim out the pitching moment due to the flaps, was added to the wing lift to give a value of trimmed lift coefficient. Superimposed on these polars is a grid of lines of constant sinking speed V_v and constant gliding speed calculated for a wing loading of 60 pounds per square foot. Although neither the drag of nacelles, landing gear, tail, and protuberances nor the effects of power is included, a comparison of the various types of flap can be made. The lowest sinking speed for any of the flapped-wing configurations would be obtained with the single slotted flaps but the lowest gliding speed would be obtained with the double slotted flaps. These data are for a 10-percent-thick wing with an aspect ratio of 9. For this particular wing, the flaps had practically no effect on the stalling characteristics.

In the estimation of full-scale flight values of maximum lift coefficient from wind-tunnel data, due account must be taken of the difference in Mach number as well as the difference in Reynolds number between the flight and wind-tunnel conditions. Although the effects of compressibility are usually associated with relatively high subsonic Mach numbers, such effects are also important at Mach numbers as low as 0.2 in studies of maximum lift. Some of the interrelated effects of Mach number and Reynolds number are shown in figure 9. (See reference 17.) These data were obtained by testing the same wing at atmospheric pressure and at a pressure of about $2\frac{1}{4}$ atmospheres. At each pressure, tests were made over the range of Mach number. The same data are plotted as a function of both Reynolds number and Mach number. The peak values of maximum lift coefficient in each case were obtained when the critical pressure coefficient, corresponding to a local Mach number of 1, was reached. At speeds lower than this critical speed, the Reynolds number had more effect; $c_{l_{max}}$ increased with increasing Reynolds number. At speeds higher than

the critical speed, Mach number had more effect; $c_{l_{max}}$ decreased with increasing Mach number. At the higher Reynolds number, the pressure coefficients were more negative and the critical pressure coefficient was reached at a lower free-stream Mach number. The pressure coefficients were still more negative with the flaps deflected and the critical pressure coefficient was reached at still lower free-stream Mach numbers. Although these data pertain to one particular wing, they do show the importance of considering both the Reynolds number and the Mach number when estimations are made of the maximum lift coefficient of a wing.

Up to this point, only unswept wings have been considered. Although many of the factors which influence the maximum-lift and stalling characteristics of unswept wings also affect the characteristics of swept wings, such effects are often masked by the effect of sweep. The characteristics of swept wings are not as amenable to calculation as those of unswept wings. Some qualitative effects of sweep, however, may be discussed. As shown in the previous paper by Toll and Diederich from calculations by lifting-surface theory, sweepback tends to load up the outboard sections of a wing while sweepforward tends to load up the inboard sections. In addition to these effects on the span loading, the spanwise component of the air flow tends to sweep the boundary layer outboard on sweptback wings and inboard on sweptforward wings. The thickened boundary layer which results is more susceptible to separation than the thinner boundary layer on an unswept wing. The effects are additive, causing severe tip stall on sweptback wings and severe root stall on sweptforward wings as shown in figure 10. (See reference 18.) For these tests the same semispan wing was rotated to give the various angles of sweep, and different tip and root sections were added for each angle. The aspect ratio was thus decreased as the sweep was increased. In addition to the loss in lateral control at the stall of the sweptback wings, sweep, either forward or backward, may cause longitudinal instability at the stall for some aspect ratios. This is discussed more fully in another paper but is mentioned here because subsequent values of maximum lift shown may not be usable because of longitudinal instability.

The effect of sweepback on maximum lift coefficient is shown in figure 11. (See reference 19.) These results were obtained in a turbulent wind tunnel and the values of Reynolds number are the so-called "effective" values obtained by multiplying the test values by a factor which is a function of the amount of turbulence in the air stream. The validity of the use of this concept of effective Reynolds number has not been established for swept wings. The important point shown by these curves is that Reynolds number must be taken into account when discussing the effect of sweep on the maximum lift coefficient of a wing and low-scale wind-tunnel results may not apply to full-scale airplanes.

Sweep also has a pronounced effect upon the increment in lift coefficient due to flap deflection as shown in figure 12. (See reference 20.) These are low-scale results obtained at a Reynolds number

of 1×10^6 to 2×10^6. All the wings tested had the same chord normal to the leading edge, were untapered, and had the same span. The aspect ratio decreased, therefore, with increasing sweepback. The increment in lift coefficient is due to the deflection of 50-percent-span, 20-percent-chord, split flaps deflected 60°. At low angles of attack, the increment in lift coefficient varies approximately as the empirical cosine-squared curve multiplied by the factor η to take into account the difference in aspect ratio. The increment in maximum lift coefficient is somewhat lower, falling to zero for 60° sweepback.

As mentioned previously, the tip stall of a sweptback wing causes a loss in lateral control and may cause longitudinal instability. It is oftentimes possible, however, to eliminate this tip stall by some stall control device. Figure 13 shows the results of using partial-span, properly located, leading-edge slats on a highly tapered, moderately sweptback wing. (See reference 14.) In this case, not only was the tip stall eliminated, but the maximum lift coefficient was increased by the addition of the slats. It should be re-emphasized that the slats must be properly located both as to span and position to improve the stalling characteristics of such a wing because improperly located slats on this same model did not give any improvement.

In conclusion, the present status and future needs of research on maximum-lift and stalling characteristics can be summarized. Theoretical methods of analysis for unswept wings have been developed for predicting the effects of variations in wing geometry. Similar methods are needed which can include the effects of sweep and low aspect ratio. Wind-tunnel experiments have been useful for determining some of the effects of sweep and of various airplane components. Further wind-tunnel investigations are desirable in which the models are allowed some degree of freedom, such as rolling, so that flight conditions can be partly simulated. Further flight tests are desirable for investigating the effects of variables which cannot be taken into account at present either by theory or in the wind tunnels and for defining more nearly exactly what are satisfactory stalling characteristics. Finally, close correlation must be maintained between the theoretical analyses, wind-tunnel experiments, and flight tests so that the information from each field of research can be applied to the others.

REFERENCES

1. Cahill, Jones F.: Summary of Section Data on Trailing-Edge High-Lift Devices. NACA RM No. L8D09, 1948.

2. Abbott, Ira H., Von Doenhoff, Albert E., and Stivers, Louis S., Jr.: Summary of Airfoil Data. NACA Rep. No. 824, 1945.

3. Jacobs, Eastman N., and Sherman, Albert: Airfoil Section Characteristics as Affected by Variations of the Reynolds Number. NACA Rep. No. 586, 1937.

4. Quinn, John H., Jr.: Tests of the NACA 64_1A212 Airfoil Section with a Slat, a Double Slotted Flap, and Boundary-Layer Control by Suction. NACA TN No. 1293, 1947.

5. Loftin, Laurence K., Jr.: Theoretical and Experimental Data for a Number of NACA 6A-Series Airfoil Sections. NACA TN No. 1368, 1947.

6. Fullmer, Felicien F., Jr.: Two-Dimensional Wind-Tunnel Investigation of the NACA 64_1-012 Airfoil Equipped with Two Types of Leading-Edge Flap. NACA TN No. 1277, 1947.

7. Fullmer, Felicien F., Jr.: Two-Dimensional Wind-Tunnel Investigation of an NACA 64-009 Airfoil Equipped with Two Types of Leading-Edge Flap. NACA TN No. 1624, 1948.

8. Sivells, James C., and Neely, Robert H.: Method for Calculating Wing Characteristics by Lifting-Line Theory Using Nonlinear Section Lift Data. NACA TN No. 1269, 1947.

9. Bollech, Thomas V.: Experimental and Calculated Characteristics of Several High-Aspect-Ratio Tapered Wings Incorporating NACA 44-Series, 230-Series, and Low-Drag 64-Series Sections. NACA TN No. 1677, 1948.

10. Sivells, James C.: Experimental and Calculated Characteristics of Three Wings of NACA 64-210 and 65-210 Airfoil Sections with and without 2° Washout. NACA TN No. 1422, 1947.

11. Neely, Robert H., Bollech, Thomas V., Westrick, Gertrude C., and Graham, Robert R.: Experimental and Calculated Characteristics of Several NACA 44-Series Wings with Aspect Ratios of 8, 10, and 12 and Taper Ratios of 2.5 and 3.5. NACA TN No. 1270, 1947.

12. Soulé, H. A., and Anderson, R. F.: Design Charts Relating to the Stalling of Tapered Wings. NACA Rep. No. 703, 1940.

13. Harmon, Sidney M.: Additional Design Charts Relating to the Stalling of Tapered Wings. NACA ARR, Jan. 1943.

14. Sweberg, Harold H., and Dingeldein, Richard C.: Summary of Measurements in Langley Full-Scale Tunnel of Maximum Lift Coefficients and Stalling Characteristics of Airplanes. NACA Rep. No. 829, 1945.

15. Anderson, Raymond F.: A Comparison of Several Tapered Wings Designed to Avoid Tip Stalling. NACA TN No. 713, 1939.

16. Sivells, James C., and Spooner, Stanley H.: Investigation in the Langley 19-Foot Pressure Tunnel of Two Wings of NACA 65-210 and 64-210 Airfoil Sections with Various Type Flaps. NACA TN No. 1579, 1948.

17. Furlong, G. Chester, and Fitzpatrick, James E.: Effects of Mach Number and Reynolds Number on the Maximum Lift Coefficient of a Wing of NACA 230-Series Airfoil Sections. NACA TN No. 1299, 1947.

18. Hieser, Gerald: Tuft Studies of the Flow over a Wing at Four Angles of Sweep. NACA RM No. L7C05a, 1947.

19. Anderson, Raymond F.: Determination of the Characteristics of Tapered Wings. NACA Rep. No. 572, 1936.

20. Letko, William, and Goodman, Alex: Preliminary Wind-Tunnel Investigation at Low Speed of Stability and Control Characteristics of Swept-Back Wings. NACA TN No. 1046, 1946.

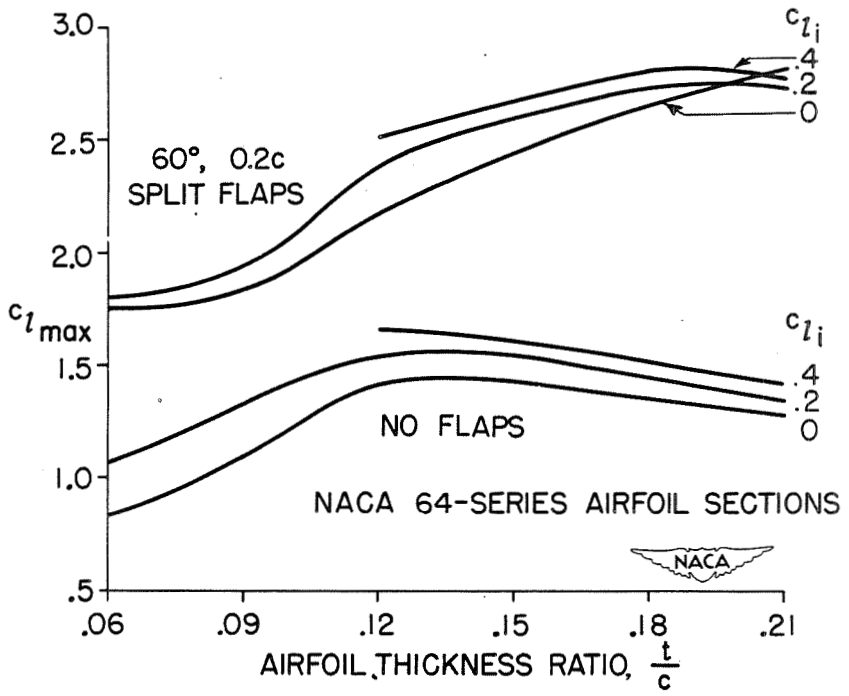

Figure 1.- Maximum-lift characteristics of NACA 64-series airfoil sections at a Reynolds number of 6×10^6.

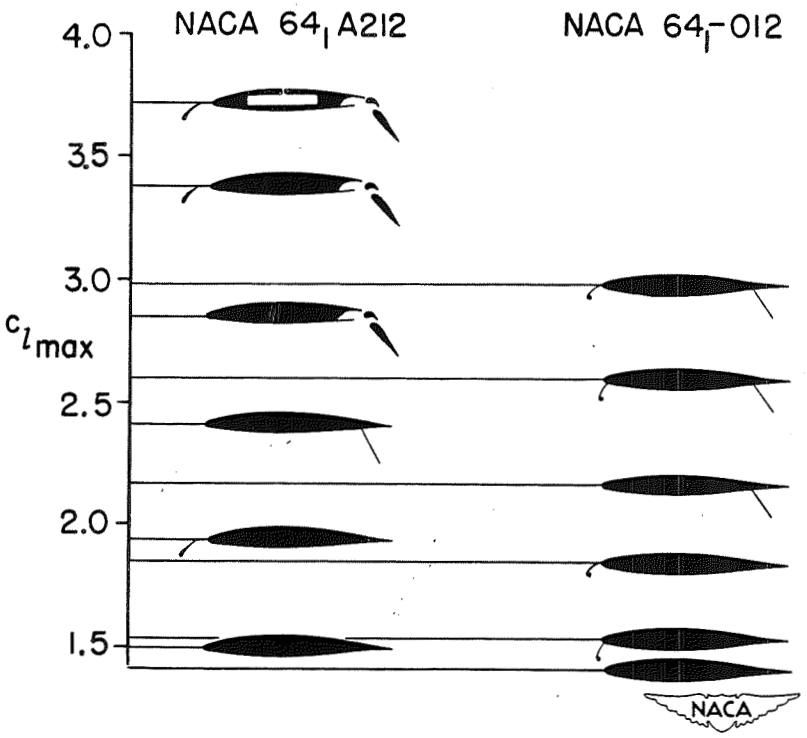

Figure 2.- Maximum lift coefficients of NACA 64_1A212 and 64_1-012 airfoil sections with various high-lift devices. Reynolds number, 6×10^6.

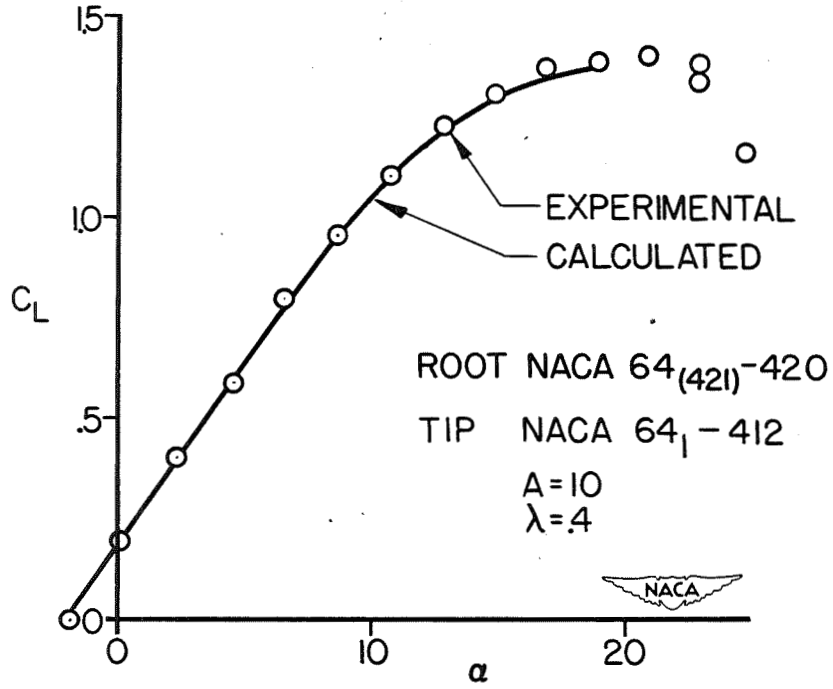

Figure 3.- Experimental and calculated maximum-lift characteristics of a wing with NACA 64-series sections.

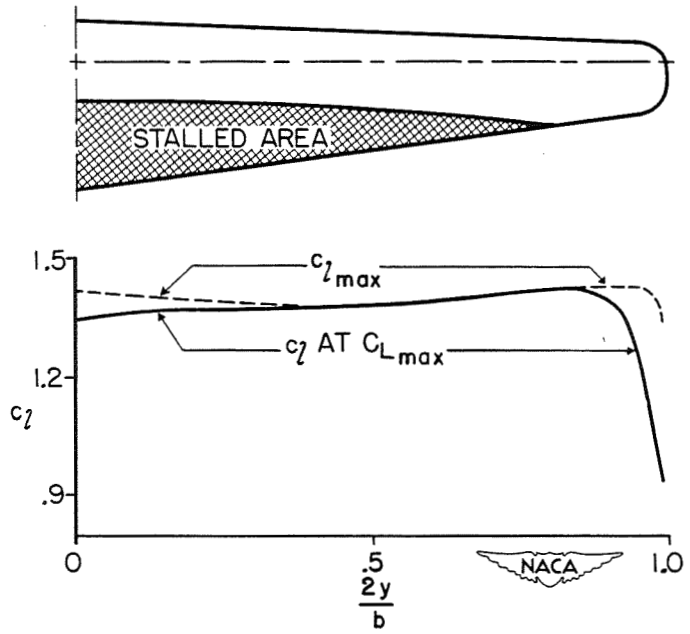

Figure 4.- Experimental and calculated stalling characteristics of a wing with NACA 64-series sections.

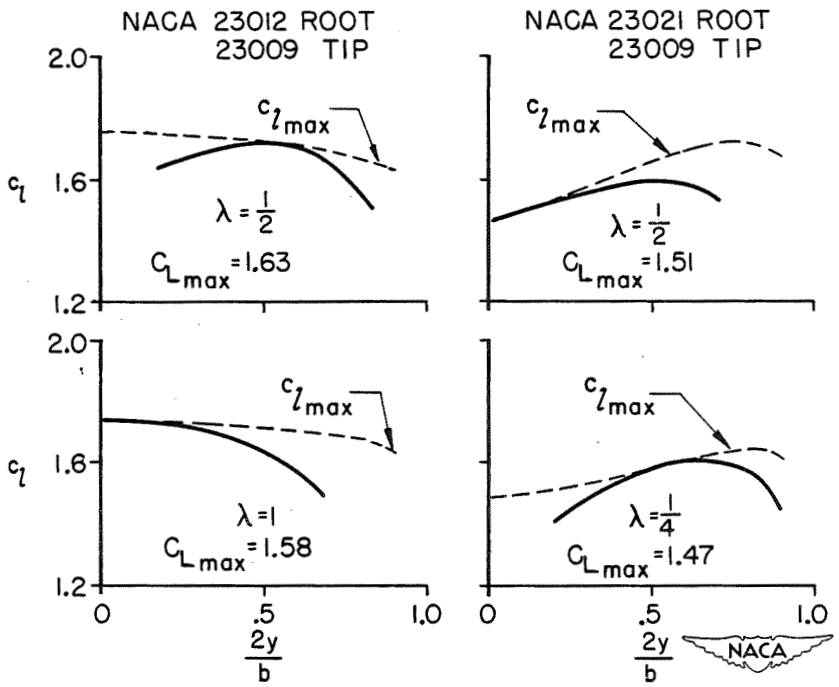

Figure 5.- Spanwise lift-coefficient distributions at maximum lift for four wings with NACA 230-series sections. Aspect ratio, 6; Reynolds number, 8×10^6.

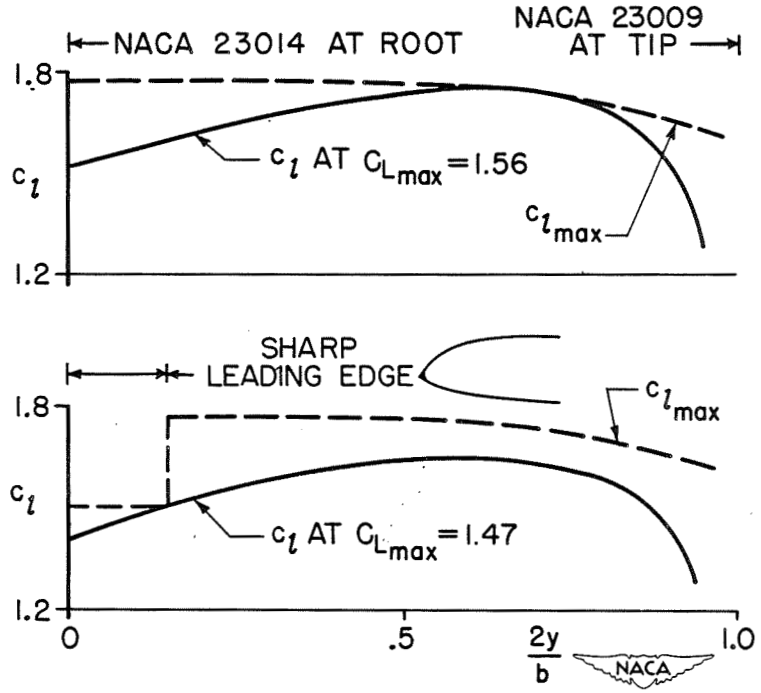

Figure 6.- Effect of a sharp leading edge on the calculated stalling characteristics of a wing.

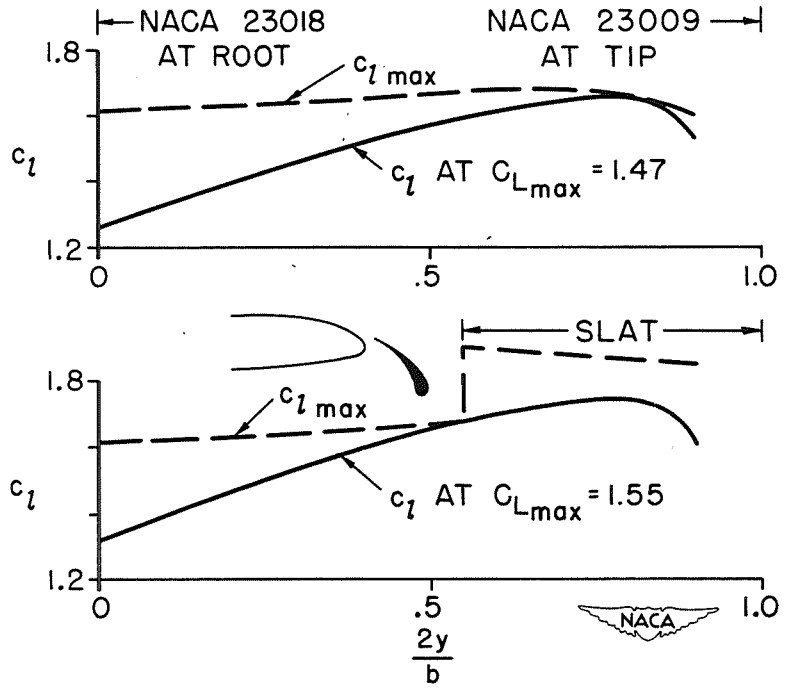

Figure 7.- Effect of leading-edge slats on the calculated stalling characteristics of a wing.

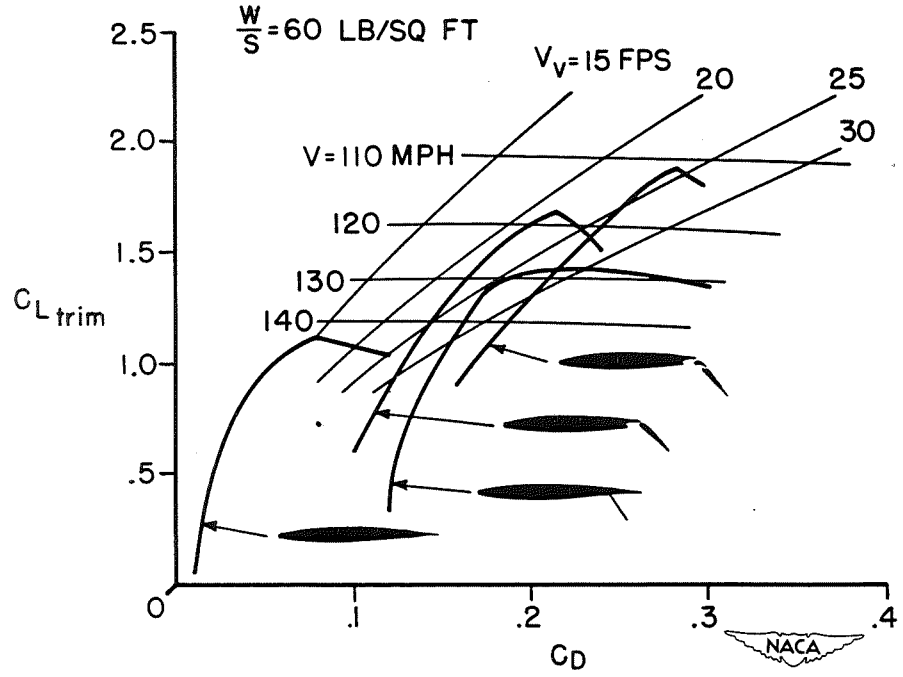

Figure 8.- Effect of split, single slotted, and double slotted flaps on the lift-drag characteristics of a wing with NACA 65-210 airfoil sections.

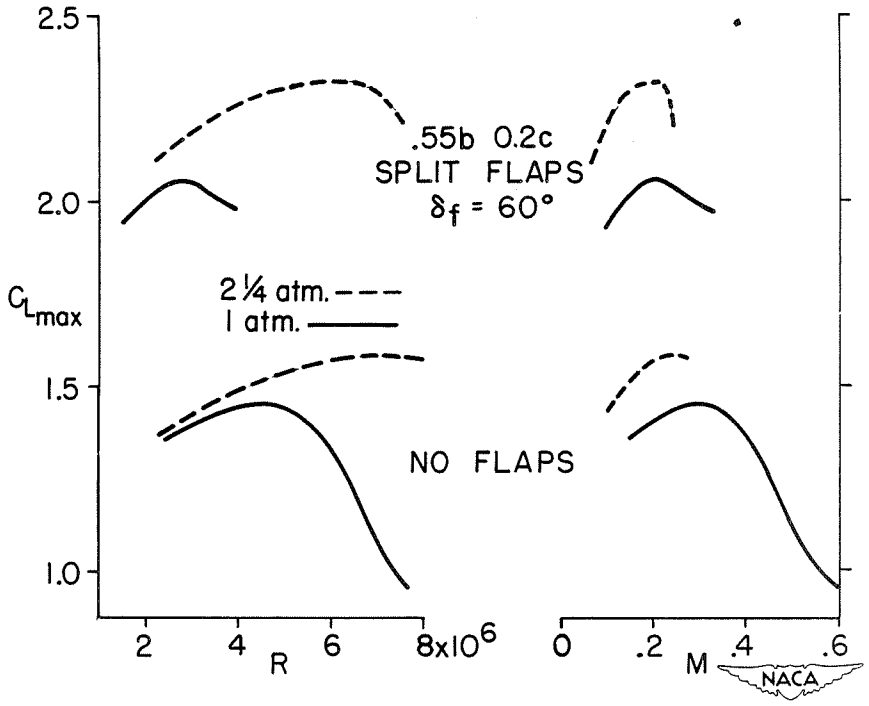

Figure 9.- Effect of Reynolds number and Mach number on the maximum lift coefficient of a wing with NACA 230-series airfoil sections.

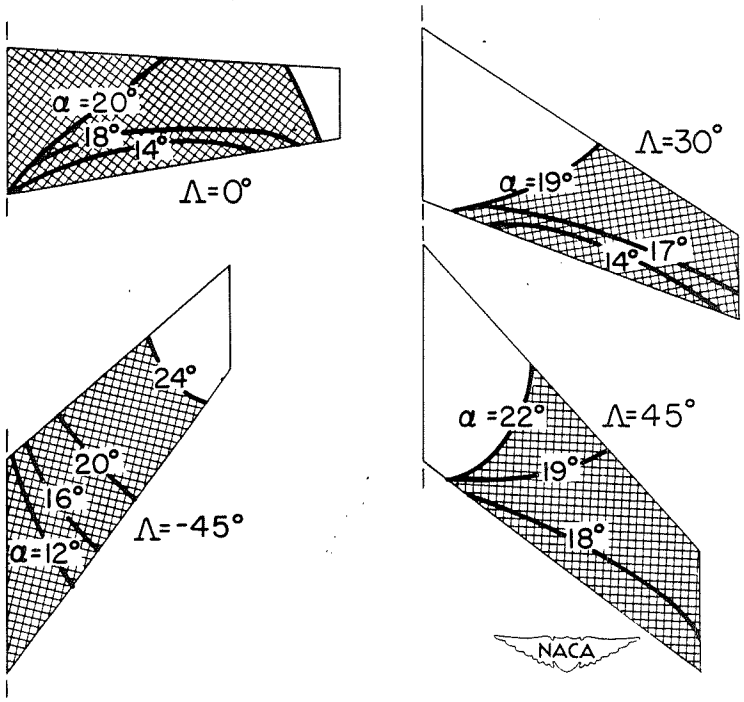

Figure 10.- Stall progressions for wings with and without sweep.

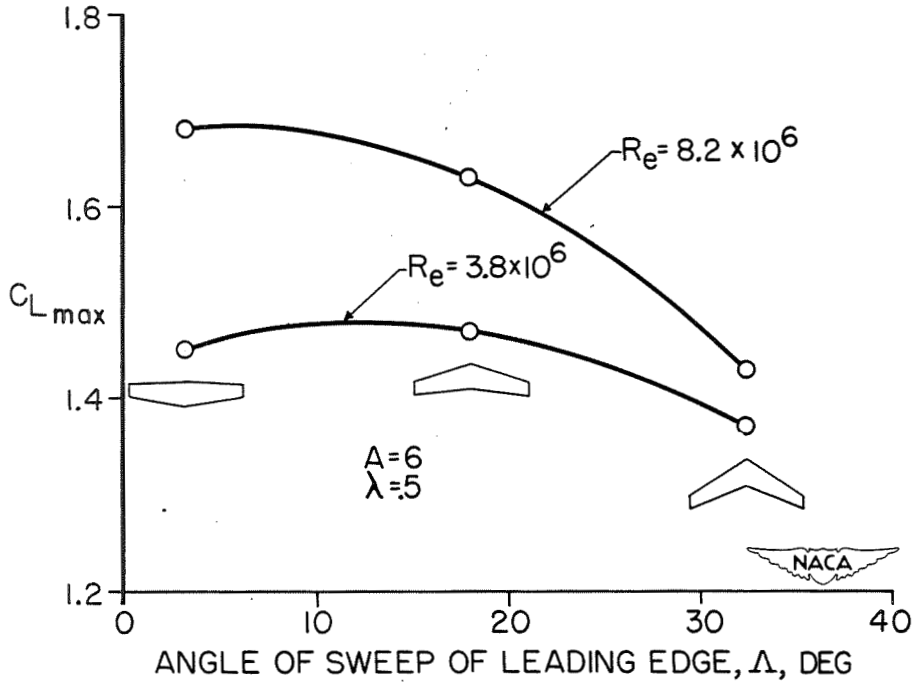

Figure 11.- Effect of sweep on the maximum lift coefficients of wings.

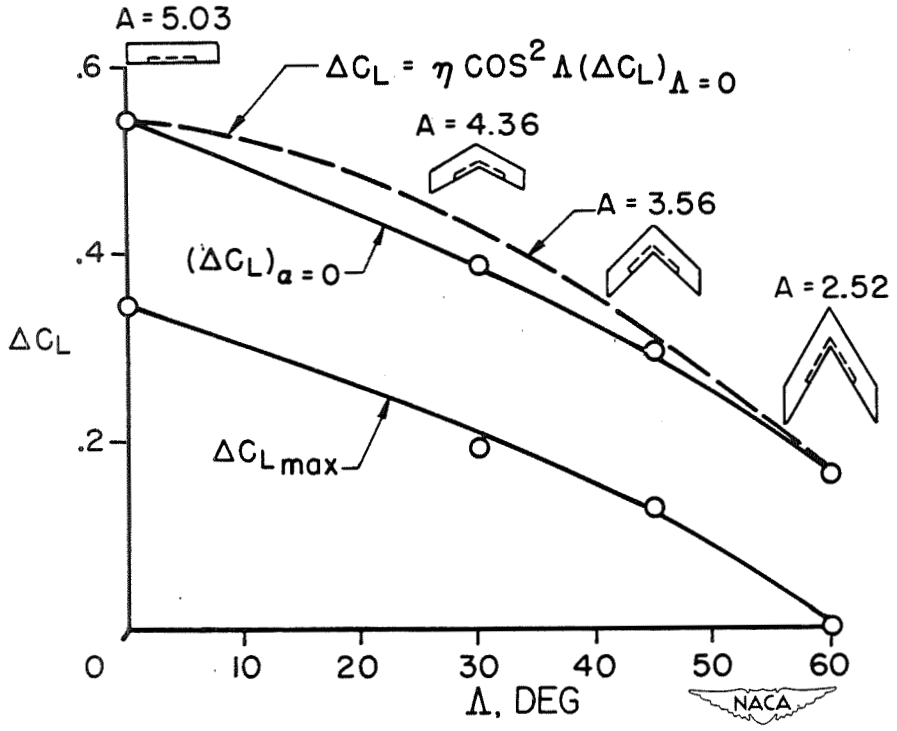

Figure 12.- Effect of sweep on the increment in lift coefficient due to flaps.

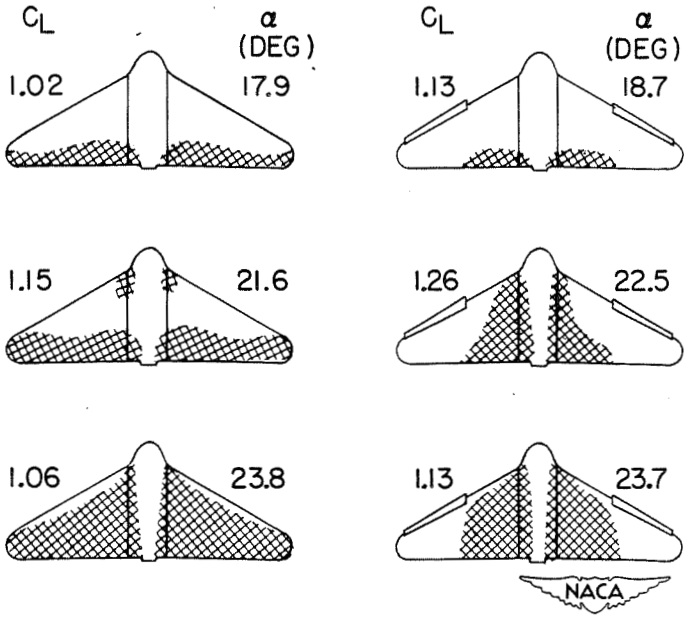

Figure 13.- Effect of leading-edge slats on the stalling characteristics of a sweptback wing.

STABILITY AND CONTROL

FACTORS AFFECTING STATIC LONGITUDINAL STABILITY AND CONTROL

By Charles J. Donlan

Langley Aeronautical Laboratory

INTRODUCTION

The purpose of this paper is to review the various factors that constitute static longitudinal stability and control and to indicate how these factors may be influenced by power effects and Mach number effects.

SYMBOLS

C_m	pitching-moment coefficient
C_L	lift coefficient
b	wing span
S	wing area
i_t	stabilizer incidence, degrees
ϵ'	increment of power-off downwash at horizontal tail (at given angle of attack) from zero-lift downwash, degrees
$\Delta\epsilon$	increment in downwash, at a given angle of attack, due to power, degrees
T_c	thrust coefficient $\left(\frac{\text{Thrust}}{\rho V^2 D^2}\right)$
ΔT_c	increment in thrust coefficient from power-off condition to a specified power condition
F	plan-form factor
M	Mach number

BASIC CONCEPTS

Static stability relates to the behavior of an airplane in a series of steady states of motion. It is of interest, therefore, to aline the

practical conditions for stability as desired by pilots with the conditions for stability that result from a mathematical treatment of the subject. From the pilot's point of view an airplane possesses stick-position stability if the stick must be moved rearward to retrim the airplane at a speed lower than the initial trimmed speed or moved forward to retrim the airplane at a speed higher than the initial trimmed speed. If the rearward movement of the stick requires a pull force or if the forward movement of the stick requires a push force, the airplane also possesses stick-force stability.

The basic mathematical condition for static stability is that the constant term E of the quartic stability equation be positive:

$$\lambda^4 + B\lambda^3 + C\lambda^2 + D\lambda + E = 0 \qquad (1)$$

The development of equation (1) for the stick-fixed condition may be found in references 1 and 2 and for the stick-free condition in reference 3.

Physically, a positive value of E indicates that one of the longitudinal modes of motion of the airplane will consist of a long-period oscillation, classically termed a phugoid oscillation. The question of the characteristics of this oscillation, and whether it is stable or unstable, is one of dynamic stability and therefore is not discussed herein. A discussion of its importance from the pilot's point of view may be found in reference 4. It will suffice to say that if E is positive, the phugoid oscillation will be present in some form but, more important, the previously mentioned relationships concerning stick-position and stick-force stability will be satisfied.

On the other hand, if E is negative, the long-period phugoid oscillation is replaced essentially by a slow divergence and the pilot will find it necessary to reverse his customary procedure for retrimming the airplane. This reversal of customary flight procedure, while not particularly desirable, is generally not catastrophic because the divergence that develops as a consequence of this type of instability depends on speed changes that take considerable time to develop.

The expression "static stability" has also been used to describe the weathercock tendencies of an airplane while flying at a constant speed. This type of stability is essentially angle-of-attack stability and is extremely important in that it prevents, for example, the airplane from developing excessive load factors when encountering a gust or other disturbances. Static stability is frequently referred to as "maneuvering stability," inasmuch as it also controls the inherent maneuverability of the airplane. The mathematical condition

for this type of stability is that the coefficient C of equation (1) be positive. Physically, if C is positive, a short-period oscillation is present; if C is negative, the oscillation is replaced by a very rapid and dangerous divergence. It should be emphasized that from the point of view of safety it is the type of stability associated with C that is most important to the pilot.

In simplified treatments of stability where power effects and compressibility effects are ignored, little misunderstanding results from the different interpretations attached to the term "static stability" because the same factor, the slope of the curve of pitching-moment coefficient against lift coefficient, usually determines the sign of both E and C. When the effects of power and compressibility are taken into account, however, the terms E and C are no longer dependent on the same parameters and a more precise interpretation of their significance is essential.

The four concepts and definitions commonly employed in current discussions of longitudinal stability are summarized in table I. The type of stability associated with E is manifested as stick-position stability or as stick-force stability. The degree of stability is measured by the static margin, defined as $-\left(\frac{dC_m}{dC_L}\right)_{C_m=0}$. The parameter $-\left(\frac{dC_m}{dC_L}\right)_{C_m=0}$ can be evaluated from wind-tunnel tests with the controls either fixed or free if the tests are conducted to simulate the appropriate power condition and flight plan. The center-of-gravity position for which the static margin vanishes for either the stick-position or stick-force condition defines the neutral point.

The type of stability associated with the term C is interpreted and measured by the pilot in terms of the control movement or control force required to effect a given acceleration at a constant speed. The degree of stability is proportional to the so-called maneuver margin. The maneuver margin can be evaluated from wind-tunnel tests as the sum of the slope of the pitching-moment curve obtained at a constant Mach number and for a fixed power condition and a term representing the damping-in-pitch characteristics of the airplane. For heavily loaded airplanes flying at high altitudes K is negligible and the maneuver margin is given essentially as $-\left(\frac{\partial C_m}{\partial C_L}\right)_M$ which can easily be obtained from wind-tunnel tests. The maneuver point coincides with the center-of-gravity position corresponding to zero maneuver margin.

If the manner in which the pitching-moment coefficient varies with the lift coefficient is known, all the essential stability parameters can be evaluated.

STABILITY AT SUBCRITICAL SPEEDS

The stability of a conventional-type airplane is determined by the relative contributions of the wing-fuselage combination and the horizontal tail. At subcritical speeds the contribution of the basic wing-fuselage combination can be estimated fairly reliably, and numerous papers and charts are available for simplifying such calculations. (See references 5 to 10.) The contribution of the horizontal tail in the absence of slipstream or jet effects can also be estimated fairly reliably for both the flaps-retracted and flaps-deflected conditions (reference 11) with the aid of downwash charts such as those prepared by Silverstein and Katzoff (reference 12). Reliable methods are also available for estimating the hinge-moment characteristics of the elevator; thus, rational estimates of the stick-free stability characteristics can be made. (See reference 13.) The addition of a propeller or a jet may, however, cause important changes in the contributions supplied by the various components, and a knowledge of the manner in which these effects are manifested is extremely helpful in design.

POWER EFFECTS

Propeller effects.- Successful methods have been developed for estimating the effects of the slipstream on the wing-fuselage characteristics (references 14 to 18), but attempts to predict the complex changes in flow at the tail plane have been less successful.

During the war years a large amount of experimental data pertaining to propeller effects were obtained particularly for single-engine airplanes. Typical investigations are reported in references 19 to 28. These data have been analyzed and a method has been developed for estimating the effects of power on the contribution of the tail to stability. The essence of the method is presented in figures 1 and 2, which were taken from an unpublished analysis.

The data of figure 1 constitute a correlation of the change in downwash angle resulting from an increment in thrust coefficient above the windmilling condition. A correlation study of 26 specific model configurations has indicated that the most powerful factors influencing the incremental downwash angle are the initial downwash angle ϵ' and a factor F

dependent on the wing plan form. It has been observed that taper ratio is of particular importance, and the manner in which the plan-form correlation factor F varies with wing taper ratio is also shown in figure 1. The dashed lines parallel to the design curve represent the order of accuracy which might be expected in applying this chart to a new design.

A correlation chart for estimating the power-on tail effectiveness is shown in figure 2. The dependency of the tail-effectiveness ratio on the relative position of the slipstream and tail position should be noted. The lines parallel to the design curve again indicate the order of accuracy of the correlation. These correlation charts at present are applicable only to single-engine tractor monoplanes with flaps retracted, but it is hoped eventually to obtain similar correlation charts for the flap-down condition.

From correlation charts such as those shown in figures 1 and 2 it is possible to construct curves of the variation of pitching-moment coefficient with lift coefficient for any power condition, and from these curves all of the essential stability parameters can be evaluated. References 29 and 30 contain graphical methods for determining the location of the neutral point.

The scarcity of systematic data on multiengine installations has thus far prevented the development of similar correlations for these configurations.

Jet effects.- The influence of jets on the longitudinal stability is, in general, not as pronounced as propellers. (See reference 31.) Direct jet effects are easily computable and charts are available for estimating the inflow field about a jet; thus, the calculation of downwash changes in the vicinity of the horizontal tail is possible (reference 32).

COMPRESSIBILITY EFFECTS

Up to the speed at which the critical Mach number of the wing is exceeded, the effects of compressibility on the stability characteristics of an airplane are relatively small, and rational estimates of these effects can be made utilizing formulas based on linear perturbation theory. The more significant changes in stability occur when the critical speed of the wing is exceeded and shock waves are found which result in large pressure changes over the wing. As a consequence, the lift and the lift-curve slope decrease rapidly, and for cambered sections the angle of attack for zero lift shifts in a positive direction. These changes are generally more pronounced for wings having greater camber.

The aerodynamic center of the wing may shift either in a forward or rearward direction depending upon the thickness and shape of the airfoil section and the wing plan form. The wing-aerodynamic-center shift associated with a particular airplane will also be affected by the fuselage or nacelles.

An example of the manner in which compressibility effects were manifested on a World War II fighter is shown in figure 3. (See reference 33.) The characteristics exhibited at $M = 0.5$ are typical of the behavior below the force break. As the critical speed of the wing was exceeded the aerodynamic center of the wing-fuselage combination moved forward as evidenced by the increased slope of the tail-off pitching-moment curve at $M = 0.76$. Despite the forward movement of the wing aerodynamic center, however, the slope $\left(\partial C_m/\partial C_L\right)_M$ for the tail-on configuration was actually increased. A noticeable change in trim is also evident. Thus, while the maneuver margin is considerably increased the static margin, as a consequence of the trim change, becomes unstable. The cause of this behavior usually is that the airplane will experience a nose-down tendency that is so great that either the elevator is not powerful enough to pull the nose of the airplane up or the control forces become too great for the pilot to handle. This behavior is referred to as the "tucking under" tendency.

If an airplane has an adjustable stabilizer, severe trim changes of this type can be compensated for without much difficulty. If the airplane has a fixed stabilizer, however, another solution to this problem is required. The solution adopted for the airplane having the characteristics shown in figure 3 involved the use of dive-recovery flaps. The essential characteristic of a dive-recovery flap is illustrated in figure 4 (reference 34). The dive flap is located on the under surface of the wing and, when deflected, causes an increase in the local downwash at the tail and a change in the angle of zero lift. The effect is the same as though the stabilizer had been moved nose downward, and a powerful positive pitching moment is created. The optimum flap deflection for a particular configuration, however, must be determined experimentally.

Severe compressibility effects may be delayed to higher Mach numbers by utilizing thinner wing sections and by employing plan forms having low aspect ratios or plan forms incorporating sweepback. (See references 35 and 36.) The incorporation of sweepback is particularly beneficial and can significantly increase the Mach number at which serious longitudinal-stability problems are encountered and might be expected also to reduce the trim changes and stability changes encountered at supercritical speeds.

One of the factors that limits the amount of sweepback that can be employed, however, is the difficulty of providing satisfactory stability and control in the landing condition.

Basic-wing characteristics.- At lift coefficients prior to that at which separated flow ensues on the wing, the position of the aerodynamic center of the wing can be estimated fairly reliably. The shift in the aerodynamic-center position that occurs at high lift coefficients is less amenable to theoretical computations, and numerous experimental investigations have been concerned with this effect. From the data examined thus far it appears that aspect ratio and sweep angle are still the two most important factors that influence the type of pitching-moment variation to be expected at the stall. The familiar manner in which sweep angle and aspect ratio affect the character of the pitching-moment variation at the stall is illustrated in figure 5, which is taken from reference 37. Combinations of sweep and aspect ratio that fall above the line in the figure have been found to yield the characteristically unstable pitching-moment variation indicated. Other factors such as airfoil section, wing taper, Reynolds number, and surface roughness have been found to influence the lift coefficient at which instability is first manifested, but the ultimate variation at the stall has still been found to be consistent with that indicated in figure 5.

While figure 5 reflects the behavior of plain wings, it has been found that the addition of trailing-edge flaps has resulted in an unstable pitching-moment variation even for wings falling in the stable region. A considerable number of investigations have, therefore, been concerned with the development of devices designed to alleviate the tip stalling that is responsible for this behavior.

Stall control devices.- Methods that have been tried in attempts to alleviate the tip stalling of sweptback wings have included wing twist, changes in wing plan form at the tip, flat-plate separators - which attempt to control the lateral flow of the boundary layer - and leading-edge flaps and slats. Combinations of these methods have also been tried on specific configurations. Perhaps the most successful stall control device thus far investigated has been the leading-edge slat. Figure 6 illustrates the behavior of this device on a moderately swept wing. (See reference 38.) It will be noticed that in this example the slat had to be extended over approximately 50 percent of the wing semispan before the desired stable pitching moment at the stall was attained. Inasmuch as the leading-edge slat modifies the span loading along the wing it might be expected that the optimum extent of flap for a particular configuration would depend on the wing plan form and the location of the wing on the fuselage.

Effect of tail location.- The attainment of satisfactory pitching-moment characteristics for the wing-fuselage combination does not guarantee that the configuration with a horizontal tail added will also be satisfactory. The optimum location of the tail must usually be found experimentally. Figure 7 which is taken from reference 39 illustrates a case where the basic wing-fuselage pitching-moment behavior was satisfactory but the resultant pitching-moment behavior with the tail in position was unsatisfactory. It is generally easier, however, to find a tail location that will result in satisfactory stability for the complete configuration if the basic wing-fuselage combination also possesses a stable pitching-moment variation at the stall.

CONCLUDING REMARKS

It must constantly be borne in mind that even if ample rigid-model wind-tunnel data are available on which to base predictions of stability, the effects of aeroelastic distortion may result in the airplane having completely different characteristics from those estimated. Some of the effects of elevator-fabric distortion are indicated, for example, in reference 40. At the same time the basic concepts of stability discussed still apply and if wind-tunnel data on an aeroelastically similar model were available reliable stability estimates could be made. There is, however, a great deal of research necessary before satisfactory methods of predicting aeroelastic effects can be developed.

REFERENCES

1. Zimmerman, Charles H.: An Analysis of Longitudinal Stability in Power-Off Flight with Charts for Use in Design. NACA Rep. No. 521, 1935.

2. Donlan, Charles J.: Some Theoretical Considerations of Longitudinal Stability in Power-On Flight with Special Reference to Wind-Tunnel Testing. NACA ARR, Nov. 1942.

3. Greenberg, Harry, and Sternfield, Leonard: A Theoretical Investigation of Longitudinal Stability of Airplanes with Free Controls Including Effect of Friction in Control System. NACA Rep. No. 791, 1944.

4. Phillips, William H.: Appreciation and Prediction of Flying Qualities. NACA TN No. 1670, 1948.

5. Anderson, Raymond F.: Determination of the Characteristics of Tapered Wings. NACA Rep. No. 572, 1936.

6. Pearson, Henry A., and Anderson, Raymond F.: Calculation of Aerodynamic Characteristics of Tapered Wings with Partial-Span Flaps. NACA Rep. No. 665, 1939.

7. Multhopp, H.: Aerodynamics of the Fuselage. NACA TM No. 1036, 1942.

8. Jacobs, Eastman N., and Ward, Kenneth E.: Interference of Wing and Fuselage from Tests of 209 Combinations in the N.A.C.A. Variable-Density Tunnel. NACA Rep. No. 540, 1935.

9. White, Maurice D.: Estimation of Stick-Fixed Neutral Points of Airplanes. NACA CB No. L5C01, 1945.

10. Gilruth, R. R., and White, M. D.: Analysis and Prediction of Longitudinal Stability of Airplanes. NACA Rep. No. 711, 1941.

11. Silverstein, Abe, Katzoff, S., and Bullivant, W. Kenneth: Downwash and Wake behind Plain and Flapped Airfoils. NACA Rep. No. 651, 1939.

12. Silverstein, Abe, and Katzoff, S.: Design Charts for Predicting Downwash Angles and Wake Characteristics behind Plain and Flapped Wings. NACA Rep. No. 648, 1939.

13. Langley Research Department (Compiled by Thomas A. Toll): Summary of Lateral-Control Research. NACA TN No. 1245, 1947.

14. Smelt, R., and Davies, H.: Estimation of Increase in Lift Due to Slipstream. R. & M. No. 1788, British A.R.C., 1937.

15. Goett, Harry J., and Delany, Noel K.: Effect of Tilt of the Propeller Axis on the Longitudinal-Stability Characteristics of Single-Engine Airplanes. NACA Rep. No. 774, 1944.

16. Ribner, Herbert S.: Notes on the Propeller and Slipstream in Relation to Stability. NACA ARR No. L4I12a, 1944.

17. Stüper, J.: Effect of Propeller Slipstream on Wing and Tail. NACA TM No. 874, 1938.

18. Katzoff, S.: Longitudinal Stability and Control with Special Reference to Slipstream Effects. NACA Rep. No. 690, 1940.

19. Weil, Joseph, and Boykin, Rebecca I.: Wind-Tunnel Tests of the 0.15-Scale Powered Model of the Fleetwings XBTK-1 Airplane. Longitudinal Stability and Control. NACA MR No. L5D27a, 1945.

20. Weil, Joseph, and Wells, Evalyn G.: Wind-Tunnel Tests of the 1/8-Scale Powered Model of the Curtiss XBTC-2 Airplane. I - Preliminary Investigation of Longitudinal Stability. NACA MR, June 1944.

21. Rogallo, Francis M., and Swanson, Robert S.: Wind-Tunnel Tests of a Twin-Engine Model to Determine the Effect of Direction of Propeller Rotation on Static-Stability Characteristics. NACA ARR, Jan. 1943.

22. Hagerman, John R.: Wind-Tunnel Investigation of the Effect of Power and Flaps on the Static Longitudinal Stability and Control Characteristics of a Single-Engine High-Wing Airplane Model. NACA TN No. 1339, 1947.

23. Wallace, Arthur R., Rossi, Peter F., and Wells, Evalyn G.: Wind-Tunnel Investigation of the Effect of Power and Flaps on the Static Longitudinal Stability Characteristics of a Single-Engine Low-Wing Airplane Model. NACA TN No. 1239, 1947.

24. Purser, Paul E., and Spear, Margaret F.: Wind-Tunnel Investigation of Effects of Unsymmetrical Horizontal-Tail Arrangements on Power-On Static Longitudinal Stability of a Single-Engine Airplane Model. NACA TN No. 1474, 1947.

25. Pass, H. R.: Wind-Tunnel Study of the Effects of Propeller Operation and Flap Deflection on the Pitching Moments and Elevator Hinge Moments of a Single-Engine Pursuit-Type Airplane.. NACA ARR, July 1942.

26. Harper, Charles W., and Wick, Bradford H.: A Comparison of the Effects of Four-Blade Dual- and Single-Rotation Propellers on the Stability and Control Characteristics of a High-Powered Single-Engine Airplane. NACA ARR No. 4F17, 1944.

27. Muttray, H.: Investigations on the Downwash behind a Tapered Wing with Fuselage and Propeller. NACA TM No. 876, 1938.

28. Hockman, Marion T., and Eisiminger, Robert E., Jr.: The Correlation of Wind-Tunnel and Flight-Test Stability and Control Data for an SB2C-1 Airplane. Jour. Aero. Sci., vol. 15, no. 1, Jan. 1948, pp. 5-17.

29. Schuldenfrei, Marvin: Some Notes on the Determination of the Stick-Fixed Neutral Point from Wind-Tunnel Data. NACA RB No. 3I20, 1943.

30. Schuldenfrei, Marvin: Some Notes on the Determination of the Stick-Free Neutral Point from Wind-Tunnel Data. NACA RB No. 4B21, 1944.

31. Abzug, Malcolm J.: Effect of Jet and Rocket Operation on Static Longitudinal and Directional Stability. A.D.R. Rep. M-35, Bur. Aero., March 1945.

32. Ribner, Herbert S.: Field of Flow about a Jet and Effect of Jets on Stability of Jet-Propelled Airplanes. NACA ACR No. L6C13, 1946.

33. Erickson, Albert L.: Investigation of Diving Moments of a Pursuit Airplane in the Ames 16-Foot High-Speed Tunnel. NACA MR, Oct. 7, 1942.

34. Erickson, Albert L.: Wind-Tunnel Investigation of Devices for Improving the Diving Characteristics of Airplanes. NACA MR No. 3F12, 1943.

35. Stack, John, and Lindsey, W. F.: Characteristics of Low-Aspect-Ratio Wings at Supercritical Mach Numbers. NACA TN No. 1665, 1948.

36. Jones, Robert T.: Wing Plan Forms for High-Speed Flight. NACA TN No. 1033, 1946.

37. Shortal, Joseph A., and Maggin, Bernard: Effect of Sweepback and Aspect Ratio on Longitudinal Stability Characteristics of Wings at Low Speeds. NACA TN No. 1093, 1946.

38. Langley Stability Research Division (Compiled by Charles J. Donlan): An Interim Report on the Stability and Control of Tailless Airplanes. NACA Rep. No. 796, 1944.

39. Purser, Paul E., Spearman, M. Leroy, and Bates, William R.: Preliminary Investigation at Low Speed of Downwash Characteristics of Small-Scale Sweptback Wings. NACA TN No. 1378, 1947.

40. Mathews, Charles W.: An Analytical Investigation of the Effects of Elevator-Fabric Distortion on the Longitudinal Stability and Control of an Airplane. NACA ACR No. L4E30, 1944.

TABLE I

TYPE	CRITERION
STICK-POSITION STABILITY	STATIC MARGIN $= -\left(\frac{dC_m}{dC_L}\right)_{C_m=0}$ WITH ELEV. FIXED
STICK-FORCE STABILITY	STATIC MARGIN $= -\left(\frac{dC_m}{dC_L}\right)_{C_m=0}$ WITH ELEV. FREE
STICK-POSITION MANEUVERING STABILITY	MANEUVER MARGIN $= -\left(\frac{\partial C_m}{\partial C_L}\right)_M + K$ WITH ELEV. FIXED
STICK-FORCE MANEUVERING STABILITY	MANEUVER MARGIN $= -\left(\frac{\partial C_m}{\partial C_L}\right)_M + K$ WITH ELEV. FREE

NACA

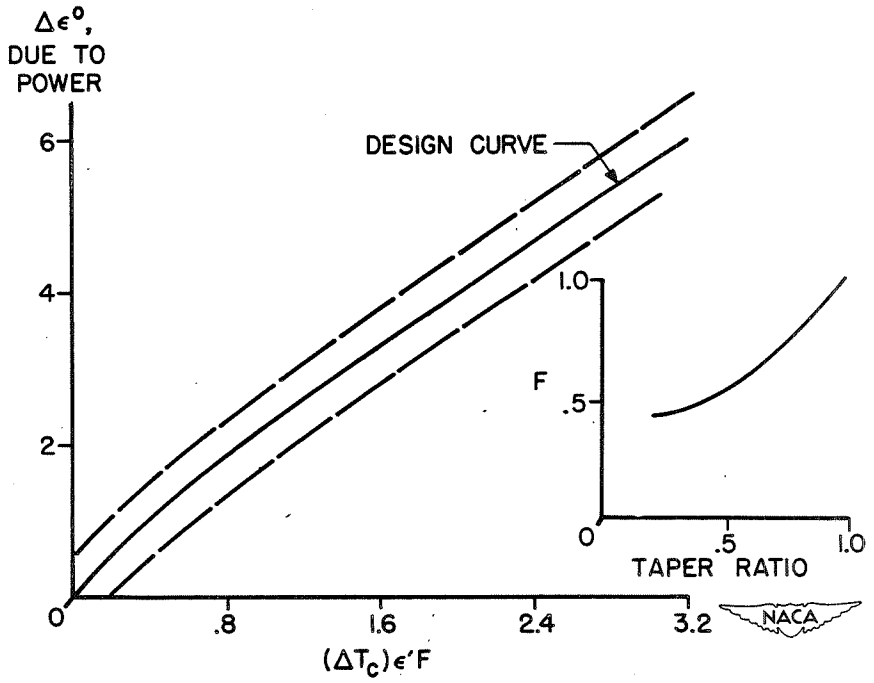

Figure 1.- Downwash correlation for single-engine tractor airplanes.

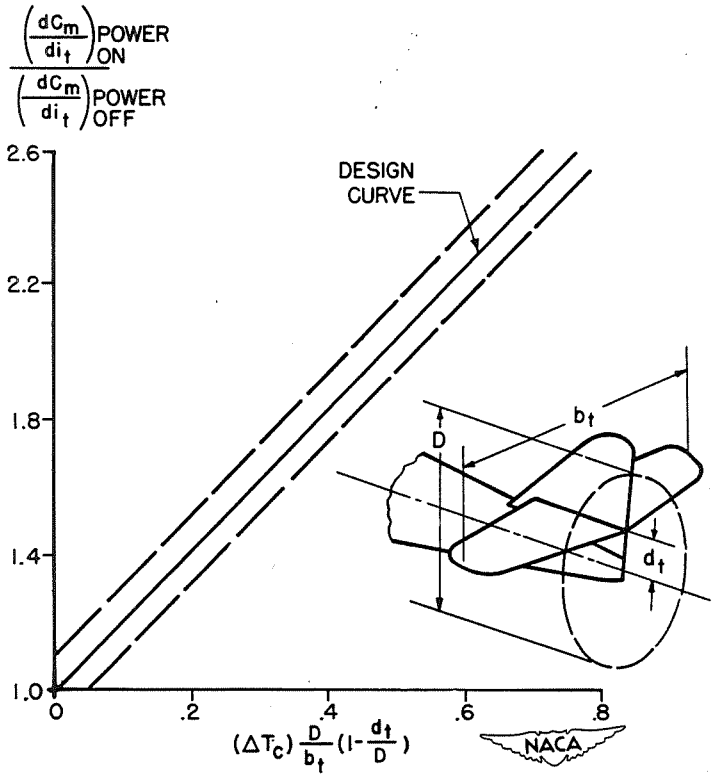

Figure 2.- Tail-effectiveness correlation for single-engine tractor airplanes.

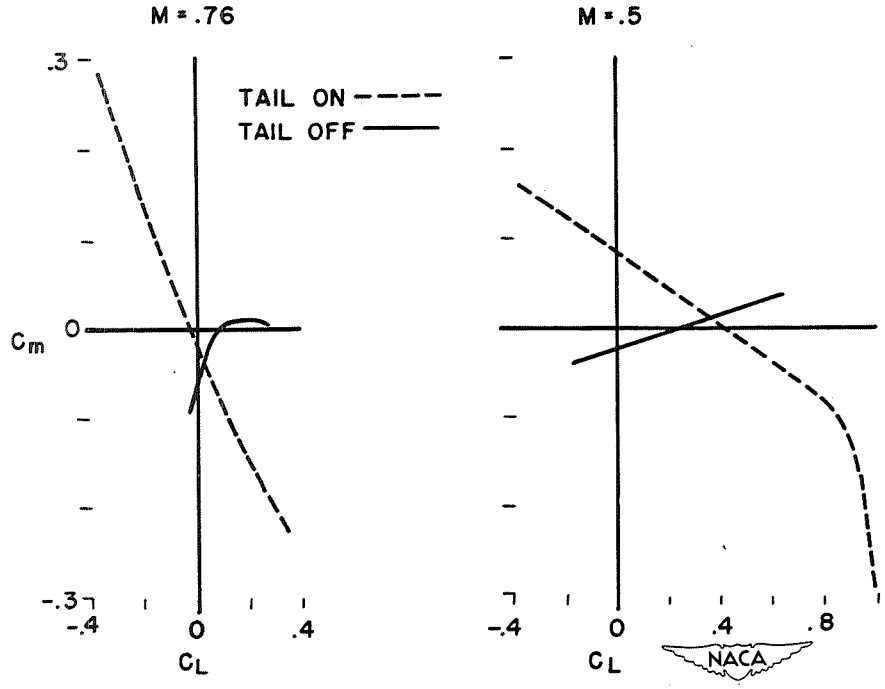

Figure 3.- Typical effect of compressibility on airplane pitching-moment characteristics.

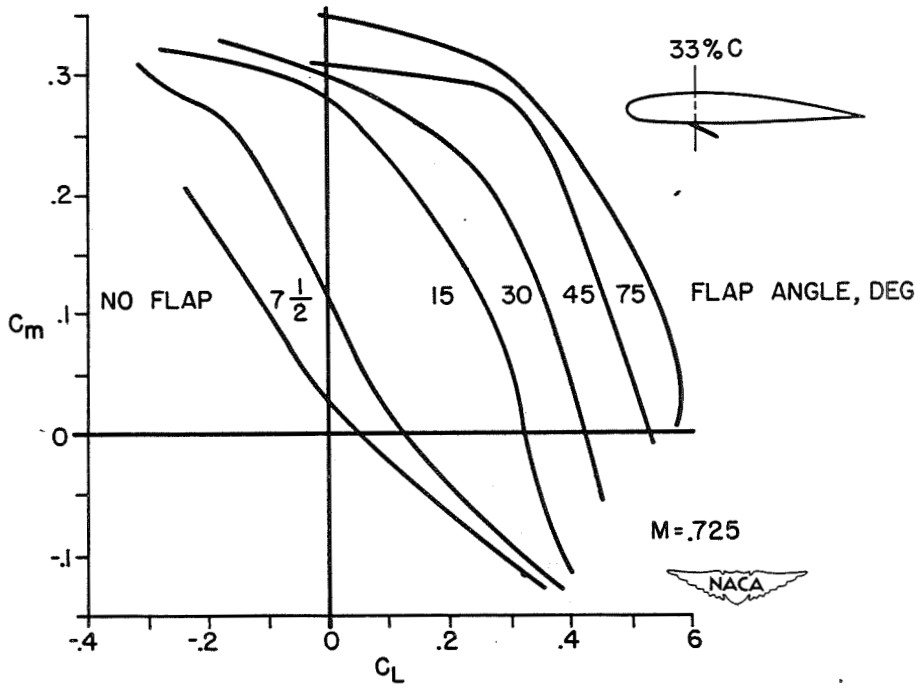

Figure 4.- Effect of dive-recovery flap on airplane pitching-moment characteristics.

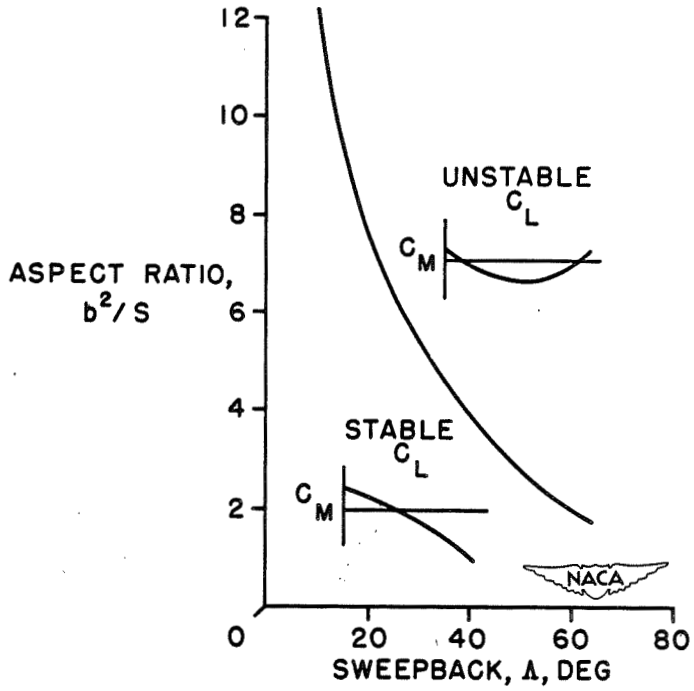

Figure 5.- Pitching-moment behavior of sweptback wings.

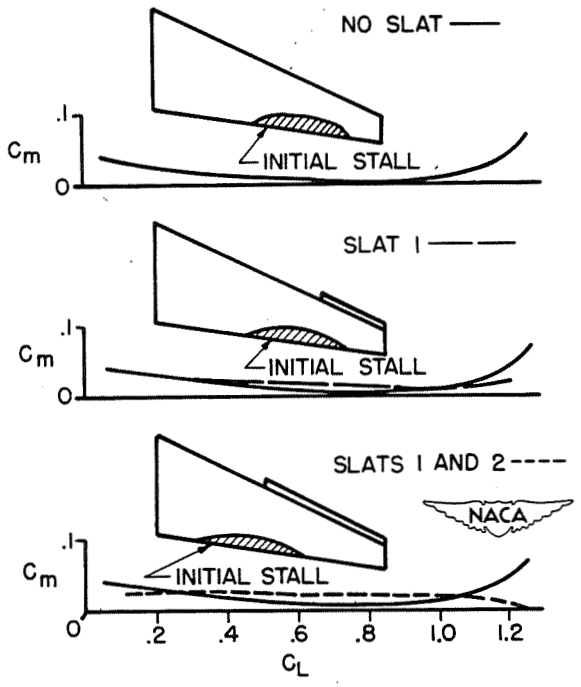

Figure 6.- Effect of leading-edge slats on pitching-moment characteristics.

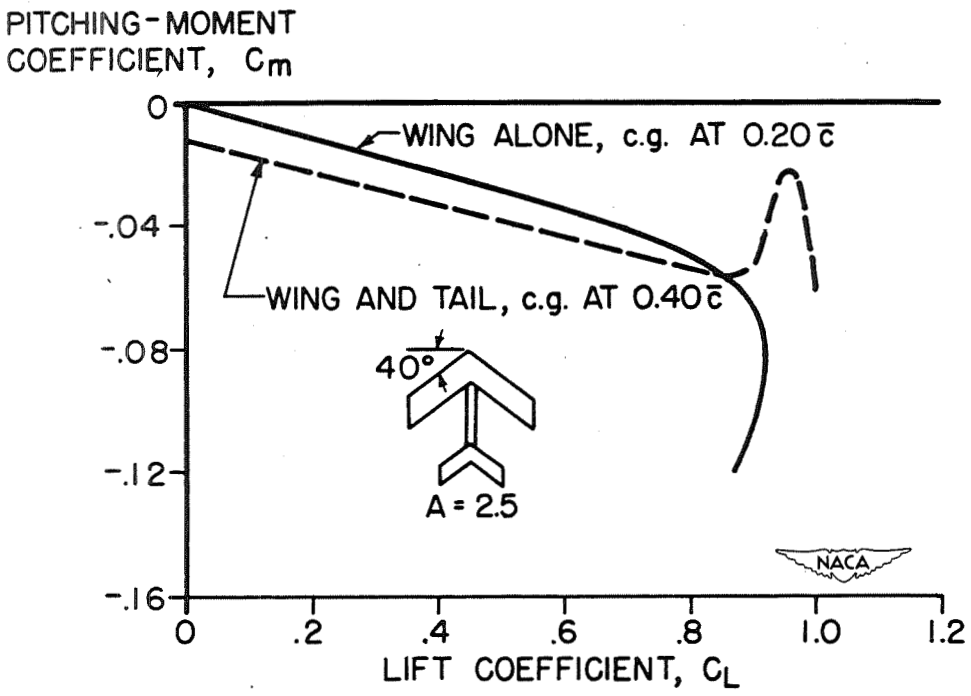

Figure 7.- Effect of tail on pitching-moment characteristics at stall.

FACTORS AFFECTING LATERAL STABILITY

By John P. Campbell

Langley Aeronautical Laboratory

INTRODUCTION

The term "lateral stability" used in this paper is intended to include all airplane stability other than longitudinal stability. That is, lateral stability includes directional (or weathercock) stability, rolling stability, bank stability (or dihedral effect) and, in fact, any form of stability that involves displacement of the plane of symmetry of the airplane by rolling, yawing, or sideslipping. Sometimes the term "lateral stability" has been used to mean only the stability associated with rolling moment due to sideslip or dihedral effect but this usage is not recommended because of the likelihood of confusion with the more general meaning of the term.

During the past few years many advances have been made toward an understanding of the complex problem of lateral stability. In the war years a great amount of experimental data on the subject was obtained from studies of military airplane designs. Analysis and correlation of these data have afforded an insight into the causes of lateral-stability difficulties and have in some cases permitted empirical methods to be set up for estimating certain stability characteristics. Basic lateral-stability research, both experimental and theoretical, was necessarily somewhat curtailed during the war but since that time this research has been accelerated to supply the ever-increasing demand for fundamental knowledge in the field of lateral stability.

SYMBOLS

C_L lift coefficient $\left(\frac{\text{Lift}}{\frac{1}{2}\rho V^2 S}\right)$

C_l rolling-moment coefficient $\left(\frac{\text{Rolling moment}}{\frac{1}{2}\rho V^2 Sb}\right)$

C_n yawing-moment coefficient $\left(\frac{\text{Yawing moment}}{\frac{1}{2}\rho V^2 Sb}\right)$

$C_{n'}$ fuselage yawing-moment coefficient $\left(\frac{\text{Yawing moment}}{\left(\frac{1}{2}\rho V^2\right)(\text{Fuselage volume})}\right)$

C_Y lateral-force coefficient $\left(\frac{\text{Lateral force}}{\frac{1}{2}\rho V^2 S}\right)$

C_{D_w} wing-drag coefficient $\left(\frac{\text{Drag}}{\frac{1}{2}\rho V^2 S}\right)$

ρ mass density, slugs per cubic foot

S wing area, square feet

b wing span, feet

z vertical height of wing above fuselage center line, feet

V airspeed, feet per second

v sideslip velocity, feet per second

β angle of sideslip

ψ angle of yaw $(\beta = -\psi)$

α angle of attack

p rolling angular velocity, radians per second

r yawing angular velocity, radians per second

$\frac{pb}{2V}$ rolling-angular-velocity factor or wing-tip helix angle generated by wing tip in roll, radians

$\frac{rb}{2V}$ yawing-angular-velocity factor, radians

C_{n_β} rate of change of yawing-moment coefficient with angle of sideslip, per degree $\left(\frac{\partial C_n}{\partial \beta}\right)$

C_{l_β} rate of change of rolling-moment coefficient with angle of sideslip, per degree $\left(\frac{\partial C_l}{\partial \beta}\right)$

C_{Y_β} rate of change of lateral-force coefficient with angle of sideslip, per degree $\left(\frac{\partial C_Y}{\partial \beta}\right)$

C_{n_p} rate of change of yawing-moment coefficient with rolling-angular-velocity factor, per radian $\left(\frac{\partial C_n}{\partial \frac{pb}{2V}}\right)$

C_{l_p} rate of change of rolling-moment coefficient with rolling-angular-velocity factor, per radian $\left(\frac{\partial C_l}{\partial \frac{pb}{2V}}\right)$

C_{Y_p} rate of change of lateral-force coefficient with rolling-angular-velocity factor, per radian $\left(\frac{\partial C_Y}{\partial \frac{pb}{2V}}\right)$

C_{n_r} rate of change of yawing-moment coefficient with yawing-angular-velocity factor, per radian $\left(\frac{\partial C_n}{\partial \frac{rb}{2V}}\right)$

C_{l_r} rate of change of rolling-moment coefficient with yawing-angular-velocity factor, per radian $\left(\frac{\partial C_l}{\partial \frac{rb}{2V}}\right)$

C_{Y_r} rate of change of lateral-force coefficient with yawing-angular-velocity factor, per radian $\left(\frac{\partial C_Y}{\partial \frac{rb}{2V}}\right)$

δ_f flap deflection, degrees

Λ angle of sweep of wing leading edge, degrees

A aspect ratio $\left(\frac{b^2}{S}\right)$

LATERAL-STABILITY DERIVATIVES

In a discussion of lateral stability it is necessary to break up this rather complex subject into its several related parts in order to get a clear picture of the advances that have recently been made in this field. One logical breakdown of lateral stability, illustrated in figure 1, involves the conventional lateral-stability derivatives used in dynamic lateral-stability work. (See references 1 to 6.) These stability derivatives are abbreviated expressions for the variations of

the rolling and yawing moments and lateral force with sideslipping, rolling, and yawing velocities. In order to make these derivatives nondimensional, the velocities v, p, and r are replaced by β $\left(\text{or } \frac{v}{V}\right)$, $\frac{pb}{2V}$, and $\frac{rb}{2V}$, respectively, as indicated at the bottom of figure 1. (See reference 1.)

The geometric designs around the derivatives in figure 1 indicate their relative importance as determined from an analysis of many theoretical and experimental studies of lateral stability. The circled derivatives have been found to be most important in that, if they are properly adjusted, the other derivatives usually have only minor effects on stability. In a discussion of lateral stability, these derivatives may logically be divided into three groups – sideslip, rolling, and yawing derivatives.

Sideslip Derivatives

The sideslip derivatives C_{n_β}, C_{l_β}, and C_{Y_β} are probably the most significant as well as the most familiar derivatives. They can be determined theoretically (references 1, 2, 6, and 7) and are also easily determined by ordinary wind-tunnel tests (references 8 to 19) in which the lateral forces and moments are measured with the model in a yawed (or sideslipped) attitude. From plots of the force-test data, the slopes $\frac{\partial C_n}{\partial \psi}$, $\frac{\partial C_l}{\partial \psi}$, and $\frac{\partial C_Y}{\partial \psi}$ (where ψ is the angle of yaw) are determined and these values are exactly equal to but opposite in sign to C_{n_β}, C_{l_β}, and C_{Y_β}, respectively. The yawing moment due to sideslip C_{n_β} is the static directional stability or weathercock-stability factor (references 20 to 34). The rolling moment due to sideslip C_{l_β} is the well-known effective-dihedral parameter which has received an increasing amount of attention in connection with highly swept wings. (See references 5, 19, 35, 36, and 37.) The lateral force due to sideslip C_{Y_β} is the effective lateral-area parameter, which is usually negligible if the weathercock stability C_{n_β} is adequate. This derivative will not be discussed further in this paper but more information on it can be obtained in references 1, 2, 6, and 38.

Rolling Derivatives

The rolling derivatives C_{n_p}, C_{l_p}, and C_{Y_p} have been treated theoretically in references 2, 6, and 39 and are measured by various experimental methods including continuous rotation tests (reference 40)

in which forces and moments are measured on a rolling model and rolling-flow tests in which the model remains stationary while the air stream in the wind tunnel is rotated (Langley stability tunnel, reference 41). Both the yawing moment due to rolling C_{n_p} and the rolling moment due to rolling (damping-in-roll factor) C_{l_p} are important from considerations of controllability as well as stability. The lateral force due to rolling C_{Y_p} is of measurable magnitude only for swept-wing airplanes and, since in all cases this derivative has been found to have an insignificant effect on stability, it will not be discussed further.

Yawing Derivatives

The yawing derivatives C_{n_r}, C_{l_r}, and C_{Y_r} are of secondary importance compared with the sideslip and rolling derivatives. These derivatives are treated theoretically in references 1, 6, 42, and 43 and have been determined experimentally by several methods including the whirling-arm method, forced-oscillation or free-oscillation method (reference 44), and the curved-flow method (Langley stability tunnel, reference 6), in which a model is held fixed in a curving air stream produced by curving the flexible side walls of the tunnel test section. The yawing moment due to yawing (damping-in-yaw parameter) C_{n_r} is the most important of the yawing derivatives but usually has no pronounced effects on stability and control if the weathercock stability C_{n_β} is adequate. Since the rolling moment due to yawing C_{l_r} and the lateral force due to yawing C_{Y_r} are even less important than C_{n_r}, no further discussion of the yawing derivatives will be given. More information on these derivatives can be found in the references 1, 6, 43, and 44.

MOST IMPORTANT LATERAL-STABILITY DERIVATIVES

The four most important derivatives C_{n_β}, C_{l_β}, C_{n_p}, and C_{l_p} will now be considered in more detail. The main emphasis will be placed on the two sideslip derivatives C_{n_β} and C_{l_β} since these derivatives have been the subject of a large part of the lateral-stability research during the past few years.

Yawing Moment Due to Sideslip C_{n_β}

The yawing moment due to sideslip C_{n_β} is a direct indication of the tendency of an airplane to weathercock, that is, to keep alined with

the relative wind. Since the wing–fuselage combination is usually unstable in this respect, a vertical tail is used which is large enough to balance out this instability and to provide a satisfactory amount of weathercock stability. This concept is very simple, but in practice proportioning an airplane to obtain a desired amount of weathercock stability has proved to be quite difficult because so many factors affect this stability. The effects of some of the more important factors will now be treated briefly.

Effect of vertical–tail aspect ratio.– One rather obvious point, but one which has not been fully appreciated until recent years, is the effect of the aspect ratio of the vertical tail on weathercock stability. This effect is illustrated in figure 2. Most airplanes prior to World War II had low–aspect–ratio vertical tails like that shown in solid lines on the sketch. The desire to get increased stability without an increase in tail area on many of our military airplanes led to use of vertical tails of higher aspect ratio which, because of their higher lift–curve slopes, gave more weathercock stability. This effect is clearly shown in figure 2 by a comparison of the slopes of yawing–moment curves $\left(\frac{\partial C_n}{\partial \psi} \text{ or } C_{n_\beta}\right)$ for a model tested with two tails of equal area but of aspect ratios of 1.0 and 2.3.

End–plate effect of horizontal tail.– Another factor which has to be taken into account in estimating vertical–tail effectiveness is the end–plate effect of the horizontal tail. Recent NACA research on this subject (references 29 and 31) has helped to put the estimation of this effect on a rational basis. In figure 3 a part of this research is summarized to show how the vertical–tail effectiveness is increased by the end–plate effect when the horizontal tail is located near the bottom or top of the vertical tail. In general, the effects of the fore and aft position of the horizontal tail and the relative sizes of the horizontal and vertical tails are small when compared with the effect of the vertical position of the horizontal tail.

Effect of wing position.– The effect of the vertical position of the wing on the fuselage on weathercock stability is illustrated in figure 4, which is a plot of the increment in C_{n_β} produced by changing from a midwing configuration to a high– or low–wing configuration. It is apparent from these data that a pronounced decrease in stability occurs as the wing is moved from a low to a high position. The amount of this reduction in C_{n_β} (over 0.001) is more than one–half the increment in C_{n_β} provided by a vertical tail of average size. This effect of wing position results primarily from the difference in the sidewash induced at the vertical tail by the high–wing and low–wing configurations. More information on this effect is given in references 9 to 13 and reference 30. Some of these references also cover the effects on C_{n_β} of flaps, wing plan form, fuselage shape, and other factors.

Effect of power.- The effect of power on the weathercock stability of propeller-driven airplanes (references 32 to 34 and 45 to 53) has been the subject of extensive study in the last few years because the tremendous increase in the power of our military airplanes has greatly increased the difficulty of obtaining satisfactory stability under all operating conditions. In the case of multiengine airplanes one of the principal problems has been to design the airplane so that directional stability and trim characteristics are satisfactory with one or two engines on the same side inoperative. (See reference 33.)

In the case of high-powered single-engine airplanes there is an asymmetry in the power-on condition that is similar to the asymmetry caused on multiengine airplanes by the failure of one engine. This asymmetry is illustrated in figure 5 by the yawing-moment curve for the single-rotation power condition for a typical high-powered single-engine airplane. The effect of power is to increase the slope of the curve (indicating an increase in weathercock stability) and to displace the curve so that at zero yaw there is a large negative or left yawing moment. A 20° right rudder deflection was found necessary in this case to trim the airplane at zero yaw. With this single-rotation condition the propeller slipstream is displaced to the right at the vertical tail so that the tail passes out of the slipstream sooner when the airplane yaws to the right than when it yaws to the left. This effect causes the yawing-moment curve to break at about 10° for right yaw and about 25° for left yaw when the tail loses effectiveness as it passes out of the slipstream. The airplane tends to become directionally unstable when the tail passes out of the slipstream because the instability of the wing-fuselage-propeller combination is greatly increased by the application of power. This increased instability is caused partly by the lateral force on the propeller itself and partly by the slipstream effect on the wing-fuselage combination.

The undesirable asymmetry with power on is of course not present on jet-propelled airplanes, and it appears that power in this case has little, if any, effect on weathercock stability. Efforts at minimizing the asymmetry on propeller-driven airplanes have been attempted by several methods, such as offsetting the vertical tail, shifting the center of gravity to the right of the thrust axis (reference 54), skewing the thrust axis (reference 55), or using dual-rotating propellers (references 32 and 47). A comparison of dual and single rotation is shown in figure 5. It is apparent that dual rotation entirely eliminates the asymmetry but that the undesirable tendency toward instability at the higher angles of yaw is still present. Since this instability, when accompanied by rudder-force reversal, can lead to the dangerous "rudder-lock" condition (reference 28), methods have been sought to improve the weathercock stability at high yaw angles. In order to improve this condition, many high-powered airplanes have dorsal or ventral fins. The functioning of these fins is explained in figure 6.

Effect of dorsal and ventral fins.- Figure 6 shows the weathercock stability of a fuselage with and without dorsal and ventral fins. The solid-line curve shows the normal fuselage instability which decreases with increasing angle of yaw. The dashed-line curve shows that the fins do not greatly affect the stability at small angles of yaw but that they make the fuselage very stable at high angles of yaw where increased stability is needed when the vertical tail loses effectiveness. This stabilizing effect of the dorsal and ventral fins has been attributed to a "spoiling" of the flow over the after part of the fuselage but a further analysis based on the experimental data of reference 25 indicates that the effect can be partly accounted for by the increasing slope of the fin normal-force curve with increasing angle of yaw. Such an effect is characteristic of surfaces having extremely low aspect ratio. (See references 56 and 57.)

Rolling Moment Due to Sideslip

The rolling moment due to sideslip C_{l_β} is known as the effective-dihedral derivative because the principal effect of varying the geometric dihedral angle of the wing is to change this derivative. (See references 35 and 36.) As pointed out in the introduction, C_{l_β} is sometimes called "lateral stability" because it is the derivative which tends to return the airplane to a wing-level attitude when it banks and starts sideslipping. Interest in this derivative has recently been greatly increased because of its extreme variation with sweepback and aspect ratio, as illustrated in figure 7.

Effect of wing plan form on C_{l_β}.- The effect of wing plan form on the variation of C_{l_β} with lift coefficient C_L is shown in figure 7. The solid-line curves are from experimental data from reference 6 and the dashed-line curves are theoretical values obtained from the same reference. The value of $-C_{l_\beta}$ for unswept wings of normal aspect ratio 5.2 increases slightly with increasing lift coefficient and the theoretical variation is in good agreement with the experimental data. In the case of the sweptback wings, at low lift coefficients $-C_{l_\beta}$ increases rapidly with lift coefficient as indicated by theory but at some moderate lift coefficient $-C_{l_\beta}$ reaches a maximum value and then drops off as the maximum lift is approached. This "drop-off," which is not predicted by the theory, is attributed to a partial separation of flow over the wing which cannot be taken into account by any of the theoretical methods now being used. The lift coefficient at which the experimental results drop off and no longer agree with the theory is influenced by many factors such as wing plan form, airfoil section, Reynolds number, and wing roughness. The drop-off occurs earliest with the more highly swept wings and with wings

having airfoils with a sharp leading edge. Increasing the Reynolds number usually makes the experimental results agree with the theory up to a higher lift coefficient but if the wing surface is rough the drop-off occurs at a fairly low lift coefficient regardless of the Reynolds number. The use of high-lift devices such as flaps and slots usually increases the maximum value of C_{l_β} for a given wing. (See reference 19.)

The data of figure 7 show that the use of sweepforward tends to reverse the variation of $-C_{l_\beta}$ with lift coefficient. For the particular wing shown, the effect of the sweepforward at low lift coefficients is to eliminate the variation of $-C_{l_\beta}$ with lift coefficient associated with the unswept wing.

Effect of wing position on C_{l_β}.- The vertical position of the wing on the fuselage has a pronounced effect on the value of C_{l_β} for a complete airplane. This effect has been treated theoretically in reference 7 and has been investigated experimentally in several NACA research studies (references 9 to 13). The results of some of this experimental work are summarized in figure 8 which is a plot of the increment in C_{l_β} produced by changing from a midwing position to a high- or low-wing position. These data show that lowering the wing causes a large reduction in effective dihedral $\left(-C_{l_\beta}\right)$ and that raising the wing causes a corresponding increase in effective dihedral. The scale at the right side of the plot indicates that changing from a low-wing to a high-wing position corresponds approximately to increasing the geometric dihedral angle of the wing by 9° or 10°. (A change of 1° in geometric dihedral angle corresponds to a change in C_{l_β} of about 0.0002.) The data presented in figure 8 are for unswept wings but the same general trends would probably be obtained with swept wings.

Effect of power on C_{l_β}.- For high-powered propeller-driven airplanes, the application of power usually causes a reduction in C_{l_β} which is most pronounced in the flap-down condition. (See references 37, 47, and 51.) This effect is illustrated in figure 9 in which rolling-moment data are presented for a high-powered single-engine airplane with power off and with single- and dual-rotating propellers operating. In the power-off condition a large amount of effective dihedral is indicated by the steep slope of the rolling-moment curve. For the single-rotation condition the application of power causes a large reduction in effective dihedral and also causes a negative rolling moment at zero yaw. The reduction in effective dihedral is caused by the fact that in a yawed or sideslipped attitude a greater portion of the propeller slipstream passes over the trailing wing than over the

leading wing. Since the dynamic pressure in the slipstream is much greater than that outside the slipstream, the trailing wing then produces a greater increment of lift due to power than is produced by the leading wing. A rolling moment therefore results which tends to raise the trailing wing. This effect is called a negative dihedral effect because it is the same as that exhibited by a wing having negative geometric dihedral. The out-of-trim rolling moment at zero yaw is caused by the propeller torque which is, of course, to the left for right-hand propeller operation.

This out-of-trim rolling moment is not obtained with the dual-rotating propeller because the propeller torques balance out. There is, however, an even more pronounced reduction in effective dihedral than in the case of single rotation. This reduction in effective dihedral with power corresponds to putting about 18° negative dihedral in the wing of this airplane. It should be pointed out, however, that this extreme effect is shown for the flap-down, power-on condition (usually called the "wave-off" condition) and that much smaller effects are usually obtained in the flap-up conditions. One proposed method for reducing the effect of power on the effective dihedral is the use of a linked differential flap system. (See reference 37.) In the case of jet-propelled airplanes the effect of power on C_{l_β} is probably negligible in all cases.

Yawing Moment Due to Rolling

The yawing moment due to rolling C_{n_p} has some effect on lateral stability but its most important effect is usually on lateral maneuverability. It is the derivative which, together with the aileron-yawing-moment factor $C_{n_{\delta_a}}$, largely determines the sideslipping tendencies in an aileron roll. For unswept wings this derivative is usually negative as shown in figure 10 which means that in a right roll it causes a left or adverse yawing moment which tends to yaw the airplane out of the turn.

The theoretical and experimental results in figure 10 which were taken from reference 6 show that the value of C_{n_p} increases with lift coefficient up to the stall which means that the adverse yawing tendency should be greatest at high lift coefficients.

For the sweptback wing (fig. 10), the theory indicates greater negative values of C_{n_p} than for the unswept wing. The experimental data, however, do not agree with the theory in this case. These data show even larger negative values of C_{n_p} at low lift coefficients than are indicated by theory, but at a moderate lift coefficient (about 0.5 in this case) the data show a sharp change which results in very large

positive or favorable values of C_{n_p} at the higher lift coefficients. As in the case of the abrupt drop-off in the value of C_{l_β} of the sweptback wings, this sharp change in C_{n_p} is attributed to a partial separation of flow over the wing which is not taken into account by this theory (reference 6). An approximate indication of the lift coefficient at which this change takes place, however, can be obtained by means of the simple expression $C_{n_p} = -\frac{C_L - 1.1 \frac{dC_{D_w}}{d\alpha}}{8}$ from reference 1.

Rolling Moment Due to Rolling

The rolling moment due to rolling C_{l_p} is called the damping-in-roll derivative because it is the factor which is a measure of the resistance of an airplane to pure rolling motions. Considerable theoretical and experimental work (references 2, 6, 39, 40, 41, 57, 58, and 59) has been done on this derivative because of its importance in both lateral stability and maneuverability. Some of the principal points regarding this derivative are illustrated in figure 11 which is a plot of the experimentally determined variation of C_{l_p} with lift coefficient for swept and unswept wings. The symbols at zero lift coefficient indicate the theoretical values of C_{l_p} for the swept and unswept wings. Theory indicates no variation in C_{l_p} with lift coefficient.

The curve shown on figure 11 for the unswept wing is for a wing of aspect ratio 5.2 but it shows characteristics that are typical of unswept wings of all aspect ratios. The experimental value of C_{l_p} is in agreement with the theory and remains essentially constant from zero lift to the stall but at the stall it abruptly decreases to zero and to positive values which indicates that the wing is unstable in roll beyond the stall and will autorotate or continue to roll once it has started. Various stall-control devices such as leading-edge slots have been used to eliminate the autorotation tendency of unswept wings at the stall because in some cases this tendency causes airplanes to become uncontrollable and to go into spins. Increasing the aspect ratio of unswept wings increases the damping in roll but does not materially alter the characteristics at the stall.

The data of figure 11 show that changing from an unswept to a swept wing causes a pronounced change in the damping-in-roll characteristics. The solid-line curve is for a 45° sweptforward wing and the dashed-line curve for a 45° sweptback wing. Both wings have an aspect ratio of 2.6.

The fact that the swept wings have a smaller value of C_{l_p} than the unswept wing at zero lift is partly because of the sweepback but mostly because the swept wings are of much lower aspect ratio. (See reference 6.) The experimental data are in agreement with the theory at zero lift. The derivative C_{l_p} for the sweptforward wing increases rapidly with lift coefficient, however, and at the stall it decreases sharply and becomes positive or unstable as in the case of the unswept wing. The rapid increase of C_{l_p} with lift coefficient is not accounted for by present theories but it can be explained by the change in span load distribution which takes place on the sweptforward wing.

In the case of the sweptback wing, a slight increase occurs in C_{l_p} with increasing lift coefficient up to some moderately high lift coefficient and then the C_{l_p} changes abruptly. This change, however, is more gradual than in the case of the unswept or sweptforward wings and the value of C_{l_p} remains negative or stable even beyond the stall. For swept wings having a very large amount of sweep or a very small aspect ratio, C_{l_p} does become unstable at the stall or at even lower lift coefficients. The fact that the sweptback wings of moderate sweep and aspect ratio maintain damping in roll at the stall is very important for it means that any roll-offs at the stall should be less violent than on most unswept wings.

EFFECT OF IMPORTANT STABILITY DERIVATIVES ON FLYING CHARACTERISTICS

The effects of the two most important stability derivatives – the directional or weathercock stability derivative C_{n_β} and the effective-dihedral derivative C_{l_β} – have been the subject of extensive studies, both experimental (references 60 to 68) and theoretical (references 69 to 71). The results of these studies have generally been in good agreement and consequently only a typical set of results will be discussed. The results of an investigation in the Langley free-flight tunnel of the effects of C_{n_β} and C_{l_β} (reference 65) are presented in figure 12. In this investigation a model was flown with a large number of combinations of vertical-tail area and geometric dihedral which provided the changes in C_{n_β} and C_{l_β}. The results are plotted in the form of a stability chart with C_{n_β} as the ordinate and $-C_{l_\beta}$ as the abscissa and with the flight behavior obtained with the different combinations of C_{n_β} and C_{l_β} indicated by the crosshatched regions on the chart.

These results are for a lift coefficient of 1.0 and for ailerons-alone control (rudder fixed) and only represent a small part of the results of the comprehensive investigation reported in reference 65.

The stability chart of figure 12 can be explained more clearly by considering the flight behavior of the model with the three combinations of C_{n_β} and C_{l_β} marked (1), (2), and (3), each within a different region on the chart. Point (1) represents a satisfactory combination because with this condition the model was easy to fly and responded satisfactorily to the controls with little adverse yawing. Point (2), which has a lower value of C_{n_β} but the same value of $-C_{l_\beta}$, was not considered entirely satisfactory because with the decreased weathercock stability excessive adverse yawing occurred during aileron rolls. This point was considered satisfactory when rudder was coordinated with the ailerons to eliminate this adverse yawing. Point (3), which has low C_{n_β} and high $-C_{l_\beta}$, represents an unflyable condition with ailerons alone. In this case, the low weathercock stability permitted excessive adverse yawing which, in combination with the large value of effective dihedral or rolling moment due to sideslip, caused reversal of aileron effectiveness. That is, when right aileron control was given, the model started to roll to the right but it also started to yaw to the left (or sideslip to the right) and the large value of rolling moment due to sideslip C_{l_β} then caused large adverse rolling moments which overpowered the ailerons and caused the model to roll to the left instead of to the right. Here again, when the rudder was coordinated with the ailerons, flights could be made but even in this case the flying characteristics were not considered satisfactory because of a weak weathercocking tendency and a lightly damped Dutch roll oscillation. This oscillation is discussed in detail in the next paper "Dynamic Stability," by Sternfield.

CONCLUDING REMARKS

During the war years and since the war, a great amount of experimental and theoretical research in the field of lateral stability was carried out and many advances were made toward a better understanding of the problems involved. Much of the information, however, is still not in a form to be used directly in airplane design, and in many cases, further correlation and analysis are required to realize the full potential usefulness of the results.

Some experimental work has been done to determine the effects of Reynolds number, and theoretical work, to determine the effects of Mach number (references 72 to 75) on the various stability derivatives. Much more research appears to be necessary, however, to determine fully these effects. Further studies should also be made of the effects on lateral stability and control of other factors such as aeroelasticity, wing airfoil section and surface roughness, and wing–fuselage–tail interference.

REFERENCES

1. Zimmerman, Charles H.: An Analysis of Lateral Stability in Power–Off Flight with Charts for Use in Design. NACA Rep. No. 589, 1937.

2. Pearson, Henry A., and Jones, Robert T.: Theoretical Stability and Control Characteristics of Wings with Various Amounts of Taper and Twist. NACA Rep. No. 635, 1938.

3. Jones, Robert T.: Notes on the Stability and Control of Tailless Airplanes. NACA TN No. 837, 1941.

4. Langley Stability Research Division (Compiled by Charles J. Donlan): An Interim Report on the Stability and Control of Tailless Airplanes. NACA Rep. No. 796, 1944.

5. Soulé, Hartley A.: Influence of Large Amounts of Wing Sweep on Stability and Control Problems of Aircraft. NACA TN No. 1088, 1946.

6. Toll, Thomas A., and Queijo, M. J.: Approximate Relations and Charts for Low–Speed Stability Derivatives of Swept Wings. NACA TN No. 1581, 1948.

7. Multhopp, H.: Aerodynamics of the Fuselage. NACA TM No. 1036, 1942.

8. Bamber, M. J., and House, R. O.: Wind–Tunnel Investigation of Effect of Yaw on Lateral–Stability Characteristics. I – Four N.A.C.A. 23012 Wings of Various Plan Forms with and without Dihedral. NACA TN No. 703, 1939.

9. Bamber, M. J., and House, R. O.: Wind–Tunnel Investigation of Effect of Yaw on Lateral–Stability Characteristics. II – Rectangular N.A.C.A. 23012 Wing with Circular Fuselage and a Fin. NACA TN No. 730, 1939.

10. House, Rufus O., and Wallace, Arthur R.: Wind–Tunnel Investigation of Effect of Interference on Lateral–Stability Characteristics of Four NACA 23012 Wings, an Elliptical and a Circular Fuselage, and Vertical Fins. NACA Rep. No. 705, 1941.

11. Recant, Isidore G., and Wallace, Arthur R.: Wind–Tunnel Investigation of Effect of Yaw on Lateral–Stability Characteristics. III – Symmetrically Tapered Wing at Various Positions on Circular Fuselage with and without a Vertical Tail. NACA TN No. 825, 1941.

12. Recant, I. G., and Wallace, Arthur R.: Wind-Tunnel Investigation of Effects of Yaw on Lateral-Stability Characteristics. IV - Symmetrically Tapered Wing with a Circular Fuselage Having a Wedge-Shaped Rear and a Vertical Tail. NACA ARR, March 1942.

13. Wallace, Arthur R., and Turner, Thomas R.: Wind-Tunnel Investigation of Effect of Yaw on Lateral-Stability Characteristics. V - Symmetrically Tapered Wing with a Circular Fuselage Having a Horizontal and a Vertical Tail. NACA ARR No. 3F23, 1943.

14. Teplitz, Jerome: Effects of Small Angles of Sweep and Moderate Amounts of Dihedral on Stalling and Lateral Characteristics of a Wing-Fuselage Combination Equipped with Partial- and Full-Span Double Slotted Flaps. NACA Rep. No. 800, 1944.

15. Purser, Paul E., and Campbell, John P.: Experimental Verification of a Simplified Vee-Tail Theory and Analysis of Available Data on Complete Models with Vee Tails. NACA Rep. No. 823, 1945.

16. Hollingworth, Thomas A.: Investigation of Effect of Sideslip on Lateral Stability Characteristics. II - Rectangular Midwing on Circular Fuselage with Variations in Vertical-Tail Area and Fuselage Length with and without Horizontal Tail Surface. NACA ARR No. L5C13, 1945.

17. Hollingworth, Thomas A.: Investigation of Effect of Sideslip on Lateral Stability Characteristics. III - Rectangular Low Wing on Circular Fuselage with Variations in Vertical-Tail Area and Fuselage Length with and without Horizontal Tail Surface. NACA ARR No. L5C13a, 1945.

18. Lange, Roy H.: Langley Full-Scale-Tunnel Investigation of the Factors Affecting the Static Lateral-Stability Characteristics of a Typical Fighter-Type Airplane. NACA RM No. L6L18, 1946.

19. Letko, William, and Goodman, Alex: Preliminary Wind-Tunnel Investigation at Low Speed of Stability and Control Characteristics of Swept-Back Wings. NACA TN No. 1046, 1946.

20. Imlay, Frederick H.: The Estimation of the Rate of Change of Yawing Moment with Sideslip. NACA TN No. 636, 1938.

21. Pass, H. R.: Analysis of Wind-Tunnel Data on Directional Stability and Control. NACA TN No. 775, 1940.

22. Shortal, Joseph A., and Draper, John W.: Free-Flight-Tunnel Investigation of the Effect of the Fuselage Length and the Aspect Ratio and Size of the Vertical Tail on Lateral Stability and Control. NACA ARR No. 3D17, 1943.

23. Fehlner, Leo F., and MacLachlan, Robert: Investigation of Effect of Sideslip on Lateral Stability Charactersitics. I – Circular Fuselage with Variations in Vertical–Tail Area and Tail Length with and without Horizontal Tail Surface. NACA ARR No. L4E25, 1944.

24. Bishop, Robert C., and Lomax, Harvard: A Simplified Method for Determining from Flight Data the Rate of Change of Yawing–Moment Coefficient with Sideslip. NACA TN No. 1076, 1946.

25. Hoggard, H. Page, Jr.: Wind–Tunnel Investigation of Fuselage Stability in Yaw with Various Arrangements of Fins. NACA TN No. 785, 1940.

26. Donlan, C. J., and Letko, W.: The Effect of Cowling Shape on the Stability Characteristics of an Airplane. NACA ARR, Sept. 1942.

27. MacLachlan, Robert, and Levitt, Joseph: Wind–Tunnel Investigation of Effect of Canopies on Directional Stability Characteristics of a Single–Engine Airplane Model. NACA TN No. 1052, 1946.

28. Thompson, F. L., and Gilruth, R. R.: Notes on the Stalling of Vertical Tail Surfaces and on Fin Design. NACA TN No. 778, 1940.

29. Katzoff, S., and Mutterperl, William: The End–Plate Effect of a Horizontal–Tail Surface on a Vertical–Tail Surface. NACA TN No. 797, 1941.

30. Recant, Isidore G., and Wallace, Arthur R.: Wind–Tunnel Investigation of the Effect of Vertical Position of the Wing on a Side Flow in the Region of the Vertical Tail. NACA TN No. 804, 1941.

31. Murray, Harry E.: Wind–Tunnel Investigation of End–Plate Effects of Horizontal Tails on a Vertical Tail Compared with Available Theory. NACA TN No. 1050, 1946.

32. Neely, R. H., Fogarty, L. E., and Alexander, S. R.: Comparison of Yaw Characteristics of a Single–Engine Airplane Model with Single–Rotating and Dual–Rotating Propellers. NACA ACR No. L4D19, 1944.

33. Pitkin, Marvin, Draper, John W., and Bennett, Charles V.: The Influence of Vertical–Tail Design and Direction of Propeller Rotation on Trim Characteristics of a Twin–Engine–Airplane Model with One Engine Inoperative. NACA ARR No. L5A13, 1945.

34. Stevens, Victor I., McCullough, George B., and Hanson, Frederick H.: An Experimental Investigation of the Effect of Propellers Used as Aerodynamic Brakes on Stability and Control. NACA ARR No. 5C01, 1945.

35. Shortal, Joseph A.: Effect of Tip Shape and Dihedral on Lateral-Stability Characteristics. NACA Rep. No. 548, 1935.

36. Maggin, Bernard, and Shanks, Robert E.: The Effect of Geometric Dihedral on the Aerodynamic Characteristics of a 40° Swept-Back Wing of Aspect Ratio 3. NACA TN No. 1169, 1946.

37. Pitkin, Marvin, and Schade, Robert O.: Tests of a Linked Differential Flap System Designed to Minimize the Reduction in Effective Dihedral Caused by Power. NACA ARR No. L5F25, 1945.

38. Drake, Hubert M.: The Effect of Lateral Area on the Lateral Stability and Control Characteristics of an Airplane as Determined by Tests of a Model in the Langley Free-Flight Tunnel. NACA ARR No. L5L05, 1946.

39. Swanson, Robert S., and Priddy, E. LaVerne: Lifting-Surface-Theory Values of the Damping in Roll and of the Parameter Used in Estimating Aileron Stick Forces. NACA ARR No. L5F23, 1945.

40. Bennett, Charles V., and Johnson, Joseph L.: Experimental Determination of the Damping in Roll and Aileron Rolling Effectiveness of Three Wings Having 2°, 42°, and 62° Sweepback. NACA TN No. 1278, 1947.

41. MacLachlan, Robert, and Letko, William: Correlation of Two Experimental Methods of Determining the Rolling Characteristics of Unswept Wings. NACA TN No. 1309, 1947.

42. Harmon, Sidney M.: Determination of the Damping Moment in Yawing for Tapered Wings with Partial-Span Flaps. NACA ARR No. 3H25, 1943.

43. Cotter, William E., Jr.: Summary and Analysis of Data on Damping in Yaw and Pitch for a Number of Airplane Models. NACA TN No. 1080, 1946.

44. Campbell, John P., and Mathews, Ward O.: Experimental Determination of the Yawing Moment Due to Yawing Contributed by the Wing, Fuselage, and Vertical Tail of a Midwing Airplane Model. NACA ARR No. 3F28, 1943.

45. Stüper, J.: Effect of Propeller Slipstream on Wing and Tail. NACA TM No. 874, 1938.

46. Rogallo, Francis M., and Swanson, Robert S.: Wind-Tunnel Tests of a Twin-Engine Model to Determine the Effect of Direction of Propeller Rotation on the Static-Stability Characteristics. NACA ARR, Jan. 1943.

47. Harper, Charles W., and Wick, Bradford H.: A Comparison of the Effects of Four-Blade Dual- and Single-Rotation Propellers on the Stability and Control Characteristics of a High-Powered Single-Engine Airplane. NACA ARR No. 4F17, 1944.

48. Tamburello, Vito, and Weil, Joseph: Wind-Tunnel Investigation of the Effect of Power and Flaps on the Static Lateral Characteristics of a Single-Engine Low-Wing Airplane Model. NACA TN No. 1327, 1947.

49. Hagerman, John R.: Wind-Tunnel Investigation of the Effect of Power and Flaps on the Static Lateral Stability and Control Characteristics of a Single-Engine High-Wing Airplane Model. NACA TN No. 1379, 1947.

50. Ribner, Herbert S.: Field of Flow about a Jet and Effect of Jets on Stability of Jet-Propelled Airplanes. NACA ACR No. L6C13, 1946.

51. Purser, Paul E., and Spear, Margaret F.: Tests to Determine Effects of Slipstream Rotation on the Lateral Stability Characteristics of a Single-Engine Low-Wing Airplane Model. NACA TN No. 1146, 1946.

52. Ribner, Herbert S.: Notes on the Propeller and Slipstream in Relation to Stability. NACA ARR No. L4I12a, 1944.

53. Ribner, Herbert S., and MacLachlan, Robert: Effect of Slipstream Rotation in Producing Asymmetric Forces on a Fuselage. NACA TN No. 1210, 1947.

54. Phillips, W. H., Crane, H. L., and Hunter, P. A.: Effect of Lateral Shift of Center of Gravity on Rudder Deflection Required for Trim. NACA RB No. L4I06, 1944.

55. Wallace, Arthur R., and Comenzo, Raymond J.: Effect of Engine Skew on Directional and Lateral Control Characteristics of Single-Engine Airplanes. NACA RM No. L6I16, 1947.

56. Zimmerman, C. H.: Characteristics of Clark Y Airfoils of Small Aspect Ratios. NACA Rep. No. 431, 1932.

57. Tosti, Louis P.: Low-Speed Static Stability and Damping-in-Roll Characteristics of Some Swept and Unswept Low-Aspect-Ratio Wings. NACA TN No. 1468, 1947.

58. Murray, Harry E., and Wells, Evalyn G.: Wind-Tunnel Investigation of the Effect of Wing-Tip Fuel Tanks on Characteristics of Unswept Wings in Steady Roll. NACA TN No. 1317, 1947.

59. Maggin, Bernard, and Bennett, Charles V.: Low-Speed Stability and Damping-in-Roll Characteristics of Some Highly Swept Wings. NACA TN No. 1286, 1947.

60. Weick, Fred E., Soulé, Hartley A., and Gough, Melvin N.: A Flight Investigation of the Lateral Control Characteristics of Short Wide Ailerons and Various Spoilers with Different Amounts of Wing Dihedral. NACA Rep. No. 494, 1934.

61. Campbell, John P., and Seacord, Charles L., Jr.: The Effect of Mass Distribution on the Lateral Stability and Control Characteristics of an Airplane as Determined by Tests of a Model in the Free-Flight Tunnel. NACA Rep. No. 769, 1943.

62. McKinney, Marion O., Jr.: Experimental Determination of the Effect of Negative Dihedral on Lateral Stability and Control Characteristics at High Lift Coefficients. NACA ARR No. L5J02, 1946.

63. Drake, Hubert M.: Experimental Determination of the Effects of Directional Stability and Rotary Damping in Yaw on Lateral Stability and Control Characteristics. NACA TN No. 1104, 1946.

64. Ankenbruck, Herman O.: Effects of Tip Dihedral on Lateral Stability and Control Characteristics as Determined by Tests of a Dynamic Model in the Langley Free-Flight Tunnel. NACA TN No. 1059, 1946.

65. McKinney, Marion O., Jr.: Experimental Determination of the Effects of Dihedral, Vertical-Tail Area, and Lift Coefficient on Lateral Stability and Control Characteristics. NACA TN No. 1094, 1946.

66. Maggin, Bernard, and Bennett, Charles V.: Flight Tests of an Airplane Model with a 42° Swept-Back Wing in the Langley Free-Flight Tunnel. NACA TN No. 1287, 1947.

67. Maggin, Bernard, and Bennett, Charles V.: Flight Tests of an Airplane Model with a 62° Swept-Back Wing in the Langley Free-Flight Tunnel. NACA TN No. 1288, 1947.

68. Forsyth, Charles M., and Gray, William E., Jr.: A Comparison of Flight-Test Results on a Scout-Bomber Airplane with 4.7° and with 10° Geometric Dihedral in the Wing Outer Panels. NACA TN No. 1407, 1947.

69. Jones, Robert T.: The Influence of Lateral Stability on Disturbed Motions of an Airplane with Special Reference to the Motions Produced by Gusts. NACA Rep. No. 638, 1938.

70. Fehlner, Leo F.: A Study of the Effects of Vertical Tail Area and Dihedral on the Lateral Maneuverability of an Airplane. NACA ARR, Oct. 1941.

71. Fehlner, Leo F.: A Study of the Effect of Adverse Yawing Moment on Lateral Maneuverability at a High Lift Coefficient. NACA ARR, Sept. 1942.

72. Ribner, Herbert S.: The Stability Derivatives of Low-Aspect-Ratio Triangular Wings at Subsonic and Supersonic Speeds. NACA TN No. 1423, 1947.

73. Jones, Arthur L., and Alksne, Alberta: The Damping Due to Roll of Trinagular, Trapezoidal, and Related Plan Forms in Supersonic Flow. NACA TN No. 1548, 1948.

74. Brown, Clinton E., and Adams, Mac C.: Damping in Pitch and Roll of Triangular Wings at Supersonic Speeds. NACA TN No. 1566, 1948.

75. Ribner, Herbert S., and Malvestuto, Frank S., Jr.: Stability Derivatives of Triangular Wings at Supersonic Speeds. NACA TN No. 1572, 1948.

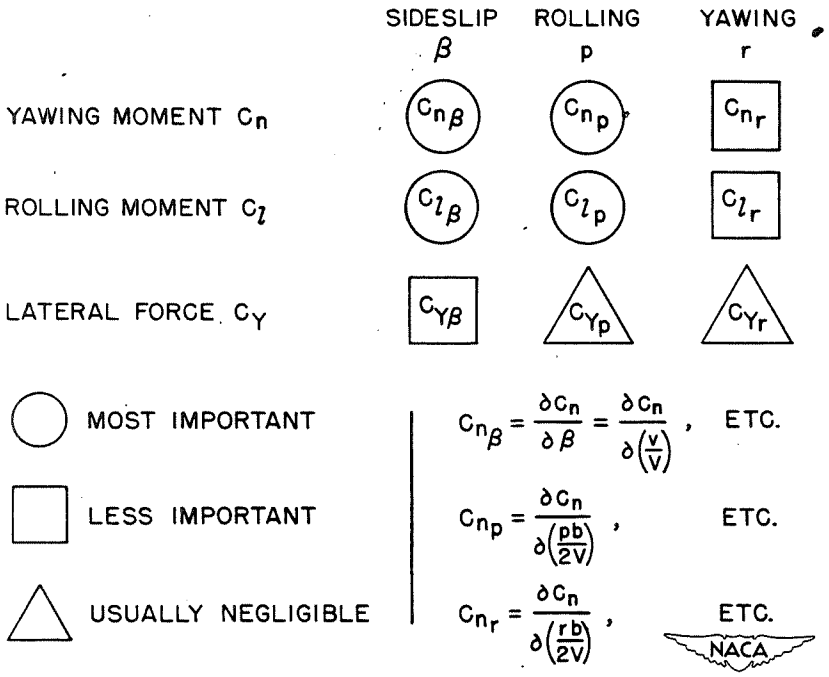

Figure 1.- Lateral-stability derivatives.

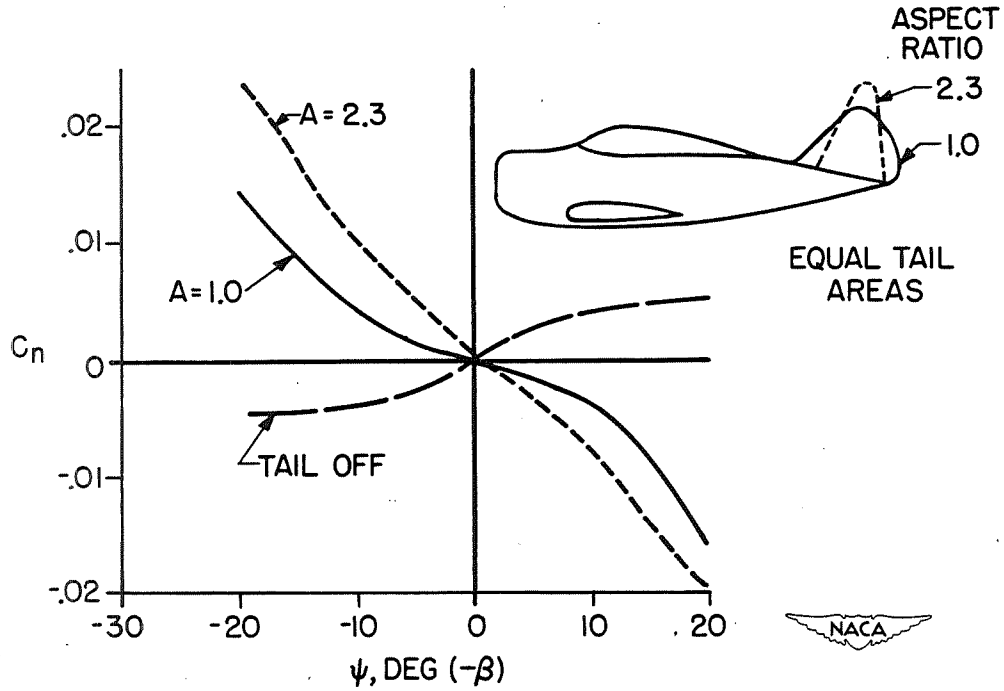

Figure 2.- Effect of aspect ratio of vertical tail on C_{n_β}.

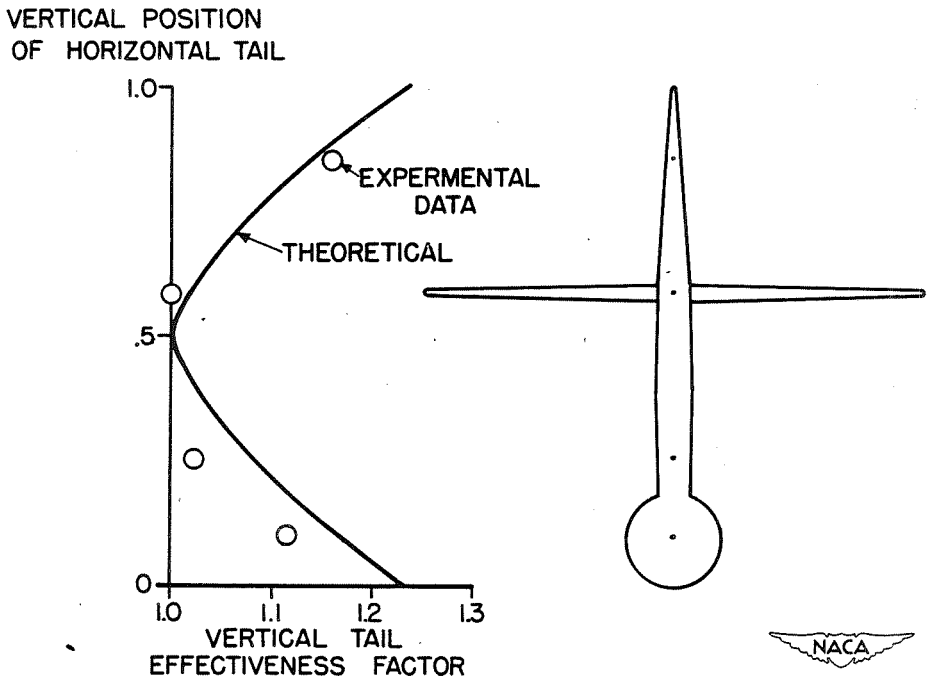

Figure 3.- End-plate effect of horizontal tail on vertical tail.

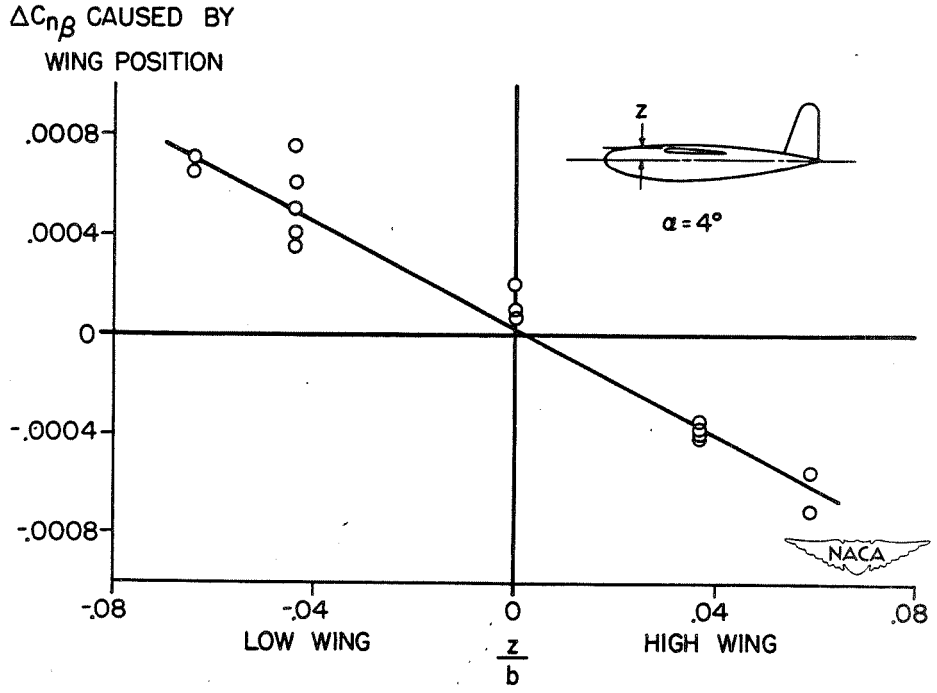

Figure 4.- Effect of wing position on C_{n_β}.

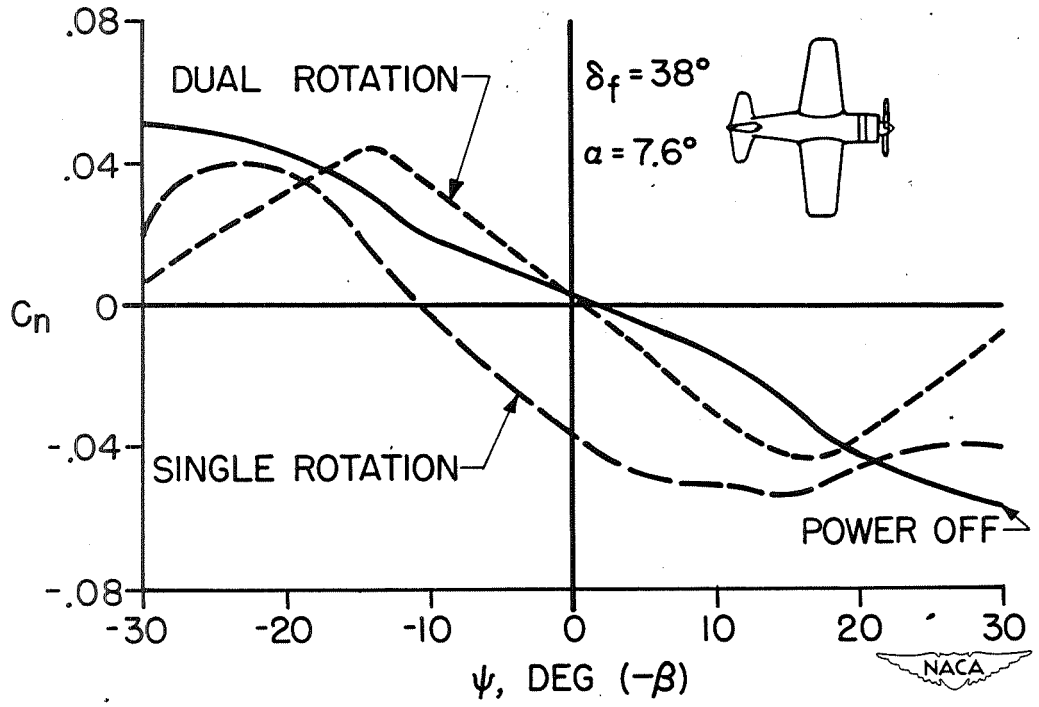

Figure 5.- Effect of power on C_{n_β} for a single-engine, propeller-driven airplane.

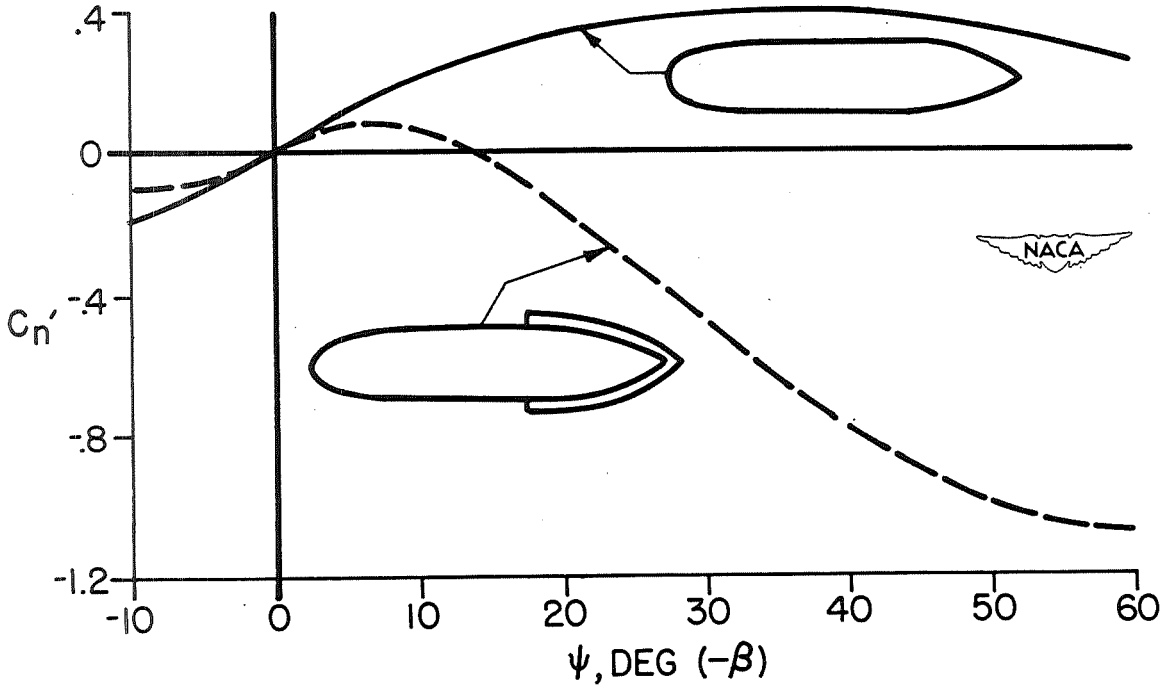

Figure 6.- Effect of dorsal and ventral fins on fuselage instability.

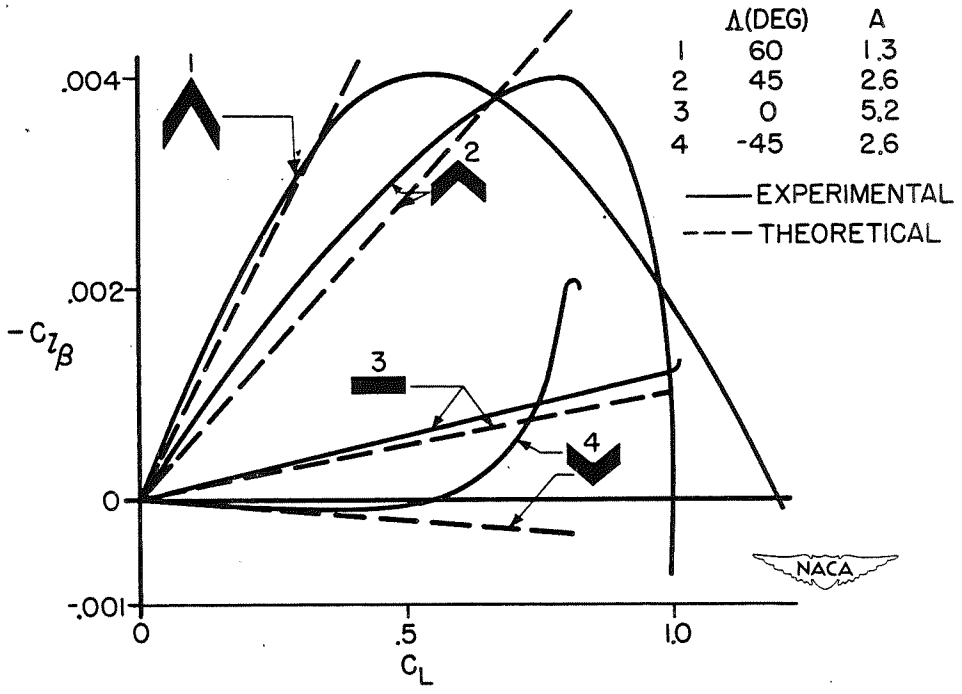

Figure 7.- Effect of wing plan form on C_{l_β}.

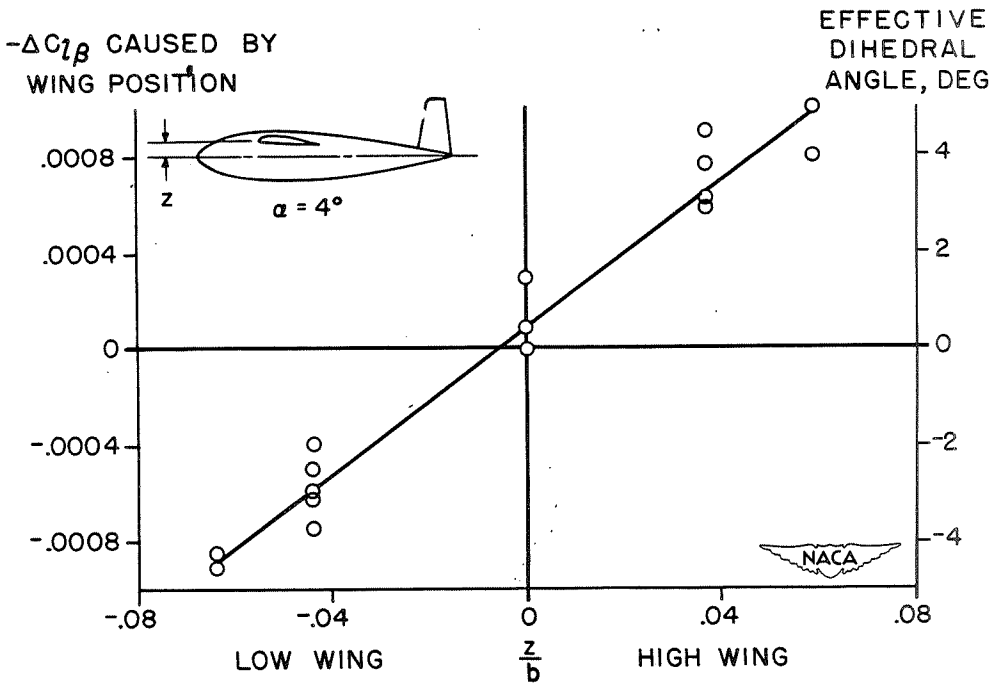

Figure 8.- Effect of wing position on C_{l_β}.

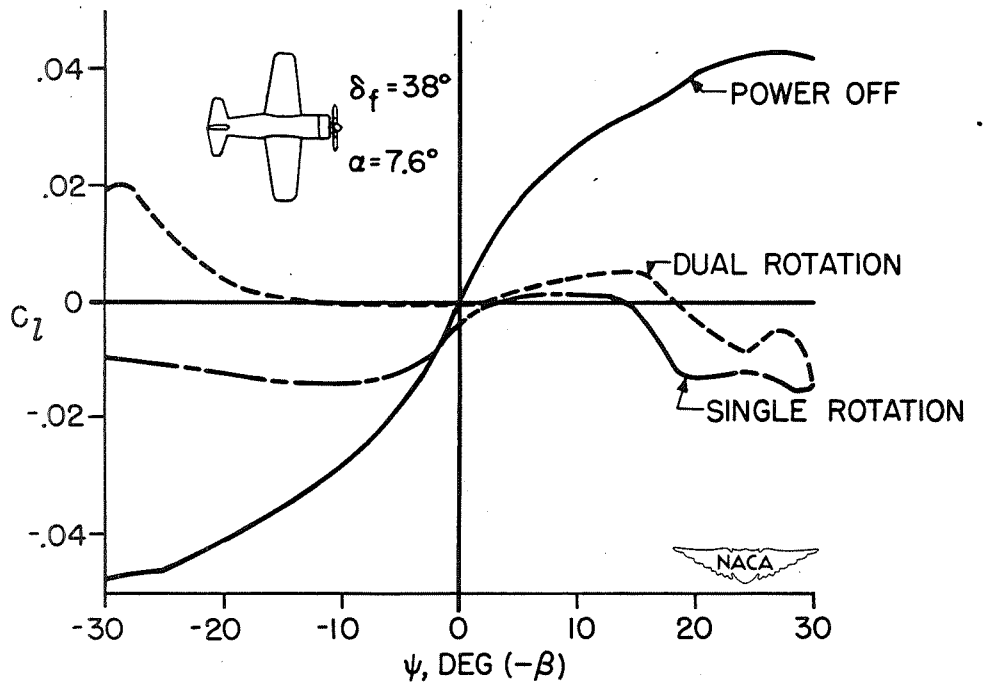

Figure 9.- Effect of power on C_{l_β} for a single-engine, propeller-driven airplane.

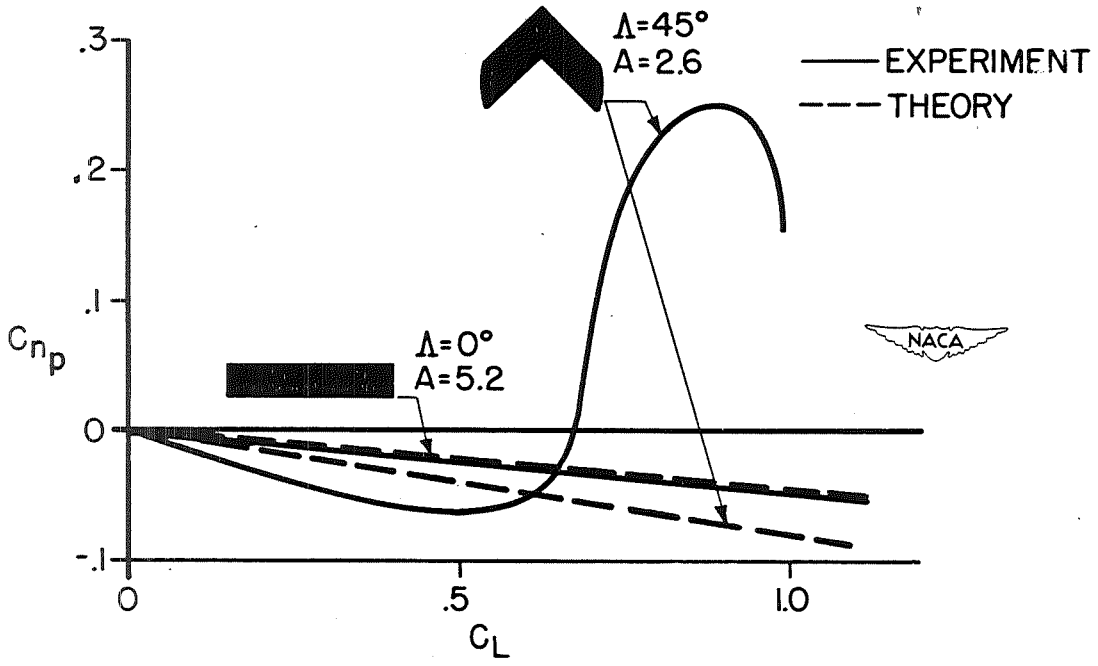

Figure 10.- Effect of wing plan form on C_{n_p}.

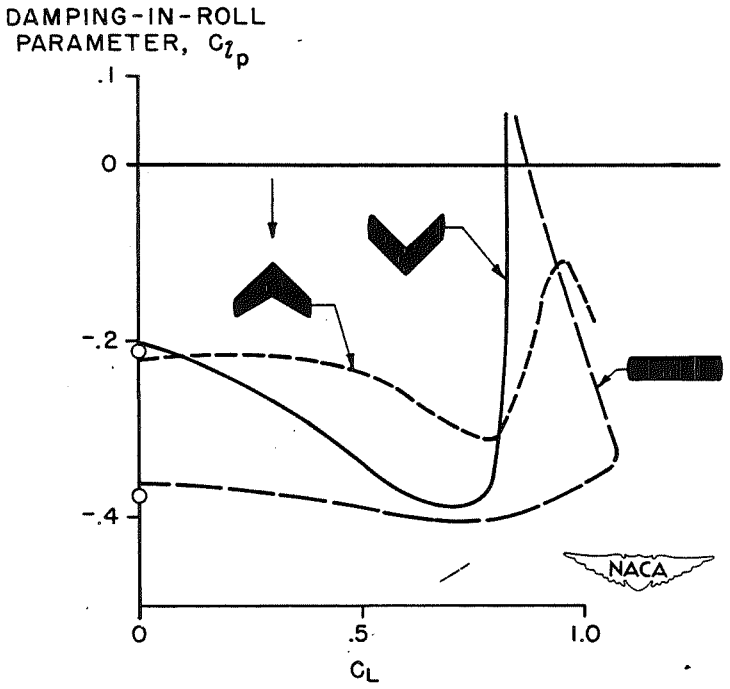

Figure 11.- Effect of wing plan form on C_{l_p}.

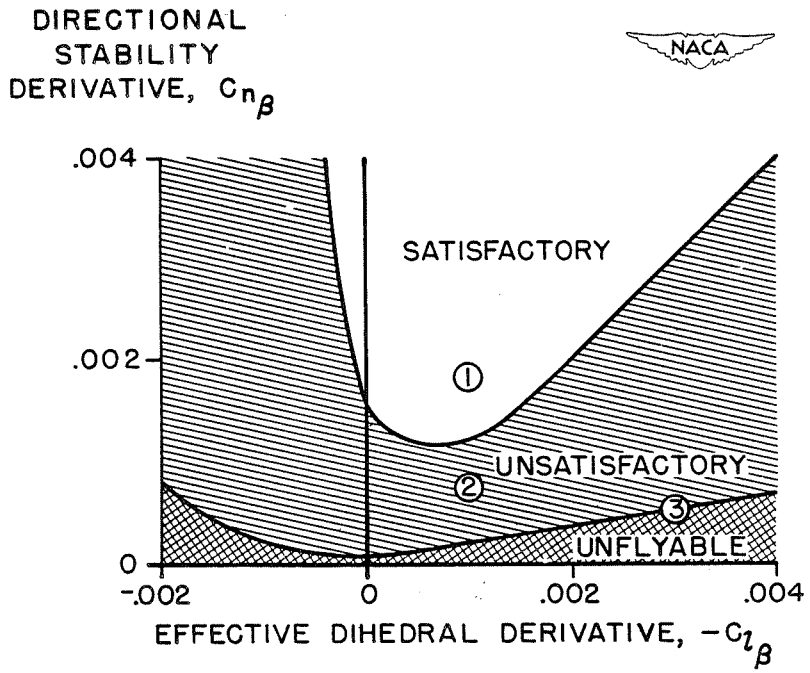

Figure 12.- Flight behavior chart based on model tests in Langley free-flight tunnel. Ailerons alone; $C_L = 1.0$.

DYNAMIC STABILITY

By Leonard Sternfield

Langley Aeronautical Laboratory

The problem of dynamic stability of airplanes is concerned with the motion of an airplane following a disturbance from an initial condition of equilibrium. Such disturbances may be caused by sudden gusts of wind or by deflection of the control surfaces. If the motion of the airplane caused by the disturbance damps, the airplane is said to be dynamically stable; if the motion caused by the disturbance builds up, the airplane is dynamically unstable. The mode of motion which may characterize dynamic instability is either an aperiodic divergence or an unstable oscillation. For many airplanes, the divergence of the aperiodic mode occurs at a slow rate and therefore pilots do not find this type of instability troublesome; hence, these airplanes are considered satisfactory, from the dynamic-stability viewpoint, even though the aperiodic mode is divergent. The oscillatory mode, however, may be objectionable to the pilot despite the fact that the oscillation is stable. The present paper on dynamic stability, therefore, will be mainly concerned with the oscillatory mode of motion.

The general equations of motion representing the motion of an airplane are referred to a system of axes which are fixed in the airplane and move with it. A system of axes that is commonly used by NACA authors is known as the stability system of axes. (See fig. 1.) The stability axes constitute an orthogonal system of axes having its origin at the center of gravity and in which the Z-axis is in the plane of symmetry and perpendicular to the relative wind, the X-axis is in the plane of symmetry and perpendicular to the Z-axis, and the Y-axis is perpendicular to the plane of symmetry. An equation of motion referred to these axes is set up for each one of the six degrees of freedom. Three of the equations are obtained by equating the aircraft mass accelerations along each axis to the aerodynamic forces and the other three equations are obtained by equating the rate of change of moment of momentum about each axis to the aerodynamic moments. (See references 1 to 4.)

A complete treatment of the dynamic stability of airplanes using the six equations would be extremely lengthy and very complex. Certain simplifying assumptions have therefore been made to facilitate the analysis. Since the airplane is symmetrical with respect to the plane that includes the fuselage axis and is perpendicular to the span axis and the steady motion about which the disturbances occur is symmetrical with regard to that plane, the six equations can be separated into a symmetric or longitudinal group consisting of three equations and an asymmetric or lateral group consisting of the other three equations, with no coupling between the two groups. The dynamic-stability investigation is therefore divided into two parts, a lateral-stability analysis and a longitudinal-stability analysis. The second assumption consists of the

application of the theory of small oscillations to both lateral and longitudinal stability, which means that second-order terms are neglected. The third assumption is that the aerodynamic forces depend solely upon the instantaneous motion of the airplane and not upon the rate at which the motion is changing. That is, it is assumed that when the angle of attack of the wing changes suddenly from one steady value to another, the lift changes instantaneously – although actually the lift approaches asymptotically the value corresponding to the new angle of attack.

The general methods involved in a dynamic-stability investigation will be presented for the lateral-stability analysis but a similar procedure is also applicable to the longitudinal-stability analysis. The linearized equations of motions, referred to the stability axes, used in the lateral-stability analysis for the condition of controls fixed are as follows:

Roll

$$2\mu_b\left(K_X^2 D_b^2\phi + K_{XZ} D_b^2\psi\right) = C_{l_\beta}\beta + \frac{1}{2}C_{l_p} D_b\phi + \frac{1}{2}C_{l_r} D_b\psi$$

Yaw

$$2\mu_b\left(K_Z^2 D_b^2\psi + K_{XZ} D_b^2\phi\right) = C_{n_\beta}\beta + \frac{1}{2}C_{n_p} D_b\phi + \frac{1}{2}C_{n_r} D_b\psi$$

Sideslip

$$2\mu_b\left(D_b\beta + D_b\psi\right) = C_{Y_\beta}\beta + \frac{1}{2}C_{Y_p} D_b\phi + C_L\phi + \frac{1}{2}C_{Y_r} D_b\psi + \left(C_L \tan\gamma\right)\psi$$

An equation of motion is presented for each one of the three degrees of freedom involved in lateral motion: roll, yaw, and sideslip. On the left-hand side of the equations are written the moment of inertia and product of inertia times the acceleration and on the right-hand side are written the aerodynamic forces or moments expressed as stability derivatives. These equations are linear differential equations with constant coefficients and, therefore, the solution of the equations of motion follows the usual procedure for linear differential equations. When $\phi_0 e^{\lambda s}$ is substituted for ϕ, $\psi_0 e^{\lambda s}$ for ψ, and $\beta_0 e^{\lambda s}$ for β in the equations written in determinant form, λ must be a root of the equation

$$A\lambda^4 + B\lambda^3 + C\lambda^2 + D\lambda + E = 0$$

Where the coefficients A, B, C, D, and E are functions of the mass and aerodynamic parameters of the equations. The roots of this stability equation determine the modes of motion. A real root indicates an aperiodic

mode and a complex root indicates an oscillatory mode. The signs of the roots determine the stability of the system. If the real roots are negative and the real part of the complex roots is negative, the airplane is dynamically stable. If any one of the real roots is positive or the real part of the complex root is positive, the airplane is dynamically unstable. The conditions for complete stability (reference 5) are that all the coefficients of the stability equation and the discriminant $R = BCD - AD^2 - B^2E$, known as Routh's discriminant, be positive. However, as mentioned previously, the mode which is of particular interest is the oscillatory mode. The first step in the analysis of the oscillatory mode is to determine the boundary for neutral oscillatory stability. This boundary is usually plotted as a function of two of the most important stability derivatives affecting lateral stability - the directional stability parameter C_{n_β}, which expresses the variation of yawing-moment coefficient with sideslip, and the effective dihedral derivative C_{l_β}, which expresses the variation of the rolling-moment coefficient with sideslip. The necessary and sufficient conditions for neutral oscillatory stability are that the coefficients of the stability equation satisfy Routh's discriminant set equal to zero and that the B- and D-coefficients have the same sign. (See reference 5.) The lateral-stability boundaries for a high-speed airplane are given in figure 2(a). The ordinate in this figure is C_{n_β} and the abscissa is C_{l_β}. The solid boundary labeled $R = 0$ is the boundary for neutral oscillatory stability. This boundary divides the quadrant into a stable and unstable region. For example, for combinations of C_{n_β} and C_{l_β} located below this boundary, that is, on the shaded side of the boundary, the oscillation of the airplane is unstable. The dashed boundary labeled $R = 0$ satisfies the condition that Routh's discriminant is zero but violates the condition that the B- and D-coefficients must be of the same sign, because the B-coefficient is positive and the D-coefficient is negative for combinations of C_{n_β} and C_{l_β} below the boundary $D = 0$. Hence this curve $R = 0$ is not a neutral-oscillatory boundary. The curve obtained by setting the E-coefficient equal to zero is known as the spiral-stability boundary. This boundary determines the stability of the numerically small real root, known as the spiral mode. For combinations of C_{n_β} and C_{l_β} on the shaded side of the line $E = 0$, the airplane is spirally unstable. There is one more mode which usually occurs in lateral motion. This mode corresponds to the heavy damping of the rolling motion due to the damping-in-roll derivative C_{l_p}. In general, therefore, the four roots obtained from the lateral-stability equation usually consist of one conjugate complex pair and two real roots. For some airplane configurations, both branches of $R = 0$ are true neutral-oscillatory-stability boundaries, as shown in figure 2(b). The significance of the two boundaries can best be understood by analyzing the modes of motion for combinations of C_{n_β} and C_{l_β} represented by the points (A), (B), (C), (D), and (E) in this figure. At point (A),

the roots of the stability equation are two negative real roots and one conjugate complex pair with the real part negative. Hence, the airplane is dynamically stable. Passing through the boundary $E = 0$ to point (B) causes one of the real roots to change sign, which indicates that the airplane is dynamically unstable because of spiral instability. Upon crossing the boundary $R = 0$ to point (C), the real part of the complex root changes sign as expected, which indicates that the oscillatory mode is unstable. Thus far, the roots consisted of two real roots and one conjugate complex pair. At point (D), however, the solution of the stability equation results in two pairs of complex roots with the real part of each pair of roots negative. The period of the oscillation which corresponds to one pair of the complex roots is about the same order of magnitude as the period of the oscillation at points (A), (B), (C) – approximately 3 seconds. The period of the other oscillation is much greater – for some airplanes, the period of this oscillation is of the order of magnitude of 15 seconds. It is this long-period oscillation which becomes unstable upon crossing the boundary $R = 0$ from point (D) to point (E). That is, at point (E), two pairs of complex roots are obtained with a positive real part of the complex roots that corresponds to the long-period oscillation so that an unstable oscillation is indicated, and a negative real part of the complex roots that corresponds to the short-period oscillation so that a stable oscillation is indicated. Thus the two curves for $R = 0$ represent neutral-oscillatory-stability boundaries, one boundary for the long-period oscillation and the other boundary for the short-period oscillation.

The second step in the analysis of the oscillatory mode is to determine the relation between the period and damping of the oscillation in the stable region. As mentioned previously, a pair of complex roots indicates an oscillatory mode. The real part of a complex root gives the damping factor and the imaginary part of the complex root gives the angular frequency of the oscillation from which the period is computed. A convenient measure of the damping is the time required for the amplitude of a disturbance to damp to half amplitude. The ratio of the time required to damp to half amplitude to the period results in the number of cycles required to damp to half amplitude. Figure 3 shows the curves of constant period and constant damping for a hypothetical airplane plotted as a function of C_{n_β} and C_{l_β}. (See reference 6.) The values corresponding to the solid curves represent the time in seconds to damp to half amplitude. As this time increases, the damping of the oscillation decreases. The solid curve labeled ∞ is the neutral-oscillatory-stability boundary; combinations of C_{n_β} and C_{l_β} located below this boundary will result in an unstable oscillation. The period of the oscillation in seconds is indicated by the values corresponding to the dashed curves. There are, at present, two schools of thought on the question as to which region in the C_{n_β}, C_{l_β} plane would result in a more satisfactory type of oscillation. For example, if the values of C_{n_β} and C_{l_β} for a given airplane correspond to point A and it is desired to improve the relation between the period and damping of the

oscillation, one group is of the opinion that the weathercock stability of the airplane should be increased. Thus, in going from (A) to (B), the damping of the oscillation is increased from 16 seconds to damp to half amplitude at (A) to 6 seconds at (B). But the period is shortened, thereby causing the number of cycles to damp to half amplitude to increase from 4 cycles at (A) to 6 cycles at (B). For this modification in the design of the airplane, therefore, the damping in seconds is improved but the damping in cycles is worsened. The opinion of the other group is that the combinations of C_{n_β} and C_{l_β} should be restricted to a small region near the origin, from point (A) to point (C). The damping in seconds is now reduced but because the period is lengthened the damping in cycles is improved, from 4 cycles at (A) to 1.67 cycles at (C). It is apparent that the desired criterion cannot be determined by the dynamic-stability investigator but must be based upon the opinions of pilots from more extensive flight-test results. Once this criterion is established, however, a figure similar to figure 3 which shows the curves of constant period and constant damping is necessary to indicate the possible combinations of C_{n_β} and C_{l_β} that will satisfy the criterion.

The dynamic-stability calculations have thus far yielded only an indication of the character of the free motion. The motion of the airplane, subsequent to a disturbance from its trimmed condition, is compounded of the several modes of motion in different proportions. The motion can be calculated by applying the Heaviside Operational Calculus or the Laplace transform to the equation of motion. The Laplace transform is considered a more powerful method than the Heaviside method because the initial conditions of the problem, initial displacements or initial velocities, are inherently taken into account by the Laplace transform. The application of these methods to the calculation of airplane motions can be found in several NACA and British reports. (See references 7 to 11.)

The present discussion has thus far been mainly concerned with the general methods of dynamic-stability analysis. The effects of some of the more important mass and aerodynamic parameters on the lateral stability will now be illustrated by showing the relative location of the neutral-oscillatory-stability boundaries in the C_{n_β}, C_{l_β} plane as these mass and aerodynamic parameters are varied.

Until recently, the product-of-inertia effect, which results from the inclination of the principal longitudinal axis of inertia relative to the flight path, has usually been neglected in lateral-stability analyses because some calculations for conventional airplanes had indicated that to neglect the angularity of the principal longitudinal axis to the flight path did not seriously affect the lateral stability. (See reference 12.) The angularity of the principal axis relative to the flight path causes the inertia forces to produce a coupling between the rolling and yawing motions so that a rolling acceleration produces a yawing moment and a yawing acceleration produces a rolling moment. Recent studies have shown, however, that the product of inertia may have a very pronounced

effect on the lateral stability of present-day airplanes designed for high-speed high-altitude flight because of high wing loadings, large differences between rolling and yawing moments of inertia, and the aerodynamic characteristics of low-aspect-ratio or swept wings. (See references 13 to 15.)

There has been a trend in the design of recent high-speed airplanes toward the use of relatively large angles of wing incidence to permit the fuselage to remain at a low angle of attack while the wing goes up to the high angles of attack required because of the high sweep and low aspect ratio. The purpose in designing the airplane so that the fuselage remains at a small angle of attack is to reduce the fuselage drag for high altitude or cruising flight or to reduce the fuselage ground angle and thereby simplify the landing-gear design. The important factor to consider in analyzing the effect of wing incidence on the lateral oscillatory stability is the inclination of the principal longitudinal axis relative to the flight path. Figure 4 shows the calculated oscillatory-stability boundaries as a function of C_{n_β} and C_{l_β} for a model tested in the Langley free-flight tunnel with the wing set at two angles of incidence, $i_w = 0^\circ$ and $i_w = 10^\circ$. In each of these configurations the model was flown at the same lift coefficient which corresponded to an angle of attack of 10° for the wing. The results indicate that when the wing was set at 0° incidence, both the wing and the principal longitudinal axis of the model, which coincided with the fuselage reference axis, were inclined 10° above the flight path to obtain the lift coefficient for trim. For that condition, illustrated by the lower sketch in the figure, the boundary falls in the lower region of the quadrant; thus, oscillatory stability is indicated for a large number of combinations of C_{n_β} and C_{l_β} located above the boundary. However, if the wing is set at an angle of incidence to obtain lift (for this case 10°), as has been proposed in several designs, and the principal axis is alined along the flight path, the oscillatory boundary falls in the upper region of the quadrant and thus it is very difficult to obtain oscillatory stability because the stable combinations of C_{n_β} and C_{l_β} are limited to the small region above this boundary. The stabilizing shift in the boundary, from $i_w = 10^\circ$ to $i_w = 0^\circ$, is caused by the fact that the principal longitudinal axis is inclined 10° above the flight path for $i_w = 0^\circ$. The boundaries indicate that the model with values of C_{n_β} and C_{l_β} shown by the test point on the figure, that is, C_{n_β} about 0.0025 and C_{l_β} approximately -0.003, is stable when the incidence is 0° and unstable when the incidence is 10°. This fact was verified by flight tests of the model in the Langley free-flight tunnel. (See reference 14.)

The important effect of the product of inertia on the oscillatory stability is emphasized by figure 5. The boundaries presented in this figure are for a high-speed airplane with a wing loading of 70 pounds

per square foot cruising at an altitude of 30,000 feet. The boundaries are again plotted as a function of C_{n_β} and C_{l_β} for two cases: The upper boundary represents the case in which the principal axis is inclined at an angle of 2° below the flight path at the nose, $\eta = -2°$, and the lower boundary represents the case in which the principal axis is alined with the flight path, $\eta = 0°$. A comparison of the two boundaries shows a large destabilizing shift in the boundary as the principal axis falls below the flight path. That is, as the boundary shifts upward from $\eta = 0°$ to $\eta = -2°$, the stable region located above the boundary is reduced. Such a marked shift in the boundary is caused by only 2° variation in the inclination of the principal longitudinal axis to the flight path.

The effect of wing loading and altitude on the oscillatory-stability boundary is illustrated by figure 6. The effects of these two parameters are treated simultaneously by considering variation in the relative-density factor μ_b, the ratio of the airplane density to air density, since this factor varies directly with both wing loading and altitude. The boundaries are shown for various values of μ_b. The values of μ_b can be interpreted in terms of wing loading and altitude as follows: A value of μ_b of 5 corresponds to a light plane with a wing loading of 10 pounds per square foot at an altitude of 10,000 feet; a value of μ_b of 30 corresponds to a World War II fighter with a wing loading of 40 pounds per square foot at an altitude of 40,000 feet; and a value μ_b of 1000 would correspond to a postwar high-speed design airplane with a wing loading of 100 pounds per square foot flying at an altitude of 60,000 feet. It is apparent from this figure that an increase in wing loading or altitude, or an increase in μ_b, shifts the boundaries upward so that a decrease in the stable region is indicated. However, it is important to note that the most pronounced effect of wing loading and altitude on stability occurs for values of μ_b less than 30, in the range of light aircraft design, whereas for values of μ_b above 30, wing loading and altitude have very little effect on stability. (See reference 16.)

One of the most important stability derivatives affecting lateral stability is the damping-in-roll derivative C_{l_p}, which becomes smaller as the sweepback is increased and as the aspect ratio is decreased. Figure 7 shows the effect of C_{l_p} on the oscillatory-stability boundary. The boundaries are plotted for several values of C_{l_p}: 0, −0.1, and −0.2. The value of C_{l_p} for a straight-wing conventional airplane is about −0.4 or −0.5. These boundaries were calculated for a hypothetical transonic airplane and are intended only to indicate the trends obtained as C_{l_p} is varied. It is evident from the boundaries that reducing C_{l_p} reduced

the lateral stability. Although the effect shown is typical for most airplane designs, calculations have indicated that the reverse effect might be present for some airplane configurations. The effect of some of the other stability derivatives and mass characteristics on the lateral oscillatory stability are presented in several NACA reports. (See references 15 and 17 to 19.)

The dynamic longitudinal stability of airplanes with controls fixed has received very extensive treatment by many authors, among whom may be mentioned Bryan, Bairstow, Wilson, and Zimmerman. (See references 1 to 3 and 20 to 22.) In general, the longitudinal motion consists of two oscillatory modes – a slightly damped long-period oscillation, known as the phugoid, and a heavily damped short-period oscillation. Because of the relation between the period and damping of each one of the oscillations, the longitudinal stability of most airplanes has been satisfactory to the pilots.

An analysis of lateral or longitudinal motion of the airplane with controls free involves an equation for an additional degree of freedom, that is, for the motion of the control itself. The discussion of control-free stability will be mainly concerned with the rudder-free case, although similar analyses have been carried out for the case of elevator free and aileron free. (See references 23 to 28.) Flight tests have shown that, under certain conditions of rudder balance, undamped lateral oscillations may occur when the rudder is freed. The oscillations involve coupling between the yawing motions of the airplane and movements of the rudder and depend on the amount of friction in the control system. Two of the most important parameters affecting the control-free stability are the restoring moment parameter C_{h_δ}, which expresses the variation of rudder hinge-moment coefficient with rudder deflection, and the floating-moment parameter C_{h_ψ}, which expresses the variation of the hinge-moment coefficient with the angle of yaw. Figure 8 shows the calculated rudder-free-stability boundaries with the effect of friction in the control system taken into account. These boundaries are plotted with C_{h_δ} as abscissa and C_{h_ψ} as ordinate. Positive values of C_{h_ψ} correspond to positive floating tendency, that is, surfaces whose free movements tend to oppose any disturbance of the airplane. The boundaries indicate that, for combinations of C_{h_δ} and C_{h_ψ} located on the shaded side of $R = 0$, the oscillation is unstable. If there is no solid friction in the system, the completely stable region is between $R = 0$ and the divergence boundary. However, if there is solid friction in the system, constant-amplitude oscillations occur for combinations of C_{h_δ} and C_{h_ψ} located between $R = 0$ and the curve labeled "friction boundary." The amplitude of the steady oscillation is proportional to the amount of solid friction in the control system. Flight tests will be necessary to indicate the maximum amount of steady oscillation that is allowable in an airplane.

The present paper indicates in general the effect of some of the mass and aerodynamic parameters on the lateral oscillatory stability. The results are illustrated for an airplane or model with a given set of values of mass and aerodynamic parameters. However, as shown in more complete lateral-stability studies, small variations in some of these parameters may cause a pronounced change in the oscillatory stability. On the basis of these detailed studies, therefore, it appears necessary to make a separate stability analysis for each airplane.

Some of the subjects that require further theoretical or experimental research are:

1. The effects of the aeroelasticity of wings on stability derivatives and hence on dynamic stability

2. The effects of power on stability

3. Analysis of the snaking or lightly damped short-period oscillations encountered recently in high-speed flight

4. Stability derivatives for transonic region

5. Analysis to determine important combinations of mass and aerodynamic parameters which affect dynamic stability

APPENDIX

SYMBOLS AND COEFFICIENTS

ϕ	angle of bank, radians
ψ	angle of azimuth, radians
β	angle of sideslip, radians $\left(\frac{v}{V}\right)$
v	sideslip velocity along the Y-axis, feet per second
V	airspeed, feet per second
ρ	mass density of air, slugs per cubic foot
q	dynamic pressure, pounds per square foot $\left(\frac{1}{2}\rho V^2\right)$
b	wing span, feet
S	wing area, square feet
W	weight of airplane, pounds
m	mass of airplane, slugs $\left(\frac{W}{g}\right)$
g	acceleration due to gravity, feet per second per second
μ_b	relative-density factor $\left(\frac{m}{\rho S b}\right)$
η	angle of attack of principal longitudinal axis of airplane, positive when principal axis is above flight path, degrees
γ	angle between flight path and horizontal axis, positive in a climb, degrees
k_{X_o}	radius of gyration in roll about principal longitudinal axis, feet
k_{Z_o}	radius of gyration in yaw about the principal vertical axis, feet
K_{X_o}	nondimensional radius of gyration in roll about principal longitudinal axis $\left(\frac{k_{X_o}}{b}\right)$

K_{Z_o} nondimensional radius of gyration in yaw about principal vertical axis $\left(\frac{k_{Z_o}}{b}\right)$

K_X nondimensional radius of gyration in roll about longitudinal stability axis $\left(\sqrt{K_{X_o}{}^2 \cos^2\eta + K_{Z_o}{}^2 \sin^2\eta}\right)$

K_Z nondimensional radius of gyration in yaw about vertical stability axis $\left(\sqrt{K_{Z_o}{}^2 \cos^2\eta + K_{X_o}{}^2 \sin^2\eta}\right)$

K_{XZ} nondimensional product-of-inertia parameter $\left(\left(K_{Z_o}{}^2 - K_{X_o}{}^2\right)(\sin \eta \cos \eta)\right)$

t time, seconds

S_b distance along flight path, in spans $\left(\frac{Vt}{b}\right)$

D_b differential operator $\left(\frac{d}{dS_b}\right)$

C_L trim lift coefficient $\left(\frac{W \cos \gamma}{qS}\right)$

C_l rolling-moment coefficient $\left(\frac{\text{Rolling moment}}{qSb}\right)$

C_n yawing-moment coefficient $\left(\frac{\text{Yawing moment}}{qSb}\right)$

C_Y lateral-force coefficient $\left(\frac{\text{Lateral force}}{qS}\right)$

C_{l_β} effective-dihedral derivative, rate of change of rolling-moment coefficient with angle of sideslip, per radian in equations and per degree in figures $\left(\frac{\partial C_l}{\partial \beta}\right)$

C_{n_β} directional-stability derivative, rate of change of yawing-moment coefficient with angle of sideslip, per radian in equations and per degree in figures $\left(\frac{\partial C_n}{\partial \beta}\right)$

C_{Y_β} lateral-force derivative, rate of change of lateral-force coefficient with angle of sideslip, per radian $\left(\frac{\partial C_Y}{\partial \beta}\right)$

C_{n_r} damping-in-yaw derivative, rate of change of yawing-moment coefficient with yawing-angular-velocity factor, per radian $\left(\frac{\partial C_n}{\partial \frac{rb}{2V}}\right)$

C_{n_p} rate of change of yawing-moment coefficient with rolling-angular-velocity factor, per radian $\left(\frac{\partial C_n}{\partial \frac{pb}{2V}}\right)$

C_{l_p} damping-in-roll derivative, rate of change of rolling-moment coefficient with rolling-angular-velocity factor, per radian $\left(\frac{\partial C_l}{\partial \frac{pb}{2V}}\right)$

C_{l_r} rate of change of rolling-moment coefficient with yawing-angular-velocity factor, per radian $\left(\frac{\partial C_l}{\partial \frac{rb}{2V}}\right)$

C_{Y_p} rate of change of lateral-force coefficient with rolling-angular-velocity factor, per radian $\left(\frac{\partial C_Y}{\partial \frac{pb}{2V}}\right)$

C_{Y_r} rate of change of lateral-force coefficient with yawing-angular-velocity factor, per radian $\left(\frac{\partial C_Y}{\partial \frac{rb}{2V}}\right)$

REFERENCES

1. Bairstow, Leonard: Applied Aerodynamics. Longmans, Green and Co., 1920.

2. Bryan, G. H.: Stability in Aviation. Macmillan and Co., Ltd., 1911.

3. Wilson, Edwin Bidwell: Aeronautics. John Wiley and Sons, Inc., 1920.

4. Jones, B. Melvill: Dynamics of the Airplane. Vol. V of Aerodynamic Theory, div. N., W. F. Durand, ed., Julius Springer (Berlin), 1935.

5. Routh, Edward John: Dynamics of a System of Rigid Bodies. Part II. 6th ed., rev. and enl., Macmillan and Co., Ltd., 1905, p. 223.

6. Brown, W. S.: A Simple Method of Constructing Stability Diagrams. R. & M. No. 1905, British A.R.C., 1942.

7. Jones, Robert T.: A Simplified Application of the Method of Operators to the Calculation of Disturbed Motions of an Airplane. NACA Rep. No. 560, 1936.

8. Jones, Robert T.: Calculation of the Motion of an Airplane under the Influence of Irregular Disturbances. Jour. Aero. Sci., vol. 3, no. 12, Oct. 1936, pp. 419–425.

9. Jones, Robert T.: The Influence of Lateral Stability on Disturbed Motions of an Airplane with Special Reference to the Motions Produced by Gusts. NACA Rep. No. 638, 1938.

10. Bryant, L. W., and Williams, D. H.: The Application of the Method of Operators to the Calculation of the Disturbed Motion of an Aeroplane. R. & M. No. 1346, British A.R.C., 1931.

11. Gandy, R. W.: The Response of an Aeroplane to the Application of Ailerons and Rudders. Part I – Response in Roll. R. & M. No. 1915, British A.R.C., 1943.

12. Zimmerman, C. H.: An Analysis of Lateral Stability in Power-Off Flight with Charts for Use in Design. NACA Rep. No. 589, 1937.

13. Sternfield, Leonard: Effect of Product of Inertia on Lateral Stability NACA TN No. 1193, 1947.

14. McKinney, Marion O., Jr., and Drake, Hubert M.: Correlation of Experimental and Calculated Effects of Product of Inertia on Lateral Stability. NACA TN No. 1370, 1947.

15. Sternfield, Leonard: Some Considerations of the Lateral Stability of High-Speed Aircraft. NACA TN No. 1282, 1947.

16. Campbell, John P., and Seacord, Charles L., Jr.: Effect of Wing Loading and Altitude on Lateral Stability and Control Characteristics of an Airplane as Determined by Tests of a Model in the Free-Flight Tunnel. NACA ARR No. 3F25, 1943.

17. Campbell, John P., and Seacord, Charles L., Jr.: The Effect of Mass Distribution on the Lateral Stability and Control Characteristics of an Airplane as Determined by Tests of a Model in the Free-Flight Tunnel. NACA Rep. No. 769, 1943.

18. McKinney, Marion O., Jr.: Experimental Determination of the Effects of Dihedral, Vertical-Tail Area, and Lift Coefficient on Lateral Stability and Control Characteristics. NACA TN No. 1094, 1946.

19. Drake, Hubert M.: The Effect of Lateral Area on the Lateral Stability and Control Characteristics of an Airplane as Determined by Tests of a Model in the Langley Free-Flight Tunnel. NACA ARR No. L5L05, 1946.

20. Zimmerman, Charles H.: An Analysis of Longitudinal Stability in Power-Off Flight with Charts for Use in Design. NACA Rep. No. 521, 1935.

21. Donlan, Charles J.: Some Theoretical Considerations of Longitudinal Stability in Power-Off Flight with Special Reference to Wind-Tunnel Testing. NACA ARR, Nov. 1942.

22. Lyon, H. M., Truscott, P. M., Auterson, E. I., and Whatham, J.: A Theoretical Analysis of Longitudinal Dynamic Stability in Gliding Flight. R. & M. No. 2075, British A.R.C., 1942.

23. Greenberg, Harry, and Sternfield, Leonard: A Theoretical Investigation of the Lateral Oscillations of an Airplane with Free Rudder with Special Reference to the Effect of Friction. NACA Rep. 762, 1943.

24. McKinney, Marion O., Jr., and Maggin, Bernard: Experimental Verification of the Rudder-Free Stability Theory for an Airplane Model Equipped with Rudders Having Negative Floating Tendency and Negligible Friction. NACA ARR No. L4J05a, 1944.

25. Maggin, Bernard: Experimental Verification of the Rudder-Free Stability Theory for an Airplane Model Equipped with a Rudder Having Positive Floating Tendencies and Various Amounts of Friction. NACA TN No. 1359, 1947.

26. Cohen, Doris: A Theoretical Investigation of the Rolling Oscillations of an Airplane with Ailerons Free. NACA Rep. No. 787, 1944.

27. Greenberg, Harry, and Sternfield, Leonard: A Theoretical Investigation of Longitudinal Stability of Airplanes with Free Controls Including Effect of Friction in Control System. NACA Rep. No. 791, 1944.

28. Phillips, William H.: A Flight Investigation of Short-Period Longitudinal Oscillations of an Airplane with Free Elevator. NACA ARR, May 1942.

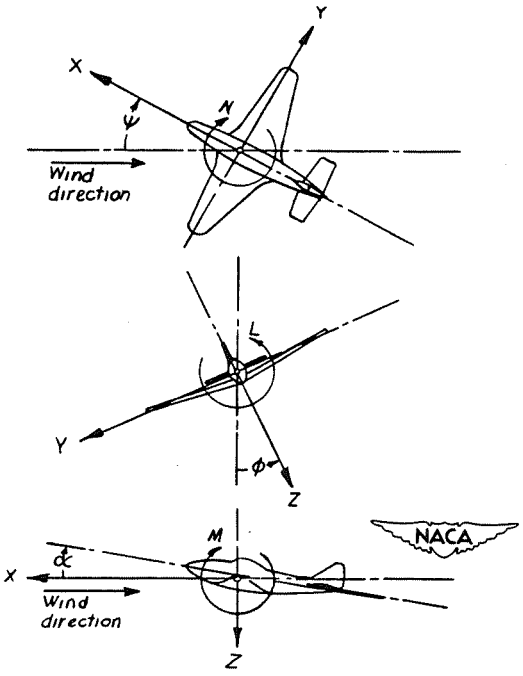

Figure 1.- The stability system of axes. Arrows indicate positive directions of moments, forces, and control-surface deflection.

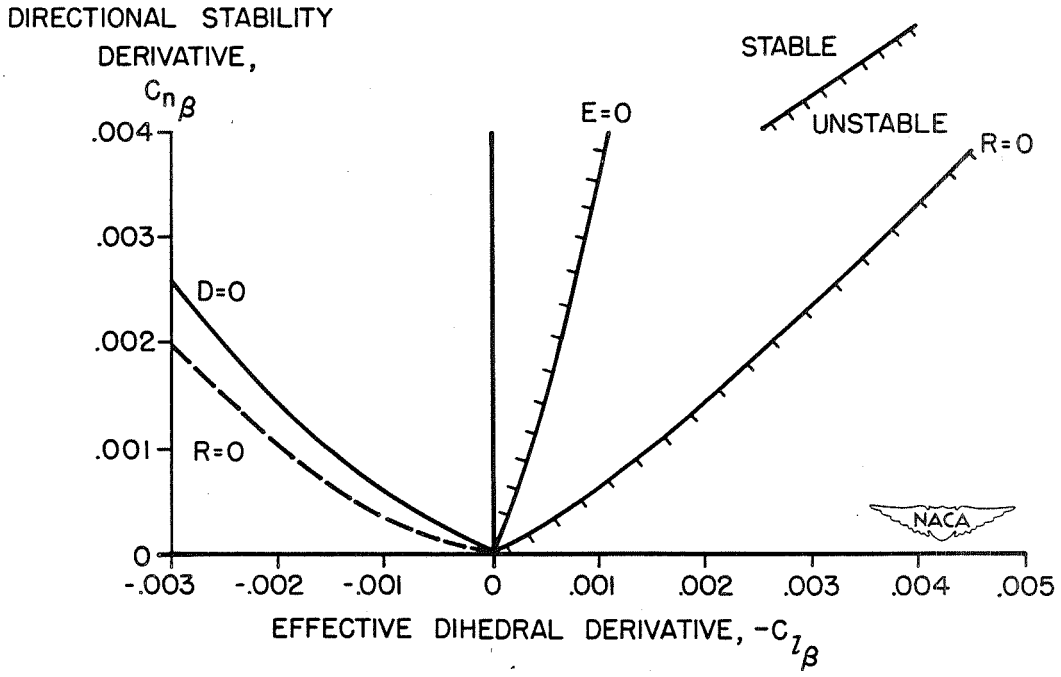

(a) The case for which only one of the two branches of the curve R = 0 is a boundary for neutral oscillatory stability.

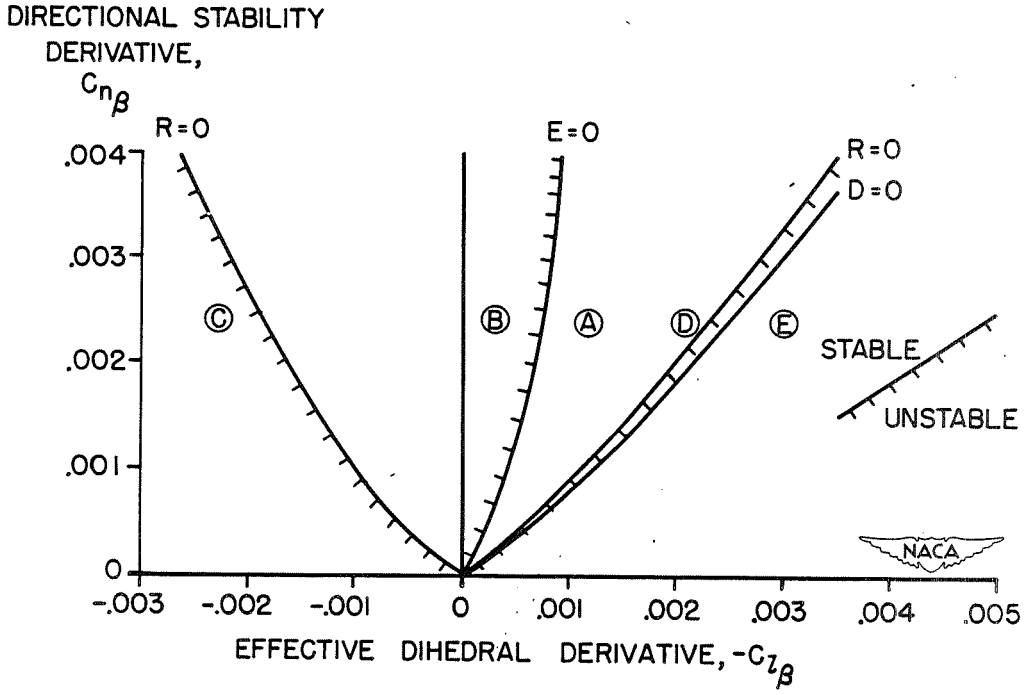

(b) The case for which both branches of the curve R = 0 are boundaries for neutral oscillatory stability.

Figure 2.- Lateral-stability boundaries for two hypothetical high-speed-airplane configurations.

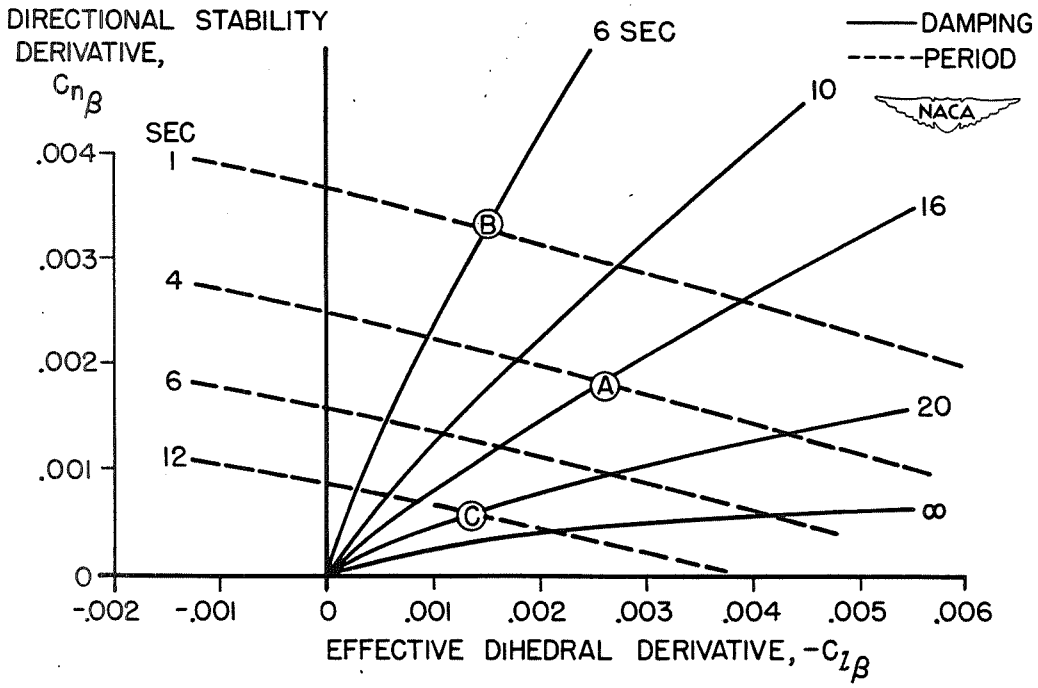

Figure 3.- Curves of constant period and constant damping.

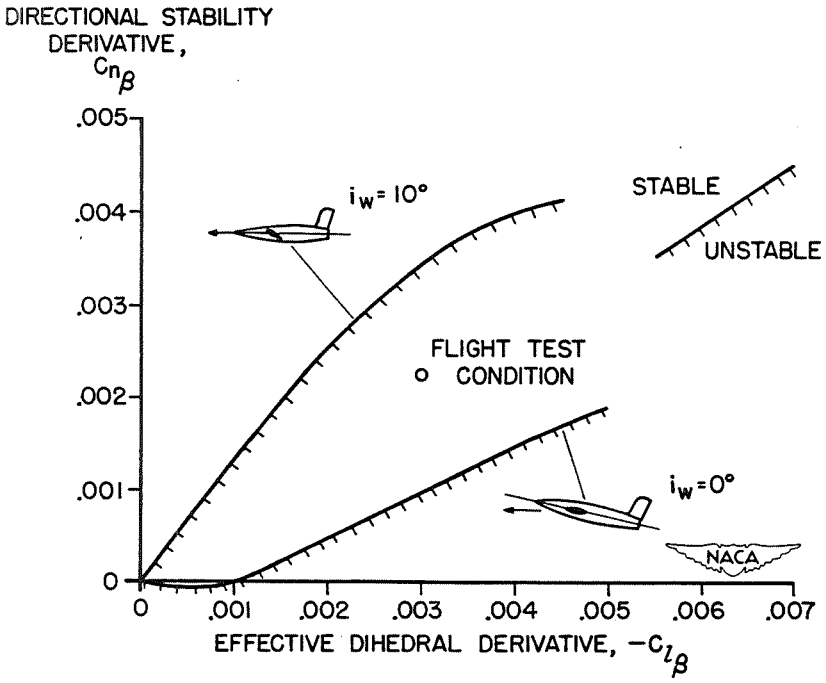

Figure 4.- Effect of wing incidence on the oscillatory stability of a model tested in the Langley free-flight tunnel.

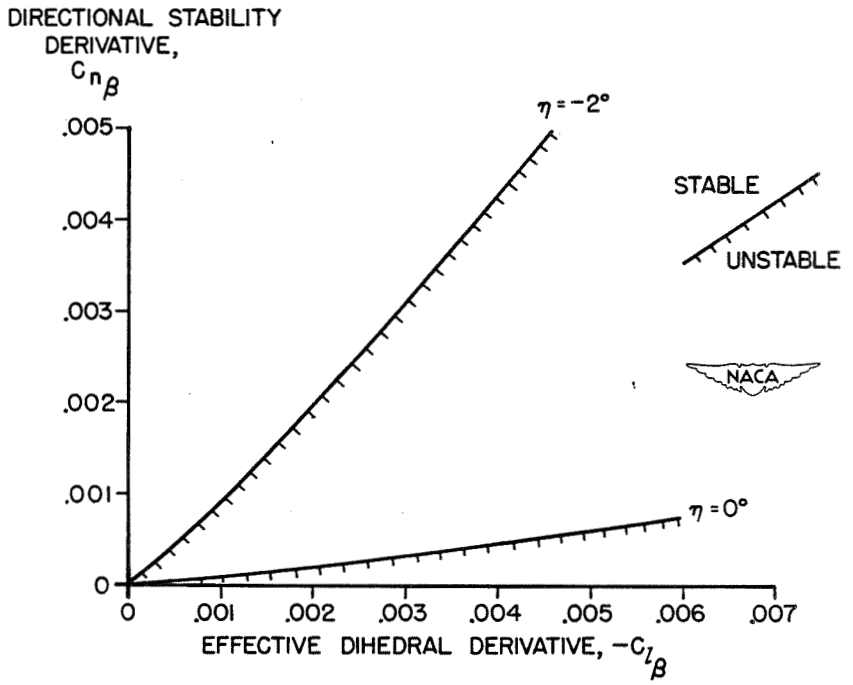

Figure 5.- Effect of the angle of attack of the principal longitudinal axis on the oscillatory-stability boundary.

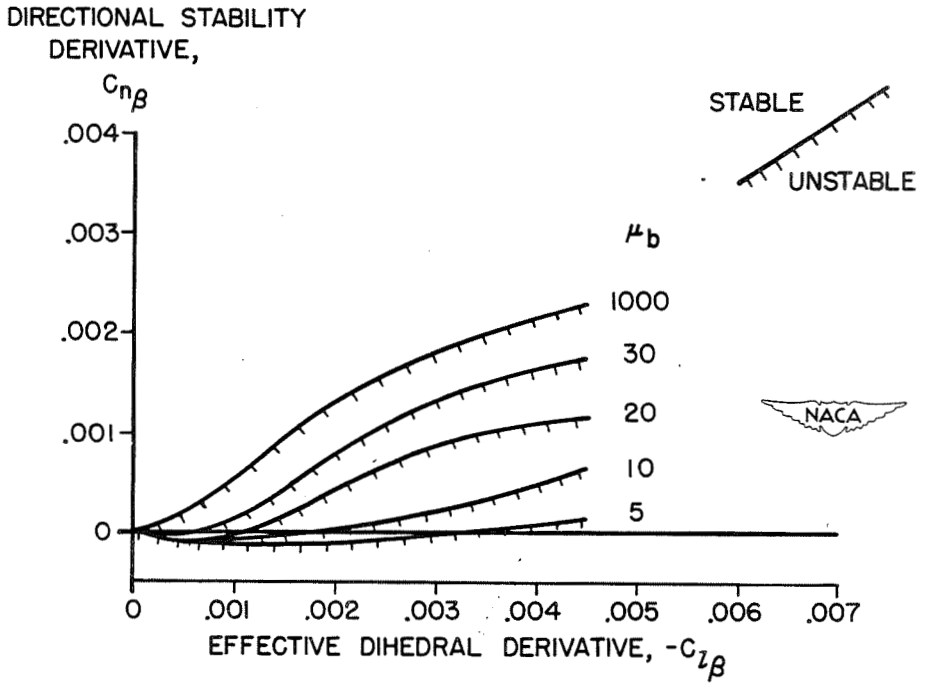

Figure 6.- Effect of the relative-density factor μ_b on the oscillatory-stability boundary.

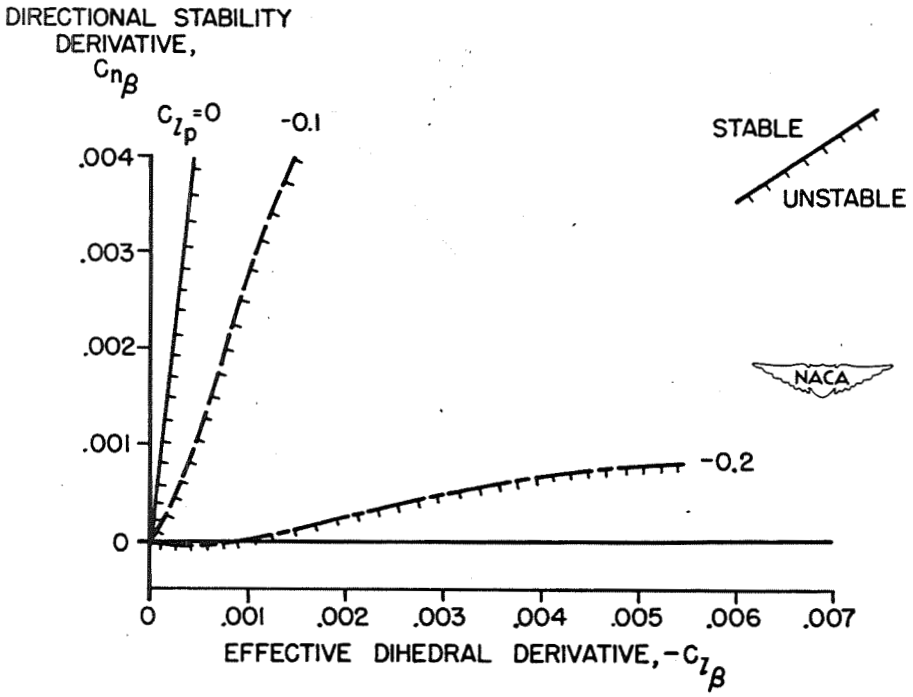

Figure 7.- Effect of damping in roll on the lateral stability of a high-speed airplane.

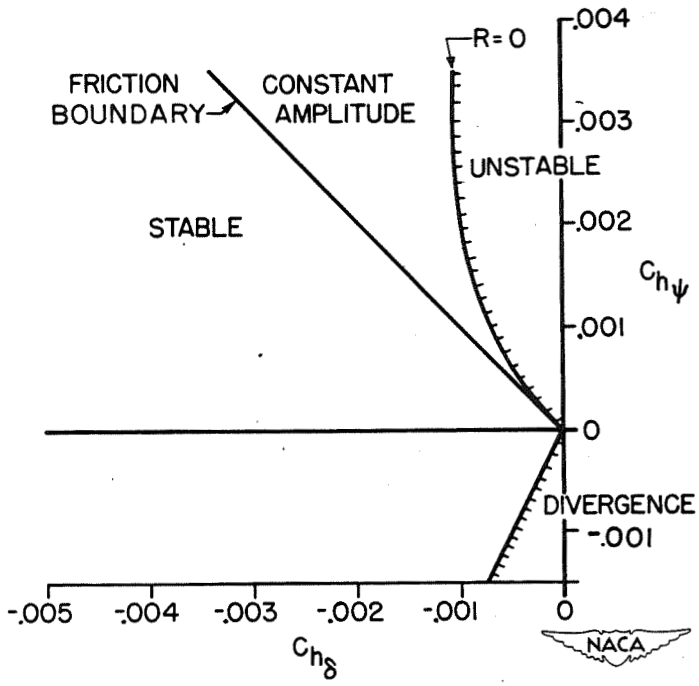

Figure 8.- Calculated rudder-free-stability boundaries for conventional attack airplane.

FLYING AND HANDLING QUALITIES OF AIRPLANES

By William H. Phillips

Langley Aeronautical Laboratory

By the flying qualities of an airplane are meant those stability and control characteristics which have an important bearing on the safety of flight and on the pilot's impressions of the ease of controlling an airplane in steady flight or in maneuvers. This paper will describe briefly the progress which has been made in setting up requirements for satisfactory flying qualities and will discuss some of the methods for predicting these qualities from calculations and wind-tunnel tests.

In the years prior to the war, relatively little was known about what characteristics of an airplane constituted satisfactory handling qualities. This does not mean that there had been no research on the subject of airplane stability. A great deal of theoretical work on this subject had been done. This theoretical work, however, was not able to take into account the characteristics of the human pilot and his relation to the airplane. On the other hand, human pilots had for many years expressed opinions with regard to the handling qualities of aircraft, and it was known that in some cases their opinions conflicted with the results of the theory. In developing a new airplane, therefore, there was no reliable procedure to provide for satisfactory flying qualities in the original design. Generally, it was necessary for a series of trial-and-error changes to be made in flight tests until the test pilot was satisfied with the qualities of the new airplane. The success of this procedure depended on the skill of the test pilot and unfortunately it did not provide a basis for avoiding poor characteristics in future designs.

It was thought that the main factors influencing the pilot's opinions of an airplane were the control motions and forces required in normal flight and in maneuvers. The first attempt to formulate a set of requirements based on these characteristics was made in 1937, but it was realized immediately that a great deal of information was required on the handling qualities of existing airplanes before a reliable set of requirements could be written. As a result the NACA undertook a program to measure the flying qualities of various airplanes. The initial results of this program are given in reference 1. Most of the available knowledge of flying qualities has been obtained from these flight tests which have been carried out on about 75 airplanes of all types, ranging from light planes to the largest bombers. In these tests, recording instruments were used to obtain quantitative measurements of control movements, control forces, and airplane motions while the pilots performed certain specified maneuvers. Procedures for making tests of this type are presented in reference 2. The results of many of these tests have been published as NACA wartime reports. From the fund of information accumulated in these reports it has been possible

to prepare a set of requirements for satisfactory handling qualities in terms of quantities that may be measured in flight or predicted from wind-tunnel tests and theoretical analyses (reference 3). When an airplane meets these requirements, it is fairly certain that the airplane will be safe to fly and desirable from the pilot's standpoint. Additional sets of requirements have been prepared by the military services (reference 4) in order to provide for the requirements of military aircraft. Similar research has been carried out in England and an attempt along these lines was also made in Germany, but the number of airplanes which were tested in flight was considerably more limited.

A report (reference 5) has been recently published which discusses the reasons for the flying qualities requirements, the design factors involved in obtaining satisfactory flying qualities, and the methods used in predicting the stability and control characteristics of an airplane. Some of the methods for predicting the handling qualities of a proposed airplane will now be described.

The flying-qualities requirements tie in with the concepts of dynamic stability in that certain requirements are specified for the characteristics of the uncontrolled motion of the airplane. The great majority of the requirements, however, pertain to the control positions and forces required in certain specified flight conditions and maneuvers. In order to predict the ability of an airplane to satisfy these requirements, solution of the equations of motion is not generally required. The required control positions and forces may be predicted by considering the airplane to be in an equilibrium condition. The forces and moments acting may then be estimated either by means of wind-tunnel tests or simply by calculations based on the dimensions of the airplane.

Investigations of varying complexity are required for these predictions depending on the flight conditions, speeds, and types of airplane involved. For conventional airplanes, the control positions required in straight flight or in steady maneuvers in conditions where the thrust coefficient is low may be estimated with sufficient accuracy for practical design purposes simply from a knowledge of the dimensions of the airplane. The effects of power on longitudinal and directional stability, in the case of propeller-driven airplanes, cannot be predicted with such a high degree of accuracy. Wind-tunnel tests of a powered model are desirable in estimating these effects. If accurate predictions of the control forces are desired, particularly on a large airplane, tests may be made of the actual control surfaces in a large wind tunnel, or at least tests of large-scale models of the control surfaces. Finally, the effects of compressibility should be determined from tests of a complete model in a high-speed tunnel. Such a complete investigation is not usually required, however, particularly for conventional airplanes, because of the large amount of data accumulated during the war on the characteristics of many airplane configurations.

Some of the data applicable to the prediction of flying qualities will now be given. Methods for predicting the longitudinal stability in the power-off condition from a knowledge of the dimensions of the airplane are given in references 6 and 7.

In these methods, the effects of the fuselage, idling propeller, wing, and tail are calculated. The effect of the upwash ahead of the wing on the fuselage and propeller pitching moments and of the downwash from the wing and propeller on the tail must be taken into account in order to obtain accurate results.

Calculation of the directional stability likewise involves estimating the contributions of the various airplane components and their mutual interference effects. The data of references 8 and 9 may be used to estimate many of these quantities. The effects of the propeller may be obtained from reference 10.

Comparison of calculated values of directional stability on a large number of airplanes with measured values has shown that this quantity may be predicted fairly accurately for airplanes with smoothly streamlined canopies. On airplanes with poorly designed canopies, the wake of the canopy passing over the vertical tail greatly reduces its effectiveness and it is rather difficult to estimate what percent of the vertical tail area should be considered effective. Some wind-tunnel data on the effects of canopies on directional stability may be found in reference 11.

Another item of importance which may be estimated quite accurately is the rolling velocity obtained in a steady roll with a given aileron deflection. Methods for making this calculation are described in detail in a report which summarizes the results of NACA lateral-control research (reference 12).

Several reports have been published comparing stability and control characteristics predicted from the dimensions of the airplane with those measured in flight (references 7, 9, and 13). In general, these results are in good agreement for flight conditions where the thrust coefficient is low. Calculations of the effects of power on the stability characteristics are more difficult, and usually it is desirable to resort to wind-tunnel tests of a powered model in order to obtain accurate results. Various attempts have been made, however, to devise semiempirical methods to determine the effects of power, based on the large number of wind-tunnel tests of powered models which were conducted during the war years (reference 14). It is also possible to estimate the effects of power by comparison with the results of tests for a similar design. The effects of power on longitudinal stability as measured in flight on a number of airplanes are given in reference 15.

The procedure for conducting wind-tunnel tests of a powered model is described in detail in reference 16. Methods for analyzing the

results of wind-tunnel tests for determination of flying qualities are given in references 17 and 18.

Several reports have been published comparing the flying qualities of aircraft as measured in flight with those predicted from wind-tunnel tests (references 19 and 20). Usually the agreement with regard to control positions is satisfactory. The prediction of control forces is subject to more uncertainty. One point which may be mentioned in connection with the prediction of control forces is that generally the hinge-moment parameters C_{h_α} and C_{h_δ} may be predicted only with a certain degree of accuracy. In cases where this much variation will cause large changes in the stick forces it is apparent that the control-force characteristics will be difficult to predict accurately. The accuracy may be improved, however, by designing the airplane in such a way that the control forces are less sensitive to small changes in the hinge-moment characteristics.

Inasmuch as in the past much emphasis has been placed on the classical theory of stability, an attempt will be made to show how the items considered important in connection with flying qualities tie in with the classical theory of stability. First, the subject of longitudinal stability and control will be considered. The theory predicts that a statically stable airplane will perform two types of oscillation: the long period or phugoid motion, which is generally poorly damped, and the short period oscillation, which is always well damped when the controls are fixed. It has been frequently demonstrated that the period of the phugoid motion is so long that the damping of this oscillation has no correlation with the pilot's opinion of the handling qualities (reference 21). This fact is so well established that any explanation of it may seem superfluous. The emphasis placed in the past on the calculations of the characteristics of this mode of motion, however, has lead many engineers to be reluctant to discount its importance. In order to demonstrate the ease with which the pilot can damp out this oscillation, therefore, figure 1 is presented. This figure illustrates that not only can the pilot damp out the phugoid motion very rapidly but that only a very small motion of control is required.

Though the short-period oscillation is always stable with controls fixed, it may become violently unstable with controls free if certain unfavorable combinations of elevator hinge-moment characteristics are employed. When this motion is unstable, it results in an oscillation which produces accelerations approaching the structural strength of the airplane within a period of 1 or 2 seconds. Flight records of the type of oscillation are shown in figure 2 for both well-damped and unstable oscillations. A condition such as this unstable oscillation obviously cannot be tolerated and it is, therefore, required that this mode of motion be well damped. A theoretical analysis of this type of oscillation presented in reference 22 indicates that the motion may become unstable if the variation of hinge-moment coefficient with deflection C_{h_δ}

(the restoring tendency of the elevator) is reduced to zero, and stability is obtained by use of a bobweight or an elevator which tends to float against the relative wind. In the example shown in figure 2, the value of C_{h_δ} was reduced to approximately zero by use of a balancing tab.

The requirement for dynamic longitudinal stability is only one of a large number of requirements which must be satisfied in order that the longitudinal stability and control characteristics should be satisfactory. The other requirements deal with the characteristics of the elevator control in steady flight, in accelerated flight, in landing, and in take-off, and also with the trim changes due to power and flaps, and the characteristics of the longitudinal trimming device. An example of one of the requirements will be given to show how a quantitative requirement of this type aids in establishing certain features of the airplane design. The requirements for longitudinal control in accelerated flight specify the variations of elevator angle and elevator force with acceleration in maneuvers in which the angle of attack is increased rapidly to produce a condition of accelerated flight without much change in airspeed. Inasmuch as the elevator force per g change in normal acceleration is fairly independent of speed on conventional airplanes, this quantity is used as one means of specifying the elevator-force characteristics. The control-force gradient should not exceed about 6 pounds per g on highly maneuverable airplanes such as fighters and should be less than 50 pounds per g on transports, heavy bombers, and so forth. In order to prevent the pilot from inadvertently overstressing the structure, a pull force of at least 30 pounds should be required to reach the allowable load factor. An excessive value of force per g will result in an airplane which is difficult to fly or maneuver, whereas a negative value will make the airplane extremely dangerous to fly because a rapid divergence would result if the pilot released the control stick. Some factors which influence the force characteristics in accelerated flight are illustrated in figure 3. From this figure it is seen that the force per g increases as the center of gravity is moved forward. The variation of force per g with center-of-gravity position may be reduced by reducing the variation of elevator hinge-moment coefficient with deflection C_{h_δ}. The curve may be shifted by a constant amount at any center-of-gravity position by changing the variation of elevator hinge-moment coefficient with angle of attack C_{h_α}. On a given airplane the range of center-of-gravity positions over which satisfactory flying qualities are obtained may be limited by this force-per-g variation. An increase in the center-of-gravity range over which satisfactory force characteristics in steady maneuvers are obtained might be provided by reducing the value of C_{h_δ} and obtaining forces in the desired range by use of a positive value of C_{h_α}. Flight tests have shown, however, that this procedure, if carried too far, may result in undesirably light control forces in rapid maneuvers, because the pilot is able to deflect the control rapidly with very little force; then the force builds up as the acceleration increases. This condition is discussed more fully in reference 23.

The desire for light control forces over a large center-of-gravity range, therefore, conflicts with the requirement for desirable control feel. The requirements may be more easily satisfied, however, if the center-of-gravity range is located well forward of the position for neutral stability with the elevator fixed.

A few of the requirements for lateral stability and control will now be discussed. Here, again, the first requirement ties in with the classical concepts of dynamic stability. There is no requirement for spiral stability inasmuch as the spiral divergence is very slow and easily controlled and also because in most conventional airplanes the friction in the control system may hold the controls in a position to cause a much more rapid divergence than the spiral divergence with the controls in the trim position. The Dutch roll oscillation has a relatively short period, however, and it should be well damped so as not to require constant attention on the part of the pilot. On practically all conventional airplanes the Dutch roll oscillation with controls fixed is sufficiently well damped. Continuous lateral oscillations, known as snaking oscillations, have, however, been encountered on many airplanes as a result of slight motion of the controls induced by the oscillation. A report which presents a theoretical analysis of this type of motion and indicates means of avoiding it is available (reference 24). While the classical Dutch roll oscillation has given little trouble in the past, it has assumed a status of increased importance in connection with recent airplane designs employing swept wings.

Other lateral stability and control requirements deal with the aileron-control characteristics, the yaw due to ailerons, the limits of rolling moment due to sideslip, the directional stability, the side-force characteristics, and the pitching moment due to sideslip. In addition, the characteristics of the rudder and aileron trimming devices are specified.

Some unusual features of airplane stability and control which have been shown to be important for many types of airplanes and which have not been given a great deal of attention in the past will now be presented.

One factor which has been found to be very important in affecting the flying qualities of many high-speed airplanes is the distortion of the control surfaces and of the airplane structure under aerodynamic loads. Data presented in figure 4 illustrate one effect which is quite frequently encountered. This figure shows the effect of stabilizer incidence on the variation of stick force with speed in straight flight. An analysis based on the assumption of a rigid airplane would indicate that there should be no change in the curve of stick force against speed due to changing the stabilizer incidence provided the airplane were retrimmed at the same speed by use of the trim tab. In practice it is found that a negative stabilizer incidence, which requires down

elevator deflection for trim in high-speed flight, usually results in rapidly increasing push forces at high speeds. This effect is caused by progressively increasing distortion of the elevator covering and twisting of the stabilizer as the aerodynamic forces are increased. This condition is very undesirable because if the pilot should release the stick at high speeds, excessive acceleration would be encountered in the pull-out. The effect of positive stabilizer incidence is to produce rapidly increasing pull forces at high speeds which violates the requirement for static longitudinal stability. These effects cannot, of course, be predicted from wind-tunnel tests of a rigid model. These distortion effects may be avoided, however, by use of the correct stabilizer setting so that the elevator is lined up with the stabilizer in high-speed flight. A similar effect of distortion on the rudder-force variation with speed is obtained by varying the setting of the vertical fin. These and other effects of distortion due to aerodynamic loads may be isolated from compressiblity effects in flight tests by making runs at different altitudes. Distortion effects set in at a given value of indicated airspeed, whereas compressibility effects occur at a given Mach number. A theoretical analysis of the effects of fabric distortion on stability is given in reference 25.

Many of the design factors which may be used to aid in meeting certain of the flight-qualities requirements are of a conflicting nature so that compromises in the design will generally have to be made in order to meet all the requirements as closely as possible. The most frequently encountered problem is that of providing sufficiently light control forces without reducing the effectiveness of the control surfaces below the specified values. All the control-force values which enter into the requirements, such as the force per g, the aileron force required in a roll, the rudder force required to offset aileron yaw, and so forth, tend to increase as the product of the span and the square of the chord of the control surface, and as the dynamic pressure. As airplanes are made larger and faster, therefore, an increasing degree of aerodynamic balance is required on all the control surfaces to meet the handling-qualities requirements. For example, figure 5 illustrates the approximate reduction in C_{h_δ} of the elevator required to meet the elevator control-force requirements as a function of airplane weight. A great deal of research has been done during the war years on means of balancing control surfaces, some of which is summarized in reference 11. Nevertheless, it is impractical to balance control surfaces more than a certain amount because variations in contours of the control surfaces of different airplanes of the same type, within production tolerances, result in variations of C_{h_δ} of the same order as the value required. On large airplanes, therefore, some aerodynamic or mechanical device is required to multiply effectively the pilot's effort by a large factor, in order that light forces may be obtained without utilizing an impractically large degree of balance. Such devices include spring tabs (reference 26) and hydraulic booster mechanisms.

Inasmuch as the handling-qualities requirements are based largely on experience with conventional airplanes, further research will probably be required to find whether additional requirements are necessary for the unconventional types of airplanes that are now being contemplated for very high speed flight. Because of the great range of speed and altitude encountered by such airplanes it may be impossible to meet the handling-qualities requirements without relying on mechanical devices to provide stability and desirable control forces. With such devices the method of the control of the airplane may differ considerably from that normally used. Research will therefore be required to find the reaction of the pilot to these unusual control forces. Preliminary research on this subject may be carried out without making actual flight tests by the use of simulators designed to behave in the same manner as the airplane.

REFERENCES

1. Soulé, H. A.: Preliminary Investigation of the Flying Qualities of Airplanes. NACA Rep. No. 700, 1940.

2. Perkins, Courtland D., and Walkowicz, T. F.: Stability and Control Flight Test Methods. AAF TR No. 5242, Materiel Command, Army Air Forces, July 14, 1945.

3. Gilruth, R. R.: Requirements for Satisfactory Flying Qualities of Airplanes. NACA Rep. No. 755, 1943.

4. Anon.: Stability and Control Characteristics of Airplanes. AAF Specification No. R-1815-A, April 7, 1945.

5. Phillips, William H.: Appreciation and Prediction of Flying Qualities. NACA TN No. 1670, 1948.

6. Gilruth, R. R., and White, M. D.: Analysis and Prediction of Longitudinal Stability of Airplanes. NACA Rep. No. 711, 1941.

7. White, Maurice D.: Estimation of Stick-Fixed Neutral Points of Airplanes. NACA CB No. L5C01, 1945.

8. House, Rufus O., and Wallace, Arthur R.: Wind-Tunnel Investigation of Effect of Interference on Lateral-Stability Characteristics of Four NACA 23012 Wings, an Elliptical and a Circular Fuselage, and Vertical Fins. NACA Rep. No. 705, 1941.

9. Sweberg, Harold H., Guryansky, Eugene R., and Lange, Roy H.: Langley Full-Scale Tunnel Investigation of the Factors Affecting the Directional Stability and Trim Characteristics of a Fighter-Type Airplane. NACA ARR No. L5H09, 1945.

10. Ribner, Herbert S.: Notes on the Propeller and Slipstream in Relation to Stability. NACA ARR No. L4I12a, 1944.

11. MacLachlan, Robert, and Levitt, Joseph: Wind-Tunnel Investigation of Effect of Canopies on Directional Stability Characteristics of a Single-Engine Airplane Model. NACA TN No. 1052, 1946.

12. Langley Research Department (Complied by Thomas A. Toll): Summary of Lateral-Control Research. NACA TN No. 1245, 1947.

13. Crane, Harold L., and Sjoberg, Sigurd A.: Comparison of Predicted and Actual Control-Fixed Stability and Control Characteristics of a Douglas A-26B Airplane. NACA MR No. L5D06, 1945.

14. Goett, Harry J., and Delany, Noel K.: Effect of Tilt on the Propeller Axis on the Longitudinal-Stability Characteristics of Single-Engine Airplanes. NACA Rep. No. 774, 1944.

15. White, Maurice D.: Effect of Power on the Stick-Fixed Neutral Points of Several Single-Engine Monoplanes as Determined in Flight. NACA CB No. L4H01, 1944.

16. Recant, Isidore G., and Swanson, Robert S.: Determination of the Stability and Control Characteristics of Airplanes from Tests of Powered Models. NACA ARR, July 1942.

17. Kayten, Gerald G.: Analysis of Wind-Tunnel Stability and Control Tests in Terms of Flying Qualities of Full-Scale Airplanes. NACA ARR No. 3J22, 1943.

18. Goett, Harry J., Jackson, Roy P., and Belsley, Steven E.: Wind-Tunnel Procedure for Determination of Critical Stability and Control Characteristics of Airplanes. NACA Rep. No. 781, 1944.

19. Kayten, Gerald G., and Koven, William: Comparison of Wind-Tunnel and Flight Measurements of Stability and Control Characteristics of a Douglas A-26 Airplane. NACA ARR No. L5H11a, 1946.

20. Hockman, Marion T., and Eisiminger, Robert E., Jr.: The Correlation of Wind-Tunnel and Flight-Test Stability and Control Data for an SB2C-1 Airplane. Jour. Aero. Sci., vol. 15, no. 1, Jan. 1948, pp. 5-17.

21. Soulé, Hartley A.: Flight Measurements of the Dynamic Longitudinal Stability of Several Airplanes and a Correlation of the Measurements with Pilots' Observations of Handling Characteristics. NACA Rep. No. 578, 1936.

22. Greenberg, Harry, and Sternfield, Leonard.: A Theoretical Investigation of Longitudinal Stability of Airplanes with Free Controls Including Effect of Friction in Control System. NACA Rep. No. 791, 1944.

23. Phillips, William H.: An Investigation of Additional Requirements for Satisfactory Elevator Control Characteristics. NACA TN No. 1060, 1946.

24. Greenberg, Harry, and Sternfield, Leonard: A Theoretical Investigation of the Lateral Oscillations of an Airplane with Free Rudder with Special Reference to the Effect of Friction. NACA Rep. No. 762, 1943.

25. Mathews, Charles W.: An Analytical Investigation of the Effects of Elevator-Fabric Distortion on the Longitudinal Stability and Control of an Airplane. NACA ACR No. L4E30, 1944.

26. Phillips, William H.: Application of Spring Tabs to Elevator Controls. NACA Rep. No. 797, 1944.

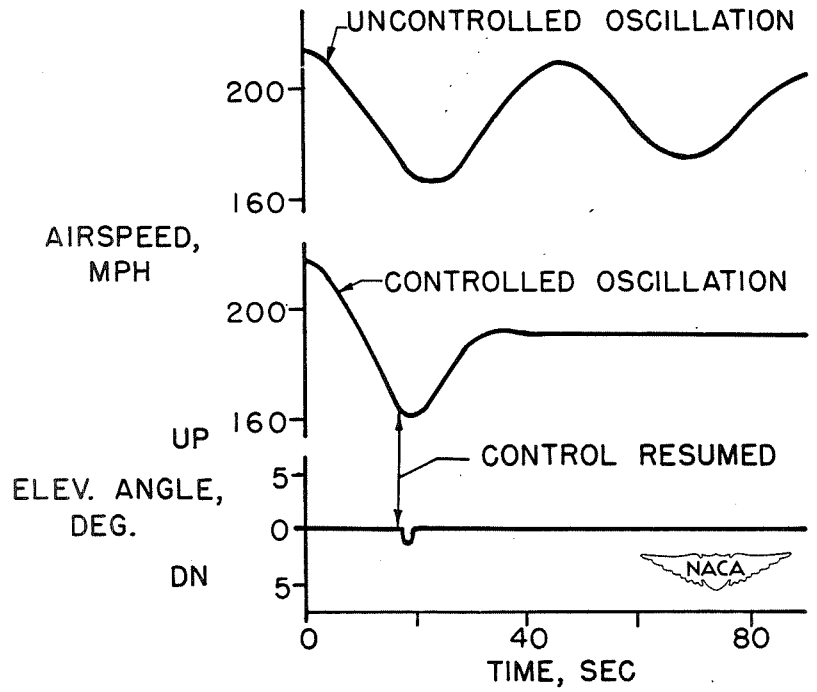

Figure 1.- Phugoid oscillations.

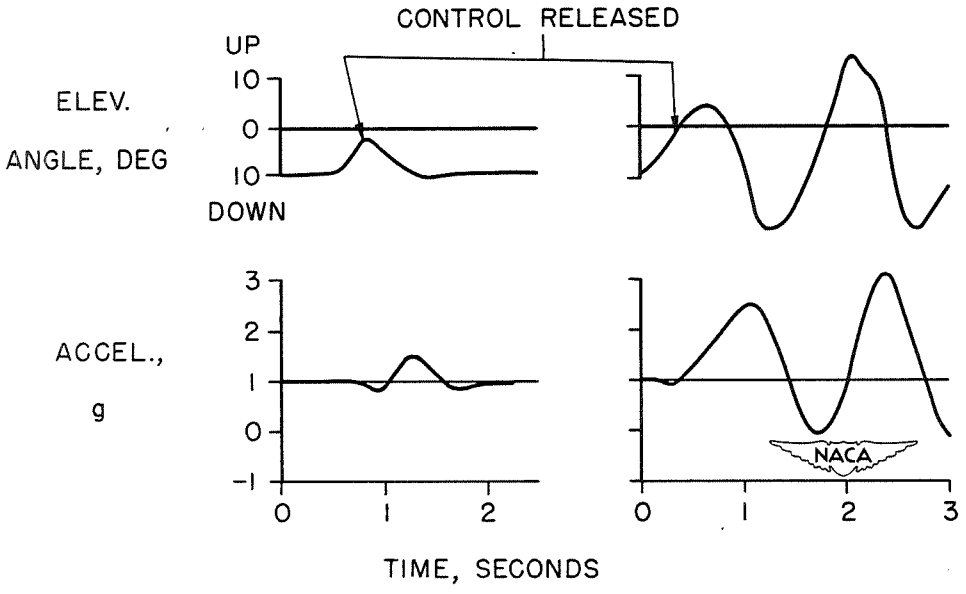

Figure 2.- Short-period oscillations.

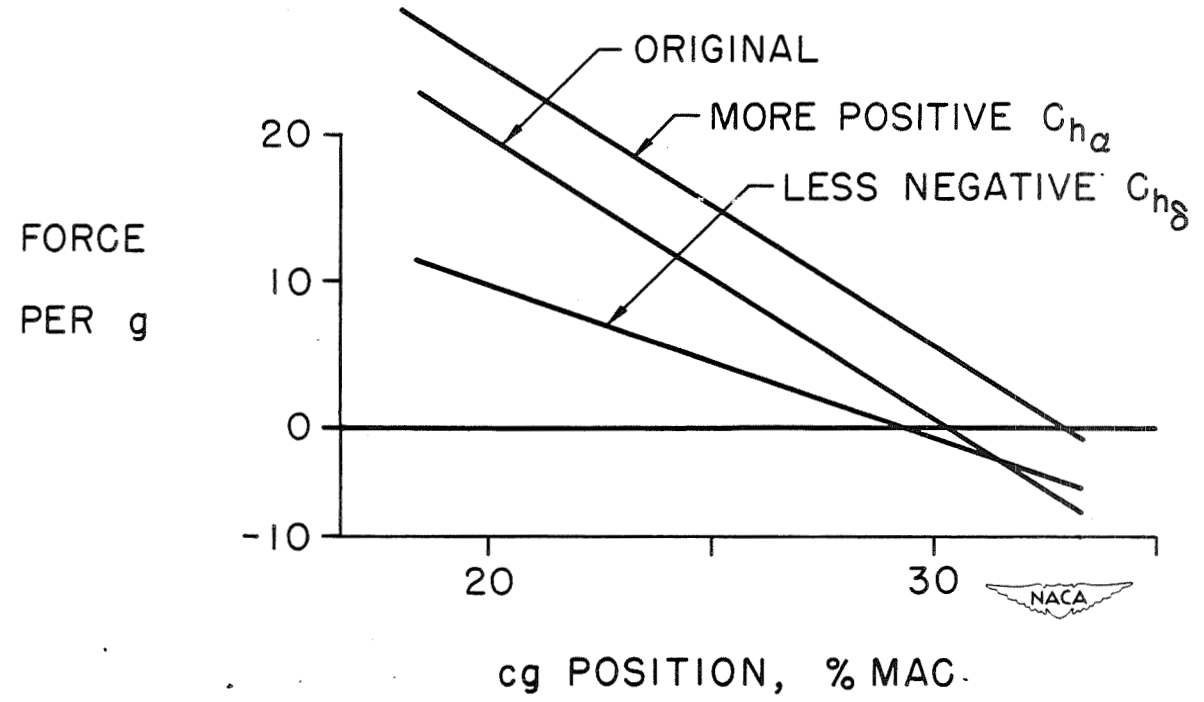

Figure 3.- Elevator forces in maneuvers.

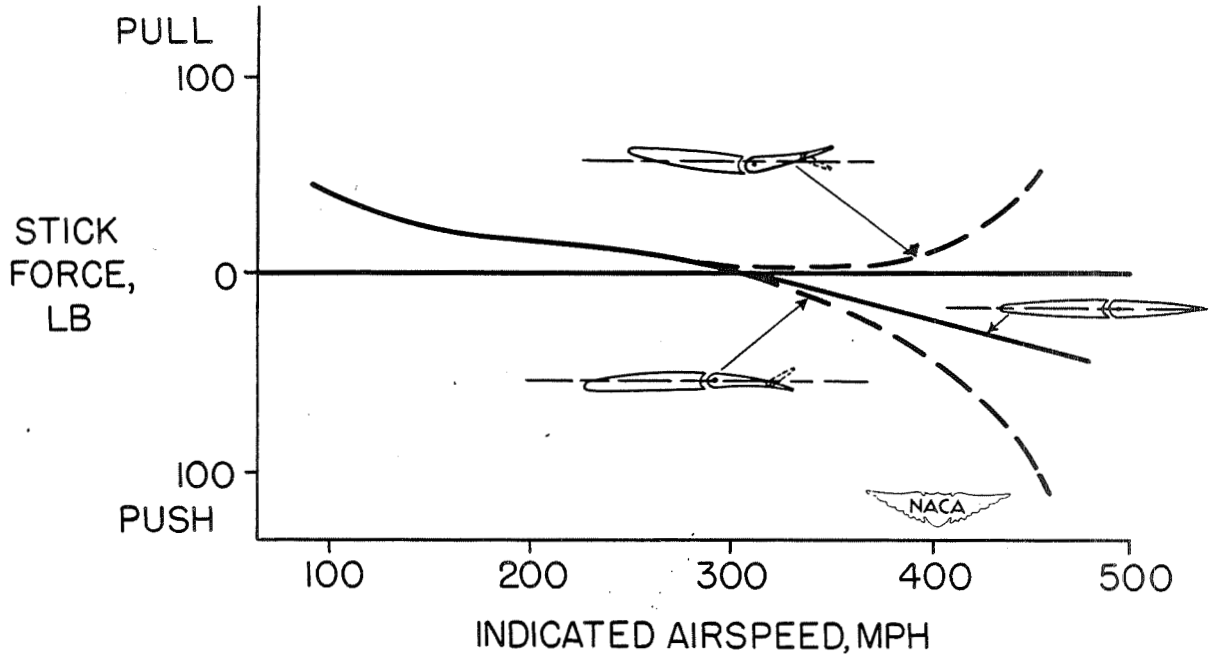

Figure 4.- Distortion effects.

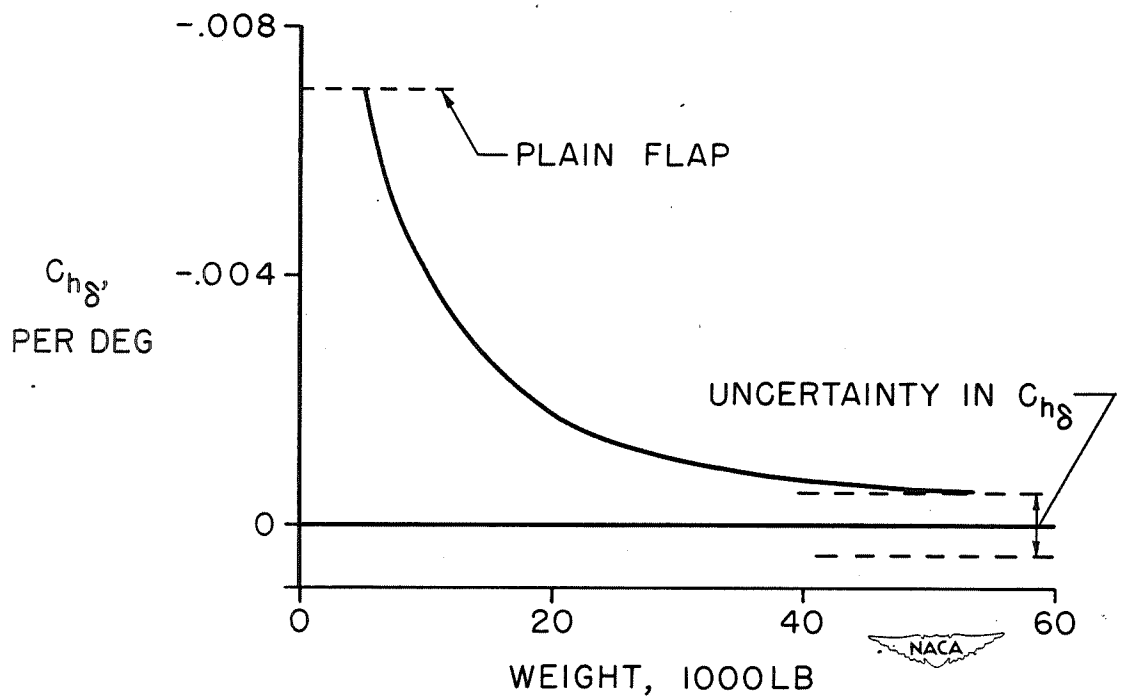

Figure 5.- Elevator balance.

HELICOPTER RESEARCH

HELICOPTER RESEARCH PROBLEMS

By Alfred Gessow

Langley Aeronautical Laboratory

INTRODUCTION

This paper is restricted to a presentation of the more important problems associated with the development of the most successful type of rotating-wing aircraft - the helicopter - and to an indication of the present status of research of these problems.

The helicopter as thought of at present is an aircraft in which lift, propulsion, and control are all provided by one or more propeller-like rotors turning about an approximately vertical axis. The fundamental advantage of such an arrangement is that the means for obtaining and controlling flight is separated from the translational speeds of the fuselage. In spite of the many advantages afforded by this feature, notably that of vertical flight, it was only during the last decade that helicopters having satisfactory performance and handling qualities have been built and flown. Their success can be attributed to improved power plants, an increased knowledge of general aerodynamics as well as the aerodynamics of rotating-wing flight, and the backlog of experience gathered from the hundreds of unsuccessful helicopter builders since the time of Da Vinci.

The present-day helicopter is still in an early stage of development. Its performance, handling characteristics, safety, and reliability, however, though still poor when judged by modern airplane standards, are already acceptable for a number of important applications where its special capabilities are at a premium. Prospects for further improvement are good and a wide field of application, both military and commercial, is assured.

DISCUSSION

The general helicopter research field is, for the present discussion, divided into four broad classifications: performance, vibration and flutter, stresses, and stability and control. A description of the problems encountered in each of these fields is given, and lines of future research are pointed out.

Performance

The problem of determining the aerodynamic characteristics of a lifting rotor for purposes of design or performance estimation is complicated by the large number of variables involved. Consequently, the approach could not be wholly empirical, and some theoretical frame work was required to correlate experimental data. The performance problem has

been attacked therefore by trying to develop a method of calculating the characteristics of the rotor from the characteristics of the blade airfoil sections. The method is similar to that of calculating propeller characteristics by blade element or strip theory but is much more complicated because of the flapping motion of the hinged blades and because the translational (edgewise) component of velocity in forward flight must also be accounted for.

In order to make the problem capable of practical solution, certain assumptions and simplifications had to be incorporated in the theory in addition to the primary one of using two-dimensional airfoil characteristics in summing up the forces acting on the blades of the rotor. A principal assumption specified that the rotor induced velocity could be calculated by the momentum theory and could be considered to be uniform across the rotor disk. (See reference 1.) The resulting calculations, which were extremely lengthy and complicated, were simplified and condensed into design charts that give a good insight as to the effects of changes in rotor design parameters. (See reference 2.) Sufficient comparisons of the theory with experimental data have been obtained from flight and full-scale tunnel tests to prove the validity of theory. (See references 3 to 9 for an experimental verification of the theory in various flight conditions.)

The accuracy of the theory is illustrated by figure 1, which shows the good agreement between the calculated and measured characteristics, as obtained in flight, of a test rotor in terms of a plot of power against velocity. It might be mentioned that model tests in general are not satisfactory for helicopter-performance work because of the effects of scale on the aerodynamic characteristics of the blade elements.

The transition region between hovering and about 30 miles per hour shown in the figure represents a speed range in which accurate data could not be obtained in flight because of instability and control difficulties or in full-scale wind tunnels because of the largely unknown interference corrections at low airspeeds. Full-scale data were obtained in this region, however, by means of a relatively new research tool - the helicopter test tower. It was found that the test-tower results checked closely with theoretical calculations over most of the transition region.

As a result of the experience gained through the use of the theory and its experimental verification, several factors were found to influence considerably the performance characteristics of rotors. One such factor was the importance of smooth, nondeformable blade surfaces in reducing the power required by the rotor in all flight conditions. (See references 9 and 10.) The importance of well-built blades arises from the fact that in cruising and high-speed flight blade profile drag accounts for from one-half to two-thirds of the total rotor losses.

Rotor theory and experiment have also shown that rotor performance is dependent to an appreciable extent on the amount of twist and taper

built into the blades of the rotor. Studies (reference 11) have indicated, for example, that the rotor induced losses, which are the penalty that must be paid for the thrust produced by the rotor, comprise approximately 75 percent of the total power losses in the hovering condition and that these losses can be reduced to the extent of increasing the hovering pay load by approximately 20 percent if the blades were designed with a moderate amount of taper and twist, instead of being untapered and untwisted.

Theory and experiment have also pointed out the values of design variables that would result in maximum performance. An example of this is illustrated in figure 2, which shows the importance of low rotor speeds and high blade lift coefficients for hovering and vertical-flight performance. The top curve shows that a reduction of tip speed from 600 feet per second to 400 feet per second would reduce the power required to hover at fixed thrust by approximately 25 percent. The lower curve shows that at a fixed power and thrust, the same reduction in tip speed results in a substantial increase in the vertical rate of climb, namely from 200 feet per minute to approximately 1150 feet per minute. The question might naturally arise as to what constitutes a lower limit to the tip speed and why the helicopter couldn't always operate at that limiting condition. The answer lies in the fact that low tip speeds are very undesirable at high speeds and that a good helicopter design must either compromise between the two conditions or must deliberately favor one at the expense of the other. (See reference 12.)

The choice of the proper tip speed and other design parameters for efficient high-speed flight must be investigated as part of the general problem of rotor-blade stalling. This problem has received and is getting a great deal of attention, inasmuch as it considerably reduces the efficiency of a helicopter flying at high speeds and is the decisive factor in limiting the top speed of present-day helicopters.

Blade stalling results from the fact that as the lifting rotor moves forward, the advancing blades encounter progressively higher velocities, whereas the retreating blades encounter progressively lower velocities. Thus, in order to maintain approximately equal lift on both sides of the rotor so as to prevent the helicopter from rolling over, the low-velocity retreating blade must operate at higher angles of attack than the high-velocity advancing blade. It follows that as the helicopter increases its forward speed, the angles of attack of the retreating blade will increase proportionally until at some value of forward speed the angles of attack of the retreating blade will reach the stall. As still higher speeds are reached, the stalling becomes progressively more severe and spreads to a larger part of the rotor disk until the severe vibrations and the loss of control brought about by the stall prevents the helicopter from flying faster.

The effect of forward speed and rotor tip speed on stalling is illustrated in figure 3. The circles represent plan views of the rotor disk, the direction of flight and direction of rotation being as shown.

The dark region at the center represents the swept area of the hub and blade shanks and the shaded crescents represent the regions where the direction of flow over the retreating blades is reversed. For this helicopter, at 40 miles per hour and 210 rotor rpm, stall is beginning to occur near the tip of the retreating blade. When the speed is increased to 70 miles per hour, still keeping the same rotor rpm, the stalled area has increased considerably. The reduction in stalled area brought about by increasing the rotor speed to 225 rpm is shown on the bottom circle. At the same forward speed, the higher rotational speed reduces the differential in speed between the advancing and retreating blades and so cuts down the stalled area.

A criterion has been developed for predicting the limiting speed due to stalling. (See reference 13.) It has been found that the operational limit can be considered as reached when the calculated angle of attack at the tip of the retreating blade exceeded the stalling angle of the blade airfoil by approximately 4°. One use of this criterion is illustrated in figure 4 which shows the variation of the minimum allowable rotor speed, as set by blade stalling, with forward speed. The minimum rotor speed was calculated for each value of forward speed by setting a 16° tip angle of attack at the retreating blade as the operational limit. Thus, for a given forward speed, a helicopter cannot be operated in the hatched portion of the plot but must increase its rotor tip speed until the tip angle of attack is 16° or less (that is, it must be operated to the right of the curve.)

Although a helicopter can be flown until the 4° tip-angle limit is exceeded, the profile-drag loss due to stalling begins as tip stalling sets in. It has been found that the profile drag approximately doubles by the time the limiting top speed is reached. (See reference 14.) The effects of stalling on rotor profile drag can be seen in figure 5, in which the profile-drag power absorbed by two sets of blades are plotted against speed. The dashed lines in the figure represent the calculated power with no allowance for blade stalling, whereas the solid lines include losses due to stalling and thus represent the actual profile-drag power absorbed. Note that stalling losses are large in comparison to the profile-drag power absorbed by the unstalled blades and that, therefore, the top speed of the helicopter is also reduced because of the additional stall power.

Once the effects of blade stalling were understood, means for alleviating or delaying these effects were investigated. A satisfactory way to delay the stall was to twist the rotor blades so that the tip sections worked at lower angles of attack than they would if the blades were untwisted. (The effects of blade twist were investigated in flight and the results are reported in reference 15.) The effectiveness of blade twist in reducing the detrimental effects of stalling can be seen in figure 5. The figure shows that an increase of about 10 percent in the limiting speed of the test helicopter appears possible with the use of -8° of blade twist. Alternatively, twist reduces the stalling profile-drag losses by approximately 40 percent of the profile-drag power absorbed

by the rotors in the unstalled condition once stalling had developed on both rotors. The use of blade twist is desirable inasmuch as, at the very least, it appears to have no detrimental effect on rotor performance in any other flight condition.

Another and somewhat obvious means for minimizing the effects of blade stalling is by increasing the blade-section stalling angle of attack. The benefits to be had by so doing, in terms of an increase in permissable load at a fixed tip speed, is shown in the left part of figure 6. It can be seen from the figure that the permissable helicopter load could be increased by a factor of 3 if the section stall angle could be increased from 12° to 20°. The successful application of various high-lift devices that would substantially increase the section stall angle without prohibitive drag increases in the high-velocity low-angle-of-attack regions of the disk will prove a fertile field for future helicopter research.

Just as blade stalling presents a lower limit to the allowable rotor tip speed, another limit exists that prevents operation at extremely high tip speeds. That limit is compressibility effects on the high-velocity tip sections of the advancing blade. For a given stalling angle, a higher section critical Mach number will permit operation at larger gross weights because it permits the use of higher tip speeds. It can be seen from the right part of figure 6 that large increases in pay load can be realized by increasing the critical Mach number of airfoil sections used in the blades.

Although most rotor blades at the present time are composed of conventional wing sections, attention is being given to the development of airfoil sections designed especially for rotors as distinguished from wings or propellers. In addition to a high stall angle and a high critical Mach number, the desirable aerodynamic characteristics of airfoil sections suitable for use as rotor-blade sections are: (1) nearly zero pitching moment, (2) low drag throughout the range of low and moderate lifts, and (3) moderate drag at high lifts.

Most of the NACA low-drag airfoils that have been developed have too high a pitching-moment coefficient to warrant consideration for use with current helicopter designs. (High pitching-moment coefficients lead to undesirable periodic stick forces and to vibrations brought about by periodic blade twist.) Although this objection is removed with the low-drag symmetrical sections, these sections are not applicable because half of the low-drag "bucket," or, in other words, half of the limited range of lift coefficients in which the important drag reductions are achieved, is below zero lift; whereas the faster moving portions of the helicopter blade are nearly always operating at positive lift coefficients.

In order to place the low-drag "bucket" in a useful range of lift coefficients and still retain zero or almost zero moment coefficient, a number of special airfoils have been derived. (See reference 16.) One of these, the NACA 8-H-12, shows the most promise. A comparison of the

NACA 8-H-12 section with the conventional NACA 23012 airfoil is given in figure 7, which shows a reduction in drag over most of the lift coefficient range combined with an earlier stall. Calculations of the performance of rotors incorporating the new section have indicated the superiority of the special section over the conventional sections. Full-scale tests of practical-construction blades incorporating the NACA 8-H-12 section are needed, however, to determine the true worth of the airfoil under actual operating conditions.

Vibration and Flutter

It is commonly accepted that where large, rotating masses are involved, vibrations of some kind are likely to appear - and the helicopter is no exception. In fact, the designers of most of the earlier types of helicopters had as much difficulty in reducing the vibration to acceptable levels as they had in obtaining adequate performance. A good deal of the trouble was caused by poorly built, unbalanced blades and was largely eliminated with more accurate designs and an increased knowledge of blade balancing and tracking procedure. A second source of the vibration difficulties encountered were inherent in the helicopter itself and could only be avoided when the phenomenon that caused it was thoroughly analyzed and understood. An example of such a phenomenon is a self-excited mechanical vibration known as "ground resonance," which has been responsible for the destruction of several autogiros and helicopters.

Essentially, "ground resonance" is a self-excited mechanical vibration that involves a coupling between the motion of the rotor blades about their drag hinges and the motion of the helicopter as a whole on its landing gear. When the frequencies of the two motions approach each other, a violent shaking of the aircraft occurs which, if undamped, would result in its complete destruction. This phenomenon was theoretically investigated and a theory was developed which suggested means for avoiding "ground resonance." (See references 17 to 19.) In order to make the theory easy to use, it was put in the form of simple charts which predicted the range of rotor speeds in which the instability occurred and the amount of damping necessary to avoid dangerous frequencies.

Another example of a vibration problem peculiar to helicopters was encountered in the operation of two-bladed rotors. The phenomenon was called blade "weaving" from the appearance of the wavy path traced by the blade tips and was found to be an aerodynamic instability or type of flutter. The problem was investigated theoretically (reference 20) and also by means of model tests. The general result of the study was that a see-saw rotor with a coning angle is more unstable than an airplane wing having corresponding parameters. The additional unstabilizing effect is associated with the difference in moments of inertia in flapping and in rotation. In fact, it was found that with certain combinations of coning angles and blade design parameters, flutter could occur even when

the chordwise center of mass of the blades was well ahead of the 25-percent-chord point. Proposed remedies for the flutter investigated included decreasing the coning angle of the blades, designing the blades so that their mass tends to be confined to the plane of rotation, increasing the control-system stiffness and forward position of the center of mass, and adding mechanical damping to the rotor system.

The helicopter is subjected to a third type of vibration that cannot be eliminated inasmuch as it is a forced vibration inherent in the aerodynamics of the rotor itself. This type of vibration is encountered, for example, with two-bladed helicopters in the transition region between hovering and forward flight wherein cyclic variations of induced and profile drag give rise to horizontal hub vibrations or, for example, when blade stalling is encountered in high-speed flight. (See reference 21.) Although inherent vibrations of these types cannot be eliminated, they can be isolated by suitably shock mounting the rotor system, and by using irreversible controls that cannot transmit vibratory forces to the pilot's controls. A great deal of work remains to be accomplished in reducing the over-all vibration level of the helicopter so that it can be flown for long periods of time without unnecessarily adding to pilot fatigue.

Stresses

Although the achievement of maximum helicopter performance and reliability calls for a thorough knowledge of the stresses imposed on the rotor and fuselage of the helicopter in all steady and accelerated flight conditions, the general field of helicopter stress analysis has been considered secondary to the aerodynamic problems. Literature on helicopter stress analysis does exist, but, in the main, conventional methods have been applied in analyzing the fuselage and rotor blades. Blade analyses, for example, have been made by propeller strip methods although an additional complication that has been taken into account is the spanwise bending of the blades, which tends to change the direction of the centrifugal loading on the blades. (See references 22 to 26 for information on blade stress analysis.) As yet, however, actual stress values, and the various assumptions regarding blade loading that are incorporated in these methods, have not been directly verified by reliable full-scale test measurements. Aside from a direct check on the actual stresses, the significance of these calculations would be greatly strengthened if experimental data were obtained on the induced flow in forward flight, so that the aerodynamic loading can be more accurately calculated. (The induced flow in hovering has been directly verified by British flight tests.)

In connection with induced-flow measurements, it might be mentioned that the over-all magnitude and general distribution of the induced velocity have been verified by rotor-blade-motion and performance tests made in flight. The induced velocity actually appears to vary nonlinearly in magnitude across the disk, however, and would therefore be expected to

influence considerably local stress values along the blade. The problem of determining induced velocities is amenable to theoretical solution; and although some work has been done along these lines (reference 27), a good deal still remains to be done before rotor-blade stresses can be predicted with confidence.

Stability and Control

The information that has been accumulated on the stability and control of helicopters during the past years has been rather limited. In their desire to establish the practicability of the helicopter as a flying machine, designers have concentrated on improving the performance and reducing the vibrations of the helicopter, while accepting marginal stability and control characteristics. As a result, the helicopter in its present stage of development is different and more difficult to fly than most fixed-wing airplanes. In response to the increasing demands placed upon the helicopter by the armed services and by commercial operators, however, the improvement of the stability and control characteristics of the helicopter and of its flying and handling qualities is perhaps the most important helicopter research problem at the present time.

A number of theoretical papers have been written on the subject of helicopter stability and control. (See references 28 to 32.) Although the theories presented in these papers are somewhat different and sometimes contradictory, it is generally agreed that (1) if the helicopter is disturbed while hovering, and if the control stick remains fixed, the helicopter will describe an oscillation about its original hovering position, and (2) the amplitude of the oscillation will increase with time. According to definition, the helicopter is thus dynamically unstable in hovering. Calculations indicate that the period of the oscillation of a two-place, 2700-pound helicopter is of the order of 10 seconds and that the rate of divergence is small. Limited flight data, obtained in this country (reference 33) and in England, have roughly checked the calculations and have indicated that the instability of the hovering oscillation is not a problem to the pilot.

The helicopter does have some handling characteristics in hovering that are frequently objectionable, especially to the novice pilot. One of the handling problems that the trainee must overcome with the smaller sized helicopter arises from the high control sensitivity of the helicopter in roll or, in other words, the high rate of roll per inch of stick displacement. This sensitivity frequently leads to over-controlling, which may result in a short-period pilot-induced lateral oscillation. Control sensitivity becomes less of a problem with large machines because for a given stick displacement the rolling velocity obtained will vary inversely as the diameter. Frequently, undesirable stick-force gradients are additional factors that add to the control problems of the unexperienced helicopter pilot.

Another control difficulty that might be mentioned has been encountered in the partial-power vertical-descent region between approximately 500 and 1500 feet per minute. In this vertical-descent range, the vibration of the helicopter becomes quite pronounced. Rather violent, random yawing motions then occur with some roll; the rate of descent apparently increases rapidly; the rotor rotational speed varies noticeably; and more often than not the helicopter eventually pitches nose down and recovers by gaining speed, despite application of considerable rearward control. There is much to be learned about this regime of operation, but preliminary indications are that the fundamental cause of the phenomenon is an unsteady, mixed flow of air through the rotor. Irregular flow in this intermediate flight condition might logically be expected inasmuch as air is blown downward through the rotor in hovering, whereas in completely power-off descent an upward flow of air takes place. Although pilots have experienced no difficulty in recovering from the maneuver at any stage desired, the phenomenon could be dangerous if it occurred at very low altitudes.

The helicopter has certain undesirable stability and control characteristics in forward flight as well as in hovering and in vertical descents. The major complaint reported by pilots is that they find it quite difficult to hold steady conditions in forward flight because of a strong tendency of the machine to diverge in pitch. Investigation has shown that this tendency results from the fact that the helicopter in general is unstable with angle of attack. There are two logical sources for this instability. The first source is the usual unstable fuselage, and the second results from the flapping of the rotor. When a flapping rotor is subjected to an angle-of-attack change in forward flight, the resulting change in blade flapping will be such as to further increase the rotor angle change.

Theoretical calculations indicate that the instability of the rotor and fuselage with angle of attack, if not overcome by a stabilizing means such as a tail surface, results in an unstable dynamic oscillation. Flight test results of stick-fixed oscillations, reported in reference 34, qualitatively checked the calculations. An example of an oscillation obtained at 40 miles per hour is shown in figure 8. The oscillation was initiated by a momentary aft motion of the stick. The period of the motion is about 14 seconds, which is long enough so that the pilot does not have trouble controlling the oscillation. The motion doubles in amplitude in about 1 cycle. Results obtained at higher speeds, however, have indicated that the motion following a disturbance is a divergence, rather than an oscillation. As you can well imagine, a divergent motion that could be brought about by a sudden gust is a dangerous maneuver if corrective action is not immediately initiated.

An example of such a maneuver obtained at 65 miles per hour is shown in figure 9. Again the helicopter was disturbed by an intentional stick motion, after which the stick was held fixed at the trim position. The helicopter nosed up mildly and then nosed down. It was still nosing down at an increasing rate, as the acceleration curve indicates, about 4 seconds

after the 1 g axis was crossed, and recovery had to be made by control application. In fact, considerable difficulty was encountered in recovering from the maneuver because the acceleration continued to build up 2 seconds after the cyclic control stick was at its forward stop. The pilot had to reduce the total pitch and had to roll the machine as in a wing-over before steady flight could be reached.

In general, it was found that though the helicopter is unstable over the entire speed range, its instability is least in the 40 to 60 miles per hour region. At higher speeds, the pilot has progressively less time to initiate recovery from a disturbance and the machine becomes rapidly more unstable.

It should be understood that the undesirable stability and control characteristics just discussed do not prohibit the present-day helicopter from being a useful tool for specialized purposes. Various means for eliminating these characteristics are under consideration in order to utilize all the potentialities of the helicopter, but the choice and application of these solutions depend upon continued research and development.

Future Research Needs

An attempt has been made herein to acquaint the reader with the present status of helicopter research. It may therefore be appropriate to conclude with a statement on future research needs.

Requirements for satisfactory flying qualities of helicopters should be established, similar to those already set up for the airplane, and means for meeting these requirements should be investigated. In particular, methods should be found to give the helicopter stick-fixed and stick-free stability in hovering and in forward flight. With this in mind, automatic-flight devices should be investigated; and the effectiveness and application of aerodynamic servocontrols and other control arrangements, including power controls, should be studied. Also, theoretical and experimental studies are needed to explain and correct the control difficulties encountered by pilots in the transition region between hovering and cruising flight and when descending vertically at partial-power conditions.

The trend toward large-diameter load-carrying helicopters calls for a more extensive knowledge of rotor-blade aerodynamic loading and blade stresses. Induced velocity and stress measurements should, therefore, be made and thoroughly analyzed. The use of more than one lifting rotor on the large load-carrying helicopters calls for a thorough investigation of the aerodynamic characteristics of the various multirotor arrangements that are being proposed. In particular, induced flow studies should be made for the various configurations that are now being used. Such studies would be useful for stability work and, also, for performance inasmuch as induced power requirements appear to be the primary unknown in computing the performance characteristics of multirotor configurations.

The application of jet propulsion to helicopters has long been considered as a desirable means for increasing the simplicity and the load-carrying ability of the helicopter. Several helicopters utilizing the jet principle have already been built and flown. A great deal of research, however, is still needed to establish the aerodynamic requirements of jet-driven helicopters and to produce an efficient jet system. The use of jets also brings about additional problems involving blade design, vibration, and stability characteristics that should be anticipated and solved.

It is hoped that an early and successful solution of these problems will make the helicopter a truly dependable and indispensable aircraft.

REFERENCES

1. Bailey, F. J., Jr.: A Simplified Theoretical Method of Determining the Characteristics of a Lifting Rotor in Forward Flight. NACA Rep. No. 716, 1941.

2. Bailey, F. J., Jr., and Gustafson, F. B.: Charts for Estimation of the Characteristics of a Helicopter Rotor in Forward Flight. I - Profile Drag-Lift Ratio for Untwisted Rectangular Blades. NACA ACR No. L4H07, 1944.

3. Gustafson, F. B.: Flight Tests of the Sikorsky HNS-1 (Army YR-4B) Helicopter. I - Experimental Data on Level-Flight Performance with Original Rotor Blades. NACA MR No. L5C10, 1945.

4. Gustafson, F. B., and Gessow, Alfred: Flight Tests of the Sikorsky HNS-1 (Army YR-4B) Helicopter. II - Hovering and Vertical-Flight Performance with the Original and an Alternate Set of Main-Rotor Blades, Including a Comparison with Hovering Performance Theory. NACA MR No. L5D09a, 1945.

5. Gessow, Alfred, and Myers, Garry C., Jr.: Flight Tests of a Helicopter in Autorotation, Including a Comparison with Theory. NACA TN No. 1267, 1947.

6. Dingeldein, Richard C., and Schaefer, Raymond F.: Full-Scale Investigation of the Aerodynamic Characteristics of a Typical Single-Rotor Helicopter in Forward Flight. NACA TN No. 1289, 1947.

7. Myers, Garry C., Jr.: Flight Measurements of Helicopter Blade Motion with a Comparison between Theoretical and Experimental Results. NACA TN No. 1266, 1947.

8. Migotsky, Eugene: Full-Scale Investigation of the Blade Motion of the PV-2 Helicopter Rotor. NACA TN No. 1521, 1948.

9. Gustafson, F. B., and Gessow, Alfred: Analysis of Flight-Performance Measurements on a Twisted, Plywood-Covered Helicopter Rotor in Various Flight Conditions. NACA TN No. 1595, 1948.

10. Gustafson, F. B.: Effect on Helicopter Performance of Modifications in Profile-Drag Characteristics of Rotor-Blade Airfoil Sections. NACA ACR No. L4H05, 1944.

11. Gessow, Alfred: Effect of Rotor-Blade Twist and Plan-Form Taper on Helicopter Hovering Performance. NACA TN No. 1542, 1948.

12. Gustafson, F. B., and Gessow, Alfred: Effect of Rotor-Tip Speed on Helicopter Hovering Performance and Maximum Forward Speed. NACA ARR No. L6A16, 1946.

13. Gustafson, F. B., and Myers, G. C., Jr.: Stalling of Helicopter Blades. NACA TN No. 1083, 1946.

14. Gustafson, F. B., and Gessow, Alfred: Effect of Blade Stalling on the Efficiency of a Helicopter Rotor as Measured in Flight. NACA TN No. 1250, 1947.

15. Gessow, Alfred: Flight Investigation of Effects of Rotor-Blade Twist on Helicopter Performance in the High-Speed and Vertical-Autorotative-Descent Conditions. NACA TN No. 1666, 1948.

16. Stivers, Louis S., Jr., and Rice, Fred J., Jr.: Aerodynamic Characteristics of Four NACA Airfoil Sections Designed for Helicopter Rotor Blades. NACA RB No. L5K02, 1946.

17. Coleman, Robert P.: Theory of Self-Excited Mechanical Oscillations of Hinged Rotor Blades. NACA ARR No. 3G29, 1943.

18. Feingold, Arnold M.: Theory of Mechanical Oscillations of Rotors with Two Hinged Blades. NACA ARR No. 3I13, 1943.

19. Coleman, Robert P., and Feingold, Arnold M.: Theory of Ground Vibrations of a Two-Blade Helicopter Rotor on Anisotropic Flexible Supports. NACA TN No. 1184, 1947.

20. Coleman, Robert P., and Stempin, Carl W.: A Preliminary Theoretical Study of Aerodynamic Instability of a Two-Blade Helicopter Rotor. NACA RM No. L6H23, 1946.

21. Seibel, Charles: Periodic Aerodynamic Forces on Rotors in Forward Flight. Jour. Aero. Sci., vol. 11, no. 4, Oct. 1944, pp. 339-342.

22. Owen, J. B. B.: The Stressing of Gyroplane Blades in Steady Flight. R. & M. No. 1875, British A.R.C., 1939.

23. Duberg, John E., and Luecker, Arthur R.: Comparisons of Methods of Computing Bending Moments in Helicopter Rotor Blades in the Plane of Flapping. NACA ARR No. L5E23, 1945.

24. Flax, Alexander H.: The Bending of Rotor Blades. Jour. Aero. Sci., vol. 14, no. 1, Jan. 1947, pp. 42-50.

25. Yuan, Shao Wen: Bending of Rotor Blade in the Plane of Rotation. Jour. Aero. Sci., vol. 14, no. 5, May 1947, pp. 285-293.

26. Horvay, Gabriel: Stress Analysis of Rotor Blades. Jour. Aero. Sci., vol. 14, no. 6, June 1947, pp. 315-336.

27. Coleman, Robert P., Feingold, Arnold M., and Stempin, Carl W.: Evaluation of the Induced-Velocity Field of an Idealized Helicopter Rotor. NACA ARR No. L5E10, 1945.

28. Sissingh: Contributions to the Dynamic Stability of Rotary-Wing Aircraft with Articulated Blades. Part I - General Principles. Translation No. F-TS-690-RE, Air Materiel Command, July 29, 1946.

29. Sissingh: The Dynamic Stability of Helicopters with Articulated Rotors - Second Partial Report. Translation No. F-TS-1002-RE, Air Materiel Command, Sept. 9, 1946.

30. Hohenemser, K.: Stability in Hovering of the Helicopter with Central Rotor Location. Translation No. F-TS-687-RE, Air Materiel Command, Aug. 1, 1946.

31. Hohenemser, K.: Longitudinal Stability of the Helicopter in Forward Flight. Translation No. F-TS-688-RE, Air Materiel Command, Aug. 2, 1946.

32. Donovan, A. F., and Goland, M.: The Response of Helicopters with Articulated Rotors to Cyclic Blade Pitch Control. Jour. Aero. Sci., vol. 11, no. 4, Oct. 1944, pp. 387-398.

33. Gustafson, F. B., and Reeder, J. P.: Helicopter Stability. NACA RM No. L7K04, 1948.

34. Reeder, John P., and Gustafson, F. B.: Notes on the Flying Qualities of Helicopters. Paper presented at the Fourth Annual Forum of the American Helicopter Society (Philadelphia, Penna.), April 22-24, 1948.

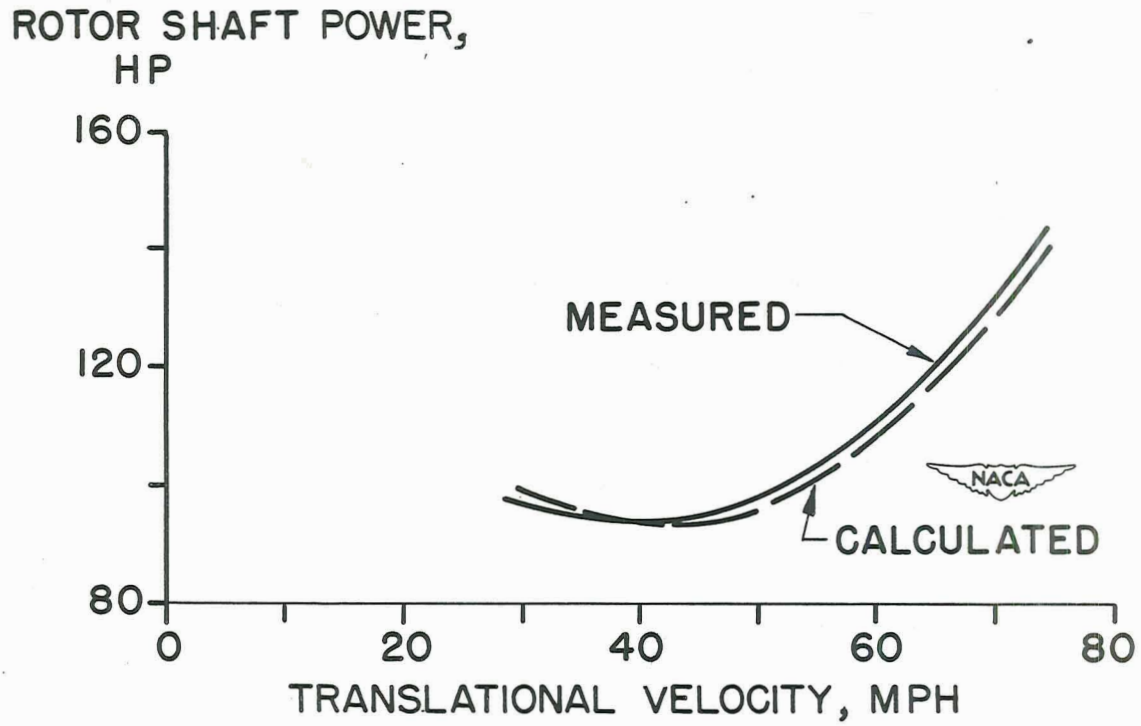

Figure 1.- Comparison of rotor characteristics as calculated and measured in flight.

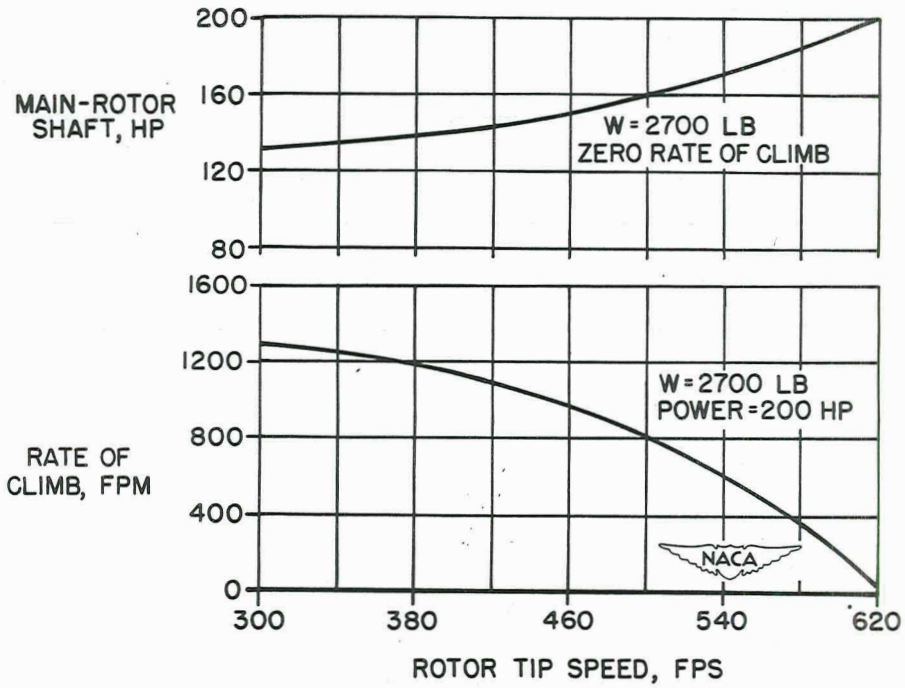

Figure 2.- Effect of rotor tip speed on hovering and vertical flight performance of sample helicopter.

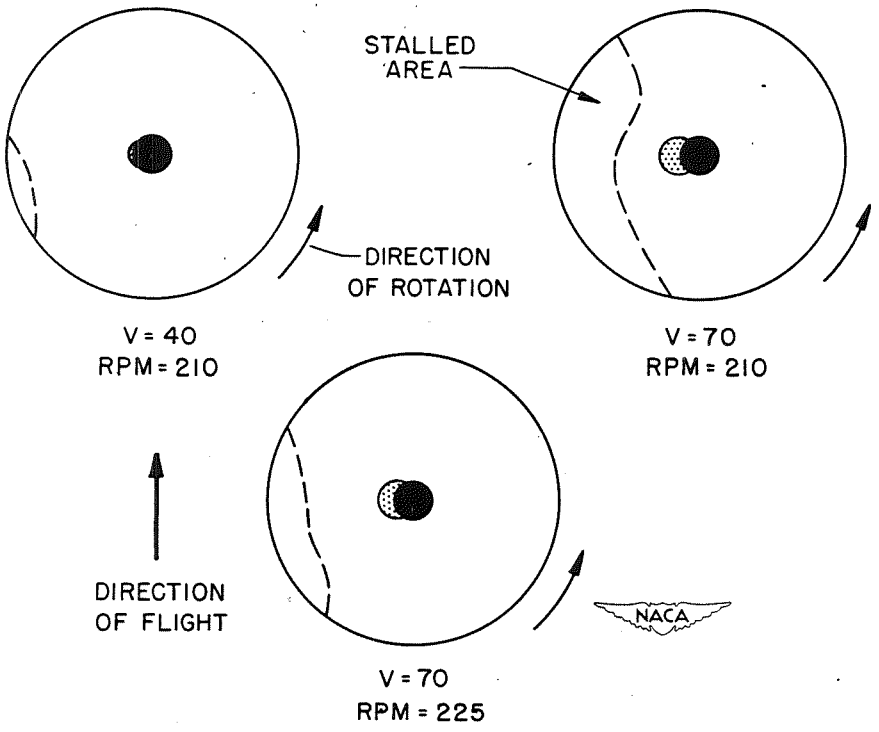

Figure 3.- Effect of forward speed and rotor tip speed on rotor-blade stall.

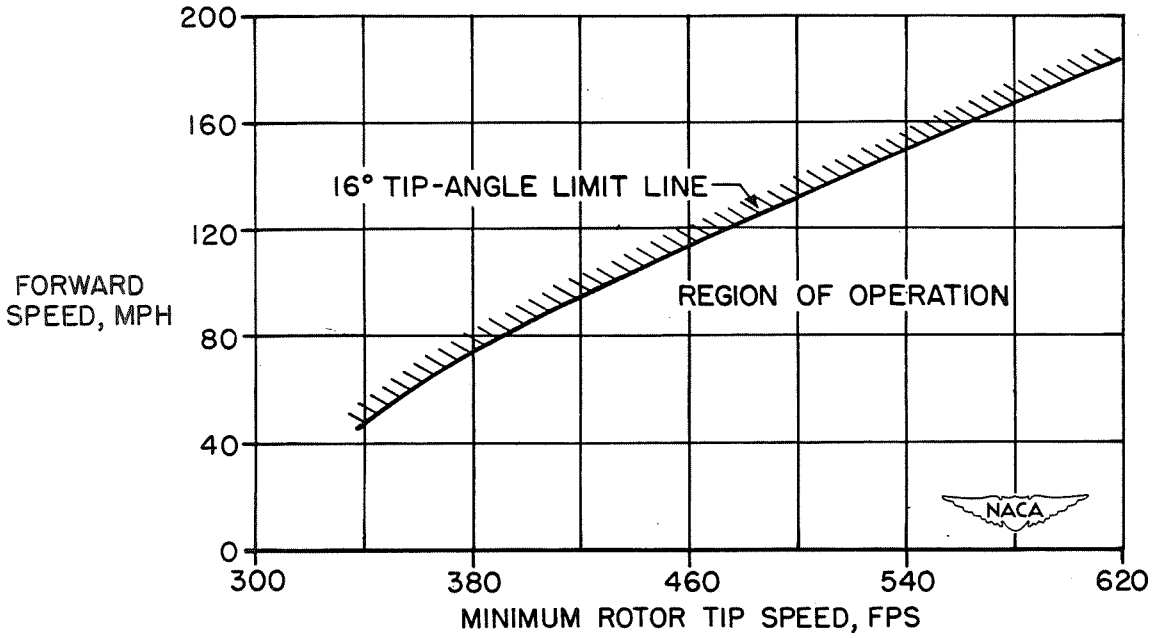

Figure 4.- Variation of minimum rotor tip speed, as set by rotor-blade stall, with forward speed.

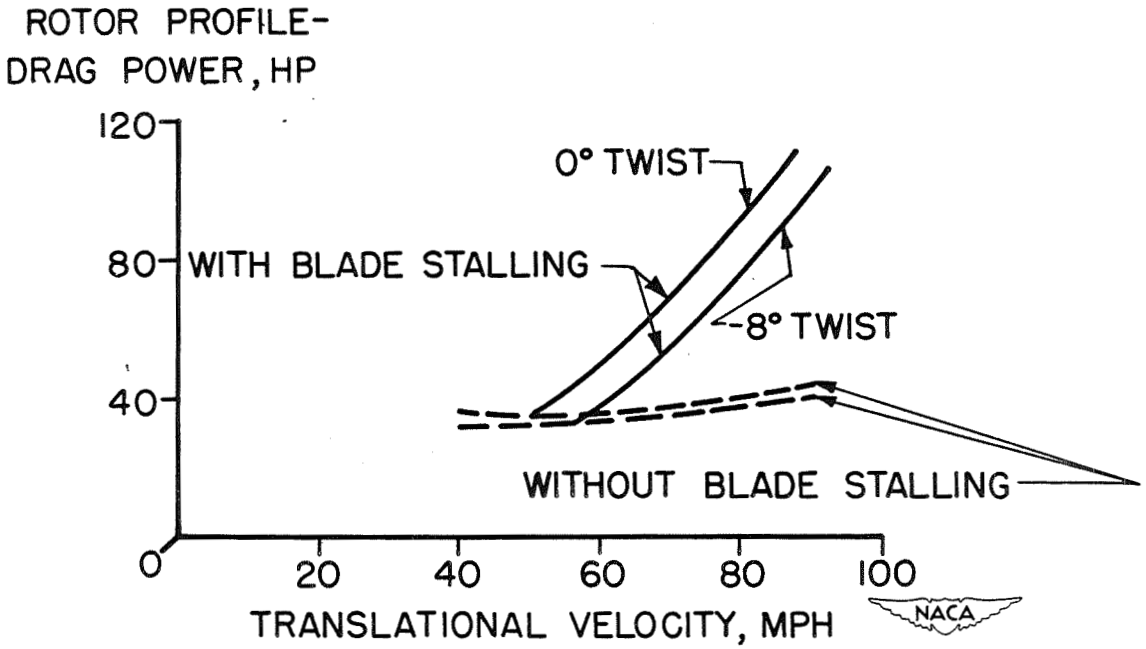

Figure 5.- Effects of rotor-blade stall and blade twist on rotor profile-drag power.

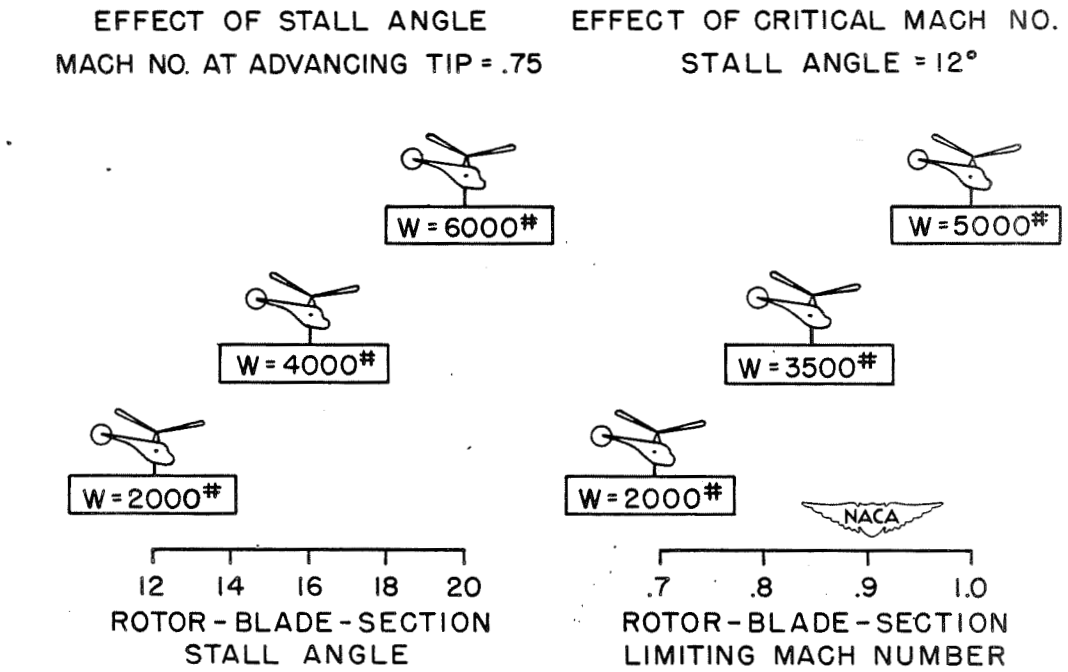

Figure 6.- Effect of rotor-blade-section stall angle and limiting Mach number on the permissible load carried by a sample helicopter.

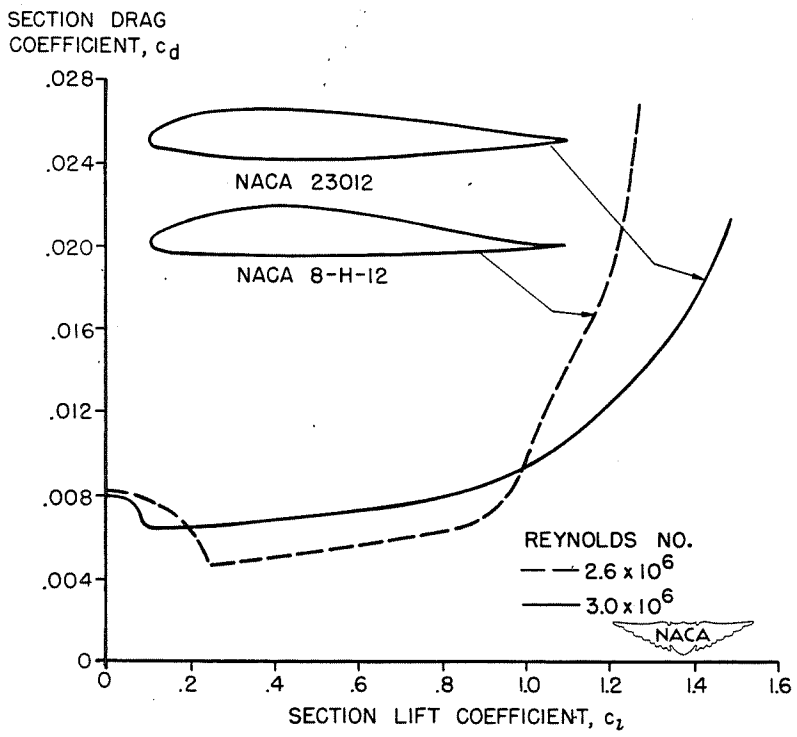

Figure 7.- Comparison of the profile-drag characteristics of the NACA 23012 and NACA 8-H-12 airfoil sections.

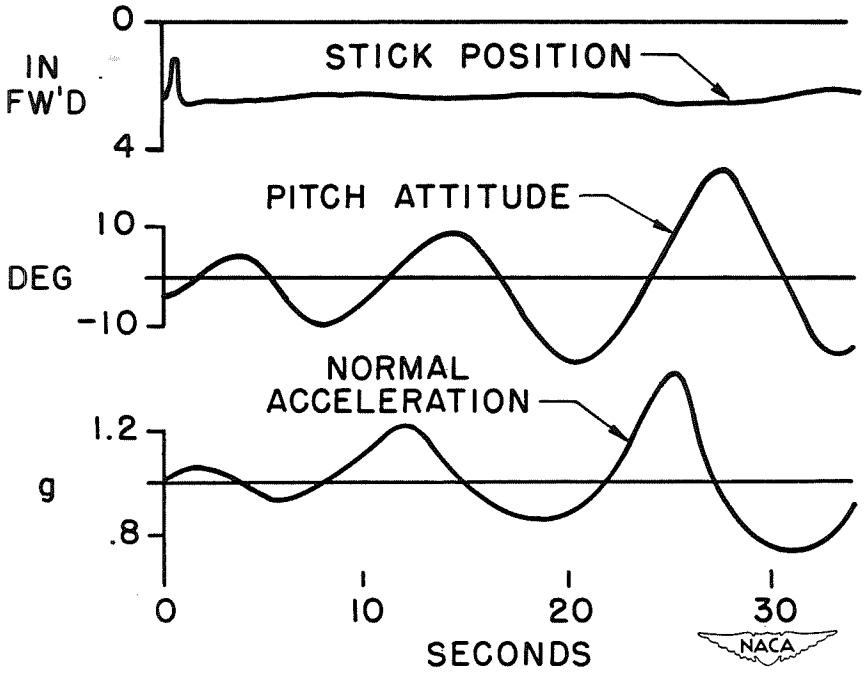

Figure 8.- Time history of a helicopter oscillation obtained in flight at 40 miles per hour.

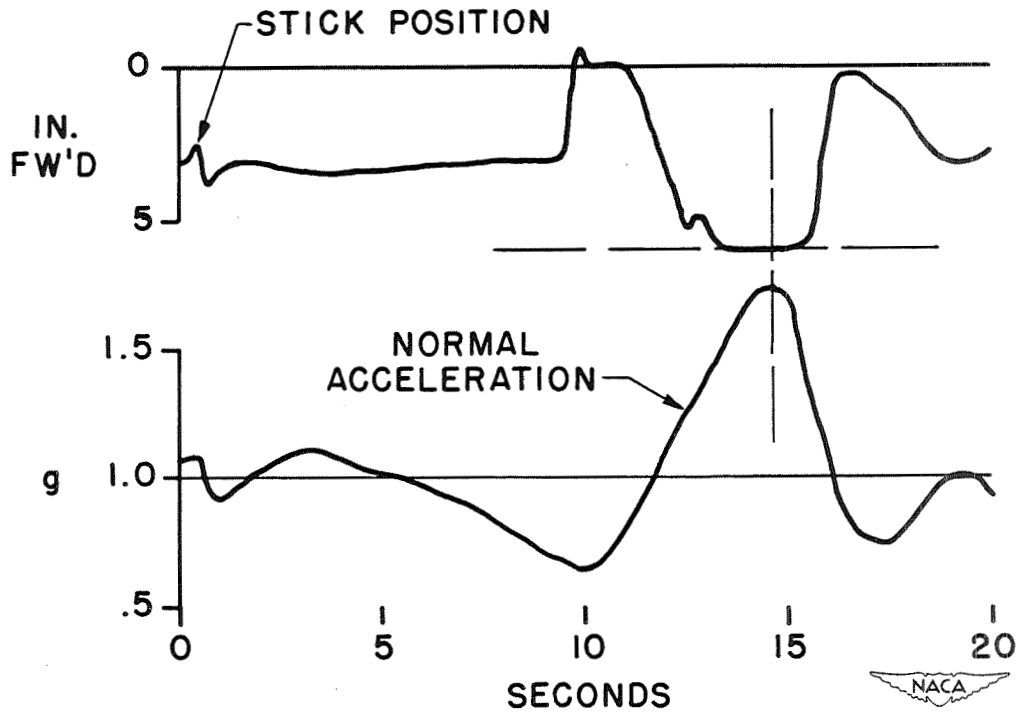

Figure 9.- Time history of the divergent motion of a helicopter obtained in flight at 65 miles per hour.

FLUTTER

D14

Preceding page blank

A SURVEY OF FLUTTER

By I. E. Garrick

Langley Aeronautical Laboratory

The field of flutter is concerned largely with a study of the circumstances whereby a complicated elastic structure such as an aircraft, or the components of an aircraft, can interact with the surrounding air stream and spontaneously extract energy to an extent that may cause damage or destruction. The problems of the flutter field have expanded with modern aircraft developments so that they involve and overlap very large parts of aerodynamics and mechanics. It is the purpose of this paper to dwell on various aspects and concepts of this broad field.

A particularly simple example of flutter is the "fish tail" motion due to mass unbalance of a control surface (common during World War I). Suppose that a very heavy mass is placed at the trailing end of a control surface. If the motion of the wing is, say, upwards the inertia of the mass tends to create a fixed point at the control-surface trailing edge. Hence the control surface deforms in such manner as to tend to increase the lift, that is, the unbalanced mass brings into being an aerodynamic force tending to increase the motion. In the downward part of the cycle, similarly, there is a force tending to increase the motion. This "tail wagging the dog" type of control-surface flutter is satisfactorily eliminated by proper dynamic mass balancing.

Modern aircraft are subject to various types of flutter troubles. There is the classical type of flutter associated with a clean efficient flow pattern, which usually, though not necessarily, involves the coupling of several degrees of freedom of the structure. And there is another type that is difficult to analyze which may involve separated flows, periodic breakaways and reattachment of the flow, stalling conditions, shocks, and various hysteresis or time-lag effects between the flow pattern and the motion. In this type of flutter only a single degree of freedom of the structure may be prominently involved (example, stall flutter). There is also a possible merging of the types.

Common cures and remedies for flutter troubles are increased stiffnesses (particularly torsional), decreased coupling as, for example, mass balancing of control surfaces, and increased damping. Because of the great number of structural parameters, however, and of the various kinds of modes and types of flutter, there is no field in which it is more true that exceptions can be found for every rule of thumb. This means that (along with usual statistical, empirical, and experimental studies) the problem should be examined analytically along fundamental lines. Since the primary source of the self-excited motion is the (uniform) air stream itself, it will perhaps be worthwhile to examine first the basis of the nonstationary potential air forces.

For the purpose of classifying the aerodynamic problems at both low and high speeds, it is desirable to look at the general nonstationary

flow equations for irrotational potential flow of a compressible fluid. The governing differential equation for the velocity potential follows from Euler's equations of motion and from the equation of continuity, with the assumption that the pressure is a function of density only and with the use of the local speed of sound as $c^2 = \frac{dp}{d\rho}$.

The general equation satisfied by the velocity potential may be put into a very pretty invariant form,

$$\frac{1}{c^2}\left(\frac{\partial}{\partial t} + \bar{v}\cdot\nabla\right)^2 \phi = \nabla^2\phi \tag{1}$$

where $\frac{\partial}{\partial t}$ and $\bar{v}\cdot\nabla$ (which is $v_x \frac{\partial}{\partial x} + v_y \frac{\partial}{\partial y} + v_z \frac{\partial}{\partial z}$ in rectangular Cartesian coordinates) operate only on ϕ, not on $\bar{v}$, and where, for example, for the adiabatic pressure–density relation, the local variable speed of sound is given by

$$c^2 = c_o^2 - \frac{\gamma - 1}{2} v^2 \tag{2}$$

Here γ is the adiabatic index (ratio of specific heats), and c_o is the velocity of sound corresponding to $v = 0$. The invariant "wave equation" form shows that the potential is propagated in the manner of a wave disturbance of finite amplitude. (For a derivation of equation (1) see appendix B of reference 1.)

Equation (1) serves to unify the discussion of the whole compressible–potential–flow picture and it shows up the difficulties inherent in the nonstationary, nonviscous flow problem in its unrestricted form. For example, when $\frac{\partial}{\partial t}$ is absent and the flow disturbances are not necessarily small, the equation becomes one treated by Rayleigh, Janzen, Poggi, and Kaplan. In a space of one dimension, for example, it reduces to the equation of Riemann for aerial plane waves of finite amplitudes.

$$\phi_{tt} + 2\phi_x \phi_{xt} - \left(\frac{dp}{d\rho} - \phi_x^2\right)\phi_{xx} = 0 \tag{3}$$

It is known that aerial plane waves of finite amplitudes cannot preserve their forms (reference 2) but that compression wave fronts steepen and rarefactions become less steep. Just as a shock condition awaits a compression front so too the past history of a rarefaction wave cannot be indefinitely prolonged without encountering discontinuities. Thus the existence of the continuous shockless pattern is for only a finite time. In a certain physical sense we must question the existence

or creation of continuous steady flow patterns in the whole of space. The steep front must be treated then by Rankine–Hugoniot relations as a shock condition. The temptation to assign similar phenomena to the general flow, of which the one–dimensional unsteady case is a special one, is very great. Then, it should not be surprising if the potential–flow equations for continuous flow impose conditions impossible of physical fulfillment just as in the Riemann case. Physical phenomena such as shocks and instabilities and mathematical phenomena such as "limiting lines" can then arise. Precise discussions of these phenomena in relation to boundary conditions are matters of great difficulty. This subject must be considered to be in an incomplete state.

If the velocity of propagation of disturbances is assumed infinite ($c = \infty$), equation (1) reduces to Laplace's equation for the incompressible fluid:

$$\nabla^2\phi = 0 \tag{4}$$

Even this deceptively simple–looking equation leads to recondite matters both of a physical and a mathematical nature, for it embraces the whole of two– and three–dimensional incompressible potential flow, stationary or nonstationary, for small or large disturbances.

Before discussing certain aspects of the physical picture, it is of special interest to look at the small–disturbance linear equation to which the original nonlinear equation may be reduced. For stability studies the main interest is often precisely in the small–disturbance form of the equations. For small disturbances from a main–stream velocity V in the x–direction and with c now regarded as a constant, the disturbance velocity potential satisfies the equation

$$\frac{1}{c^2}\left(\frac{\partial}{\partial t} + V\frac{\partial}{\partial x}\right)^2 \phi = \nabla^2\phi \tag{5}$$

This equation contains, for $V = 0$, the equation for the propagation of sound. For steady flow, $\frac{\partial\phi}{\partial t} = 0$, it is the general equation for linearized subsonic and supersonic flow which leads, for example, to the Prandtl–Glauert rule for subsonic flow and to the Ackeret rule for supersonic flow. In the general nonstationary case it is the theoretical basis for much of the existing work on the aerodynamical background of flutter, both at subsonic and supersonic speeds. This is perhaps the proper place to mention that equation (5) can also be associated with the purely acoustical problem of moving sources of sound.

In the near–sonic region, however, the linearized theoretical basis clearly requires modification as indicated by the Prandtl–Glauert and

Ackeret rules leading to infinite slopes of the lift curve at $M = 1$. It is likely that in this region it is necessary to employ iterative methods and to take into account second-order and other effects including viscosity and shape factors, but even the small-disturbance equation appears differently. Thus if all velocities are only slightly different from the critical local velocity of sound c^* $\left(c^* = \sqrt{\frac{2}{\gamma + 1}}\, c_o \right)$ and if the main stream is in the x-direction, there is obtained for the equation satisfied by the velocity potential

$$\frac{1}{c^{*2}}\left(\frac{\partial}{\partial t} + c^*\frac{\partial}{\partial x}\right)^2 \phi = \nabla^2\phi + (\gamma + 1)\,\frac{\partial^2\phi}{\partial x^2}\left(1 - \frac{1}{c^*}\frac{\partial\phi}{\partial x}\right) \qquad (6)$$

or

$$\phi_{tt} + 2c^*\phi_{xt} - (\gamma + 1)(c^{*2} - c^*\phi_x)\,\phi_{xx} - c^{*2}\left(\phi_{yy} + \phi_{zz}\right) = 0$$

This equation reduces in the steady case to a nonlinear equation leading to the transonic similarity rules discussed recently by Von Kármán and others. Its use in conjunction with boundary conditions for solving flow problems has not as yet been attempted. Clearly, difficulties of mathematical and physical conceptions arise here too. There is a noteworthy similarity of the structure of this equation with that of equation (3).

Physical conceptions bearing on the origin of lift and the genesis of flow patterns are of special interest for nonstationary flows. The role of the trailing edge in subsonic aerodynamics in distinguishing an airfoil from a nonlifting body cannot be overstated. It is remarkable that the nature of the Kutta-Joukowski condition for smooth flow at the trailing edge has not been more deeply studied but rests only on descriptive and plausible grounds. A fuller study of the flow mechanism must of course involve, in some measure, dissipation, the boundary layer, and the wake.

The trailing edge may be considered the means for separating a zero circulation into equal positive and negative parts, one part being left bound to the airfoil, the other free floating in the wake. It may be recalled that the total circulation – the bound circulation over the airfoil and the free circulation over the surface of discontinuity which the airfoil has left behind – satisfies the Helmholtz-Kelvin theorem and vanishes. It is instructive to describe this key mechanism in another way. Consider the nature of the disturbance flow pattern of a flat-plate airfoil of infinite span undergoing a vertically downward motion; the main features are the acceleration of the fluid downward on the top and bottom sides and the spilling of fluid upwards along both edges, the whole pattern akin to that of two equal and opposite vortices. This flow pattern superposed

with a uniform stream yields the noncirculatory flow pattern past a straight-line airfoil at an angle of attack. Then the further effect of the forward motion and of the trailing edge consists in effectively "sliding ahead and slicing off" the back part of the disturbance flow pattern thus leaving a bound circulation on the airfoil and a countercirculation in the wake. Of course, the influence of the field of floating vortices left behind in the wake must also be taken into account in analyzing the resulting pattern at the airfoil.

These conceptions are not self-evident but have since Lanchester slowly evolved and are still crystallizing. It is of some interest to note that without these concepts everyday natural phenomena such as the dynamic nature of the flight of birds, which supposedly first stirred man's imagination to attempt imitation of flight, remain imperfectly understood. (See reference 3.)

The potential type of flow is actually more nearly realized physically in the nonstationary than in the steady case. Thus for quick movements, very high lift coefficients and more nearly theoretical values of the slope of the lift curve can be realized. All this appears to be related to the nonstationary processes in the boundary layer which "effectively" yield a thinner boundary layer for higher frequencies; though to bring in these effects directly is a highly complex affair. A basic nondimensional parameter for comparing similar flows in the harmonically oscillating case, directly relating in a significant manner frequency, size, and velocity, is the "reduced" frequency defined by the ratio of the circular frequency times the half-chord to the main-stream velocity:

$$\left(k = \frac{\omega b}{V}\right)$$

In the incompressible nonstationary case there are two basic procedures which turn out to be completely equivalent: (a) the Birnbaum method followed up in particular by Cicala and Küssner and (b) the Wagner method followed up in particular by Glauert and Theodorsen. (See references 4 to 10.)

In the Birnbaum method a distribution of vorticity over the mean chord is assumed in a particular form of an infinite series (implicitly going to zero at the trailing edge); relations between the bound vorticity and the free vorticity are evaluated with consideration of the conditions at the trailing edge and the boundary condition that the main flow plus the induced flow at the airfoil surface corresponds with the actual motion of the airfoil, so that the resulting combined flow is at all times tangential to the airfoil surface. Knowledge of the local pressures is obtained directly from the vorticity distribution. It is of considerable mathematical interest that an explicit solution can be obtained in the two-dimensional incompressible case. (For example, see reference 1.)

In the Wagner method (which conveniently utilizes the principles of conformal mapping) the trailing-edge condition plays a more explicit

role. The flow pattern may be thought of as built up by superposition of many elementary flows, each elementary flow being that of the straight-line airfoil with an infinitesimal segment locally deflected; each elementary flow is composed of two parts, a noncirculatory flow pattern corresponding to a source-sink or doublet distribution in the presence of a finite line and the wake flow pattern corresponding to a distribution of vortices generated at the trailing edge during the past history of the motion. Again, from the local pressures, the integrated forces and moments follow by integration.

It is instructive to point out that in the Wagner approach to the problem, the velocity potential or response to a sudden change of angle of attack plays an important part while in the Theodorsen developments the steady-state response for the harmonically oscillating airfoil is significant, and that these two functions are mated ones in the sense of the Laplace or Fourier integral transforms. (See reference 12.) This observation is an aid to the further application of the superposition theorem and to the treatment of gusts and other transient conditions. (See reference 13.)

The extension of the procedures to higher Mach numbers has been the objective of much of the more recent work. Solutions of the original linearized compressible-flow equations (equation (5)) are sought which can serve to solve the boundary problem. Main references in the subsonic case are the original paper by Possio, a subsequent general formulation by Küssner, and a calculation procedure by Dietze (references 14 to 16). It is noteworthy that the methods of the acceleration potential have found prominent application in these subsonic-flow studies. Difficulties, even in the plane case, arise: (1) The elementary solutions corresponding to sources and doublets have a different structure and (2) the boundary conditions lead to an integral equation with a highly complicated kernel function. (It should be remarked that the problem has also been treated by utilizing directly the velocity potential. (See reference 17.) A simpler kernel function occurs, but certain Mathieu functions are required for further practical developments.)

Several procedures have been tried to obtain numerical solutions of the integral boundary equation. Frazer and Skan (references 18 and 19) give a method of collocation in which boundary conditions are satisfied at a set of points, leading to n equations in n unknowns. Another procedure, a more flexible one, is the iteration procedure of Dietze which in contrast with the other procedures also lends itself to aileron calculations. Applications to flutter problems have been made in several papers (for example, references 19 and 20). Of practical interest are the facts that the Prandtl-Glauert rule appears as a limiting case for static instabilities and for low "reduced" frequency cases corresponding to high-density wings and high altitudes and that, while in general the compressibility effects are very complicated, the magnitudes of the effects are not large in the range of validity of the linearized theory (approximately $M < 0.75$) for structural parameters of normal and practical concern.

Of much interest too is the study of nonstationary air forces at supersonic speeds. (See reference 21.) There is a peculiar reversal of the role of the leading and trailing edges as compared with subsonic conditions. Thus, there are the conditions necessary for an attached shock at the leading edge that require a sufficiently sharp leading-edge angle. Otherwise a detached shock ahead of the body and a mixed supersonic-subsonic type of flow are involved. The trailing edge need play no determining role as it does in the subsonic case and, in fact, a compression-expansion wave mechanism is involved in the generation of lift. In general the flow pattern must be pieced together (as in method of characteristics) of several regions with various edge conditions and various conditions at the Mach lines.

In the small-disturbance linearized treatment of oscillating air forces (with no strong shocks or other large disturbances assumed present in the underlying steady flow pattern) elementary source-type solutions play a key role. The elementary source effect may be associated with a locally deflected flow pattern and, in accordance with the similarity of the acoustical and hydrodynamical problem as already observed, behaves as a source of spherical sound waves in motion uniformly through the medium with supersonic speed.

The moving-source solutions have a considerable interest in themselves. Historically, they are involved in the Doppler effect and were encountered also in electrodynamics at the turn of the century (reference 22), in somewhat disguised fashion from present forms, in the study of electrons moving at speeds both above and below that of light. (The doctrine of special relativity was still young.)

In order to illustrate briefly the source effects at supersonic speeds there are presented figure 1 and the velocity potential relation (reference 1):

$$\phi = \frac{1}{r}\left[f(t - \tau_1) + f(t - \tau_2)\right]$$

where

$$r = \frac{1}{M^2 - 1}\sqrt{(x - \xi)^2 - (M^2 - 1)\left[(y - \eta)^2 + (z - \zeta)^2\right]}$$

$$\tau_{1,2} = \frac{M}{c}\frac{x - \xi}{M^2 - 1} \mp \frac{r}{c}$$

The field point (x,y,z) at any time t is influenced by two waves which originated at times τ_1 and τ_2 earlier. A given field point

at successive times $T + \tau_1$ and $T + \tau_2$ experiences, respectively, the effect of penetration into the spherical wave front of a pulse created at the origin at time T and the emergence out of the same wave front. At penetration of the wave front for a positive source there is a compression and subsequent equal expansion and, at emergence, the opposite effect. The distance r occurring in the velocity-potential relation, which in the case of a fixed source is the actual distance from the source to the field point, is shown geometrically in figure 1. At subsonic speeds there is only the single effect of penetration into the wave front because the field point never emerges from within the wave front.

The synthesis of solutions of boundary problems in terms of the source solution (and its normal derivative corresponding to a doublet solution) is of considerable general scope and validity. The applications form a wide field of research activity and it is regretted that they must be passed by with so few words at this time. It is of interest to mention that there are many papers now appearing in Russian dealing with similar problems. (See for example, reference 23.)

These aerodynamic considerations have been dwelt on because the motivating source of energy for flutter is the air stream itself and it is necessary to have some ideas of the nature of the oscillating air forces and moments which act, and their relative phases and amplitudes, in order to assess or analyze flutter effects.

Attention is now diverted to the mechanical nature of the flutter problem. For simplicity a configuration as in figure 2, an idealized wing on springs, is first considered. Corresponding to the two degrees of freedom, vertical deflection h and rotation α, there are two simultaneous differential equations, representing the equilibrium of vertical forces and of moments about the axis of rotation:

$$\ddot{h}A + \ddot{\alpha}B + hC = P$$

$$\ddot{\alpha}D + \ddot{h}B + \alpha E = M_o$$

where A and D are structural inertia terms, B is the coupling term due to mass unbalance about the axis of rotation, C and E are elastic restoring terms, and P and M_o are terms of aerodynamic origin.

If the air forces appropriate to small sinusoidal motions are employed, the flutter solution appears as a certain determinant put equal to zero, (which represents the condition for a nontrivial solution of the algebraic equations in h and α):

$$\begin{vmatrix} A_{a\alpha} & A_{ah} \\ A_{c\alpha} & A_{ch} \end{vmatrix} = 0$$

The individual terms are combinations of the inertia, elastic, and aerodynamic effects. This solution states that mechanical equilibrium is possible, that is, the laws of motion are satisfied, in the border sinusoidal case at a certain airspeed with a certain frequency and with certain amplitude and phase relations between the degrees of freedom. The question of whether the border stability condition, corresponding to a vanishing of the damping for the particular sinusoidal motion, separates a damped oscillation from a growing (negatively damped) oscillation, or vice versa, or is merely a resonance condition, is answered by other considerations – for example, by further study of the effects of the parameters, particularly structural damping, at the border condition, or by physical arguments.

The flutter determinantal equation (which contains complex elements, and hence is really two simultaneous equations) yields information on both the flutter frequency and the flutter speed. Several procedures, numerical, graphical, algebraic, and vectorial, for obtaining its solution, or for varying the parameters in the neighborhood of a definite solution have been developed. This phase of the flutter problem is a popular one and is the subject of many papers in the literature. One procedure which deserves special mention is the plotting of structural damping against airspeed as in reference 24 which treats directly the complex roots of the equation. The imaginary parts can be interpreted as the damping needed to obtain a flutter condition, negative damping then meaning that external energy must be added, stability thus being indicated. The plots of the imaginary parts of the complex roots against airspeed serve to measure the nearness to flutter and to give an indication of the violence and the type of flutter involved. (Of course after the flutter condition is encountered and small disturbance limits are exceeded, nonlinear effects may take over to limit the amplitude of oscillation, provided the structure holds together.) It should be briefly mentioned at this point that in addition to the dynamic instability conditions, the determinantal equation also contains the static instability conditions corresponding to wing divergence or control reversal. As pointed out previously, in these static cases in particular, the theoretical values need modifications to represent more closely experimental values for example, of the slope of the lift curve, center-of-pressure location, and hinge-moment coefficients.

In order to improve the foregoing idealized simple picture it is necessary to take into account a larger number of degrees of freedom and to bring in three-dimensional structural considerations. (See references 24 to 28.) This end is readily accomplished by the classical methods of Lagrange in which each degree of freedom may represent a spanwise mode of vibration (generalized coordinate) and the kinetic energy and the potential energy of the mechanical system play a central role. The terms representing the aerodynamic energy are obtained from the work done by the air forces in each coordinate.

The Lagrangian equations of motion representing the equilibrium in the chosen degrees of freedom then lead, as before in the sinusoidal case, to a characteristic flutter-stability equation in which the spanwise-mode

effect is properly weighted and, conveniently, the mechanical potential energy (as in the Rayleigh vibration-mode methods) may involve the natural uncoupled frequencies of the structure. In this approach, matrix methods arise in a very natural manner. In recent years the matrix methods have become increasingly popular even with "practical" vibration people and it is believed this trend should be fostered rather than feared. It is however always a matter of taste and judgment and often very difficult to choose the degrees of freedom and their number to compromise properly between time, labor, physical grasp, and accuracy.

The problem of a continuous wing structure can also be set up as an integro-partial differential equation (instead of a system of simultaneous ordinary differential equations) in which the modes of vibration in the flutter condition are solved for rather than assumed. It is recognized however that, in general, the problem involves elastic problems which are too complex to be exactly handled even without consideration of the air forces and includes aerodynamic problems which are complicated enough even in the steady case and for rigid structures. In practice the procedures are iterative or approximate. (See reference 29.) The uniform cantilever wing has recently been given such a treatment (reference 30) with two-dimensional air forces assumed.

In fact in most flutter treatments two-dimensional air forces have been employed, frequently with over-all corrections for finite span inserted. Appropriate corrections for finite-span effects have occupied the attention of several authors. (See references 31 to 35.) The subject, however, is not in a too satisfactory state mainly because of complexity. The nonstationary effects attributed to aspect ratio are, in general, fairly small for moderate aspect ratios. There is room for both theoretical and experimental contributions in this field for wings of small aspect ratio.

A few words should perhaps be devoted to the subject of flutter of sweptback wings, a study which has been only lightly touched on by several writers. With sweepback the problem is complicated in both its structural and its aerodynamic aspects. Structurally, there exists a greater degree of coupling between bending and torsion as, for example, for a curved or bent-back elastic axis. Even the conception of an elastic axis, commonly used for unswept wings without large cut-outs, may, because of cross-stiffness effects, need to be replaced by the more general conception of influence-coefficients. In its aerodynamic aspect there is a greater degree of coupling in the air forces; for example, the bending deformation (dihedral effect) enters into the angle of attack of a wing section. Thus a small dihedral leads to second-order effects for unswept wings and to first-order effects for highly swept wings.

For an infinite uniform yawed wing (yawed at an angle not near 90°) two-dimensional (low speed) considerations indicate that the flutter speed increases by a factor of one over the cosine of the angle of yaw or sweep. A finite yawed wing, mounted on springs permitting it to

move vertically and to rotate about an axis, would be expected to have a flutter speed with a factor of sweep higher than one over the cosine. However, for a finite sweptback wing clamped at its root, the combined effect of the elastic and aerodynamic coupling adversely affects the flutter speed so that, in general, the factor is considerably lowered.

There are many indications, however, that the static instability aileron reversal (in which the rolling power vanishes at a certain airspeed) rather than the dynamic instability may impose more severe design requirements for sweptback wings (for example, reference 35) at high speeds.

It has been possible to present here only a selection of aspects of the flutter field. The whole story of modern experimental techniques and research has had to be omitted. It is clear that measurement of aerodynamic coefficients for nonstationary flow throughout the subsonic, near-sonic, and supersonic speed ranges requires very exacting experimental techniques and critical tests. In testing for flutter in some of these speed ranges, it has been found convenient to employ, in addition to wind-tunnel research, techniques utilizing bomb drops and rocket missiles. Also required are the modern developments in pressure cells, strain gages, and electronic, telemeter, and vibration equipment.

In closing this survey of flutter, it is again emphasized that the physical classification of the flutter problem of a given structure is not easy for an attempt must be made to recognize which of the abundant sources of modes may be significantly involved and whether the type of flow is primarily of the potential classical type or includes a merging with other types of flow. In the near-sonic range, in particular, there is a clash between the potential and separated flows and a susceptibility to both kinds of flutter troubles. It is believed that refinements made in the aerodynamic and mechanical aspects of the flutter problem to be significant should to an extent keep in step with each other. It is hoped that some of the many facets and challenges of the flutter problem have been indicated.

REFERENCES

For a more complete list of references, see also bibliographies contained in the references.

1. Garrick, I. E., and Rubinow, S. I.: Theoretical Study of Air Forces on an Oscillating or Steady Thin Wing in a Supersonic Main Stream. NACA TN No. 1383, 1947. (Contains 21 references.)

2. Rayleigh, (Lord): Aerial Plane Waves of Finite Amplitude. Scientific Papers, vol. V, Cambridge Univ. Press, 1912, pp. 573–610.

3. Garrick, I. E.: Propulsion of a Flapping and Oscillating Airfoil. NACA Rep. No. 567, 1936.

4. Birnbaum, W.: Das ebene Problem des schlagenden Flügels. Z.f.a.M.M., Bd. 4, Heft 4, Aug. 1942, pp. 277–292.

5. Cicala, Placido: Le Azioni aerodinamiche sui profili di ala oscillanti in presenza di corrente uniforme. Extract from Mem. della R. Accad. delle Sci. di Torino, ser. 2, pt. I, t. 68 (1934–35).

6. Küssner, H. G.: Zusammenfassender Bericht über den instationären Auftrieb von Flügeln. Luftfahrtforschung, Bd. 13, Nr. 12, Dec. 20, 1936, pp. 410–424.

7. Wagner, Herbert: Über die Entstehung des dynamischen Auftriebes von Tragflügeln. Z.f.a.M.M., Bd. 5, Heft 1, Feb. 1925, pp. 17–35.

8. Glauert, H.: The Force and Moment on an Oscillating Aerofoil. R. & M. No. 1242, British A.R.C., 1929.

9. Theodorsen, Theodore: General Theory of Aerodynamic Instability and the Mechanism of Flutter. NACA Rep. No. 496, 1935.

10. Von Kármán, and Sears, W. R.: Airfoil Theory for Non-Uniform Motion. Jour. Aero. Sci., vol. 5, no. 10, Aug. 1938, pp. 379–390.

11. Küssner, H. G., and Schwarz, L.: The Oscillating Wing with Aerodynamically Balanced Elevator. NACA TM No. 991, 1941.

12. Garrick, I. E.: On Some Fourier Transforms in the Theory of Non-Stationary Flows. Proc. Fifth Int. Cong. Appl. Mech. (Cambridge, Mass., 1938), John Wiley & Sons, Inc., 1939, pp. 590–593.

13. Küssner, H. G.: Das zweidimensionale Problem der beliebig bewegten Tragfläche unter Berücksichtigung von Partialbewegungen der Flüssigheit. Luftfahrtforschung, Bd. 17, Lfg. 11/12, Dec. 10, 1940, pp. 355–361.

14. Possio, Camillo: L'Azione aerodinamica sul profilo oscillante in un fluido compressible a velocità iposonora. L'Aerotecnica, vol. XVIII, fasc. 4, April 1938, pp. 441–458. (Available as British Air Ministry Translation No. 830.)

15. Küssner, H. G.: General Airfoil Theory. NACA TM No. 979, 1941.

16. Dietze, F.: The Air Forces of the Harmonically Vibrating Wing in a Compressible Medium at Subsonic Velocity (Plane Problem). Translation No. F–TS–506–RE, Air Materiel Command, U.S. Army Air Forces, Nov. 1946.
and
Part II: Numerical Tables and Curves. Translation No. F–TS–948–RE, Air Materiel Command, U.S. Army Air Forces, March 1947.

17. Reissner, E., and Sherman, S.: Compressibility Effects in Flutter. Curtiss–Wright Research Lab., Rep. No. SB–240–S–1, Jan. 1944.

18. Frazer, R. A.: Possio's Derivative Theory for an Infinite Aerofoil Moving at Sub–Sonic Speeds. 4932, 0.205 (Rev.), British A.R.C., Jan. 23, 1941.

19. Frazer, R. A., and Skan, Sylvia W.: Influence of Compressiblity on the Flexural–Torsional Flutter of Tapered Cantilever Wings. 5916, 0.274 (Rev.), British A.R.C., June 30, 1942.

20. Garrick, I. E.: Bending–Torsion Flutter Calculations Modified by Subsonic Compressiblity Corrections. NACA Rep. No. 836, 1946.

21. Garrick, I. E., and Rubinow, S. I.: Flutter and Oscillating Air–Force Calculations for an Airfoil in a Two–Dimensional Supersonic Flow. NACA TN No. 1158, 1946.

22. Schott, G. A.: Electromagnetic Radiation. Cambridge Univ. Press, 1912.

23. Krasilschickova, E. A.: Disturbed Motion of Air Caused by Vibration of a Wing Moving at Supersonic Speed. Appl. Math. and Mech. (Moscow), vol. XI, no. 1, 1947, pp. 147–164.

24. Smilg, Benjamin, and Wasserman, Lee S.: Application of Three–Dimensional Flutter Theory to Aircraft Structures. ACTR No. 4798, Materiel Div., Air Corps, July 9, 1942.

25. Loring, S. J.: Outline of a General Approach to the Flutter Problem. SAE Jour., vol. 49, no. 2, Aug. 1941, pp. 345–355.

26. Loring, Samuel J.: Use of Generalized Coordinates in Flutter Analysis. SAE Jour., vol. 52, no. 4, April 1944, pp. 113–132.

27. Bleakney, William M.: Three–Dimensional Flutter Analysis. Jour. Aero. Sci., vol. 9, no. 2, Dec. 1941, pp. 56–63.

28. Flax, Alexander H.: Three–Dimensional Wing Flutter Analysis. Jour. Aero. Sci., vol. 10, no. 2, Feb. 1943, pp. 41–47.

29. Küssner, Hans Georg: Schwingungen von Flugzeugflügeln. Jahrb. 1929 der DVL, E. V. (Berlin–Adlershof), pp. 313–334.

30. Goland, M., and Luke, Y. L.: The Flutter of a Uniform Wing with Tip Weight Rep. No. 1–S36–E–4, Midwest Res. Inst., Kansas City, Mo., Jan. 2, 1947.

31. Jones, Robert T.: The Unsteady Lift of a Wing of Finite Aspect Ratio. NACA Rep. No. 681, 1940.

32. Cicala, Placido: Lo Stato attuale delle ricerche sul moto instazionario di una superficie portante. L'Aerotecnica, vol. XXI, no. 9–11, Sept.–Nov., 1941.

33. Reissner, Eric: Effect of Finite Span on the Airload Distributions for Oscillating Wings. I – Aerodynamic Theory of Oscillating Wings of Finite Span. NACA TN No. 1194, 1947.

34. Jones, W. Prichard: Aerodynamic Forces on an Oscillating Aerofoil–Aileron-Tab Combination. R. & M. No. 1948, British A.R.C., 1941.

35. Collar, A. R.: Aeroelastic Problems at High Speed. Jour. R.A.S., vol. LI, no. 433, Jan. 1947, pp. 1–34.
(Contains 30 references to the British literature.)

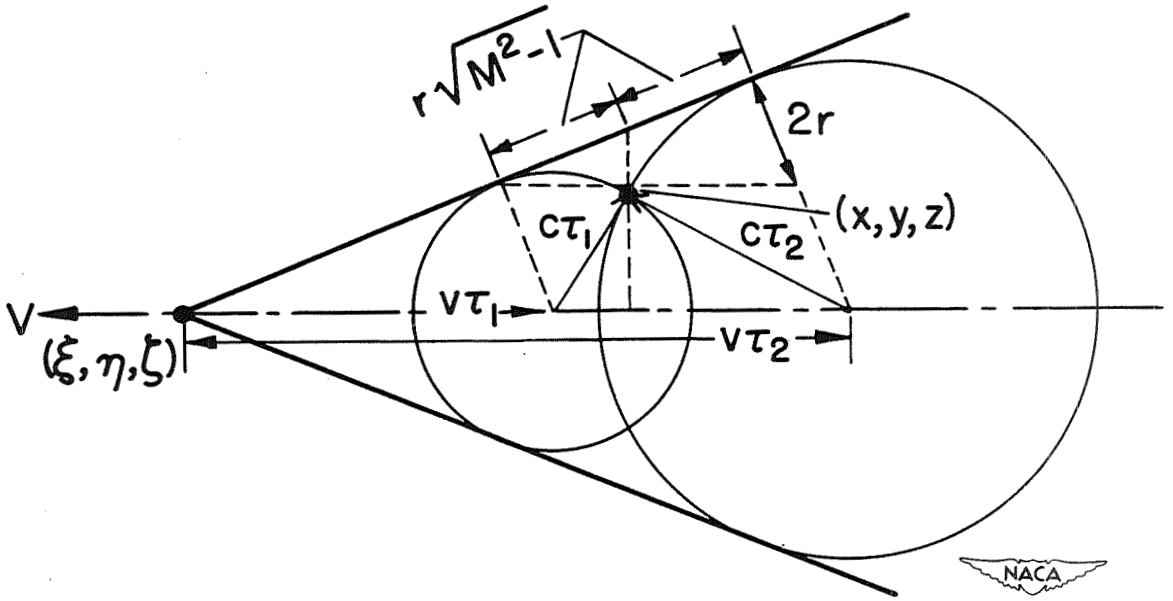

Figure 1.- Field of influence of a spherical source moving at a constant supersonic velocity.

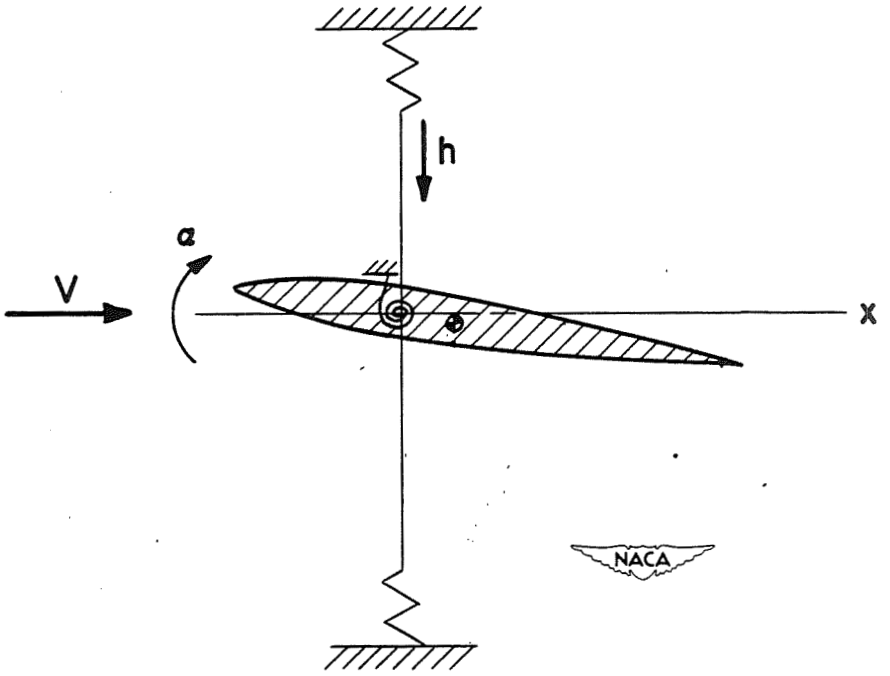

Figure 2.- Idealized wing configuration with two degrees of freedom.

AIR INLETS

D/5

Preceding page blank

AIR INLETS

By Norman F. Smith

Langley Aeronautical Laboratory

The first radial-engine cowling, developed by the NACA in 1927 (fig. 1), marked the transition from the external to the internal cooling system. This development provided an important improvement in airplane performance by removing engine and heat-exchanger components, which are poor aerodynamic shapes, from the full velocity of the air stream and by providing gains in cooling efficiency and control of engine temperature.

Some years later, airplane speeds had advanced to the point where the critical speed of components became important. The critical speed of the original cowling was recognized as being low, and an investigation was initiated in 1939 to develop a shape having as high a critical speed as possible and proportions to fit then-existing radial engines. The result of this effort was NACA cowling C (fig. 1), which has a critical Mach number of 0.63 (480 mph at sea level) and has been virtually a standard on American radial-engine aircraft since its development (reference 1). A short time later, nose B was developed (reference 2 and fig. 1). This shape is a longer nose inlet designed for use with submerged engine designs or jet propulsion installations, and has a critical Mach number of 0.84 (640 mph at sea level). These two inlets, NACA cowling C and nose B, were derived on the same basis, that is, to have a flat pressure distribution and, therefore, the optimum critical speed for the particular proportions involved.

The fuselage nose position for air inlets has received considerable attention at the Langley Laboratory because of the aerodynamic advantages offered by this position. Such an air intake is located in a natural stagnation region wherein external compression can be accomplished at an efficiency of 100 percent. Also, no boundary-layer problem is encountered, and there exists the fact that the external drag of a body with a properly designed nose inlet is as low as or lower than the drag of a streamlined body. Experimental data (from reference 2) illustrating this last item are shown in figure 2. The tick at the left is the drag coefficient of the basic body, whereas the curve shows the external drag of the body with nose B inlet through a range of internal flow. At flow rates above a certain minimum value, the external drag is clearly seen to be equal to or slightly less than the drag of the basic body. The higher drag at low flow rates is due to the fact that a pressure peak exists at the lip for this condition, and this peak fixes transition at a point well forward and produces higher skin-friction drag.

From the aircraft designer's point of view, it was highly desirable to expand the information available on nose inlets to permit design of a nose inlet for any desired subsonic Mach number. Upon examination, the nose B and NACA cowling C ordinates, reduced to nondimensional form, were found to be practically the same. Since the very different critical speeds of these air inlets were apparently due to the different geometric proportions, it appeared possible that a whole series of nose inlets might be based upon common ordinates. By use of the nose B ordinates, therefore, the systematic family of nose inlets shown in figure 3 was designed and was tested to determine the effects of proportions on critical speed characteristics (reference 3). The length ratio (X/D) is shown across the top and the inlet diameter ratio d/D down the side. The inlet shown in the upper left is approximately nose B, whereas the one in the lower right is very close to NACA cowling C.

The results of tests of one of these nose inlets are shown in figure 4. In the left figure are the pressure distributions over the external surface of the inlet at three values of inlet velocity ratio, which is the ratio of inlet velocity to free-stream velocity. It can be seen that the pressure distribution remains flat, with a low peak value, down to some low value of V_1/V_0, below which the high local angle of attack of the lip causes a pressure peak to occur. This peak continues to increase in height as V_1/V_0 is further decreased. The estimated critical Mach numbers obtained from these pressure distributions are shown in the right half of figure 4 plotted against inlet-velocity ratio. It can be seen that the critical Mach number of the nose inlet remains approximately constant as the inlet-velocity ratio is decreased until the point is reached where a pressure peak appears at the lip. Below this value of inlet-velocity ratio, the critical Mach number decreases rapidly.

The values of critical Mach number below the "knee" of the curve are of course in need of qualification because they were estimated from sharp local peak pressures, and it has been shown in various wind-tunnel tests of airfoils and bodies that such local peaks may disappear at higher Mach numbers or have little effect upon the Mach number at which adverse compressibility effects occur. This phenomenon is discussed in connection with airfoils in the paper by Becker entitled "Characteristics of Wing Sections at Transonic Speeds." It is, however, desirable aerodynamically to avoid this condition for reasons of possible compressibility effects, separation, or, as was shown in figure 2, higher skin friction.

The region to the right of the knee of the critical Mach number curve of figure 4, therefore, is of primary interest. Since in most airplane installations the minimum inlet-velocity ratio is encountered at the maximum speed of the airplane, the knee of the curve becomes

a logical "design point" for the particular nose inlet. In other words, an airplane for which maximum Mach number and air-flow requirements at the maximum Mach number correspond to the "knee" of the curve will, at speeds other than maximum, be operating below and to the right of the design point in the region where a flat pressure distribution exists.

The values of M_{cr} and V_1/V_0 at the design point was found in the wind-tunnel tests to be a function of the proportions of the nose inlet. Accordingly, the design points of the series of nose inlets shown in figure 3 have been arranged in the form of design charts, from which the proportions of a nose inlet can be selected to fulfill any design requirements of air flow and critical Mach number. The design chart is shown as figure 5. A sample selection is shown by the arrows. Entering the lower section with the desired value of mass flow ratio and proceeding vertically to the value of critical Mach number desired, the entrance diameter ratio d/D can be read. Continuing to the top section of the chart, the length ratio X/D is obtained. Combining these proportions with the 1-series ordinates the required nose inlet shown at left center is obtained. Two other selections, for Mach numbers of approximately 0.63 and 0.9, are shown to scale and illustrate the variation in proportions with Mach number.

The design charts actually cover a number of different types of inlets, the first of which is of course the plain open-nose inlet as applied to a jet machine. Mention has been made previously of the excellent drag characteristics of this type of installation.

Two additional types of installations which can be designed from these charts are shown in figure 6. The upper one is a more or less conventional configuration where the propeller is located on a spinner ahead of the air inlet. An analysis (reference 3) of existing data from various cowling tests provides an indication that the effects of a spinner of reasonable size upon the characteristics of a cowling are small. Cowlings for use with spinners can therefore be selected from the design charts, taking into account only the flow area blocked out by the spinner. An additional problem exists with this type of inlet, however, in that the boundary layer on the spinner will separate if the inlet-velocity ratio is too low. This phenomenon is purely a result of the pressure gradient ahead of the air inlet, produced principally by the inlet-velocity ratio. Analysis (reference 3) of data from tests of many cowlings indicates that a value of inlet-velocity ratio of at least 0.4 is required to eliminate separation from the spinner. This value is, of course, higher than that which might otherwise be used in order to minimize internal losses. More on this problem is presented herein in connection with fuselage scoops.

The lower installation shown in figure 6 is an NACA rotating cowling in which the forward part of the cowling rotates with the

propeller (reference 4). Although more complicated mechanically, this type of installation offers several aerodynamic advantages. The problem of boundary-layer separation at the entrance (due to inlet-velocity ratio) is eliminated since no surface protrudes beyond the inlet. Also, the propeller shanks, which are often difficult to make optimum both aerodynamically and structurally, can be housed in generous fairings in the lower velocity region within the spinner. By this means, the internal efficiency is improved, particularly on installations of high power where a large number of wide blades are needed. The propulsive efficiency is also improved because only the more efficient outboard sections of the propeller are exposed to the air stream. Several tests of these types of installations have indicated that the aerodynamic advantages of the rotating type are larger than the weight and structural penalties incurred, particularly for installations of very high power.

Another type of "stagnation inlet" is, of course, the wing-leading-edge inlet. The problems involved in the design of wing inlets are more numerous than for other types. The effective-angle-of-attack range through which the inlet must operate is higher because of the induced angle of attack which occurs ahead of the wing. If the inlet is located behind a propeller, the effective angle will also be affected by propeller power. The inlet must have a high critical Mach number at one end of the speed range and a high value of maximum lift at the other, while maintaining reasonable drag characteristics throughout the operational range of lift coefficient and inlet-velocity ratio. The wing inlet is of interest primarily for aircraft having wings of high or medium thickness since the very thin wings of high-speed aircraft do not offer the thickness or internal space for inducting the large volume of air required.

Because of the large number of variables and problems involved, design data for wing inlets are not available from which an inlet can be chosen without a development program being required. However, the general physical configuration required for satisfactory characteristics is known from numerous development programs. Figure 7 compares such a configuration (reference 5) with an earlier and less satisfactory development (reference 6). The early inlet shown in the sketch at the lower left is characterized by relatively sharp lips, a large opening height, and no lip stagger. The pressure distribution over the upper lip at zero lift is flat, with a value of peak pressure which, although not shown, appears low. At a lift coefficient of 0.55, however, a high pressure peak exists at the lip, which is undesirable from the standpoint of drag (transition), critical speed, and, at a still higher angle of attack, maximum lift.

The inlet at the right shows a more rounded pressure distribution, although a slightly higher value of peak pressure, and it evinces only a small pressure peak at a lift coefficient of 0.66. This inlet possesses thicker lips, a small inlet height, and a noticeable lip stagger.

The maximum lift characteristics of these two configurations and of a basic airfoil section are shown in the left half of figure 8. As might be expected, the sharp-edge inlet (a) has a very low maximum lift at low flow rates, rising to about the same as the basic airfoil section when the favorable effects of air flow are felt at the higher inlet-velocity ratios. The air inlet (b) has a higher maximum lift than inlet (a) or the basic airfoil section through a wide range of air-flow quantity.

The inlet losses for inlets (a) and (b) are shown in the right half of figure 8. Again, the sharp lips of inlet (a) have produced large losses outside a narrow range of lift coefficient. Inlet (b), however, shows essentially zero inlet losses through a wide range of lift coefficient, adequate for the particular airplane involved.

Thus, a wing-leading-edge inlet which has good aerodynamic characteristics has a small entrance-to-thickness ratio and relatively thick, staggered inlet lips well-rounded into a bell-mouth shape.

Several advantages of the stagnation type of air inlet have already been listed and discussed. In spite of these advantages, it often happens that other factors dictate the use of an air scoop or air inlet located aft on the fuselage. Such factors may include armament in the nose, pilot visibility, ducting length and weight, over-all structural weight, and airplane stability.

The two primary problems involved in scoop design are boundary layer and interference. Figure 9 illustrates the boundary-layer phenomena (reference 7). In the upper left is a sketch of a fuselage and scoop. Below the sketch is plotted the boundary-layer thickness along the fuselage ahead of the scoop for three values of inlet-velocity ratio. At the highest value, 0.9, the boundary layer grows at a normal rate up to the scoop entrance. At an inlet-velocity ratio of 0.5 some thickening at the entrance is found; and at the lowest inlet-velocity ratio, 0.2, the boundary layer has apparently separated and has reached a thickness equal almost to the scoop entrance height. A cross plot of the boundary-layer thickness shown at the right indicates that separation apparently occurs when the inlet-velocity ratio is decreased below approximately 0.6. This phenomenon is the same as that which was previously mentioned as occurring on cowling spinners. The consequences of the separation shown were, of course, a reduction in air-flow quantity and a substantial increase in inlet losses. Providing the scoop shown with a boundary-layer bypass which removed a thickness slightly more than the boundary-layer thickness for $\frac{V_1}{V_0} = 0.9$ eliminated the separation entirely and restored the pressure recovery to essentially 100 percent.

In figure 10 (from reference 3) is shown the critical Mach number characteristics of three longitudinal planes of the scoop with boundary-layer removed: the bottom plane, shown by the solid line, the side plane, shown by short dashes, and the fillet plane, shown by long dashes. The scoop was designed by use of the NACA 1-series nose inlet ordinates. For comparison, the critical Mach number curve for the corresponding NACA 1-series nose inlet is shown as the top curve. The curves for the two lower planes have essentially the same shape as the curve for the nose inlet but are displaced downward because the scoop is located in the flow field of the wing. The curve for the fillet plane is displaced still farther and its shape is changed somewhat. These data show that the external contour of a fuselage scoop can be designed with the aid of the NACA 1-series nose inlet charts provided that proper allowance is made for the interference of wing or fuselage.

While problems do exist in the design of efficient air exits, their magnitude and number are by no means comparable to those involved in the design of air inlets. The optimum location for emitting air is, of course, at the tail of the fuselage or body, since here mutual interference of fuselage and the air jet are minimized. In cases where the air exit must be located elsewhere, a few simple rules should be followed: First, the air exit should be located in a region of low induced velocity to minimize interference effects; second, the air should be directed outward parallel to the passing air stream; and third, the body aft of the exit should be undercut to allow for the thickening effect of the air jet.

Figure 11 illustrates this third item and shows pressure distributions over an air exit with and without undercutting (reference 8). It should be noted that a pressure peak (solid line) is induced at the exit by the effective bump produced by the mass of air flowing from the exit. Undercutting the exit (dashed line) reduced this peak to only a small increment above the value of pressure coefficient measured with the exit faired over. Doubtless, this dashed profile could be improved by still more undercutting and the superstream velocities eliminated altogether, at least for certain operating conditions.

Although this paper deals primarily with the subject of air inlets, it is appropriate to include several references on duct and internal-system design (references 9 to 11). These references do not in themselves constitute complete coverage of the subject, but, like many of those listed at the end of this paper, provide a digest of much of the available information. Each paper contains a list of references which may be used in an extended study of the subject.

In considering briefly the problem of supersonic air inlets, it is interesting to consider the case of a subsonic nose inlet operating at transonic and supersonic speeds. (See fig. 12.) At supersonic

speeds, a conventional nose inlet with rounded lips is found to have a bow wave ahead. Through this bow wave there is a loss in total pressure of the air, both that entering the inlet and that going around the body. The total pressure loss through a normal shock, which approximates the loss through the center part of a bow wave, is shown in the upper right corner of figure 12. It can be seen that the loss is small at low supersonic Mach numbers – of the order of 2 percent at $M = 1.3$. This means that the losses encountered at low supersonic Mach numbers with this type of inlet will be small. This inlet is suitable for use, then, in the transonic range, with the added advantage of good characteristics through the subsonic range.

At higher supersonic Mach numbers, however, the losses increase significantly, and other types of inlets must be considered. If the blunt lips of the subsonic inlet are replaced with suitable sharp-edged lips and if the inlet–velocity ratio is increased to 1.0, the bow wave may be eliminated and replaced by an external oblique shock and by a normal shock in the diffuser, as shown in the lower half of figure 12.

If a normal diverging subsonic diffuser is used, the shock will occur at a Mach number equal to or higher than the flight Mach number. This means that, although the external conditions may be improved by using this type of inlet, the internal losses will be higher than for the subsonic configuration of figure 12.

The configuration shown in figure 13 incorporates a converging-diverging diffuser (reference 12) in an attempt to compress the flow supersonically and cause the shock in the diffuser to occur at a lower Mach number.

The upper curve at the right gives the contraction ratio between entrance and throat for isentropic compression to $M = 1$ at the throat. This throat area is, however, too small for the establishment of supersonic flow in the converging section, since in order to "swallow" the shock, the throat must first pass the mass flow required for an inlet–velocity ratio of unity at the reduced density and total pressure due to the bow wave. The lower curve gives the maximum contraction ratio which can be used if a diffuser is to start or "swallow" the shock. The permissible contraction ratio is seen to be about half that required at $M = 1.6$ and less at higher Mach numbers. Thus, the requirements for starting a converging–diverging diffuser reduce the effectiveness of this configuration seriously in that large losses are still encountered through the normal shock in the diffuser at higher supersonic Mach numbers.

The type of air inlet shown schematically at the lower left was suggested by Oswatitsch in Germany (reference 13) and makes use of the more efficient compression through several oblique shocks on a conical body ahead of the inlet. After compression to a low supersonic Mach

number ahead of the entrance, the flow enters a converging-diverging diffuser in which a normal shock occurs as in the previous case, but at a very low supersonic Mach number with, of course, improved pressure recovery.

The following statements are made in summary:

Design charts are available from which optimum-critical-speed nose inlets can be selected for any required subsonic Mach number. These charts may also be used in the design of rotating cowlings, cowlings for use with spinners, and to aid in the design of fuselage scoop contours. In configurations where boundary layer exists ahead of an air inlet, either the inlet-velocity ratio must be kept high enough to prevent separation or a suitable scoop or bypass must be provided to remove the boundary layer.

Wing-inlet shapes have been developed which have maximum lift higher than plain airfoil sections and which have critical Mach number and internal pressure-recovery characteristics adequate for the airplanes involved.

The subsonic nose inlet can be used effectively at low supersonic Mach numbers because losses through the normal shock (or bow wave) are small at low supersonic Mach numbers. At higher supersonic Mach numbers a different configuration is needed which has sharp leading edges and which utilizes the most efficient arrangement of shocks possible for compressing the inlet flow. One such configuration utilizes a series of oblique shocks on a central conical body for compression to low supersonic Mach numbers ahead of the inlet.

REFERENCES

1. Robinson, Russell G., and Becker, John V.: High-Speed Tests of Conventional Radial-Engine Cowlings. NACA Rep. No. 745, 1942.

2. Becker, John V.: Wind-Tunnel Tests of Air Inlet and Outlet Openings on a Streamline Body. NACA ACR, Nov. 1940.

3. Baals, Donald D., Smith, Norman F., and Wright, John B.: The Development and Application of High-Critical-Speed Nose Inlets. NACA ACR No. L5F30a, 1945.

4. McHugh, James G.: Progress Report on Cowlings for Air-Cooled Engines Investigated in the NACA 19-Foot Pressure Wind Tunnel. NACA ARR, July 1941.

5. Racisz, Stanley F.: Development of Wing Inlets. NACA ACR No. L6B18, 1946.

6. Smith, Norman F.: High-Speed Investigation of Low-Drag Wing Inlets. NACA ACR No. L4I18, 1944.

7. Smith, Norman F., and Baals, Donald D.: Wind-Tunnel Investigation of a High-Critical-Speed Fuselage Scoop Including the Effects of Boundary Layer. NACA ACR No. L5B01a, 1945.

8. Becker, John V., and Baals, Donald D.: Wind-Tunnel Tests of a Submerged-Engine Fuselage Design. NACA ACR, Oct. 1940.

9. Rubert, Kennedy F., and Knopf, George S.: A Method for the Design of Cooling Systems for Aircraft Power-Plant Installations. NACA ARR, March 1942.

10. Becker, John V., and Baals, Donald D.: Analysis of Heat and Compressibility Effects in Internal Flow Systems and High-Speed Tests of a Ram-Jet System. NACA ACR, Sept. 1942.

11. Henry, John R.: Design of Power-Plant Installations. Pressure-Loss Characteristics of Duct Components. NACA ARR No. L4F26, 1944.

12. Kantrowitz, Arthur, and Donaldson, Coleman duP: Preliminary Investigation of Supersonic Diffusers. NACA ACR No. L5D20, 1945.

13. Oswatitsch, Kl.: Pressure Recovery for Missiles with Reaction Propulsion at High Supersonic Speeds (The Efficiency of Shock Diffusers). NACA TM No. 1140, 1947.

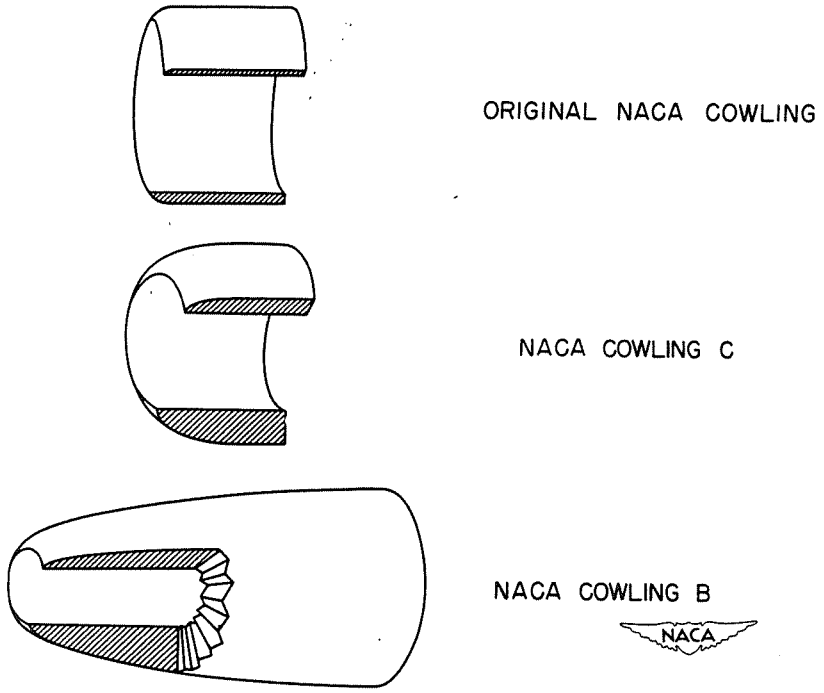

Figure 1.

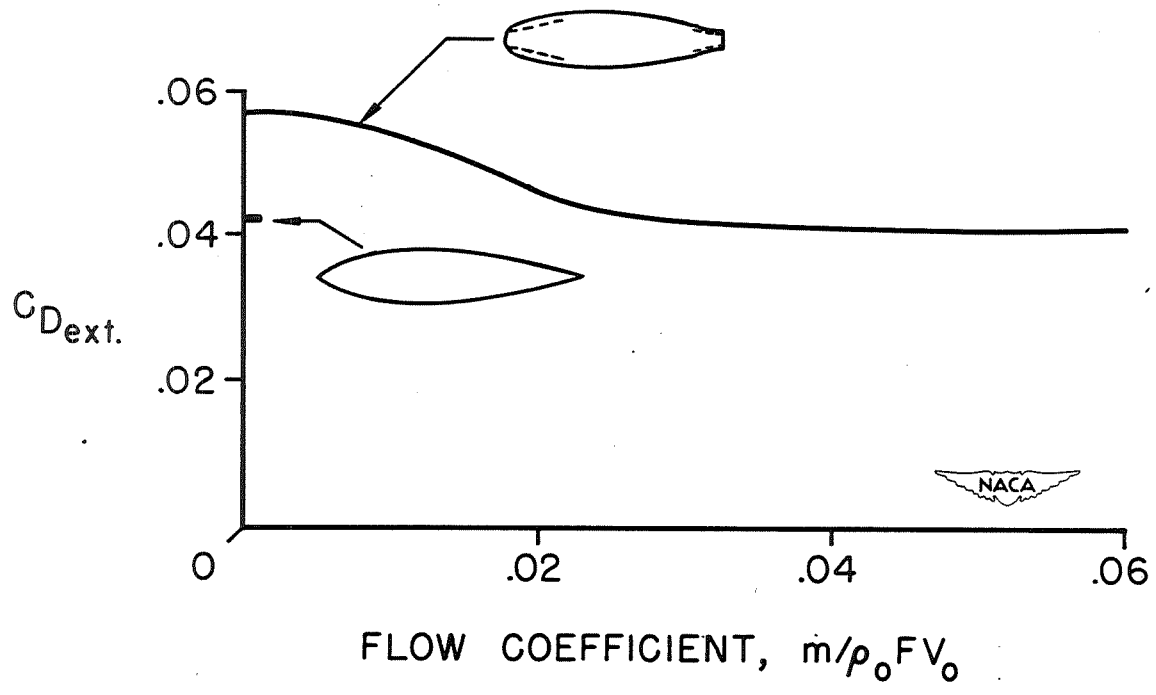

Figure 2.- External drag of body with and without nose inlet.

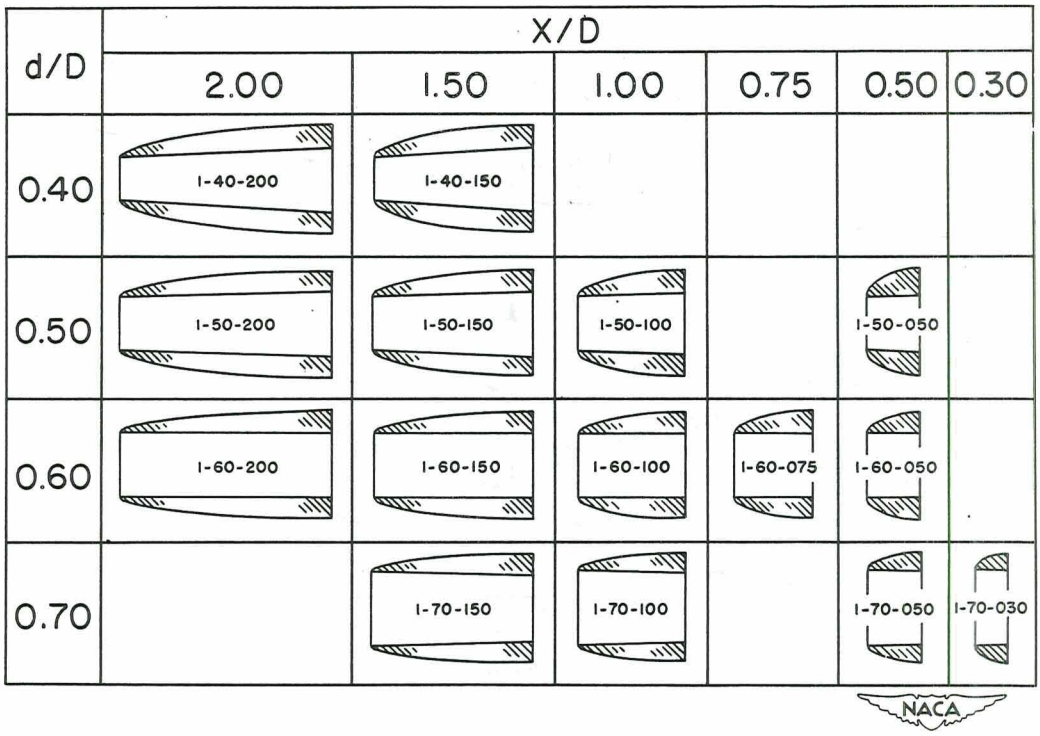

Figure 3.- NACA 1-series nose inlets tested.

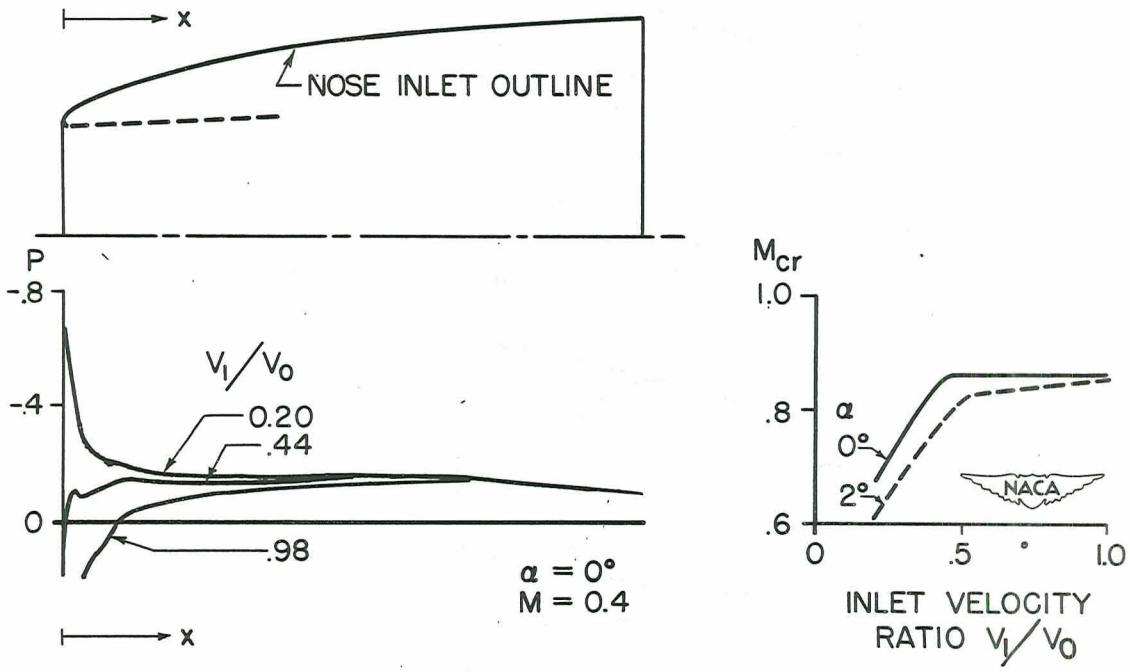

Figure 4.- Characteristics of typical NACA 1-series nose inlet. (1-50-150).

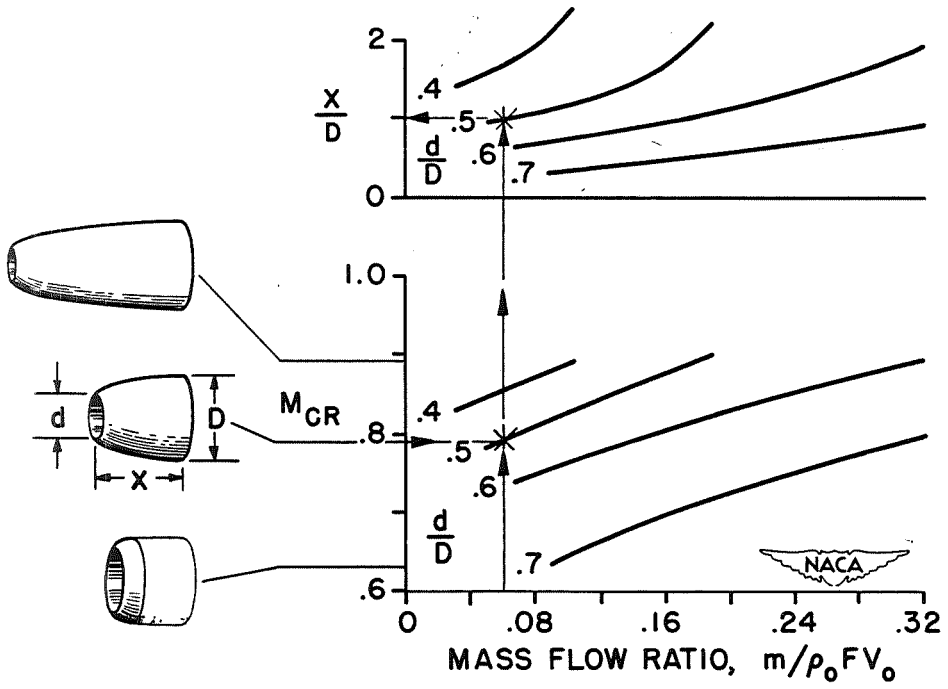

Figure 5.- NACA 1-series design chart.

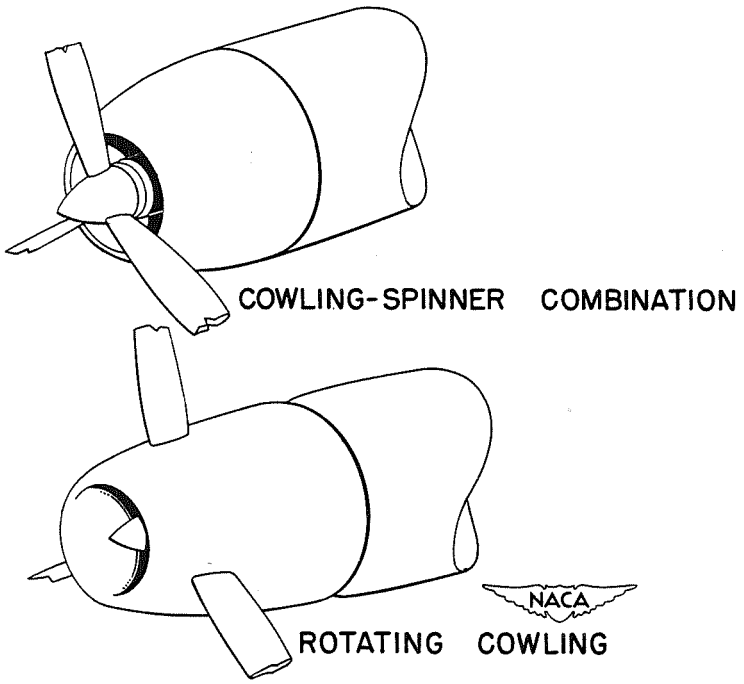

Figure 6.

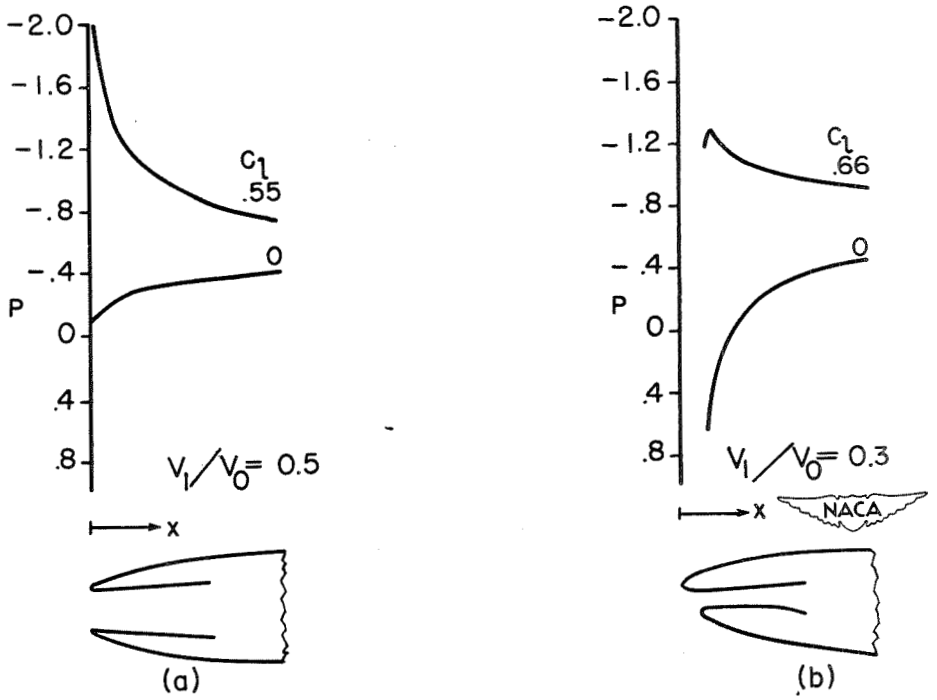

Figure 7.- Pressure distributions over upper lip of two wing inlets.

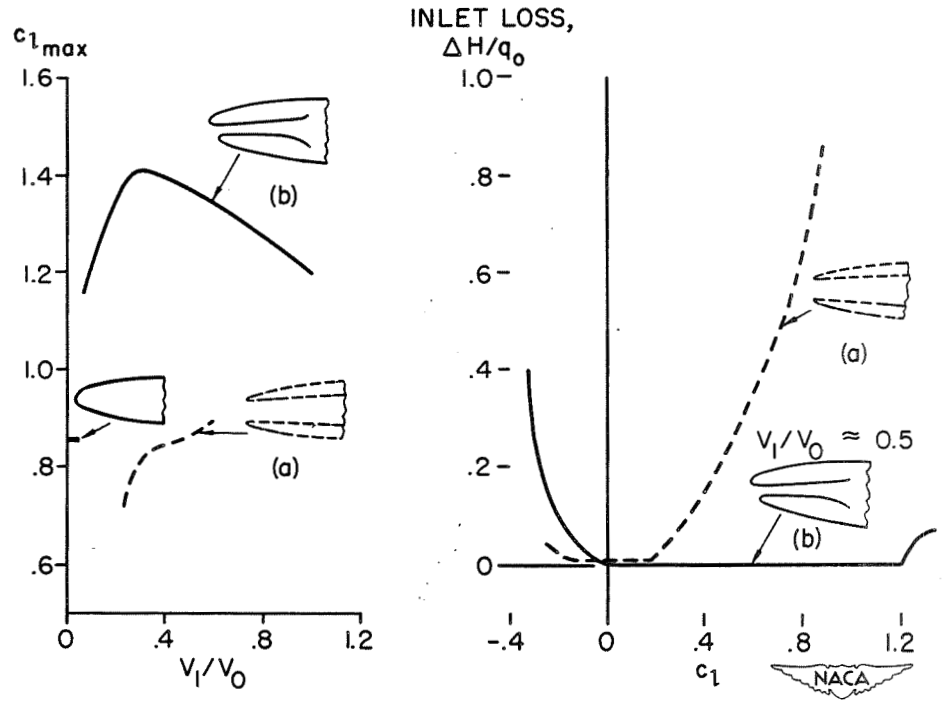

Figure 8.- Maximum lift and inlet losses for two wing inlets.

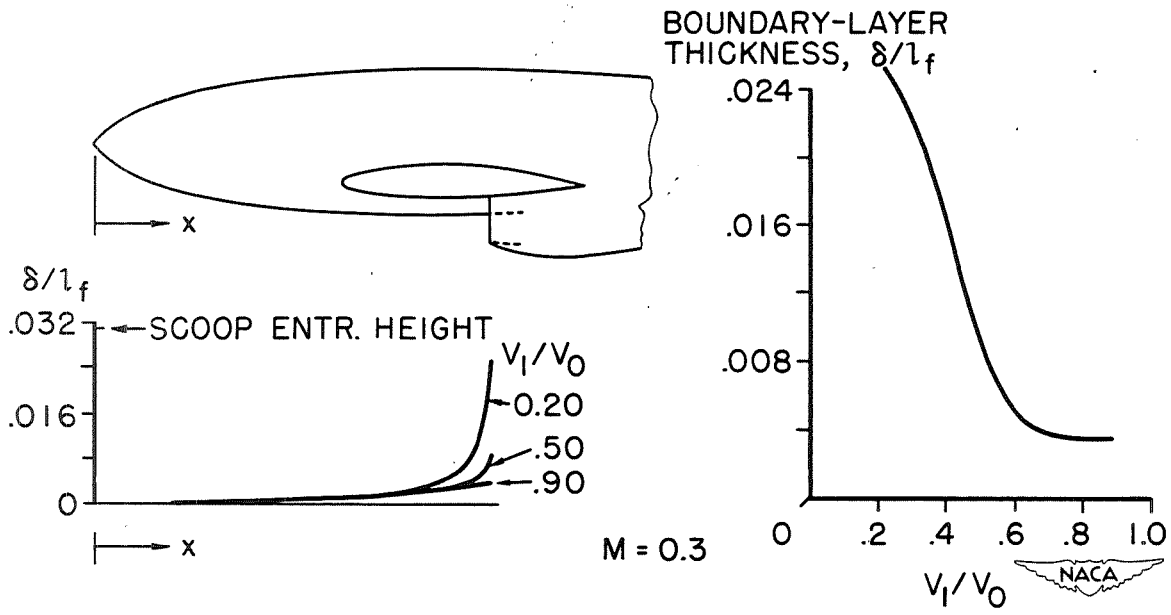

Figure 9.- Boundary-layer thickness ahead of fuselage scoop.

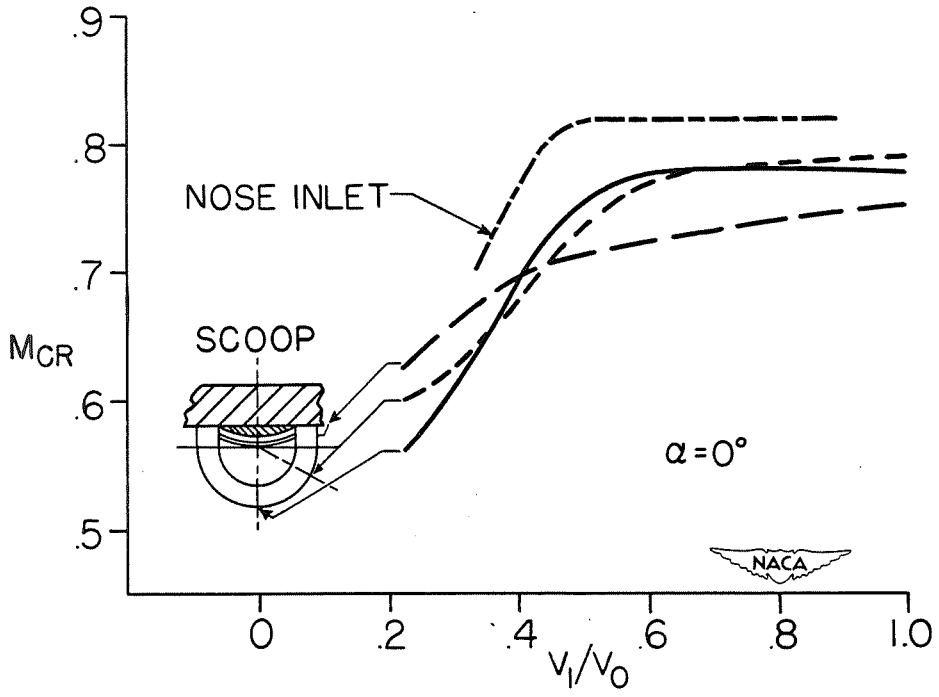

Figure 10.- Critical Mach numbers of nose inlet and scoop.

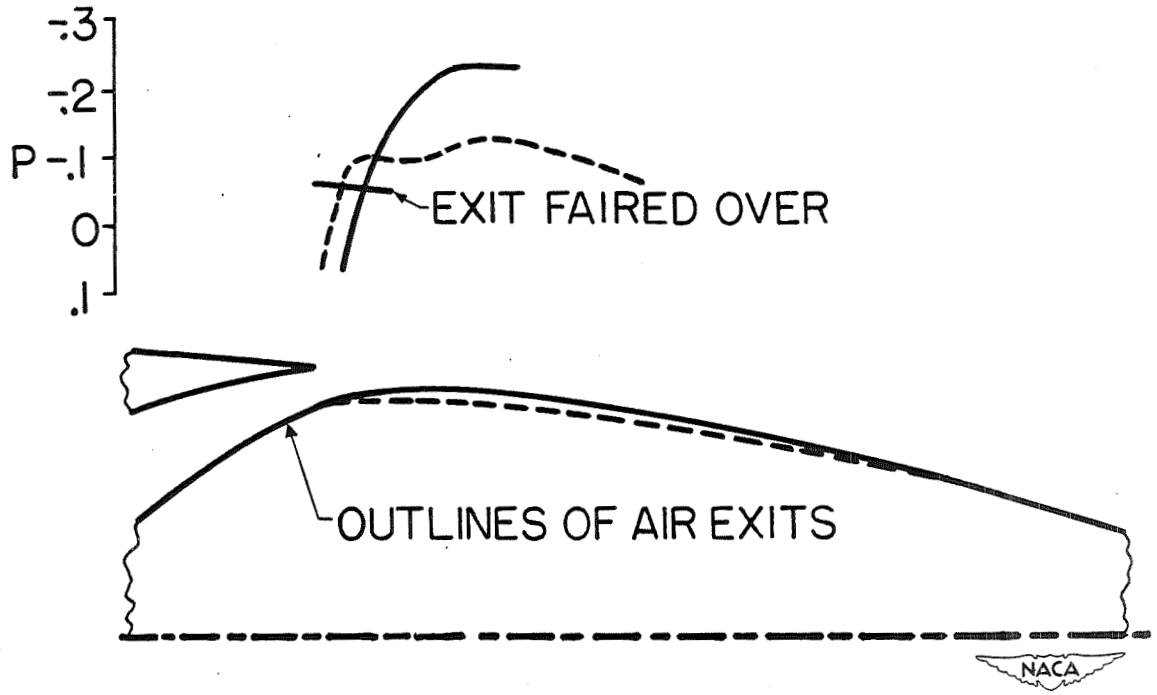

Figure 11.- Pressure distributions over air exits.

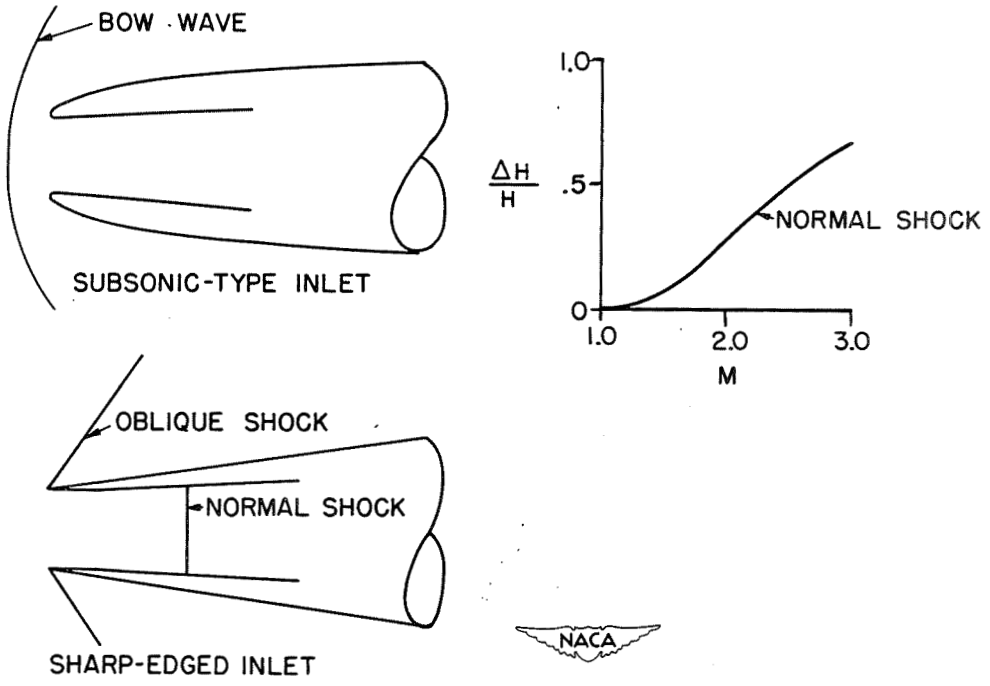

Figure 12.- Air inlets at supersonic speeds.

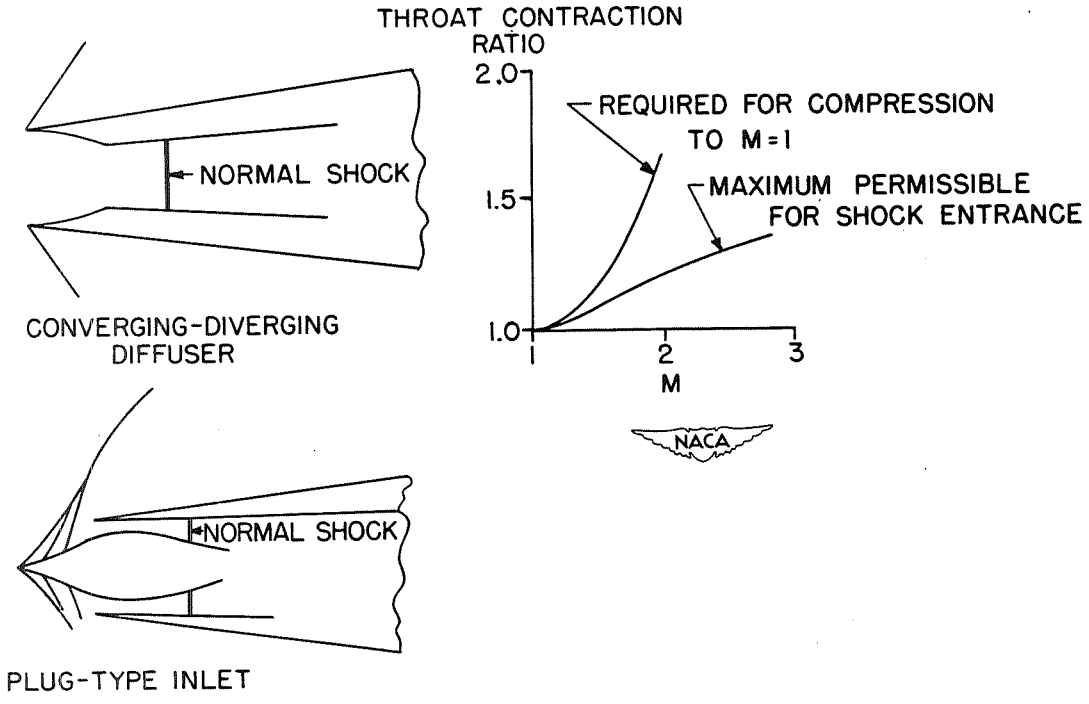

Figure 13.- Air inlets at supersonic speeds.

SUPERSONICS

D16

Preceding page blank

TWO-DIMENSIONAL SUPERSONIC WING THEORY

By Walter G. Vincenti

Ames Aeronautical Laboratory

INTRODUCTION

The problem of an airfoil section in two-dimensional supersonic flow, which is fundamental to a consideration of other, more general wing problems in supersonic flight, was first treated theoretically in a paper by Ackeret published in Germany in 1925. Shortly thereafter - in 1928 - experimental results were reported in England by Stanton. As a result of the work of these and a number of later investigators, the fundamentals of the problem were well, though perhaps not widely, understood before the beginning of World War II. During the wartime and postwar periods, detailed advances in both theory and experiment have been made, as well as increased application of the available knowledge, usually on classified projects. The fundamental ideas in the field, however, can be discussed almost completely in terms of results available prior to 1940.

FUNDAMENTAL CONSIDERATIONS OF SUPERSONIC FLOW

Before proceeding to the discussion of the theory, it is desirable to review briefly the fundamental difference between subsonic and supersonic flow (references 1 to 4). This difference is illustrated in figure 1, which shows the wave pattern set up by a disturbance point in both a steady subsonic stream and supersonic stream. In either case, if the disturbances from the point are small, each elementary disturbance is propagated spherically at the speed of sound relative to the moving stream. Because of the motion of the stream, however, the center of each elementary sphere is at the same time carried downstream relative to the original source of the disturbance. If the speed of the stream is less than the speed of sound, as shown on the left in figure 1, the elementary disturbances will travel upstream against the flow faster than their centers are swept downstream. As a result, the disturbances move ahead of their source and affect all parts of the flow field. In a supersonic stream, as shown on the right in this figure, the centers of the disturbance spheres are carried downstream faster than the disturbance itself can be propagated forward. As a result, all disturbances in the supersonic stream are confined to the interior of a cone known as the Mach cone. The flow outside this region is, so to speak, unaware of the presence of any disturbance. It is apparent that the greater the supersonic speed, the smaller the included angle at the apex of the Mach cone. These simple considerations must be modified somewhat if the disturbances are not small; however, the results serve as a reasonable first approximation in most actual cases.

The concept of the Mach cone has important implications with regard to the applicability of two-dimensional theory and data to parts of three-dimensional wings. The relationship of this concept to three-dimensional wings is illustrated in figure 2. In the case of the straight wing, for example, the effect of the finite span of the wing is confined approximately to conical regions extending downstream from the leading edge of each tip. The flow over the remainder of the wing (shaded area) is not influenced by the presence of the tips and this shaded area is thus a region of two-dimensional flow. For the more complex plan forms shown, the flow over the shaded regions is similarly unaffected by the presence of the tips and, for these examples, of the root of the wing as well. Within these regions the flow can be treated as essentially two-dimensional by utilizing the components of the flow quantities and deflection angles normal to the swept straight-line elements which generate the wing surface (reference 5).

FLOW FIELD ABOUT AN AIRFOIL SECTION

With this background, consider the general character of the two-dimensional flow field about an airfoil section at supersonic speed. Figure 3 is a diagram of the idealized, inviscid flow around a simple, double-wedge section at angle of attack for a free-stream Mach number of approximately 2. The pattern shown is that predicted by theory when the local velocity in the flow field is everywhere supersonic. In accordance with the previous considerations of supersonic flow, the oncoming stream (fig. 3) continues undisturbed until it reaches the region of influence of the airfoil. Within this region the flow changes are of two general kinds. When the flow is turned around a concave corner, as on the lower surface at the leading edge, a compression takes place. When the flow is turned around a convex corner, as on the upper surface at the same location, an expansion results. The compression from the concave corner takes place discontinuously through an oblique shock wave with an accompanying dissipation of energy - that is, with an increase in entropy. The expansion takes place continuously and isentropically in a fan-shaped region originating at the convex corner. Thus, if the flow is along a streamline some distance above the present airfoil, the air first undergoes reductions in pressure through two successive expansion regions, one originating at the leading edge and one at the ridge line, and is then recompressed by a shock wave originating at the trailing edge. The air beneath the lower surface is, in the same general manner, first compressed through a shock wave and then successively expanded through two expansion regions. It is interesting to note that along the surface of the airfoil itself the expansions as well as the compressions take place discontinuously. Thus, contrary to the condition which would exist in subsonic flow, there is no stagnation point in the vicinity of the leading edge and no tendency toward an infinite velocity at the sharp convex corners.

As the angle of attack of the airfoil is changed, the flow pattern will, of course, change correspondingly. In particular, the flow

disturbance on a given surface at the leading or trailing edge will change from an expansion to a compression, or vice versa, as the required deflection of the stream is altered. Of more importance, as the angle of attack is increased, a condition is eventually reached in which the flow behind the shock wave at the leading edge is no longer supersonic but becomes subsonic instead. At a slightly higher angle of attack, the wave detaches and moves forward of the airfoil. These latter effects also occur at a given angle of attack when the Mach number is reduced toward unity. Once such changes have taken place, the entire character of the flow pattern is altered and the purely supersonic considerations of the foregoing discussion no longer apply.

For simplicity, the discussion herein has been carried out in terms of a simple, flat-sided section. The same considerations apply to a curved profile so long as the leading edge is sharp, except that in such a case the expansion along the convex curved surface takes place gradually rather than discontinuously. (The restriction of the discussion to airfoils with a sharp leading edge is of no serious consequence, since an edge of this type appears desirable for optimum performance in the two-dimensional case when the velocity is more than slightly supersonic.)

METHODS OF ANALYSIS

Several theoretical methods are available for determining the characteristics of an airfoil in a two-dimensional supersonic flow. The methods all assume that the fluid is inviscid, that the leading and trailing edges of the airfoil are sharp, that any shock waves originating from these edges are attached to the airfoil, and that the flow behind the leading-edge shock wave is supersonic. They differ only in the degree of mathematical accuracy involved. In order of decreasing accuracy, the methods may be described as the shock-expansion theory, the second-order theory, and the linear (or first-order) theory.

Shock-Expansion Theory

The shock-expansion method follows directly from the application to the airfoil problem of known analytical results for an oblique shock wave and an expansion region (references 1 to 3 and 6 to 9). From simple considerations of momentum, energy, and continuity, the change in pressure and Mach number across a single shock wave can be calculated in terms of the Mach number of the oncoming flow and the angle of deflection of the flow in passing through the wave. Similar results can be obtained for an isolated expansion region. On the basis of these results together with the assumption that interaction effects between the individual shock waves and expansion regions are negligible, the pressure distribution over the airfoil surface can be calculated by a step-by-step procedure beginning at the leading edge and proceeding rearward (references 10 and 11). For example, on the lower surface of the double-wedge

section in figure 3, if the free-stream Mach number and the deflection angle at the leading edge are known, the pressure and Mach number on the forward lower surface can be found from the equations for an oblique shock wave. By use of these quantities to provide the initial conditions for the flow approaching the ridge line, the pressure on the rear lower surface can then be found from the known results for an expansion. Because of the nature of the equations for an expansion, the procedure applies equally well to a section with a curved profile. Once the complete pressure distribution is known, the lift, pitching moment, and pressure drag of the airfoil are determined by graphical or numerical integration.

As compared with the theories to be discussed later, the shock-expansion method has the advantage of greater mathematical accuracy; in fact, in instances for which the assumption of no effective interference between the shock waves and expansion regions is satisfied, the method provides the complete inviscid solution to the problem. (The case illustrated in figure 3 can be shown to be of this type since the regions of flow influenced by the eventual intersections of the different disturbances lie completely downstream of the airfoil.) In other instances, notably on airfoils with curved surfaces, some interference does occur with a resulting approximation in the theory. The main disadvantage of the method, however, is that no analytical expressions are provided for the section characteristics, a separate set of calculations being required for each airfoil at each angle of attack.

Second-Order and Linear Theories

The disadvantage of the shock-expansion theory is overcome, at the expense of further approximation, by the second-order and linear theories (references 12 to 15). The relationship upon which these theories are based is given as equation (1) in figure 4. This equation, which is derived by series approximation to the complete equations for two-dimensional supersonic flow, expresses the pressure coefficient P at any point on the airfoil in terms of ascending powers of the local deflection angle η. The coefficients of the terms in the series are functions primarily of the free-stream Mach number M_o and, secondarily of the ratio of the specific heats of the gas γ. By proper definition of the sign of the angle η - positive when the surface is facing toward the oncoming free stream and negative when facing away from the oncoming free stream (see diagram in fig. 4) - and by limitation of the power series to the first two terms, the same equation can be made to serve for both a compression and an expansion. This result illustrates the fact that in a given supersonic stream the pressure at a point on an airfoil in two-dimensional flow is, to the second order of approximation, determined solely by the local inclination of the airfoil surface. This is contrary to the situation in subsonic theory, in which the conditions at one point on an airfoil section depend, even to the first order, upon conditions at every other point.

On the basis of the foregoing simple result for the surface pressure, general second-order expressions for the lift, pitching-moment, and pressure-drag characteristics of any airfoil section can be obtained by direct integration. The final equations involve the coefficients C_1 and C_2, the angle of attack of the airfoil, and certain simple integrals which depend upon the airfoil shape only. These equations have been worked out in their most general form by Lock (references 15 and 8). For cases in which the shape of the airfoil can be expressed analytically, the integrals involved are readily evaluated to obtain direct equations for the airfoil characteristics in terms of the parameters which define the profile. These results are especially useful in studying the effects of systematic variation in thickness and camber for families of sections.

When both the terms C_1 and C_2 are retained, the general equations (see fig. 4) constitute the second-order theory. If the coefficient C_2 is in all cases set equal to zero, a linear (or first-order) theory is obtained. This latter approximation, which is sufficient for many purposes, is also known as the Ackeret theory since the linear theory was first proposed by Ackeret in his original treatment of the supersonic airfoil problem (reference 12). This elementary theory leads to certain exceedingly simple results. It indicates, for example, that the aerodynamic center of the airfoil is at midchord irrespective of the shape of the section and that the minimum pressure drag for a family of sections of given thickness distribution varies as the square of the thickness ratio. The second-order approximation, which modifies these results somewhat, was developed by Busemann (reference 14) at a later date when it was found that certain of the first-order results were not in complete accord with experiment. It is interesting to note, however, that even to the second order the lift-curve slope (per radian) for any airfoil section has the simple value of $2C_1$ or $\frac{4}{\sqrt{M_o^2 - 1}}$.

COMPARISON BETWEEN THEORY AND EXPERIMENT

Since the various theoretical methods have been reviewed, a comparison of the theoretical and experimental results for specific airfoils can now be made.

Pressure Distribution

Of first interest is an examination of a typical pressure distribution. Calculated and measured results are shown in figure 5 for a 10-percent-thick symmetrical, biconvex section at a Mach number of 2.13 and an angle of attack of 10°. The local pressure is plotted in

coefficient form as a function of the chordwise position; positive pressures are plotted below the horizontal axis and negative pressures, above. The pressure distributions calculated by the three theories are indicated by different lines in the figure. Experimental data obtained, as part of an extensive investigation, by Ferri (reference 16) are shown as individual points.

A noticeable improvement is seen in the accuracy of the theoretical calculations in going from the linear to the more refined theories. Over most of the section, both the second-order and shock-expansion theories show reasonable agreement with experiment although the check is slightly better when the shock-expansion theory is used. Over the rear 40 percent of the upper surface, however, the experimental pressures depart noticeably from the values given by any of the theories.

The discrepancy between the theoretical pressure distributions calculated by the linear theory and those calculated by the more precise theories has, curiously enough, little effect upon the value of the integrated lift. In fact, the area between the curves for the upper and lower surfaces, which gives a representation of the lift, is exactly the same for the linear and second-order theories. In other words, these two theories, although they disagree in chordwise lift distribution, agree in the value of the total lift for the present section. It is apparent from the difference in lift distribution, however, that the second-order theory gives a position of the center of pressure (or aerodynamic center) forward of that predicted by the linear theory. (The discrepancies noted between the various theories would, of course, be smaller for thinner airfoils and at lower angles of attack.)

The failure of even the higher-order theories to predict the pressure distribution over the rear part of the upper surface is known to be due to shock-wave, boundary-layer interaction (reference 16). As was previously indicated (see fig. 3), the idealized inviscid flow over a lifting airfoil section is characterized by an oblique compression wave originating on the upper surface at the trailing edge. In the real, viscous fluid the flow pattern is modified by an interaction between this trailing wave and the boundary layer on the airfoil surface. The boundary layer separates from the upper surface some distance ahead of the trailing edge, with the formation of a weak compression wave at the separation point and a consequent increase in pressure between this point and the trailing edge.

The difference between the pressure distributions shown herein and those characteristic of an airfoil in subsonic flow is apparent. Here, the pressures on both surfaces of the section decrease progressively toward the trailing edge with no pressure recovery such as that which occurs in the subsonic case. This lack of pressure recovery over the rear of the section at supersonic speeds gives rise, even in the theoretical inviscid flow, to an appreciable pressure drag. In the subsonic case the drag in a two-dimensional inviscid flow is, of course, exactly zero.

Over-All Aerodynamic Characteristics

With the foregoing results in mind, consider the over-all characteristics of a typical airfoil. Figure 6 presents theoretical and experimental lift and moment results, at the same Mach number as before, for a cambered, double-wedge airfoil of 6.3 percent thickness. A straight-sided airfoil was chosen here, instead of the previous biconvex section, in order to simplify the calculations by the shock-expansion method.

As indicated from the plot of lift coefficient and angle of attack, the three theories give approximately the same lift-curve slope, at least at small angles. A curve through the experimental points, taken again from the results of Ferri (reference 16), would have a slope about 10 percent less than the common theoretical value. This reduction is due to the shock-wave, boundary-layer interaction previously discussed. With regard to the angle of zero lift, the linear theory shows a value of exactly zero. The higher-order theories show a small positive value in agreement with experiment. (This experimental result, incidentally, is in direct contrast with the result in subsonic flow, where positive camber leads to a negative angle for zero lift.) In general, it may be said that the check between theory and experiment with regard to lift is within acceptable practical limits.

The agreement with regard to pitching moment is generally less satisfactory. In figure 6 the moment coefficient of the double-wedge airfoil - for moments taken about the midchord point - is plotted as a function of the lift coefficient. The inclination of the moment curves toward the right may be taken as an approximate measure of the displacement of the aerodynamic center forward of the midchord. The experimental moment coefficients are seen to be more positive than the theoretical at all lift coefficients. A straight line through the experimental data would indicate a position of the aerodynamic center forward of the midchord by about 9 percent of the airfoil chord. This displacement is significantly greater than the theoretical displacement of zero according to the linear theory or of 4 percent according to the second-order and shock-expansion theories. Both the general positive shift in the experimental moment coefficients and the relatively forward displacement of the aerodynamic center are attributable to shock-wave, boundary-layer interaction on the upper surface near the trailing edge.

Drag results for the double-wedge airfoil are shown in figure 7 as a function of the lift coefficient. Theory indicates that the variation of pressure drag with lift is essentially parabolic - exactly so in the case of the linear and second-order theories, nearly so in the case of the shock-expansion method. The second-order and shock-expansion theories give virtually coincident curves. It is seen that the experimental data agree fairly closely with these latter results. The exact agreement in the magnitude of the minimum drag is at first surprising. The effect of skin friction, which is completely neglected in the theory, would be expected to raise the measured minimum drag relative to the

theoretical value. This tendency is opposed, however, by the unexpectedly high pressures in the vicinity of the trailing edge as the result of shock-wave, boundary-layer interaction. These two effects are probably compensating in the present case. Such compensation is not to be expected, however, on all airfoils or at all Mach numbers and Reynolds numbers.

The results of the foregoing figures are all for a single Mach number. Figure 8 illustrates the typical effect of variation in Mach number upon a given section characteristic, in this case the drag coefficient at zero angle of attack. The theoretical curves show an increase in the pressure drag coefficient as the Mach number decreases toward unity. (The linear and second-order theories give identical results in the present case, though this fact is not always true.) The two available experimental points confirm the theoretical tendency. The theoretical results are, as previously implied, valid down to the Mach number at which the flow behind the leading-edge shock wave becomes subsonic. Below this point, the problem is one of mixed subsonic and supersonic flow; the theoretical solutions to this problem are only now being developed.

CONCLUDING REMARKS

Only a brief outline of existing knowledge regarding the basic two-dimensional wing problem at supersonic speeds has been presented. Many subsidiary problems have been studied on the basis of the available theories, including the effects of systematic variations in airfoil shape (reference 17), the properties of flaps (reference 18), the influence of sweepback for cases in which two-dimensional theory is applicable (reference 19), and the characteristics of two-dimensional biplanes (references 20 and 21). For many such problems, valuable results have been obtained with one or another of the inviscid theories, depending upon the degree of accuracy required. In other cases, however, such as those concerning the determination of the optimum airfoil shape for a given operating condition, consideration of the effects of viscosity and the boundary layer is essential (reference 22). In the study of the effects of viscosity and the boundary layer, in particular, there is an opportunity for much valuable research.

APPENDIX

SYMBOLS

C_1, C_2	coefficients in series expansion for P
c_l	section lift coefficient
$c_{m_{c/2}}$	section pitching-moment coefficient for moments about the midchord point
c_d	section drag coefficient
$c_{d_{\alpha=0}}$	section drag coefficient at zero angle of attack
M_o	free-stream Mach number
p	local static pressure at point on airfoil
P	local pressure coefficient $\left(\frac{p - p_o}{q_o}\right)$
p_o	free-stream static pressure
q_o	free-stream dynamic pressure
α	angle of attack
γ	ratio of specific heats of gas $\left(c_p/c_v\right)$
c_p	specific heat at constant pressure
c_v	specific heat at constant volume
η	local inclination of surface of airfoil measured relative to free-stream direction

REFERENCES

1. Liepmann, Hans Wolfgang, and Puckett, Allen E.: Introduction to Aerodynamics of a Compressible Fluid. John Wiley & Sons, Inc., 1947.

2. Taylor, G. I., and Maccoll, J. W.: The Mechanics of Compressible Fluids. Vol. III of Aerodynamic Theory, div. H, W. F. Durand, ed., Julius Springer (Berlin), 1935, pp. 209-250.

3. Sauer, Robert: Theoretical Gas Dynamics. Edwards Brothers, Inc. (Ann Arbor, Mich.), 1947.

4. Von Kármán, Theodore: Supersonic Aerodynamics - Principles and Applications. Jour. Aero. Sci., vol. 14, no. 7, July 1947, pp. 373-409.

5. Busemann, A.: Aerodynamischer Auftrieb bei Uberschallgeschwindigkeit. Luftfahrtforschung, Bd. 12, Nr. 6, Oct. 3, 1935, pp. 210-220. (Available as British A.R.C. 2844, Ae. Techl. 1201, Feb. 3, 1937.)

6. Laitone, Edmund V.: Exact and Approximate Solutions of Two-Dimensional Oblique Shock Flow. Jour. Aero. Sci., vol. 14, no. 1, Jan. 1947, pp. 25-41.

7. Lighthill, M. J.: Two-Dimensional Supersonic Airfoil Theory. R. & M. No. 1929, British A.R.C., 1944.

8. The Staff of the Ames 1- by 3-Foot Supersonic Wind-Tunnel Section: Notes and Tables for Use in the Analysis of Supersonic Flow. NACA TN No. 1428, 1947.

9. Moeckel, W. E., and Connors, J. F.: Charts for the Determination of Supersonic Air Flow against Inclined Planes and Axially Symmetric Cones. NACA TN No. 1373, 1947.

10. Ivey, H. Reese, Stickle, George W., and Schuettler, Alberta: Charts for Determining the Characteristics of Sharp-Nose Airfoils in Two-Dimensional Flow at Supersonic Speeds. NACA TN No. 1143, 1947.

11. Edmonson, N., Murnaghan, F. D., and Snow, R. M.: The Theory and Practice of Two-Dimensional Supersonic Pressure Calculations. Bumblebee Rep. No. 26, The Johns Hopkins Univ., Appl. Phys. Lab., Dec. 1945.

12. Ackeret, J.: Air Forces on Airfoils Moving Faster Than Sound. NACA TM No. 317, 1925.

13. Taylor, G. I.: Applications to Aeronautics of Ackeret's Theory of Aerofoils Moving at Speeds Greater Than That of Sound. R. & M. No. 1467, British A.R.C., 1932.

14. Busemann, A., and Walchner, O.: Airfoil Characteristics at Supersonic Speeds. R.T.P. Translation No. 1786, British Ministry of Aircraft Production. (From Forschung auf dem Gebiete des Ingenieurwesens, March-April, 1933, vol. 4, pp. 87-92.)

15. Lock, C. N. H.: Examples of the Application of Busemann's Formula to Evaluate the Aerodynamic Force Coefficients on Supersonic Aerofoils. R. & M. No. 2101, British A.R.C., 1944.

16. Ferri, Antonio: Experimental Results with Airfoils Tested in the High-Speed Tunnel at Guidonia. NACA TM No. 946, 1940.

17. Ivey, H. Reese: Notes on the Theoretical Characteristics of Two-Dimensional Supersonic Airfoils. NACA TN No. 1179, 1947.

18. Collar, A. R.: Theoretical Forces and Moments on a Thin Aerofoil with Hinged Flap at Supersonic Speeds. R. & M. No. 2004, British A.R.C., 1943.

19. Ivey, H. Reese, and Bowen, Edward N., Jr.: Theoretical Supersonic Lift and Drag Characteristics of Symmetrical Wedge-Shape-Airfoil Sections as Affected by Sweepback outside the Mach Cone. NACA TN No. 1226, 1947.

20. Lighthill, M. J.: A Note on Supersonic Biplanes. R. & M. No. 2002, British A.R.C., 1944.

21. Moeckel, W. E.: Theoretical Aerodynamic Coefficients of Two-Dimensional Supersonic Biplanes. NACA TN No. 1316, 1947.

22. Ivey, H. Reese, and Klunker, E. Bernard: Considerations of the Total Drag of Supersonic Airfoil Sections. NACA TN No. 1371, 1947.

BIBLIOGRAPHY

Ferri, A.: Experiments at Supersonic Speed on a Biplane of the Busemann Type. R.T.P. Translation No. 1407, British Ministry of Aircraft Production. (From Atti di Guidonia, No. 37-38, 1940, pp. 517-557.)

Hilton, W. F., and Pruden, F. W.: Subsonic and Supersonic High Speed Tunnel Tests of a Faired Double Wedge Aerofoil. R. & M. No. 2057, British A.R.C., 1943.

Hooker, S. G.: The Pressure Distribution and Forces on Thin Airfoil Sections Having Sharp Leading and Trailing Edges, and Moving with Speeds Greater Than That of Sound. R. & M. No. 1721, British A.R.C., 1936.

Kahane, A., and Lees, Lester: The Flow at the Rear of a Two-Dimensional Supersonic Airfoil. Jour. Aero. Sci., vol. 15, no. 3, March 1948, pp. 167-170.

Lighthill, M. J.: The Conditions behind the Trailing Edge of the Supersonic Aerofoil. R. & M. No. 1930, British A.R.C., 1944.

Stanton, T. E.: A High Speed Wind Channel for Tests on Aerofoils. R. & M. No. 1130, British A.R.C., 1928.

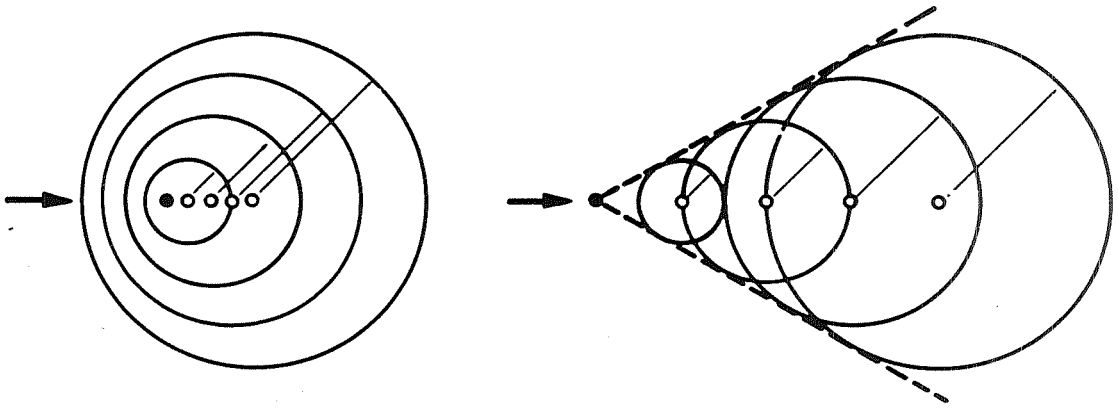

Figure 1.- Disturbance point in subsonic flow and supersonic flow.

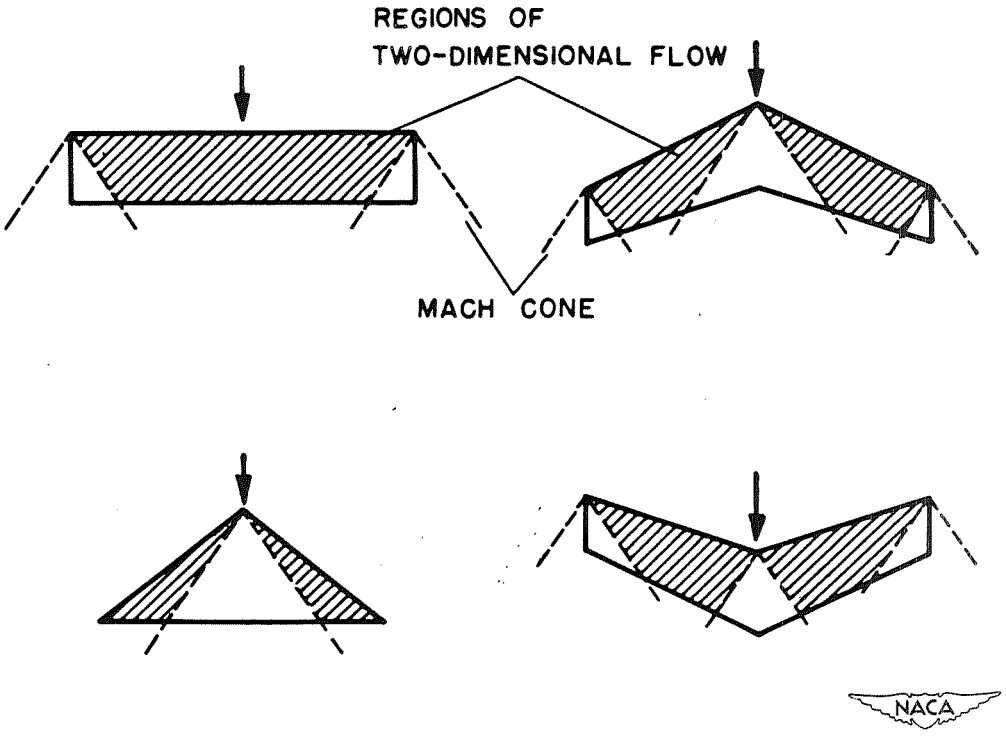

Figure 2.- Regions of two-dimensional flow.

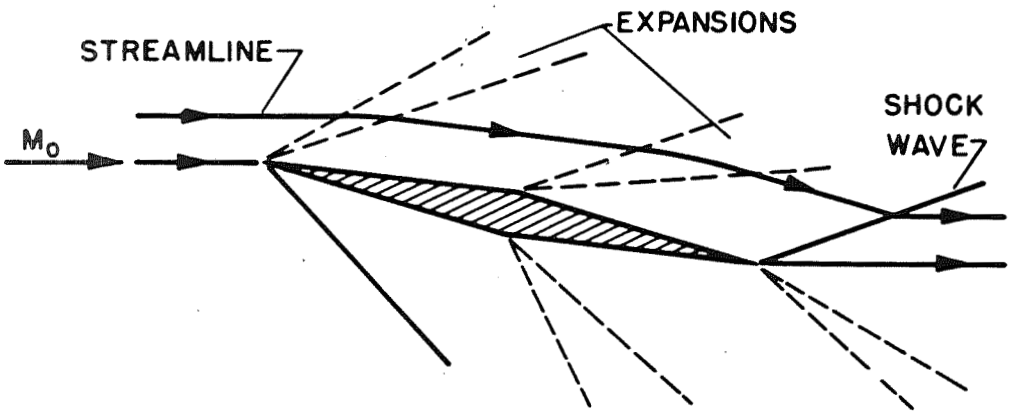

Figure 3.- Idealized flow pattern about a double-wedge section at $M_o \approx 2$.

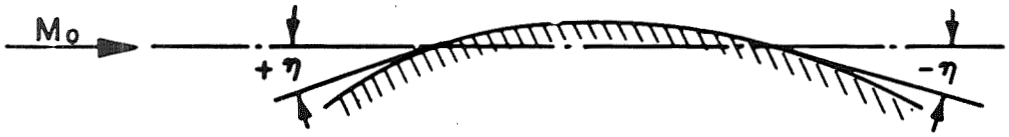

$$P = \frac{p - p_o}{q_o} = C_1 \eta + C_2 \eta^2 + \cdots \qquad (1)$$

WHERE $C_1 = \dfrac{2}{\sqrt{M_o^2 - 1}}$ (ACKERET) (2)

$$C_2 = \frac{(\gamma+1) M_o^4 - 4 (M_o^2 - 1)}{2 (M_o^2 - 1)^2} \quad \text{(BUSEMANN)} \quad (3)$$

NACA

Figure 4.- Basic equations for linear and second-order theories.

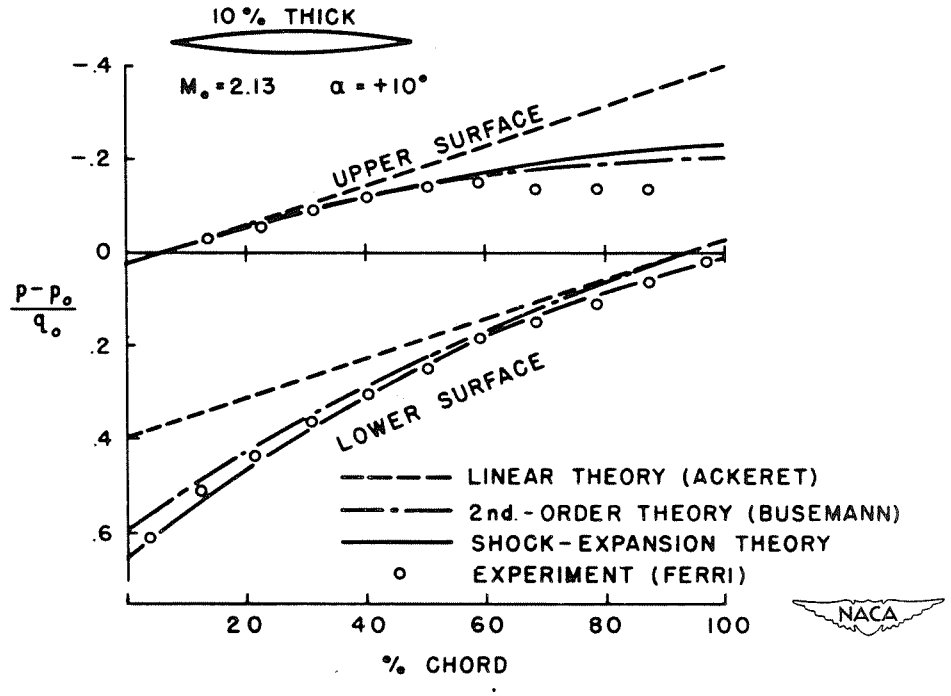

Figure 5.- Pressure distribution for symmetrical biconvex section.

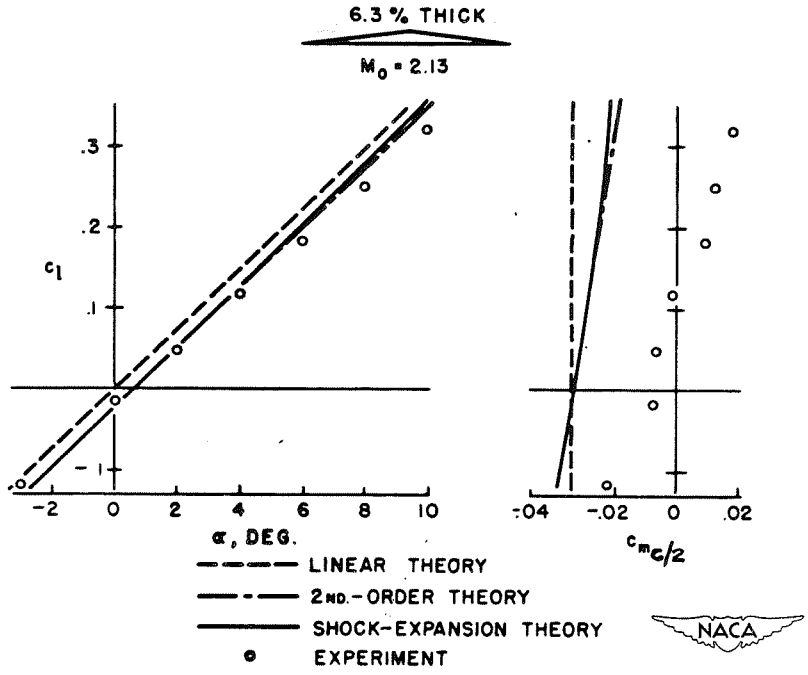

Figure 6.- Lift and pitching moment for cambered double-wedge section.

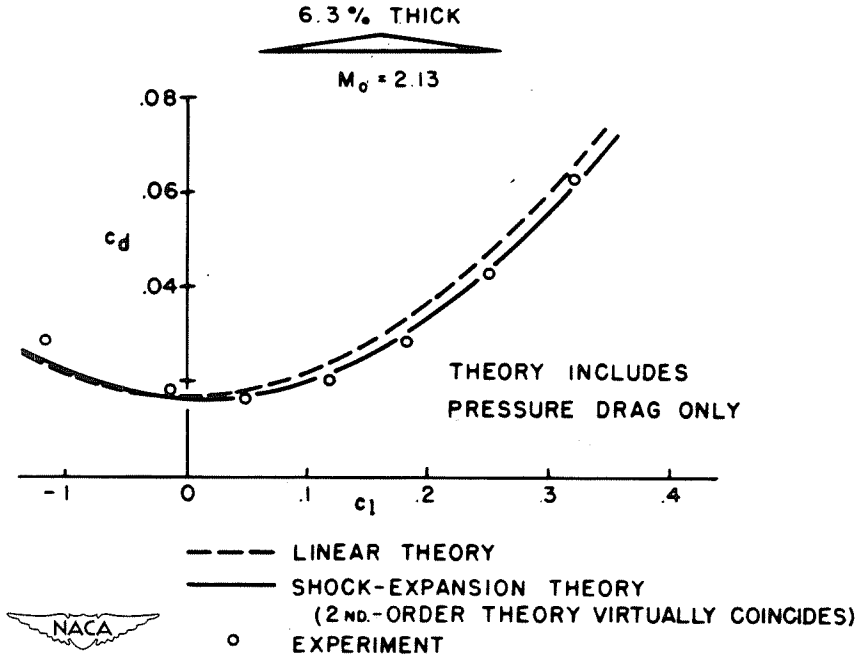

Figure 7.- Drag for cambered double-wedge section.

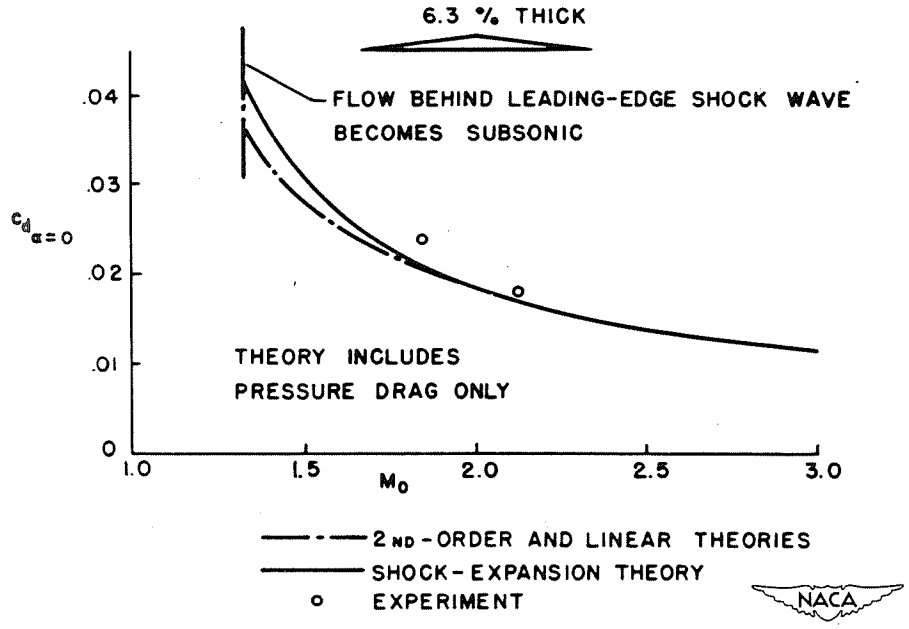

Figure 8.- Variation with Mach number of drag at zero angle of attack.

THE USE OF CONICAL AND CYLINDRICAL FIELDS IN SUPERSONIC WING THEORY

By Robert T. Jones

Ames Aeronautical Laboratory

Some of the recent advances in the theory of thin airfoils are presented with particular reference to extensions of the theory to three-dimensional flows and to supersonic speeds.

The thin-airfoil theory is essentially a linearized theory of small disturbances and the orgin of the concepts may be traced back to the older theories of Munk and Ackeret. The present emphasis on three-dimensional flows arose from the discovery that the type of two-dimensional supersonic flow considered by Ackeret is aerodynamically inefficient. The search for aerodynamically efficient forms for supersonic flight also focuses attention on the linear, or small-disturbance, theory since bodies and wings creating large disturbances are thought to be aerodynamically inefficient.

The newer development of the theory is the work of many investigators. The present discussion, however, is based largely on the conical-flow theory first employed by Busemann (reference 1).

The term "thin airfoil" is used to denote a thin, essentially flat body, the surface of which departs only slightly from the xy-plane. In the general problem no restriction is made on the shape of the plan form, but it is essential that the body be thin and flat in all vertical cross sections; hence, slender bodies of revolution are avoided.

The problem discussed herein is the calculation of the small disturbance velocities u, v, and w in the external field produced by the flight velocity V of the airfoil.

As is well known in acoustics, air motions of small amplitude are governed primarily by the simple properties of elasticity of volume and density. In order to depict such motions mathematically, a frictionless, perfectly elastic fluid is, therefore, adopted and a velocity field uvw must be found which is consistent with Newton's laws and which agrees at the airfoil surface with the outward, or normal, velocity imparted by the motion of the airfoil. The application of Newton's laws to the motions of small elements of such a simplified model fluid results in the familiar wave equation for the velocity potential φ,

$$\varphi_{xx} + \varphi_{yy} + \varphi_{zz} = \frac{1}{c^2}\varphi_{tt} \tag{1}$$

where c is the velocity of sound and $\varphi_x = u$, $\varphi_y = v$, $\varphi_z = w$.

The description of the whole velocity field by a single scalar potential φ is, of course, a great simplification and, as explained in text books on hydrodynamics, this scalar potential occurs in every case of frictionless motion in which the density ρ is a function of the pressure only. The elements of such a fluid move only under the action of "buoyancy" or pressure forces. When the density is dependent on the pressure only, variations of density occur only along the direction of the buoyant force. This force then passes through the center of gravity of each element and no rotation is produced. The existence of φ follows from the absence of rotation.

Of first interest in the airfoil problem are steady flows. The steady flow consists of a fixed pattern of streamlines attached to the airfoil and moving with it. In order to represent the steady flow, it will be necessary to transform the stationary axes of equation (1) to axes moving with the airfoil at the flight velocity V. The quantity $\frac{1}{c^2}\varphi_{tt}$ is then replaced by $\frac{V^2}{c^2}\varphi_{xx}$ and the equation becomes, after transposition,

$$\left(1 - \frac{V^2}{c^2}\right)\varphi_{xx} + \varphi_{yy} + \varphi_{zz} = 0 \qquad (2)$$

in which $\frac{V}{c}$ is the Mach number M. The problem is now the mathematical one of finding a solution of equation (2) which agrees with the normal boundary velocity imparted by the airfoil. When the thin airfoil as specified is used, it is found sufficient to replace the actual boundary condition by an equivalent condition on the vertical velocity w in the chord plane; that is,

$$(w)_{z=0} = V\frac{dz}{dx}$$

where $\frac{dz}{dx}$ is the slope of the airfoil surface. It is important to note that the sliding component of the airfoil surface imparts no motion to the fluid since the fluid is frictionless. The error made in the equivalent boundary condition at $z = 0$ becomes appreciable only at distances of the order of one wing thickness from the edge. The pressure distribution over the airfoil surface may likewise be taken as the pressure in the chord plane and is obtained from the well-known formula for the pressure in a sound wave

$$\Delta p = -\rho\frac{\partial\varphi}{\partial t}$$

or, in steady flow

$$\Delta p = -\rho V \frac{\partial \varphi}{\partial x}$$

from which

$$\frac{\Delta p}{q} = -2\frac{u}{V}$$

Thus far, nothing has been said about subsonic- or supersonic-flight velocities. This distinction arises in equation (2) and in the form of its solutions when $M \gtrless 1$.

Except for this distinction, variations of M are of no consequence mathematically since they can be represented by an equivalent change in the scale of x relative to the other coordinates. This change of scale is known as the Prandtl-Glauert transformation and is given as

$$x' = \frac{x}{\sqrt{1 - M^2}}$$

or

$$x' = \frac{x}{\sqrt{M^2 - 1}}$$

The formula to be used depends on whether the flight velocity is subsonic or supersonic. In the latter case, the significance of the transformation is easily seen, since this transformation serves to maintain the correct inclination of the Mach waves to the line of flight at different speeds. It should be noted that the sudden transition of the differential equation from the elliptic to the hyperbolic type at $M = 1.0$ is a feature of the steady-flow equation (equation (2)) and does not, of course, arise in connection with equation (1).

The essential features of the steady flow at subsonic or supersonic speeds can then be ascertained from solutions of the reduced or normalized equations. For $M = 0$,

$$\varphi_{xx} + \varphi_{yy} + \varphi_{zz} = 0 \qquad (3)$$

and for $M = 1.41$,

$$\varphi_{xx} - \varphi_{yy} - \varphi_{zz} = 0 \tag{4}$$

As may be shown by direct differentiation, equations (3) and (4) possess the primary solutions

$$\varphi = f(\alpha x + \beta y + \gamma z)$$

where α, β, and γ are quantities determined so that for equation (3)

$$\alpha^2 + \beta^2 + \gamma^2 = 0$$

and so that for equation (4)

$$\alpha^2 - \beta^2 - \gamma^2 = 0$$

The cylindrical flow field, which is the basis of the two-dimensional or wing section theory, is obtained by specializing the primary solution to the two coordinates x and z. In this case for equation (3) $\alpha = 1.0$ and $\gamma = i$; and for equation (4) $\alpha = 1.0$ and $\gamma = 1.0$ so that the general solutions for the cylindrical or two-dimensional flow field become

$$\varphi = f(x \pm iz)$$

or

$$u = f'(x \pm iz)$$

$$w = \pm iu$$

The general solution is the basis of the Munk theory, as well as the more exact wing section analyses which depend on the theory of functions of a complex variable. At supersonic speeds the corresponding solutions are

$$\varphi = f(x \pm z)$$

or

$$u = f'(x \pm z)$$

$$w = \pm u$$

This latter form of solution, which represents a plane sound wave of arbitrary intensity at 45° to the normalized coordinate axes, is the basis of the Ackeret theory.

The general form of flow field given by solutions of the two foregoing types is illustrated in figure 1. The sketch on the left-hand side is the familiar subsonic streamline pattern for a symmetrical biconvex wing section. In the subsonic pattern the velocity and pressure disturbances diminish uniformly with distance and in the case of steady flow the field possesses a fore and aft symmetry which results in no pressure drag or wave drag. The sketch on the right-hand side (fig. 1) illustrates the marked difference in streamline pattern that arises when the crosswise velocity of the cylindrical field is supersonic. In this case the phase relation of u and w is shifted (from 1 to i) and the pressure distribution is antisymmetric, resulting in a wave drag. This drag appears as the energy in the plane sound waves emanating from the airfoil. The change from subsonic to supersonic type of flow field arises when the rate of progress of the flow pattern through the still fluid exceeds the velocity of sound. With cylindrical flow, the field is not affected by an axial velocity of the cylinder and the pattern progresses at a rate determined only by the crosswise motion of the cylinder. Hence, the subsonic type of flow may persist on a yawed wing even though the flight velocity is supersonic. (See reference 2.)

The sketch in the lower part of figure 1 represents a cross section of a conical flow field of the type originated by Busemann. The particular case used for illustration herein is the flow produced by a flat plate of triangular plan form moving point foremost at a small angle of attack (fig. 2). The Mach cone originates, of course, at the apex of the triangle and the field inside this cone is geometrically the same in all downstream cross sections except for an expansion in scale along the x-axis. The conical flow field may be obtained by the superposition of primary solutions of the form

$$u = F(\alpha x + \beta y + \gamma z)$$

If $\mu = e^{i\theta}$, then the solution

$$u = F\left[-2\mu x + (1 + \mu^2)\gamma + i(1 - \mu^2)z\right]$$

represents a plane sound wave at an angle θ to the y–, z–axes. Superposition of such waves of strength $f'(\mu)$ from $\theta = 0$ to $\theta = 2\pi$ results in a solution analogous to Whittaker's solution; that is,

$$u = \oint f'(\mu)\, F\left[-2\mu x + (1 + \mu^2)y + i(1 - \mu^2)z\right] d\mu$$

The quantity $-2\mu x + (1 + \mu^2)y + i(1 - \mu^2)z$ may be factored into $(\mu - \epsilon)\left(\mu - \frac{1}{\epsilon}\right)(y - iz)$ where

$$\epsilon = \frac{y + iz}{x + \sqrt{x^2 - y^2 - z^2}}$$

The general solution for 0^o is obtained when F is replaced by log; that is,

$$u = \oint f'(\mu)\, \log\left[(\mu - \epsilon)\left(\mu - \frac{1}{\epsilon}\right)(y - iz)\right] d\mu$$

$$= \oint f(\mu)\left[\frac{1}{\mu - \epsilon} + \frac{1}{\mu - \frac{1}{\epsilon}}\right] d\mu$$

$$= 2\pi i\left[f(\epsilon)\right]$$

if the contour does not include $\frac{1}{\epsilon}$ and if $\oint f(\mu)\, d\mu = 0$ or, in other words, if f is an analytic function (see reference 3).

If the flight velocity is subsonic, the argument ϵ is replaced by $\frac{y + iz}{x + \sqrt{x^2 + y^2 + z^2}}$. The latter solution was given by W. F. Donkin in 1857 (see reference 4). In either case the form of the argument shows an essential similarity to an expanding cylindrical field (see reference 5). In fact, for the slender conical field, where $y^2 + z^2$ may be neglected in comparison with x^2, the argument becomes simply $\frac{y + iz}{2x}$.

Although no analytic function of ϵ which removes the distortion of the conical field relative to the cylindrical field can be found, it is possible to transform the field in such a way that the distortion is removed in the neighborhood of the airfoil in the plane $z = 0$. The desired transformation is obtained from the fact that

$$\frac{y + iz}{x} = \frac{2\epsilon}{1 + \epsilon\bar{\epsilon}}$$

Since $\epsilon\bar{\epsilon}$ approaches ϵ^2 near $z = 0$, the analytic variable

$$z = \frac{2\epsilon}{1 + \epsilon^2}$$

will approach $\frac{y + iz}{x}$ in the neighborhood of the chord plane inside the Mach cone. The new variable z greatly simplifies the boundary conditions inasmuch as the Mach cone is transformed into the positive and negative branches of the real axis outside ± 1 and the interior of the Mach cone is mapped into the whole plane. Figure 3 illustrates the effect of this change of variable.

The relation between u and w in the conical field is found from the conditions for irrotational flow; that is,

$$\frac{\partial w}{\partial x} = \frac{\partial u}{\partial z}$$

In terms of the variable ϵ

$$dw = \frac{i}{2}\left(\epsilon - \frac{1}{\epsilon}\right) du$$

or in terms of the variable z

$$w = -i\int \frac{\sqrt{1 - z^2}}{z}\, du$$

It is interesting to note that the condition for a flat airfoil surface in two-dimensional flow holds also for the conical field. In the two-dimensional flow $w = iu$ and the condition for a flat surface (constant w) is simply that the function adopted for u has no imaginary part over the region of the real axis covered by the airfoil (assuming that the real

solutions for u and w are used). In the conical flow, the quantity $\frac{\sqrt{1 - z^2}}{z}$ is a real number over that part of the real axis between ± 1 so that in this region the condition is unchanged.

Figure 4 illustrates the solution for the flat triangular airfoil at a small angle of attack as obtained by H. J. Stewart and M. I. Gurevich (references 6 and 7) and also by Bartels and LaPorte (reference 8). The constant value of w, denoted by w_c, must be calculated to give the relation between the lifting pressure and the angle of attack. The quantity m is the cotangent of the sweepback angle for $M = \sqrt{2}$; for other Mach numbers $m = \sqrt{M^2 - 1}$ times the cotangent of the sweep angle.

Other wing forms generally require the superposition of conical and cylindrical fields. Thus, in the case of the rectangular wing of wedge-shaped section (fig. 5) the field is cylindrical up to the Mach cone originating at the corner of the wing and is conical inside this cone.

The solution for the flat triangular wing can be used as a starting point to obtain the pressure distribution over a sweptback wing. In this process, which is explained in references 9 and 10, the desired wing plan form is, in effect, cut out of the triangle by the superposition of conical fields which cancel the lifting pressure over portions of the triangular area extending beyond the desired outline. The process is simplified in the supersonic case by the limited zone of influence of the superimposed fields. The lifting pressure distribution over a wing with 63° sweepback is shown in figure 6. It will be noted that the lift distribution over the foremost section is flat, as in the Ackeret theory, while farther along the span the subsonic type of pressure distribution appropriate to the reduced crosswise velocity appears. In this example the wing tips were cut off in a direction parallel to the air stream and, in such cases, the lift drops sharply to zero in the region behind the Mach cone from the tip corner.

The solution for a sweptback wing having curvilinear sections cannot be obtained by the superposition of a finite number of conical fields but requires an integration. Such a case is illustrated in figure 7, which shows the pressure distributions at several sections of a symmetrical biconvex wing at 0° angle of attack. This example serves to illustrate the change in proceeding from subsonic to supersonic speed. Since the angle of sweepback is large, the change is not pronounced and occurs primarily at the center sections of the wing. It is interesting to note that the center sections of the wing have a pressure drag at subsonic speeds.

REFERENCES

1. Busemann, A.: Infinitesimal Conical Supersonic Flow. NACA TM No. 1100, 1947.

2. Jones, Robert T.: Wing Plan Forms for High-Speed Flight. NACA TN No. 1033, 1946.

3. Whittaker, E. T., and Watson, G. N.: A Course of Modern Analysis. Fourth ed., Cambridge Univ. Press (London), 1927, p. 403. (Reprinted 1940.)

4. Bateman, H.: Partial Differential Equations of Mathematical Physics. American ed., Dover Publications, 1944, pp. 357-358.

5. Jones, Robert T.: Properties of Low-Aspect-Ratio Pointed Wings at Speeds below and above the Speed of Sound. NACA Rep. No. 835, 1946.

6. Gurevich, M. I.: Lift Force of an Arrow-Shaped Wing. Appl. Math. and Mech. (Moscow), vol. X, no. 4, 1946, pp. 513-520.

7. Stewart, H. J.: The Lift of a Delta Wing at Supersonic Speeds. Quarterly Appl. Math., vol. IV, no. 3, Oct. 1946, pp. 246-254.

8. LaPorte, O., and Bartels, R. C. F.: An Investigation of the Exact Solutions of the Linearized Equations for the Flow past Conical Bodies. Bumblebee Rep. No. 75, Univ. Michigan, Eng. Res. Inst., Feb. 1948.

9. Cohen, Doris: The Theoretical Lift of Flat Swept-Back Wings at Supersonic Speeds. NACA TN No. 1555, 1948.

10. Lagerstrom, P. A.: Linearized Supersonic Theory of Conical Wings. J.P.L. Progress Rep. No. 4-36, Calif. Inst. Tech., 1947.

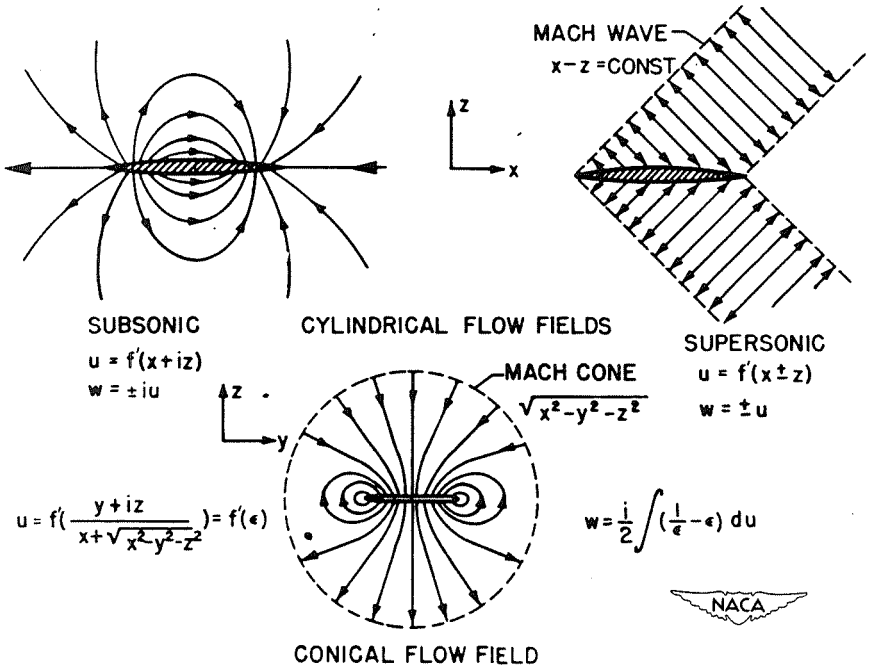

Figure 1.- General form of cylindrical and conical flow fields.

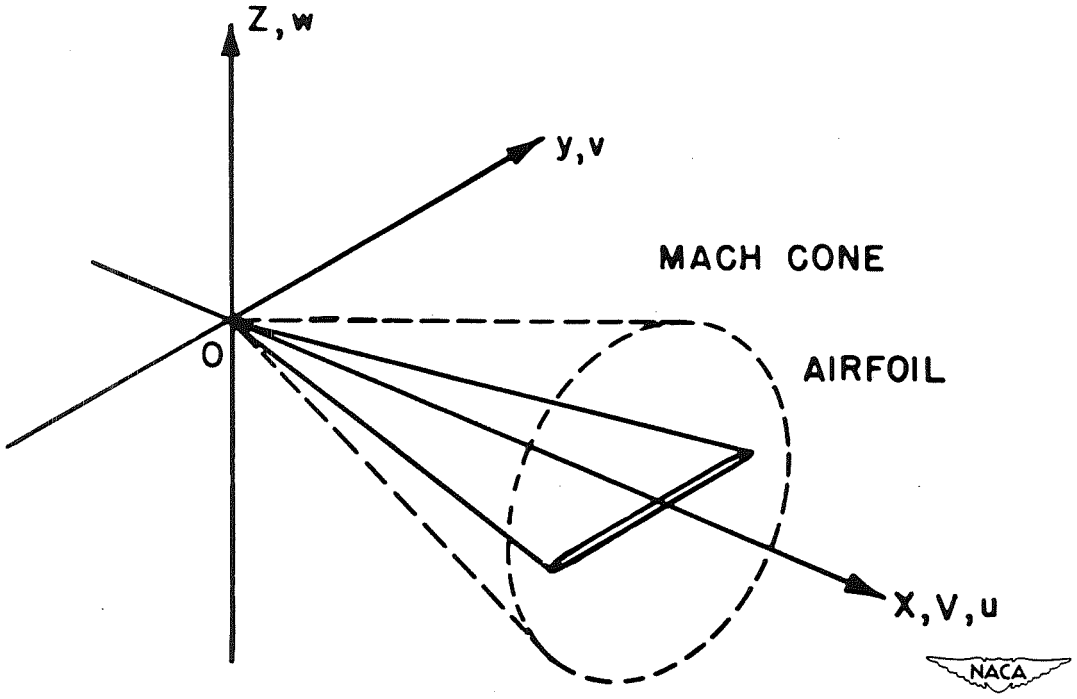

Figure 2.- Flat plate of triangular plan form in conical flow field.

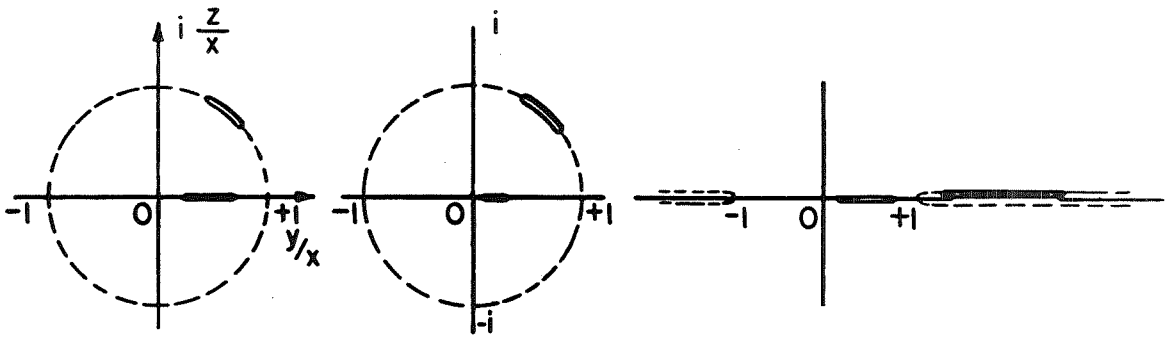

Figure 3.- Transformation of flow field to the $z = 0$ plane.

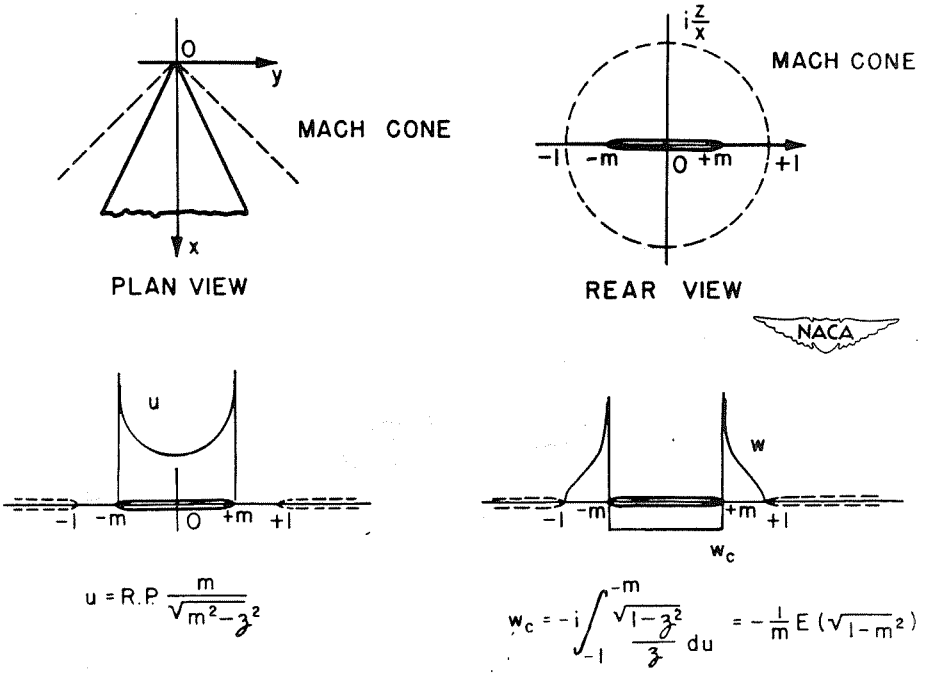

Figure 4.- Solution for flat triangular airfoil at small angle of attack.

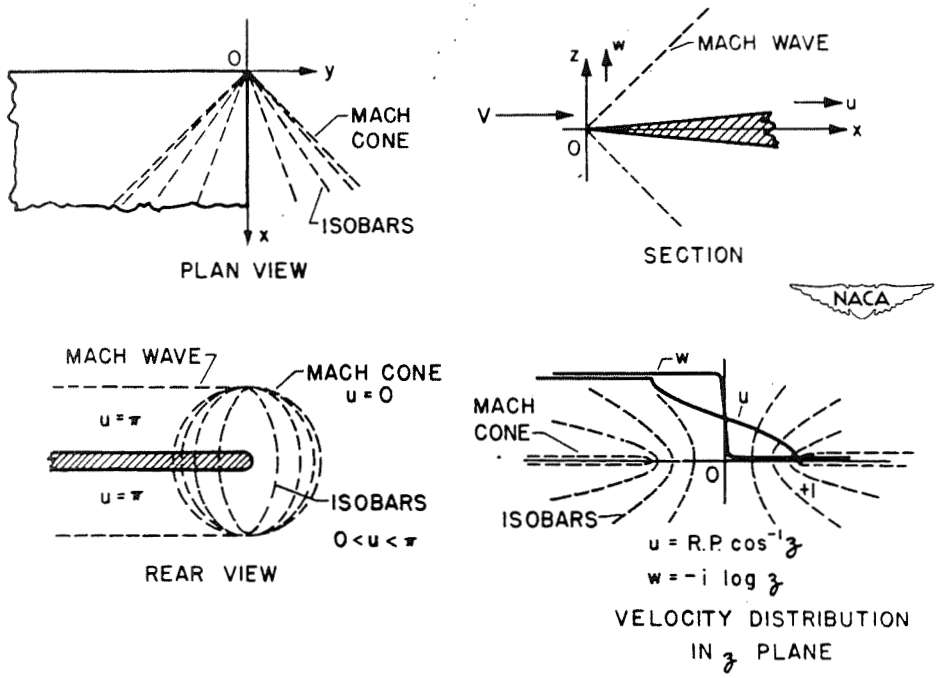

Figure 5.- Cylindrical and conical flow fields about a rectangular wing having a wedge-shape section.

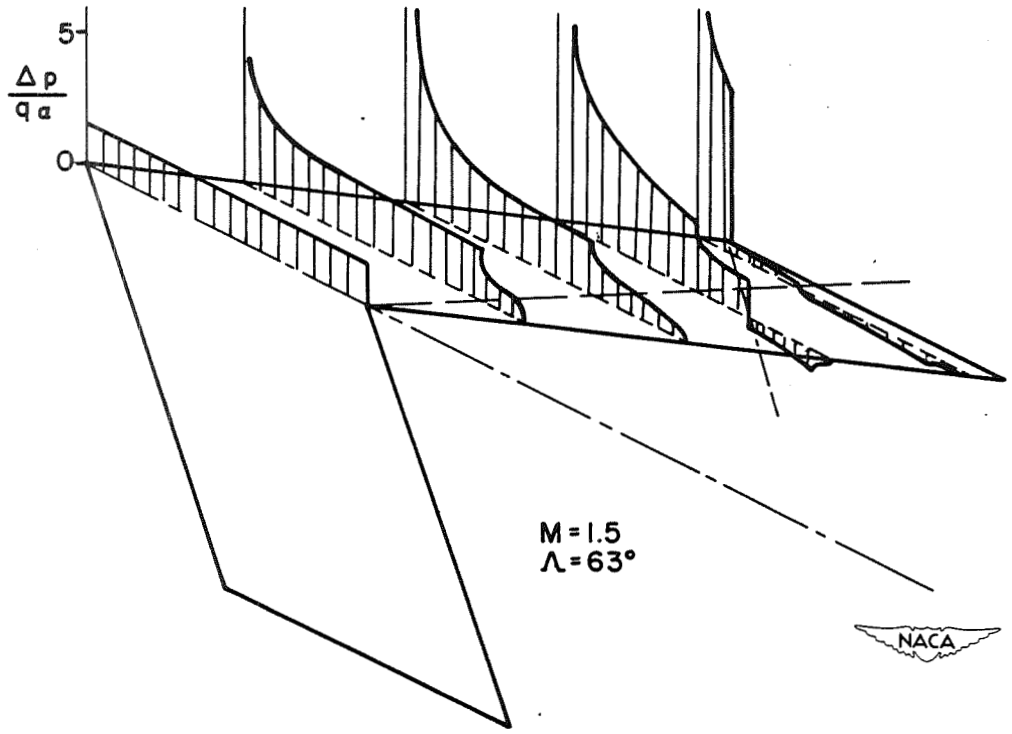

Figure 6.- Lifting pressure distribution over a wing with 63° sweepback.

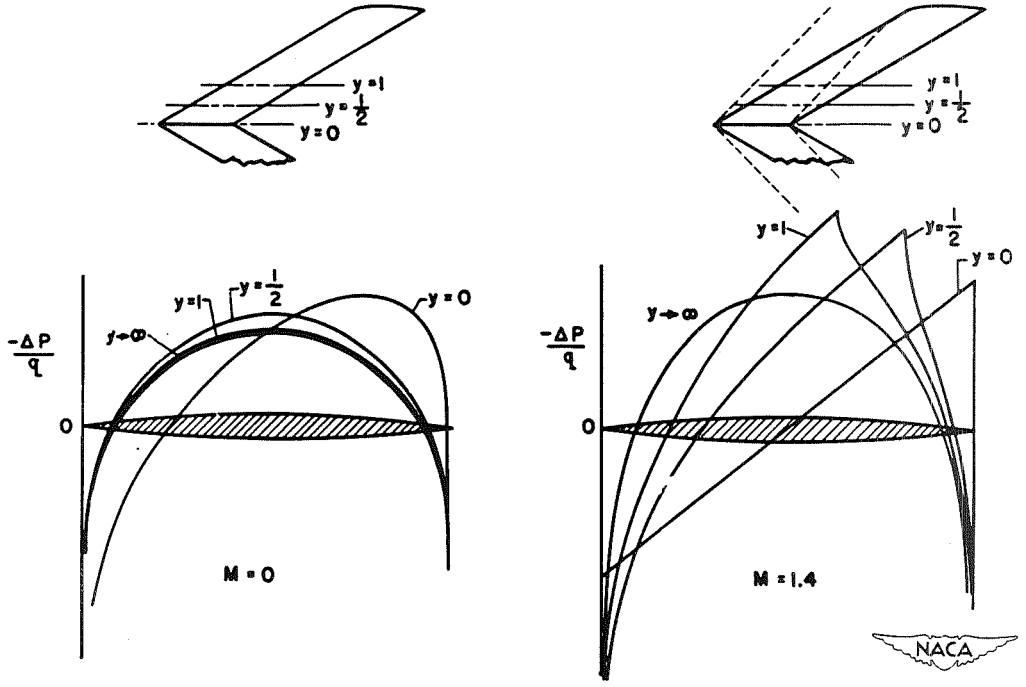

Figure 7.- Pressure distributions at several sections of a symmetrical biconvex wing at 0° angle of attack.

D/13

Preceding page blank

THE USE OF SOURCE AND SINK CONCEPTS IN THE CALCULATION OF WING CHARACTERISTICS AT SUPERSONIC SPEEDS

By Clinton E. Brown

Langley Aeronautical Laboratory

The calculation of wing characteristics within the linear theory is performed by a superposition of known solutions of a more elementary nature. In incompressible flow the use of source and vortex solutions has proven very useful, perhaps because the elementary solutions themselves have been easy to visualize; certainly the idea of building up a body of revolution by a continuous distribution of sources and sinks is a natural one. At supersonic speeds the use of sources, doublets, and vortices can lead to many simplifications and give the student a physical picture of what is occurring in the flow. Von Kármán and Moore (reference 1) were first to introduce source and sink concepts to supersonic aerodynamics when they calculated the flow about bodies of revolution by an axial distribution of sources. In 1935, at the Volta Congress, Von Kármán (reference 2) suggested the use of surface source distributions in the calculation of wing characteristics and thus laid the ground work for much of the present work.

Unfortunately, the spherical symmetry of incompressible source flow is lost as the velocity of the stream becomes greater than the speed of sound, as may be seen by comparison of the potential function ϕ of a source in incompressible flow and supersonic flow:

$$\phi_{M=0} = \frac{K}{\sqrt{x^2 + y^2 + z^2}} \tag{1}$$

and

$$\phi_{M>1} = \frac{K}{\sqrt{x^2 - (M^2 - 1)(y^2 + z^2)}} \tag{2}$$

where K is the strength of the source and M is Mach number of the undisturbed stream. Prandtl (reference 3) has given a very good derivation of the potential function of a supersonic source system that uses a superposition of sources fixed in the fluid but varying in strength with time. Consider a body moving at supersonic speed through a compressible fluid originally at rest. The motion produced must satisfy a differential equation which, upon restriction to motions that are small

compared with the velocity of sound, becomes the wave equation in three dimensions, well-known in mathematical physics. That is,

$$\frac{1}{c^2}\frac{\partial^2\phi}{\partial t^2} = \frac{\partial^2\phi}{\partial x^2} + \frac{\partial^2\phi}{\partial y^2} + \frac{\partial^2\phi}{\partial z^2} \tag{3}$$

where c is the speed of sound.

The solution of this equation representing a fixed source of fluid is also known and more complicated solutions may be built up by distributing sources in the fluid. In order to get to the solution for a body or disturbance moving through the fluid, Prandtl assumes the x-axis or flight axis to be covered with sources, each source being fixed and having strength vary with time. (See fig. 1.) As a given disturbance moving along the z-axis reaches any source, that source starts to flow, flows according to a common law, and ceases to flow when the disturbance has passed. The potential at any point (x,y,z) in the fluid is then made up of the contribution from each source in accordance with the known expression for the potential function of the source flow. This expression is given in figure 1 for a source located at a point on the x-axis and is as follows:

$$d\phi = -\frac{f\left(t - \tau - \frac{R}{c}\right)}{R}\,dx'$$

where t is the time, τ is the time at which the source started to flow, c is the speed of sound, R is the distance between the source and field point, and f is the law which governs the strength of the source flow. As no disturbance can be produced at the point (x,y,z) until the sound or pressure wave reaches the field point, the potential is only affected by those sources, the initial waves of which have already reached the field point at the time t. It should be noticed that lines from the initial point of the disturbance tangent to the wave fronts from the sources form the Mach cone or region of influence of the disturbance. The potential will then be expressed as an integral and will be a function of the space coordinates and time. If, however, the observation point is allowed to move along at the same speed as the disturbance, the time element disappears, and finally an integral expression is obtained for a system of sources moving at a supersonic Mach number M. The following expression was used by Von Kármán and Moore (reference 1) in computing the flow over slender bodies of revolution at supersonic speeds:

$$\phi = -2\int_{a_1}^{a_2} \frac{f(x_1)\,dx_1}{\sqrt{(x - x_1)^2 - (M^2 - 1)(y^2 + z^2)}} \tag{4}$$

In this equation, the field point is at (x,y,z) and the position on the axis x_1 may be considered to be the location of a supersonic point source having as its potential field the expression of equation (2).

For wing problems, however, lifting surfaces, and therefore surface source distributions, are of interest. The potential at any point in the space will then be made up of the contributions from sources distributed over a region of the xy-plane and may be written as a double summation or integral:

$$\phi_S = -\int_{b_1}^{b_2}\int_{a_1}^{a_2} \frac{g(x_1,y_1)\,dx_1\,dy_1}{\sqrt{(x-x_1)^2 - (M^2-1)\left[(y-y_1)^2 + z^2\right]}} \tag{5}$$

In this expression the quantity $g(x_1,y_1)$ is the expression describing the source intensity at the point (x_1,y_1). Care must be taken in choosing the limits in the integral so that the area of integration includes only those sources which can effect the field point, that is, the sources which contain the field point in their Mach cones.

The velocity component normal to the xy-plane containing the sources is obtained by differentiating the potential function with respect to z. Puckett (reference 4) and others have shown that this normal velocity at a point on the surface $z = 0$ is affected only by the sources in the immediate vicinity of the point and is given by the expression

$$\underset{\pm z \to 0}{v_z} = \frac{\partial \phi}{\partial z} = \pm \pi g(x,y) \tag{6}$$

It is seen that the normal velocity is discontinuous at the surface and of magnitude proportional to the local-source strength. This result is not surprising if it is remembered that the source solutions used in the previous derivation produced a radial flow and therefore could not produce a velocity normal to the plane containing the source except directly at the source itself.

At the surface, the slope of the streamlines is given to a first approximation by

$$\frac{v_z}{V_0} = \tan\theta \approx \theta \tag{7}$$

The source distribution over the surface then produces a splitting of the flow streamlines and is therefore capable of representing the effect of thickness on a wing plan form. For example, on a wing of given plan form the surface slopes are known and, hence, from equations (6) and (7) the source distribution is known. The potential function for the wing can therefore be calculated by inserting for $g(x_1,y_1)$ in equation (5) the expression obtained from equations (6) and (7) to obtain

$$\phi_S - = \frac{V_0}{\pi}\int_{b_1}^{b_2}\int_{a_1}^{a_2} \frac{\theta(x_1,y_1)dx_1dy_1}{\sqrt{(x-x_1)^2-(M^2-1)\left[(y-y_1)^2+z^2\right]}} \tag{8}$$

Once the potential function is known, it is possible to obtain the velocities by differentiation. The method for calculating the pressure distribution and drag of symmetrical wings at zero angle of attack is thus direct and involves only the solution of definite integrals. This method has numerous applications in calculating the drag of supersonic wings. Rectangular wings, triangular wings, and tapered and untapered sweptback wings having various airfoil sections have been calculated and are available.

As has been seen, a source distribution produces a parting of the flow and hence an identical flow pattern above and below the xy-plane. Sources alone, therefore, will not produce a lifting force on a body.

What is needed is a potential function which is discontinuous at the plane of the wing and which will, therefore, produce a difference of pressure or lift on the wing. If the vertical velocity produced by a source distribution is used as a new potential function, this type of potential function can be obtained because, as demonstrated previously, the normal velocity is discontinuous at the plane of the sources. The new potential function, which is the derivative of a source potential, is called a doublet potential because it can be formed by an operation on a double sheet of positive and negative sources. The doublet potential may be written now as

$$\phi_D = \frac{\partial \phi_S}{\partial z} = \frac{\partial}{\partial z}\left\{-\int_{b_1}^{b_2}\int_{a_1}^{a_2} \frac{k(x_1,y_1)dx_1dy_1}{\sqrt{(x-x_1)^2-(M^2-1)\left[(y-y_1)^2+z^2\right]}}\right\} \tag{9}$$

and by referring again to equation (6) it is seen that the potential at the surface $z = 0$ is

$$\underset{\pm z \to 0}{\phi_D} = \pm \pi k(x,y) \tag{10}$$

where $k(x,y)$ is the doublet- or source-distribution function. At the surface, the x-, y-, and z-component velocities may be written as follows:

$$\underset{\pm z \to 0}{v_x} = \frac{\partial \phi}{\partial x} = \pm \pi \frac{\partial k}{\partial x} \tag{11}$$

$$\underset{\pm z \to 0}{v_y} = \frac{\partial \phi}{\partial y} = \pm \pi \frac{\partial k}{\partial y} \tag{12}$$

$$v_z = \frac{\partial \phi}{\partial z} = \frac{\partial^2}{\partial z^2} \left\{ -\int_{b_1}^{b_2} \int_{a_1}^{a_2} \frac{k(x_1,y_1)\,dx_1\,dy_1}{\sqrt{(x - x_1)^2 - (M^2 - 1)\left[(y - y_1)^2 + z^2\right]}} \right\} \tag{13}$$

Inasmuch as the pressure is proportional to the x-component velocity, it can be seen that there is a difference in pressure or lift wherever $\frac{\partial k}{\partial x}$ exists. The z-component of the disturbance velocity is found to be continuous at the surface and the streamlines above and below the surface are therefore deflected in the same direction. The doublet distribution is thus capable of representing the effects of camber and angle of attack of wings.

In problems in which the camber or angle of attack is given and the pressure distribution is required, the doublet-distribution method is rather difficult to use because the doublet distribution function is not known but is beneath the integral signs, as in equation (13). The camber or angle of attack can give the value of the vertical velocity v_z, but the function $k(x_1,y_1)$, the doublet distribution, is not known. This type of equation, called an integral equation, is often quite difficult to evaluate.

When the pressure distribution is given, the potential on the surface and, therefore, the doublet distribution can be calculated directly. The camber can then be obtained by calculating the vertical velocity at each point. The difficulty of solving an integral equation is therefore not met in this case.

In order to illustrate briefly the manner in which camber lines may be calculated, consider a uniformly loaded triangular wing. The pressure coefficient may be prescribed as a constant A and, therefore, from the pressure equation, v_x is constant; that is,

$$\frac{\Delta p}{q} = -\frac{2v_x}{V_0} = A \tag{14}$$

Inasmuch as the potential is the integral of the velocity v_x by definition, the potential on the surface becomes

$$\phi_{z=0} = \int v_x \, dx = -\frac{AV_0}{2}\left[x + F(y)\right] \tag{15}$$

At the leading edge, however, $\phi = 0$ and, therefore, the unknown function $F(y)$ may be evaluated as follows:

$$x = |y| \tan \Lambda \tag{16}$$

hence

$$F(y) = -|y| \tan \Lambda \tag{17}$$

where Λ is angle of sweepback.

Since the surface potential distribution and doublet distribution are equal except for a constant factor π, the potential of the complete flow is given by the doublet distribution as

$$\phi = \frac{\partial}{\partial z}\left\{\int_{b_1}^{b_2}\int_{a_1}^{a_2} \frac{AV_0}{2\pi} \frac{\left(x_1 - |y_1| \tan \Lambda\right) dx_1 dy_1}{\sqrt{(x - x_1)^2 - (M^2 - 1)\left[(y - y_1)^2 + z^2\right]}}\right\} \tag{18}$$

This integral can now be evaluated and, from the potential function obtained, the vertical velocity at the surface may be computed; thus the camber lines can be found. The camber on such a wing has been given already by Jones in reference 5.

In the solution of the integrals used in this paper the order of integration and differentiation is found to be quite important. The solutions are difficult because the elementary solution is not defined at its Mach cone. Hadamard (reference 6) has treated such problems, however, and Heaslet and Lomax (reference 7) have applied his procedure to the solution of wing problems.

The foregoing method of doublet distributions can be tied in with the familiar vortex-theory concept of incompressible flow. Consider a three-dimensional wing represented by a certain doublet or surface-potential distribution. The circulation Γ about a chordwise strip can be computed in the usual manner by integrating the velocities along a line directly above and below the surface. The circulation thus becomes

$$\Gamma = \int_{L.E.}^{T.E.} \left(v_{x_u} - v_{x_l} \right) dx = \phi_u - \phi_l \tag{19}$$

The integration is complete at the trailing edge because the x-component-velocity difference vanishes at this point. The potential difference in the wake becomes, then, only a function of y. The pressure on the strip is given by the relation

$$\Delta p = - \rho V_0 v_x \tag{20}$$

The lift on the strip of width dy is then

$$\frac{dL}{dy} = \int_{L.E.}^{T.E.} (\Delta p_l - \Delta p_u) dx = \rho V_0 \Gamma \tag{21}$$

This equation shows that the Joukowski hypothesis is valid also in the supersonic range of flight and the familiar concepts of vortex flow must apply. It will be interesting to show how a horseshoe vortex can be found

by a doublet distribution. In the sketch, consider the area in the xy-plane enclosed by the straight lines to be uniformly covered by doublets.

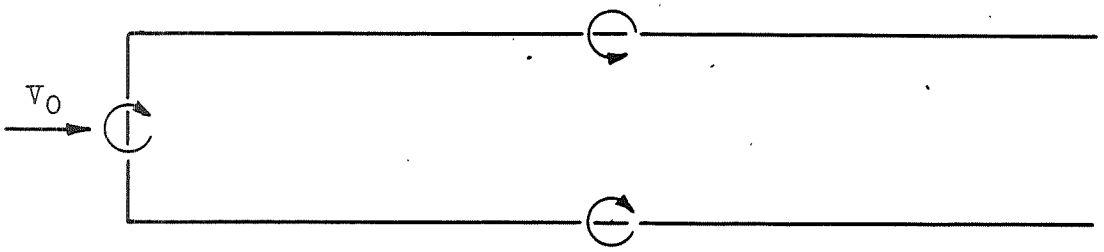

The surface potential in this region will also be constant as discussed previously. The circulation computed along any circuit enclosing the boundary of the region will then be a constant which is proportional to the strength of the doublet distribution. The doublet distribution is therefore seen to be equivalent to a single vortex line along the boundary of the region considered. This result is directly analogous to that found in incompressible flow; however, the induced velocity fields in the two cases are different except at a large distance behind the lifting line where they become the same. Any wing and its wake may be represented by a vortex distribution in the usual manner, although for supersonic wing problems the lifting-line theory is unsatisfactory because of the discontinuities present in the solutions which make the assumptions used in lifting-line theory very poor indeed. The alternative is, of course, to proceed to a surface distribution of vortices or doublets in which case the objections are overcome. Calculations of this type have been performed by Schlichting. (See reference 8.) At a great distance behind the wing, the change in potential with respect to the flight direction approaches zero and the differential equation of motion

$$(M^2 - 1)\frac{\partial^2 \phi}{dx^2} = \frac{\partial^2 \phi}{dy^2} + \frac{\partial^2 \phi}{dz^2}$$

approaches Laplace's equation in two dimensions involving only the cross-flow velocities. The downwash produced by the wing is then seen to be affected by only the trailing vortex system as in incompressible flow. (See reference 9.) It might be supposed that the induced drag of the wing could be calculated from the energy in the wake; however, an additional amount of energy due to lift is found to be transported to infinity by the sound waves produced at the wing. (See reference 10.) The calculation of the induced drag for certain cases requires the use of second-order terms, which were originally dropped in the analysis. The use of such terms is, therefore quite a controversial subject. Available information on the subject, however, indicates that a procedure in which these terms are included is at least qualitatively correct.

Puckett and others have demonstrated that under certain conditions the flow over lifting surfaces may be obtained by source distributions instead of doublet distributions which involve integral equations. Such conditions arise when the flow component normal to a leading edge is supersonic; then, the two sides become independent. This fact is illustrated by the first sketch of figure 2. The region of influence of a disturbance on one side of the triangular wing does not intersect the leading edge; hence, the effect of the disturbance is not felt on the opposite side. The pressure distribution on the surface for the case in which the opposite surface forms a wedge is the same as that for the case in which the opposite side is coincident with the original surface. The potential can therefore be found for both cases by the source-distribution method.

The second sketch in figure 2 indicates that when the flow component normal to the leading edge is subsonic, the two surfaces are not independent, and the source distribution method cannot be used without further consideration. Evvard (reference 11) has found a very ingenious way to extend the source-distribution method for calculating lift to those cases in which the leading-edge components of velocity become subsonic. It is assumed that the wing leading edge is extended until the normal component of flow is supersonic and the two sides become independent. The problem is then to determine the proper source distribution over the wing extension that makes the potential difference in this region zero. In figure 2 the region on the wing extension affecting the field point shown is labeled A. Evvard discovered that the effect of the proper source distribution over this area was equal but opposite in sign to the effect produced by the sources in region B. The potential at the field point can therefore be calculated by performing an integration of the sources over region C. Problems involving the use of two interacting wing extensions are no longer as simple but can still be done. The aforementioned method is indeed of great utility as it is very simple to apply and obviates the necessity for solving integral equations.

The theoretical work discussed herein must be carefully checked experimentally before it can be trusted to any great extent. At this time it is too early to set down the limits of applicability, such as the Mach number range, maximum angle of attack, or thickness ratios; however, the fact that the theory is of great value cannot be questioned inasmuch as the results provide analytic expressions from which trends and the effects of variation of parameters may be found.

REFERENCES

1. Von Kármán, Theodor, and Moore, Norton B.: Resistance of Slender Bodies Moving with Supersonic Velocities with Special Reference to Projectiles. Trans. A.S.M.E., vol. 54, no. 23, Dec. 15, 1932, pp. 303–310.

2. Von Kármán, Th.: The Problem of Resistance in Compressible Fluids. GALCIT Pub. No. 75, 1936. (From R. Accad. d' Italia, cl. sci. fis., mat. e nat., vol. XIV, 1936.)

3. Prandtl, L.: Theorie des Flugzeugtragflügels im zusammendrückbaren Medium. Luftfahrtforschung, Bd. 13, Nr. 10, Oct. 12, 1936, pp. 313–319.

4. Puckett, Allen E.: Supersonic Wave Drag of Thin Airfoils. Jour. Aero. Sci., vol. 13, no. 9, Sept. 1946, pp. 475–484.

5. Jones, Robert T.: Estimated Lift–Drag Ratios at Supersonic Speed. NACA TN No. 1350, 1947.

6. Hadamard, Jacques: Lectures on Cauchy's Problem in Linear Partial Differential Equations. Yale Univ. Press (New Haven), 1923.

7. Heaslet, Max A., and Lomax, Harvard: The Use of Source–Sink and Doublet Distributions Extended to the Solution of Arbitrary Boundary Value Problems in Supersonic Flow. NACA TN No. 1515, 1948.

8. Schlichting, H.: Airfoil Theory at Supersonic Speed. NACA TM No. 897, 1939.

9. Lagerstrom, P. A., and Graham, Martha E.: Downwash and Sidewash Induced by Three–Dimensional Lifting Wings in Supersonic Flow. Rep. No. SM–13007, Douglas Aircraft Co., Inc., April 14, 1947.

10. Von Kármán, Theodore: Supersonic Aerodynamics – Principles and Applications. Jour. Aero. Sci., vol. 14, no. 7, July 1947, pp. 373–409.

11. Evvard, John C.: Distribution of Wave Drag and Lift in the Vicinity of Wing Tips at Supersonic Speeds. NACA TN No. 1382, 1947.

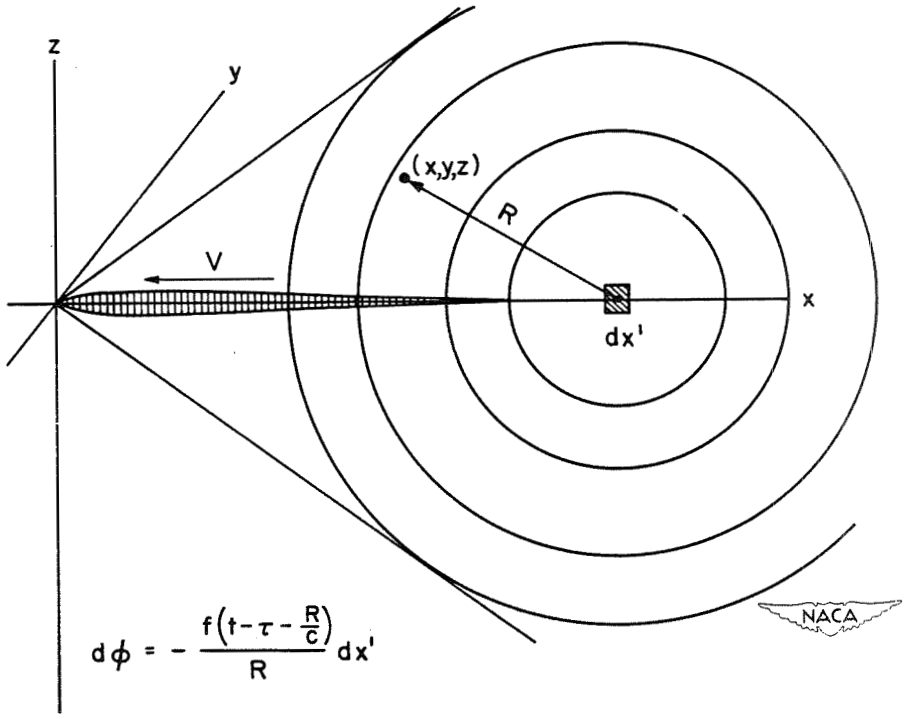

Figure 1.- Source system in motion.

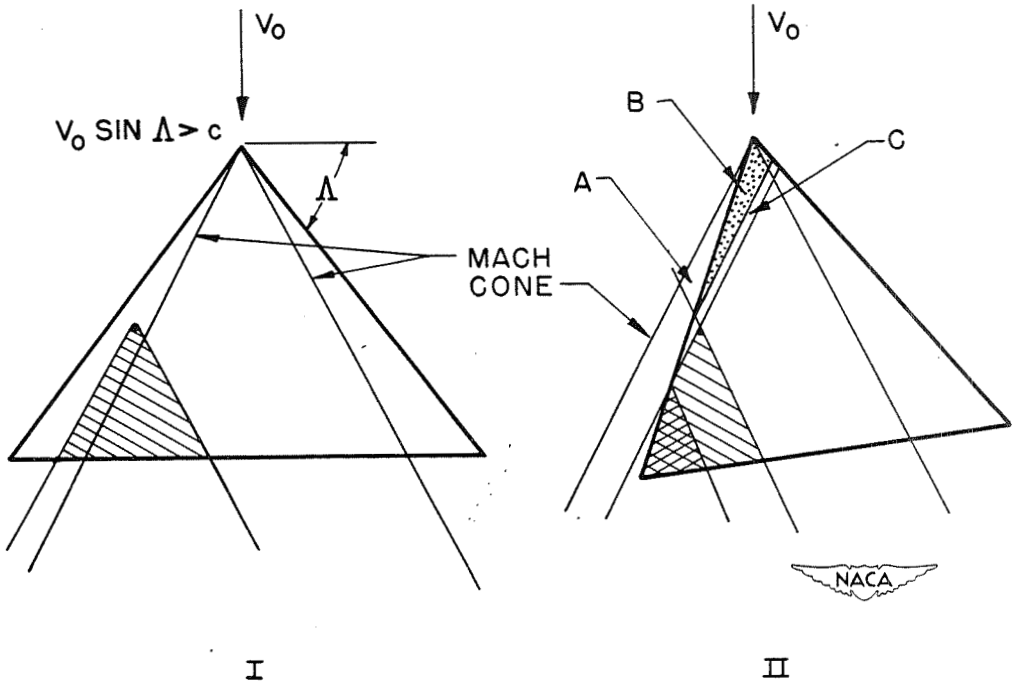

Figure 2.- Illustration of Evvard's method.

UNSTEADY LIFT IN HIGH-SPEED FLIGHT

By Harvard Lomax

Ames Aeronautical Laboratory

The problems discussed in this paper involve the initial time history of forces on a two-dimensional flat-plate wing section. The first of these problems is the calculation of the transient pressure on the flat plate starting from rest and continuing at a constant speed and angle of attack. This can correspond physically to a sudden angle-of-attack change. The second problem is the calculation of the transient pressure on the flat plate entering a sharp-edge gust. For large values of time, both of these solutions approach the more familiar steady-state value of the lift on the plate at a given angle of attack.

The problem involving the angle-of-attack change is the same as that studied by Wagner (reference 1) for the case of incompressible flow. In the present paper, this well-known solution is extended to include the effects of both subsonic and supersonic Mach numbers. This study shows that the effect of Mach number on the load distribution is entirely different at the beginning of the motion than at the end of the motion when the Prandtl-Glauert or Ackeret formula applies.

Previous studies have been made in the field of high-speed unsteady lift by Garrick and Rubinow (reference 2), and by Chang (reference 3).

The method of solution employed in this paper differs from that used by Garrick and Rubinow in their study of flutter in that emphasis is placed on the development of lift following a sudden unit change in angle of attack rather than on the lift of a harmonically oscillating wing. This unit-angle-of-attack method was used by Heaslet and Lomax (reference 4) and proceeds as follows: First, the basic partial differential equation is obtained and simplified to its linearized form; then a solution for a sudden "unit" displacement is found in terms of the pressure distribution; finally, since the basic equation has been linearized, these solutions for the unit displacement are superimposed with the result that the pressures on a flat plate undergoing any arbitrary motion can be found. The usefulness of the result is greatly increased by its ready adaptation to the operational methods used in similar problems by Jones (reference 5) and presented in detail by Churchill (reference 6).

The solutions which this type of analysis yields is given the name "indicial solutions." As an example, consider that the unit displacement is the angle of attack of the wing. This means by definition that α is zero for negative values of time and equal to unity for all positive values of time. The load distribution resulting from such a unit displacement is called the indicial angle-of-attack load. Similarly, the integrated value of this loading is called the indicial angle-of-attack lift.

Proceeding now in the manner which has been outlined, the basic partial differential equation is obtained. This governing equation used in the study of unsteady lift problems comes from a combination of the equations of motion, continuity, and state. The approximations used in reducing these equations to the linearized form suitable for analysis are simply that the induced velocities are small enough to be neglected in comparison with the free-stream velocity and that the velocity gradients are all of similar magnitude. These assumptions in simplifying the partial differential equation are consistent with those of thin airfoil theory in simplifying the boundary conditions - namely, that the boundary conditions be specified in the plane $Z = 0$ and that the tangent of the angle of attack be replaced by the angle. Such approximations result in an indeterminate error in the induced velocities of the solutions, so that for terms like the lift, velocity of sound, and entropy which can be expanded in terms of, say, the induced velocity u, only the lowest nonzero power of u should be used in the expansion.

The resulting linearized partial differential equation is the same as that studied by the various authors mentioned. The two-dimensional form of this equation for the perturbation velocity potential in terms of the space coordinates X', Z', the time t' and the free-stream velocity of sound a_o and Mach number M_o can be written as follows:

$$\left(1 - M_o^2\right) \frac{\partial^2 \Phi}{\partial X'^2} + \frac{\partial^2 \Phi}{\partial Z'^2} - \frac{2M_o}{a_o} \frac{\partial^2 \Phi}{\partial X' \, \partial t'} - \frac{1}{a_o^2} \frac{\partial^2 \Phi}{\partial t'^2} = 0 \quad . \quad . \quad . \qquad (1)$$

In such a form, it is rather formidable, but by use of the transformation

$$\left.\begin{aligned} X &= X' - M_o a_o t' \\ Z &= Z' \\ t &= a_o t' \end{aligned}\right\} \qquad (2)$$

it can be reduced to

$$\frac{\partial^2 \Phi}{\partial t^2} - \frac{\partial^2 \Phi}{\partial X^2} - \frac{\partial^2 \Phi}{\partial Z^2} = 0 \qquad (3)$$

the normalized form of the wave equation.

The wave equation, of course, has been extensively studied, since it is one of the most important equations of mathematical physics. Most of this study, however, has been directed toward problems in which the boundary conditions are given for $t = 0$. (See, for instance, reference 7.) In such cases both the function and the initial values of its derivatives must be specified in order that a unique solution can be obtained. This is the so-called Cauchy problem. In unsteady lift problems, on the other hand, the boundary values are known only in the plane $Z = 0$; that is, the slope of the lifting surface is specified for all values of time. This difference in orientation completely changes the nature of the problem. And, in fact, it can be shown that when boundary values are specified for $Z = 0$, a unique solution can be found, just as in Laplace's equation, by specifying only the derivative of the function. This same situation — that of having the data given in another than the classical $t = 0$ plane — arose in the study of three-dimensional supersonic lifting-surface problems and a rather complete discussion of it in that connection is given in reference 8.

This analogue with the supersonic lifting-surface problem can be quite useful in establishing the data necessary for the unsteady lift cases. In order to construct this analogy, however, it is first necessary to discuss the boundary values for some typical unsteady lift problems. Consider a wing at an angle-of-attack α starting suddenly from rest at $t = 0$. (See fig. 1.) In the X,t plane, this wing would sweep out a region shown as the shaded area in figure 1(a). It is to be remembered from the transformation given as equation (2) that the coordinate t represents true time t' except for the stretching factor a_o, and, for a given t, a change in the coordinate X represents a change in the true distance X'. Thus at $t = 0$, the shaded area extends from $X = 0$ one chord length back to $X = c_o$. At some later time, the wing will have moved in the negative X-direction to a new position such as the point A in figure 1(a). The trailing edge at such a time remains one chord length behind at the point C. The dash lines in the figure represent the traces of the characteristic cones. Physically, these lines represent the foremost and rearmost positions to which a pressure disturbance starting at their apex can travel in a given time. Thus a disturbance starting on the leading edge at $t = 0$ can be felt only between the points B and D when the wing has traveled so that its leading edge is at A. Hence, for a wing traveling at supersonic speeds, point A will fall to the left of the characteristic line and for a wing traveling at subsonic speeds it will fall to the right.

If the wing is to attain its unit angle of attack without rotation, then the boundary values are such that the vertical induced velocity is a constant over the entire shaded region of figure 1(a), and the loading is zero over the rest of the plane $z = 0$.

Compare these boundary conditions with those for a supersonic three-dimensional, flat-plate, lifting-surface problem. If the shaded region is thought of as a wing plan form, the problems are identical. The characteristic cones represent the familiar Mach cones; and since the dash lines have a 45° slope, the equivalent Mach number is $\sqrt{2}$. The wing in unsteady lift flying at supersonic speeds has for its equivalent a three-dimensional lifting surface with supersonic edges. The solution to such a lifting-surface problem is relatively simple to find. On the other hand, the wing in unsteady lift flying at subsonic speeds has for its equivalent a three-dimensional lifting surface with some subsonic edges. Although this complicates the problem considerably, still by methods such as those introduced by Evvard (reference 9), solutions can be found.

Another type of boundary-value problem is shown in figure 1(b). This figure represents a wing at zero angle of attack traveling at supersonic speeds entering a sharp-edge gust the front of which is situated along the line $X = 0$. The vertical induced velocity over the shaded region is a constant, the value of which is equal and opposite to the gust intensity, and is zero in the unshaded region between the t-axis and the trailing-edge trace. Over the rest of the plane, the loading must be zero. Again by constructing the analogue with the three-dimensional lifting-surface problem a solution can easily be obtained.

The solution for the load coefficient for a wing starting from rest and continuing at supersonic speeds - that is, the indicial load coefficient for α - is shown in figure 2(a). At $t = 0$ the wing suddenly attains an angle of attack (without rotation). Immediately the load coefficient jumps to a constant value of magnitude $4\alpha/M_o$ over the entire chord. At a subsequent time this value moves off the chord with the trailing characteristic trace, the apex of which is at the origin. Between the traces of the characteristic cone a transition occurs, the load falling below the value $4\alpha/M_o$ and then rising to the higher value $4\alpha \Big/ \sqrt{M_o^2 - 1}$. This latter value is the familiar steady-state two-dimensional value for load commonly called the Ackeret loading. As the leading characteristic trace leaves the wing, the Ackeret loading covers the chord and the wing has reached its steady-state value.

Compare this loading with the indicial load coefficient due to angle of attack for a wing flying at subsonic speeds (fig. 2(b)). Again at $t = 0$, the incremental load jumps immediately to the constant value $4\alpha/M_o$ over the entire chord. However, in this subsonic case, the load near the trailing edge immediately falls so that for all values of time greater than zero the loading at the trailing edge is continuous and zero. That is to say, the Kutta-Joukowski condition is

satisfied except at the instant $t = 0$. Subsequently, the load distribution approaches asymptotically the normal additional load distribution associated with steady two-dimensional subsonic theory – that is, very high values near the leading edge fall to zero at the trailing edge.

Figure 3 shows the indicial load coefficient due to angle of attack for a restrained wing flying at supersonic speeds and entering a sharp-edge gust. The gust is located in the region from $X = -\infty$ to $X = 0$. Initially the loading over the chord is zero. As the leading edge begins to penetrate the gust, however, in the region between the characteristic traces the load begins to rise from zero to the Ackeret loading, and again as the loading characteristic trace crosses the trailing edge the wing has reached its final steady-state Ackeret value.

Further discussion of these phenomena can best be completed by considering the integrated values of these loadings plotted against a variable representing time. Thus figure 4 shows a plot of lift-curve slopes against s, the number of half-chords traveled by the wing, for a wide range of Mach number. The curve for $M = 0$ – that is, the curve for the two-dimensional wing with incompressible flow – was first studied by Wagner. Since the starting value is always $4/M$, this incompressible flow value of C_{l_α} must initially jump to infinity. The infinite value, which results from the infinite acceleration imposed in the boundary conditions by the step function, lasts only for an infinitesimal time; however, C_{l_α} then falls to π and rises gradually to the asymptotic value 2π. The calculations for the curves in the region $0 < M_o < 1$ were completed only to the time necessary for a pressure signal to travel from the trailing to the leading edge. Further computations are possible but would have been more complex. On the other hand, the qualitative nature of the curves for larger values of time is fairly obvious. Thus at a Mach number of 0.8 the starting value is 5. The lift-curve slope falls linearly for the time required to travel about a half-chord length and then rises to approach asymptotically the value $2\pi/\sqrt{1 - M^2}$. The curve for a Mach number of 0.4 is similar. Such a behavior obviously invalidates the use of the Prandtl-Glauert Mach number correction to unsteady lift analysis. Between $t = 0$ and $t = \infty$ the correction factor must lie between $1/M$ and $1/\sqrt{1 - M^2}$, but the exact value is quite complex. The variation of this transient C_{l_α} with Mach number is accentuated most sharply by considering the value at $M = 1$.

The curve in figure 4 for $M = 1$ presents the build-up of lift-curve slope for a wing starting from rest and traveling at the speed of sound. Since the Mach number is unity, the starting value of C_{l_α} is 4. The magnitude of C_{l_α} increases with time and is infinity at $s = \infty$. However, since the whole theory is based on the assumption

that the induced velocities are small compared with the free-stream velocity, the number of half-chords traveled before the theory breaks down is severely limited. Just how much so depends, of course, on the angle-of-attack change chosen. Nevertheless, some insight into the nature of sonic flow has been gained.

Curves for supersonic Mach numbers of 1.2 and 1.4 are also plotted in figure 4. At a Mach number of 1.2 the variation of C_{l_α} with time approximates rather closely Wagner's curve for $M = 0$. In the supersonic case, however, C_{l_α} is initially constant at $4/M$ for about one-half chord length traveled and then rises and reaches its steady-state Ackeret value of $4/\sqrt{M^2 - 1}$ after a few chord lengths; whereas, in the subsonic case, the value is nowhere constant and approaches its steady-state value asymptotically. For higher supersonic Mach numbers, the magnitudes of the curves decrease and the difference between the starting and final values becomes less.

So far, the discussion has been limited to the indicial lift for a sudden angle-of-attack change. A comparison between this lift and that developed by a supersonic wing entering a sharp-edge gust is given in figure 5. The curves shown are both for a Mach number of 1.2, the dash curve representing the change in lift coefficient for the wing entering the gust. The principal difference between the curves is in the initial value, the gust curve starting at zero and the angle-of-attack curve starting at $4/M$. After about 12 chord lengths, however, the curves are identical, since both have assumed the Ackeret value.

A simple but important dynamic maneuver can be studied by means of the two indicial lift functions, the one for α and the other for a gust. This maneuver is the response of an unrestrained airfoil to a gust when the effects of pitching are neglected. Such a maneuver for sharp-edge gusts has been studied in reference 4.

The study of the unsteady lift problem is far from being complete. It is believed that the effect of the indicial lift on the downwash at the vertical tail plane at supersonic speeds has not been touched, nor has the effect of gusts on wings traveling at high subsonic speeds. Furthermore, the methods described in this paper might be used as another approach to the study of compressible flutter problems for Mach numbers less than 1 - especially the problem of aileron flutter. Another type of research, the study of which has just been started at the Ames Aeronautical Laboratory, is that of the two-dimensional wing accelerating through the speed of sound. The results already presented for the indicial lift around a Mach number of 1 indicate that further research along these lines might produce worthwhile results.

REFERENCES

1. Wagner, Herbert: Über die Enstehung des dynamischen Auftriebes von Tragflügeln. Z.f.a.M.M., Bd. 5, Heft 1, Feb. 1925, pp. 17–35.

2. Garrick, I. E., and Rubinow, S. I.: Theoretical Study of Air Forces on an Oscillating or Steady Thin Wing in a Supersonic Main Stream. NACA TN No. 1383, 1947.

3. Chang, Chieh–Chien: The Transient Reaction of an Airfoil Due to Change in Angle of Attack at Supersonic Speed. Preprint No. 134, Inst. Aero. Sci., 1948.

4. Heaslet, Max. A., and Lomax, Harvard: Two–Dimensional Unsteady Lift Problems in Supersonic Flight. NACA TN No. 1621, 1948.

5. Jones, Robert T.: The Unsteady Lift of a Wing of Finite Aspect Ratio. NACA Rep. No. 681, 1940.

6. Churchill, Ruel V.: Modern Operational Mathematics in Engineering. McGraw–Hill Book Co., Inc., 1944.

7. Hadamard, Jacques: Lectures on Cauchy's Problem in Linear Partial Differential Equations. Yale Univ. Press (New Haven), 1923.

8. Heaslet, Max. A., and Lomax, Harvard: The Use of Source–Sink and Doublet Distributions Extended to the Solution of Arbitrary Boundary Value Problems in Supersonic Flow. NACA TN No. 1515, 1948.

9. Evvard, John C.: Theoretical Distribution of Lift on Thin Wings at Supersonic Speeds (An Extension). NACA TN No. 1585, 1948.

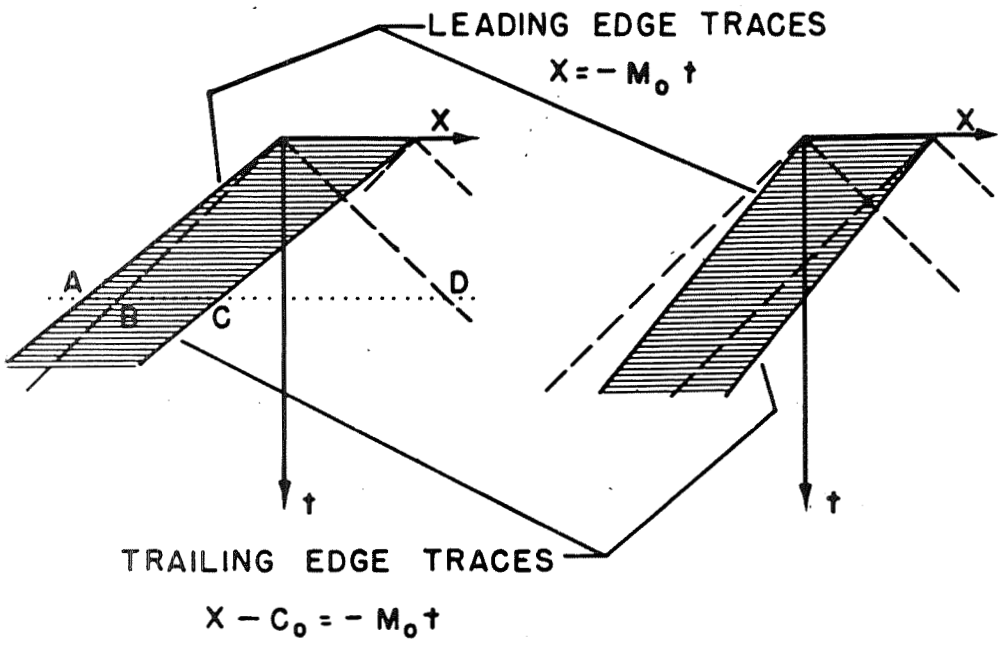

(a) Subsonic and supersonic wing receiving sudden angle-of-attack change at $t = 0$.

Figure 1.- Sketches showing different types of boundary conditions for two-dimensional unsteady lift problems.

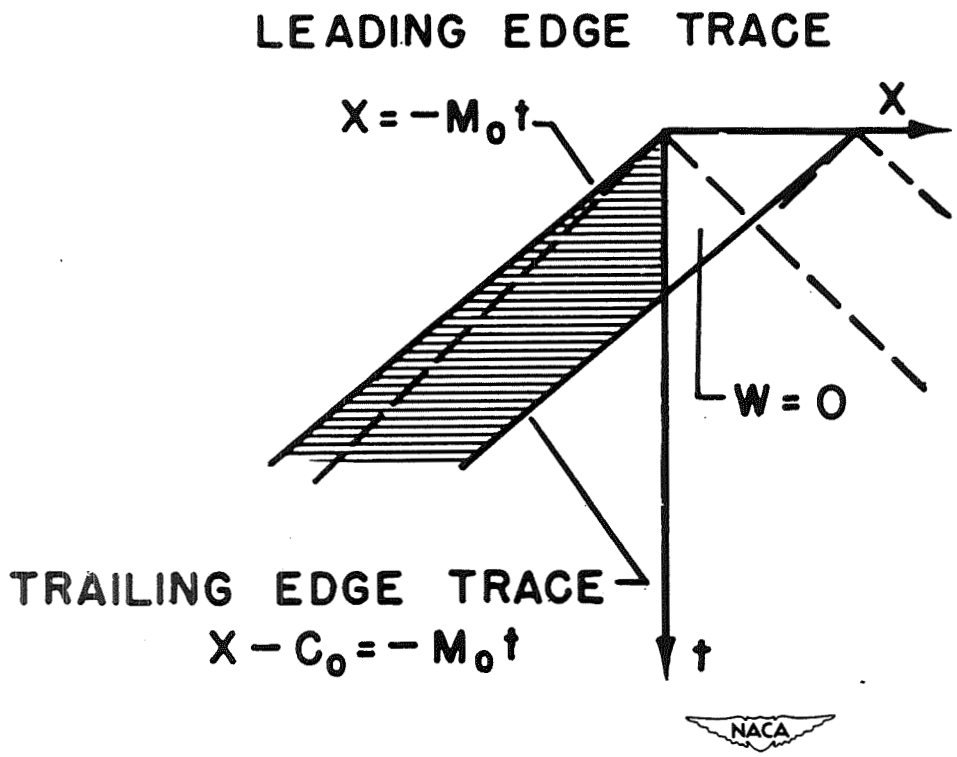

(b) Supersonic wing entering sharp-edge gust at $X = 0$.

Figure 1.- Concluded.

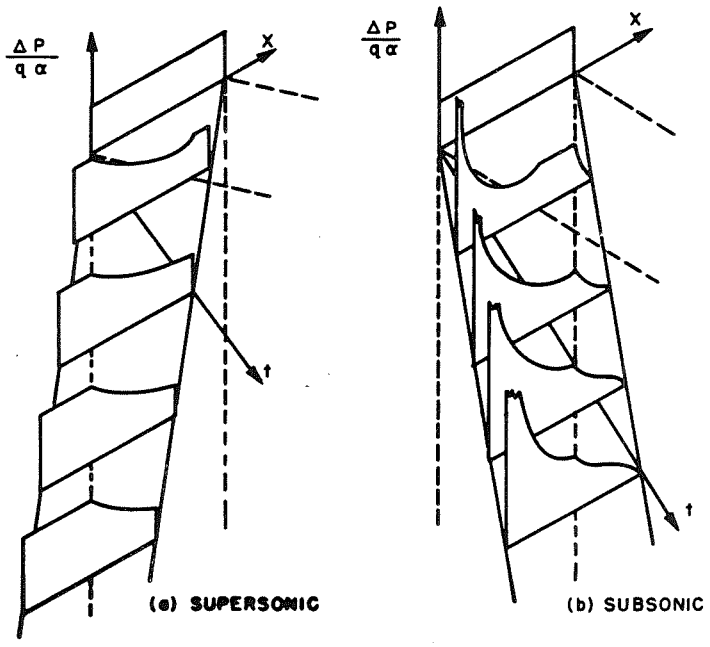

Figure 2.- Pressure distributions on wing receiving sudden angle-of-attack change at $t = 0$.

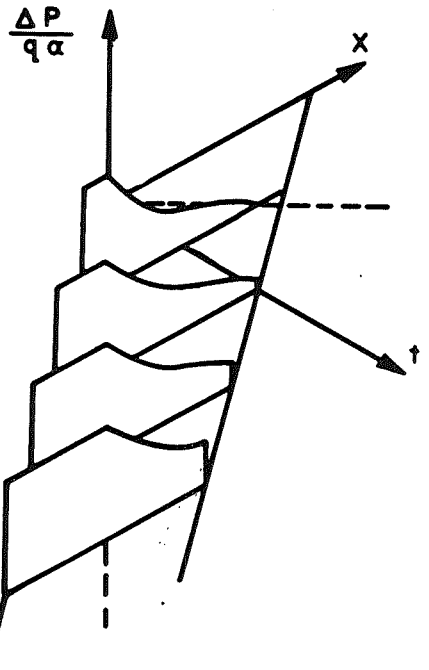

Figure 3.- Pressure distribution on supersonic wing entering sharp-edge gust at $X = 0$.

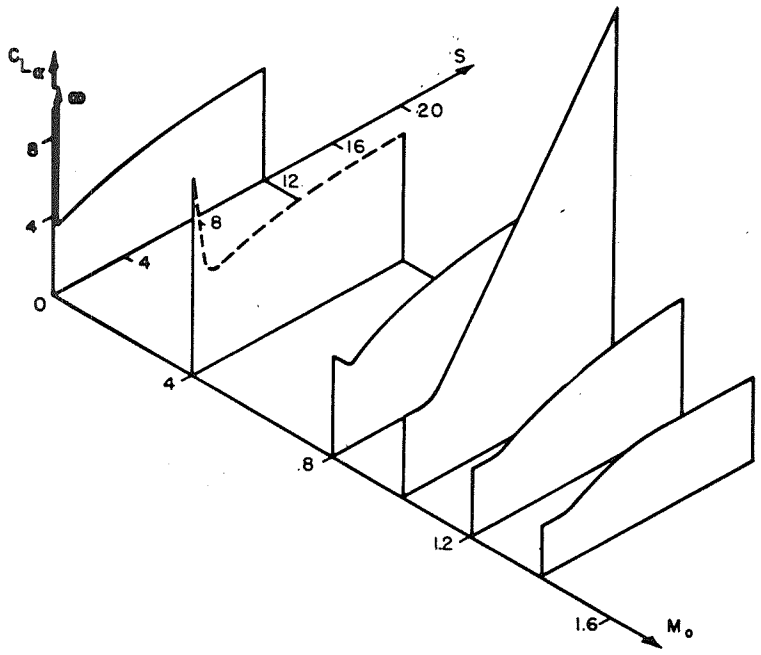

NACA

Figure 4.- Indicial lift-curve slope for Mach numbers between 0 and 1.4 shown to time required to travel 12 half-chords.

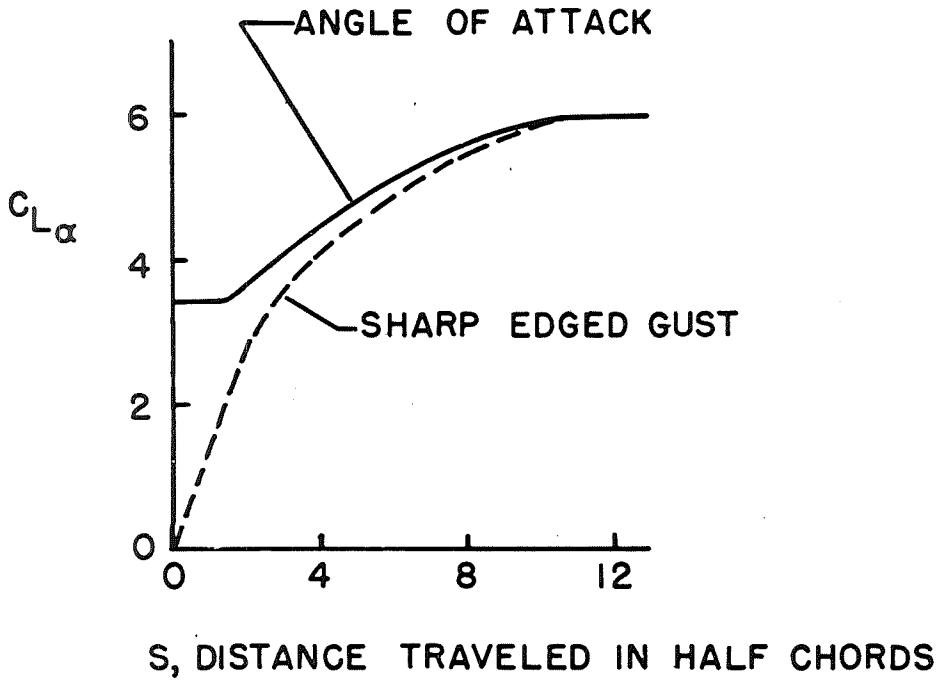

NACA

Figure 5.- Indicial lift-curve slopes for restrained wing.

A SURVEY OF METHODS FOR THE CALCULATION OF FLOW AROUND BODIES OF REVOLUTION AT SUPERSONIC SPEEDS

By Antonio Ferri

Langley Aeronautical Laboratory

The theoretical determination of aerodynamic characteristics of bodies traveling at supersonic speed has been considered only recently in relation to flying problems but has been for a long time an important problem in ballistics. For this reason and because, for bodies of revolution, the problem is sensibly more simple, the bodies considered in the theoretical work are bodies having circular cross section, while small attention has been given heretofore to bodies having a cross section different from the circular, although these bodies are important for practical applications. A bibliography of information on this subject is presented at the end of this paper.

For bodies of revolution of good aerodynamic shape, in general the physical phenomena are well understood and the analysis of the flow phenomena can be made with good approximation when the boundary layer along the body does not separate. If the body analyzed is a sharp, slender body of revolution axially alined with the direction of the undisturbed stream, an axial-symmetrical shock is produced at the apex of the body (fig. 1). If the body is a cone of revolution, the generatrix of the shock is a straight line, while in the general case it is a curve that becomes more inclined with the direction of the undisturbed stream, moving away from the body and tending to become parallel to the Mach line.

Across the shock an increase of entropy occurs that corresponds to a variation of momentum in the flow, and, therefore, the shock produces a drag called shock drag. Because the variation of entropy changes with the inclination of the shock, the flow behind a curved shock is not any longer an isentropic flow. The entropy is constant along every streamline in the zone between two shocks, but a variation of entropy exists in a direction normal to the streamlines and, therefore, the flow is rotational flow.

Along the surface of the body, when the generatrix of the body is a curved line, the pressure decreases. If the radius of curvature of the generatrix of the body is small, in the zone in which the generatrix becomes parallel to the undisturbed stream the local pressure is lower than the free-stream pressure. If a cylindrical part of some extent follows the ogive, along the cylindrical part, the pressure increases and tends to become equal to the static pressure. If the back part of the body finishes with a tail as shown in figure 1, the pressure along the tail continues to decrease and at the end of the body another shock wave is produced.

At the surface of the body the boundary layer grows and a wake exists at the tail of the body. The wake changes the actual shape of the streamlines at the end of the body, and, therefore, in this zone a theoretical analysis of the phenomenon made with perfect-flow theory cannot reproduce correctly the physical phenomenon.

However, the phenomenon can be foreseen theoretically with good accuracy in the zone of the flow in which the effect of the boundary layer on the shape of the streamlines is negligible.

When the body has an angle of attack the phenomenon changes and the axial symmetry disappears; the theoretical analysis then becomes more difficult.

For small (infinitesimal) angles of attack the shock that is produced at the apex of the body remains approximately a surface of revolution, but its axis is not coincident with the axis of the body nor with the direction of the undisturbed stream. Because the phenomenon is not the same in every meridian plane passing through the axis of the body, a velocity component in a direction normal to the meridian plane exists, and a force component normal to the undisturbed stream can be found. This component produces a lift and a moment on the body. At the tail of the body when the body has an angle of attack, the wake produced by the boundary layer is not symmetrical with respect to the axis of the body. The wake has an effect on the value of the lift; therefore, because the lift is related to the boundary-layer phenomena, the lift of a body of revolution that ends with a point cannot be analyzed with good approximation if only perfect-flow theory is used.

If an open-nose body of revolution is considered, the analysis of the flow phenomena does not change if the flow enters the body with supersonic speed. In this case, at the lip of the body the phenomenon is two dimensional. The shock moving far from the lip decreases in intensity in a similar way to that of the pointed nose of revolution.

The theories used for the determination of pressure along a body of revolution are of two types: the small-disturbance theory and the characteristics theory. Both systems deal with adiabatic perfect flow, and the effect of viscosity and conductivity are neglected. The small-disturbance theory uses more simple hypotheses in the flow determination and allows in some cases analytical expressions for the aerodynamic phenomena, whereas the characteristics theory takes into account all the physical aspects of the phenomena for adiabatic perfect flow but does not solve practical problems of axial symmetrical flow in an analytical form and requires a numerical determination of every particular case considered.

The simplification accepted by the small-disturbance theory is that the variations of velocity components produced by the presence of the body in the stream are so small that the square terms of the disturbance velocities and of their derivatives can be neglected with respect to the first-order terms in the equation of motion. In this approximation the entropy remains constant throughout the stream and a velocity-potential function can be used. The equation of motion for potential flow and cylindrical coordinates (fig. 2), is expressed as:

$$\left(1-\frac{u^2}{a^2}\right)\frac{\partial^2\phi}{\partial x^2}+\left(1-\frac{v^2}{a^2}\right)\frac{\partial^2\phi}{\partial y^2}+\left(1-\frac{w^2}{a^2}\right)\frac{1}{y^2}\frac{\partial^2\phi}{\partial\varphi^2}-\frac{2uv}{a^2}\frac{\partial^2\phi}{\partial x\,\partial y}-\frac{2uw}{a^2}\frac{1}{y}\frac{\partial^2\phi}{\partial x\,\partial\varphi}$$

$$-\frac{2vw}{a^2}\frac{1}{y}\frac{\partial^2\phi}{\partial y\,\partial\varphi}+\frac{v}{y}\left(1+\frac{w^2}{a^2}\right)=0 \qquad (1)$$

where ϕ is the total-velocity potential; u, v, and w are velocity components; and a is the speed of sound. Then, in the small-disturbance approximation the expression becomes:

$$\left(1-M_1^2\right)\frac{\partial^2\phi'}{\partial x^2}+\frac{\partial^2\phi'}{\partial y^2}+\frac{1}{y^2}\frac{\partial^2\phi'}{\partial\varphi^2}+\frac{1}{y}\frac{\partial\phi'}{\partial y}=0 \qquad (2)$$

where M_1 is the Mach number of the undisturbed stream assumed parallel to the x-direction, and ϕ' is the potential function that represents the variations of velocity components produced in the stream by the movement of the body (disturbance velocities). The theory of small disturbances can be used in every case in which the more simple hypotheses are respected, and, therefore, for every free-stream Mach number considered. However, from a practical point of view it is necessary to remember that the theory cannot be used in the neighborhood of $M_1 = 1$, while the precision of the results decreases at high Mach numbers because for a given geometrical shape of the body the disturbance velocities increase in intensity when the Mach number increases.

The equation of motion in the simplified form (equation (2)) is a linear differential equation of second order with constant

coefficients and therefore permits a superimposition of solutions that simplifies notably the problem. The solution of any problem in the approximation of equation (2) can be obtained by the superimposition of simple solutions, known from sound-wave theory, that in aerodynamics represent sources, sinks, and doublets. The problem of determining the flow properties of a given phenomenon is transformed in this way to the problem of determining the correct distribution of sources or doublets that respect the boundary conditions considered in the problem.

For bodies of revolution axially alined with the undisturbed stream, the solution of the problem can be obtained by considering a source-sink distribution along the axis of the body, the intensity of which depends upon the free-stream Mach number and upon the shape of the body. The intensity of the source-sink distribution can be obtained generally by a step-by-step calculation of simple form or in some cases in analytical form. The step-by-step calculation is usually required when the boundary conditions are exactly fulfilled by imposing the condition that the disturbance-velocity components at the surface of the body must produce a stream that, when superimposed on the undisturbed stream, must be exactly tangent to the body. For very slender bodies of revolution with a generatrix having finite curvature the step-by-step calculation can be avoided. In the neighborhood of the axis of the body the component of the disturbance velocity normal to the axis can be determined directly from the intensity of the source distribution along the axis, and vice-versa. Now, if the body is a slender body of revolution, the component of the disturbance velocity normal to the axis at the surface of the body is essentially equal to the same component in the neighborhood of the axis. But the component of the disturbance velocity normal to the axis at the surface of the body is given by the boundary conditions and depends upon the stream velocity and upon geometrical parameters of the body and, therefore, is known. In this case, the intensity of the source distribution can be obtained directly from the shape of the body without a step-by-step calculation.

The intensity of the source distribution is given in this approximation by

$$f(x) = \frac{V_1}{2\pi} \frac{ds(x)}{dx}$$

where $s(x)$ is the cross-sectional area of the body at the abscissa x. The value of the drag obtained by this approximation is independent of the Mach number.

This result depends upon the simplifications assumed; however, it gives an indication that the effect of variation of Mach number in the aerodynamic phenomena of slender bodies of revolution is not very large.

When the body of revolution has a small (infinitesimal) angle of attack, the solution is obtained by considering two potential functions, the potential function ϕ_1 that represents the phenomenon dependent on the component of the stream in line with the axis of the body, and the potential function ϕ_2 that considers the part of the phenomenon dependent on the component normal to the axis. The first potential function is identical in the approximation accepted to the function used in the axial symmetrical phenomena, while the second potential function corresponds to the potential of a doublet distribution placed along the axis of the body. The intensity of the doublet distribution must be determined as a function of the boundary conditions. Again, for very slender bodies of revolution having generatrices with finite curvature, the doublet distribution depends only on geometrical parameters of the body considered and can be determined directly. In this case, the lift coefficient is dependent only on the end section of the body and is independent of the Mach number. The lift obtained with the small-disturbance theory for bodies pointed at both ends is zero but is different from zero if the end section is different from zero. This result depends on the assumptions made; however, it shows that the lift is a function of the dimension of the wake and, therefore, of the phenomena in the boundary layer. Indeed, the cross section of the wake corresponds physically for the flow outside of the boundary layer to an end section of the body.

By use of the small-disturbance theory, it is possible to determine some general properties of bodies of revolution and to obtain some indications of the shapes of bodies having low shock drag. For example, if the length and diameter of an ogive body are fixed, the shape that corresponds to minimum drag has a blunt nose. The radius of curvature of the meridian curve at the nose is very small, and, therefore, the zone in which the nose is blunt is very small. This result is found also when more approximate treatment is used.

In order to give an idea of the approximation of the small-disturbance theory, comparison between the pressure coefficients $\Delta p/q$ given by this theory for different stream Mach numbers and the results obtained by exact-perfect-flow theory is shown in figure 3. The bodies considered are cones of revolution with different apex angles.

In the small-disturbance theory it is assumed that all the disturbances are transmitted along surfaces that have constant

inclination with respect to the axis of the body. The inclination corresponds to the free-stream Mach angle. In this approximation no shock waves can be found.

When phenomena of bodies at an angle of attack are considered, the Mach cones move rigidly with the body or in some cases do not move with respect to the direction of the stream.

In order to obtain the effect of the presence of the shock and in order to determine with greater precision the phenomena outside of the boundary layer, the characteristics system must be used. The principal idea of the characteristics method is based on the fact that every small disturbance produced in a supersonic stream is transmitted only in the flow inside the Mach cone from the point in which the disturbance is produced; therefore, the Mach cone from the point in which the small (infinitesimal) disturbance is produced is a surface across which the phenomenon changes. In mathematical language this surface is a characteristic surface, because as the disturbance is small and the phenomenon continuous, the flow properties represented, for example, by the stream velocity components must be the same at the inside and outside surface of the Mach cone; since the analytical expression of the flow properties must change across the surface, therefore, the partial derivative of the flow properties (in our case the velocity components) must change in discontinuous form. The characteristic surfaces exist only if the flow is anywhere supersonic because only in this case the disturbances are transmitted along the surface correspondent to the Mach cone.

The characteristic surfaces are constituted by the envelope of all the Mach cones that have their vertices at the points in which a disturbance is produced. They separate the zone of the flow in which the perturbation is transmitted from the undisturbed zone. Because the Mach angle is not constant in the flow, the characteristic surfaces are curved and at the inclination any point is a function of the local velocity. When the body considered is a body of revolution at zero angle of attack, the phenomenon has axial symmetry and also the characteristic surfaces are surfaces of revolution. The velocity at any point is defined by two velocity components and the analysis of the phenomenon can be made by determining the motion in a meridian plane. In place of the characteristic surfaces the characteristic lines are considered. These lines are obtained by the intersection of the characteristic surfaces with the meridian plane.

At every point of the meridian plane the characteristic lines are inclined at the local Mach angle with the local direction of the velocity, and at every point two characteristic lines pass correspondent to the two directions in which a Mach line can be drawn with respect to the direction of the velocity. If μ is the local Mach

angle and θ the local inclination of the velocity with respect to the axis of the body, a characteristic line is inclined at $\mu + \theta$ and the other at $\theta - \mu$. The value of μ and θ is different at different points of the flow; therefore, the characteristic lines are curved.

The characteristics theory consists in the analysis of the changes of flow properties along characteristic surfaces or, for bodies of revolution, along characteristic lines.

By use of the law of continuity, the law of conservation of energy, or the law of variation of momentum, a partial differential equation for the law of motion can be obtained. Because of the presence of curved shocks in the flow, the flow analyzed is rotational and, therefore, in general in the analysis the use of a potential function is not possible. For two-dimensional or axial symmetrical phenomena a special stream function can be used which permits the obtaining of a partial differential equation correspondent to the equation of motion for potential flow. This stream function for rotational flow, or differential expressions for the velocity components, the pressure, and the density can be used to obtain the equations of motion in differential form. The equation which defines the motion becomes much simpler if the variation of the flow properties is analyzed along the characteristic surfaces, because some terms of the differential equation disappear.

If a body of revolution axially alined with the free stream is analyzed, the variation of flow properties must be analyzed along the characteristic lines. Because across every point of the flow two characteristic lines pass, two equations are obtained which give in differential form the variation of the flow properties along the lines. Because the flow properties at any point are defined if two quantities (for example, the two velocity components) are known, the two equations permit the problem to be defined.

The equations that give the law of motion along the characteristic lines still are differential equations with variable coefficients but permit the numerical determination of the problems if a method of finite differences is used in place of the differential equation in order to determine the variation of flow properties along the characteristic line.

The equation of motion along the characteristic line can be given in the following form (see fig. 4):

$$\frac{dy}{dx} = \tan(\mu + \theta) \tag{3a}$$

$$\frac{dV}{V} - \tan\mu\, d\theta + dx\left[\frac{\sin^3\mu}{\cos(\theta+\mu)}\frac{dS}{dn}\frac{1}{\gamma R} - \frac{\sin\theta\sin\mu\tan\theta}{\cos(\theta+\mu)}\frac{1}{y}\right] = 0 \tag{3b}$$

and

$$\frac{dy}{dx} = \tan(\theta - \mu) \tag{3c}$$

$$\frac{dV}{V} + \tan\mu\, d\theta - dx\left[\frac{\sin^3\mu}{\cos(\theta-\mu)}\frac{dS}{dn}\frac{1}{\gamma R} + \frac{\sin\theta\sin\mu\tan\theta}{\cos(\theta-\mu)}\frac{1}{y}\right] = 0 \tag{3d}$$

where V is the intensity of velocity, θ the inclination of velocity with respect to the axis, $\frac{dS}{dn}$ the gradient of entropy in normal direction to the streamlines, and γ and R are constants.

From the equations (3), the flow property at a given point can be determined, when the flow properties at two points near to the point considered and along the characteristic lines are known (fig. 4).

If the flow properties in P_1 and P_2 near each other are known, the values of θ and μ are also known; therefore, from P_1 the tangent to the characteristic line given by equation (3a) and from P_2, the tangent to the characteristic line given by (3c) can be drawn, and a point P_3 can be determined. On the assumption that in the first approximation the coefficients in equations (3d) and (3b) are constants between P_1 and P_2 and P_2 and P_3, and applying equation (3b) between P_1 and P_3 and equation (3d) between P_2 and P_3 allows two equations to be obtained that permit determination of the variation $d\theta$ and dV between P_3 and P_1 (equation (3b)) and the variation dV and $d\theta$ between P_3 and P_2 (equation (3d)). Indeed, the variation dx is known, and all the coefficients are constants and known. When the values of V and θ at P_3 in the first approximation are determined, a second approximation can be obtained by assuming for the coefficients in equations (3b) and (3d), and for the direction of the characteristic in equations (3a) and (3b) the average values between the values at the points P_1 and P_2 and the values obtained in the first approximation for the point P_3. In equations (3b) and (3d),

the term $\frac{dS}{dn}$ appears only if the flow is rotational flow. This term can be determined at every point because the entropy is constant along every streamline between shock waves, and the equation of the shock gives the variation of entropy that occurs when a streamline crosses a shock wave.

The system permits the determination of the phenomenon when shock exists and allows any required precision to be obtained, because the precision depends on the distance between the points P_3 and P_2 or P_3 and P_1, a distance that can be reduced to any value.

The system is numerical but the solution can be obtained in computing machines of large size that can give numerical results in a very short time. The only approximations introduced are that viscosity and conductivity can be neglected.

In order to apply the characteristic system to any body of revolution the flow must be determined initially along a characteristic line. If the body is a sharp-nosed body of revolution the calculation starts with the determination of the flow at the apex, flow that is conical flow; while if the body is an open-nosed body of revolution the calculations start by determining the shock at the lip of the nose with the two-dimensional theory. Figure 5 shows a comparison between experimental results and values determined with the characteristic system for a body of revolution of simple shape. Figure 6 shows a practical determination of the supersonic part of the flow inside a conical diffuser. The shock produced at the lip of the body increases in intensity and becomes normal at the axis. The increase in intensity of disturbances produced at the wall of circular tubes is a general phenomenon and is important for supersonic circular tunnels.

When the body is not a body of revolution or has an angle of attack, the characteristic system can still be applied but becomes much more involved, because it is necessary to determine the flow variations not along two characteristic lines, but along two characteristic surfaces. Practically, the determination of the flow properties at any point can be obtained by the analysis of the variations along the intersections with a meridian plane of two characteristic surfaces that pass at the point considered and along the intersection of one of two characteristic surfaces with a plane perpendicular to the axis. In this way a system of three linear equations is obtained, when the method of finite differences is used, that permits the determination of one of the flow properties, for example, of the velocity at the point considered.

The numerical solution becomes very involved, especially if the flow with shock is analyzed, and requires that the initial conditions can be determined at the front part of the body.

When a body of revolution with small angle of attack is analyzed, the hypothesis can be accepted that the effect of cross flow is very small and in this case a cross flow can be superimposed to the axial flow, the characteristic lines of the two flows are coincident, and the calculations can be simplified. For example, this system can be used easily in order to determine the flow around a cone of revolution in yaw.

In this approximation the velocity component in normal direction to every meridian plane of the body changes with the sine of the angle that defines the position of the meridian plane as in the small-disturbance theory.

This is the status of the analysis along bodies of revolution. Both theories can probably be extended to similar problems. The extension of the small-disturbance theory to bodies of cross section different from the circular but having constant shape must not be too difficult.

The use of the small-disturbance theory for interference problems seems also possible, and some results of this application are yet to be obtained.

For the small-disturbance theory a complete analysis of the approximations that can be obtained would be very useful. Discrepancy of opinions exists especially on the possibility for this theory of evaluating the Mach number effect on phenomena for bodies unclined at an angle of attack.

In order to give an idea of the precision that can be obtained from the theory of small disturbances, a comparison of the lift-coefficient-curve slope $dC_L/d\alpha$ given with the assumption of small disturbances and without this assumption is presented in figure 7 for different Mach numbers. The bodies are cones of revolution of different apex angles η_0.

The development of an analytical theory having higher approximation than the small-disturbance theory for bodies of revolution would be very useful but seems at present very difficult. The characteristics theory can be extended to the analysis of any shape of body having anywhere supersonic flow, if the initial conditions can be determined; therefore, the determination of general conical flow in more exact form is essential for the extension of the field of application of this theory.

Interference problems can be analyzed with the characteristics theory. This analysis, however, requires a large amount of numerical work in every application. This obstacle, which exists at the present time, can perhaps be eliminated by using for the numerical calculations large size computing machines. The characteristics system can probably be extended to viscous-flow phenomena or to phenomena with variable total energy.

BIBLIOGRAPHY

Small-Disturbance Theory

1. Von Kármán, Theodor, and Moore, Norton B.: Resistance of Slender Bodies Moving with Supersonic Velocities, with Special Reference to Projectiles. Trans. A.S.M.E., vol. 54, no. 23, Dec. 15, 1932, pp. 303–310.

2. Von Karman, Th: The Problem of Resistance in Compressible Fluids. Atti dei Convegni Volta, 5 Convegno di Sci. Fis., Mat. e Nat., R. Accad. d'Italia (Rome), second ed., 1940, pp. 210–269.

3. Ferrari, C.: Campi di corrente ipersonora attorno a solidi di rivoluzione. L'Aerotecnica, vol. XVII, fasc. 6, June 1937, pp. 507–518.

4. Tsien, Hsue-Shen: Supersonic Flow over an Inclined Body of Revolution. Jour. Aero. Sci., vol. 5, no. 12, Oct. 1938, pp. 480–483.

5. Brown, Clinton E., and Parker, Hermon M.: A Method for the Calculation of External Lift, Moment, and Pressure Drag of Slender Open-Nose Bodies of Revolution at Supersonic Speeds. NACA ACR No. L5L29, 1946.

6. Haack, W.: Geschossformen kleinsten Wellenwiderstandes. Bericht 139 der Lilienthal-Gesellschaft für Luftfahrtforschung, 1941, pp. 14–28.

7. Lighthill, M. J.: A Note on Supersonic Biplanes. R. & M. No. 2002, British A.R.C., 1944.

8. Jones, Robert T., and Margolis, Kenneth: Flow over a Slender Body of Revolution at Supersonic Velocities. NACA TN No. 1081, 1946.

9. Ferrari, Carlo: Sulla determinazione del proietto di minima resistenza d'onda. Nota I. Atti R. Accad. Sci. Torino, vol. 74, 1938–39.

10. Ferrari, Carlo: Sul problema del proietto di minima resistenza d'onda. Atti R. Accad. Sci. Torina, vol. 75, 1939–40.

Characteristic System for Bodies of Revolution in Axis with the Flow

11. Crocco, L.: Una nuova funzione di corrente per lo studio del moto rotazionale dei gas. Rend. della R. Accad. dei Lincei. Vol. XXIII, ser. 6, fasc. 2, Feb. 1936

12. Busemann, A.: Drücke auf kegelförmige Spitzen bei Bewegung mit Überschallgeschwindigkeit. Z.f.a.M.M., Bd 9, Heft 6, Dec., 1929, pp. 496–498.

13. Taylor, G. I., and Maccoll, J. W.: The Air Pressure on a Cone Moving at High Speeds. Proc. Roy. Sec. (London) ser. A, vol. 139, no. 838, Feb. 1, 1933, pp. 278–311.

14. Ferrari, C.: Campo aerodinamico a velocita iperacustica attorno a un solido di rivoluzione a prora acuminata. L'Aerotecnica, vol. XVI, fasc. 2, Feb. 1936, pp. 121–130.

15. Ferrari, C.: The Determination of the Projectile of Minimum Wave-Resistance. R.T.P. Translation No. 1180, British Ministry of Aircraft Production. (Part II from Atti R. Accademie Sci. Torino, vol. 75, Nov.-Dec. 1939, pp. 61–96).

16. Guderley, G.: Die Charakteristikenmethode für ebene und achsen-symmetrische Überschallströmungen. Jahrb. 1940 der deutschen Luftfahrtforschung, R. Oldenbourg (Munich), pp. I 522 – I 535.

17. Sauer, R.: Charakteristikenverfahren für räumliche achsensymmetrische Überschallströmungen. Forschungsbericht Nr. 1269, Deutsche Luftfahrtforschung (Aachen), 1940.

18. Tollmein, W.: Anwendung der rechnerischen Behandlung von Stossfront und Wirbelströmung auf einen aus Kegel und Zylinder zusammengesetzten Körper. Archiv. Nr. 44/14, Technischen Hochschule Dresden, Sept. 23, 1944.

19. Temple, G.: The Method of Characteristics in Supersonic Flow. R. & M. No. 2091, British A.R.C., 1944.

20. Ferri, Antonio: Application of the Method of Characteristics to Supersonic Rotational Flow. NACA TN No. 1135, 1946.

Characteristic System for Bodies of Revolution in Yaw

21. Ferrari, C.: Determination of the Pressure Exerted on Solid Bodies of Revolution with Pointed Noses Placed Obliquely in a Stream of Compressible Fluid at Supersonic Velocity. R.T.P. Translation No. 1105, British Ministry of Aircraft Production. (From Atti R. Accad. Sci. Torino, vol. 72, Nov.-Dec. 1936, pp. 140–163.)

22. Sauer, R.: Überschallströmung um beliebig geformte Geschoszspitzen unter kleinem Anstellwinkel. Luftfahrtforschung, Bd.19, Lfg. 4, May 6, 1942, pp. 148–152.

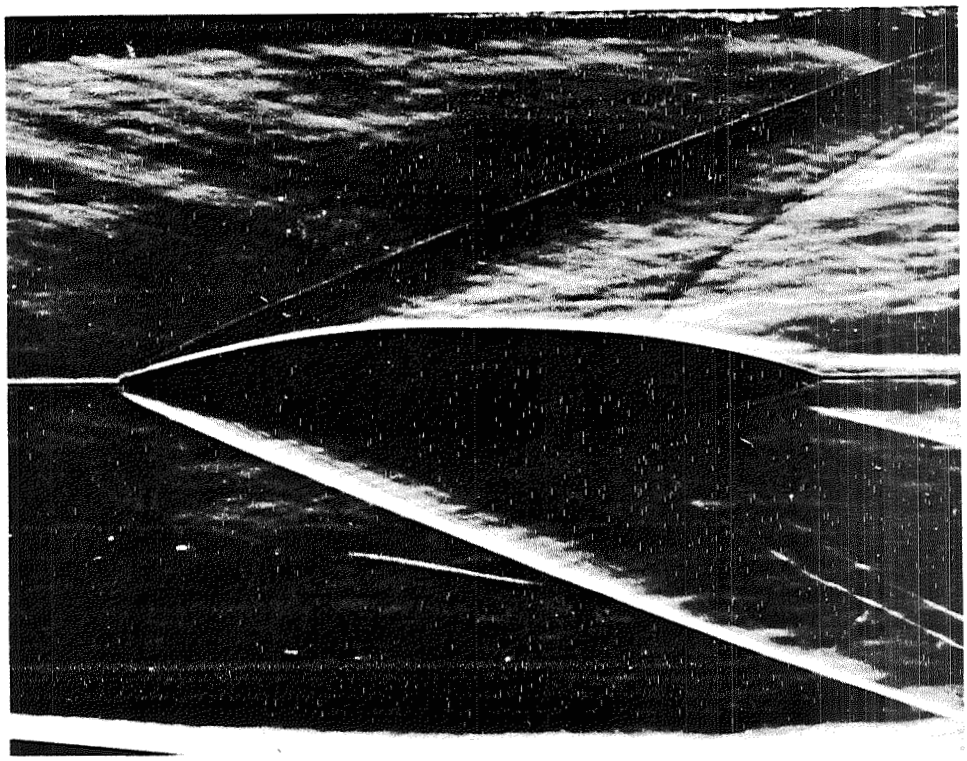

Figure 1.- Axial-symmetrical shock at apex of slender body of revolution.

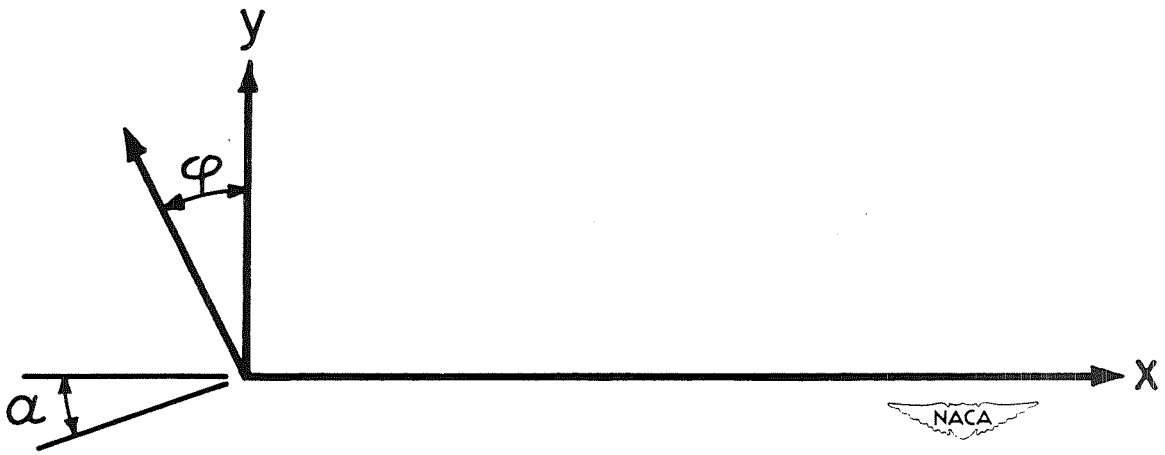

Figure 2.- Coordinate system.

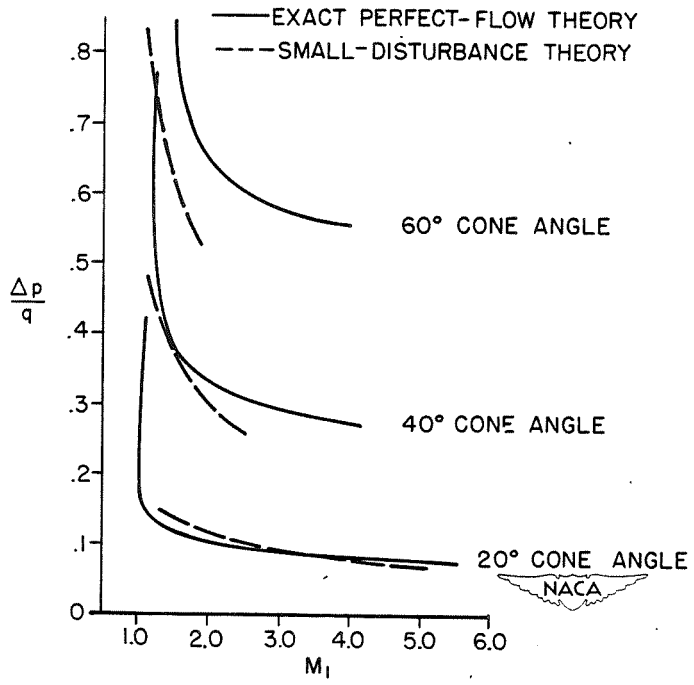

Figure 3.- Variation of $\Delta p/q$ with M_1 for various cone angles.

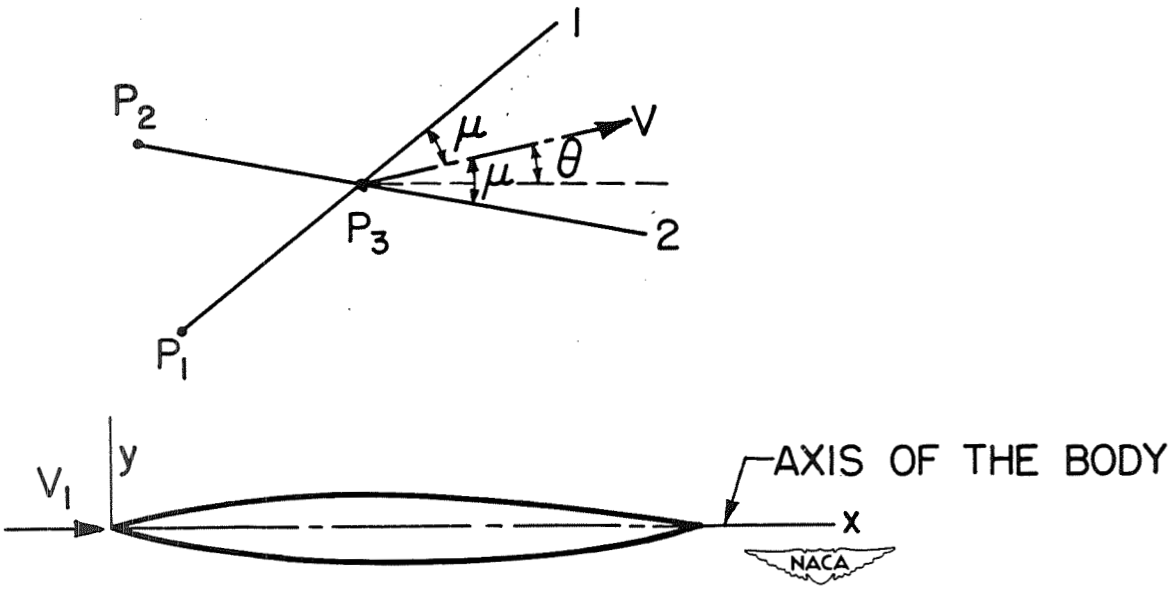

Figure 4.- Diagram illustrating scheme of characteristics method.

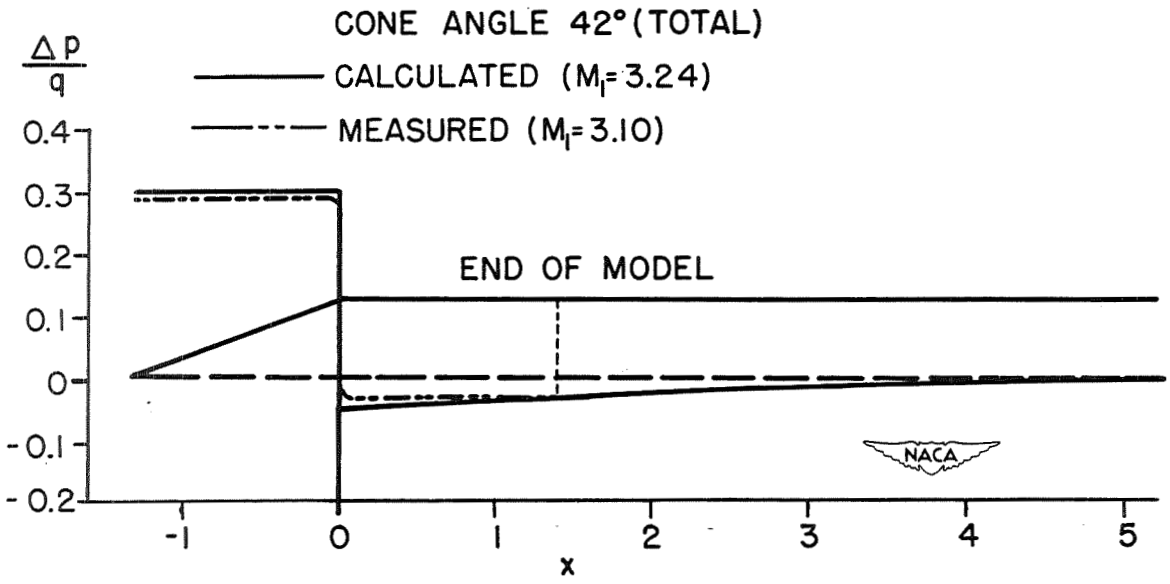

Figure 5.- Comparison of experimental and calculated results.

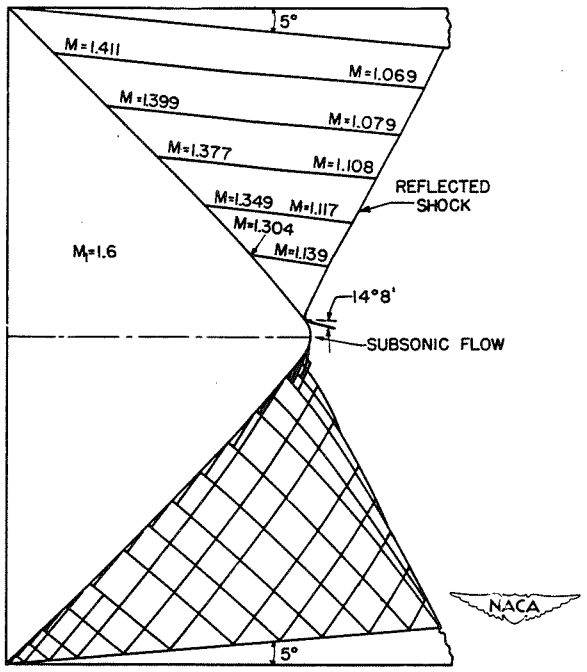

Figure 6.- Determination of supersonic flow in a conical diffuser.

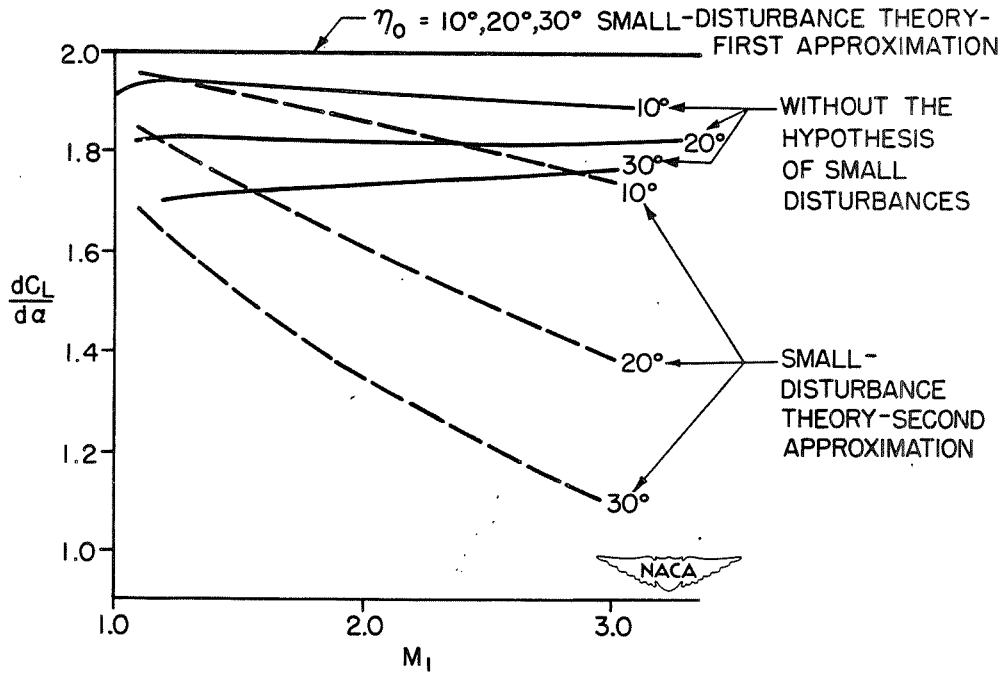

Figure 7.- Comparison of results obtained with and without assumption of small disturbances for cones in yaw.

AERODYNAMIC HEATING

SOME CONSIDERATIONS OF AERODYNAMIC HEATING

By Coleman duP. Donaldson

Langley Aeronautical Laboratory

With the contemplation in recent years of flight at ever-increasing Mach numbers, the problem of aerodynamic heating has become increasingly important to the aeronautical engineer. Unfortunately, much of the work on this subject has not been done from the point of view of the aerodynamicist but has been based on the conventions of the varied branches of specialized fields of heat exchange. From considerations, therefore, of this difficulty and of the increasing importance of this subject to the aerodynamicist, a brief review of boundary-layer heating phenomena appears to be desirable at this time.

If air is brought to rest near the surface of an insulated plate and no energy is assumed to be transferred to or from any element of mass, then from the equation for the conservation of energy

$$T + \frac{U^2}{2c_p} = \text{Const} = T_s$$

where T is the local temperature, U is the local velocity, c_p is specific heat at constant pressure, and T_s is the stagnation temperature. Then, the temperature rise from the free stream to the surface ΔT is found to be

$$\Delta T = \Delta T_{ad} = \frac{U^2}{2c_p}$$

This temperature rise is called the adiabatic temperature recovery and is used as a reference temperature rise in most heat-transfer discussions.

The importance of this temperature rise at high Mach numbers is clear if the equation for the stagnation temperature is written

$$T_s = T\left(1 + \frac{M^2}{5}\right)$$

which is the equation relating this adiabatic stagnation temperature T_s to the free-stream temperature T, where M is the stream Mach number. At a Mach number of 5.0 the surface temperature is six times the free-stream temperature, so that the problem of aerodynamic heating requires serious attention.

Consider now the energy per unit area transferred into an element of height dy while the air is brought to rest first by the temperature

gradient set up and secondly by the friction work done. The energy transferred into the element by heat conduction per second is, then,

$$- k \frac{\partial^2 T}{\partial y^2} dy$$

and that by frictional work is

$$\mu \left[\left(\frac{\partial u}{\partial y} \right)^2 + u \frac{\partial^2 u}{\partial y^2} \right] dy$$

where k is thermal conductivity, μ is viscosity, and u is the velocity component in the x-direction.

These two effects are of opposite sign and if they are equal in magnitude the energy per element remains constant and the energy equation holds through the boundary layer. If the two effects are assumed equal, then

$$k \frac{\partial^2 T}{\partial y^2} = \mu \left[\left(\frac{\partial u}{\partial y} \right)^2 + u \frac{\partial^2 u}{\partial y^2} \right]$$

Now, from the energy equation

$$\frac{\partial^2 T}{\partial y^2} = \frac{1}{c_p} \left[\left(\frac{\partial u}{\partial y} \right)^2 + u \frac{\partial^2 u}{\partial y^2} \right]$$

or

$$\frac{\mu c_p}{k} = 1$$

The quantity $\frac{\mu c_p}{k}$ is called the Prandtl number σ and is a measure of the relative magnitude of the friction and heat-conduction effects in an insulated flow. This parameter is very important in all heat-transfer phenomena. If the Prandtl number is 1.0, the temperature recovery on an insulated body is equal to the adiabatic recovery ΔT_{ad}; thus,

$$\Delta T = \Delta T_{ad} = \frac{U^2}{2c_p}$$

The value of the Prandtl number for air has been variously measured and placed at between 0.72 and 0.76 and hence the temperature recovery on an insulated body should be lower than the adiabatic recovery. The ratio of the actual recovery to the adiabatic recovery $\Delta T / \Delta T_{ad}$ is called the temperature-recovery factor.

If the Prandtl number is not equal to 1.0 or if there exists a heat transfer in or out through the surface at which the velocity is zero, then, in order to solve for the temperatures that exist for a particular velocity profile, three differential equations may be set up. The first two are the well-known continuity and momentum equations.

$$\frac{\partial(\rho u)}{\partial x} + \frac{\partial(\rho v)}{\partial y} = 0 \tag{1}$$

and

$$\rho\left(u\,\frac{\partial u}{\partial x} + v\,\frac{\partial u}{\partial y}\right) = \frac{\partial}{\partial y}\left(\mu\,\frac{\partial u}{\partial y}\right) \tag{2}$$

where ρ is density.

The third equation is an expression of the fact that all the energy transferred into an element by frictional work, conduction, and convection must be carried away by these same processes so that the temperature of the element does not increase with time. For simplification, variations of v in the x- and y-directions are neglected as well as variations of u in the x-direction, with the result that

$$k\,\frac{\partial^2 T}{\partial y^2} + \mu\left(\frac{\partial u}{\partial y}\right)^2 = \rho c_p\left\{u\,\frac{\partial T}{\partial x} + v\,\frac{\partial T}{\partial y}\right\} \tag{3}$$

In order to solve these three equations Eckert and Drewitz (reference 1) assumed that the continuity equation could be satisfied by the use of a stream function and then, use can be made of the new variables

$$\xi = \frac{1}{2}\,y\sqrt{\frac{u_o}{\nu x}}$$

and

$$\zeta = \frac{\psi}{\sqrt{\nu u_o x}}$$

where u_o is free-stream velocity, ν is kinematic viscosity, and ψ is the stream function. Equations (2) and (3) can be put into convenient form by use of these variables and the solution can then be obtained. The

result for the heat transfer per unit area h through the surface, when $0.5 < \sigma < 2$, was

$$h \approx 0.332\, k \sqrt{\frac{u_o}{\nu x}}\, \sqrt[3]{\sigma} \left[(T_w - T_o) - \frac{u_o^2}{2c_p} \sqrt{\sigma} \right]$$

where T_w is the wall temperature and T_o is free-stream temperature. This result is all that is needed for comparison with the results of experimental measurements on an insulated flat plate, for when $h = 0$,

$$T_w - T_o = \frac{u_o^2}{2c_p} \sqrt{\sigma}$$

and the temperature-recovery factor is

$$\frac{\Delta T}{\Delta T_{ad}} = \sqrt{\sigma}$$

For air with a Prandtl number $\sigma = 0.72$ the theoretical temperature-recovery factor is 0.85.

Figures 1 and 2 show the full solution by Eckert and Drewitz (reference 1) for the local temperature rise and stagnation temperature for the laminar-boundary-layer profile. It may be seen from figure 2 that, since the air near the surface of the plate has a stagnation pressure less than free stream, conservation of energy requires the air in the outer portion of the boundary layer to have a stagnation temperature greater than free stream.

The temperature recoveries measured experimentally on an insulated flat plate are shown in figure 3 as a function of local Reynolds number R. The theoretically determined recovery factor $\frac{\Delta T}{\Delta T_{ad}} = 0.85$ agrees well with the experimental values in the laminar region, but as the Reynolds number increases along the plate, transition occurs and the temperature-recovery factor increases from the laminar value to a value at the beginning of the turbulent layer of 0.90.

Before further discussion is made of the results of this laminar analysis to predict the temperature recoveries about bodies other than flat plates, some discussion should be given to one of the methods of analyzing the heat-transfer characteristics of the turbulent boundary layer.

Figure 4 is an illustration of the type of velocity profile that will be assumed. The method of solution is as follows (reference 3): The laminar sublayer will be assumed to have a linear velocity profile and

a parabolic temperature profile $T = A + By + Cy^2$. The local heat and momentum transfers of this layer are determined and, when made to agree with the local heat and momentum transfers of the turbulent layer at the outer edge of the laminar sublayer, a unique solution for the heat transfer through the combined layers results.

For the analysis of the turbulent layer the following equations are at our disposal. They are the continuity equation

$$\frac{\partial(\rho u)}{\partial x} + \frac{\partial(\rho v)}{\partial y} = 0 \tag{4}$$

the momentum equation

$$\rho \frac{du}{dt} = - \frac{\partial \tau}{\partial y} \tag{5}$$

and the energy equation

$$\rho \frac{d}{dt}\left(c_p T + \frac{u^2}{2}\right) = - \frac{\partial}{\partial y}(u\tau) - \frac{\partial h}{\partial y} \tag{6}$$

where

$$\tau = \overline{\rho v' l_y} \frac{\partial u}{\partial y}$$

$$= A \frac{\partial u}{\partial y}$$

$$h = c_p \overline{\rho v' l_y} \frac{\partial T}{\partial y}$$

$$= \Lambda \frac{\partial T}{\partial y}$$

The transfer term $\overline{\rho v' l_y}$ is assumed to be equal in both the transfer of heat and momentum; that is, the mixing length l_y in the two cases is the same so that

$$\Lambda = c_p A$$

The momentum and energy equations (equations (5) and (6)) then become

$$\rho \frac{du}{dt} = - \frac{\partial}{\partial y}\left(A \frac{\partial u}{\partial y}\right)$$

$$\rho \frac{d}{dt}\left(c_p T + \frac{u^2}{2}\right) = - \frac{\partial}{\partial y}\left[A \frac{\partial}{\partial y}\left(c_p T + \frac{u^2}{2}\right)\right]$$

and the total energy and the velocity satisfy the same linear differential equation, a significant fact first pointed out by Crocco. (See reference 3.) All boundary conditions may be satisfied if

$$c_p T + \frac{u^2}{2} = au + b$$

where a and b are constants independent of y.

Frankel used the foregoing procedure to obtain the following result for the heat transfer through a turbulent boundary layer:

$$\frac{h_w}{\tau_w} = \frac{c_p\left(T_o - T_w\right) + \frac{u_o^2}{2} + \frac{u_1^2}{2}(\sigma - 1)}{u_o + u_1(\sigma - 1)}$$

Again, if the case of an insulated plate is considered, the temperature recovery is

$$\Delta T = \frac{u_o^2}{2c_p} - \frac{(1 - \sigma)u_1^2}{2c_p}$$

or

$$\frac{\Delta T}{\Delta T_{ad}} = 1 - (1 - \sigma)\left(\frac{u_1}{u_o}\right)^2$$

From the work done on the turbulent boundary layer at low speeds the value of the square of the ratio u_1/u_o is found to be proportional to the friction stress at the wall divided by twice the dynamic pressure

$$\left(\frac{u_1}{u_o}\right)^2 = 135 \frac{\tau_w}{2q}$$

The temperature-recovery factor for air becomes

$$\frac{\Delta T}{\Delta T_{ad}} = 1 - 37.8 \frac{\tau_w}{2q}$$

Figure 5 is a plot of this relationship for values of $\tau_w/2q$ usually encountered. The results are found to be of the right order of magnitude for the temperature-recovery factors of turbulent layers. Experimental measurements on turbulent layers have given temperature-recovery factors ranging from 0.89 to 0.93 but no such linear dependence as is indicated by the equation has been shown experimentally. Research is needed to determine the proper relationship between u_l and u_o at high speeds as the use of the low-speed relationship at high Mach numbers is not at all logical.

The next step is to determine whether it is possible to apply the results just obtained for insulated flat plates to the prediction of temperatures in insulated bodies of other shapes.

If the velocity distribution about a body is known, the local temperature distribution outside the boundary layer can be found; each element of the body is then assumed to have the flat-plate recovery factor based on its own local conditions. The temperature rise above local temperature for a laminar boundary layer is then

$$\Delta T_l = 0.85 \frac{u_l^2}{2c_p}$$

and the local recovery factor will be 0.85. The recovery factor based on free-stream temperature and the adiabatic recovery of the free-stream velocity is

$$\frac{\Delta T_o}{\Delta T_{ad_o}} = 1 - 0.15\left(\frac{u_l}{u_o}\right)^2$$

Figure 6 shows this last recovery factor $\Delta T_o/\Delta T_{ad_o}$ as measured around a circular cylinder at a Mach number of 0.526 and a Reynolds number of 1.81×10^5. The only part of these data that can be compared with our analysis are those obtained at stations less than 80° from the leading edge, because at larger angles the vortex street shed by the body completely alters the phenomena with the result that surface temperatures are much lower. When these data are converted into the form $\Delta T_l/\Delta T_{ad_l}$ (the dashed line) the agreement with the flat-plate results is good except

in the region near the stagnation point. This result seems to indicate that it is permissible to use flat-plate results to predict temperature distributions over insulated bodies of different shape.

Finally, the measurements on this cylinder over a large range of Mach number indicate that the theoretical prediction - namely, that the local temperature-recovery factor is independent of Mach number - is correct for all moderate Mach numbers. This result is shown in figure 7, which is a plot of the local temperature-recovery factor at a station 70° from the leading edge of the cylinder for a range of free-stream Mach numbers. Since the local Mach numbers are well in excess of unity, these data indicate that the local recovery factor is independent of Mach number up to local Mach numbers approaching 2.0.

These results indicate that the theoretical analysis of the laminar boundary layer on a flat plate presented is an adequate tool for predicting the temperature recoveries on the surfaces of insulated bodies moving at high speeds. It may also be used for calculating moderate heat transfers, but the theory fails if the heat transfer is of a magnitude large enough to change appreciably the common laminar-boundary-layer profile of figures 1 and 2.

The analysis of the turbulent boundary layer indicates that the temperature-recovery factor of an insulated flat plate depends upon the friction stress at the wall and that experimentally it is desirable to measure this quantity simultaneously with the temperature-recovery factor. Certainly further research is needed on the nature and extent of the laminar sublayer of the turbulent boundary layer at high speeds.

Finally, it must be pointed out that the methods of analysis presented herein are not the most refined available to the specialist in the field of heat transfer today (see references 4 to 6) but are presented because they represent the basic methods of approach and serve as an introduction to the problems of aerodynamic heating.

REFERENCES

1. Eckert, E., and Drewitz, O.: The Heat Transfer to a Plate in Flow at High Speed. NACA TM No. 1045, 1943.

2. Eckert, E., and Weise, W.: Messungen der Temperaturverteilung auf der Oberfläche schnell angeströmter unbeheizter Körper. Jahrb. 1940 der deutschen Luftfahrtforschung, R. Oldenbourg (Munich), pp. II 25 - II 31.

3. Frankl, F.: Heat Transfer in the Turbulent Boundary Layer of a Compressible Gas at High Speeds. NACA TM No. 1032, 1942.

4. Fluid Motion Panel of the Aeronautical Research Committee and Others: Modern Developments in Fluid Dynamics. Vol. II, S. Goldstien, ed., The Clarendon Press (Oxford) 1938, chs. XIV and XV.

5. Emmons, H. W., and Brainerd, J. G.: Temperature Effects in a Laminar Compressible-Fluid Boundary Layer along a Flat Plate. Jour. Appl. Mech., vol. 8, no. 3, Sept., 1941, pp. A-105 - A-110.

6. Tifford, Arthur N.: The Thermodynamics of the Laminar Boundary Layer of a Heated Body in a High Speed Gas Flow Field. Jour. of Aero. Sci., vol. 12, no. 2, April 1945, pp. 241-251.

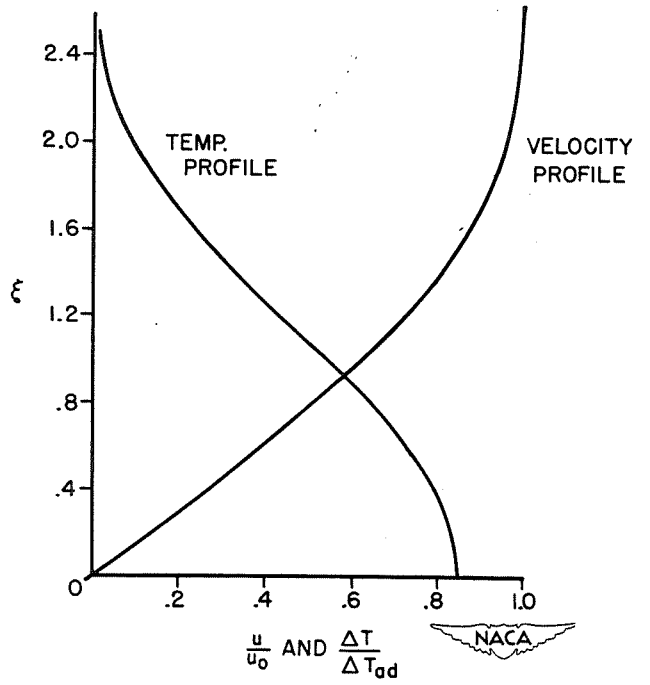

Figure 1.- Local temperature-recovery factor and velocity profile for laminar boundary layer.

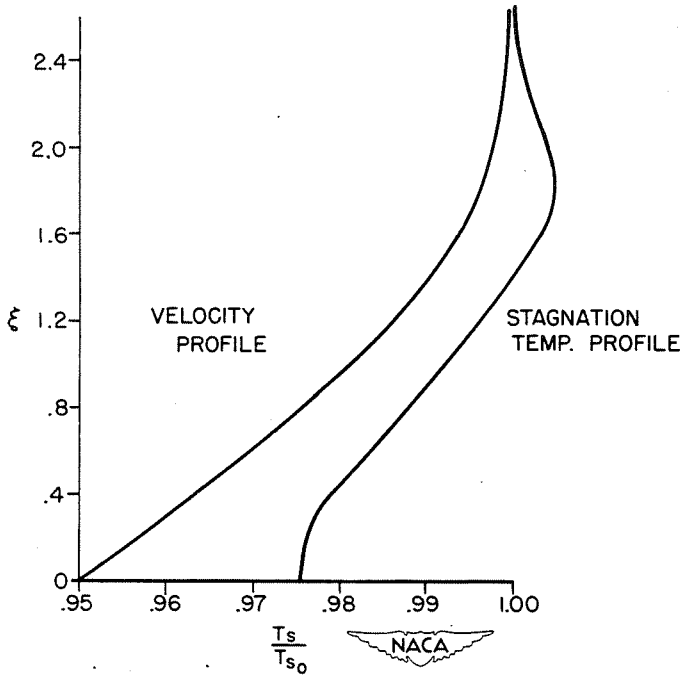

Figure 2.- Stagnation-temperature ratio and velocity profile for laminar boundary layer.

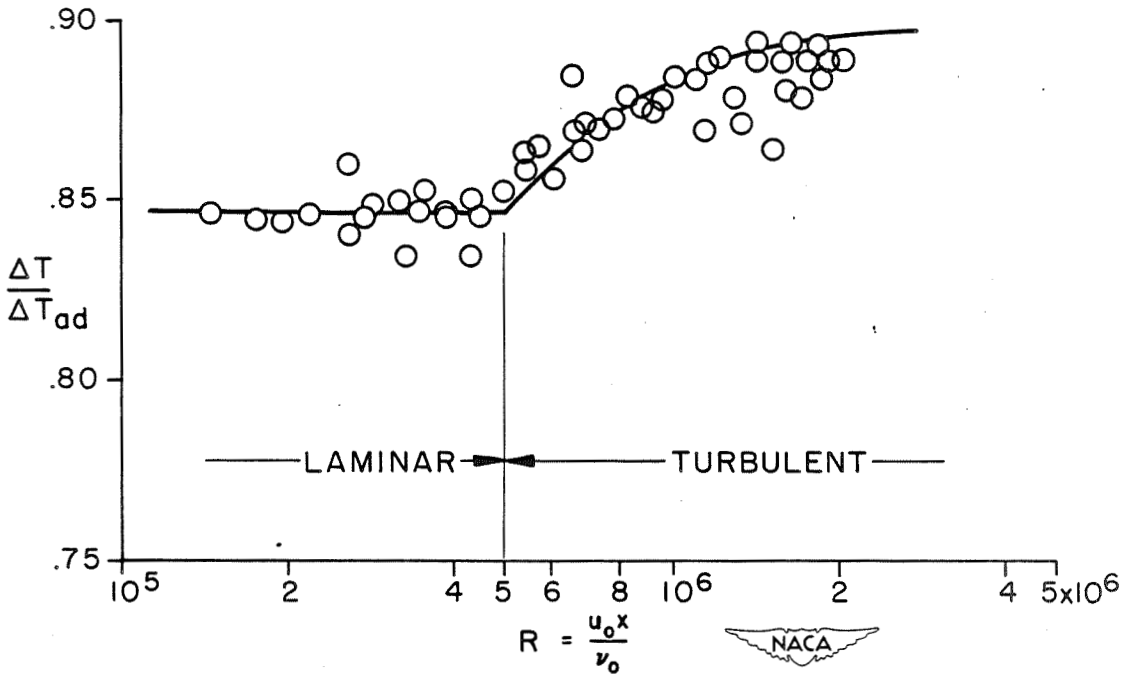

Figure 3.- Temperature recoveries on a flat plate.

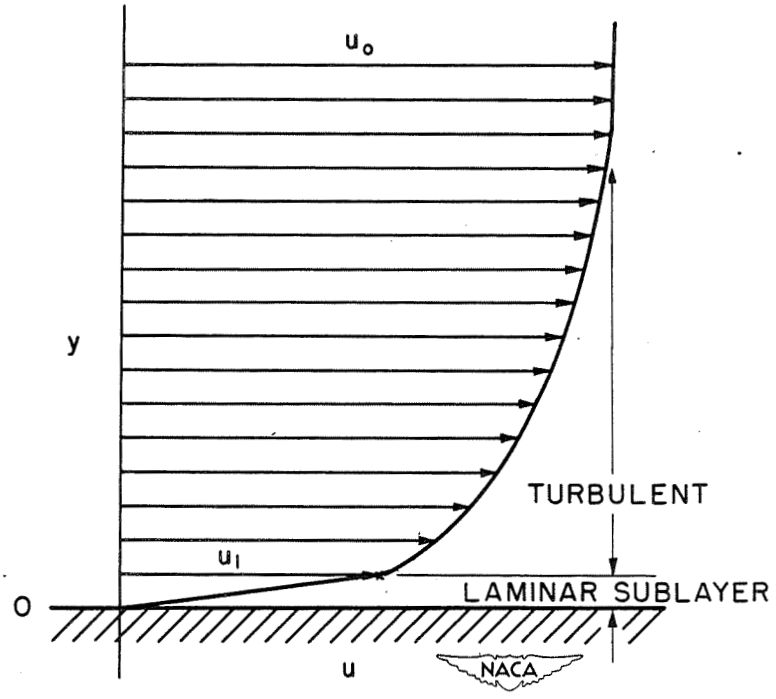

Figure 4.- Assumed turbulent-velocity profile.

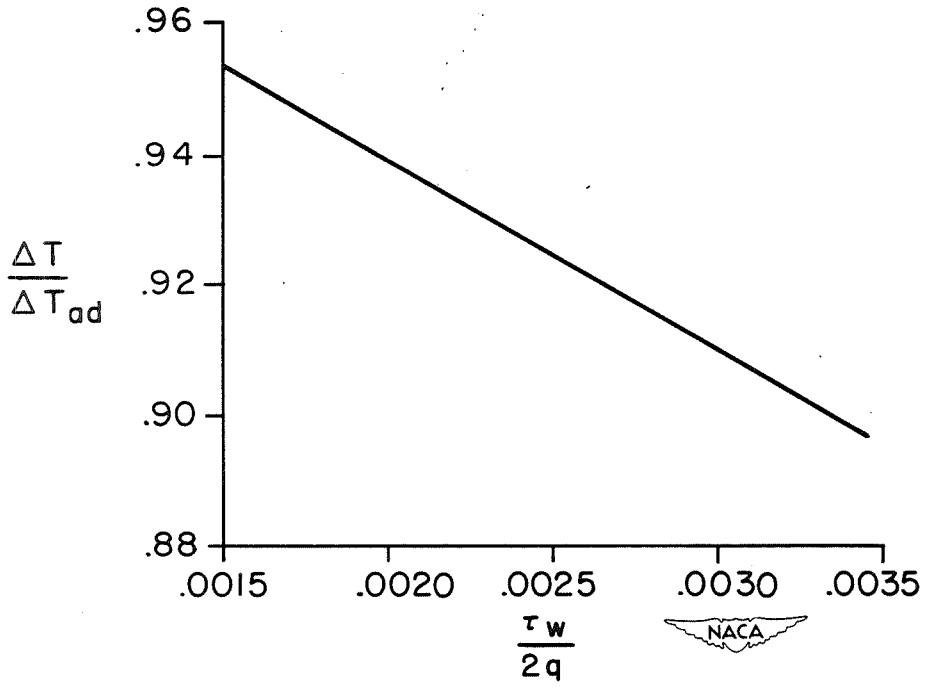

Figure 5.- Theoretical temperature recovery for turbulent boundary layer.

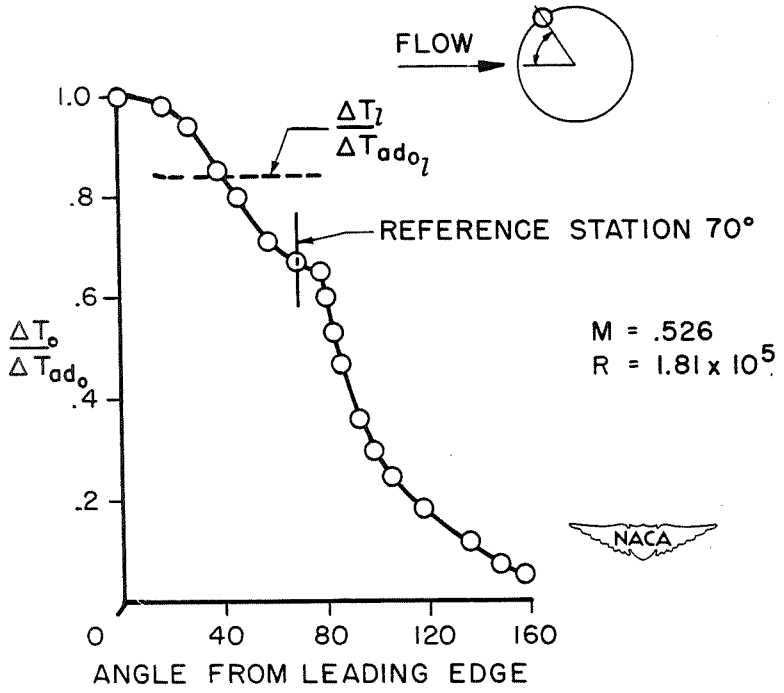

Figure 6.- Temperature recovery on circular cylinder.

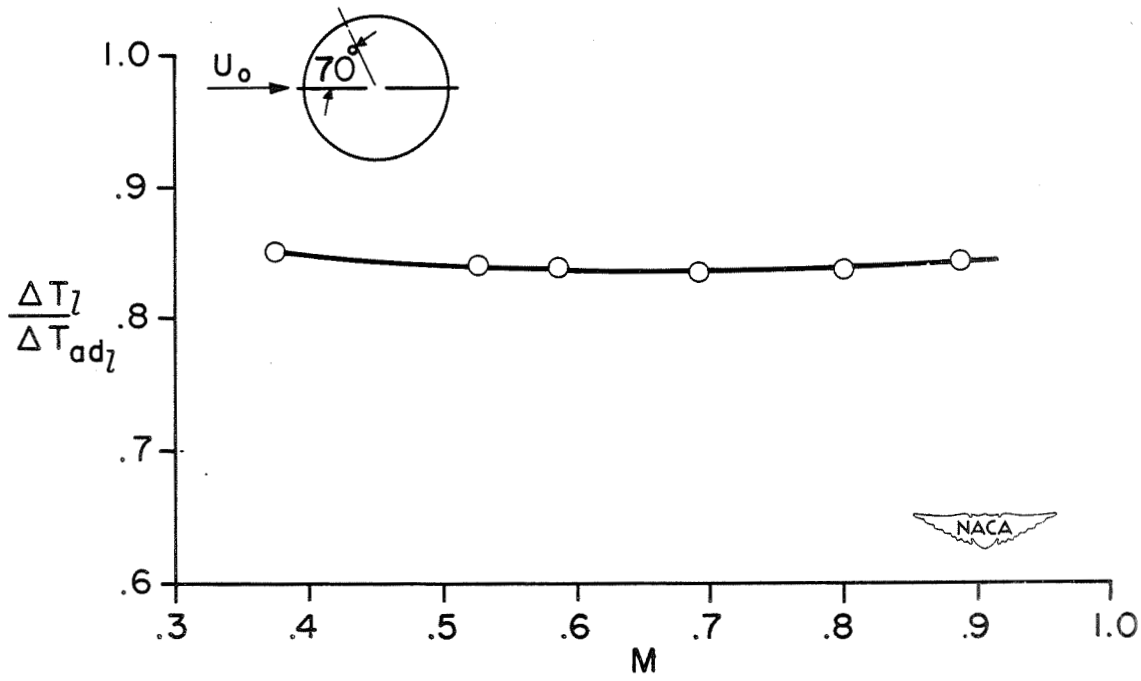

Figure 7.- Temperature recovery at 70° station on circular cylinder at various free-stream Mach numbers.